

UNCLASSIFIED

AD NUMBER
AD488995
NEW LIMITATION CHANGE
TO Approved for public release, distribution unlimited
FROM Distribution authorized to U.S. Gov't. agencies and their contractors; Critical Technology; AUG 1966. Other requests shall be referred to Air Force Flight Dynamics Lab., Attn: FDTS, Wright-Patterson AFB, OH 45433.
AUTHORITY
AFWAL ltr dtd 29 Nov 1988

THIS PAGE IS UNCLASSIFIED

113834

AFFDL-TR-65-230 ✓

AFRL-TR-65-230

**HYDROGEN TANKAGE
FOR
HYPERSONIC CRUISE VEHICLES
- PHASE I**

John H. Heathman, et al

GENERAL DYNAMICS
Convair Division

TECHNICAL REPORT AFFDL-TR-65-230

August 1966

"This document is subject to special export controls and each transmittal to foreign governments or foreign nationals may be made only with prior approval of the Air Force Flight Dynamics Laboratory AFFDL/FDTS."

AIR FORCE FLIGHT DYNAMICS LABORATORY
RESEARCH AND TECHNOLOGY DIVISION
AIR FORCE SYSTEMS COMMAND
WRIGHT-PATTERSON AIR FORCE BASE, OHIO

20070925189

NOTICES

When Government drawings, specifications, or other data are used for any purpose other than in connection with a definitely related Government procurement operation, the United States Government thereby incurs no responsibility nor any obligation whatsoever; and the fact that the Government may have formulated, furnished, or in any way supplied the said drawings, specifications, or other data, is not to be regarded by implication or otherwise as in any manner licensing the holder or any person or corporation, or conveying any rights or permission to manufacture, use, or sell any patented invention that may in any way be related thereto.

Copies of this report should not be returned to the Research and Technology Division unless return is required by security considerations, contractual obligations, or notice on a specific document.

**HYDROGEN TANKAGE
FOR
HYPERSONIC CRUISE VEHICLES
- PHASE I**

John H. Heathman, et al

"This document is subject to special export controls and each transmittal to foreign governments or foreign nationals may be made only with prior approval of the Air Force Flight Dynamics Laboratory AFFDL/FDTS. "


FOREWORD

This is the Final Report on Phase I, of a three phase program, performed under Contract AF33(615)-2048. This report covers work performed during the period from July 1964 to September 1965.

This contract, with General Dynamics Convair, San Diego, California, was initiated under Project and Task Number 651G. The work was administered under the direction of the Air Force Flight Dynamics Laboratory, with Mr. L. G. Kelly, FTDS, as Project Monitor.

Project Leader for General Dynamics Convair on this program is Mr. J. H. Heathman of Advanced Launch and Reentry Systems, under the administration of Mr. R. A. Nau, Manager. Others who contributed in studies and preparation of this report include Messrs. G. Yates, Thermodynamics; W. Egli, Fuel and Insulation Systems; T. L. Stockham, Testing; J. L. Christian, Material Evaluation; D. Neff, Strain Gage Evaluation; and J. Rose, Tank Fabrication.

This technical documentary report has been reviewed and is approved.


R. L. Cavanagh
Applied Mechanics Branch
Research and Technology Division
Air Force Flight Dynamics Laboratory

(ABSTRACT)

This is the Final Report on Phase I, of a three phase program, under contract AF33(615)-2048 (Reference 1) to design, fabricate and experimentally verify non-integral, insulated, liquid hydrogen tankage for manned hypersonic cruise vehicles. The vehicles mission data, fuel quantity and usage rates were supplied by the Research and Technology Division of the Air Force Flight Dynamics Laboratory. This report presents design criteria, results of large scale tank design studies, an optimization program, supporting test and evaluation work, and an experimental test program to determine the design requirements for a lightweight, reliable tankage system. Design studies covered structural materials and concepts, insulation systems, and fuel system requirements. Results of the optimization program on the large scale designs provided the basis for the design and fabrication of the two thin-gage, 130 gallon, subscale experimental tanks. The recommended tank design, which employed the 718 alloy and the all-Microquartz insulation system in a helium environment, was then tested in a simulated vehicle environment. This testing gave data on transient temperature rise and stratification of the ullage, transient heating rates to and stratification of the liquid, boil-off cooling effects on tank wall temperature, and a comparison of actual thermal performance with analytical predictions. This work provides the basis for establishment of the design requirements of a large-scale tank to be designed, fabricated and proof tested in Phase II. This tank will then be tested in Phase III to a simulated vehicle environment which includes programmed liquid hydrogen defueling.

TABLE OF CONTENTS

<u>Section</u>	<u>Page</u>
1.0 Introduction	1
2.0 Mission Data and Design Criteria	3
2.1 Mission Data and Vehicle Configuration	3
2.2 Temperature Trajectory	3
2.3 Structural Criteria	3
2.4 Insulation System Criteria	8
2.5 Fuel System Criteria	9
3.0 Preliminary Large-Scale Tank Designs	11
3.1 Structural Material Evaluation	11
3.2 Tank Structure	15
3.3 Insulation Systems	33
3.4 Fuel System	61
4.0 Optimization of Large-Scale Tank Design	67
4.1 Input Data	67
4.2 Optimization Analysis	68
4.3 Results	74
5.0 Experimental Test Program	93
5.1 Tank Structure Design	93
5.2 Insulation Design and Fabrication	105
5.3 Subscale Tank Testing	123
5.4 Thermal Test Results	140
5.5 Correlation of Test Results	163
6.0 Phase I Conclusions and Large-Scale Tank Recommendations	199
7.0 References	203
Appendix I - Cryotherm Testing	205
Appendix II - Strain Gage Evaluation	233
Appendix III - Evaluation of the Effects of Hydrogen Exposures on the Mechanical Properties of Titanium 5Al 2.5 Sn ELI Alloys	291

LIST OF FIGURES

<u>Figure</u>		<u>Page</u>
1	Representative Vehicle Configuration	4
2	Equilibrium Skin Temperatures	5
3	Simulated Temperature Profile for Testing - Radiation Shield	6
4	Fuel Flow Schedule	10
5	Ultimate Tensile Strength/Density vs. Temperature for Candidate Materials	13
6	Yield Strength (0.2%)/Density vs. Temperature for Candidate Materials	14
7	Tank Supports - Material Selection	16
8	Preliminary Design - Tank Structure	19
9	Tank Skin vs. Operating Pressure	20
10	Maximum Ultimate Shear and Axial Load Intensities	21
11	Tank Skins - Compression Buckling vs. Frame Spacing	22
12	Tank Skins - Shear Buckling vs. Frame Spacing	23
13	Skin/Stiffener to Tank Skin Area Ratio vs. Operating Pressure	24
14	Plate-Stringer Area and Radius of Gyration vs. Stringer Spacing to Stringer Depth Ratio	26
15	Ellipsoidal Dome ($a/b = \sqrt{2}$) - Meridian and Hoop Load Intensities as a Function of Pressure	28
16	Preliminary Design - Tank Supports	30
17	Tank Structural Weight vs. Operating Pressure	31
18	Thermal Conductivity (K) of Dynaquartz in He	36
19	Thermal Conductivity (K) of Dynaquartz in N ₂	37
20	Composite Insulation Systems	38
21	Thermal Conductivity (K) of Low Temperature Insulations	40
22	Thermal Conductivity (K) - Linde Super-Insulation Vacuum Panels and Compressed Super-Insulation	41
23	Thermal Conductivity Times Density (Kρ) of Low Temperature Insulations	42
24	Composite Insulation Schematic	43
25	Ground-Hold Heat Fluxes to LH ₂ vs. Insulation Thickness	47
26	Hydrogen Mass in Tank after 30 Minutes Ground-Hold	49

LIST OF FIGURES (CONTINUED)

<u>Figure</u>		<u>Page</u>
27	Equivalent LH ₂ Mass Loss During 30 Minute Ground-Hold - Self Pressurization	50
28	Heat Flux to LH ₂ vs. Flight Time - Microquartz (He)	51
29	Heat Flux to LH ₂ vs. Flight Time - Top Surface - Microquartz (He)	52
30	Heat Flux to LH ₂ vs. Flight Time - Microquartz (N ₂)/Foam Composite	53
31	Tank Wall Temperature (Top Surface) vs. Trajectory Time	54
32	Heat Flux to Ullage Through Top Surface - 520°R Tank Wall Temperature	56
33	Time Top Tank Wall Reaches 520°R - Start of Spray Cooling	57
34	Temperature Distribution Along Tank Support Members - Ground-Hold Condition	59
35	Tank Support Members - Temperature Distribution (In-flight)	60
36	Ground-Hold Storage Options	62
37	Tank Fill and Ground-Hold Fuel Levels	64
38	Area and Volume Relationships of Tank	69
39	Optimization Program - Computer Flow Diagram	71
40	Total Tank Weight Breakdown vs. Bottom Insulation - Microquartz (He)	75
41	Total Tank Weight Breakdown vs. Vent Pressure - Microquartz (He) Insulation	76
42	Flight Time at Which LH ₂ Boiling Starts	77
43	Take-off Weight vs. Insulation Thickness - Microquartz (He) 0.5-Inch Top Insulation	78
44	Take-off Weight vs. Insulation Thickness - Microquartz (He) 1.0-Inch Top Insulation	79
45	Take-off Weight vs. Insulation Thickness - Microquartz (He) 2.0-Inch Top Insulation	80
46	Take-off Weight vs. Insulation Thickness - Microquartz (He) 3.0-Inch Top Insulation	81
47	Take-off Weight vs. Venting Pressure - Microquartz (He)	83
48	Optimum Take-off Weight vs. Top Insulation Thickness - Microquartz (He)	84

<u>Figure</u>	LIST OF FIGURES (CONTINUED)	<u>Page</u>
49	Total Tank Weight Breakdown vs. Bottom Insulation - Micro-quartz (N ₂)/Foam Composite	85
50	Take-off Weight vs. Insulation Thickness - Microquartz (N ₂)/Foam Composite (1.0 Inches)	86
51	Take-off Weight vs. Insulation Thickness - Microquartz (N ₂)/Foam Composite (1.5 Inches)	87
52	Take-off Weight vs. Insulation Thickness - Microquartz (N ₂)/Foam Composite (2.0 Inches)	88
53	Take-off Weight vs. Venting Pressure - Microquartz (N ₂)/Foam Composite	89
54	Optimum Top Insulation - Microquartz (N ₂)/Foam Composite	90
55	Subscale Tank #1 Configuration	94
56	Subscale Tank #2 Configuration	95
57	Bipod Tank Support System - Installed	97
58	Fill/Drain and Vent Line Assemblies	98
59	Subscale Tank Manufacturing Breakdown and Assembly Sequence	100
60	Subscale Tank #1 Structure Assembly	102
61	Microquartz Insulation System - Tank #1	107
62	Stitching of the Insulation Blankets	109
63	Close-up View of Insulation Blanket Stitching	109
64	Insulation Blanket Assembly - Cone Ends	110
65	Insulation Blanket Assembly - Cylindrical Section	110
66	Insulated Subscale Tank #1 in Support Fixture	111
67	Cryopumping and Overheating Criteria for Foam/Microquartz Insulation	113
68	Microquartz/Foam Composite Insulation - Foam Thickness Required to Maintain the Interface Temperature at 150°R During Ground-Hold Condition	116
69	Microquartz/Foam Composite Insulation System - Tank #2	117
70	Sealed Foam Test Specimens	119
71	Sealed Foam Specimens - Environmental Tests	121
72	Tank #1 Helium Mass Spectrometer Leak Check	125
73	Schematic Diagram of Test Tank Installation	132

LIST OF FIGURES (CONTINUED)

<u>Figure</u>		<u>Page</u>
74	Subscale Tank Fuel System Schematic	133
75	Subscale Tank Instrumentation Location	138
76	Subscale Tank #1 - Liquid Level and Temperature Sensors	139
77	Test Tank Installed in Environmental Chamber	141
78	Radiation Shield Temperature - Top - Test 3	143
79	Subscale Test Tank Pressure - Test 3	145
80	Subscale Tank Liquid Level - Test 3	146
81	Liquid Heat Flux Rate - Test 3	147
82	Altitude Chamber Pressure - Test 4	148
83	Radiation Shield Temperature - Bottom - Test 4	149
84	Subscale Test Tank Pressure - Test 4	150
85	Liquid Heat Flux - Test 4	151
86	Top Tank Skin Temperature - Test 4	152
87	Bottom Insulation Temperature - Test 5	154
88	Subscale Tank Liquid Level - Test 6	155
89	Liquid Heat Flux Rate - Test 6	156
90	Ullage and Vent Gas Temperature - Test 6	157
91	Top Insulation, Skin and Ullage Temperature - Test 6	158
92	Test Tank and Chamber Pressure - Test 7	159
93	Subscale Tank Liquid Level - Test 7	160
94	Liquid Heat Flux Rate - Test 7	161
95	Liquid/Ullage Temperature - Test 7	162
96	Subscale Test Tank Pressure - Test 8	164
97	Subscale Tank Liquid Level - Test 8	165
98	Liquid Heat Flux Rate - Test 8	166
99	Test Tank Pressure - Test 9	167
100	Subscale Tank Liquid Level - Test 9	168
101	Heat Flux Rate to Cylindrical Area - Tank #1	170
102	Heat Flux Rate to Cone End - Tank #1	172
103	Heat Flux Through Penetrations - Tank #1	173

LIST OF FIGURES (CONTINUED)

<u>Figure</u>		<u>Page</u>
104	Heat Flux to Liquid - Tank #1	174
105	Thermal Conductivity Ratio of Microquartz in Helium vs. Pressure - Tank #1	175
106	Top Insulation, Tank Skin and Ullage Temperature - Test 9	176
107	Bottom Insulation Temperature - Test 3	177
108	Bottom Insulation Temperature - Test 8	178
109	Heat Flux Rate to Liquid - Test 6	180
110	Convective Heat Loss in Subscale Tank at Ground-Hold	181
111	Forward Longitudinal Support Temperature - Test 8	182
112	LH ₂ Stratification at Ground-Hold - Test 7	187
113	Top Tank Skin Temperatures - Mid-Section	189
114	Nitrogen Ullage Temperatures - Test 3	190
115	Hydrogen Ullage Temperatures - Test 8	191
116	Deviation in Measured Boil-off Rate from Predicted Boil-off Rate	195
117	Cryotherm Specimen Configuration	207
118	Insulation Blanket-Test Specimen GD/C 65-59341-1	209
119	Details for Insulation Test Specimen GD/C 65-59343-3	210
120	Mounting Plate - Insulation Test Specimen	211
121	Cryotherm Apparatus	213
122	Temperature and Pressure Program - Subscale Tank Tests	214
123	Thermal Conductivity (K) of Polyurethane Foam (Freon Blown) - Corrected for Adhesive Penetration	217
124	Thermal Conductivity (K) at 760 mm Hg in Nitrogen	218
125	Thermal Conductivity (K) at 8 mm Hg in Nitrogen	219
126	Thermal Conductivity (K) at 760 mm Hg in Helium	220
127	Thermal Conductivity (K) at 8 mm Hg in Helium	221
128	Temperature Profiles for -5 Specimen - Cryotherm Tests	224
129	Temperature Profiles for -803 Specimen - Cryotherm Tests	225
130	Heat Flux Rate and Accumulative Heat Flux for -803 Specimen (Run #2) - Cryotherm Tests	226
131	Temperature Profiles for -5 Specimen with Thermal Barrier - Cryotherm Tests	227

<u>Figure</u>	LIST OF FIGURES (CONTINUED)	<u>Page</u>
132	Temperatures of the -5 Specimen at the Microquartz/Foam Interface - Adhesive Failure	228
133	Thermal Conductivity (K) of Foam and Associated Gases	232
134	Mounting of FNB-50-12E Strain Gauge, Prior to Spraying on Protective Coat Cover	236
135	Strain Gage Installation on Tensile Coupons	238
136	FNB-50-12E Strain Gauges in Various Phases of Mounting on Test Coupons	239
137	Typical Circuit for FNB-50-12E Strain Gauge	240
138	Instrumentation and Specimen Being Lowered into LN ₂ for $\frac{\Delta T}{\Delta G}$ Determination	242
139	Zero Shift vs. Ballast Resistor - Inconel (72 to -320 ^o F)	244
140	Zero Shift vs. Ballast Resistor - Titanium (72 to -320 ^o F)	245
141	Circuit Sensitivity vs. R _B Resistance	247
142	Thermal Output vs. Temperature - Strain Gage on Inconel 718	248
143	Thermal Output vs. Temperature - Strain Gage on Inconel 718	249
144	Thermal Output vs. Temperature - Strain Gage on Titanium	250
145	Thermal Output vs. Temperature - Strain Gage on Titanium	251
146	FNB-50-12E Strain Gage Thermal Output	252
147	Constant Strength Beam Apparatus	254
148	Gage Factor vs. Temperature FNB 50-12E Strain Gage	257
149	Resistance Change of Copper Wire	259
150	Curing Strain Gage Installations on Tank #1	266
151	Strain Gage Installation - Subscale Tank #1	267
152	Inside Instrumentation - Subscale Tank #1	268
153	Outside Instrumentation - Subscale Tank #1	269
154	Strain Gage & Thermocouple Installation - Tank #2	270
155	Hoop Strain - Water Proof Test (Inconel 718)	271
156	Hoop Strain - Water Proof Test (Inconel 718)	272
157	Longitudinal Strain - Water Proof Test (Inconel 718)	273

LIST OF FIGURES (CONTINUED)

<u>Figure</u>		<u>Page</u>
158	Hoop Strain - LN_2 Proof Test (Inconel 718)	274
159	Hoop Strain - LN_2 Proof Test (Inconel 718)	275
160	Longitudinal Strain - LN_2 Proof Test (Inconel 718)	276
161	Hoop Strain - Water Proof Test (Titanium)	278
162	Longitudinal Strain - Water Proof Test (Titanium)	279
163	Strain Gage Output (194) - LN_2 Tests	281
164	Strain Gage Output (194) - LH_2 Tests	282
165	Strain Gage Output (195) - LN_2 Tests	283
166	Strain Gage Output (195) - LH_2 Tests	284
167	Strain Gage Output (196) - LN_2 Tests	285
168	Strain Gage Output (198) - LN_2 Tests	286
169	Strain Gage Output (198) - LH_2 Tests	287
170	Strain Gage Output (199) - LN_2 Tests	288
171	Strain Gage Output (199) - LH_2 Tests	289
172	Standard Tensile Specimens for Smooth and Notched ($K_t = 6.3$) Tests	297
173	Schematic View of Hydrogen Exposure Apparatus	298
174	General View of Gaseous Exposure Test Apparatus	299
175	Retort for Gaseous Hydrogen Exposures	300
176	Schematic View of Load Applicator	301
177	Mechanical Properties at 75°F , After Exposure to 1.0 psig H_2 Gas for 5 Hours	302
178	Mechanical Properties at -423°F , After Exposure to 1.0 psig H_2 Gas for 5 Hours	303
179	Mechanical Properties at 75°F , After Exposure to 1.0 psig H_2 Gas for 50 Hours	304
180	Mechanical Properties at -423°F , After Exposure to 1.0 psig H_2 Gas for 50 Hours	305
181	Mechanical Properties at 75°F , After Exposure to 1.0 psig H_2 Gas for 5 Hours with 10 KSI Load	306
182	Mechanical Properties at -423°F , After Exposure to 1.0 psig H_2 Gas for 5 Hours with 10 KSI Load	307

LIST OF FIGURES (CONTINUED)

<u>Figure</u>		<u>Page</u>
183	Mechanical Properties at 75 ⁰ F, After Exposure to 1.0 psig H ₂ Gas for 50 Hours with 10 KSI Load	308
184	Mechanical Properties at -423 ⁰ F, After Exposure to 1.0 psig H ₂ Gas for 50 Hours with 10 KSI Load	309
185	Photomicrograph of Titanium (Heat #3930498) - As Received	310
186	Photomicrograph of Titanium (Heat #3930498) - After Exposure to 1.0 psig H ₂ Gas at 200 ⁰ F, for 50 Hours, with 10 KSI Load	310
187	Photomicrograph of Titanium (Heat #3930498) - After Exposure to 1.0 psig H ₂ Gas at 300 ⁰ F, for 50 hours, with 10 KSI Load	311
188	Photomicrograph of Titanium (Heat #3930498) - After Exposure to 1.0 psig H ₂ Gas at 500 ⁰ F, for 50 hours, with 10 KSI Load	311
189	Photomicrograph of Titanium (Heat #3930498) - After Exposure to 1.0 psig H ₂ Gas at 600 ⁰ F, for 5 hours, with 10 KSI Load	312

LIST OF TABLES

<u>No.</u>		<u>Page</u>
1	Critical Tank Loading - Ultimate	17
2	Penetration Heat Leak Rates	58
3	Sealed Foam Specimens - Test Results	120
4	Subscale Tank Instrumentation	135
5	Typical Boil-off Losses During a Test	184
6	Heat Flux Rates Resulting from LH ₂ Stratification Tests	186
7	Test Results Summary	216
8	Thermal Cycling Test Results, 65-59343-5 Specimen	229
9	Microquartz/Foam Test Specimen Temperatures	231
10	History and Chemical Analysis of Titanium 5Al 2.5 Sn ELI Alloy	313
11	Mechanical Properties of Titanium 5Al 2.5 Sn ELI Alloy (Heat No. 3930498, 0.032 Inch Thick Sheet)	314
12	Mechanical Properties of Titanium 5Al 2.5 Sn ELI Alloy (Heat No. D-3274, 0.006 and 0.013 Inch Thick Sheet)	321
13	Mechanical Properties of Titanium 5Al 2.5 Sn ELI Alloy (Heat No. D-5907, 0.032 Inch Thick Sheet)	322

1.0 INTRODUCTION

This report presents work accomplished in Phase I of a three-phase program to design, fabricate and obtain experimental verification of liquid hydrogen tankage applicable to manned hypersonic vehicles. The programs flow diagram on the three phases is shown at the end of this introduction. This diagram also shows the interrelating of tasks performed in Phase I and their influence on Phase II work.

The objective of the Phase I work was to arrive at design recommendations for a large-scale, flight-weight, non-integral liquid hydrogen fuel tank, designed for use in a hypersonic vehicle with long-time cruise capability.

Design criteria were established, based upon mission data, vehicle configuration, and fuel usage requirements for the hypersonic cruise vehicle specified.

Preliminary large-scale tank design studies were carried out with the view to investigating aspects of the tankage system having an influence on the total performance. Tank structural concepts and material candidates were evaluated as a means of providing minimum tankage weight, compatible to the environmental conditions. Survey of insulation systems was made to determine suitable candidates, having sufficient thermal data on which to conduct a reliable thermal analysis. Fuel system requirements were investigated in order that they would provide maximum thermal performance provisions for minimum weight. Large scale tank geometry consists of a main shell 20 feet long with a cross-section of two intersecting circles 64 inches in diameter providing a total width of 8 feet. An influencing ground rule was that the tank would have the capability to support the load factors associated with the taxi condition without pressure-stabilization. This requirement gives the tank a capability of handling all flight loading without the need for internal pressure.

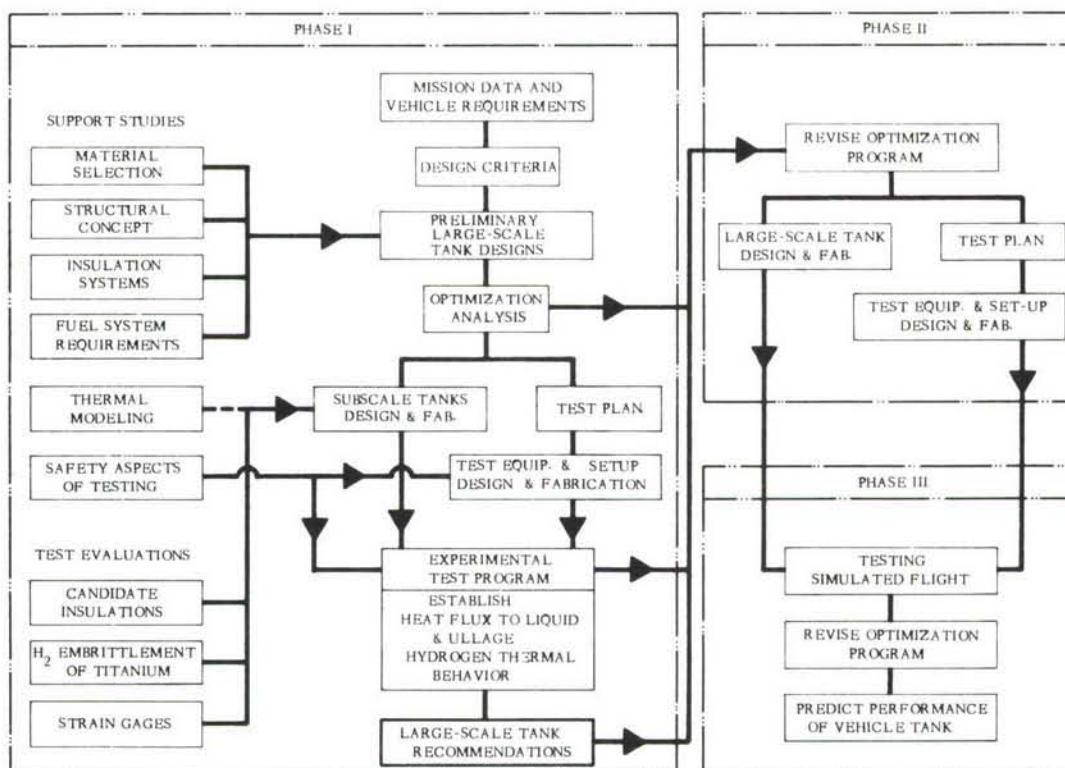
Testing and evaluation studies were carried out on strain gages, and the potential embrittlement of titanium under hydrogen gas exposures. These testing programs were necessary in order to define these possible problem areas and support the work to be accomplished in Phase II.

An optimization analysis was performed, with the use of a computer program, on the basis of the design criteria and the results of the large-scale tank investigations, for minimum take-off weight and the capability to carry fuel in the amount specified for the time required. Parameters used in the optimization were tank pressure, fuel boil-off, and the weight of structure, insulation and fuel system. The program assumed the use of a boost pump to handle saturated fuel conditions and that the tank wall is limited to room temperature by spray cooling.

Thermal modeling was investigated with the view to establishing the degree to which the testing of models can be employed in predicting vehicle tank performance and feasibility of using liquid nitrogen to simulate liquid hydrogen in testing. This investigation revealed that neither of these considerations were feasible, since dimensioning fluid and materials and/or environmental conditions cannot be independently varied within the limits of the thermal laws.

Two subscale tanks were designed and fabricated from the results of the optimization analysis, large scale tank designs and test requirements. These tanks employed the two candidate insulation systems, the all Microquartz (helium environment) system and the foam/Microquartz (nitrogen environment) composite sealed system, and structural material candidates 718 nickel super alloy and the 5 Al 2.5 Sn titanium alloy ELI termed Tank #1 and Tank #2, respectively. Investigation into the composite system revealed the need to do some preliminary testing under the specific environment conditions being employed by this program. This testing was accomplished in a cryotherm apparatus. These tests established thermal conductivities, and determined durability under cyclic temperature and pressure conditions. The effects of variation in conductivity, manufacturing tolerances and fabrication procedures for the composite system were also evaluated. Testing of the composite system revealed extreme sensitivity to overheating at the interface from small variation in conductivity, relative thickness and density of the composite elements and fabrication methods used. This, together with the small amount of additional data that would be obtained from testing this tank, resulted in the termination of further work after the structural proof test of Tank #2. Testing of Tank #1, utilizing the all Microquartz insulation system and the 718 alloy, provided information on the transient temperature rise and stratification in the ullage, transient heating rates to the liquid, and boil-off cooling effects on tank wall temperatures. Performance evaluation determined from tests was then compared with analytically predicted performance.

PROGRAM FLOW DIAGRAM



2.0 MISSION DATA AND DESIGN CRITERIA

2.1 MISSION DATA AND VEHICLE CONFIGURATION

Mission data and vehicle configuration were supplied by the AFFDL and are typical of a manned hypersonic cruise vehicle. The representative vehicle configuration is shown in Figure 1. The insulated liquid hydrogen tank to be optimized is located in the forward fuselage section between stations 30 and 50. The fuselage is described as an elliptical cone with an 8° half angle in the profile view and a 10° half angle in the plan view. The flight angle of attack is 5° .

2.2 TEMPERATURE TRAJECTORY

Based on provided mission data and vehicle geometry, equilibrium skin temperatures were calculated along the trajectory on the top, bottom, and side of the fuselage. Equilibrium temperatures at station 40 are shown in Figure 2. Temperatures from station 30 to 50 vary by only about 30° ; since this variation is not considered significant, a constant temperature along the fuselage length was assumed. The fuselage was divided into upper and lower zones for the purpose of analysis and test. The upper and lower temperature profiles as a function of time are shown in Figure 3. Since the fuselage structure is assumed to be an all metal honeycomb with no insulation, temperature drop through the fuselage structure was assumed to be negligible.

Heat is transferred from the fuselage to the tank insulation primarily by convection during ground hold and by radiation during the cruise portion of the flight. The fuselage was assumed to contain a dry inert environment of either helium or nitrogen depending on the insulation system in use.

2.3 STRUCTURAL CRITERIA

2.3.1 PRESSURIZATION LOADS. The following criteria on pressurization complies with MIL-A-8861 (Reference 2) paragraph 3.1.7 and is consistent with Reference 1.

The tank and supporting structure will be designed for all fuel levels from full to empty for the following conditions:

Limit Design -

- a) Any possible combination of differential pressure with limit ground and flight loads without harmful permanent deformation.
- b) 1.33 times any possible combination of differential pressures with 1.0 'g' flight loads without harmful permanent deformation.

The tank is not dependent on pressurization for its structural integrity during fueling or before take-off.

The differential pressure includes any tolerance due to relief valve operation, etc.

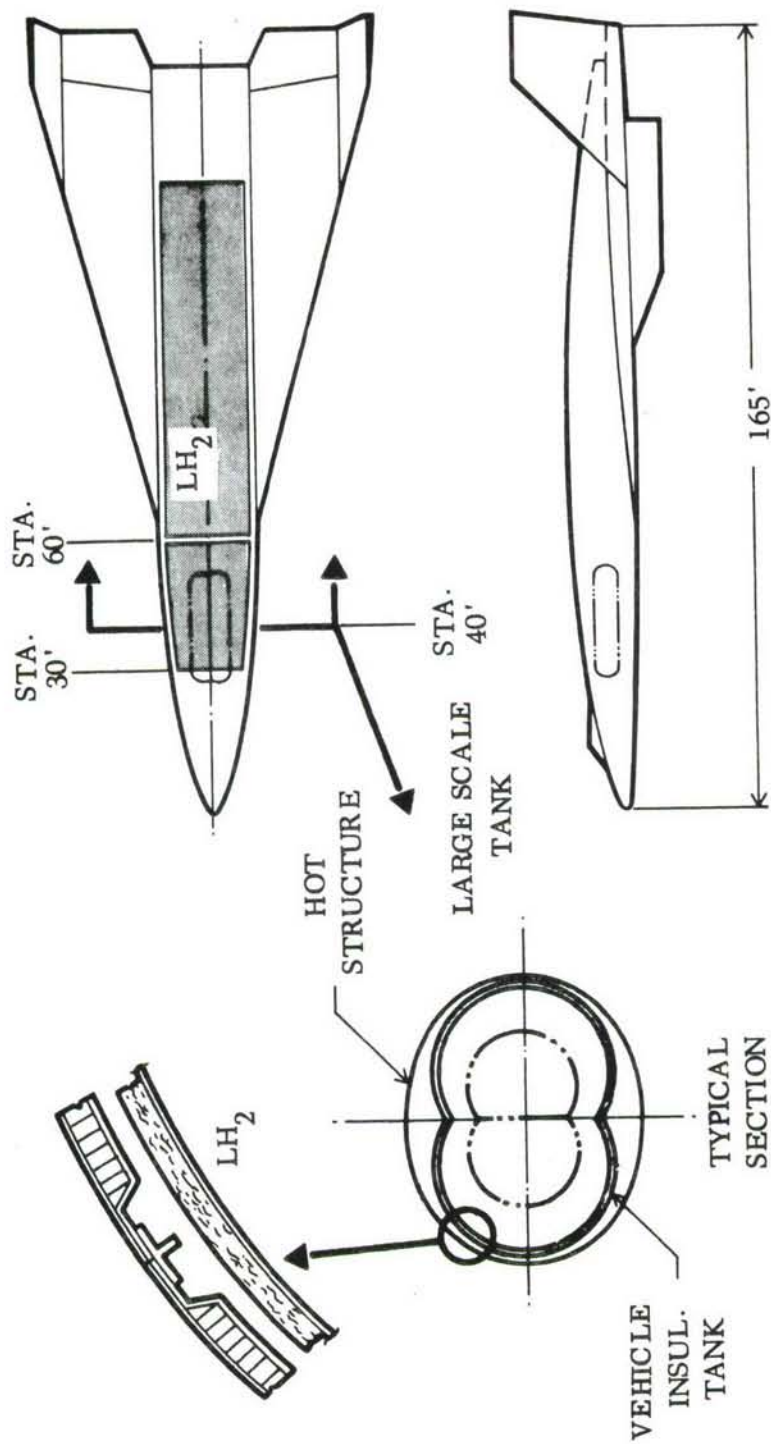


FIGURE 1. REPRESENTATIVE VEHICLE CONFIGURATION

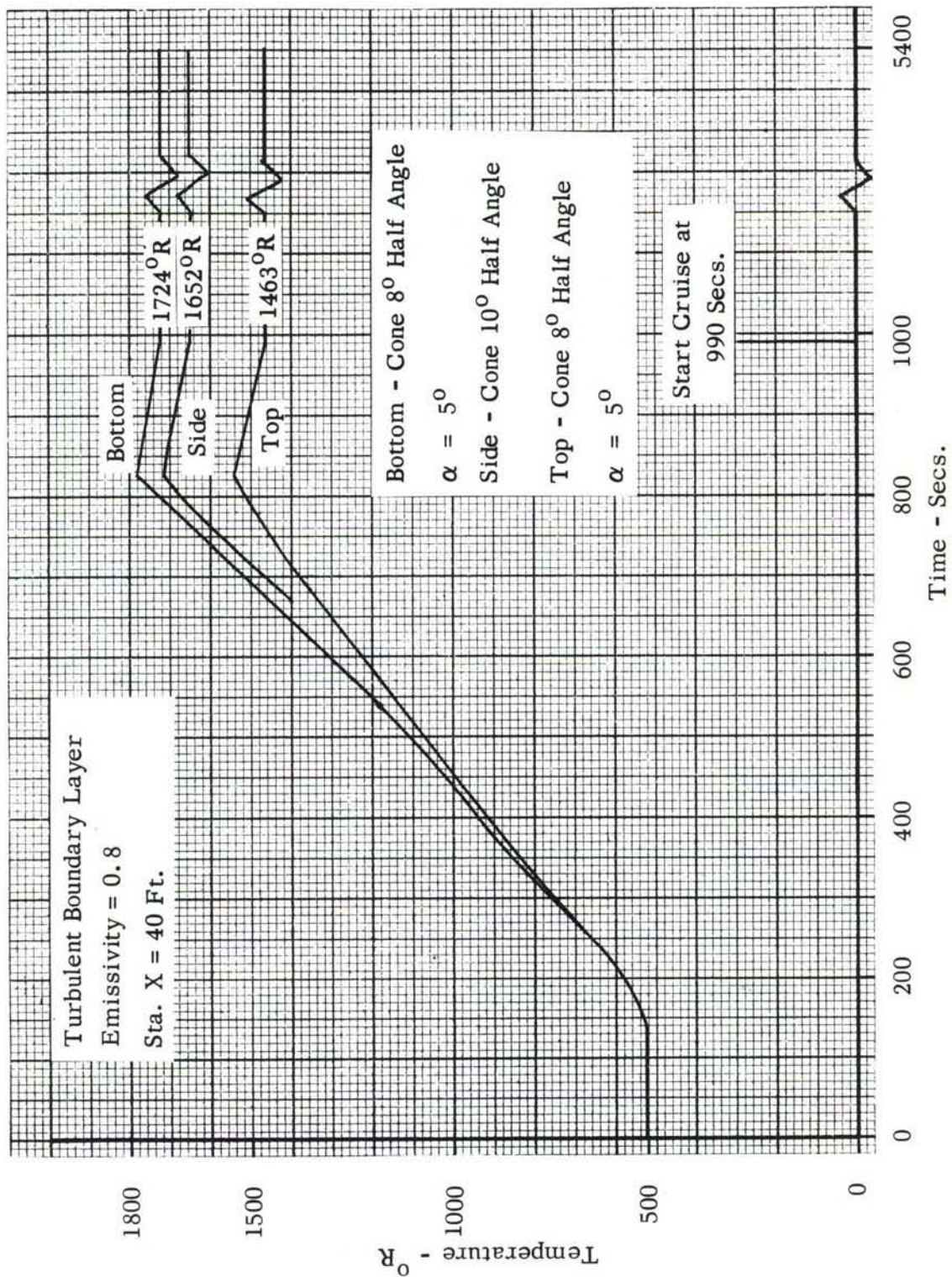


FIGURE 2 - EQUILIBRIUM SKIN TEMPERATURES

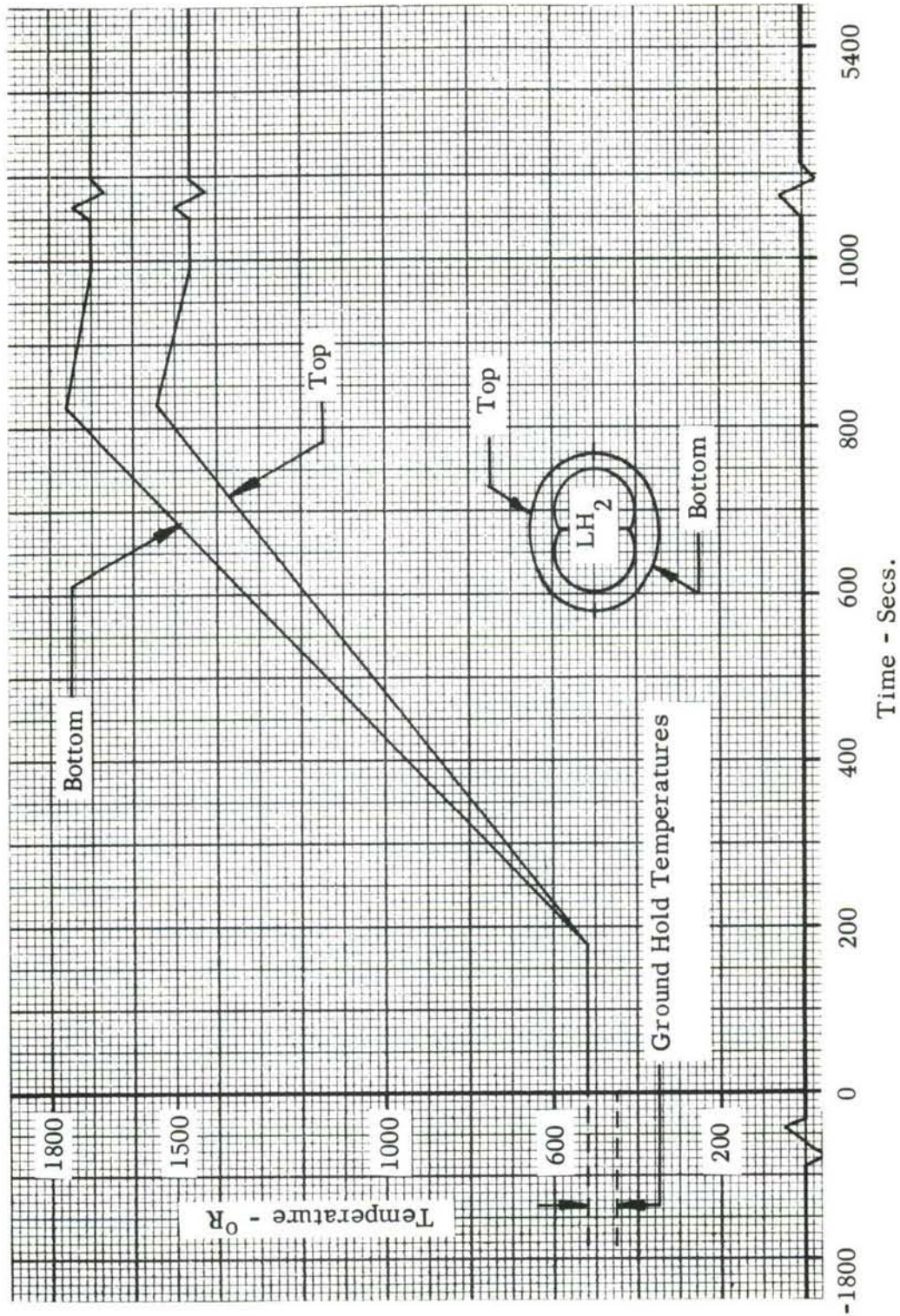


FIGURE 3 - SIMULATED TEMPERATURE PROFILE FOR TESTING - RADIATION SHIELD

2.3.2 FLIGHT LOAD FACTORS. The following limit load factors act independently. They represent the maximum flight inertia load factors experienced by the vehicle during its flight trajectory. Tank full to empty conditions apply.

Longitudinal:	0.5 forward and aft
Lateral:	0.5 right and left
Vertical:	2.0 down, 0.0 up

The following load factors are ultimate, act independently and apply only to tank supports, attachments and carry-through structure. These factors are in agreement with MIL-A-8865 (Reference 3, paragraph 3.3.3) and apply through tank full to empty conditions.

Longitudinal:	3.0 forward 1.5 aft
Lateral:	1.5 to right and to left
Vertical:	4.5 down, and 2.0 up

2.3.3 TAXI LOAD FACTORS. The following limit load factors apply to the ground-hold and taxi conditions, act independently and apply to a full tank for both zero and full pressurization.

Longitudinal:	0.8 forward, 0.5 aft
Lateral:	0.5 right and left
Vertical:	2.0 down, 0.0 up

2.3.4 ALLOWABLE STRESSES. The criteria of allowable stresses shall be as follows:

a) LIMIT

The structural components shall not yield under maximum operating conditions.

b) ULTIMATE

The structural components shall not fail or experience instability under ultimate loads. The ultimate factor of safety shall be:

$$\text{Ultimate Factor of Safety} = 1.5$$

c) FATIGUE

Structural components shall withstand 500 flight cycles. Room temperature allowable stresses will be used except where the design temperatures are more critical.

2.3.5 PRESSURE TEST INFLUENCE ON STRUCTURAL CRITERIA. The tank is to be tested with water and liquid nitrogen at a pressure of 1.33 times the maximum

design pressure to substantiate structural integrity. Water testing is safe in that water under pressure has very little stored energy. A tank failure would not be catastrophic because the initial opening in the tank would relieve the pressure limiting the damage to the initial failure. Testing with the liquid nitrogen serves the same purpose as the water test except that it also proves the tank integrity at cryogenic temperatures. Since water is approximately 14 times denser, and liquid nitrogen 11 times denser than liquid hydrogen, filling the tank with either in the horizontal position will overload the structure in shear and bending. Since the tank will be designed for liquid hydrogen and not the water or liquid nitrogen condition, test procedures such as water immersion, liquid displacement, on-end testing, or additional supporting will be developed.

2.3.6 TANK SUPPORTS CRITERIA. The tank support system will be designed to the following criteria:

- a) The tank is supported in such a manner as to allow for differential thermal expansion of the tank and supporting structure.
- b) Tank supports are designed to minimize heat leak into the liquid hydrogen. The maximum allowable heat leak will be no more than 30% of total heat leak.
- c) Tank supports are the minimum number to satisfy static equilibrium.

2.4 INSULATION SYSTEM CRITERIA

All insulation systems shall conform to the following design criteria:

- a) The insulation system shall have a service life of 500 normal missions without refurbishment or major repair.
- b) Multiple-component insulations must be designed to prevent cryopumping of N_2 during all phases of operation.
- c) Sealed and evacuated systems must be capable of being checked for vacuum tightness prior to refueling.
- d) Localized damage to the insulation must be repairable in the field without disturbing the undamaged portion of the system.
- e) All supports and connections to the tanks are to be capable of connection or disconnection without disturbance of the basic tank insulation.
- f) The insulation must be capable of withstanding flexing of the tank, as well as stresses introduced by thermal gradients across the system.

2.5 FUEL SYSTEM CRITERIA

Significant criteria for fuel system design are:

A. Operational Requirements

1. 30-minute ground hold disconnected from any ground support facilities.
2. Fuel flow schedule - scaled from Reference 1 to meet 90-minutes of usable fuel flow to engine (see Figure 4).
3. 3245 lbs. of usable fuel.
4. 500 flight minimum system life.

B. Environment

1. Ambient pressure vs. time obtained from a given vehicle trajectory, (Reference 1, using ARDC Model Atmosphere).
2. Inert atmosphere in the space between tank and outer vehicle structure.
3. Compartment temperature ranges from 400 to 1700°R.
4. Tank internal environment temperature: from 36°R to upper temperature limit of tank structural material or insulation system.
5. Pressure: 0 to 80 psig.

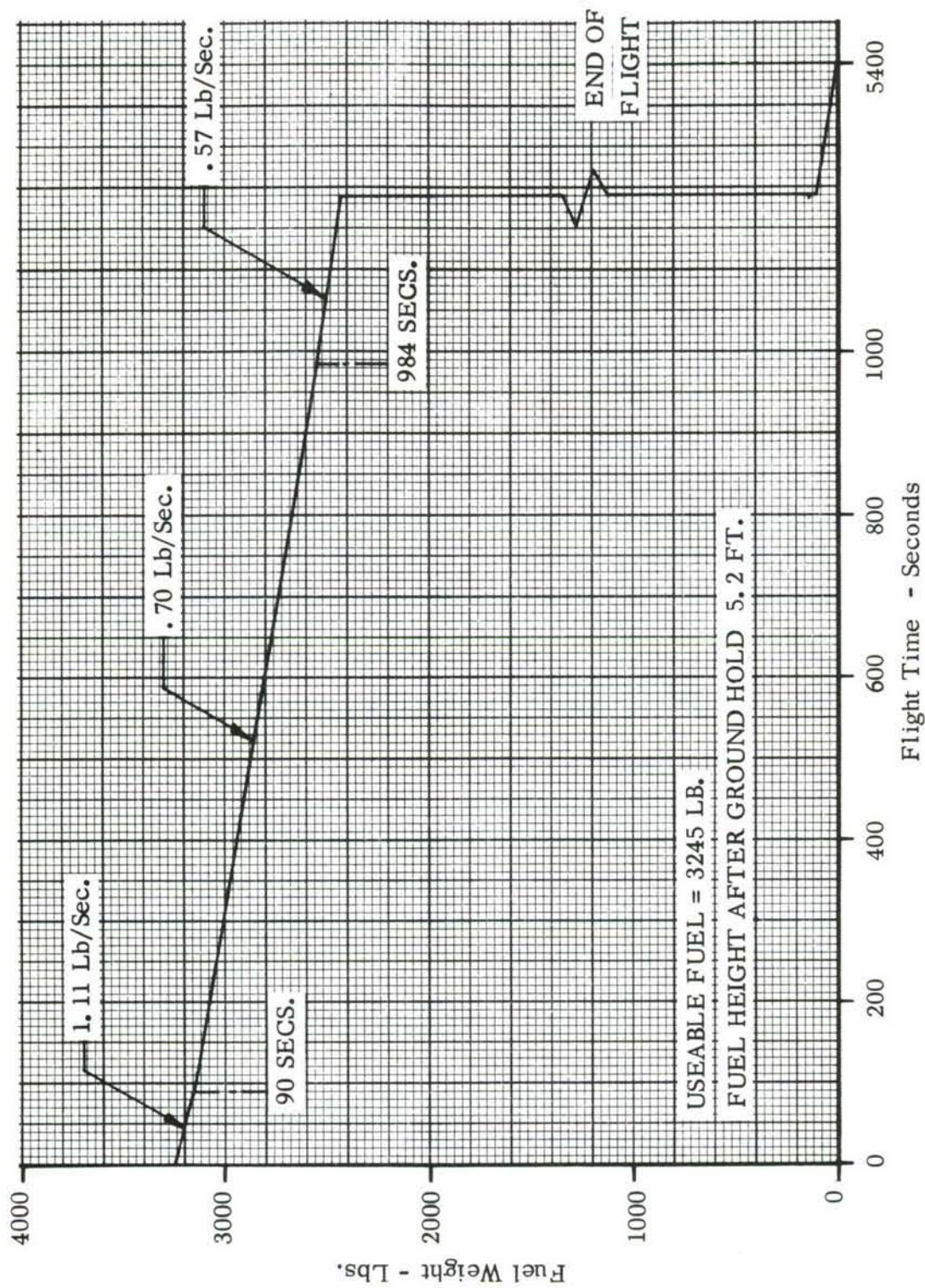


FIGURE 4 - FUEL FLOW SCHEDULE.

3.0 PRELIMINARY LARGE-SCALE TANK DESIGNS

Preliminary large-scale tank design studies were carried out with the view to investigating all aspects of the overall tankage system having an influence on the total performance. Tank structural concepts and material candidates were evaluated as a means of providing minimum tankage weight, for a pressure range of 20-80 psig, compatible to the environmental conditions. Survey of insulation systems was made to determine suitable candidates having sufficient thermal data on which to conduct a reliable thermal analysis. Fuel system requirements were investigated in order that they would provide maximum thermal performance provisions for minimum weight. Large-scale tank is 20 feet in length and has a cross-section of two intersecting circles 64 inches in diameter, provided a total tank width of 8 feet. An influencing ground rule was that the tank would have the capability to support the load factors associated with the taxi condition without pressure stabilization. Relative load factors of flight and taxi gives the tank capability of handling all flight loading without the need of internal pressurization.

3.1 STRUCTURAL MATERIAL EVALUATION

Material selections were made on the basis of mechanical, physical and chemical properties to suit the environmental conditions involved, and also provide good fabricability. Evaluation of the mechanical properties were based primarily on strength and toughness properties from -423° F to upper design temperature. Fabricability included the ability of the materials to be formed, machined, chemically milled and welded. Material procurement lead times and availability were also factors in the materials evaluation.

Tank Material

Selection of candidate materials for this application were made from the following list:

1. 718 nickel alloy, 30% cold rolled and aged
2. 5 Al 2.5 Sn titanium alloy ELI
3. 2014-T6 aluminum alloy
4. 2219-T87 aluminum alloy
5. 310SS, 75% cold rolled
6. Hastelloy X annealed
7. Haynes-Stellite 25 annealed

Since the major portion of the structural weight is dependent upon the yield and ultimate tensile strength-to-density ratios, these values were plotted against temperature for all material listed, Figures 5 and 6. From these graphs the 718 alloy, titanium and the aluminum alloys had the best potential as final material candidates. The 310SS has lower allowables than the 718 nickel alloy and is without any significant qualities to offset this disadvantage. Strength at elevated temperatures is desirable in a candidate material. Ullage stratification and empty tank considerations give rise to high temperatures, and tank wall will require continual active cooling if room temperatures are to be maintained. Since all candidate insulation systems were temperature limited at the time of this evaluation, it was decided to proceed on the basis of room temperature allowables and determine influence of elevated temperatures after the insulation system evaluation.

The 718 nickel alloy, in the 30% cold rolled condition, has the highest strength/density ratio of all the materials considered at -50° F and above. This material has also good toughness and strength at cryogenic temperatures, good fabricability and welding properties. Weld strength is less than the parent metal and forming must be done in a reduced strength material condition. This requires use of doublers or material build-up at welds, and reduces materials efficiency for formed parts.

Titanium 5 Al 2.5 Sn ELI (extra low interstitials) alloy has excellent strength and toughness at cryogenic temperatures. This alloy is not heat-treatable. Use of this material in the annealed condition produces a 100% weld efficiency and forming requirements do not impose any penalties. A potential problem area with this material is its sensitivity to embrittlement from exposure to a hydrogen atmosphere at elevated temperatures. To more accurately define this occurrence and evaluate exposure conditions under which it is anticipated to occur, particular in regard to the temperature, a test evaluation program was performed. This work is reported on in Appendix III. The test results were not consistent with previous testing data and hence did not supply any conclusive answers on this problem area.

Aluminum alloy 2219-T87 was chosen over the 2014-T6 alloy on the basis of its better fabrication qualities. Extensive welding studies on these two aluminum alloys, Reference 4, show inconsistent weld properties for the 2014 alloy at cryogenic temperatures and poor weld repair qualities. The 2219 alloy is readily fabricated and possesses good strength and toughness properties through the temperature range considered. The T87 condition is achieved by solution heat treatment, cold working and artificially aging the material. Welding reduces the strength to its annealed condition locally and forming cannot be done in the T87 condition. Formed parts can be heat treated to a T62 condition when in small subassemblies. Welds will require doublers or material build-up.

Room temperature properties of the materials, selected for preliminary design investigation, are presented below:

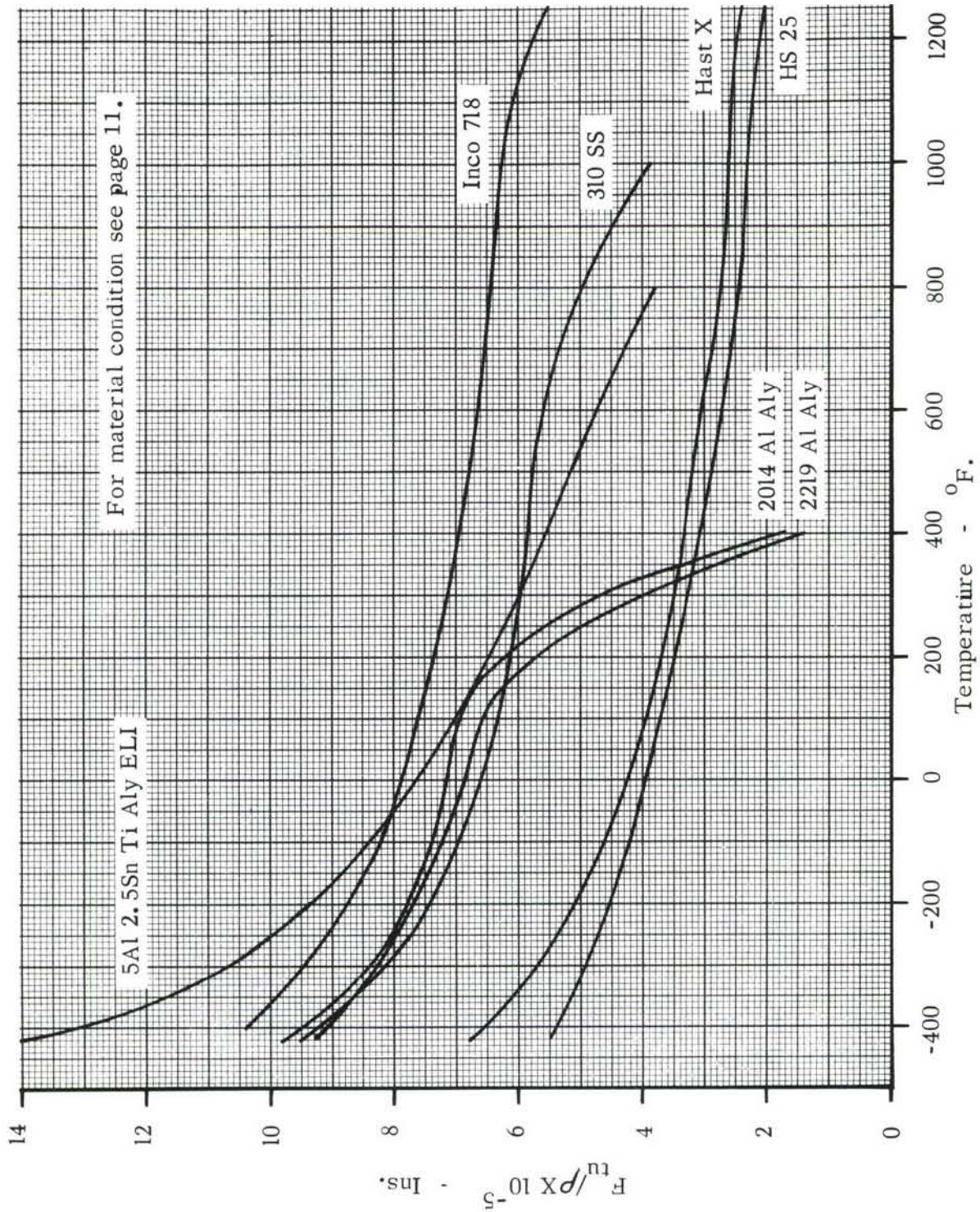


FIGURE 5. ULTIMATE TENSILE STRENGTH/ DENSITY Vs TEMPERATURE FOR CANDIDATE MATERIALS.

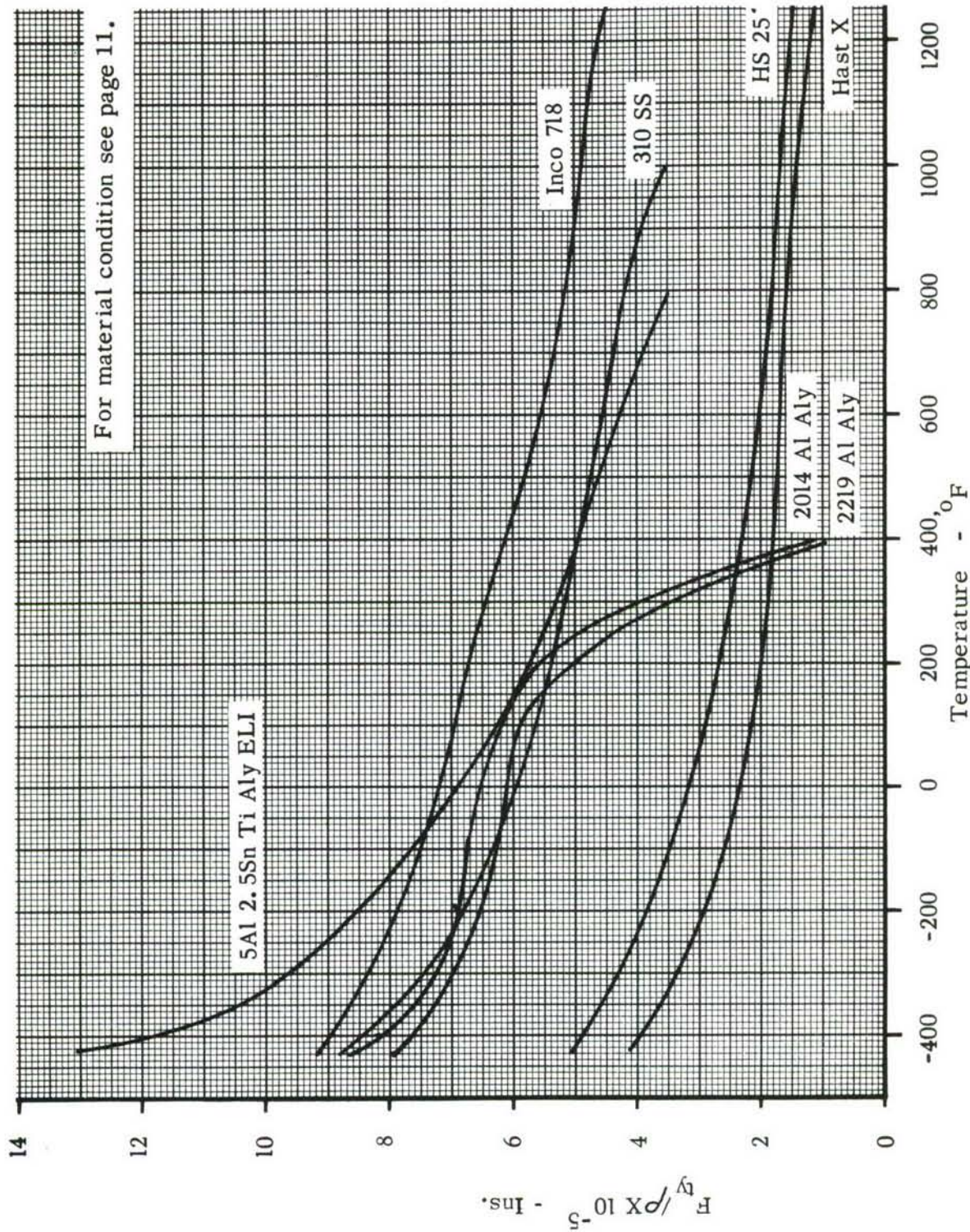


FIGURE 6. YIELD STRENGTH (0.2%)/ DENSITY Vs TEMPERATURE FOR CANDIDATE MATERIALS.

Material	Condition	F_{tu} (psi)	F_{ty} (psi)	E (psi)	ω lbs/in ³
5 Al 2.5 Sn titanium alloy ELI	Annealed	110,000	100,000	15.5×10^6	.162
718 nickel alloy	30% cold rolled and aged	220,000	200,000	29.4×10^6	.297
	Annealed and double aged	180,000	150,000		
2219 aluminum alloy	T87	62,000	50,000	10.5×10^6	.102
	T62	54,000	36,000		

The preliminary design investigation provided tankage weight as a function of operating pressure for these three material candidates. Input of this data into the optimization program resulted in the choice of the 718 nickel alloy and titanium alloy materials for further evaluation in the design and fabrication of two subscale tanks. The 718 nickel alloy, in the 30% cold rolled plus aged condition, was the final choice as the tankage structural material. This was due to its higher strength at temperature and because potential embrittlement of titanium to hydrogen gas exposures could not be resolved.

Tank Support Material

Candidate materials considered for the support system were:

718 nickel alloy, annealed and double aged
Rene 41
Hastelloy C annealed

These tank support material candidates were initially evaluated on the basis of their thermal conductivity (K) to mechanical properties (F_{tu} , F_{cy} and E) ratios, shown in Figure 7, in order to provide low conductivity. However, thermal evaluation showed heat leaks through supports do not present a problem area for hypersonic vehicles and hence do not justify any elaborate design investigations. This resulted in the choice of the 718 alloy, in the annealed and double aged condition, on the basis of its better fabricability and material properties for the temperature range considered (-423° F to 1300° F).

3.2 TANK STRUCTURE

The critical conditions determined from the design criteria, Section 2.0, are: 1) inertia loadings combined with maximum operating gage pressures; 2) inertia loading for the unpressurized fill condition; and 3) proof testing and burst strength requirements. Critical loading cases for the tank and support system are given in Table 1.

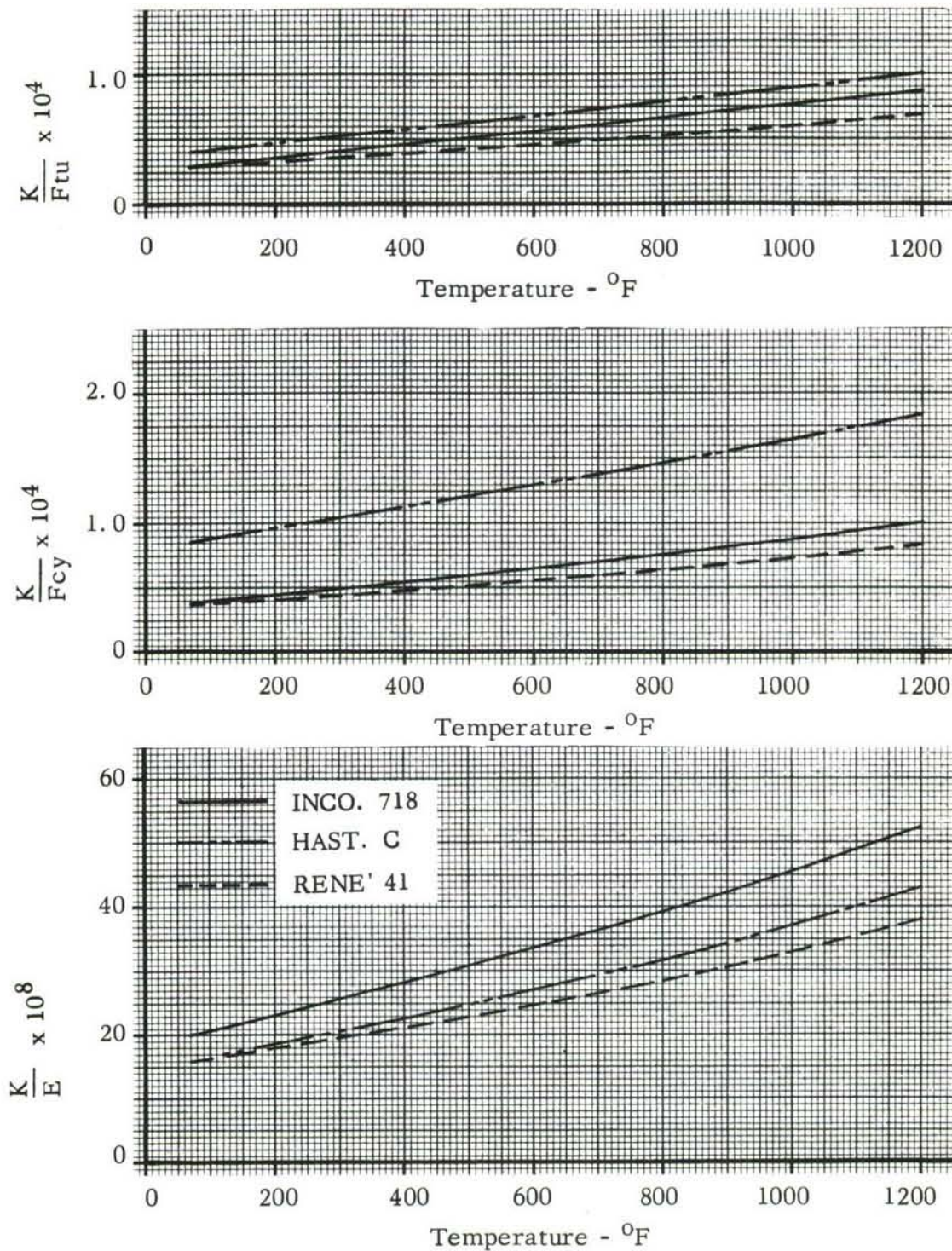


FIGURE 7.- TANK SUPPORTS - MATERIAL SELECTION

Table I. CRITICAL TANK LOADING - ULTIMATE

Total tank weight used to determine the maximum loading conditions are as follows:

Empty Tank Weight = 1100 Lb.

Load factors are from Section 2.3

Fuel Weight = 3780 Lb

N = Load Factor

P = Loading

Total Tank Weight = 4880 Lb.

Subscripts X, Y & Z denote longitudinal, transverse and vertical directions.

BASIC TANK STRUCTURE

CONDITION	N _X	N _Y	N _Z	TANK WEIGHT	P _X	P _Y	P _Z
FLIGHT *	-0.75	0.75	0.0	4880	-3660	3660	0
	0.75	-0.75	3.0		3660	-3660	-14,640
TAXI *	-1.20	0.75	0.0	4880	-5860	3660	0
	0.75	-0.75	-3.0		3660	-3660	-14,640

TANK SUPPORTS, ATTACHMENTS & CARRY-THROUGH STRUCTURE

FLIGHT *	-3.0	1.5	2.0	4880	-14,640	7,320	9,760
	1.5	-1.5	-4.5		7,320	-7,320	-22,000
CRASH *	-8.0	1.5	2.0	1100	-8,800	1,650	2,200
	1.5	-1.5	-4.5		1,650	-1,650	-4,950

* These loadings act independently.

The basic objective of this investigation is to establish a realistic minimum tankage weight, as a function of operating gage pressure, for each of the material candidates. An operating tank pressure range of 20 to 80 psig was used for this investigation. Tank skins were not allowed to buckle, since the insulation system will be bonded to the tanks outer surface. Design conditions with internal pressure would require a tank with only membranes if the gage pressure is equal to or greater than 4.3 psi; at this pressure there would be no compression in the skins. With gage pressures less than 4.3 psi the tank skins must carry compressive stresses. Internal stiffeners must then be used to stabilize the skins, unless the skins are very thick, to satisfy the no-buckling requirements. Frame/stringer and frames-only stiffening concepts were chosen for detailed analysis. These concepts allow the effects of longitudinal and transverse stiffening to be studied independently and the resulting weights can then provide a basis for comparison with other structural concepts. These two concepts are shown, together with the rest of the preliminary tank design structure, in Figure 8. Other structural concepts investigated were honeycomb sandwich and integral skin stiffening. The honeycomb sandwich concept considered has a fiber glass phenolic core and metallic outer face sheet. At lower pressures this concept showed good efficiency when also considered as an insulation element to prevent cryopumping of N_2 in a composite insulation system. Thermal data, however, is not available for the range of environmental conditions it would encounter in this program. Since testing to secure such data is outside the limits of this program, this concept was eliminated. However, it remains a good candidate for future research programs into composite insulation systems for tankage. Integral skin stiffening was also eliminated. The radius of gyration requirements for stiffening were not obtainable, due to practical machining limitations, for the effective skin thicknesses involved. The structural approach that considers only the center beam in bending, a possible minimum weight candidate, was not considered due to the requirements of bonding the insulation to the tank shell surface.

Material candidates used in the structural analysis were 5 Al 2.5 Sn titanium alloy ELI, 718 nickel alloy in the 30% cold rolled and aged condition, and the 2219-T87 aluminum alloy. The required skin thickness is determined by the maximum differential tank pressure, as shown in Figure 9, for the candidate materials. Also shown in this figure is the pressure at which the structural concept changes for each of these materials. Maximum shear and axial loading intensities for the tank are presented in Figure 10. Critical compressive and shear buckling stresses as a function of frame spacing are presented in Figure 11 and 12. Stiffening requirements for the tank skin, shown in Figure 13, includes intermediate frames, and stringers where applicable.

STRUCTURAL CONCEPTS
BASED ON A NON-BUCKLING SHELL CRITERIA

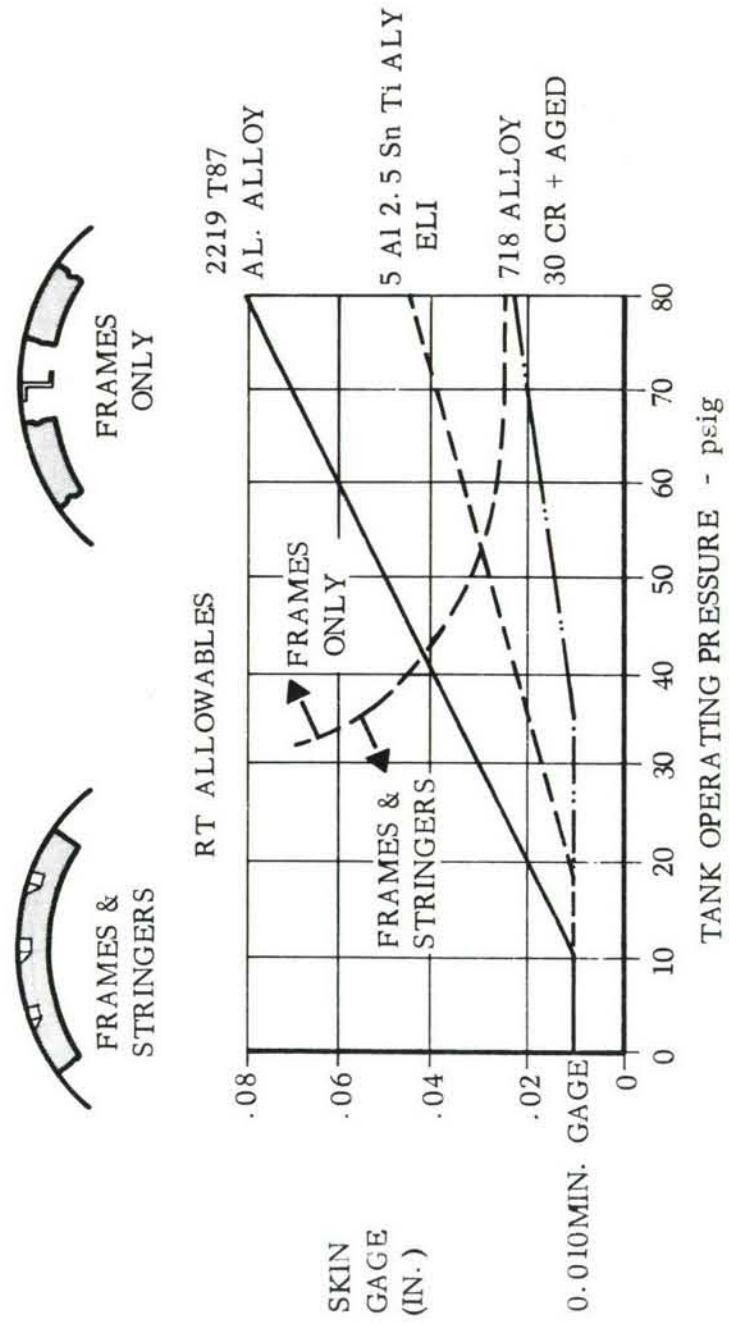
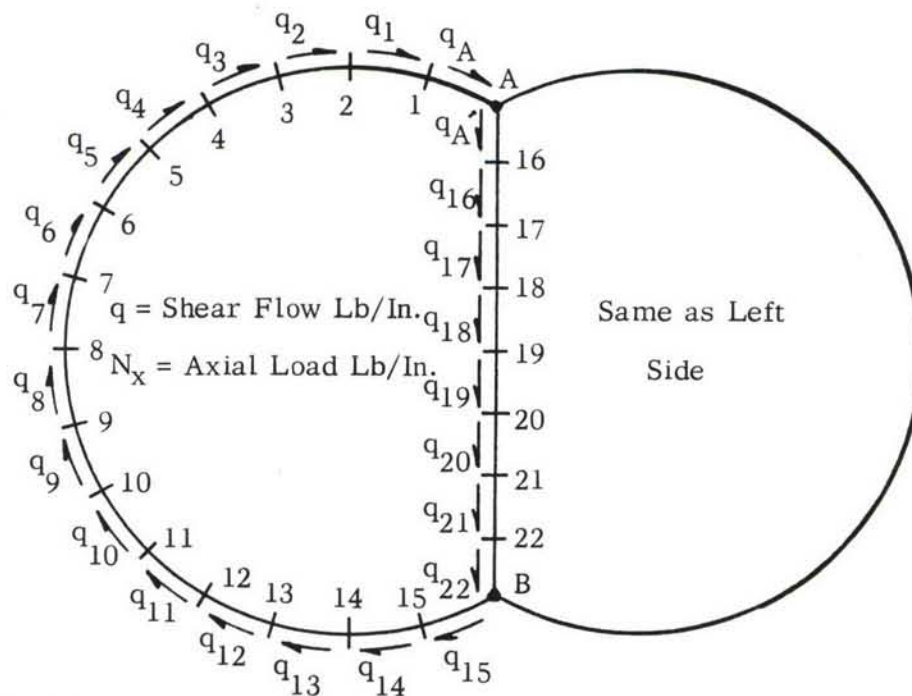


FIGURE 9 - TANK SKIN VERSUS OPERATING PRESSURE



NON PRESSURIZED CONDITION $N_Z = 3g$ $W = 4880$ lbs.

$$S_Y = 0, S_Z = -7320 \text{ Lb.}$$

$$M_X = 0, M_Y = 439.9 \times 10^6 \text{ In. Lb.} \quad M_Z = 0$$

	q	N_x		q	N_x		q	N_x
A	-13.685	-68.109	9	40.974	20.355	A'	-40.736	-
1	-3.133	-75.966	10	35.513	39.324	16	-46.599	-51.081
2	7.785	-78.645	11	27.794	55.614	17	-50.512	-34.053
3	18.337	-75.966	12	18.337	68.109	18	-52.466	-17.028
4	27.794	-68.109	13	7.785	75.966	19	-52.466	0
5	35.513	-55.614	14	-3.133	78.645	20	-50.512	17.028
6	40.974	-39.324	15	-13.685	75.966	21	-46.599	34.053
7	43.803	-20.355	B		68.109	22	-40.736	51.081
8	43.803	0						

FIGURE 10 - MAXIMUM ULTIMATE SHEAR AND AXIAL LOAD INTENSITIES

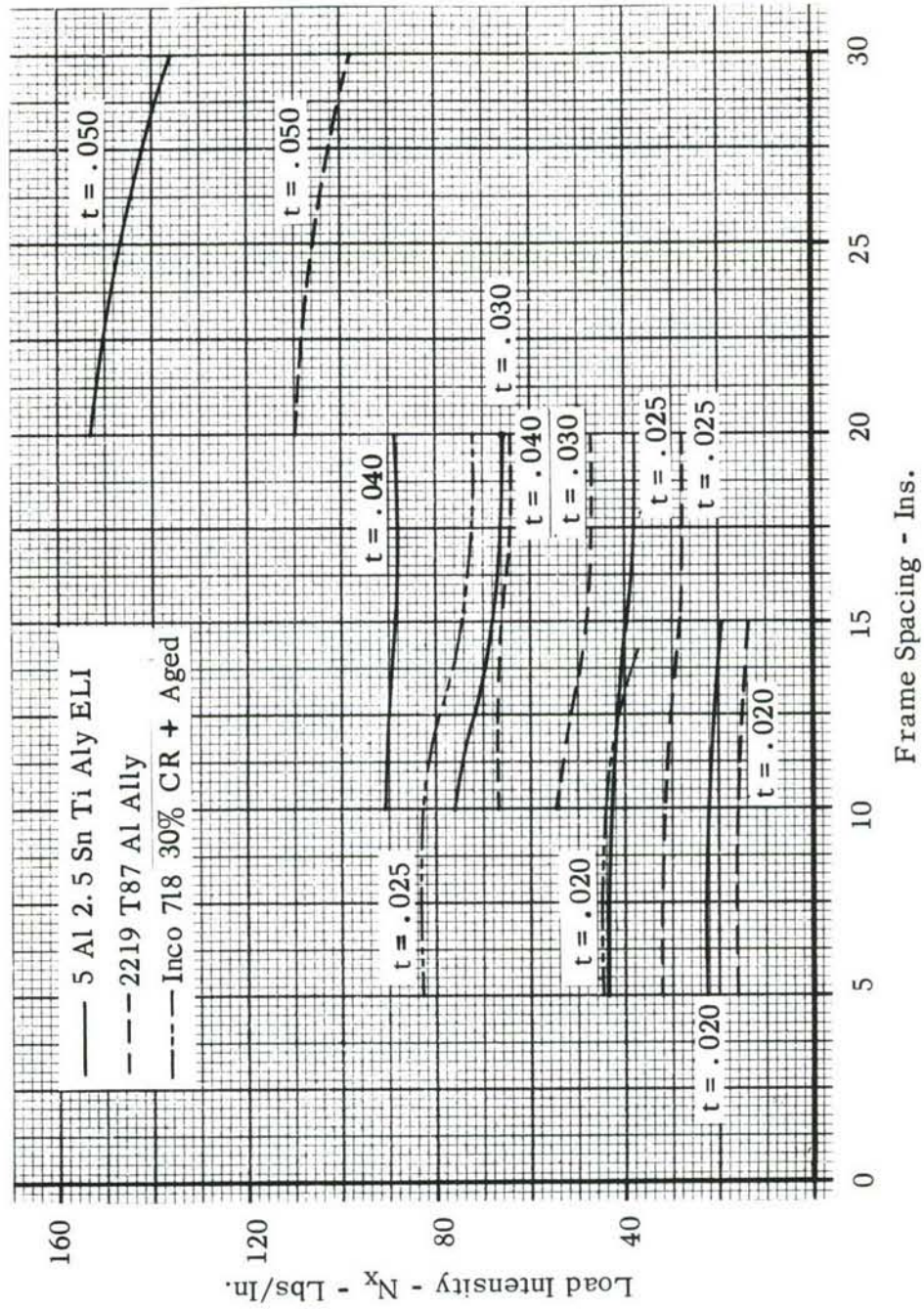


FIGURE 11 - TANK SKINS - COMPRESSION BUCKLING VS FRAME SPACING

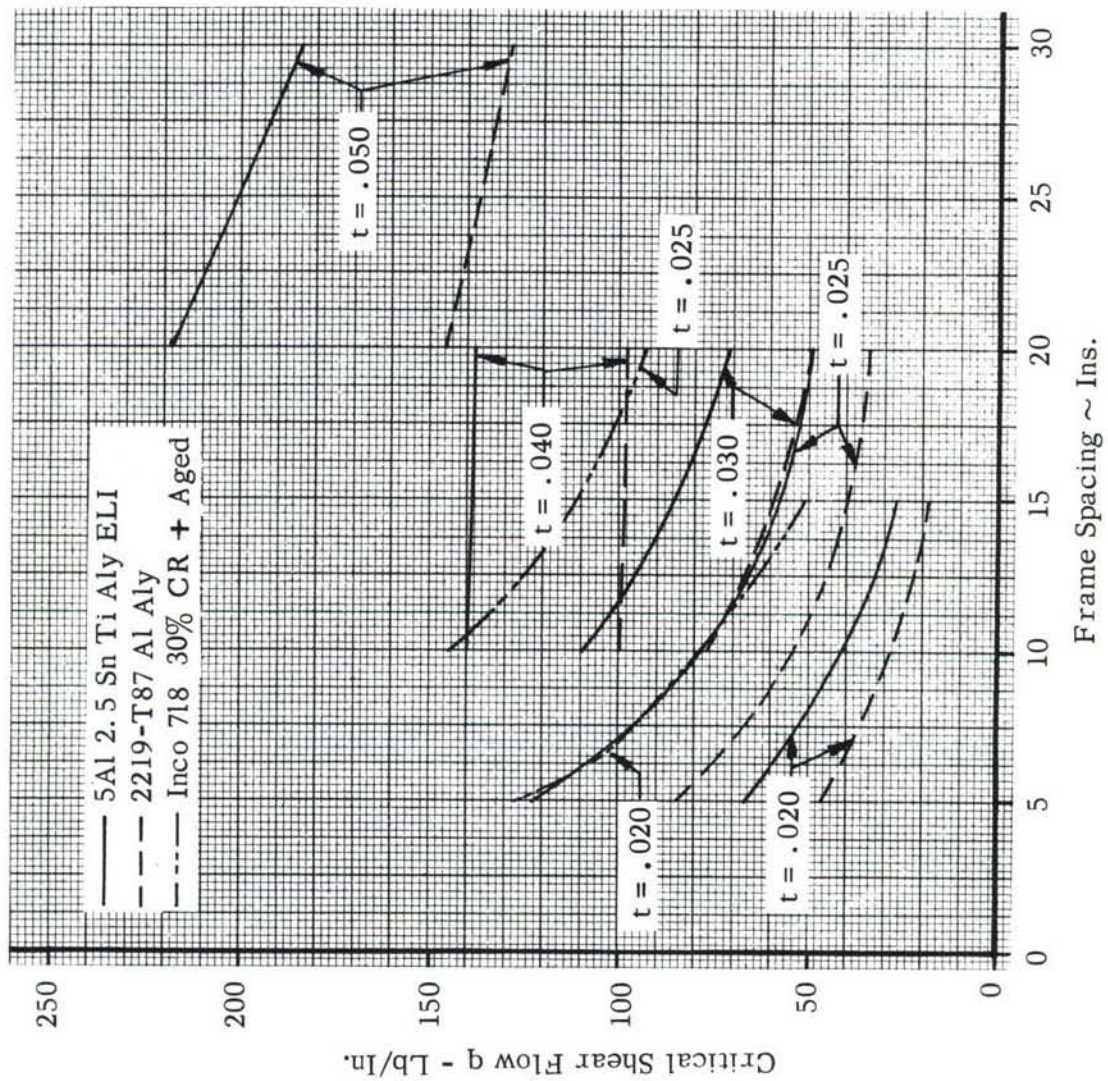


FIGURE 12 - TANK SKINS - SHEAR BUCKLING VS FRAME SPACING

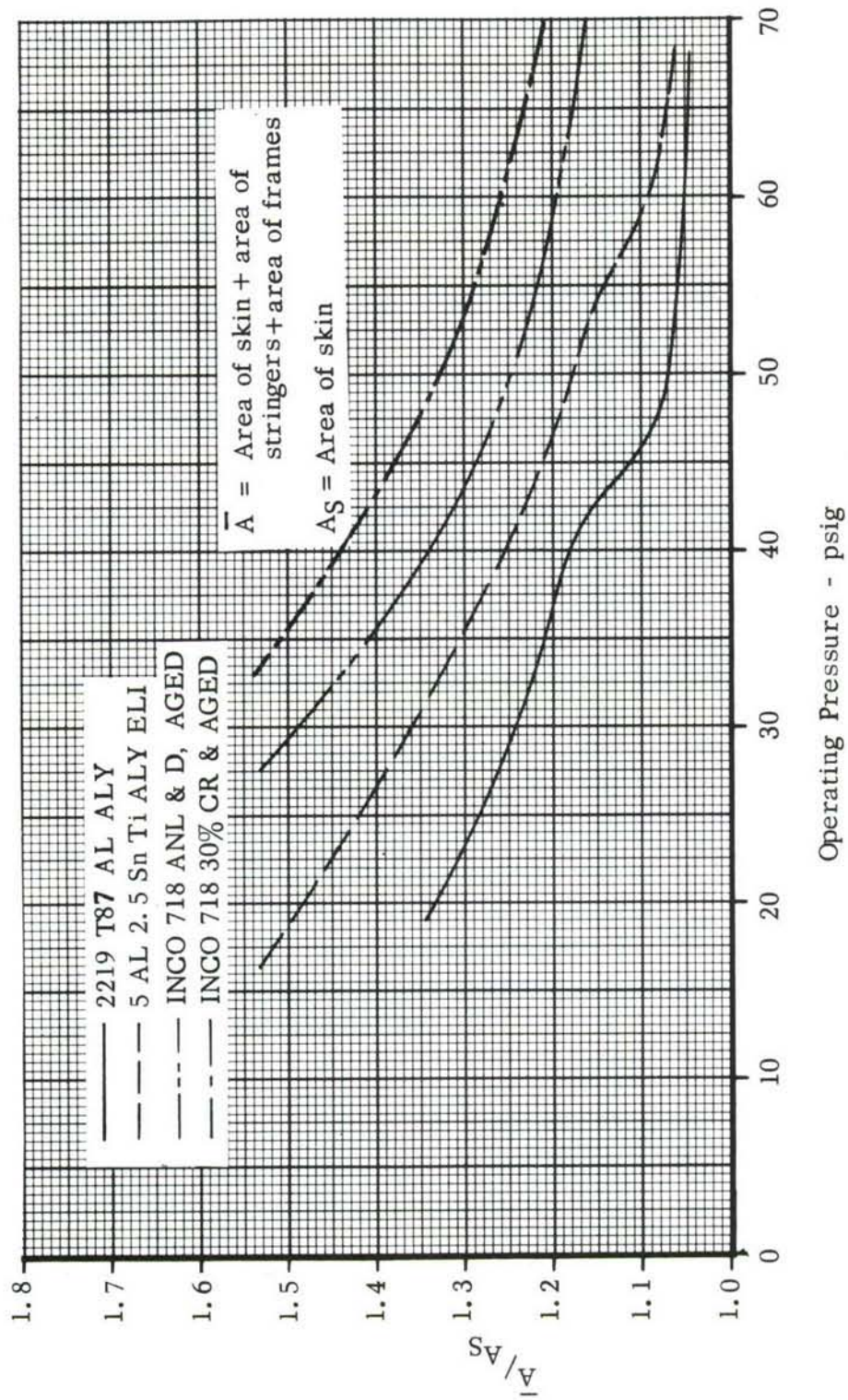


FIGURE 13 - SKIN/STIFFENER TO TANK SKIN AREA RATIO VS OPERATING PRESSURE

Stringer/Frame Stiffened Shell Concept

The upper pressure limit to which this concept was used is dependent upon the material and its associated R/t relationship. If frame spacing less than 10 inches is required to stabilize the tank skin against shear and compressive buckling, this concept is employed. This cutoff represents a minimum structural weight consideration. For the candidate materials these upper pressure limits are:

Titanium alloy	50 psig
Aluminum alloy	40 psig

The 718 nickel alloy is confined to this concept for the full pressure range considered, 20 - 80 psig, due to the associated high R/t values resulting from thin gages required.

Frame spacing is 30 inches. Although this is not necessarily optimum spacing, weight sensitivity was shown to be small for variation about this frame spacing. Intermediate frames are rolled "Z" sections, attached to skin with spot or seam welds, depending on material employed, and spliced through center web for shear and bending moment continuity. Frame height is taken as twice the stringer height and the frame flanges as one-third the frame height. Stringers have a "Z" section and are continuous, passing through cut-outs in the frames. Stringer height is half that of the intermediate frames, actual dimension being dependent upon material and pressure involved. Stringer spacing and cross sectional areas were determined by first calculating stringer spacing to preclude skin compression and shear buckling at peak load, then calculating the stringer cross sectional areas required to carry ultimate axial compression with a 30-inch frame spacing.

Stringer cross sectional areas were determined using the non-dimensional design curves presented in Figure 14. To use the non-dimensional design curve the required radius of gyration as well as the stringer spacing must be known. The radius of gyration is calculated by using the Euler column formula for the design compression stress and frame spacing. Design stresses are low, and as such are in the Euler formula range. After the ratio of radius of gyration to stringer spacing has been calculated, the non-dimensional design curve is used to determine the ratio of total skin stringer area and the ratio of stringer spacing to stringer height.

Frame Stiffened Shell Concept

For the pressure range being considered, 20 to 80 psig, this concept is only applicable to the titanium and aluminum materials. This concept is employed where a frame spacing 10 inches or greater would stabilize the skin against compressive and shear buckling loads. Actual frame spacing employed, at a particular pressure, is dependent upon material and skin thickness involved. Intermediate frames are similar

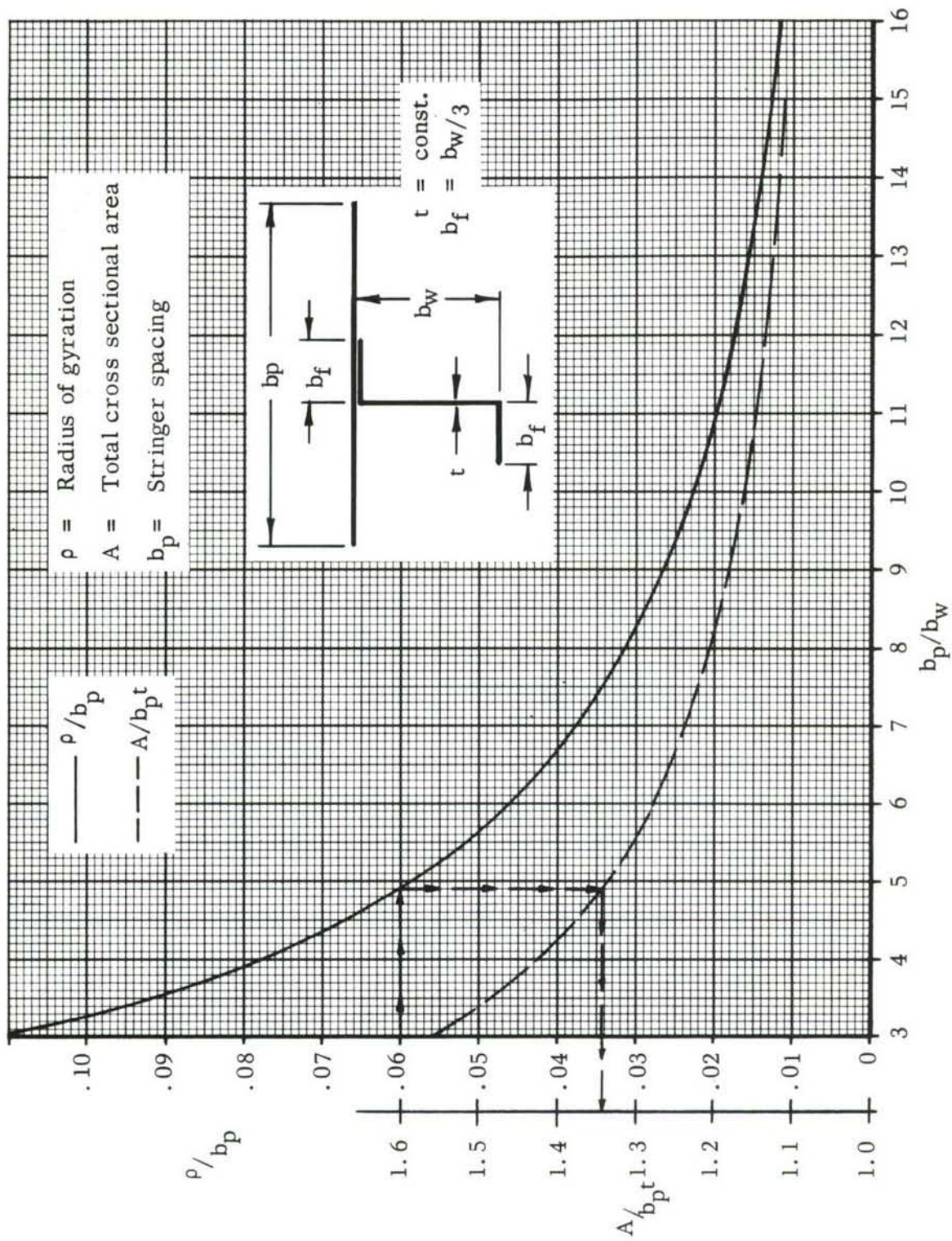


FIGURE 14 - PLATE-STRINGER AREA AND RADIUS OF GYRATION VS STRINGER SPACING TO STRINGER DEPTH RATIO

to those employed by the stringer/frame concept, being of "Z" section and splicing through the center web to maintain bending and shear continuity. Cross sectional areas of the intermediate frames are determined from a frame analysis.

Skin Splices

Skin splice designs are dependent upon the material candidate. Titanium uses butt splices, since the fusion welds of this annealed alloy are as good as the parent material. When lap splicing is required, a resistance spot and seam weld pattern is employed. Spot welds are avoided in titanium due to the low tensile/shear strength ratio at cryogenic temperatures (-423°F). Both the 718 nickel alloy and the aluminum alloys use lap splices in the transverse direction and doublers either side of the skin in the longitudinal direction. These splices have a center seam weld with spot welds either side. These splice designs account for the loss of material properties, from the initial cold work or heat treated condition, when welded.

Dome Ends

Dome ends are primarily dependent upon the maximum pressure differential loading case. Geometry is ellipsoidal with a major/minor axis ratio of 1.414. This configuration gives zero hoop stresses at the attachment to end frames with consequent reduction of stress discontinuities. This dome end also gives minimum surface area while still retaining only tensile stresses under pressure; any ratio greater than 1.414 would develop compressive stresses under pressure and hence require stiffening. A plot of meridional and hoop load intensity, as a function of the distance from the axis of symmetry to the surface, is presented in Figure 15. From this plot it can be seen that the maximum load intensity of the bulkhead is only 70% of that in tank shell. For a constant skin thickness bulkhead, the skin thickness will be 70% of the tank skin thickness. Bulkhead weights were calculated using a constant skin thickness. Mechanical properties of the bulkhead materials used in the weight evaluation are those obtainable in a formed part. Material conditions used are: Titanium 5 Al 2.5 Sn ELI annealed, 718 nickel alloy annealed and double aged, and aluminum 2219-T62. Access hatches are provided in the dome ends, 24 inches in diameter, using metal "O" rings for sealing. For design purposes it was assumed that only two hatches would be required.

End Frames

End frame weights were calculated using the frame bending moments determined from analysis. A frame section with a flange $1/3$ of the height was used. Frame height was used as the variable parameter to calculate minimum frame weight.

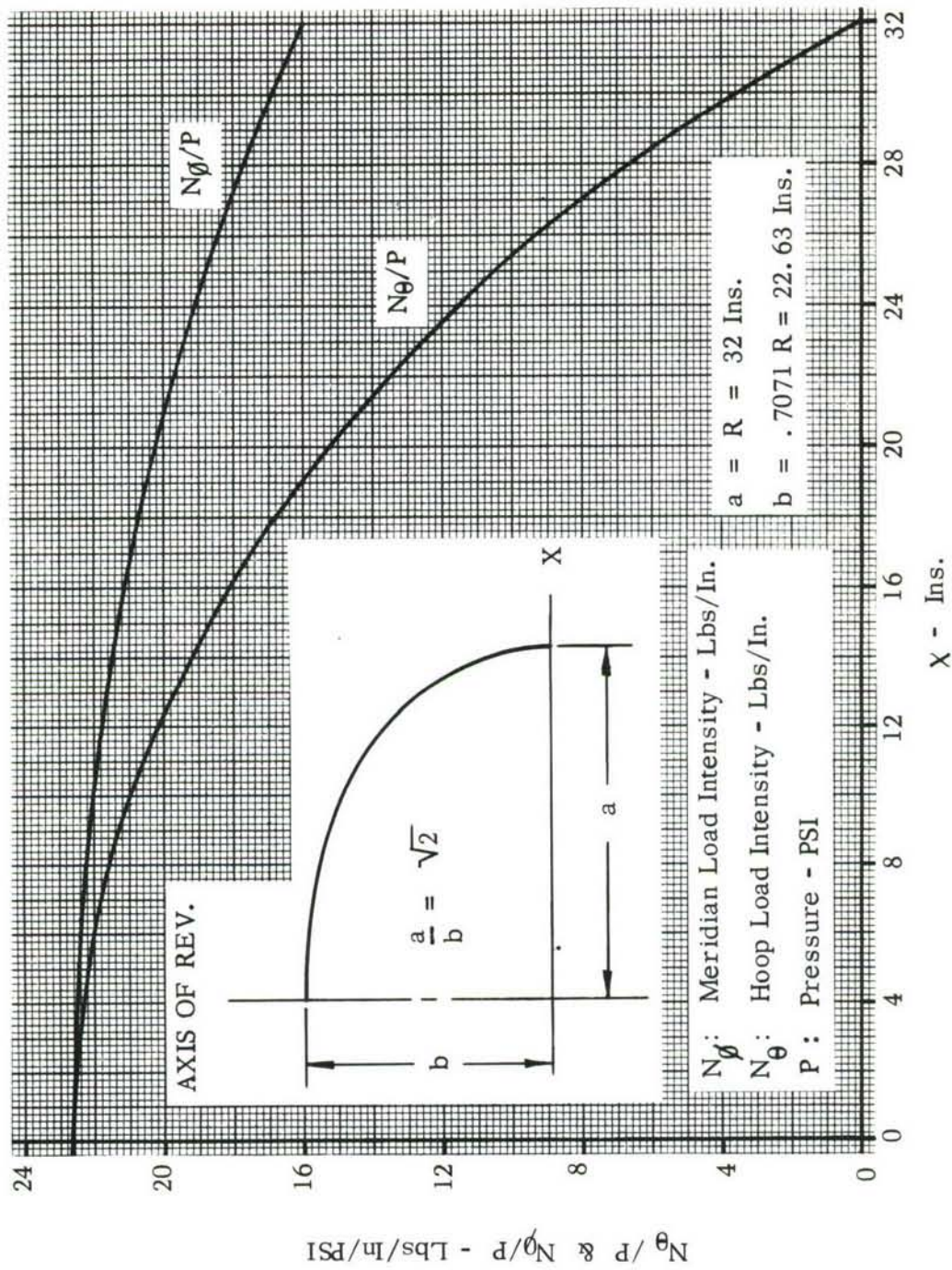


FIGURE 15 - ELLIPSOIDAL DOME ($a/b = \sqrt{2}$) - MERIDIAN AND HOOP LOAD INTENSITIES AS A FUNCTION OF PRESSURE

Tank Support System

The tank support system design is shown in Figure 16. This support design allows for free movement between the tank and vehicle structure resulting from relative thermal contractions and expansions, provides for a minimum number of supports to satisfy static equilibrium, and minimizes heat leaks to the liquid hydrogen. Support members were designed based upon the loading defined in Table 1. This design locates the supports at the bottom of tank on the end frames, a natural hard point for support. The forward support system consists of two side supports for vertical loads and a tripod at the centerline for side load and drag. The side supports are located at BL 33.0 (left and right) and allow for transverse thermal contraction and expansion. The tripod provides the fixed portion of tank support system, the only movement being vertical rise of tank from tripod structure along a bearing slide. This capability is required to prevent induced loading from side supports. The drag member of the tripod is inclined 60° from the vertical. This angle was selected so that the resulting kick load on the side load members was no greater than that produced by the side loading case. The optimum angle is 24° from the vertical for the bipod members. This was determined by equating column compressive allowable and axial load as a function of column length, then calculating length for minimum weight. The aft support system is like the forward except for the drag strut. The main difference is that the longitudinal thermal expansion and contractions of both the tank and vehicle structure are compensated for at this end. These movements are accomplished without inducing loads into the tank structure by ball-jointed side supports and the use of a linkage on the bipod.

Tank supports are insulated for the Microquartz (N_2)/Foam insulation systems to prevent cryopumping. The temperature distribution along support members is given in Section 3.3.8. Each support is insulated with sealed foam a distance out from the tank sufficient to prevent cryopumping. The need for movement is required at the supports, and an evacuated bellows system is assumed to best accomplish this purpose.

Tank support materials were evaluated in Section 3.1. Since heat leaks through the tank supports are small, nickel alloy 718 was chosen over Rene 41 on the basis of its better fabrication qualities.

Tank Structure Weight Analysis

Tank structural weight as a function of operating pressure is presented in Figure 17. These weights are based on a 20 foot tank shell length. To account for variation of structural weight as a function of tank length, within $\pm 5\%$ of 20 feet, a structural weight equation was derived. This equation, given below, provided the structural weight input to the optimization computer program.

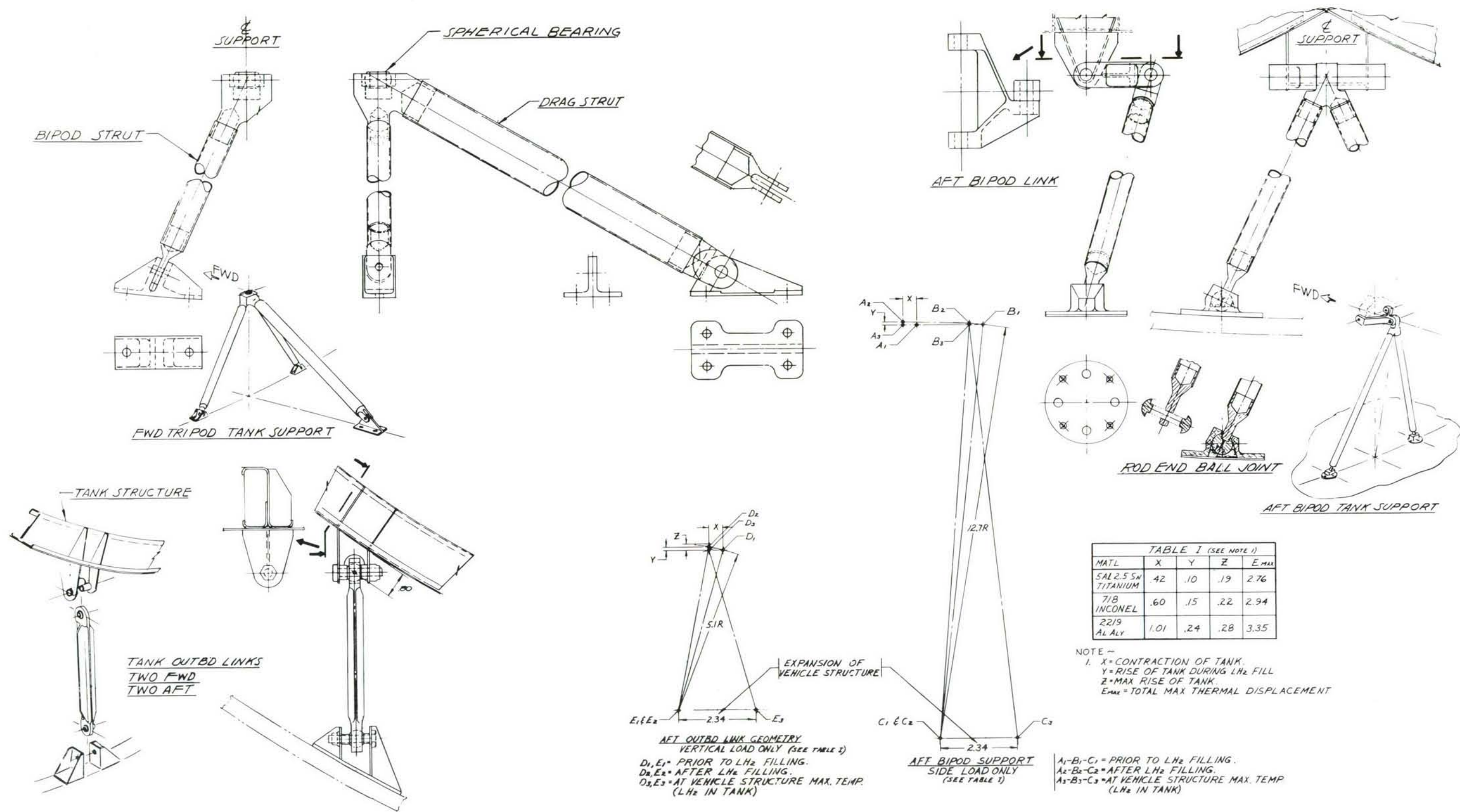


FIGURE 16. PRELIMINARY DESIGN - TANK SUPPORTS

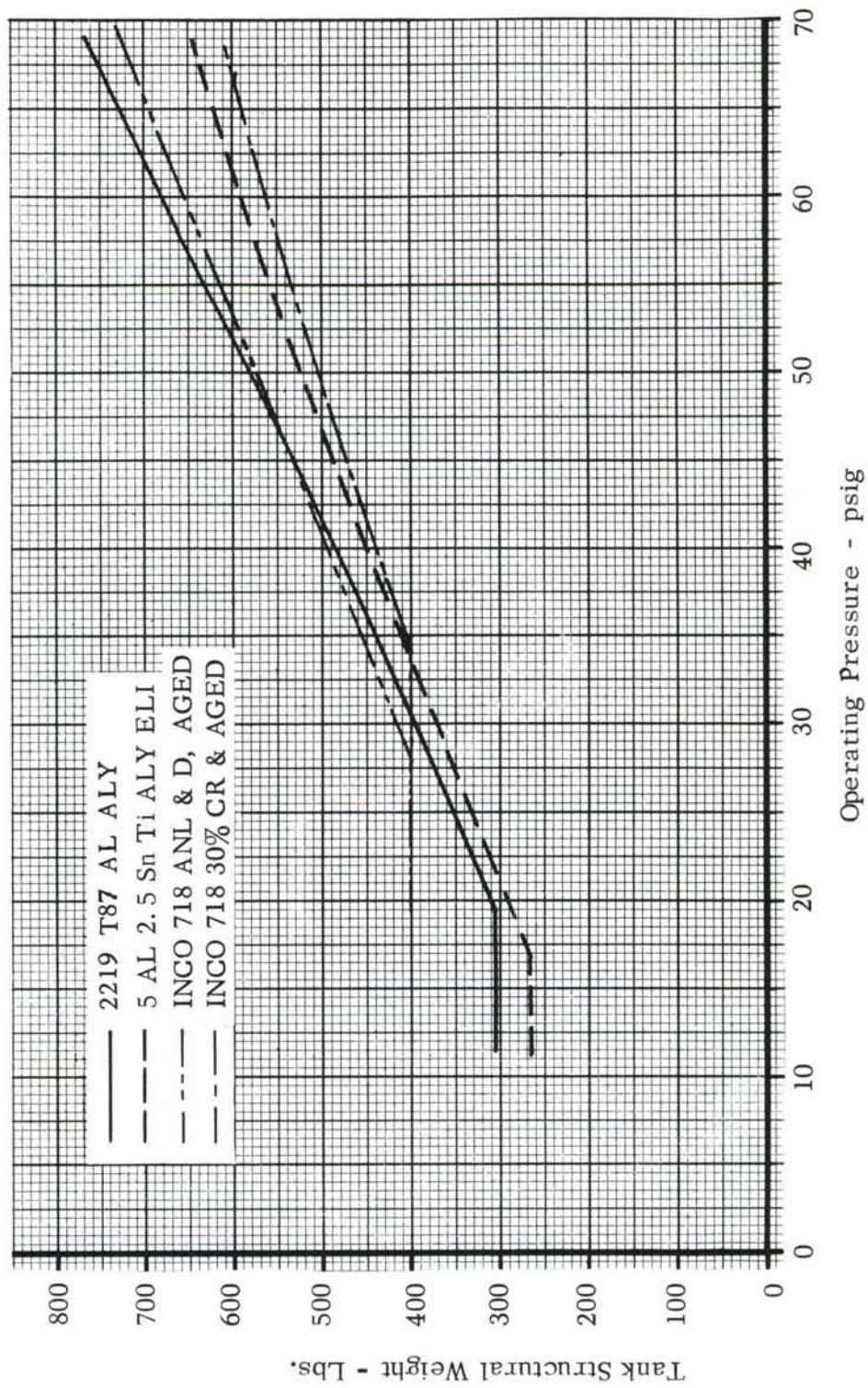


FIGURE 17 - TANK STRUCTURAL WEIGHT VS. OPERATING PRESSURE

$$W = p \frac{\rho}{F_{tu}} \left[.248 \left(\frac{A}{A_s} \right) L + .711 \right] \times 10^6 \text{ lbs}$$

where

W = Tank Structural Weight, lb.

p = Operating Pressure, psig.

ρ = Material Density, lbs/cu.ins. (Pg 15)

F_{tu} = Ult. Tensile Stress, PSI (Pg 15) L = Tank Length, Ft.

$\frac{A}{A_s}$ = Stiffening/Skin Ratio, (Figure 13)

To account for minimum gage influence a restriction is placed on operating pressure employed in above equation. This restricted lower pressure for each material candidate is:

2219-T87 aluminum alloy	10.0 psig
5A1 2.5 Sn titanium alloy	17.5 psig
718 nickel alloy, annealed + double aged	28.0 psig
718 nickel alloy, 30% cold rolled + aged	40.0 psig

When operating pressure is less than above values, the restricted pressure must be employed in the weight equation.

Results of the optimization program gave low operating optimum pressures for both tankage systems. At these pressures the frame/stringer structural concept has the highest structural efficiency for all of the candidate materials, see Figure 9. The structural concepts employed were based on a non-buckling criteria to comply with the requirements of the sealed element composite insulation system. However, when the choice of the all-Microquartz helium environment insulation system was made and the adhesive bonding requirement was removed, a new minimum weight structural concept presented itself. This recommended structural concept uses a frame-only stiffening concept and allows for elastic buckling of the skin while the majority of tank bending is taken by the center beam. This concept provides minimum structural weight where skin buckling can be tolerated, and helps deviate thermal stress development

3.3 INSULATION SYSTEMS

The primary functions of a liquid hydrogen tank insulation system are to limit the boil-off of propellant, prevent freezing of moisture, and avoid liquefaction of surrounding gas on the tank surface. For the specific application in a hypersonic cruise vehicle with hot structure and non-integral tankage, a secondary function of the insulation is to limit the temperature of the tank wall. The insulation must be lightweight, thermally efficient, and capable of withstanding the environment imposed for 500 flights, with high reliability.

The annular gap between the outer vehicle structure and the tank forms a natural vessel for introduction of an inert purge gas to prevent moisture condensation or air liquefaction. Furthermore, by inerting this annulus, the hazards due to potential hydrogen leakage from the tank or propellant lines are minimized. The inerting purge gases chosen were helium for the permeable insulation systems and dry nitrogen for the sealed or evacuated composite systems. Helium is required in the permeable systems, where the gas comes in contact with the tank wall, since it is the only gas which does not condense at liquid hydrogen temperatures. The disadvantages of this gas are its high conductivity and shortage in supply. Nitrogen was chosen for the composite insulation systems on the basis of its significantly lower conductivity, inertness and ready availability. Liquefaction of the nitrogen gas is prevented by sizing the lower sealed element to give a temperature greater than 160° R at the interface of the composite system.

A large number of insulation systems appeared potentially available for use in this program. Selection of a candidate insulation system required that sufficient thermodynamic data was available to support an analysis of performance throughout the environmental conditions encountered. Insulation systems in the early development stage, where insufficient data was available, were eliminated. These systems, some of which had unique qualities, have been included to provide information on their future potential for hypersonic cruise vehicle applications.

Remaining candidate systems were examined in further detail regarding the availability of sufficient thermodynamic and design data to allow performance and weight calculations. All candidate insulation systems employed a high temperature fibrous blanket. The material chosen for this blanket was Microquartz, manufactured by Johns-Manville. This is a high silica, fibrous insulation having low conductivity and density, good temperature compatibility, available thermal data, and provides good fabrication qualities due to its inherent flexibility. The systems were examined for configuration complexity, reliability and manufacturing feasibility, and weight comparisons were made based on a typical flight heat flux condition.

3.3.1 DEVELOPMENTAL SYSTEMS. These systems involve recent developments in insulation technology, and although found to lack sufficient data for evaluation purposes, are presented for reasons of interest and future potential.

Marshield. The Marshield insulation consists of aluminum radiation shields separated by dimpled fiberglass spacers. A helium environment is required for use in the atmosphere. A Microquartz protective blanket is required to prevent overheating of the fiberglass. The Marshield thermal conductivity is about 0.6 BTU-in./hr-ft² °R at a mean temperature of 275 °R (ground hold). This is essentially the same as helium purged Microquartz. Since the density of the Marshield system is 10.0 lbs/ft³ and the Microquartz is 4.5 lbs/ft³, the all Microquartz system results in a lower weight than a composite of Marshield and Microquartz.

Jackson CO₂ System. The Jackson CO₂ system, under development by NASA/Langley, is a new research program. It consists of a fibrous insulation blanket which is cryo-pumped full of CO₂ frost during ground hold, and then allowed to sublime and out-gas during flight. No useful thermal conductivity or density data is available at this time.

Linde Opacified Paper. The Linde opacified paper system is a recent development, consisting of quartz paper with dispersed metal fibers. Multiple layers of the paper are applied to the tank to obtain the desired thickness. A helium environment is needed to prevent cryopumping. The material has the same temperature compatibility range as Microquartz. As indicated by Linde, the kρ values for this material are probably comparable to Microquartz. General Dynamics Convair's experience with layer-type insulations has shown that thermal performance can vary considerably depending on the method of application and resultant density (thickness) after installation. Although the quartz type paper may provide a better over-all insulation than the quartz fiber batts, additional test data and application experience is needed to demonstrate the capability of this insulation.

Multishielding. This is not an insulation, per se, but rather a means of reducing the heat input to the tank by intercepting the heat flux with conductive fins attached to the vent line. The refrigeration capacity of the boil-off gas is thereby utilized, allowing a reduction of the passive insulation weight. The system is ideally suited for a long-time ground or space storage where the cryogen is maintained at the boiling point for long periods of time and vented slowly and continuously. However, the tank insulation under study will be used for only two hours and vented only during the latter part of operation. In order to minimize the number of insulation penetrations, only one or two vent tubes would be utilized on the tank. Therefore, it becomes questionable if the vent gas refrigeration can be utilized efficiently. The design and ultimate weight of this heat exchanger installation to meet the reliability and environmental conditions imposed on this system have not been determined. The use of multishielding for this application would probably not be greatly superior to passive insulation from a thermal standpoint, and the reliability would be adversely affected due to the required system complexity.

3.3.2 MICROQUARTZ BLANKET IN HELIUM ENVIRONMENT. This system consists of 3 lb/ft³ quartz fiber felt, enclosed between two layers of quartz cloth and stitched with quartz thread to obtain a final density of 4.5 lb/ft³. The resulting blanket is then

bonded to the tank wall. Helium is introduced into the annular space between the vehicle structure and insulation to prevent cryopumping and ice accumulation.

The thermal conductivity used for evaluation is shown in Figures 18 and 19. This is test data developed under Contract AF33(657)-9444 (Reference 5) and is actually for Dynaquartz. This data was used since comparable test results were not available at this time for Microquartz. Dynaquartz is made from Microquartz by a sintering process resulting in the formation of rigid material. Since the two materials are identical in composition and density, the use of Dynaquartz data was considered acceptable. Subsequent testing has shown that Microquartz has a lower conductivity than Dynaquartz. The conductivity values used, thus provided conservative results.

3.3.3 COMPOSITE SYSTEMS IN N_2 ENVIRONMENT. These systems consist of a layer of low-temperature insulation adjacent to the tank wall, an impermeable sealing membrane, and a layer of high-temperature insulation to protect the sealing membrane from the high temperature environment. This protection is required, since currently available low temperature insulation materials and sealing membranes have definite temperature limits well below the external insulation temperatures encountered in this application. The composite systems show a performance advantage due to: a) the high efficiency of the low temperature insulation materials, and b) the improved efficiency (reduced conductivity) of the fibrous high temperature insulation in a nitrogen environment, as opposed to a helium environment. For this increased thermal efficiency, greater complexity and reduced reliability are involved. Since only temperature limited materials are available for the sealing layer and lower insulation element, a basic incompatibility problem exists for composite systems in a hypersonic cruise vehicle environment.

The insulation materials investigated for the lower element were polyurethane foam, cork board, honeycomb, super-insulation, and the Linde vacuum panel. The insulation is either evacuated by an external source or through the cryopumping effect of the low temperature of the liquid hydrogen in the tank. The outer high temperature layer is a Microquartz blanket similar to the type described earlier. Typical construction details for composite systems are shown in Figure 20.

Super-insulation is not compatible as an element of a composite system, nor is sufficient data available for a reliable thermal analysis. Installed as an evacuated system, it would be compressed by the atmospheric pressure during the ground hold condition. This pressure would decrease to 8 mm Hg at the cruise altitude. The effect of load relaxation is to reduce the conductivity due to decrease of the conductive heat path through the multiple layers of material. The actual thermal conductivity during flight is difficult to establish since the conductivity is a function of compression loading which, in turn, varies with ambient pressure, weight of the external Microquartz blanket, and the amount of spring back of the sealing membrane. This system also suffers from excessive weight due to the thick Microquartz blanket necessary to protect the low temperature element from overheating during the cruise condition.

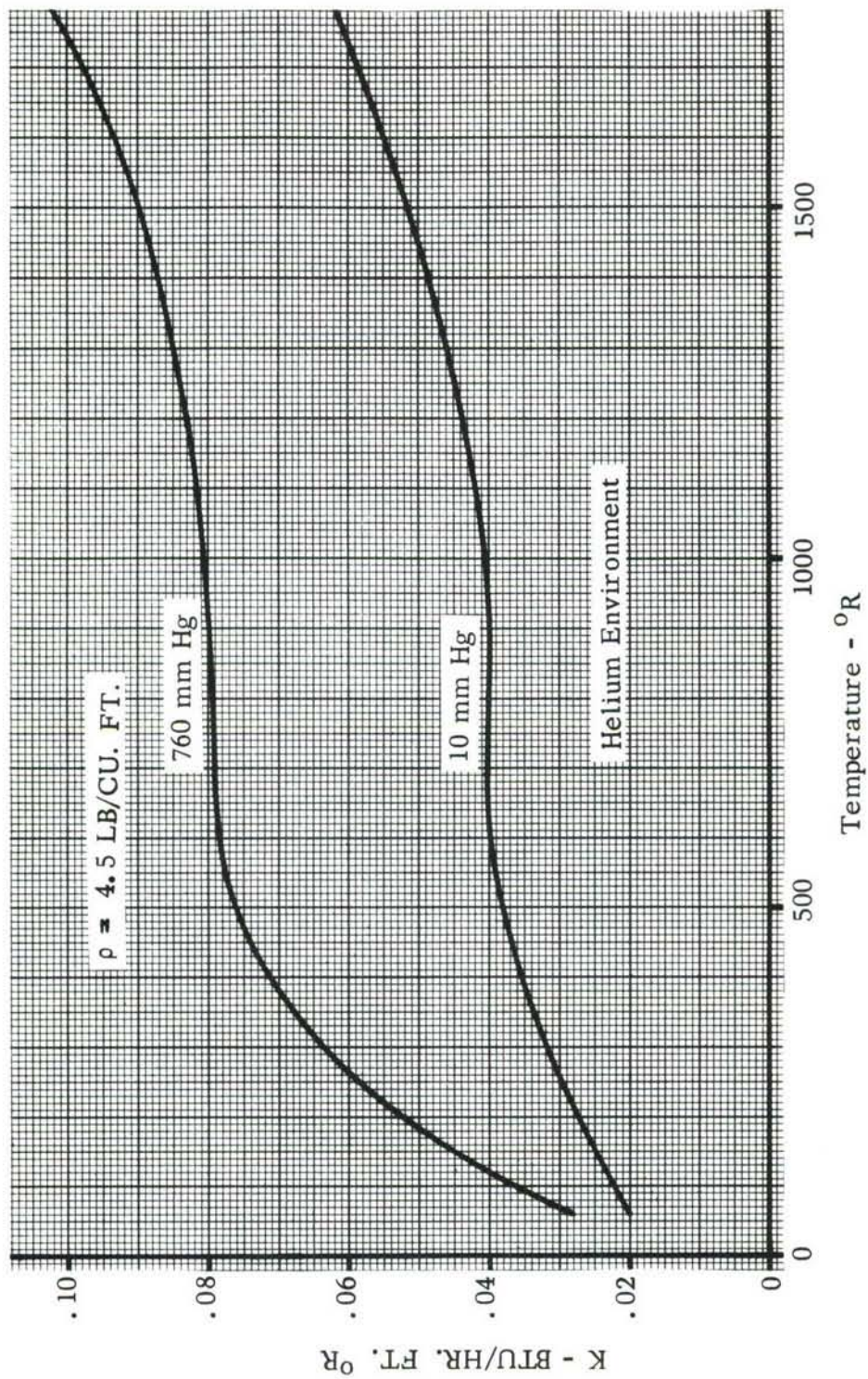


FIGURE 18 - THERMAL CONDUCTIVITY (K) OF DYNAQUARTZ IN He

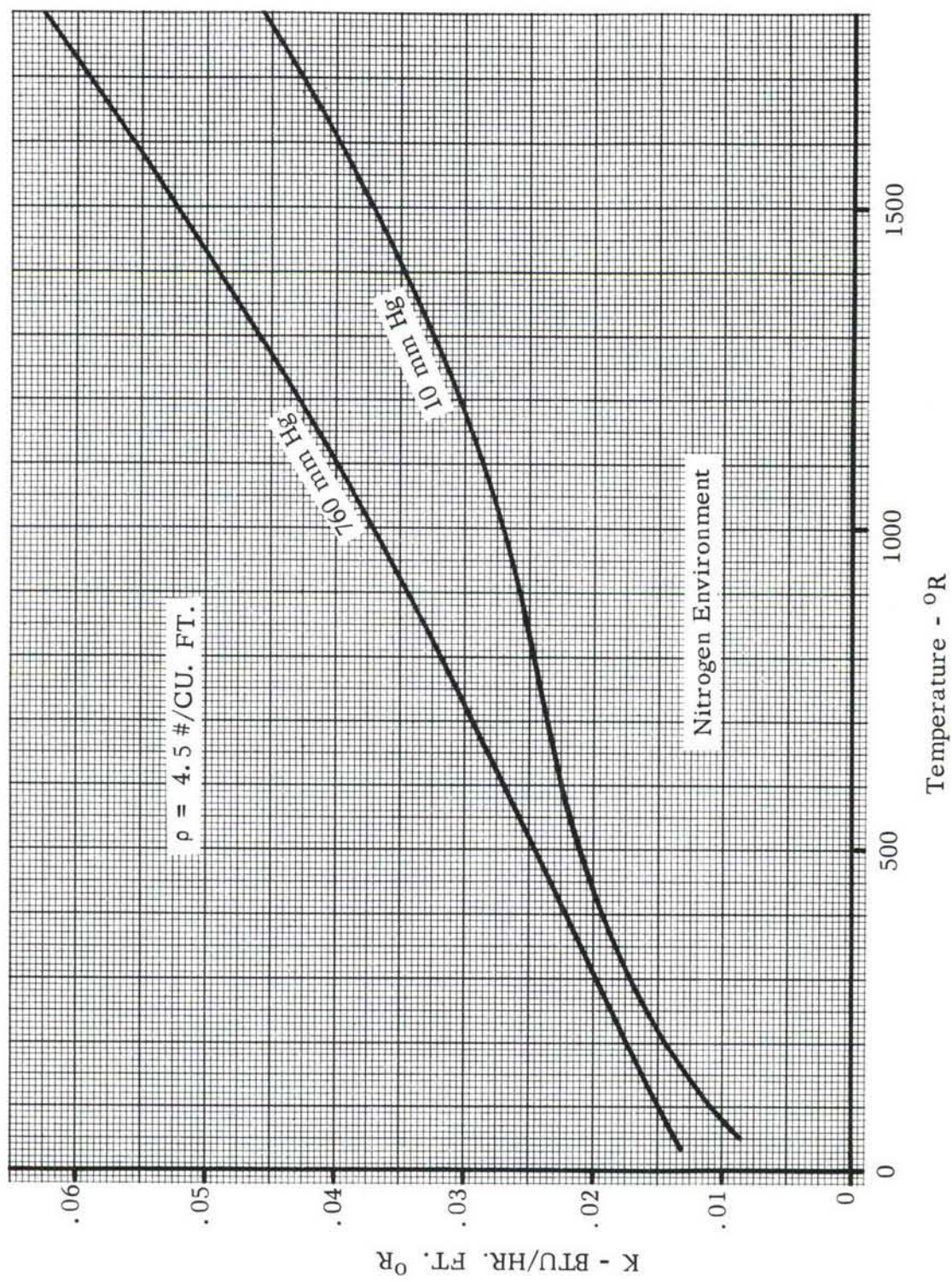


FIGURE 19 - THERMAL CONDUCTIVITY (K) OF DYNAQUARTZ IN N_2

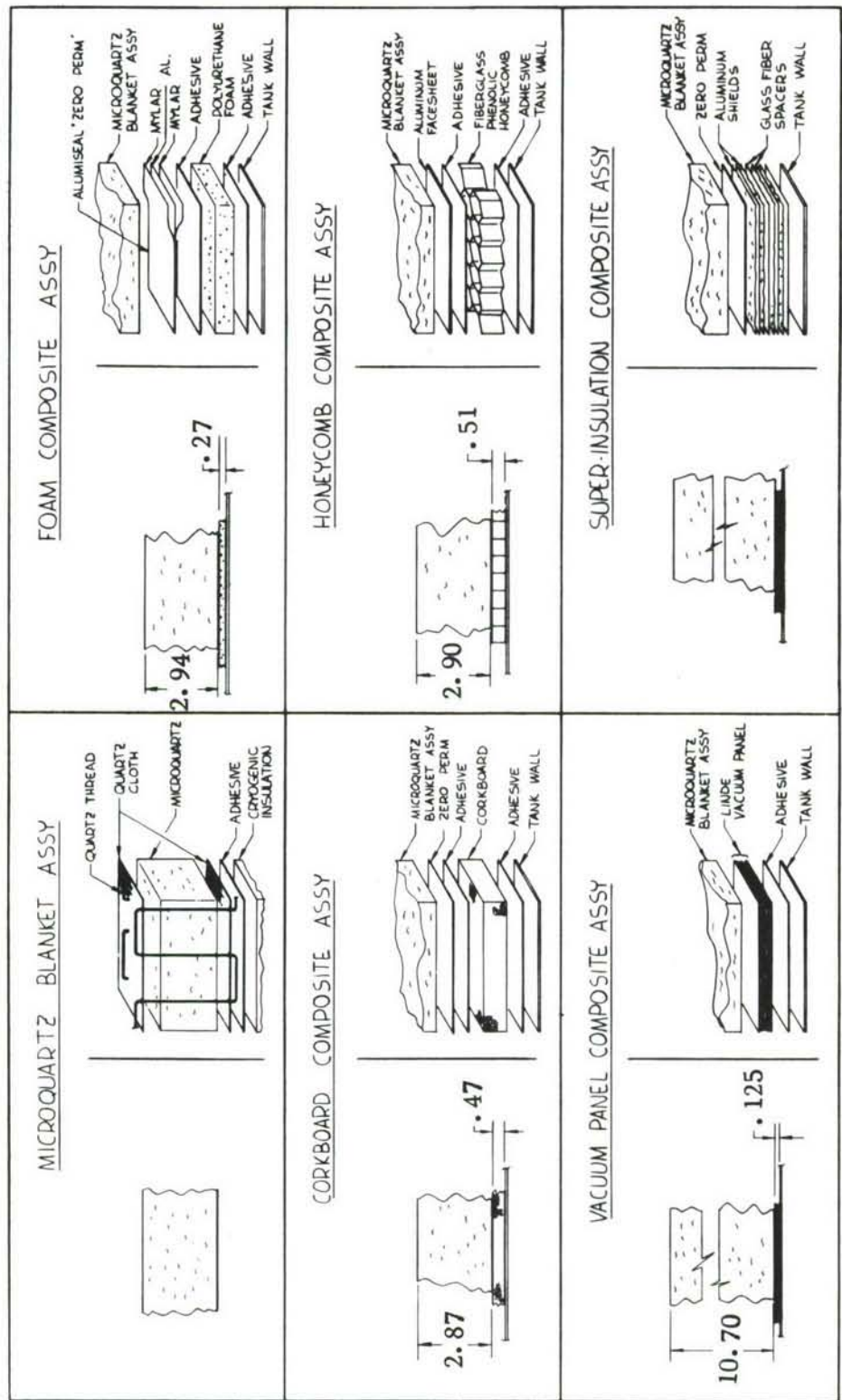


FIGURE 20 - COMPOSITE INSULATION SYSTEMS

The Linde vacuum panel evaluation provides an explanation of the problems associated with this condition.

The available data on honeycomb insulation is inadequate for evaluation on a parametric basis, primarily due to lack of systematically developed test data. Honeycomb can be utilized in a number of configurations, and fabricated from various materials. Variables that affect the conductivity and weight are cell size, thickness of core, filler material (if used), core material, type and amount of adhesive, and emissivity of facing sheets. In addition, the cells can be purged with helium, sealed to allow self-evacuation, or evacuated from an external source. Currently available test data covers only a few of these variables. An extensive experimental program would be required to generate sufficient information for system optimization. Since such an effort is beyond the scope of this contract, subsequent work on the honeycomb was limited to a single configuration, utilizing extrapolated conductivity values.

The thermal conductivity (k) for the lower element insulation materials are shown on Figures 21 and 22. From these graphs, it is apparent that the Linde vacuum panel has an extremely low conductivity value when compared with the other candidates. However, of greater concern is the lower element's compatibility with the total system composite and its $k\rho$ product. The thermal conductivity times density ($k\rho$) values for the same materials are shown on Figure 23. The $k\rho$ value is a useful measure of insulation efficiency, since the system with lowest $k\rho$ product has the least weight for a fixed heat flux. Provided it has compatibility with the total composite, the Linde vacuum panel is again shown to be the most efficient element on the basis of this comparison, with the foam, honeycomb and corkboard following in that order of preference. Sufficient thermal data is available to support an analysis on foam, corkboard, and the Linde vacuum panel, while extrapolated data has been used of a specific honeycomb construction to assess the future potential of this system.

Compatibility of the lower sealed element with the total insulation system composite was an important factor in the selection of suitable candidates. Evaluation of compatibility was made on the composite being capable of preventing cryopumping of the nitrogen gas environment at ground hold and not becoming subject to overheat at interface during the cruise condition with a dry tank wall. Figure 24 shows the composite insulation schematic with the interface temperature limits of 160°R minimum for the cryopumping condition and 600°R maximum for the overheat condition.

The minimum thickness ratios of the low and high temperature elements, shown in the table below, were determined by the cryopumping condition. Using these ratios, the upper tank wall temperature was determined that would prevent overheat of the composite interface during the cruise condition.

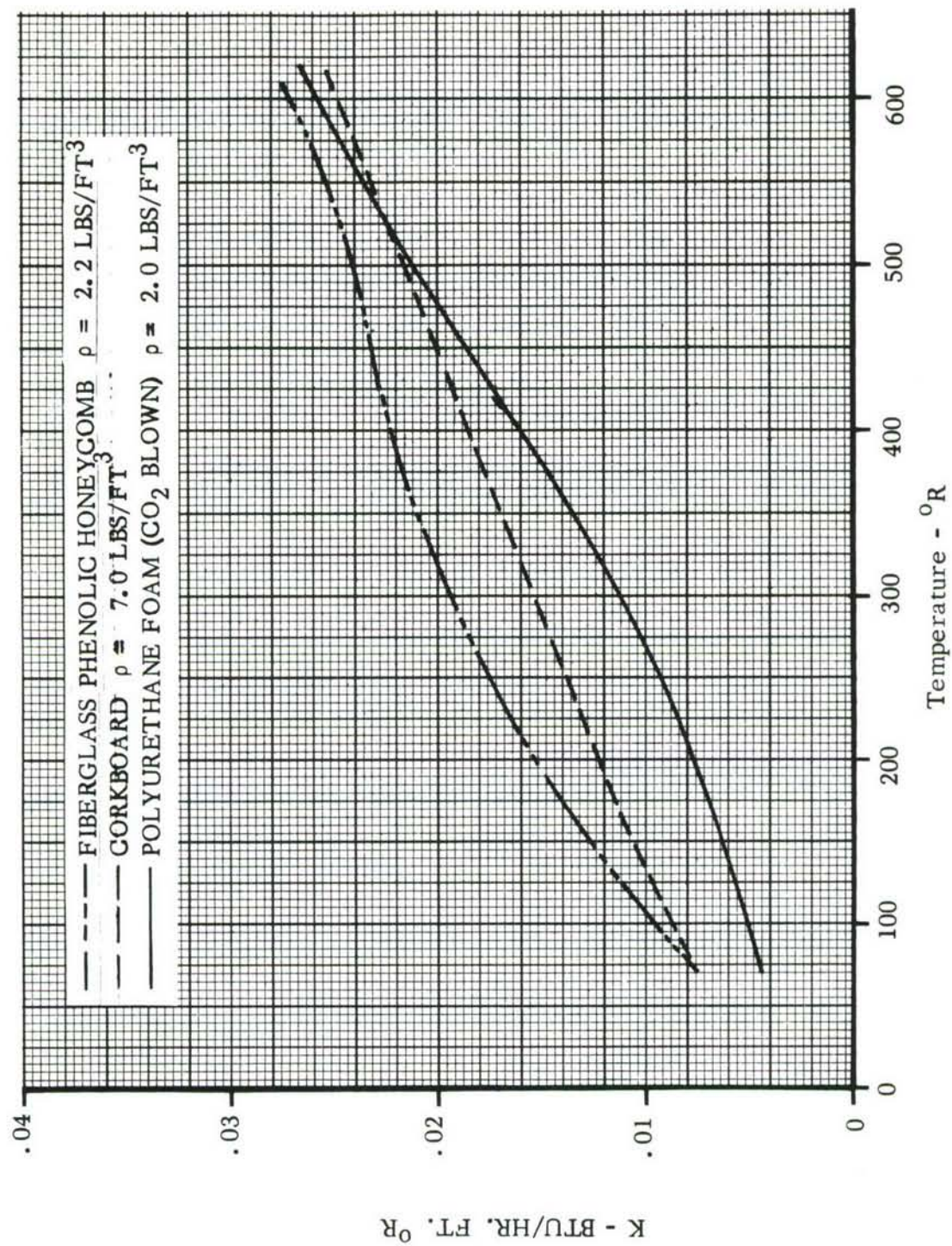


FIGURE 21 - THERMAL CONDUCTIVITY (K) OF LOW TEMPERATURE INSULATIONS

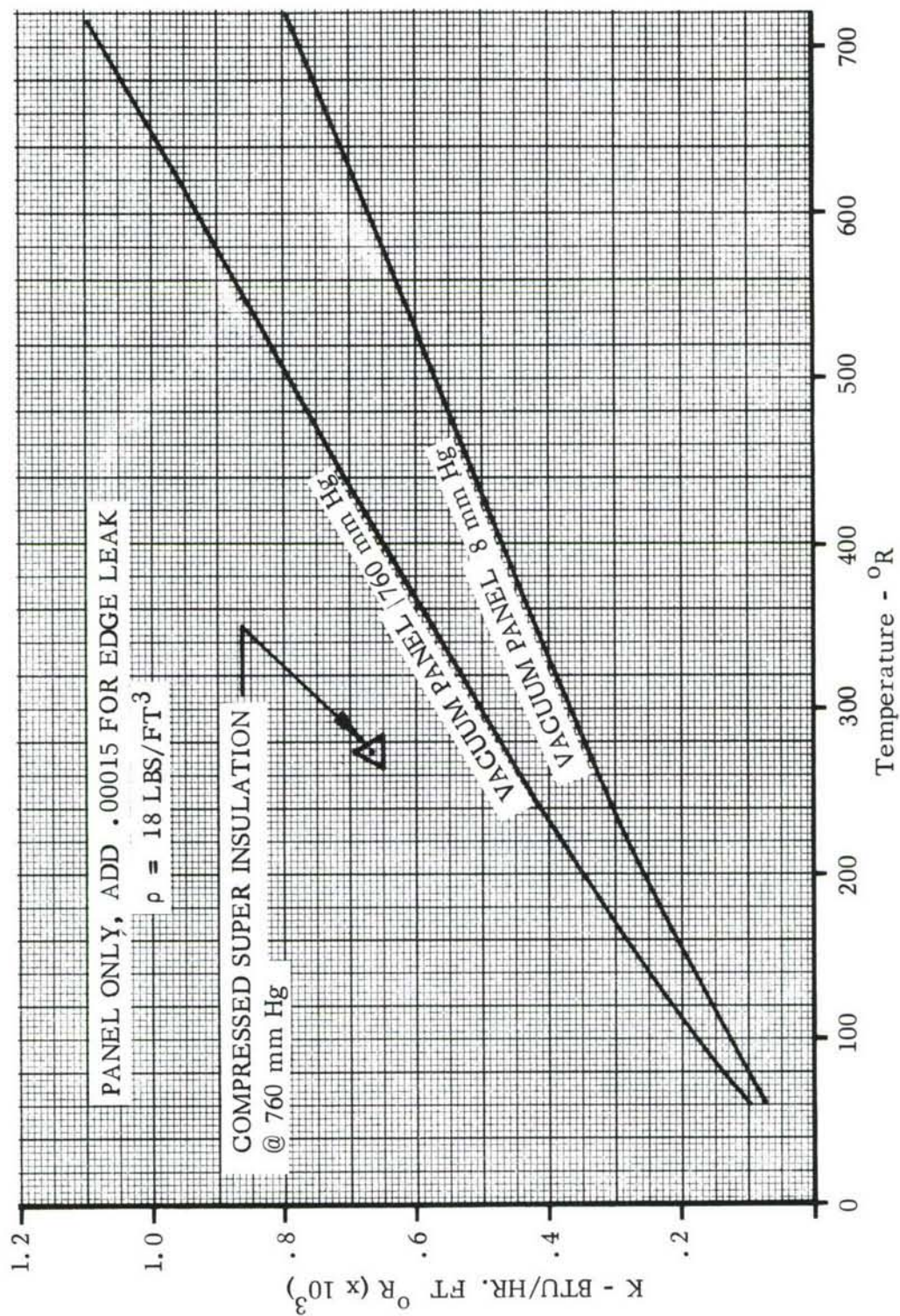


FIGURE 22 - THERMAL CONDUCTIVITY (K) - LINDE SUPER INSULATION VACUUM PANELS AND COMPRESSED SUPER INSULATION

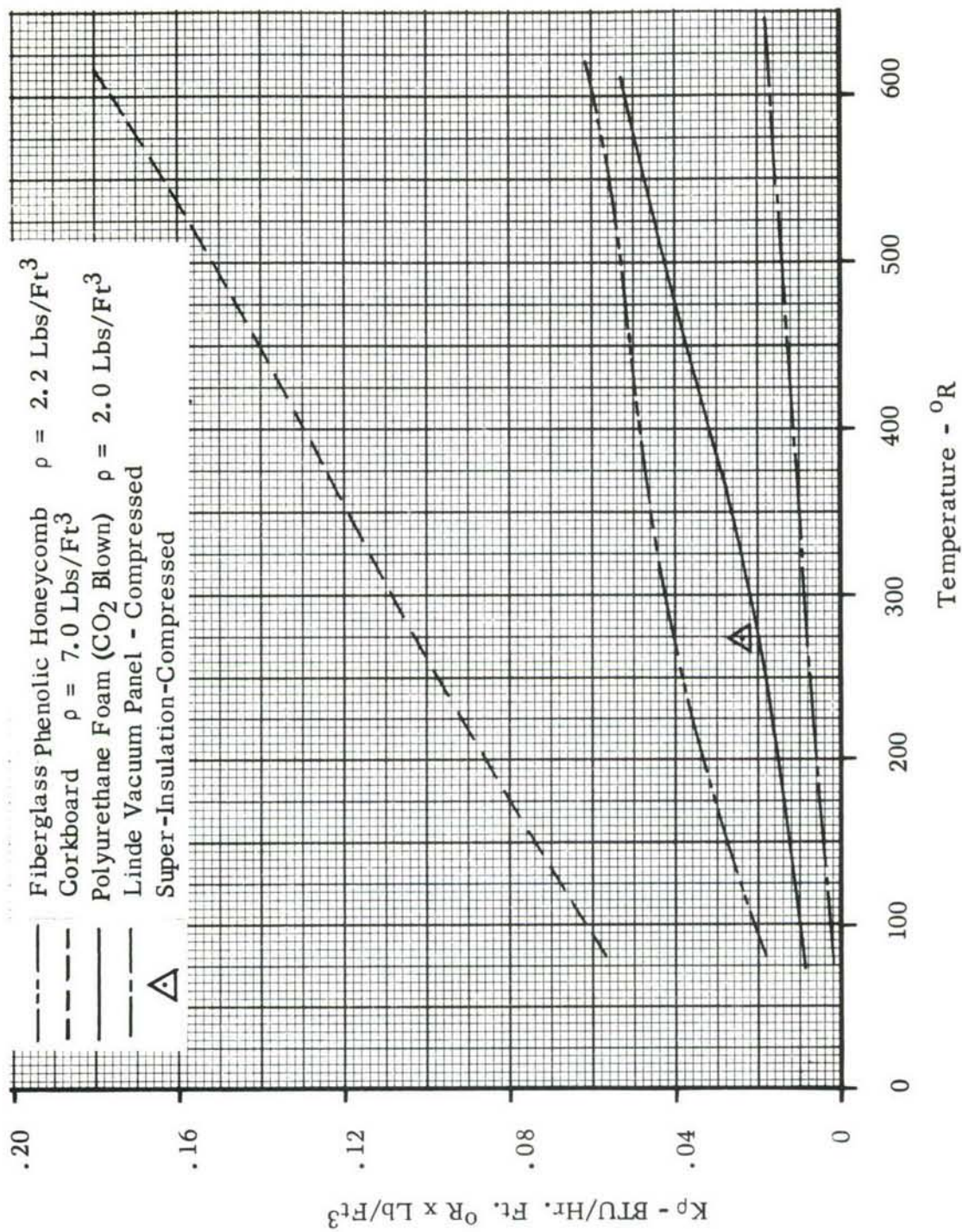


FIGURE 23 - THERMAL CONDUCTIVITY TIMES DENSITY ($K\rho$) OF LOW TEMPERATURE INSULATIONS

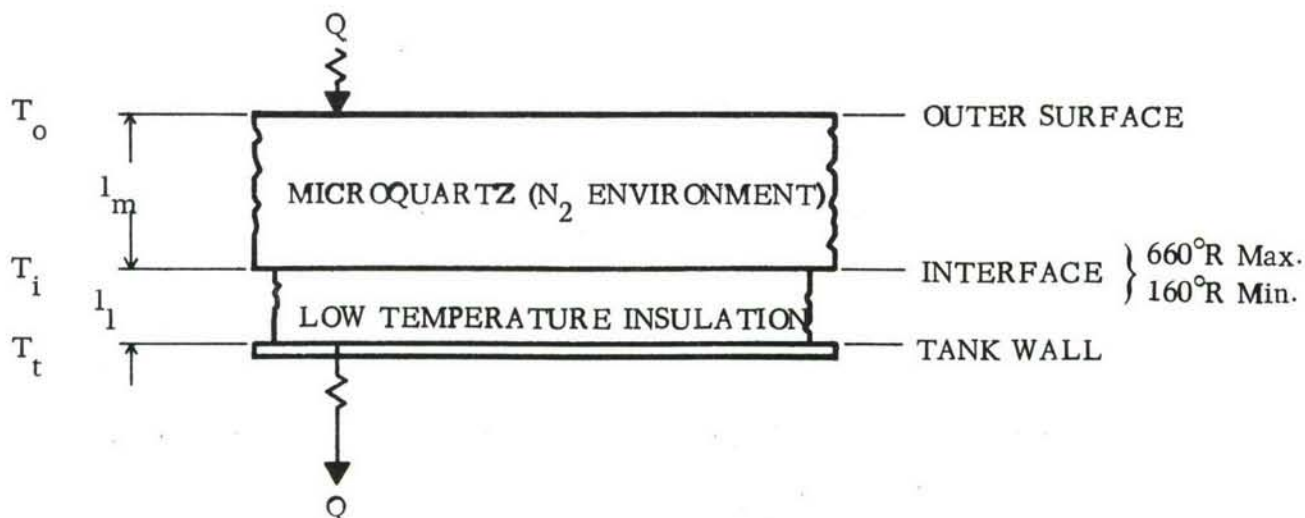


FIGURE 24. COMPOSITE INSULATION SCHEMATIC

Material	l_l/l_m	Cruise (Upper Surface)		
		T_t	T_i	T_o
Foam	.092	580°	660°	1460°
Honeycomb	.178	510°	660°	1460°
Cork board	.160	510°	660°	1460°
Linde Vacuum Panel	.0031	555°	660°	1460°

The limiting tank wall temperature is close to ambient for all the low temperature sealed elements. Since ullage gas stratification and empty tank considerations will give rise to higher temperatures than this, some form of active cooling is mandatory for all composite systems considered.

Linde vacuum panel thickness required is less than one percent of the total thickness of the composite insulation. A practical minimum thickness for the panel is about .125 inches. The resulting Microquartz thickness would, therefore, be 40.00 inches, which is obviously not aligned to minimum weight considerations. If we take an extreme approach and control the tank wall temperature to slightly above LH_2 temperatures, 40° R, a revised thickness ratio of .0116 could be employed. This, however, results in a Microquartz blanket 10.7 inches thick in order to prevent overheating of the interface. The Linde vacuum panels are, therefore, not practical system elements for this application with current state-of-the-art material restrictions on temperature capability.

3.3.4 WEIGHT COMPARISON. The previously developed conductivity and thickness ratio data allows a weight comparison between the systems of interest. The weights of the low-temperature insulation elements are shown below:

Item	Weight, lb/ft ²					
	Foam, 2 lb/ft ³		Cork, 7 lb/ft ³		Honeycomb 3/8 in. Cell	
	Variable	Fixed	Variable	Fixed	Variable	Fixed
Insulation	.167 x l_1	-	.583 x l_1	-	.183 x l_1	-
Adhesive	-	.150	-	.150	-	.110
Sealing Membrane	-	.022	-	.022	-	-
Face Sheet, .005 in. Al.	-	-	-	-	-	.072
Total	.167 l_1 + .172		.583 l_1 + .172		.183 l_1 + .182	

l_1 = thickness of insulation, inches

A representative flight condition with a steady flux of 150 BTU/hr-ft² through the lower tank surface was selected as the basis for comparison. The temperature of the tank wall and insulation outer surface are 40°R and 1720°R, respectively. System weight comparisons results are shown below:

System	Conductivity (BTU/Hr-Ft-°R)		Thickness (Inches)		Weight (Lb/Ft ²)		
	Low Temp. Insul.	High Temp. Insul.	Low Temp. Insul.	High Temp. Insul.	Low Temp. Insul.	High Temp. Insul.	Total
Microquartz in He Environment	-	.0400	-	5.37	-	2.28	2.28
Foam-Microquartz Composite	.0093	.0280	.270	2.94	.22	1.34	1.56
Honeycomb Microquartz Composite	.0168	.0282	.510	2.90	.26	1.32	1.58
Cork Board Microquartz Composite	.0139	.0285	.467	2.87	.44	1.31	1.75

The effect of the helium environment on the Microquartz performance is illustrated by the increased conductivity and higher system weight.

Breakdown of the Microquartz blanket's element weights and the weight equation employed in the optimization program is given below:

FIXED WEIGHT	LB/FT ²	VARIABLE WEIGHT	LB/FT ²
Quartz Thread	.012	Microquartz Felt (4.5 lb/ft ³)	.375 x l _m
Quartz Cloth	.140	Quartz Thread	.012 x l _m
Adhesive	.050		

$$W = (.202 + .387 \times l_m) \text{ lb/ft}^2$$

where l_m = blanket thickness, inches.

For the foam/Microquartz composite insulation system, the weight equation used in the optimization program was:

$$W = [.374 + .363 l_t] \text{ lbs/ft}^2$$

where l_t = total composite thickness, inches.

3.3.5 FINAL SYSTEM SELECTION. The helium environment Microquartz system was selected on the basis of least complexity, high inherent reliability, absence of thermal stress problems and availability of thermal properties. The higher weight of this system is offset by its simplicity and excellent temperature compatibility.

The honeycomb low temperature element of a composite system does not have sufficient thermal data available, nor have its structural implications been sufficiently investigated to be recommended as a final system insulation choice, at this time. The purpose in its being considered up to this point is to provide comparison data for future evaluation purposes, especially in light of its potential as a structural element for stiffening. The composite systems potentially applicable are then the foam-Microquartz and the corkboard-Microquartz systems. Both of these approaches are similar in design concept. A vacuum-tight membrane is required between the low-temperature and the high-temperature insulation layers. Sealing problems are likely to be encountered around penetrations and tank access covers. Both systems have a low tolerance for overheating due to the presence of temperature limited adhesives and membranes. The high temperature gradient across the low temperature insulation will lead to thermal stresses and possible premature failures. The foam composite shows a slight weight advantage over the corkboard and easier application to compound curvature surfaces due to the hot forming capability of the foam. It was therefore selected as the other system for detailed optimization and application to a

subscale tank. This system operates in a nitrogen gas environment, and showed improved thermal performance at the cost of increased complexity and reduced reliability.

Preliminary test evaluation of these two selected systems, conducted in a guarded liquid nitrogen calorimeter, was performed to establish thermal conductivity and durability under cyclic temperature and pressure conditions. This work is reported on in Appendix I. Evaluation of the effects of variation in conductivity, manufacturing tolerances, and fabrication procedures was also made on the foam/Microquartz composite insulation system. Evaluation testing on the composite insulation system revealed its extreme sensitivity to overheating at the sealing interface. This resulted in the termination, by the AFFDL, of further work on this system, prior to being installed on an experimental tank and tested in an experimental chamber.

Final choice of insulation, for hypersonic cruise vehicle application, is the Microquartz helium environment system. This system is state-of-the-art, compatible with environment involved, relatively easy to fabricate, and when bonding requirements are removed, is not temperature limited.

3.3.6 HEAT FLUX THROUGH CANDIDATE INSULATION SYSTEMS. The heat flux through the all Microquartz and the foam/Microquartz insulation systems was determined for the trajectory environmental conditions and used as input data for the optimization. Three environmental conditions were investigated:

- (1) ground hold (radiation shield temperature, 490°R)
- (2) flight-upper surface (cruise structure temperature, 1460°R)
- (3) flight-lower surface (cruise structure temperature, 1700°R)

The analysis includes all liquid hydrogen losses, which are a function of insulation design and thickness:

- (1) Expansion space for the liquid as it is heated during ground hold.
- (2) Boil-off during flight.
- (3) Amount of spray necessary to maintain a 520°R tank wall temperature during flight.

3.3.6.1 Ground Hold. The steady state heat flux through the insulation to the liquid during ground hold for the Microquartz in a helium environment and for the Microquartz/foam composite in a nitrogen environment are shown in Figure 25.

Two methods were considered at ground hold to absorb the incoming heat flux. The tank can be filled to a pre-determined level, locked up, and allowed to self-pressurize.

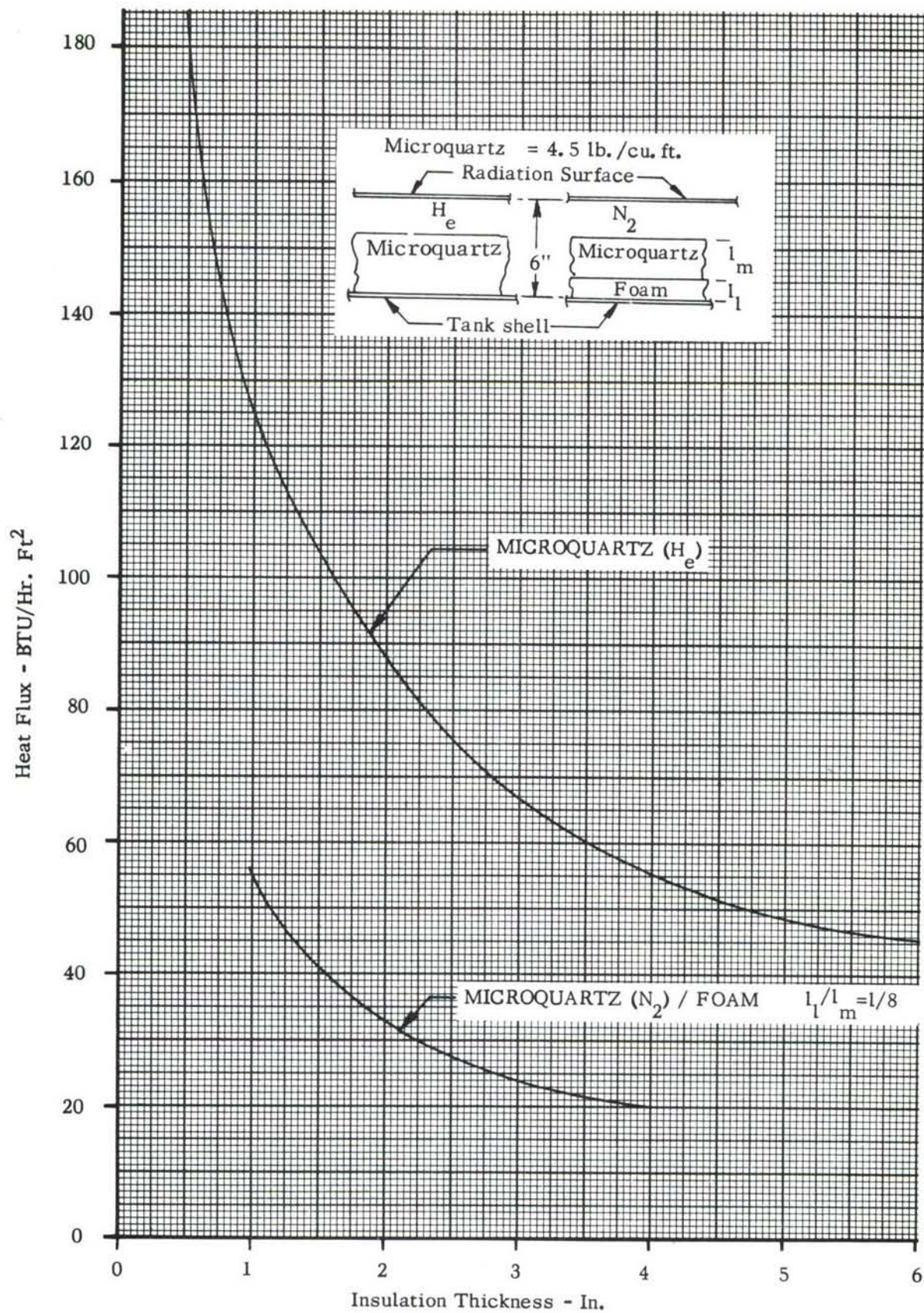


FIGURE 25 - GROUND HOLD HEAT FLUXES TO LH₂ VERSUS INSULATION THICKNESS

The liquid will increase in temperature and expand (density decrease) to fill the tank at the end of ground hold. The amount of space necessary for liquid expansion is then lost volume (or LH_2 mass). The other method for absorbing the ground hold heat leak is to fill the tank and allow it to boil off during the ground hold time. Boiling liquid hydrogen contains vapor bubbles which substantially reduce the bulk density. Tests by GD Convair on Centaur³ indicate that hydrogen, boiling at one atmosphere (36.5°R) has a bulk density of 4.3 lb/ft^3 , whereas the saturated liquid has a density of 4.4 lb/ft^3 . The mass of liquid hydrogen in the tank at the end of a 30-minute ground hold is shown in Figure 26 for the case where the tank is self-pressurized and for boil-off at one atmosphere. It is evident that the self-pressurized case provides considerably more liquid at the start of flight. Thus, the optimization was based on self-pressurization during ground hold. Typical liquid hydrogen penalties associated with self-pressurization for various heat fluxes on the top and bottom of the tank during ground hold are shown in Figure 27.

3.3.6.2 Flight. The upper and lower tank surfaces are subjected to different temperature environments, thus different heat rates, during flight. About half of the upper tank surface area is not in contact with the liquid during the entire cruise period. The bottom tank surface is in contact with the liquid and kept cold throughout the flight. For these reasons the upper and lower surfaces are treated separately in the optimization analysis. The thickness of insulation on the upper half and lower half of the tank, respectively, were parameters in the determination of optimum insulation weight.

The heat flux to the liquid through the upper and lower surfaces as a function of flight time and insulation thickness is shown in Figures 28 and 29 for the all Microquartz system, and in Figure 30 for the composite Microquartz/foam system. This data was input to the optimization program.

3.3.7 ULLAGE AND TANK WALL TEMPERATURES. A sample calculation was made to determine the magnitude of the ullage and upper wall temperatures in the tank. The upper tank wall temperatures through the trajectory were calculated for insulation thicknesses of 3 and 6 inches of Microquartz (helium). The GD Convair transient heat conduction computer program (Reference 6) and the North American tank pressurization computer program (Reference 7) both predicted a final temperature of about 1100°R for the upper tank wall with 3 inches of insulation. The GD Convair program assumed no heat transfer from the wall into the ullage. The NAA program included convective heat transfer from the wall to the ullage. The NAA program indicates that the ullage will stratify and have little or no cooling effect on the wall when the liquid is not boiling. The top tank wall temperature profiles are shown in Figure 31. The tank wall reaches the design temperature of 520°R after 1900 seconds with 3 inches of insulation. About 6 inches of insulation is required to limit the tank wall to a temperature of 520°R after 5400 seconds.

Neither of the above calculations included radiation from the upper tank surface to the liquid. A literature search was made to find the absorptivity of LH_2 , but no values were found. The NBS Cryogenic Labs in Boulder and the NBS Spectroscopy Section in Washington were contacted. Dr. Lide (NBS Washington) offered the opinion

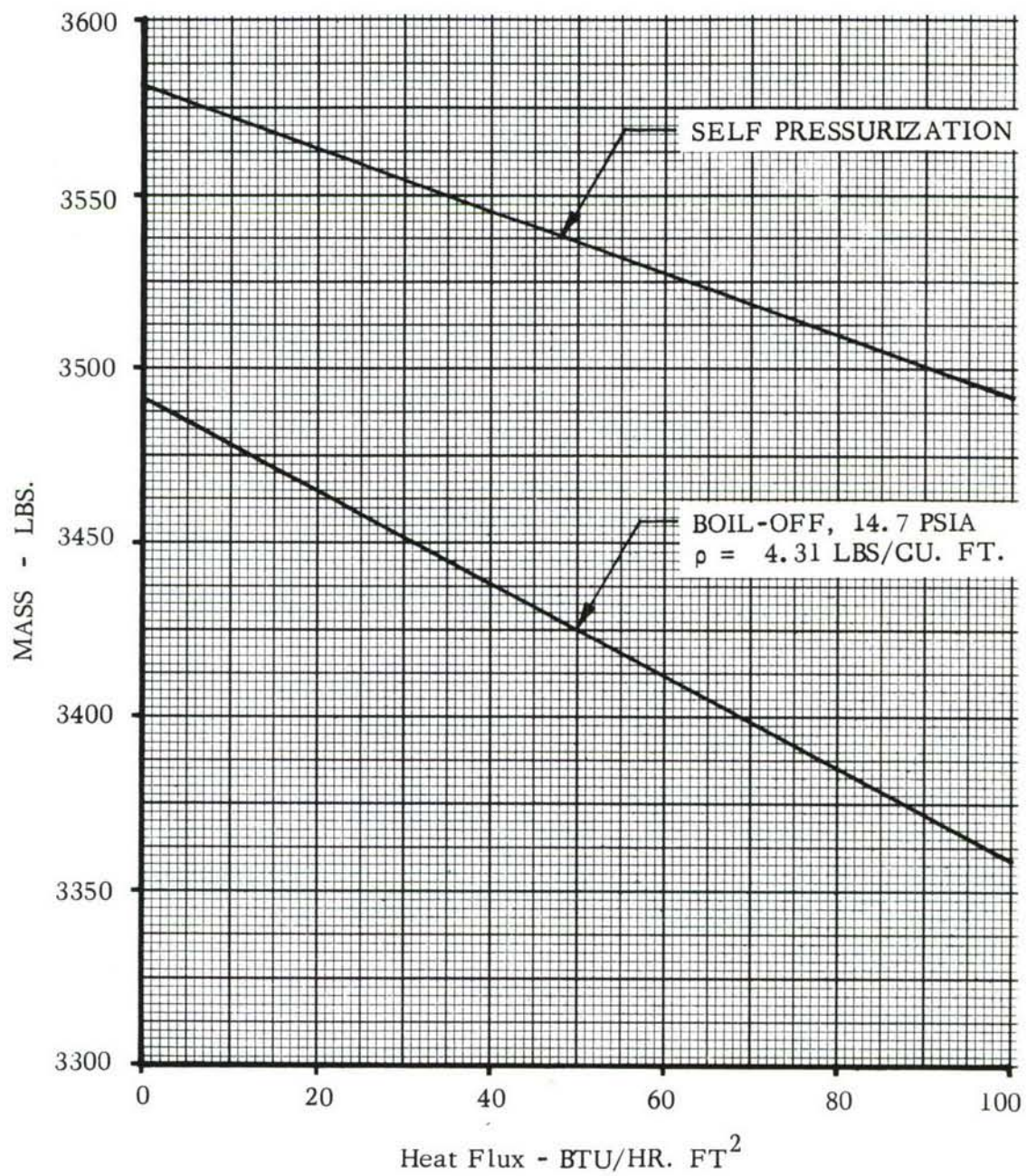


FIGURE 26 - HYDROGEN MASS IN TANK AFTER 30 MINUTES GROUND-HOLD

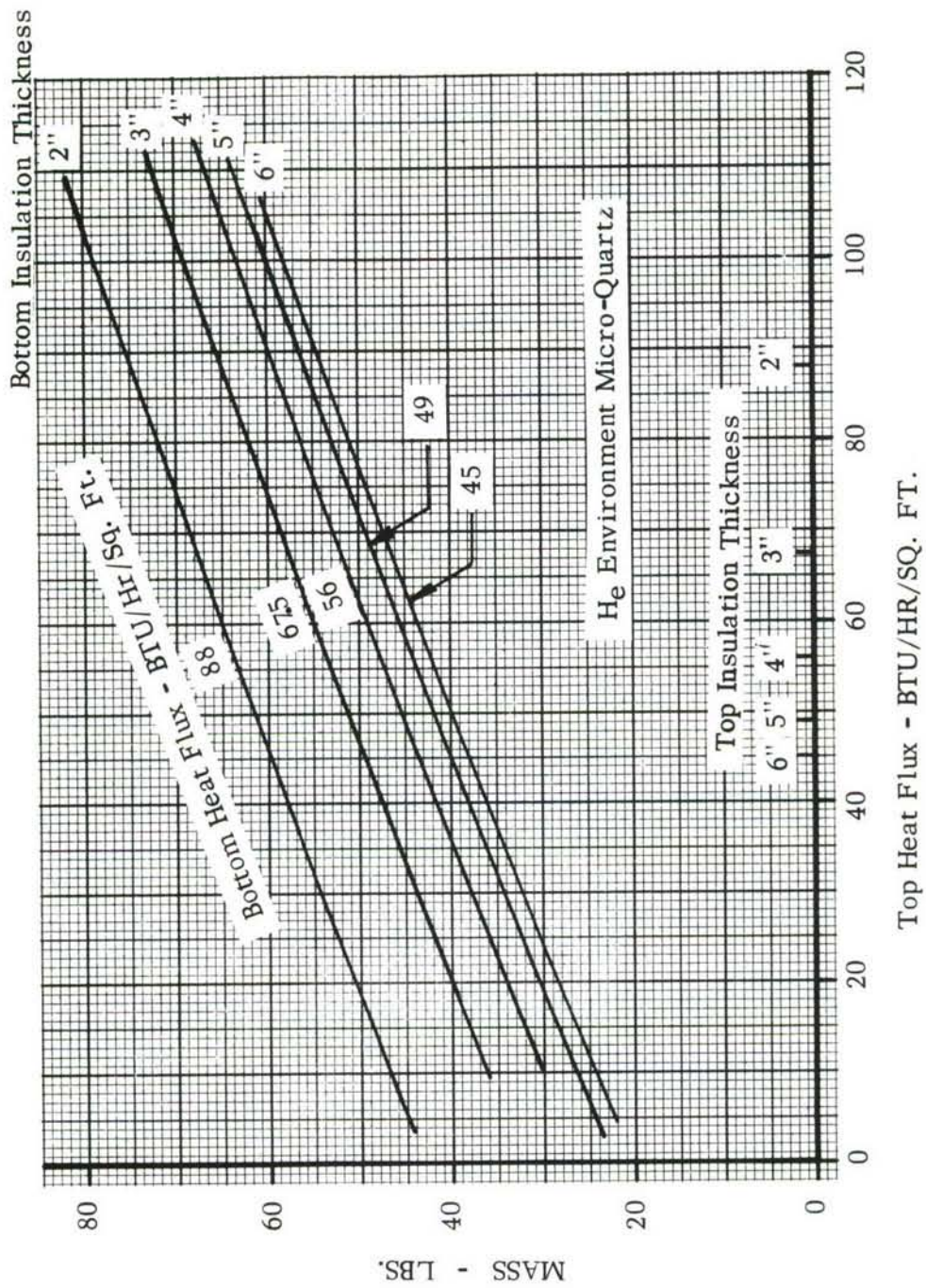


FIGURE 27. EQUIVALENT LH₂ MASS LOSS DURING 30 MINUTE GROUND HOLD - SELF PRESSURIZATION

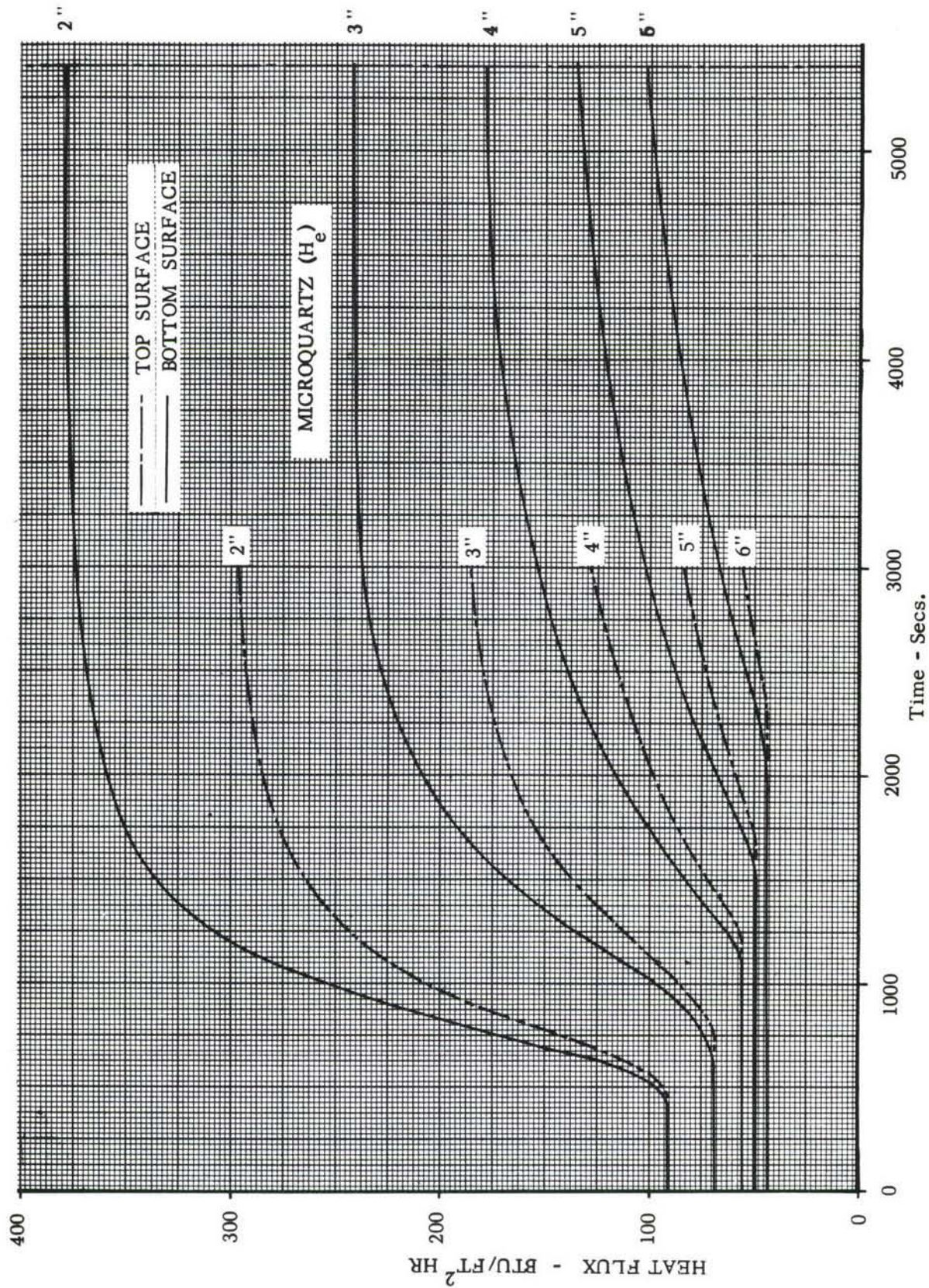


FIGURE 28 - HEAT FLUX TO LH₂ VS FLIGHT TIME - MICROQUARTZ (H_e)

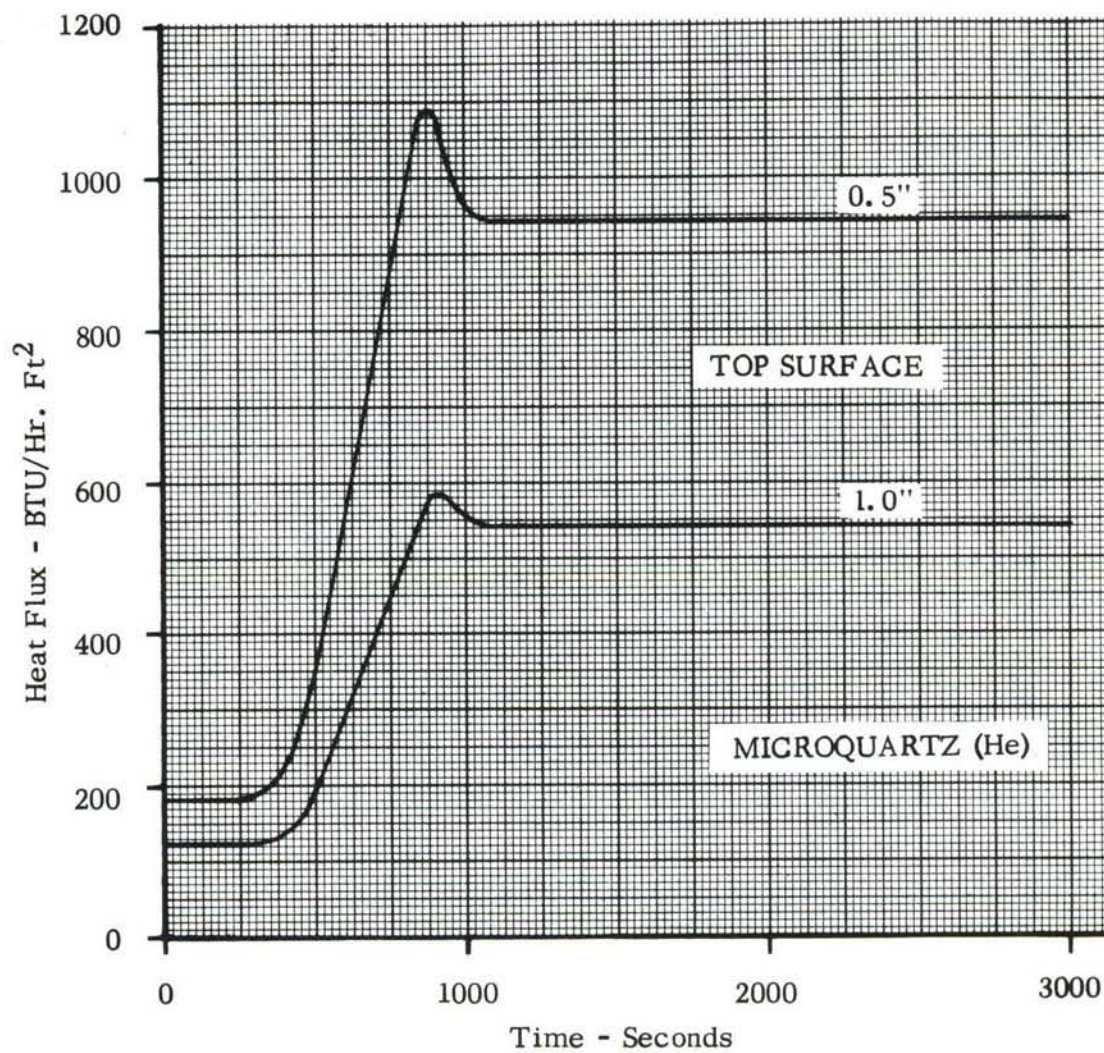


FIGURE 29 - HEAT FLUX TO LH₂ VS FLIGHT TIME - TOP SURFACE
- MICROQUARTZ (He)

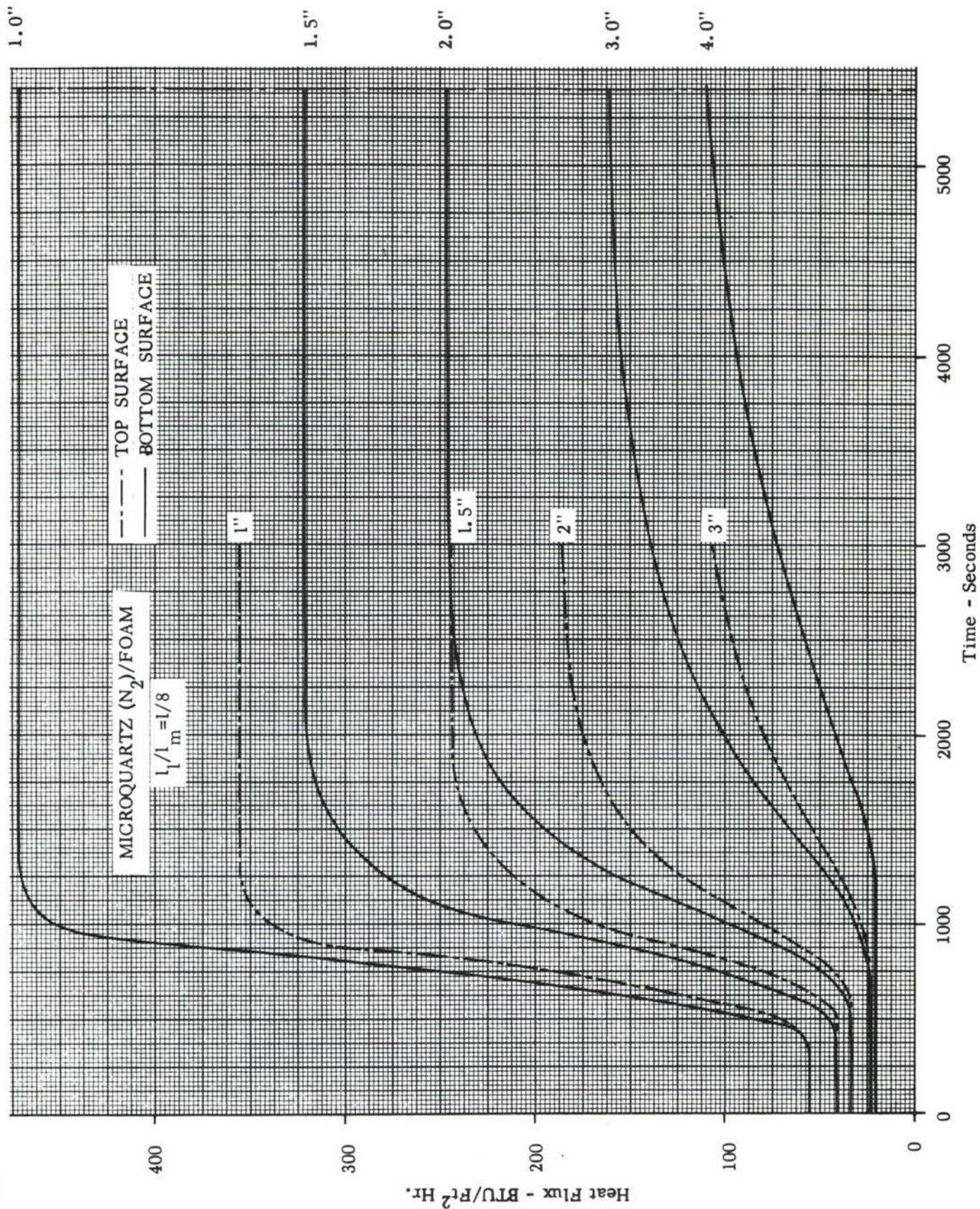


FIGURE 30 - HEAT FLUX TO LH₂ VS FLIGHT TIME - MICROQUARTZ (N₂)/FOAM COMPOSITE

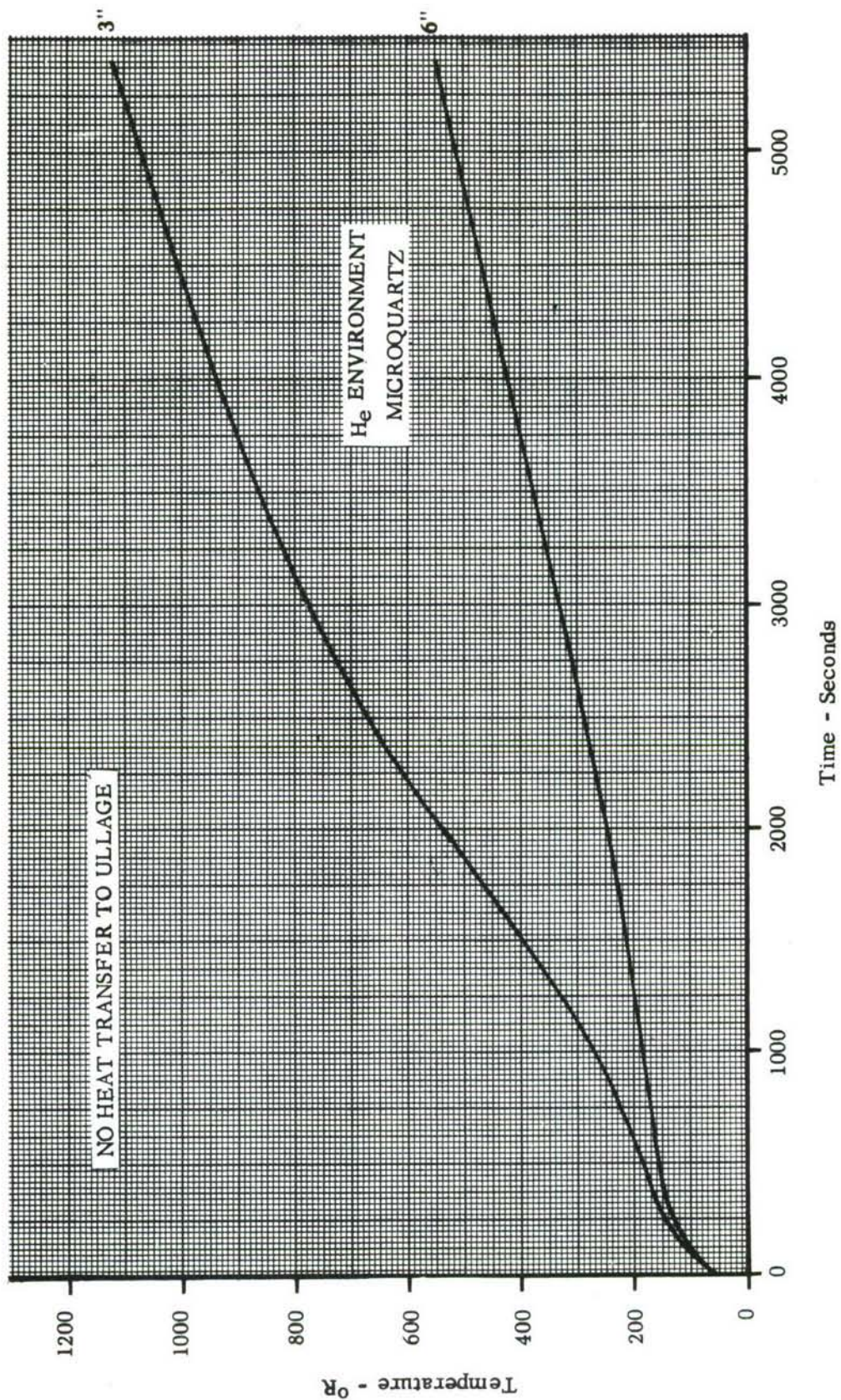


FIGURE 31 - TANK WALL TEMPERATURE (TOP SURFACE) VERSUS TRAJECTORY TIME

that LH_2 may be transparent to infrared radiation. If this is correct, the radiation heat transfer will be between the warm upper and cold lower tank wall. The emissivity of titanium at low temperature is about 0.1. The heat transfer between parallel planes at 520°R and 40°R is about 6.5 BTU/hr-ft^2 ($\epsilon = 0.1$). The effect of radiation from the upper tank wall will not be significant in reducing its temperature, because the heat flux through the insulation on the upper surface is more than 100 BTU/hr-ft^2 .

Provision was made in the analysis to include spray cooling the top of the tank to maintain a wall temperature of 520°R . The heat flux to the ullage from the upper surface with a 520°R tank wall is shown in Figure 32. The time at which the upper tank wall reaches 520°R is shown in Figure 33. Advantage is taken of both the heat of vaporization and sensible heat of the vapor in the use of spray cooling. This results in a minimum quantity of spray being required. Spray cooling is used only from the time the upper tank wall reaches 520°R to the time at which liquid boiling starts. Once boiling starts, the cold vapor addition is assumed to provide adequate tank wall cooling. The start of liquid boiling depends both on tank vent pressure and the insulation thickness. The rate of temperature rise of the tank wall is also dependent upon the insulation thickness.

Tank pressure can be reduced (for any reasonable insulation thickness; i.e., > 1.0 inch) such that boiling will start early, thus limiting the tank temperature to less than 520°R without spray cooling. This is not necessarily optimum as the optimization analysis has shown. It is also assumed that sufficient residual (unusable) fuel will remain to provide boil-off cooling during letdown; 'end-of-flight' parameters are not being investigated in this study.

3.3.8 HEAT LEAKS THROUGH SUPPORTS AND PENETRATIONS. The heat leakage rates for the various tank penetrations are shown in Table 2 for the ground hold and the flight conditions. The rates given are the steady state heat transfer rates to the liquid hydrogen.

The magnitudes of the total penetration heat leak, 41 BTU/hr and 195 BTU/hr for the ground hold and flight conditions, respectively, are less than 1% of the total heat which enters the liquid hydrogen through the insulated walls of the tank. For this reason, the penetration heat leaks were neglected in the optimization of the tank insulation system.

The distribution of temperature in the supports is of interest primarily in the foam/Microquartz system where it is possible to liquefy the nitrogen atmosphere upon the surface of the supports. Figure 34 shows the temperature distribution along the three support members and indicates the minimum length of support which must be insulated to prevent cryopumping during the ground hold condition. Figure 35 shows the temperature distribution along the supports during flight and illustrates that the support insulation will not exceed the composite insulation temperature limit of 200°F during the flight trajectory.

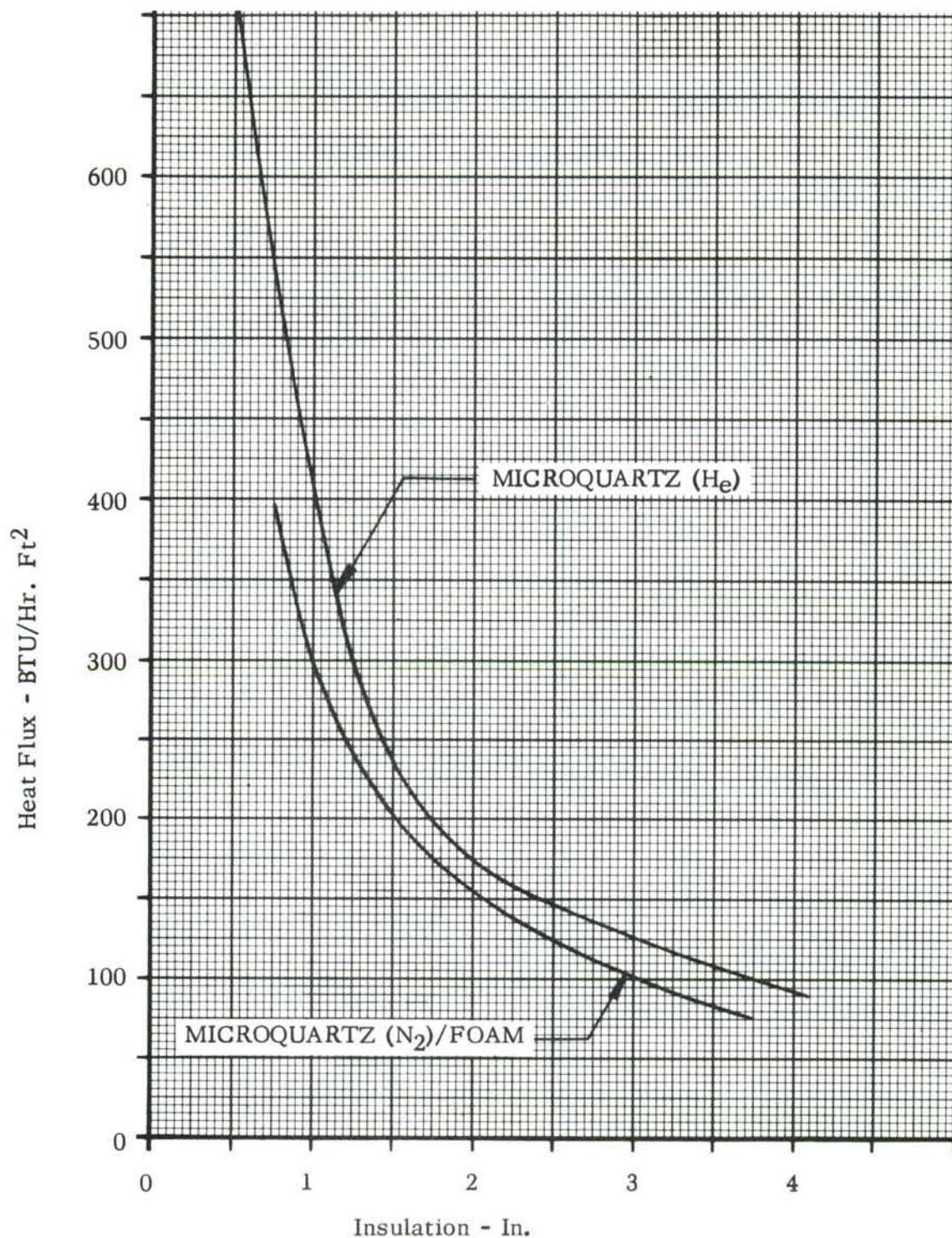


FIGURE 32 - HEAT FLUX TO ULLAGE THROUGH TOP SURFACE -
520°R TANK WALL TEMPERATURE

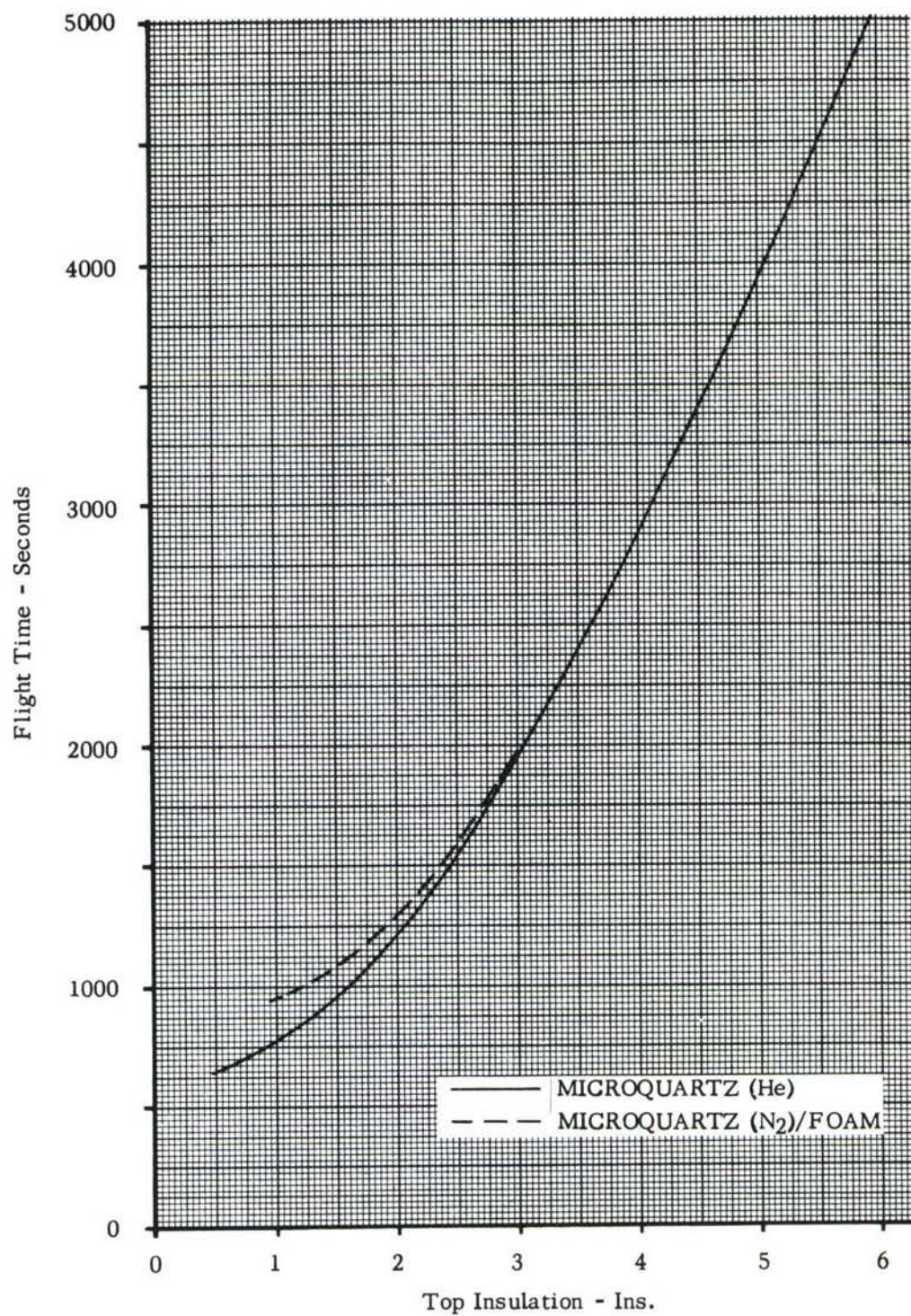


FIGURE 33 - TIME TOP TANK WALL REACHES 520°R - START OF SPRAY COOLING

TABLE 2

PENETRATION HEAT LEAK RATES

	Ground Hold (BTU/hr.)	Flight (BTU/hr.)
Forward tripod support with drag link	1.5	10.0
Aft bipod support	1.2	9.3
Outboard support links (four)	4.6	41.2
Piping penetrations (estimated)		
Vacuum jacket drain pipes (two)	17	135
Vent pipes (two)	17	0*
	41	195

*Vent pipes at top of tank will not affect heat flux to liquid in-flight.

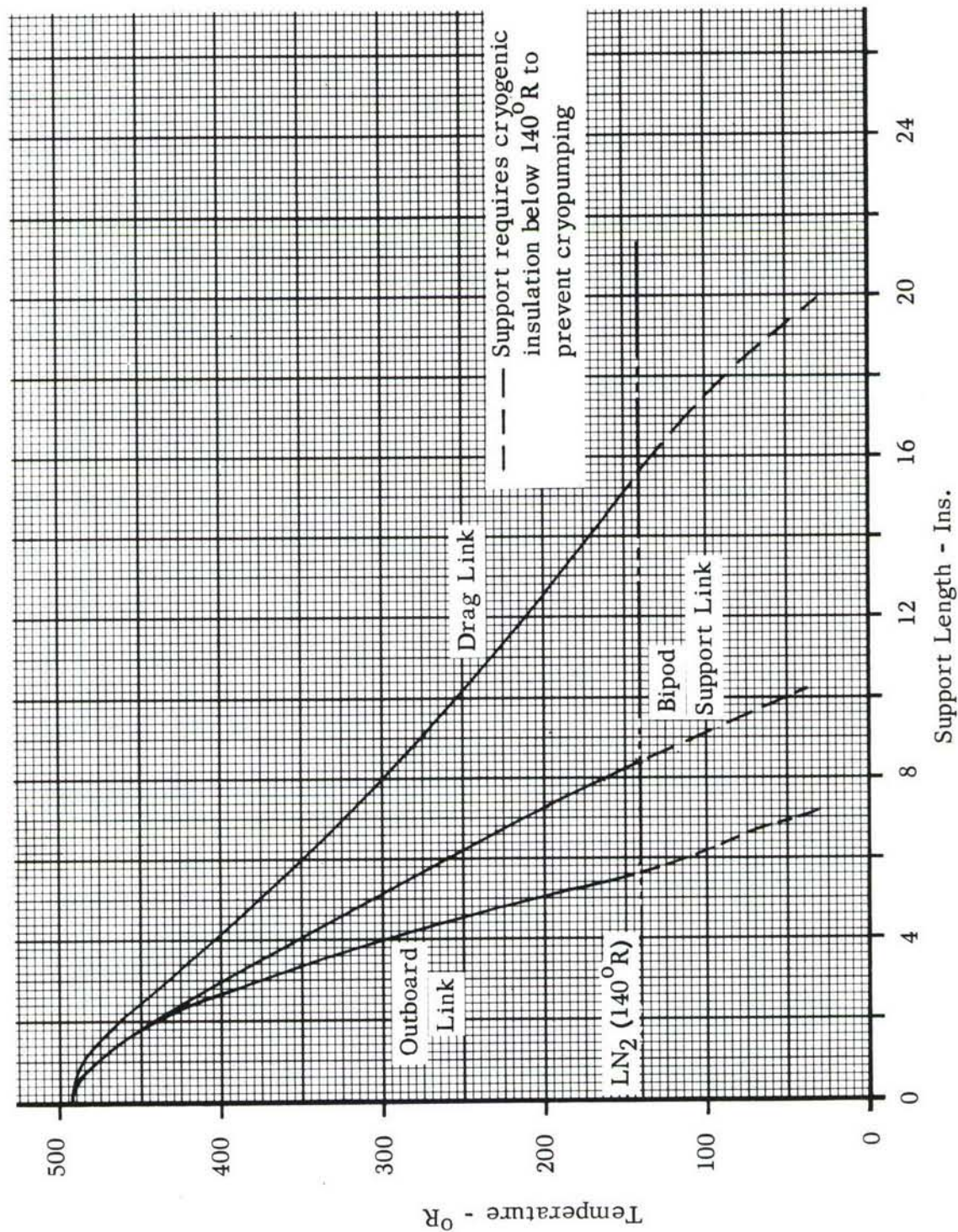


FIGURE 34 - TEMPERATURE DISTRIBUTION ALONG TANK SUPPORT MEMBERS - GROUND HOLD CONDITION

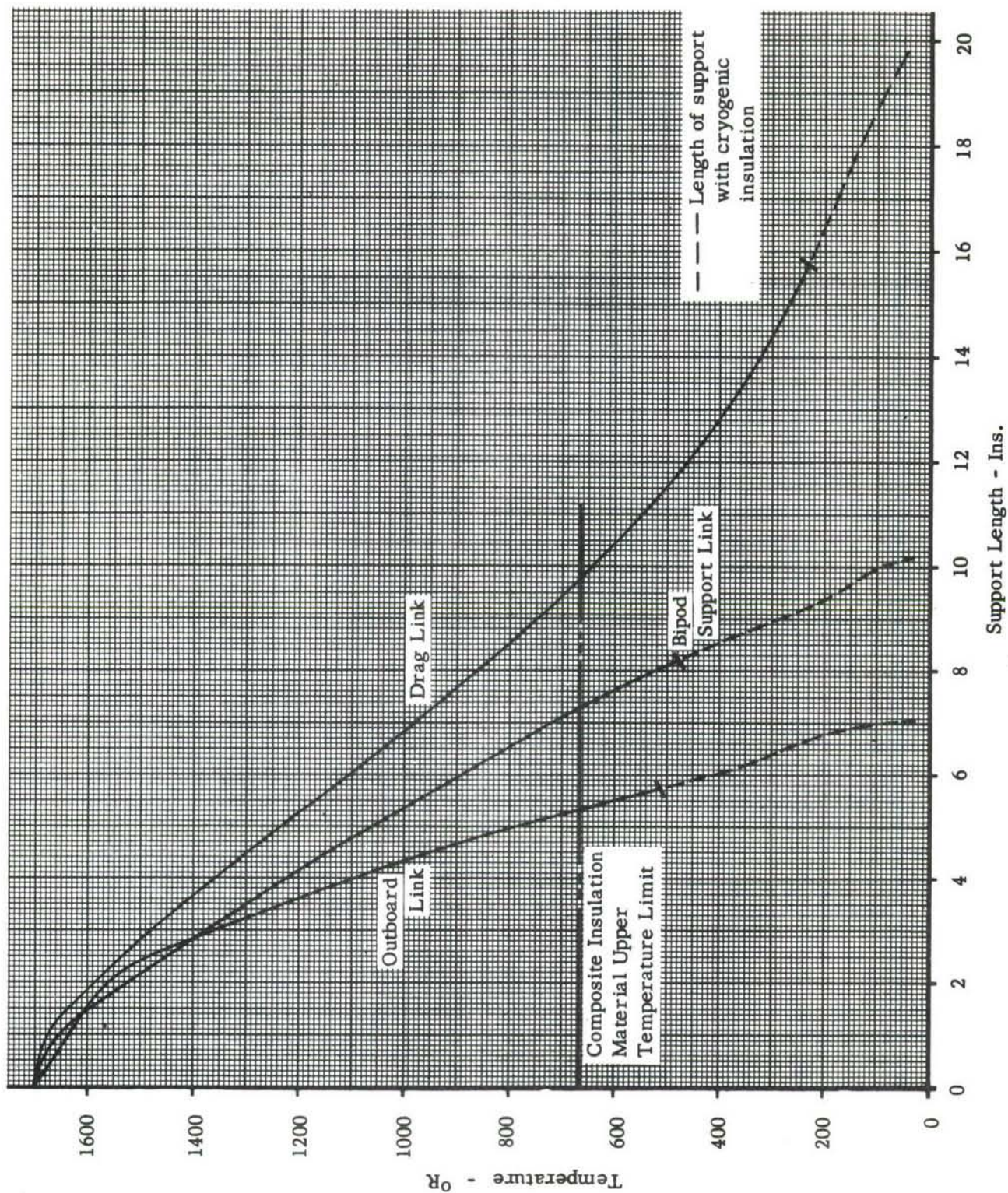


FIGURE 35 - TANK SUPPORT MEMBERS - TEMPERATURE DISTRIBUTION (IN-FLIGHT)

3.4 FUEL SYSTEM

The fuel system was studied to provide performance and design criteria for the optimization procedure and design of the test tanks. The study ground rule was to provide maximum thermal performance for minimum system weight.

3.4.1 DESIGN APPROACH. The ground hold period was reviewed to arrive at a storage method providing maximum utilization of available tank volume. For the in-flight phase, boost pump and pressure feed methods were examined to transfer fuel to the high pressure engine pump. Typical tank pressure and wall temperature histories were examined to establish the requirements for pressurization and tank wall cooling methods.

Ground Hold Storage - The two methods of ground hold storage investigated, Figure 36, were the self-pressurization and boil-off approaches. In the self-pressurization approach, the vent valve controls the ullage pressure to prevent boiling of the bulk liquid. The heat flux, therefore, results in sensible heating of the liquid, and liquid expansion due to density decrease. The ullage volume is minimum at takeoff. Sufficient ullage space must be allowed for at end of the fill condition to provide for this liquid expansion.

In the boil-off approach, heat is absorbed by boiling at atmospheric pressure; vapor is vented overboard. Boil-off results in poor tank volume utilization due to a combination of effective density decrease (volume displaced by vapor bubbles) and vented propellant.

The self-pressurization approach provided the maximum utilization of tank volume, and was, therefore, selected for this program.

In Flight Storage and Fuel Transfer - The two basic methods available for LH_2 transfer are pressure feed and booster pump feed. Choice of transfer method determines storage conditions.

Pressure feed has been employed to transfer fuel for vertical take-off boosters. The ullage pressure is maintained well above bulk liquid vapor pressure in order to supply single-phase fuel to the engine high-pressure pump.

Pressure feed resulted in higher tank pressures, greater insulation thickness, and a sizeable unusable fuel quantity -- particularly in horizontal tankage. Temperatures at the upper tank skin would also be higher due to ullage stagnation.

Booster pump feed allows boiling of the liquid, since the tank-mounted pumps will suppress the vapor phase, thus ensuring transfer of 100 percent liquid. The booster pump feed approach provides a greater difference between total pressure and fuel vapor pressure (defined as NPSH, or net positive suction head) at the tank outlet,

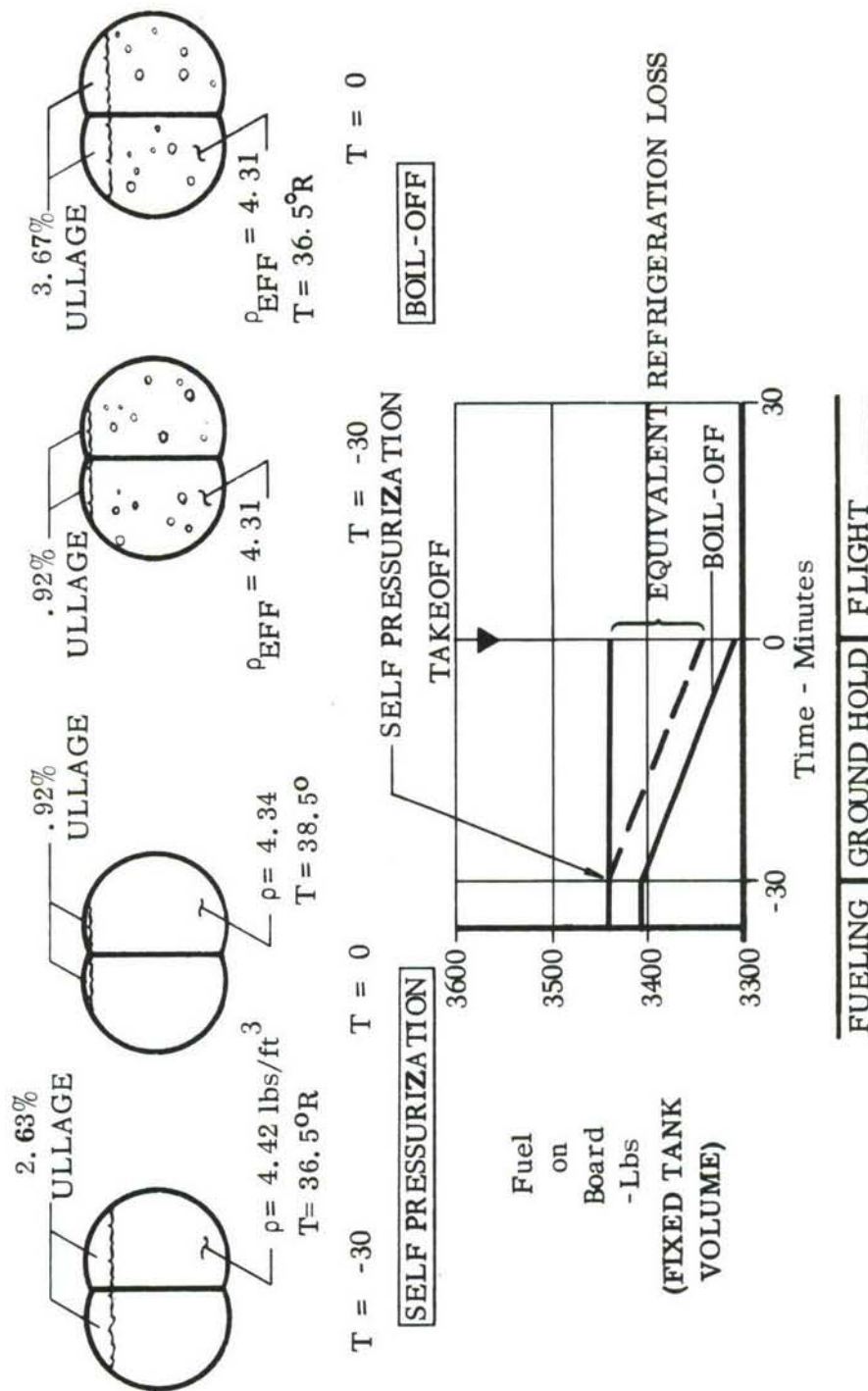


Figure 36. GROUND HOLD STORAGE OPTIONS

thereby allowing a safety margin for transfer line heat leak and pressure drop, as well as reasonable size main pumps.

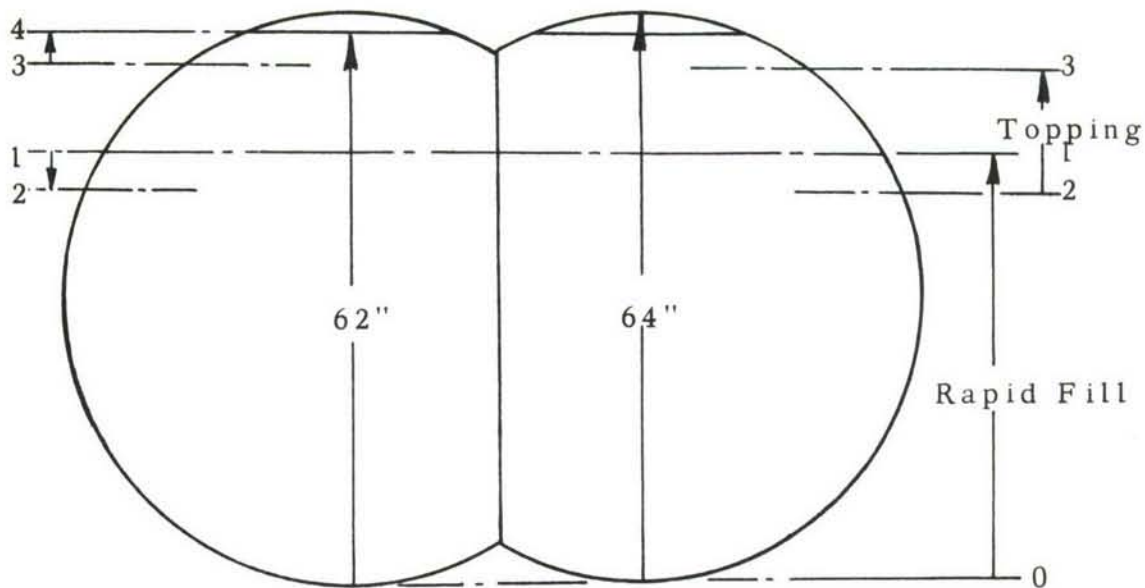
The boost pump system was chosen due to the lower resulting tankage weight, increased tank cooling capability from boil-off, and pump-fed spray system capability.

Operational Sequencing - On the basis of the chosen ground-hold and in-flight approaches, the operational sequencing of the fuel during the specified mission is as follows.

- A. Purge - Warm He is used to purge air or N₂ from the tank.
- B. Chillover - Accomplished with LH₂ at a flow rate compatible with thermal stress tolerance of the tank material - vent open.
- C. Tank filling and ground hold. A graphic presentation of the events during this phase is shown in Figure 37.
- D. Take-off, climb and cruise. Fuel is emptied from the tanks by the booster pump to the main pumps at the prescribed engine use rate. Venting will occur as the liquid boils. The tank is maintained at a constant absolute pressure by self-pressurization from expansion of the ullage and by the boil-off gas. For this tank, depletion of usable fuel coincides with the end of cruise.
- E. Letdown and landing. Residual fuel is allowed to vent at a reduced absolute pressure. As ambient pressure rises, He or N₂ gas is used to maintain positive internal pressure.
- F. Ground Operations. Remaining hydrogen is purged with He or N₂ to render tank atmosphere safe for maintenance, checkout or repair operations.

3.4.2 VEHICLE FUEL SYSTEM CONFIGURATION. A preliminary configuration study was made of a vehicle tank in order to establish subsystem weight sensitivity to tanks operating pressure, and to allow design of a representative test tank fuel system. Significant subsystems are fuel supply, fill and drain, vent, pressurization, fuel jettison and tank wall cooling.

Fuel Supply. The main components are the two tank-mounted booster pumps, located one per tank lobe at the aft tank end. Each pump is sized to handle total take-off fuel flow rate. Additional components of this subsystem are check valves, tank shut-off valve and fuel transfer line.



Level

- 0 - 1 Rapid refueling to 80% useful capacity with vent open. Fuel is boiling.
- 1 - 2 Lock-up, self-pressurization with accompanied suppressed boiling and bulk volume reduction.
- 2 - 3 Topping-up under pressure to a pre-determined level that will prevent liquid rise above 62 inches during ground hold.
- 3 - 4 Liquid expansion due to density decrease as bulk temperature rises during 30-minute ground hold. The final fill level at the end of ground hold is to be 62 inches. Insulation system performance predicts topping level required to meet this condition.

FIGURE 37 - TANK FILL AND GROUND-HOLD FUEL LEVELS

Fill and Drain. This system is required for refueling and defueling of the tank. Components were sized for a 5-minute refuel time to fill the tanks to 80% capacity. A high LH₂ velocity was chosen to reduce line size to 2 inch diameter. The refuel line is connected into the fuel supply manifold so that a single tank pierce point can be used for both systems. Main components in the system are the tank-mounted refuel-defuel valve, the vacuum jacketed line, and a ground disconnect valve. The system will also be used for introduction of purge gases.

Vent System. Functions of this system can be classified under normal and emergency operations. The normal operating functions are: 1) Venting of purge gases; 2) Venting of GH₂ on chardown and refueling; 3) Venting of boil-off during flight; and 4) Venting of residual hydrogen gas after completion of fuel delivery to the engines.

The emergency functions are: 1) Vent boil-off in case of booster pump or thermal protection system failure; and 2) Relieve tank pressure in case of failure of the refuel system causing tank overflow.

An examination of the above functions showed that the refuel overflow is the critical sizing condition.

The system consists of two vent valves at the aft tank end to handle venting on the ground, and two forward for in-flight venting. The valves would probably be installed internally to avoid the severe temperature environment outside the tank. External vent lines are used to route the gas to the aft end of the vehicle.

Pressurization. The function of this system is to maintain positive gage pressure in the tank in situations where hydrogen vapor pressure is not sufficiently high. After landing, external pressurization is required since residual gas temperature will decrease resulting in negative pressures. A small amount of helium will be adequate to maintain the tank pressure. Pressurization will not be required during any other phase of the mission.

Fuel Jettison. A fuel dump system is almost mandatory for manned, winged flight vehicles. The performance requirements are established from operational studies, vehicle aerodynamic characteristics, abort conditions, and CG control requirements. Since these considerations fall outside of the scope of the contract, the jettison system was not included in the optimization procedure. Arbitrary selection of jettison system performance would obscure the basic tank pressure weight relationship being sought.

Tank Wall Cooling. A cooling system is required to control the tank wall temperature to 520°R maximum for all insulation systems bonded to the tank wall. The most positive way to accomplish this function is by means of an internal spray system. A preliminary analysis shows that the required coolant flow-rate can be supplied by the booster pumps already in the tank, feeding several longitudinal tubes fitted with spray nozzles. Cooling is effected by generating a fine mist in the ullage space, thereby

maintaining low ullage and tank wall temperatures. The spray flow rate is regulated by thermostatically controlled valves. The spray method allows flexibility for cooling local "hot spots" as well as positive control of coolant flow rate. In the case of spray system failure, the tank can be cooled by venting to a lower pressure causing boil-off to occur.

Another cooling method of interest consists of a vent manifold line with multiple bell-mouths, causing boil-off vapor to flow across the tank's surface in a reasonably uniform fashion, thereby cooling the tank structure. The system does not have the flexibility for cooling local stagnation areas, however, and a lengthy analytical and experimental calibration procedure would be required to obtain the desired uniform degree of cooling. The weight of the system would be about equal to the spray system weight. The vent manifold approach is applicable primarily to a tank using high-temperature structure and insulation materials without adhesives for insulation attachment. Since the selected tank design consists of Inconel with unbonded Microquartz blanket insulation, this cooling approach is preferred on the basis of least complexity and greater reliability.

Weight Sensitivity. None of the above subsystems showed any significant sensitivity to tank operating pressure. Consequently, the weights were omitted from the optimization procedure.

3.4.3 TEST TANK FUEL SYSTEM. The test tank will necessarily have a simplified system configuration. This is due to lack of components designed specifically for the application and the fact that the tank will be tested in a static, horizontal position. A single booster pump has been made available and will be used. The flow control valves for fill/drain and vent functions will all be located externally to the test chamber. The vent manifold system which gives increased tank wall cooling will also be used as the basic tank vent outlet. A spray system will not be incorporated since the Inconel-Microquartz combination has a high temperature capability. No provisions will be made for rapid fuel dump. A helium pressure source will be incorporated externally to pressurize the tank through the vent system, primarily as a safety precaution.

4.0 OPTIMIZATION OF LARGE SCALE TANK DESIGN

Cryogenic tank design depends on the conventional interrelating factors of temperature, stress, and pressure. The degree of dependency is great when the tankage system has to operate over wide environmental extremes associated with high speed flight up to high altitudes. Optimization techniques must be employed to assure minimum weight. An optimization procedure was established to answer the following question: Which combination of tank pressure, insulation weight, tank structural weight, fuel boil-off and fuel system weight will yield a minimum take-off weight, provided a specified total amount of fuel is supplied to the engine for a specified fuel flow schedule. A computer program has been developed to establish total system weight at take-off as a function of top and bottom insulation thickness and tank vent pressure. The solution is based on computations of the time history of the properties of the liquid in the tank during ground hold and flight. The program requires input data defining the heat flux through the insulation, tank geometry, tank structure weight, insulation weight and fuel system weight. The following paragraphs describe the input data employed, the computation process, and the results obtained.

4.1 INPUT DATA

a) The structural weight data developed from the preliminary tank design was reduced to equation form with tank pressure as the independent variable. The tank length was allowed to vary within $\pm 5\%$ to account for volume variations without radius change. Equation is given on Page 32.

b) The weight of both selected insulation systems was reduced to equation form with over-all thickness as the independent variable. Equations are given on Page 45. For the composite system, the ratio of foam to Microquartz thickness was 1:8.

c) The fuel system components for the large scale tank were evaluated to determine weights and any sensitivity of these weights to the tank operating pressure. The sensitivity was found to be minor; therefore, constant weights were used in the optimization study.

d) The heat flux to the LH_2 at the top and the bottom of the tank was determined in Section 3.3.6. This data was used in tabular form for the program, with heat flux as a function of flight time. The ground hold heat flux, was assumed constant during the 30-minute hold time. Additional inputs were the heat fluxes to the ullage, consisting of a top area which is always dry, and the remaining area, which becomes dry as the liquid is depleted; the time to start spray based on conduction data; and the enthalpy change of the evaporated liquid spray. The penetration heat leak was neglected since it represents less than 1% of the total heat input to the liquid.

e) A geometry table specified the tank wetted area and liquid volume in dimensionless ratios involving length and radius as a function of a dimensionless liquid height, h/R . Tank length and radius can thereby be changed without the need of recomputing the area and volume relationships. The ratio for the elliptical tank ends are specified separately from the cylindrical section. Figure 38 gives the area and volume relationships of the liquid as a function of height for a 20-foot tank shell length.

f) The thermodynamic properties of the liquid as a function of temperature were reduced to tabular form. The properties are vapor pressure, liquid density, liquid enthalpy and heat of vaporization.

g) The fuel flow schedule was established by scaling the full size vehicle fuel flow given by the contract work statement. The flow-rate as a function of flight time, shown on Figure 4, was used as input to the computer program.

h) The input values held constant during the analysis were the fuel level at the end of ground hold; the tank radius; ground hold time of 1800 seconds; flight time of 5400 seconds; and the initial LH_2 density of 4.421 lb/ft^3 (14.7 psia saturation).

4.2 OPTIMIZATION ANALYSIS

A computer solution has been developed to predict the time history properties of the liquid in the hydrogen propellant tank during ground hold and flight. The program was compiled so that a minimum take-off weight system might be selected, considering insulation thickness and the pressure at which venting occurs as the variables to optimize. Constraints on the solution were a fixed mass of useful fuel and a selected fuel schedule; thus a constant flight time resulted. The smaller insulation thicknesses result in larger amounts of boil-off and therefore require more initial mass aboard, as well as a larger tank. Variable volume tanks must be considered in order to satisfy constant flight time; this was accomplished by varying the length of the cylindrical tank section. The volume of the elliptical ends is a function of radius only and was not varied during this optimization. An initial tank length was selected as a starting point for the iterative process.

The following nomenclature is used throughout this section:

A	Tank inner surface area, sq. ft.
H	Enthalpy, BTU/lb.
L	Tank length, ft.
M	Mass aboard, lb.
\dot{M}	Fuel flow rate, lb/sec.
P	Vapor pressure, psia
Q	Total heat input, BTU

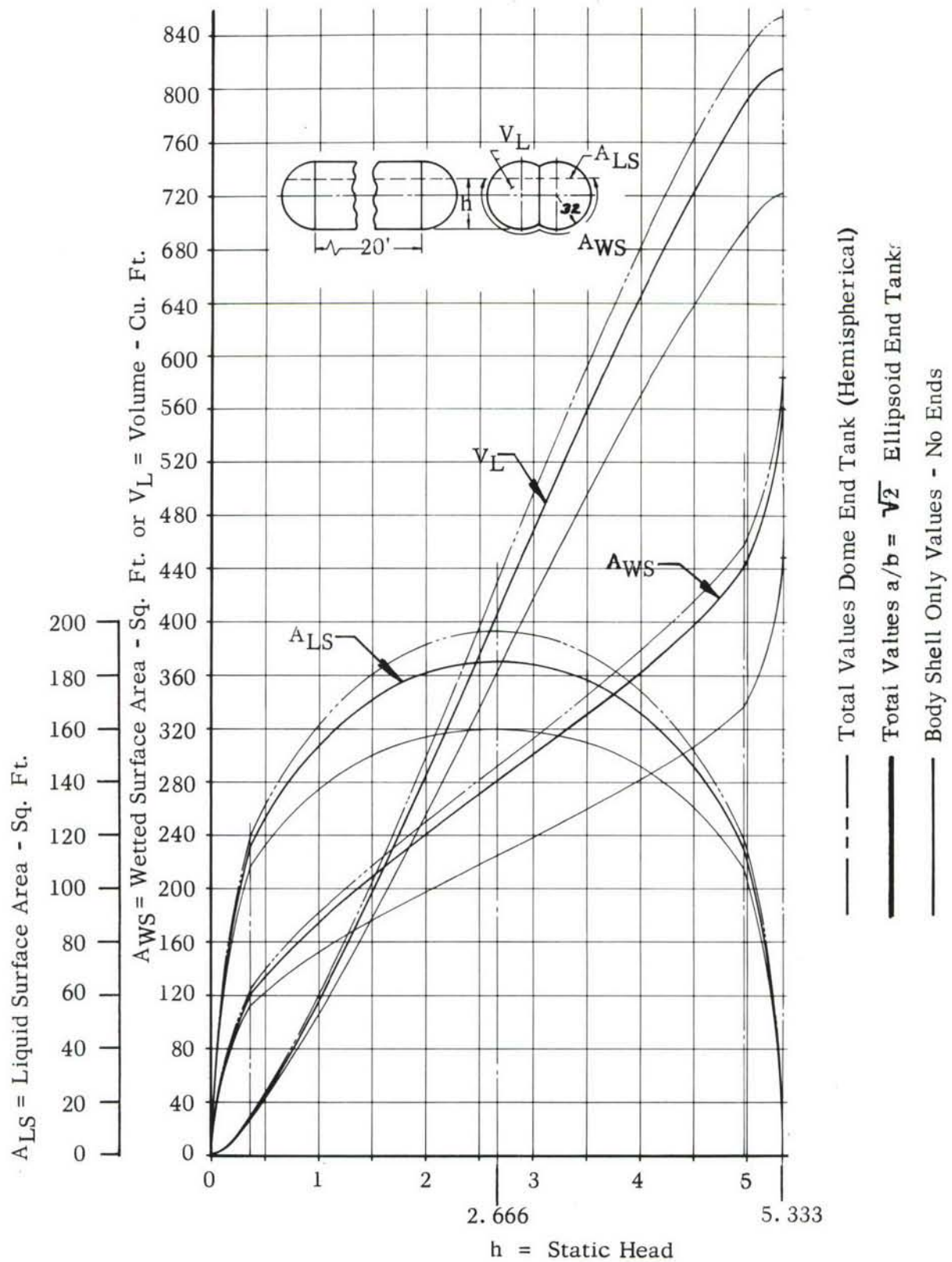


FIGURE 38 - AREA AND VOLUME RELATIONSHIPS OF TANK

R	Tank radius, ft.
T	Liquid temperature, °R
V	Volume, cu. ft.
h	Height in tank, ft.
q	Heat flux, BTU/hr. - sq. ft.
Δ	Incremental change during time interval
λ	Heat of vaporization BTU/lb.
θ	Ground hold or flight time, sec.
ρ	Density, lb/ft ³

Subscripts:

av	Average evaluation of property
b	Bottom half of tank
e	Effective length used to determine these variables
h	Current liquid height
L	Liquid
m	Properties evaluated at maximum (vent) pressure conditions
o	Boil-off value
2R	Value for full tank
s	Spray, side-wall (dry)
t	Top half of tank
w	Wetted surface
1	Initial ground hold conditions
2	End of ground hold conditions
3	End of flight
θ	Time property evaluated
$\theta + \Delta\theta$	Time property evaluated

The problem is divided into the ground hold portion and the flight portion. Each portion is an iterative solution, which will be shown in the following development. The program flow sheet is shown in Figure 39.

The fuel level at the end of ground hold is a constant, 5.20 feet. The fill level to which the tank is topped is calculated based on the expansion space needed as the fuel heats during ground hold. These two levels establish the heat transfer areas; the mass aboard can be determined from the defined volumes. The density at the end of ground hold, ρ_2 , is assumed and the initial mass of LH₂ in the tank is calculated

$$M = \rho_2 V_2 = \rho_1 V_1 \quad (1)$$

where

V_1 = liquid volume at start of ground hold

V_2 = liquid volume at end of ground hold

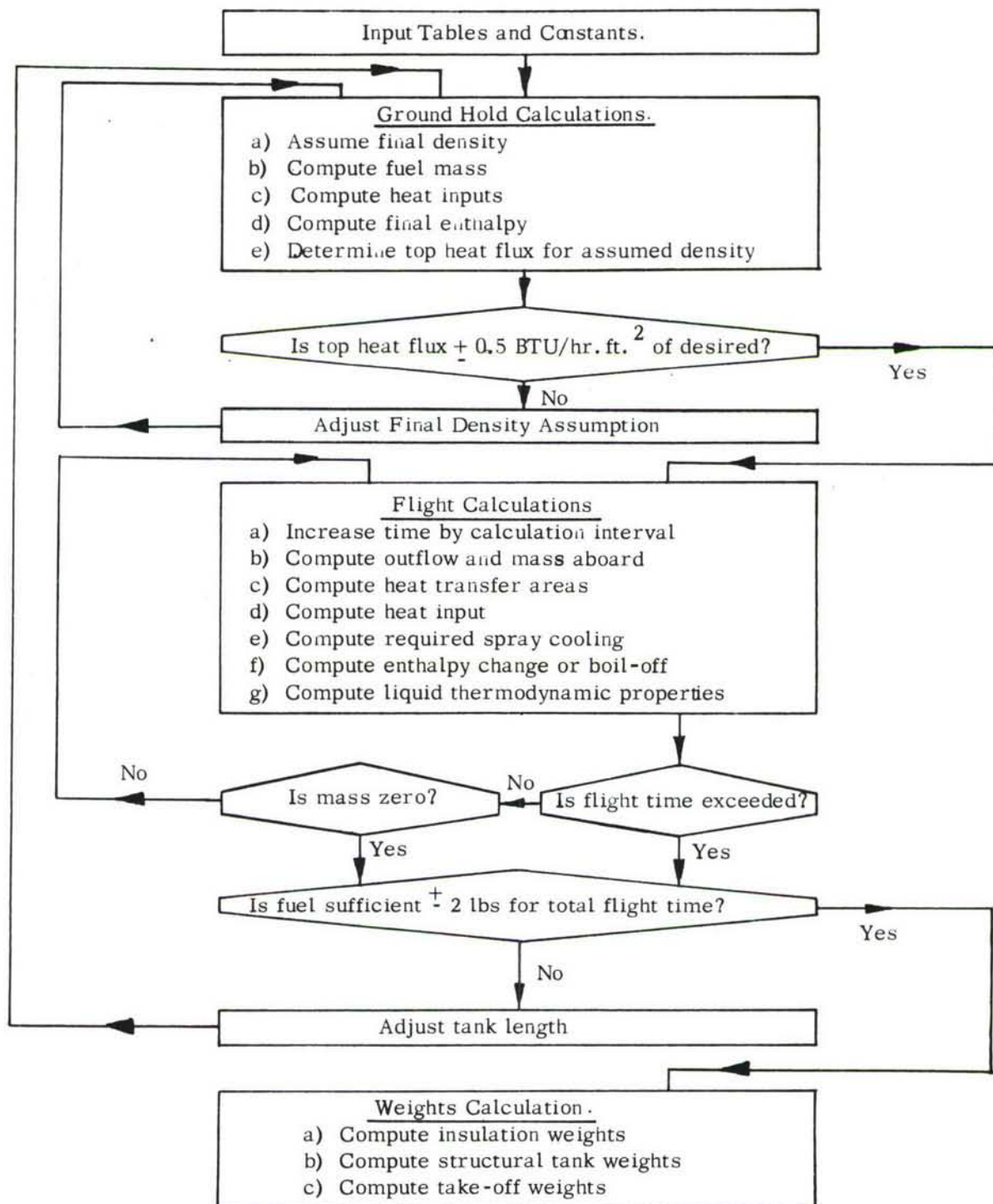


FIGURE 39 OPTIMIZATION PROGRAM-COMPUTER FLOW DIAGRAM.

The areas are established since

$$A_{w, 1} = f(V_1) \text{ and } A_{w, 2} = f(V_2) \quad (2)$$

The top and bottom areas where insulation thickness may vary are determined

$$A_{w, b} = 0.5 A_{w, 2R} \quad (3)$$

$$A_{w, 1, t} = A_{w, 1} - A_{w, b} \quad (4)$$

$$A_{w, 2, t} = A_{w, 2} - A_{w, b} \quad (4a)$$

$$A_{w, av, t} = 0.5 (A_{w, 1, t} + A_{w, 2, t}) \quad (5)$$

From the initial density and estimate of final density, the enthalpy is

$$H_1 = f(\rho_1) \text{ and } H_2 = f(\rho_2) \quad (6)$$

The total heat input during ground hold is

$$Q = M (H_2 - H_1) \quad (7)$$

Now the top heat flux corresponding to the assumed density is determined using the average top area during ground hold

$$q_t = (Q/\theta_2 - q_b A_{w, b})/A_{w, av} \quad (8)$$

Since both top and bottom heat fluxes were known input quantities, the calculated value of q_t can be compared to input q_t to see if another iteration on estimated density is required.

With this series of iterations complete, the flight program is commenced with known property data, geometry, liquid fuel level, and a known flight heat flux schedule. At this point it is not known if the fuel aboard is sufficient to fulfill the fuel schedule at 5400 seconds.

For the flight calculation, the change in wetted area with time is significant and a time increment solution is utilized; for these calculations 25 second intervals were used. Since ground hold was a single time interval calculation, flight time was initialized to zero at the beginning of these calculations. An in-flight effective heat transfer area is selected different from the wetted area used in ground hold, since in-flight the tank receives radiation heating from the hot structure (not from tank ends). This effective area is the cylindrical side area of a tank whose length is

$$L_e = L + 2 (0.707) R \quad (9)$$

$$A_e = f(R, L_e) \quad (9a)$$

where

L = tank cylindrical length

R = tank radius

In these calculations, the time-average areas are used for heat transfer which allows for decrease in area caused by fuel flow and boil-off during the time interval.

$$Q = (q_b A_{e, b} + q_t A_{e, t}) (\Delta \theta) \quad (10)$$

For liquid vapor pressure less than the vent pressure, i.e., $P < P_m$, the heating results only in a sensible temperature increase in the liquid with no boil-off. The saturated liquid properties of pressure, temperature, density, and enthalpy are all defined when one value is known. This analysis assumes no liquid stratification, i.e., the bulk liquid is at a uniform temperature. For the time interval in the flight program, using heat input from Equation (10)

$$\Delta H = Q / (M_{\theta} - 0.5 \dot{M} \cdot \Delta \theta) \quad (11)$$

$$H_{\theta + \Delta \theta} = H_{\theta} + \Delta H \quad (12)$$

Since no boil-off occurs for $P < P_m$,

$$M_{\theta + \Delta \theta} = M_{\theta} - \dot{M} \cdot \Delta \theta \quad (13)$$

When $P = P_m$, sensible heating no longer occurs and the heat addition, Equation (10), results in boil-off, as defined by

$$\Delta M_o = Q / \lambda_m \quad (14)$$

In this instance

$$M_{\theta + \Delta \theta} = M_{\theta} - \dot{M} \Delta \theta - \Delta M_o \quad (15)$$

For all θ after which the top tank surface is greater than a given temperature, a spray is utilized to cool this surface. The amount of spray required in a time increment is determined from the heat input to the dry surfaces; the enthalpy change is selected for a liquid vaporizing and approaching some temperature near that of the dry wall. For the area of the top inner wall, which is always dry, (125 sq. ft.), and the portion that has become dry prior to spray commencing, the heat transfer is

$$Q_s = \left[125 q_{s, t} + (A_{e, h} = 2R - 125 - A_{e, av}) q_{s, s} \right] \Delta \theta \quad (16)$$

From this the mass of spray is determined

$$M_s = Q_s / H_s \quad (17)$$

For the time interval, final mass is

$$M_{\theta + \Delta \theta} = M_{\theta} - \dot{M} \Delta \theta - \Delta M_o - \Delta M_s \quad (18)$$

If $M_{\theta + \Delta\theta}$ goes to zero prior to end of flight, θ_3 , it is necessary to resize the tank larger and to return to ground hold calculations. For this resizing, only changes in tank cylindrical section length are made. If $M_{\theta + \Delta\theta}$ is positive at θ_3 , a smaller tank will accomplish this mission and again tank size is changed and the program returns to ground hold calculations. This procedure is repeated until fuel mass ± 2 lbs. approaches zero at the desired flight time, θ_3 . This completes the iteration steps for the program and the weight analysis for this selected tank length is then calculated.

4.3 RESULTS

The components making up the take-off weight include spray, boil-off, tank structure, insulation, and useful fuel (3245 pounds). The independent variables which affect these component weights are venting pressure, top insulation thickness and bottom insulation thickness. In order to optimize the system (obtain a minimum take-off weight), plots were made of take-off weight versus bottom insulation thickness with pressure as the parameter for each top insulation thickness. The minimums from the curves representing the preferred bottom thickness were next plotted versus pressure with top insulation as the parameter. The minimums of these curves indicated the preferred venting pressure. Finally, a cross-plot of the minimum take-off weights from these curves versus top insulation thickness yielded the preferred top insulation thickness for a minimum take-off weight system.

The results from the analysis will be presented for the microquartz (helium) system followed by the microquartz/foam system. Typical results for the former system with one top insulation thickness (2-inch) are presented in Figures 40 and 41 to show how bottom insulation thickness and venting pressure affect the various component weights. The component weights add to give the take-off weight.

The effects of the independent variables on the component weights is similar for both systems. Tank weight increases with pressure but decreases slightly with thicker insulations which are associated with smaller tank sizes. Insulation weights also decrease with increasing pressure because of smaller tank size. Boil-off decreases with increased pressure because the total boiling time is decreased; it also decreases with increased insulation thickness. The primary variable effecting spray is the top insulation thickness which is not illustrated in these figures. The length of time during which spray occurs may be determined from Figures 33 and 42. The former indicates when the upper surface reaches 520°R and the latter when the vapor pressure of the liquid reaches the venting pressure and spray ceases.

The total tank weights at take-off are shown in Figures 43 through 46 for the microquartz (helium) system for top insulation thicknesses analyzed of 0.5, 1, 2 and 3 inches. Observe that the minimum weights for the lower pressure occur at about 4.0 inches of bottom insulation independent of upper insulation thickness. These minimum weights are cross-plotted versus venting pressure in Figure 47. Minimum take-off weights result for pressures of 30 psia. This lower pressure optimization reflects the influence of low

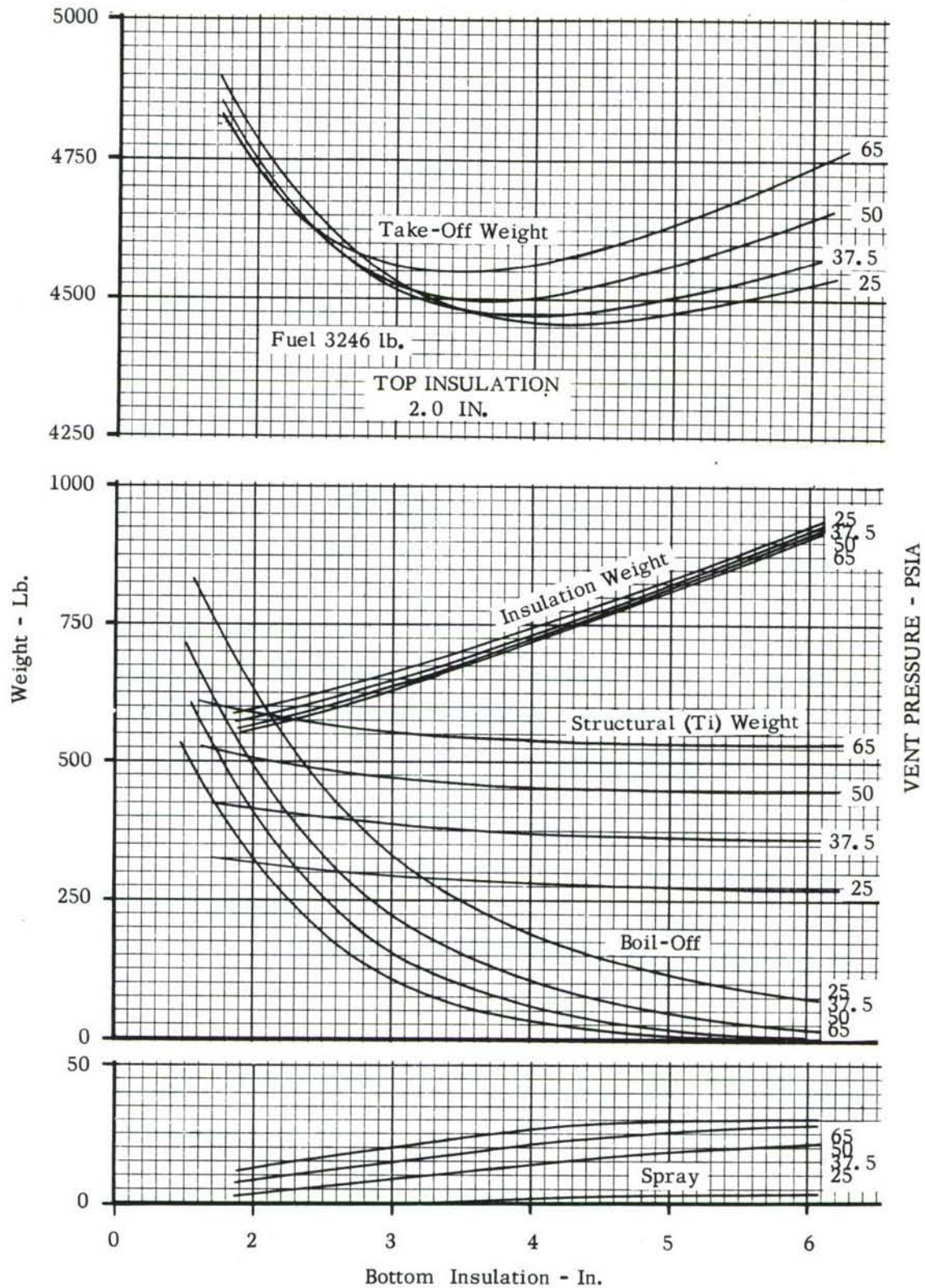


FIGURE 40 - TOTAL TANK WEIGHT BREAKDOWN VERSUS BOTTOM INSULATION - MICROQUARTZ (H_e)

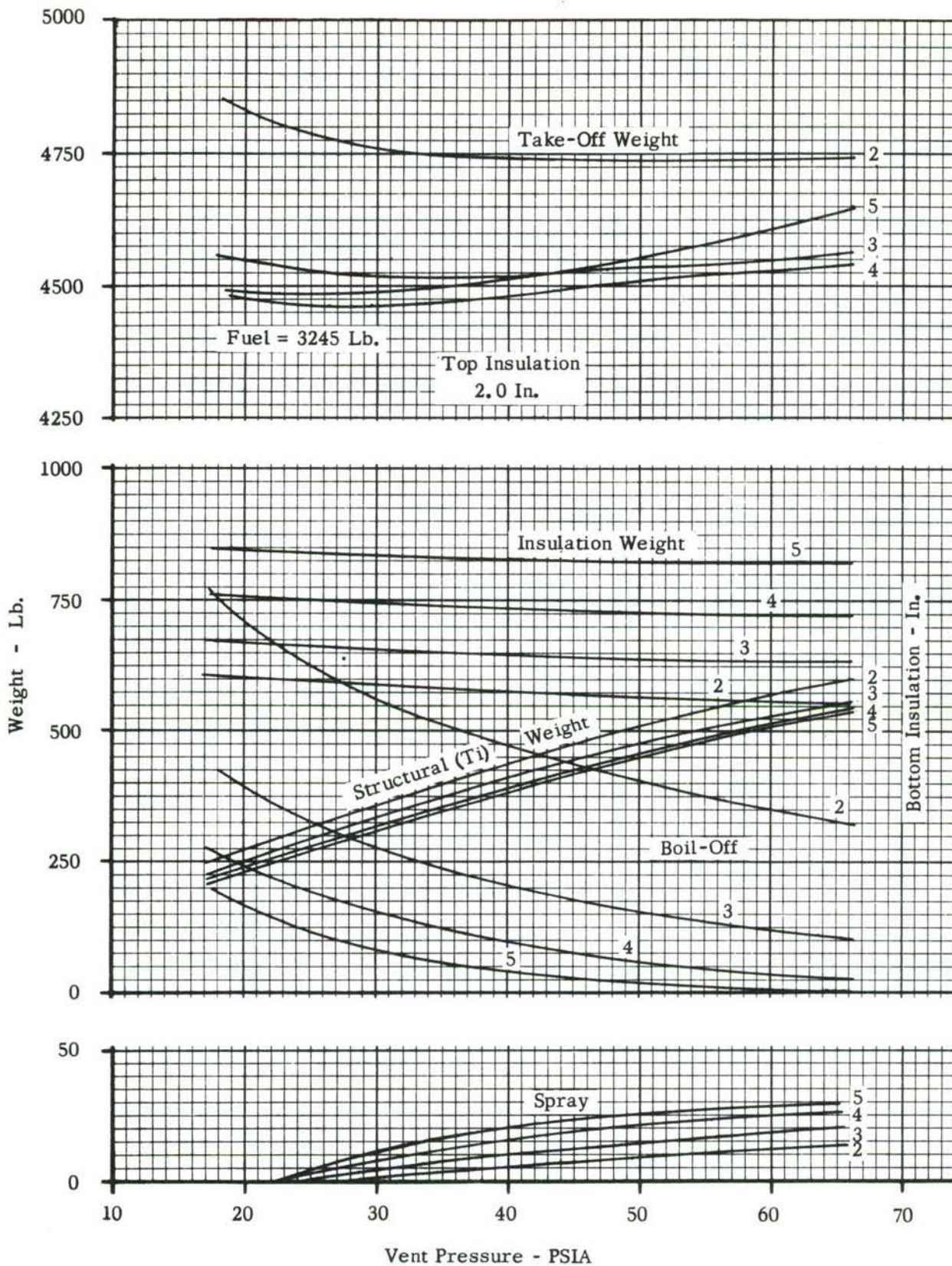


FIGURE 41 - TOTAL TANK WEIGHT BREAKDOWN VS VENT PRESSURE-MICROQUARTZ (He) INSULATION

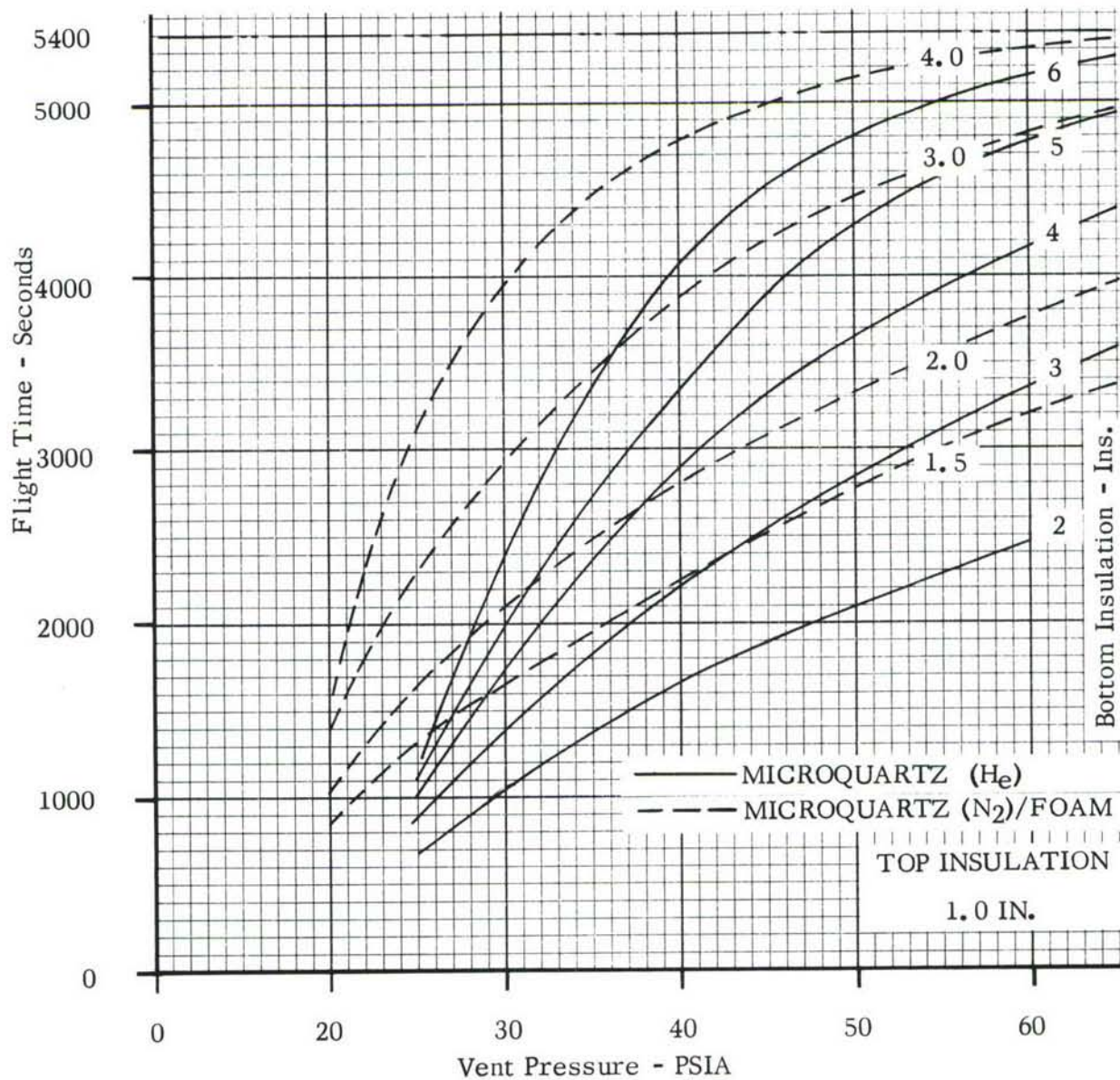


FIGURE 42 - FLIGHT TIME AT WHICH LH₂ BOILING STARTS.



FIGURE 43 - TAKE-OFF WEIGHT VS INSULATION THICKNESS -
MICROQUARTZ (He) 0.5-INCH TOP INSULATION

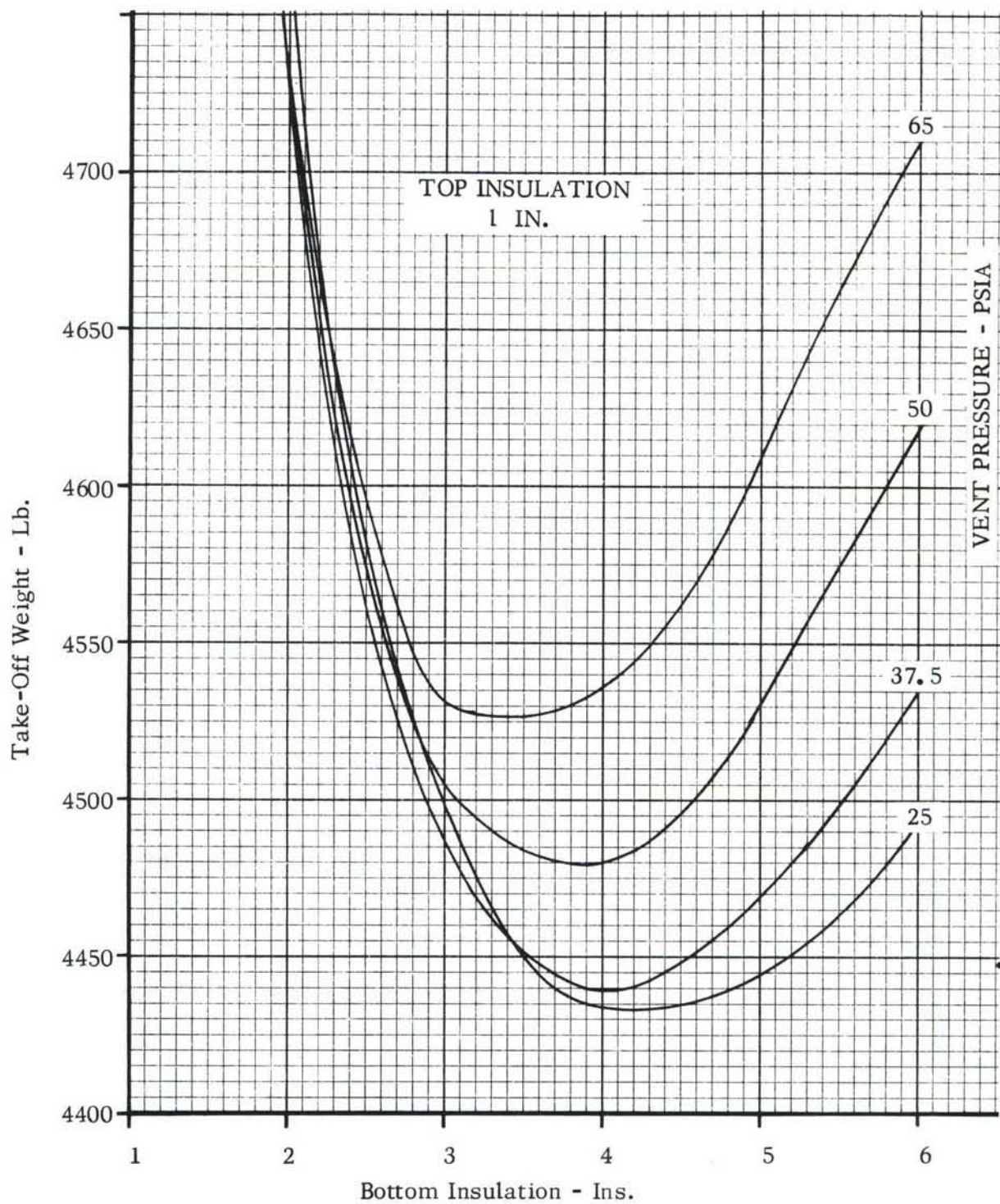


FIGURE 44 - TAKE-OFF WEIGHT VS INSULATION THICKNESS -
MICROQUARTZ (He) 1.0-INCH TOP INSULATION

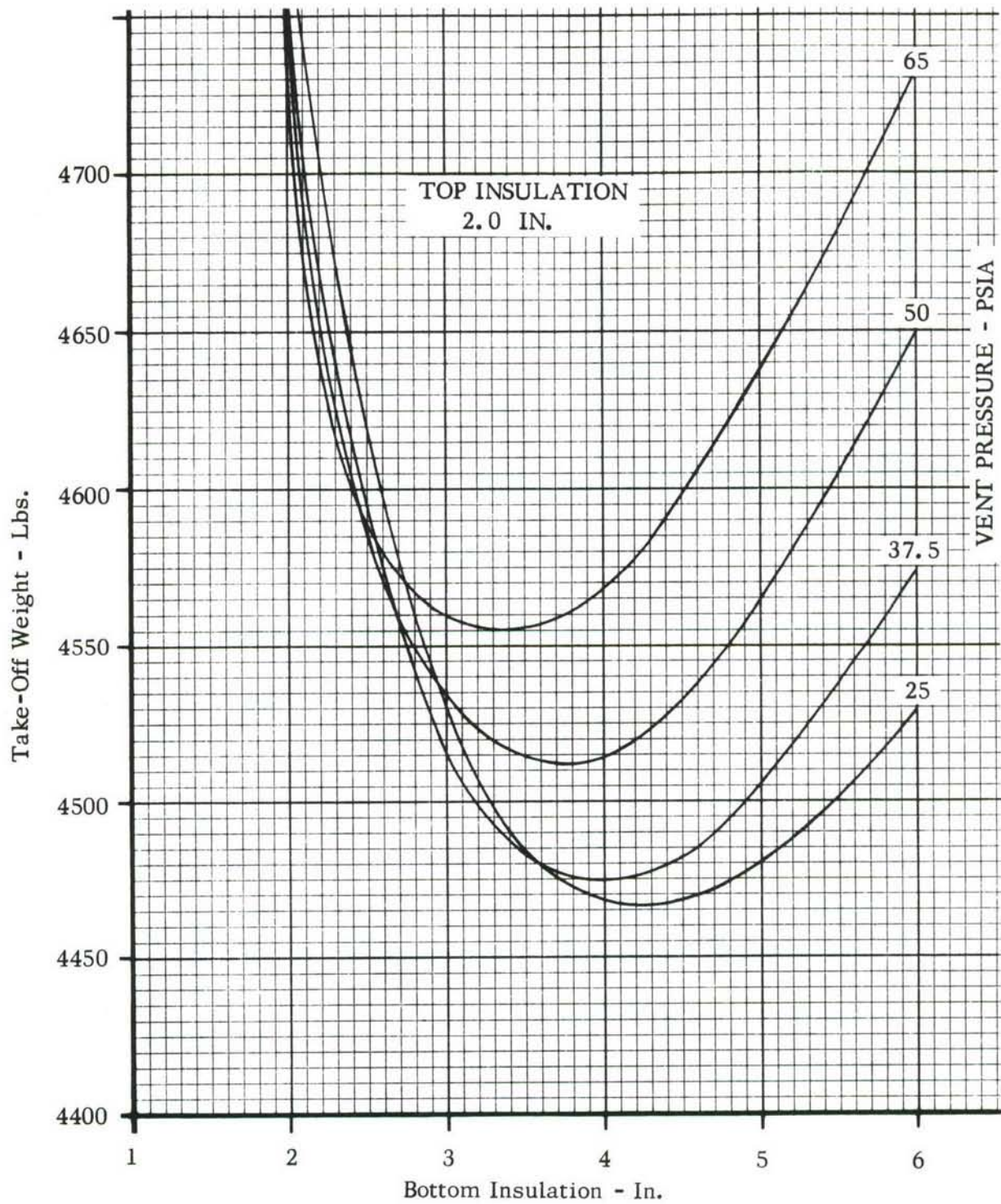


FIGURE 45 - TAKE-OFF WEIGHT VS INSULATION THICKNESS - MICROQUARTZ (He) 2.0-INCH TOP INSULATION

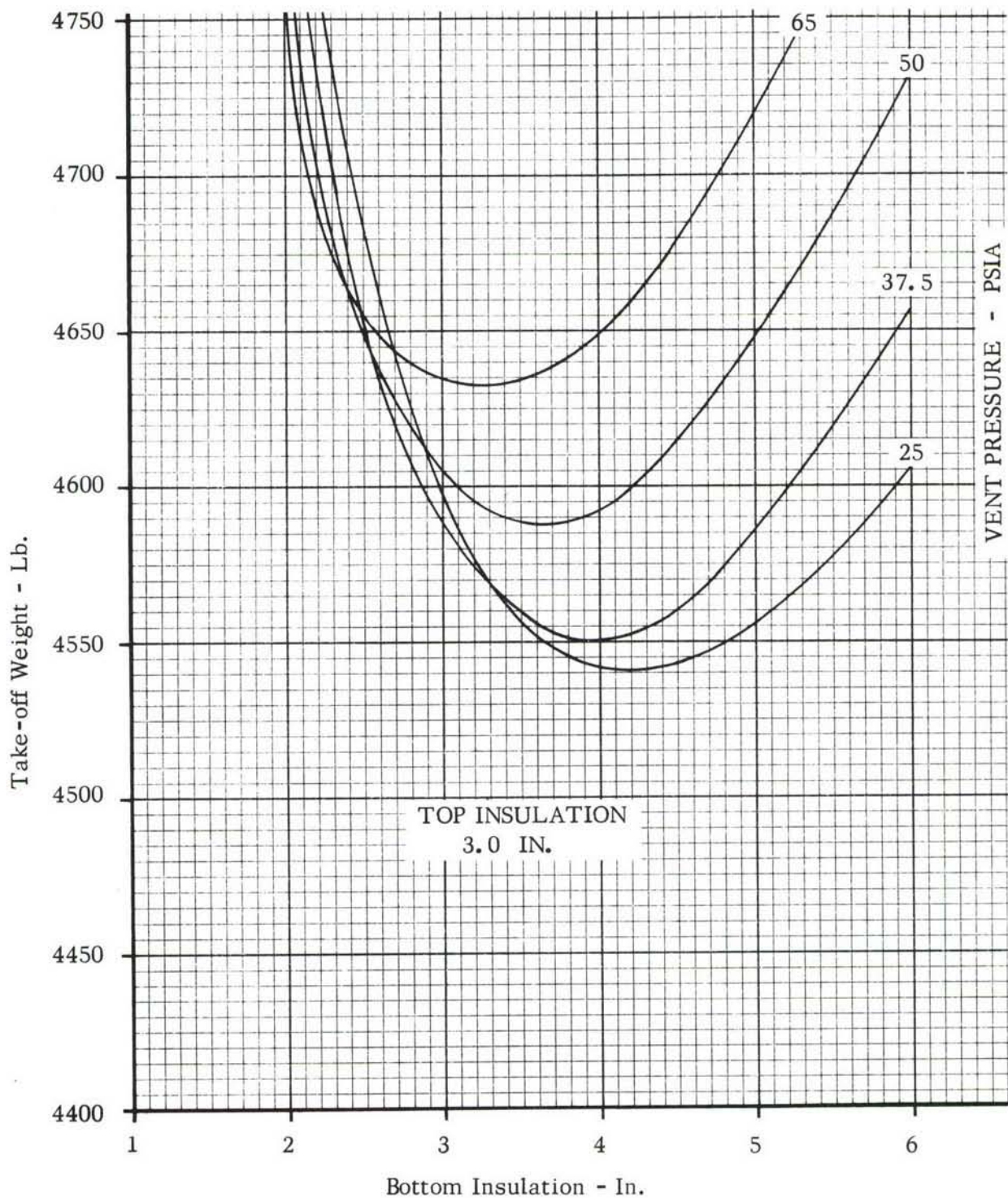


FIGURE 46 - TAKE-OFF WEIGHT VS INSULATION THICKNESS - MICROQUARTZ (He) 3.0-INCH TOP INSULATION

tank weight at lower pressures. The optimum top insulation is illustrated in Figure 48 where the minimum points of Figure 47 are used; a thickness for top insulation of about 1.3 inches results. In summary, the microquartz (helium) insulation system optimizes at 4 inches bottom and 1.3 inches top insulation with a vent pressure of 30 psia.

The microquartz/foam insulation system was optimized in a similar manner. Typical component weights are presented in Figure 49. The total weights are shown in Figures 50 through 52 for top insulation thickness of 1, 2 and 3 inches. An optimum bottom insulation thickness of 3.6 inches results at low pressures. When these minimum weights are plotted versus venting pressure in Figure 53, the minimum weight results at the minimum practical operating pressure limit (20 psia), which was selected to keep the tank pressure above the liquid vapor pressure at the end of the 30-minute ground hold period. In Figure 54, the minimum weight occurs at the minimum top insulation thickness used in this analysis (1 inch) which was considered to be the minimum practical thickness for this composite system. As a result, the optimum microquartz/foam system is a bottom and top insulation thickness of 3.6 and 1.0 inches, respectively, at a vent pressure of 20 psia.

In the breakdown below, storage penalties are expressed as a percentage of useful fuel weight. The lower boil-off weights for the foam/Microquartz system reflect the lower heat fluxes with this system. The higher tank weight for the all Microquartz (helium) system results from the higher pressure at which the system optimized, 30 versus 20 psia. The Microquartz/foam system provides a weight advantage of 168 pounds.

WEIGHT BREAKDOWN USEFUL FUEL - 3,245 LB.	MICROQUARTZ (He)		MICROQUARTZ/FOAM (N) ²	
	Lbs.	%	Lbs.	%
Insulation	671	20.7	645	19.9
Structure	365	11.2	280	8.6
Boil-off	186	5.7	134	4.1
Spray	10	.3	5	.3
Storage Penalty	1232	37.9	1064	32.8

From the results of the computer program, optimum values of venting pressure and insulation thicknesses were established, and associated tank length and volume determined for the two large-scale tank designs.

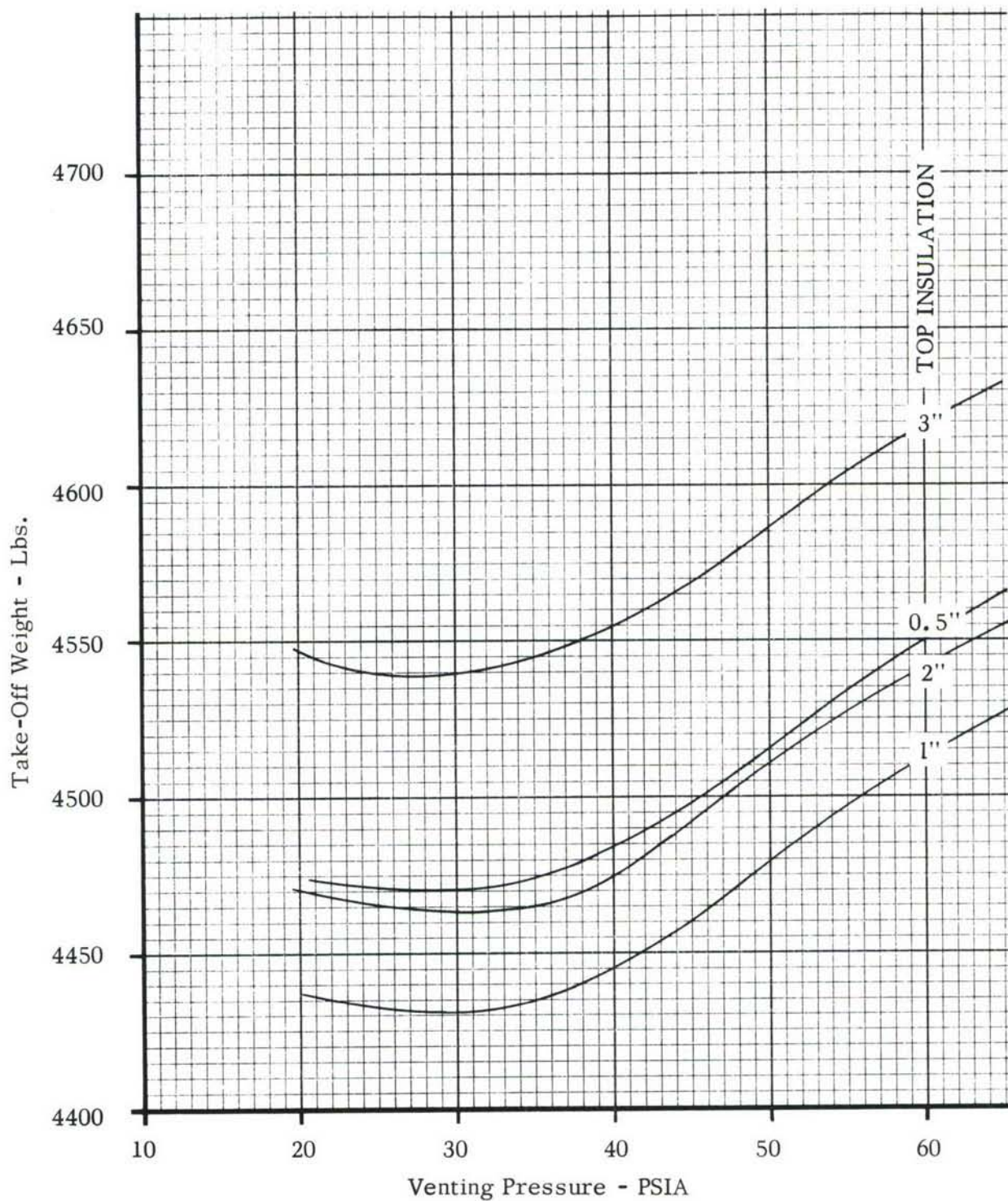
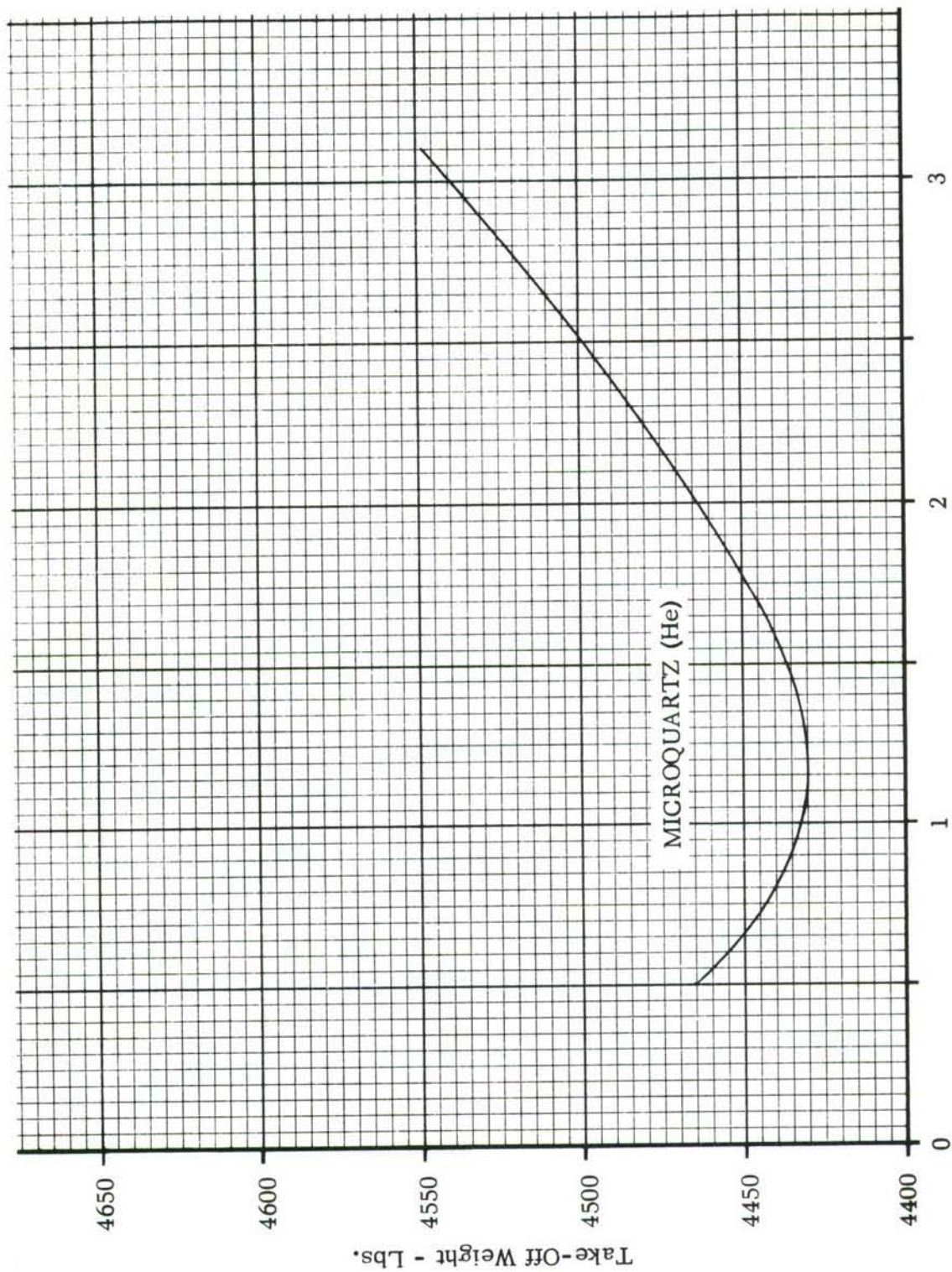


FIGURE 47 - TAKE-OFF WEIGHT VS VENTING PRESSURE - MICROQUARTZ (He)



Top Insulation - Inches

FIGURE 48 - OPTIMUM TAKE-OFF WEIGHT VS TOP INSULATION THICKNESS - MICROQUARTZ (He)

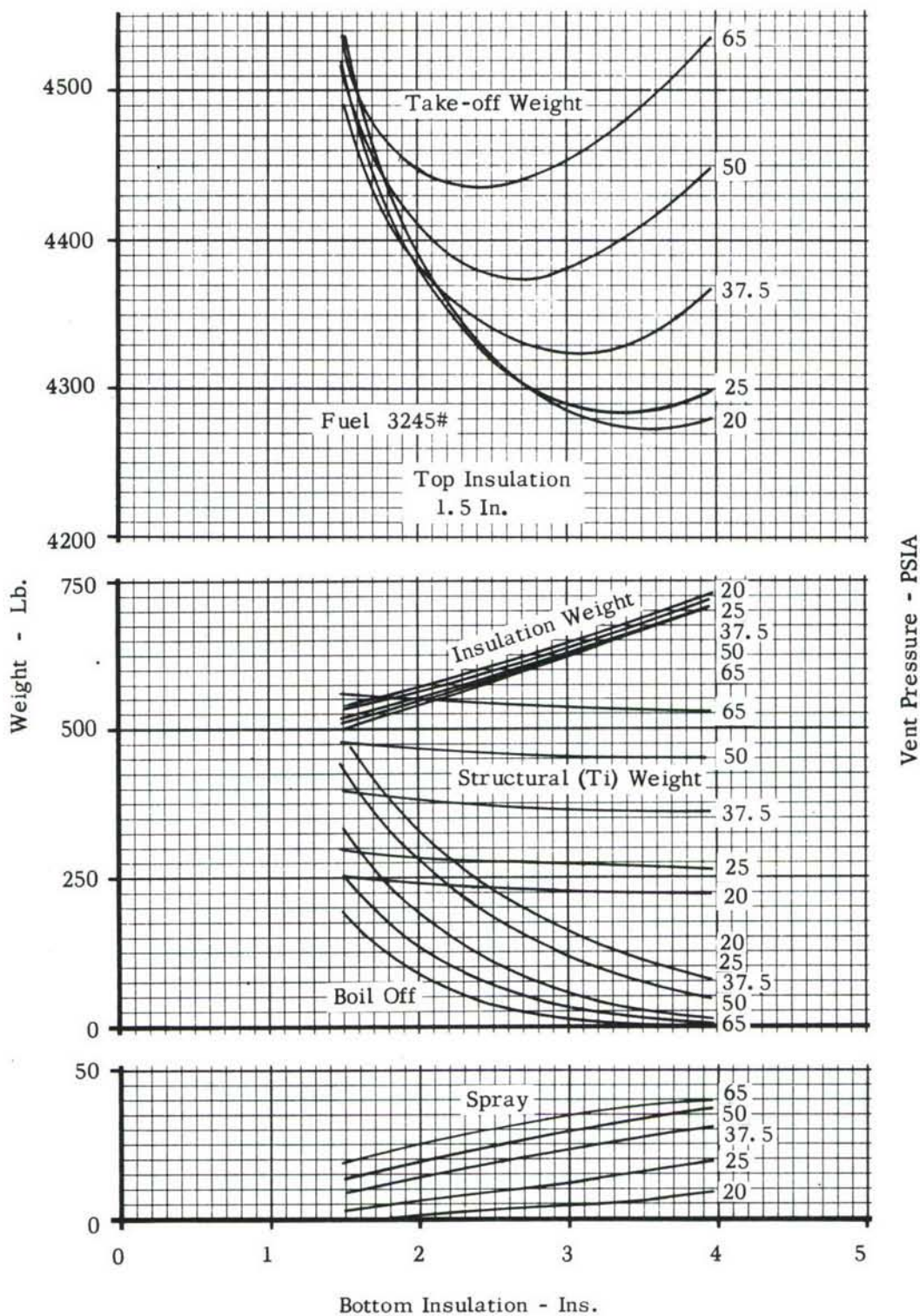


FIGURE 49 - TOTAL TANK WEIGHT BREAKDOWN VS BOTTOM INSULATION MICROQUARTZ (N₂)/FOAM COMPOSITE

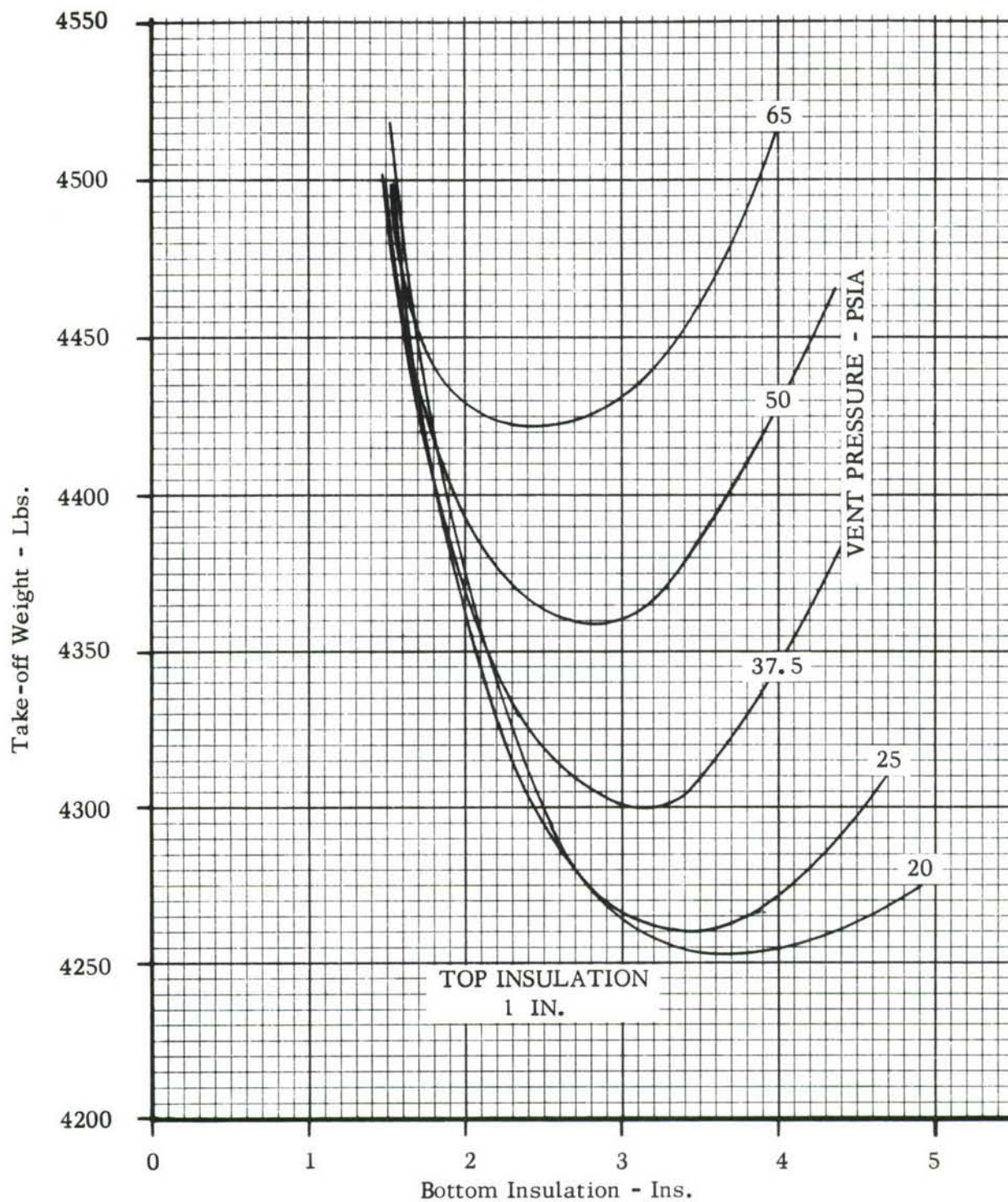


FIGURE 50 - TAKE-OFF WEIGHT VS INSULATION THICKNESS -
MICROQUARTZ (N₂)/FOAM COMPOSITE (1.0 INCHES)

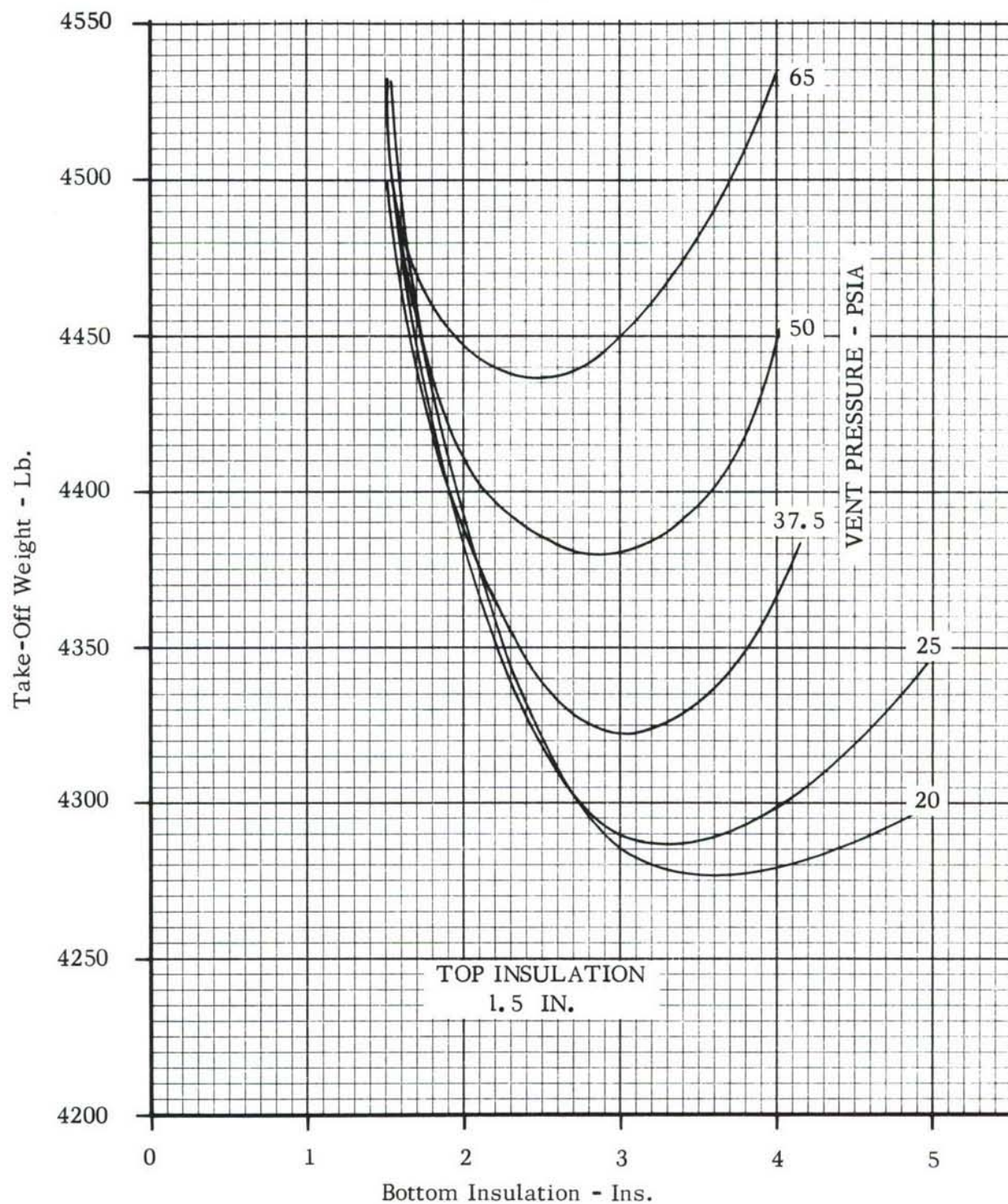


FIGURE 51 - TAKE-OFF WEIGHT VS INSULATION THICKNESS -
MICROQUARTZ (N₂)/FOAM COMPOSITE (1.5 INCHES)

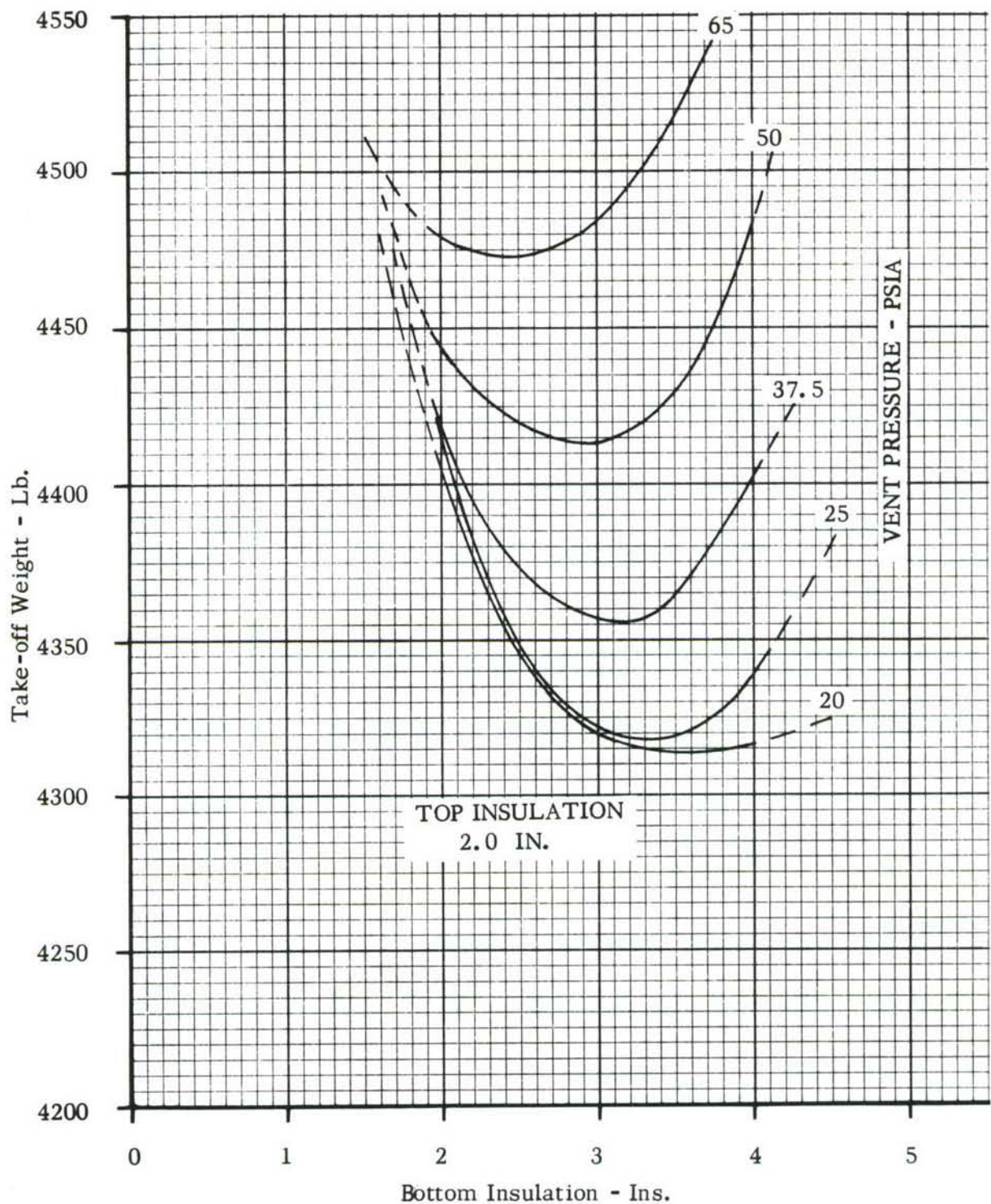


FIGURE 52 - TAKE-OFF WEIGHT VS INSULATION THICKNESS -
MICROQUARTZ (N₂)/FOAM COMPOSITE (2.0 INCHES)

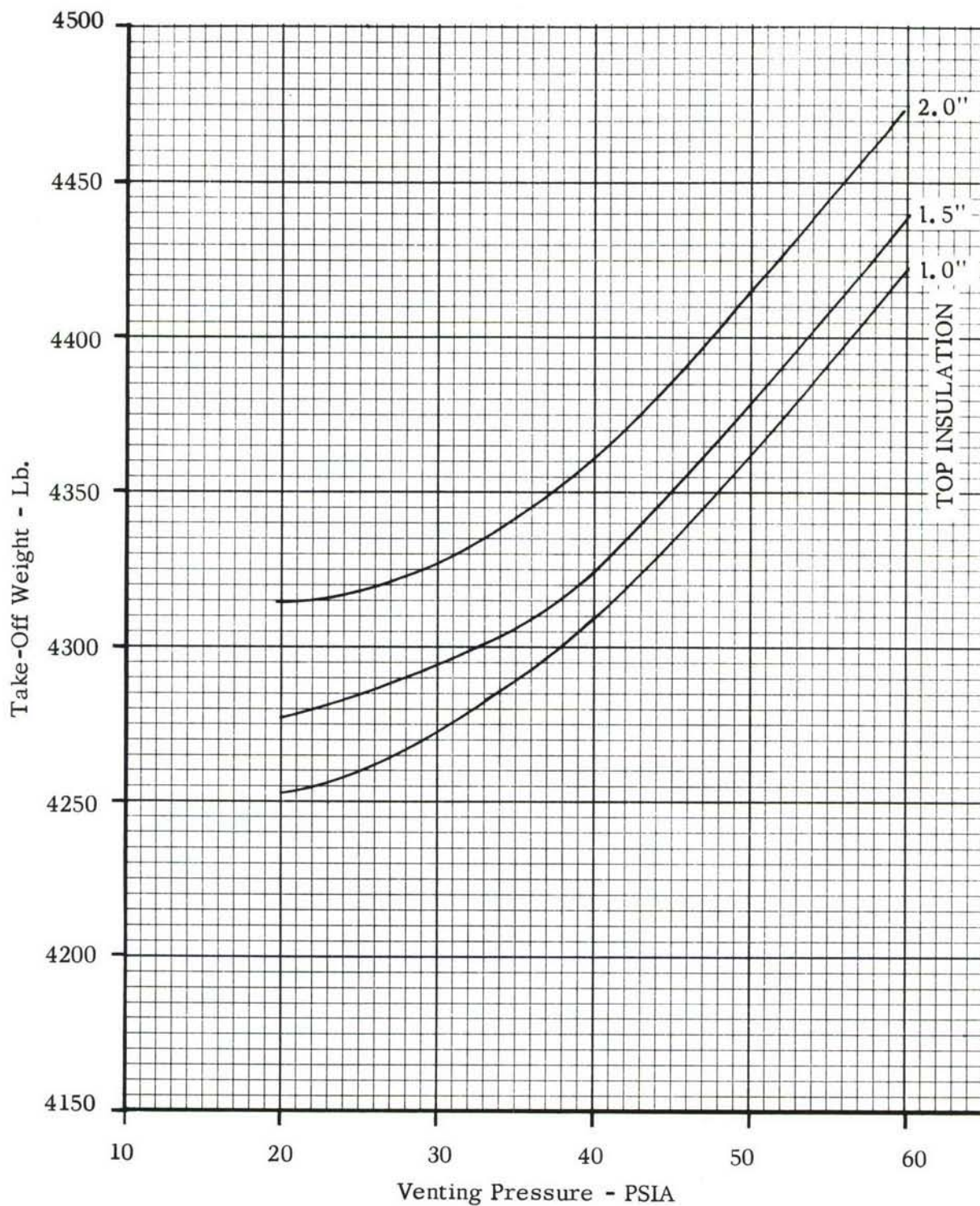


FIGURE 53 - TAKE-OFF WEIGHT VS VENTING PRESSURE - MICROQUARTZ (N₂)/FOAM COMPOSITE

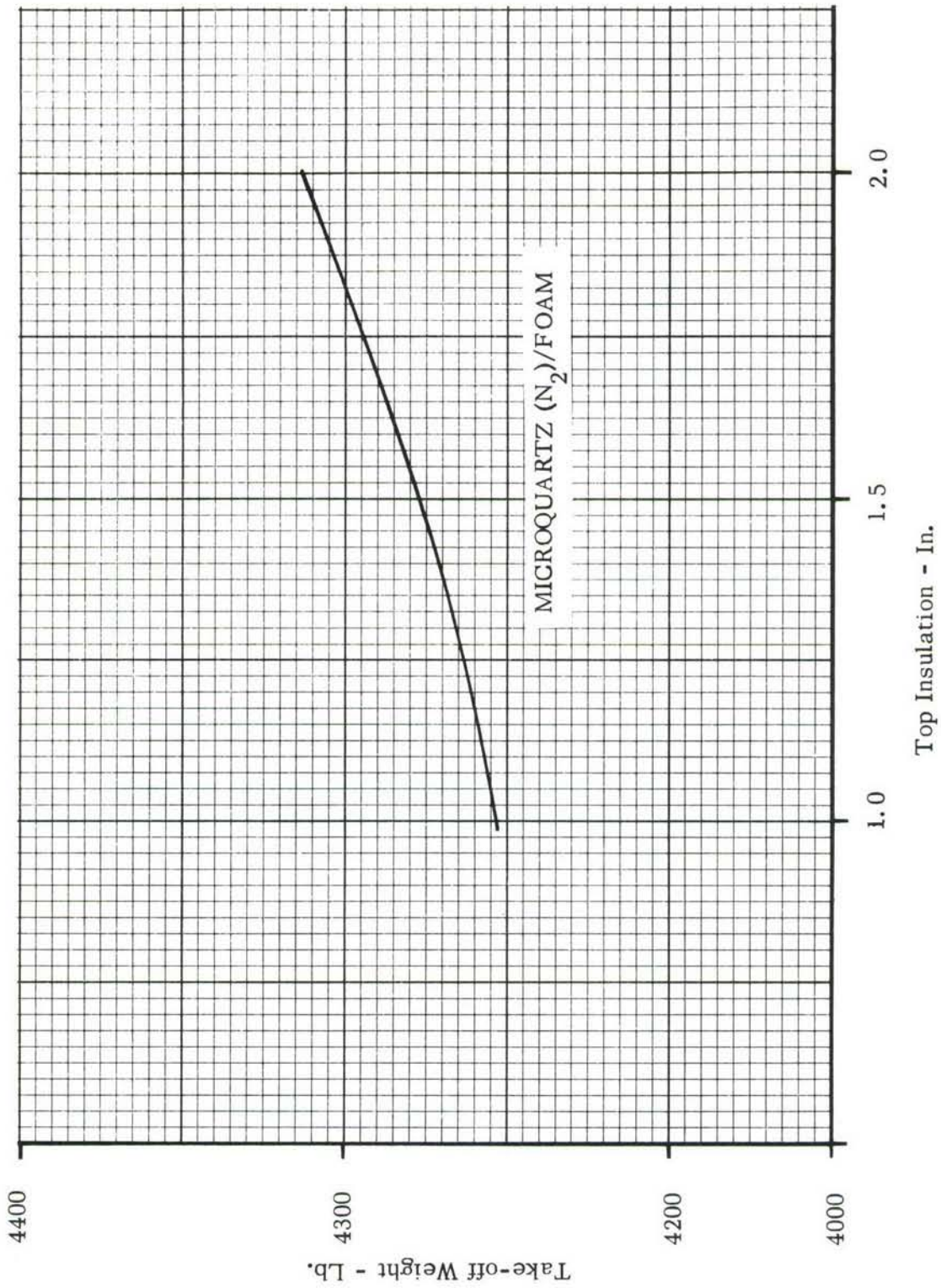


FIGURE 54 - OPTIMUM TOP INSULATION - MICROQUARTZ (N₂)/FOAM COMPOSITE

OPTIMIZED PARAMETERS		MICROQUARTZ (He)	MICROQUARTZ/FOAM (N ₂)
Venting Pressure	- psia	30	20
Top Insulation	- in.	1.3	1.0
Bottom Insulation	- in.	4.0	3.6
Tank Volume	- cu. ft.	801	778
Length	- ft.	19.64	19.00

5.0 EXPERIMENTAL TEST PROGRAM

The objective of the experimental test program was to prove the operational and thermal performance of the insulation system, uncover possible problem areas involved in the designs, establish hydrogen thermal behavior for hypersonic vehicle applications, and provide a comparison of tankage thermal performance against analytical predictions. The results of this fabrication and testing phase give substance to the selection of a final, large-scale tank design. This work was accomplished through the following steps:

a) Design and fabrication of two subscale tanks, using the two candidate structural materials and insulation systems, established by the preliminary large scale tank designs, results of the optimization analysis, and requirements of testing. Consideration was originally given to these tanks being thermally scaled models of the large tanks but investigations showed that dimensioning, fluid and material properties and/or environmental conditions could not be independently varied within the limits of the thermal laws. Preliminary insulation testing, reported in Appendix I, revealed the composite systems extreme sensitivity to overheating at its sealing interface and was partially responsible for termination of work on Tank #2 prior to it being tested in the environmental chamber.

b) Test equipment and instrumentation were designed and fabricated, and the environmental chamber modified to conform with testing objectives, procedures, and safety requirements. The requirements of safety were established from a study made to determine the possible hazards involved in a test of this nature. To support strain gage applications in tank testing, an evaluation program was performed to the environmental conditions anticipated. This program determined the type of gage to be employed, substantiated bonding procedures, established reliability and provided calibration data. This work is reported on in Appendix II.

c) Subscale tanks were proof-tested with water and liquid nitrogen, and helium mass spectrometer leak-checked to establish structural integrity. Tank #1 was instrumented and installed into the test furnace fixture within the environmental test chamber. The experimental test program was then run to the established test procedures, determining transient heating rates to liquid and ullage, thermal behavior of hydrogen, and establishing tank thermal performance for comparison with the analytical predictions.

5.1 TANK STRUCTURE DESIGN

The two subscale tank designs, Tank #1 and Tank #2, are shown in Figures 55 and 56. These designs are based upon the results of the optimization analysis, preliminary large-scale tank designs, and testing requirements. The tanks are identical in geometry, having a main shell two feet in diameter and five feet long with conical

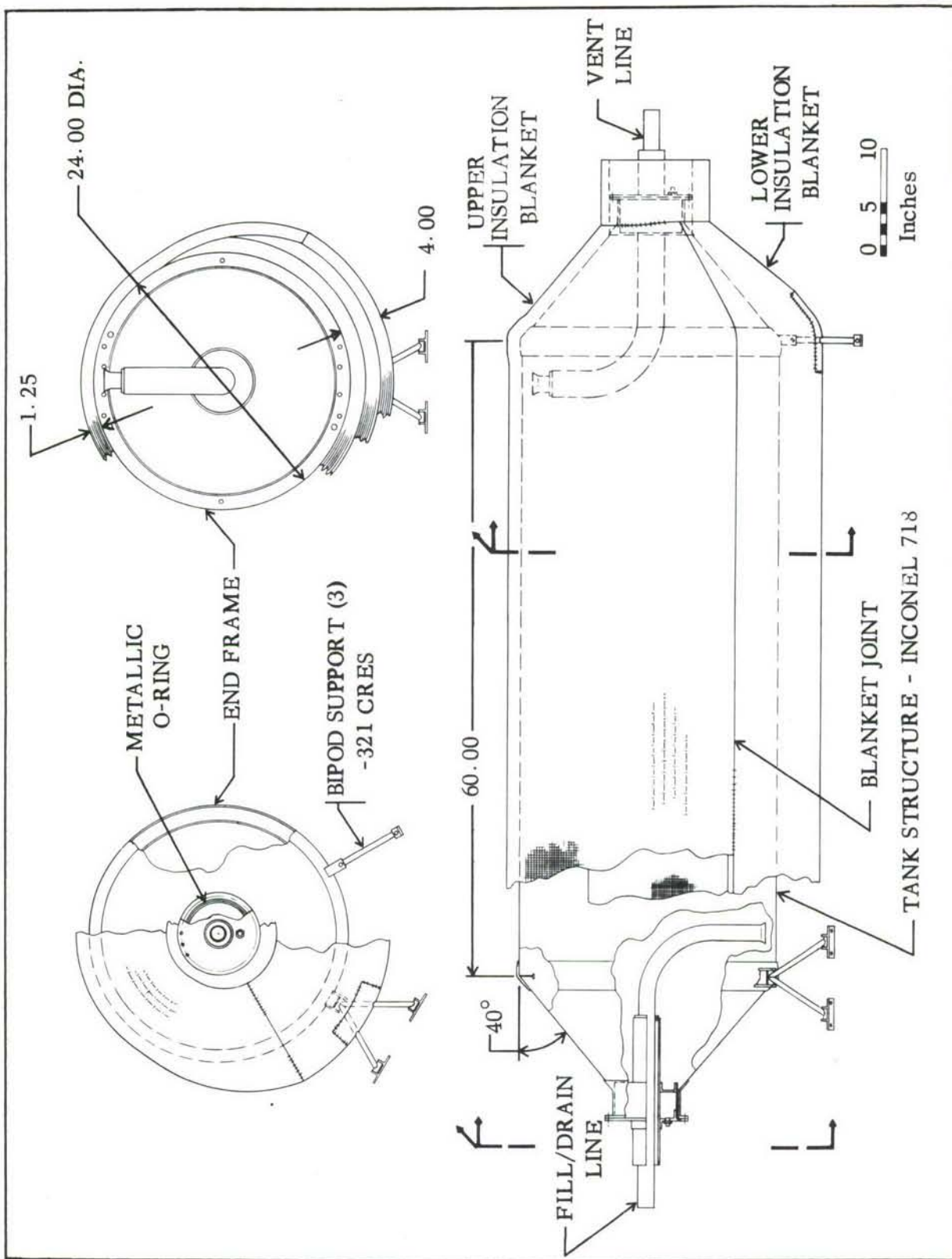


FIGURE 55 - SUBSCALE TANK #1 CONFIGURATION

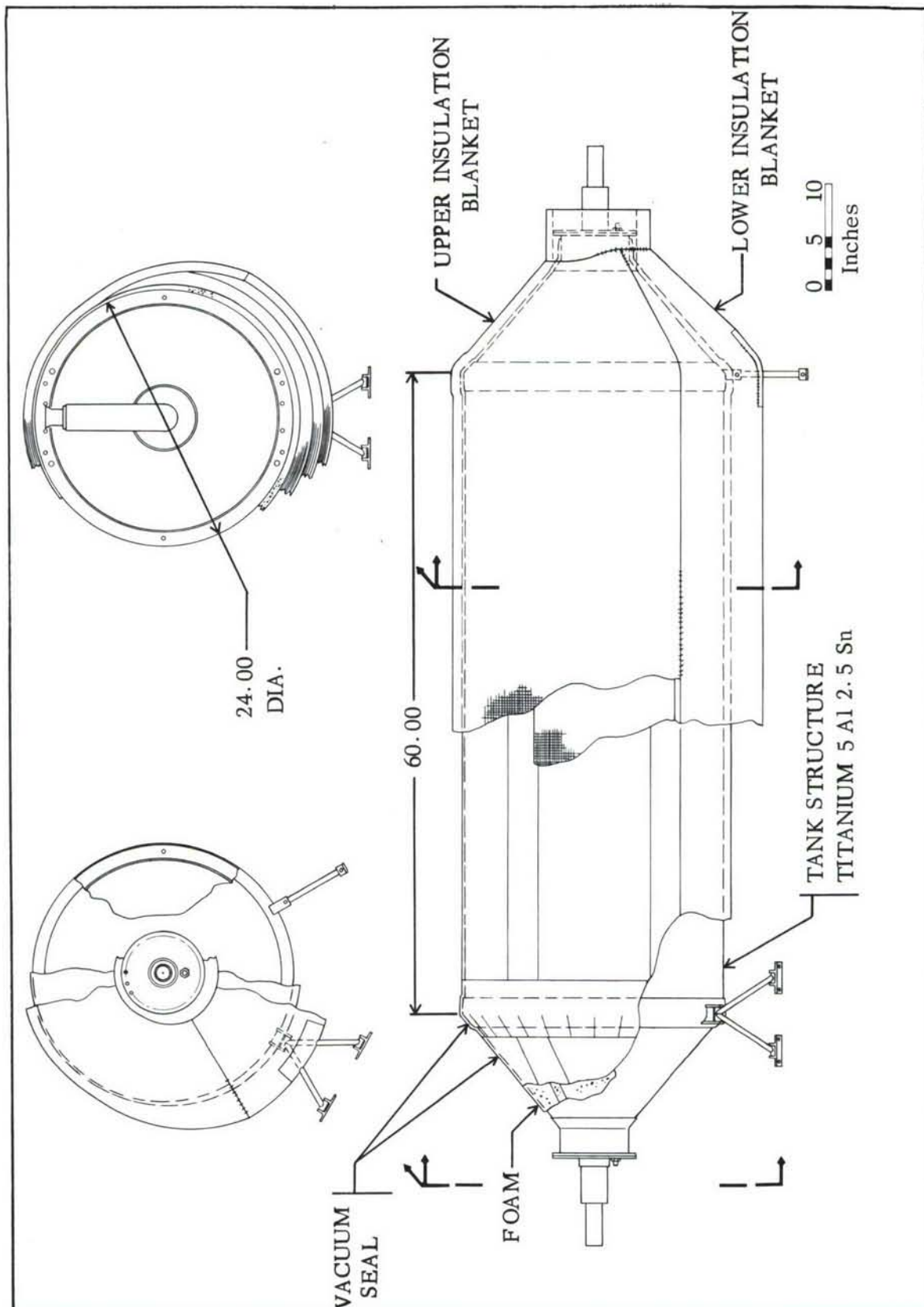


FIGURE 56 - SUBSCALE TANK #2 CONFIGURATION

end closures. The conical end closures allow for simple manufacturing methods and low tooling costs without violating any of the test objectives. Tank #1 used the 718 nickel alloy as its structural material and the all-Microquartz, helium environment, insulation system. Tank #2 used the 5 Al 2.5 Sn titanium alloy, ELI, as its structural material and the foam/Microquartz, nitrogen environment, composite insulation system. The 718 nickel alloy was associated with the all-quartz insulation system, in view of the potential high temperature tolerance a system using these materials would have. The venting pressures established by the optimization analysis, 20 and 30 psig for Tanks #1 and #2, respectively, were used as a performance parameter for the testing program but were not the basis of the tanks design. The tanks were designed to withstand operating pressures of 100 psig to comply with testing requirements. The subscale tank shell did not require stiffening except for the end frames. These end frames redistribute support loading from tank weight and react compression loading from the conical end closures. Detailed discontinuity analyses of the two subscale test tank configurations were conducted to verify structural integrity for design and proof requirements. In addition, an analysis of the non-axisymmetric thermal stresses induced during test were conducted to examine their effects on the pressurized tank wall.

The support system, Figure 57, consists of two forward supports and one aft; all are identical bipods and pinjointed at both ends. The support system is identical for both tanks and is fabricated from 321 CRES material. The forward transverse and longitudinal bipods react the loading in these directions, together with the vertical loading, which gives this end a fixed condition. Pinjointing of the longitudinal bipod allows for transverse thermal contractions and expansions of the tank structure. The aft support is a transverse bipod which reacts side and vertical loading and provides for longitudinal thermal contractions and expansions. The lower portion of these supports were subjected to 1260° F during the test. To provide free movement of the joints in this high temperature environment, they were treated with a special lubrication process.

Fill/drain and vent line assemblies, Figure 58, are common to both tanks. The assembly consists of a vacuum pot that attaches to a vacuum jacketed line. The vent and fill/drain assemblies are identical except for the amount of vacuum jacketing on the line. These assemblies attach to the end closures by bolted flanges, the vent line assembly at the forward or fixed end and the fill/drain line assembly at the aft end, the sealing being accomplished by means of metallic "O" rings. The material chosen for fabrication of these assemblies is 321 CRES. The use of different materials at the flanged joint did not present any sealing problems. All the wiring required for internal instrumentation of the test tanks passed through the vent line. Access to the inside of the tank is provided by the removal of the fuel line assemblies.

5.1.1 TANK #1 STRUCTURE FABRICATION. The subscale Tank #1 was fabricated from the 718 nickel alloy material in the annealed condition, using a skin gage

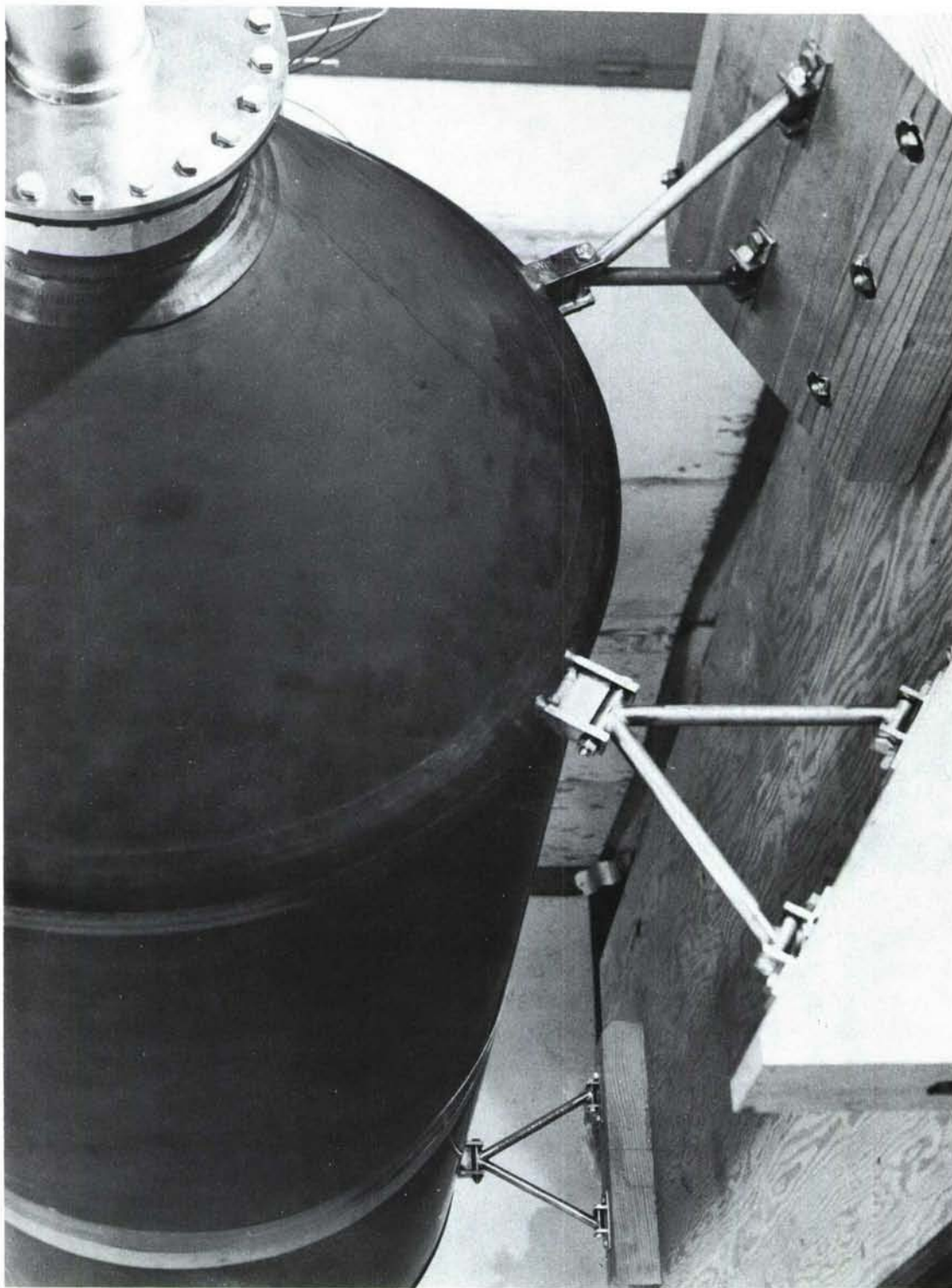


Figure 57 BIPOD TANK SUPPORT SYSTEM - INSTALLED

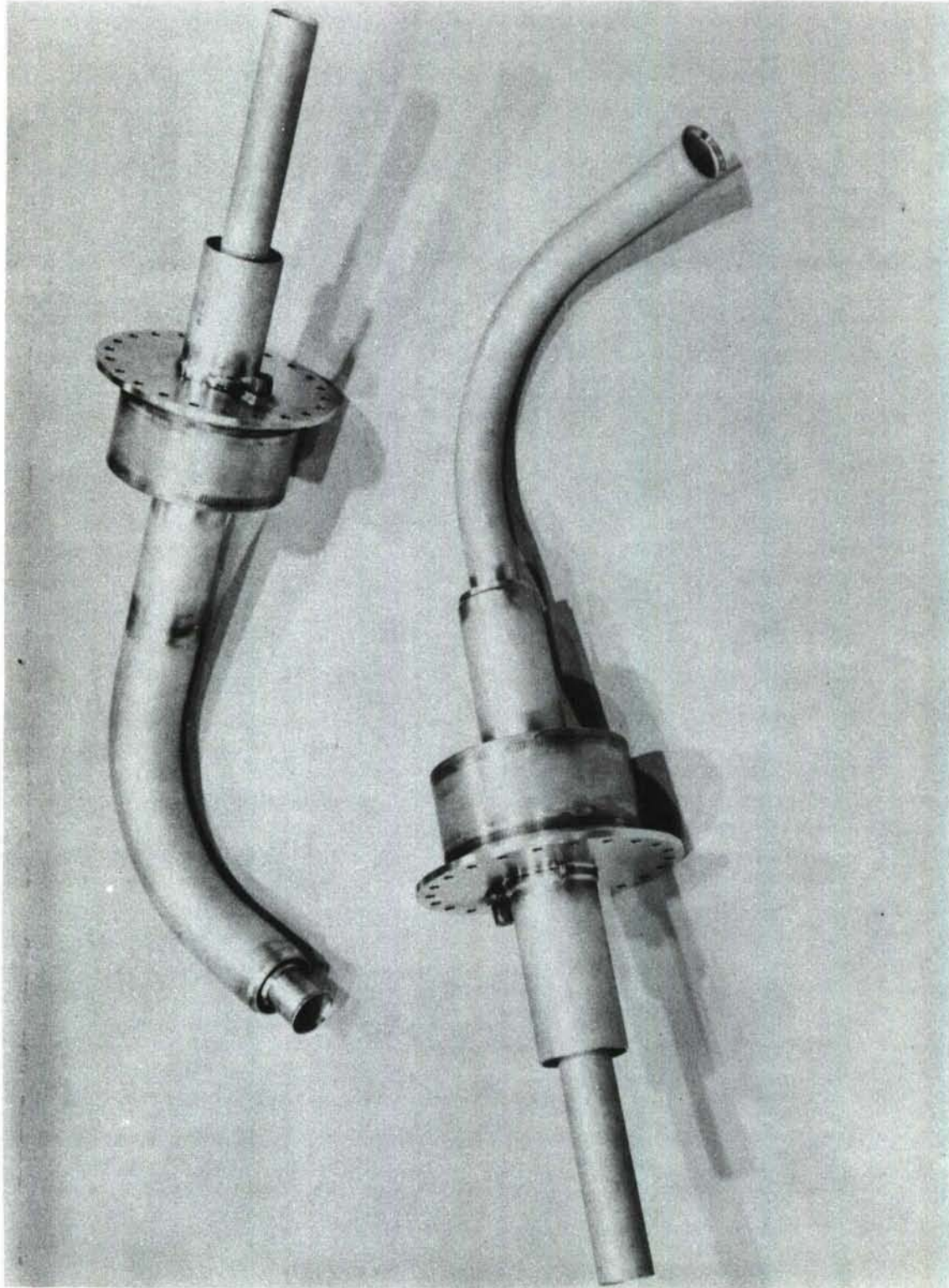


Figure 58. FILL/DRAIN AND VENT LINE ASSEMBLIES

of .020 for the main shell and end closures. The manufacturing breakdown and assembly sequence used in the tank's fabrication is shown in Figure 59. The tank was fabricated in two major assemblies, giving good access for installation of internal instrumentation and providing frame inspection after heat treatment. The final closure was accomplished by a fusion butt weld at the forward frame.

Frames were made from several parts welded together to form an assembly. The outer frame cap was made in three parts, each being brake formed, annealed, stretch formed with an intermediate anneal, and then hot sized to relieve stresses and give dimensional stability. These parts were then trimmed, fusion butt welded together and machined. Machining of these rings required tooling aids to prevent deflection of the part from the heavy cutting-tool loads. The outer frame caps were resistance welded to the cone assemblies. The frame subassemblies, consisting of a web and inner frame cap, were then welded to the outer frame cap. The aft cone assembly was then joined to the main cylindrical section of the tank, which also included a portion of the forward frame cap, resulting in two major assemblies.

The two major assemblies for the tank were heat-treated to obtain an aged condition for the tank material. The aging of the tank material gives it increased strength, provides maximum weld efficiency for the fusion and resistance welds, and removes the need for doublers which reduces fabrication task. The heat treatment for the tank incorporated a stress relieving sequence. This requirement was based on some recent data that indicated this alloy has a tendency to crack around welds, due to gradual decrease of elongation, at the aging temperature of 1350° F. While this effect has only been noted in heavier gages, 0.25 and above, it was considered a point of good practice to stress-relieve welded assemblies prior to aging. The stress relieving operation was accomplished by charging the assemblies into the preheated furnace at 1650° F causing the material to heat rapidly through the aging zone, and then reducing to aging temperature. After aging, the circumferential lap splice which employed two resistance seam welds showed deformation in the form of bubbles. This deformation was caused by moisture, entrapped between the two gas tight welds during fabrication, being expanded during the elevated temperatures of heat treatment. This, in turn, caused the deformation of the tank material, which had little resistance to deformation under the elevated temperatures and high stresses. This discrepant area was removed and a repair section was spliced in using a spot/seam/spot resistance weld pattern. Splices employing two seam welds were removed from both tank designs, in view of the above problem, and also because of the potential entrapment they offer to liquid hydrogen. Should the first seam leak liquid hydrogen into the space between the lines of the weld, and this space become subject to the high heat fluxes associated with tank testing with the liquid level having fallen below level of entrapment, the rapid change of state to gas could produce a rupture of the tank. For weld joints involving one seam weld, the local failure of the weld would leak hydrogen and not represent such a potential catastrophic failure. The lap joint configuration, using two resistance seam welds, was originally advocated on the basis of its improved fatigue capability from the removal of spot welds which

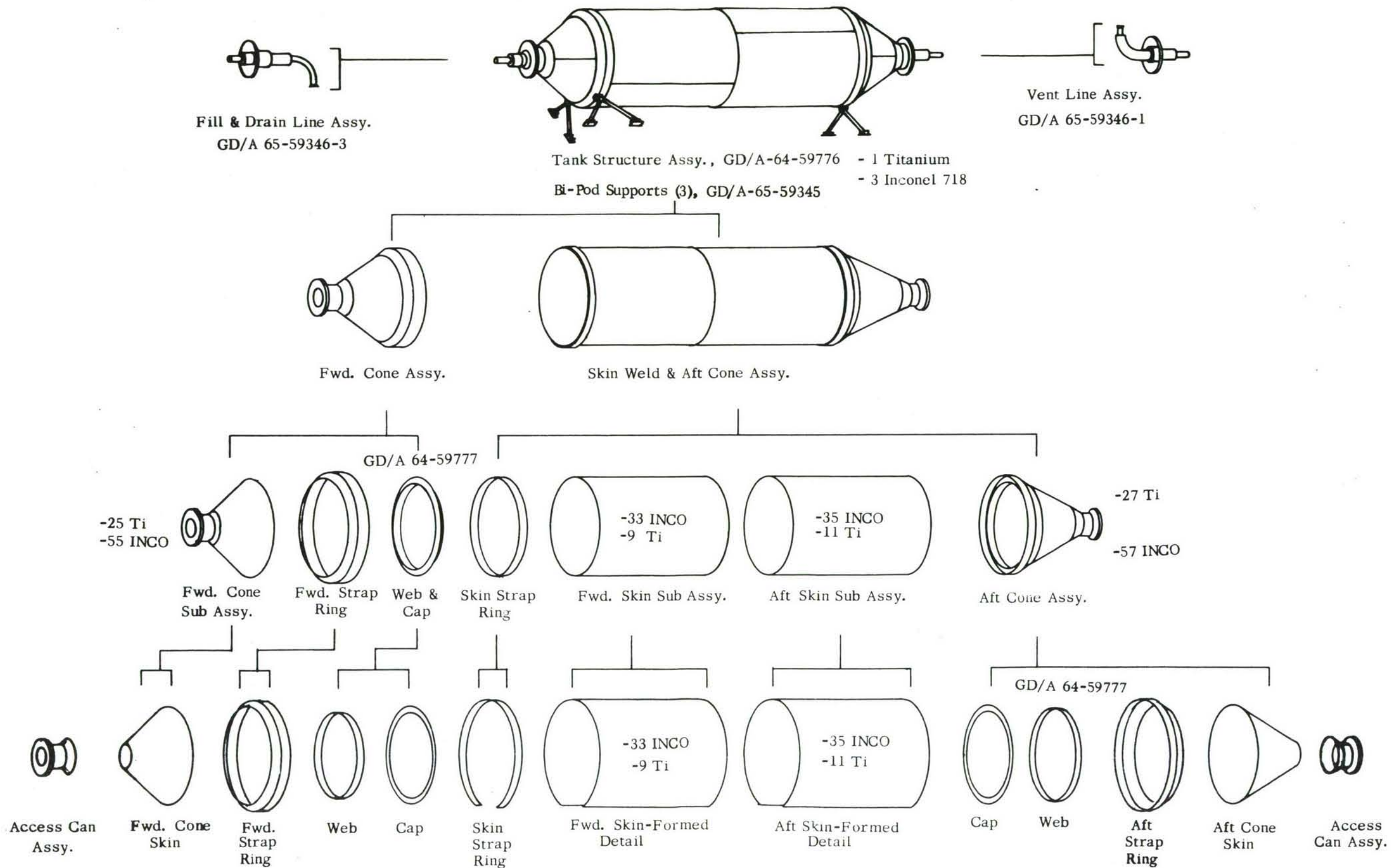


Figure 59 SUBSCALE TANK MANUFACTURING BREAKDOWN AND ASSEMBLY SEQUENCE.

represent stress raisers and a source of crack initiation. This was especially significant for the titanium tank, since the tension capability of its spot welds is below the acceptance standards of MIL-W-6858. Figure 60 shows the completed tank, mounted on its transportation skid.

718 Nickel Alloy

The 718 nickel alloy has good elongation and forming characteristics in the annealed condition. After forming, this alloy can be age-hardened to relatively high tensile values. Welding can be done in both the annealed and aged condition because of its slower aging response compared to other age hardenable alloys. TIG butt welds in the annealed and aged condition have a reduced weld efficiency; however, this can be brought up to approximately that of the parent metal by aging in subassemblies. The 718 alloy can be resistance spot-welded to itself. Toughness values, as evaluated by tension shear ratio, are above the MIL-W-6858 requirement of 0.25 for all temperatures. This alloy allows for welds to be repaired, which is a significant advantage over many of the other nickel alloys.

The specification used for sheet and plate material procurement is GD/A 0-71038. This specification covers the two conditions, "annealed" and "annealed plus age hardened." The mechanical properties at RT are specified as:

Condition	F_{tu}	F_{ty}	e, %
Annealed < .187	140,000 Max.	80,000 Max.	30 Min.
> .187	150,000 Max.	90,000 Max.	40 Min.
Age Hardened	180,000 Min.	150,000 Min.	15 Min.

The specification used for bar and forging material is GD/A 0-71037.

Heat Treatment

Annealing consists of heating to 1950° F., holding this temperature for sufficient time to obtain uniform temperature in the material, followed by cooling to room temperature at a rate equivalent to air cool or faster.

Age hardening consists of:

- a) Heating to 1350° F.
- b) Holding at 1350° F. \pm 25° for 8 hours
- c) Furnace cooling to 1200° F. (cooling rate not critical)
- d) Holding at 1200° F. \pm 25° F. until the total of (b) + (c) + (d) is 18 hours.

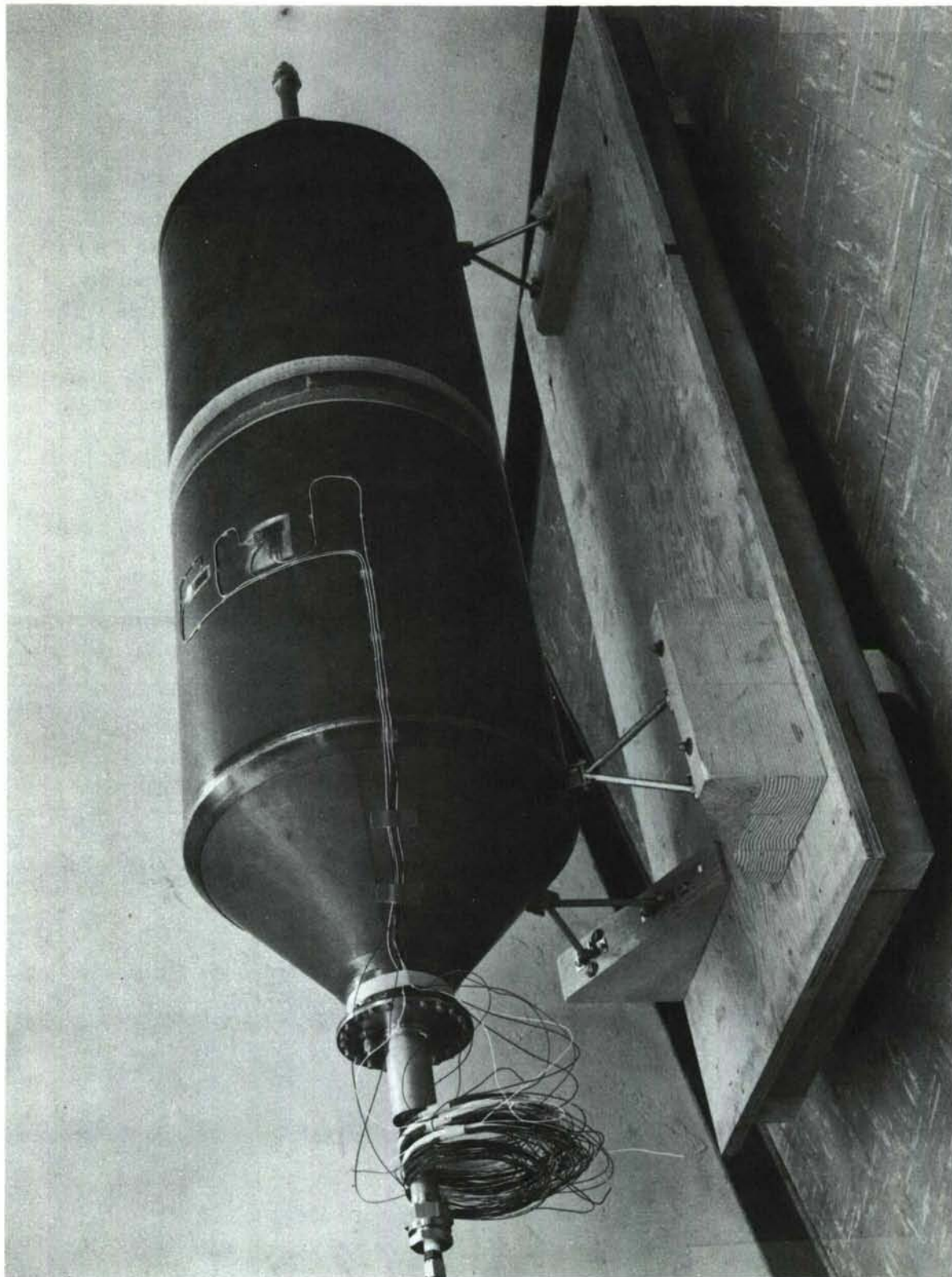


Figure 60. SUBSCALE TANK #1 STRUCTURE ASSEMBLY.

5.1.2 TANK #2 STRUCTURE FABRICATION. Subscale Tank #2 was fabricated from the 5 Al 2.5 Sn titanium alloy ELI, and employed a skin gage of .030 for the main shell and end closures. The manufacturing breakdown and assembly sequence used in tank fabrication is shown in Figure 59. The method of fabrication for the tank, frame build-up and installation were similar to Tank #1.

Procurement difficulties were encountered with this material, 14 weeks delivery time after ordering. Reasons given by vendor were priority and difficulties in obtaining a material chemical analysis to GD Convair ELI (extra low interstitials) specification. Longitudinal splices on the tank are all fusion butt welds. Since the material is in the annealed condition, this alloy not being responsive to heat treatment, these butt welds do not require doublers. Circumferential lap splices, for reasons explained for Tank #1, are made using a spot/seam resistance weld pattern. This joint configuration was tested to support its application in this tank, since no test data exists to corroborate the analysis. Results of these structural tests, to substantiate this new splice configuration, are given below.

Four GD Convair standard 36 inch long tensile test specimens, with a 4-inch nominal width, were fabricated using the same .030 gage 5 Al 2.5 Sn titanium alloy sheet stock being used for Tank #2 manufacture. Three specimens were subjected to static tests to failure at room temperature, -320°F and -423°F ., respectively. The fourth specimen was cycled once to 75 ksi at room temperature, and once to 75 ksi at -320°F to simulate the H_2O and LN_2 proof pressure tests to be performed on the tank. The specimen was then subjected to a 1000 cycle fatigue test, followed by a tensile test to failure at -423°F . The test results are shown below.

Test No.	Specimen	Test Type	Failure Stress
1	A	Room temperature static tensile test	123 ksi
2	B	-320°F static tensile test	196 ksi
3	C	-423°F static tensile test	184 ksi
4	D	Room temperature static tensile test to 75 ksi	No failure
5	D	-320°F static tensile test to 75 ksi	No failure
6	D	Fatigue @ -423°F - 0-50-0 ksi	No failure no leak @ 1000 cycles
7	D	-423°F static tensile test	150 ksi

Material: 5 Al 2.5 Sn titanium alloy, .030" gage

Titanium 5 Al 2.5 Sn Alloy ELI

The ELI designation stands for extra low interstitials. Investigations have shown that certain interstitial alloying elements cause this alloy to be brittle at liquid hydrogen (-423°F) temperatures. The specification, GD/A 0-71010, which limits the amount of the interstitial elements, has been used for material procurement. This alloy has excellent strength to weight ratio, exhibits good toughness characteristics and good weldability. It is characterized by large increases in both ultimate and yield strength and very small decreases in elongation with decreasing temperature down to -423°F . Welded joints are as strong as the parent metal. This eliminates the need for doublers, which saves weight, and reduces the need for spotwelds which act as stress raisers and sources of crack initiation in fatigue. The minimum guaranteed mechanical properties at RT given by GD/A 0-71010 specification are:

Condition	F_{tu}	F_{ty}	$e, \%$
Annealed < .015			4
.015 - .025	110,000	100,000	7
> .025			10

5.1.3 CONCLUSIONS AND RECOMMENDATIONS FROM FABRICATION OF SUB-SCALE TANKS

1) Tooling and fixturing needs were greater than anticipated to meet dimensional and reliability requirements. Fixturing was required to stabilize parts for machining operations, prevent distortion during welding and heat treat operations, and provide good gas coverage and chill-down characteristics during weld operations.

2) Manual weld operations were found unreliable for obtaining consistent weld quality and automatic weld operations were performed, where possible, at the expense of increased tooling.

3) Radiographic examinations do not reveal locations of spot weld failures. Exact location of these discrepant areas were found extremely difficult to ascertain. Method finally employed was localized helium soap bubble checking.

4) Development of a TIG fusion spot weld procedure, for repair of resistance spot welds, was developed and gave satisfactory results for the limited access considerations under which it was employed. The developed procedure gave a small heat affected zone at the welds.

5) Repair of resistance welded joints, other than repair of isolated spot

welds, is limited for both materials due to their sensitivity to impurities between faying surfaces.

6) Rigid welding procedures were found essential for both the 718 alloy and the titanium alloy, especially cleanliness requirements. The 718 alloy was sensitive to fit-up, producing expulsion if not controlled.

7) Welded joints that involve double seam welds are considered hazardous for tankage applications, due to the potential entrapment of LH_2 between the seams.

8) Development of weld schedules for both the 718 alloy and titanium was a large task. This was due to the testing and microscopic examination requirements for each schedule run and the need to establish schedules for every variation in gage combination and material condition. Both materials used were essentially development alloys, with limited fabrication data available.

9) Fabrication of parts by weld build-up; i.e., frames, was found to be expensive and time consuming. Future work will give greater consideration to forgings or plate stock, from which parts will be machined.

10) Quality of teflon coating on "O" rings, used in sealing access areas, require improvement. Uncoated rings will be evaluated and a survey made on improved sealing methods.

11) Material quantity requirements were many times greater than originally estimated, to contend with overage, spare parts, extensive weld schedules, and forming development.

12) Extensive machining of the 718 alloy produces a high degree of work hardening which requires intermediate heat treatment to provide good surface finish and prevent cracking during any subsequent weld operations.

13) Material lead times supplied by vendors were found to be unreliable, resulting in delays of fabrication start dates. This was attributed to the development nature of the materials, priority, and difficulties in meeting specifications.

5.2 INSULATION DESIGN AND FABRICATION

5.2.1 HELIUM ENVIRONMENT MICROQUARTZ SYSTEM. This insulation system was chosen for subscale Tank #1. From the optimization program, thicknesses of 1.3 and 4 inches were established for the upper and lower surfaces, respectively. These thicknesses were employed as the basis of the insulation design, dependent upon manufacturing and procurement influences.

Design

The typical Microquartz blanket cross section is shown on Figure 61. The insulation on the tank bottom consists of three individually machine-sewed blankets joined together by hand tufting on 4-inch centers. This was necessary due to thickness limitation imposed by existing sewing machines, which are capable of handling a maximum build-up of 1-3/8 inches. The top insulation consists of a single blanket 1.25 inches thick. In order to minimize discontinuities, the upper blanket extends over the lower blanket for 60° of arc on each side. The conical ends are joined to the cylindrical segment by overlapping the individual Microquartz layers. The tank ends are insulated with removable cylindrical muffs. Originally, the proposed insulation attachment consisted of adhesive bonding along the entire faying surface to the tank. This approach was modified since the adhesive imposed a temperature limitation of 200° F, and precluded removal of the blankets for inspection or repair. The revised attachment consists of several tension bands, supplemented by localized bonding along the lower tank half to prevent sagging of the blankets.

Materials

The choice of materials was dictated by the high temperature environment, and the physical characteristics required to allow adequate handling properties during manufacture and installation.

The Microquartz felt employed has a basic density of 3.0 lb/ft³, and a thickness of 3/16 inches. Stitching compresses the material to a nominal density of 4.5 lb/ft³, equivalent to a layer thickness of 1/8 inch. The structural properties of the Microquartz, such as amount of compression under load and spring-back characteristics, show that some amount of residual thread tension is required for a structurally acceptable blanket. Experiments have shown that a thickness reduction of 30% to 40% is desirable to obtain adequate handling properties. A final density of 4.5 lb/ft³ was therefore selected.

Glass cloth is used for the inner face of the blanket, and also intermediate layers where the temperature will not exceed 600°F. The selected style is 116 plain weave, at 3.16 oz/sq. yard and strength of 123 x 120 lb/inch. High temperature intermediate layers of cloth and the outer facing were made with J. P. Stevens style 593 quartz cloth, with an actual weight of 7.0 oz/square yard. This material is 5H satin-weave, and possesses an adequate balance of strength and weight to resist handling and separation by thread tension. This cloth has a washed low residue finish (residue is .1% to .15% net weight). The quoted tensile strength is 150 x 145 lb/inch.

Other materials were considered for this application, such as Refrasil (H. I. Thompson) and Astrosil (J. P. Stevens) high-silica leached glass cloth. These materials have adequate temperature resistance properties, but their strength and abrasion resistance was found to be extremely poor compared to quartz cloth, and they were therefore eliminated.

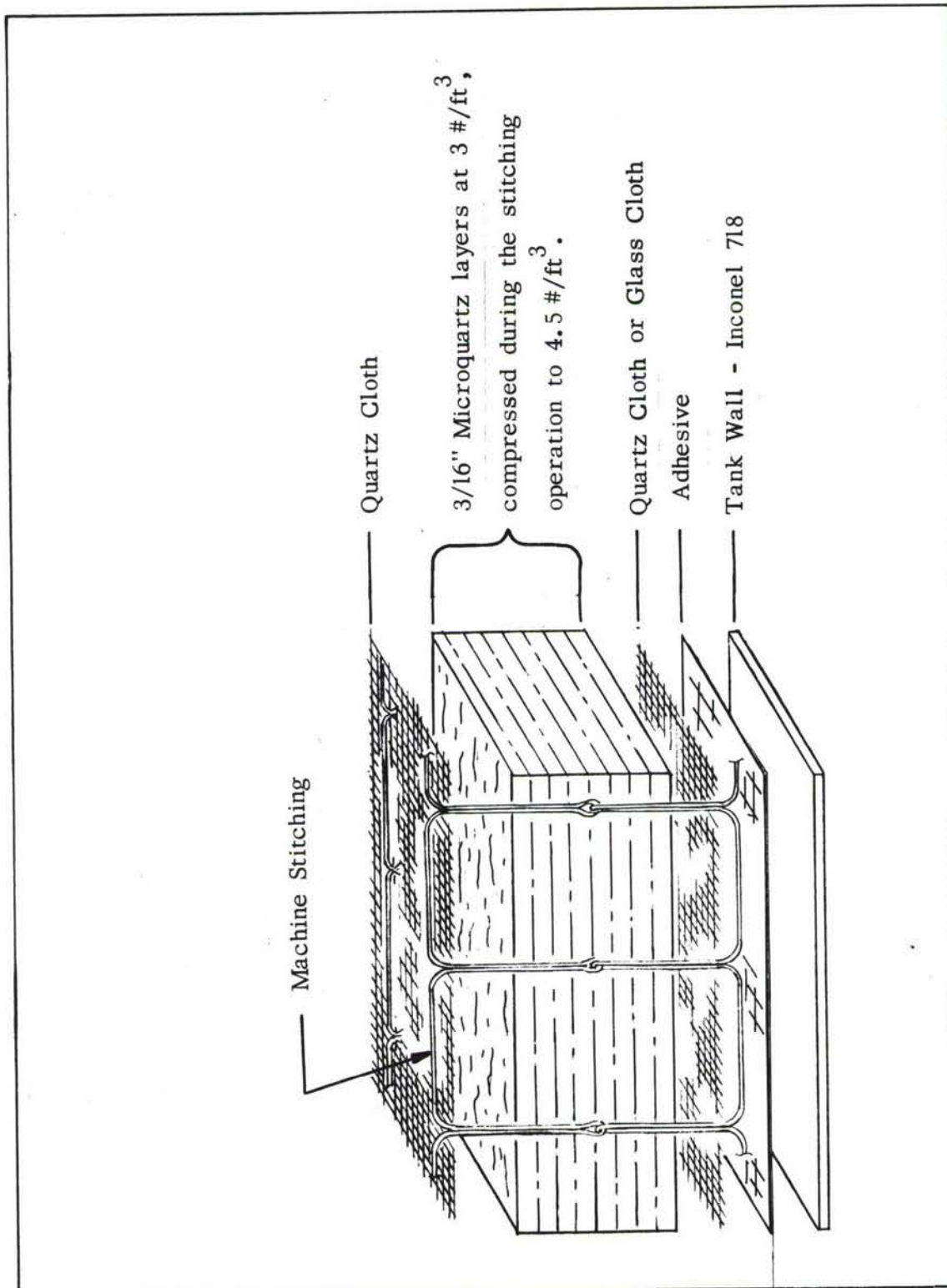


Figure 61 MICROQUARTZ INSULATION SYSTEM - TANK #1

Considerable difficulty was encountered in procuring a high temperature thread suitable for machine sewing. The lack of adequate thread for cryotherm specimen fabrication required the use of hand-sewing the blankets. This approach was not practical for the subscale tank insulation in view of the amount of labor required. Inquiries were made among the leading thread and fabric manufacturers, and two candidate materials were found. Johns-Manville supplied a silica thread covered with a Mylar sleeve to allow sewing. Dodge Fibers Company supplied a quantity of quartz thread with teflon coating to provide a smooth, low friction finish. Both types of thread were tufted into a cryotherm specimen and subjected to a simulated flight environment. After the test, the Mylar sleeve on the J-M thread was charred and the basic thread had no useful strength. Combustion of the Mylar apparently overheated the thread. The quartz thread survived the test without any apparent change in physical properties, although the teflon coating had vaporized. Sewing experiments showed that the Dodge Fibers thread can be processed successfully by machine. The knot strength is not as high as for equivalent size glass thread, but still adequate for the current application. The Dodge Fibers thread was therefore selected for blanket fabrication. The thread designation is RQ 752-12, with a yield of 3000 yards/lb.

Fabrication

A survey of currently available sewing machine capability revealed that several modifications would be required in order to allow stitching of 1-3/8 inch thick blankets. A Singer Model 7-31 machine in the GD/C factory was therefore modified by adaptation of a redesigned foot and use of a longer needle. The new foot was shortened to provide adequate clearance between the lower surface of the foot and the table, and was provided with a 2 inch x 2 inch plexiglass surface to distribute the pressure over a wide area and still allow observation of stitching.

A wood mockup was fabricated to aid insulation blanket sizing layup, and handstitching in critical areas. The mockup is basically a half-shell incorporating the conical ends. Strategically located cutouts in the skin allow access to the inner blanket face for stitching.

The blanket fabrication sequence consisted of cloth and felt layup and sizing on the mockup, hand tufting on several points to allow moving of the assembly to the sewing table, and then machine sewing with the blanket laid out flat. The cylindrical and conical segments were then reinstalled on the mockup for hand splicing of the joints and final sizing. Figures 62 through 65 show various phases of the insulation blanket manufacture. The completed assembly on the tank is shown in Figure 66.

Difficulties were encountered initially, such as quartz thread breakage, missed stitches, and broken needles. The problem was solved by changing to a larger diameter needle with the eye hand-polished to remove the sharp edges which tended to abrade the quartz thread.

The stitching resulted in somewhat greater overall density than 4.5 lb/ft^3 , although the proper thickness was maintained. This was due to decreased blanket width and length resulting from the quilting effect between stitches.



Figure 62 STITCHING OF THE INSULATION BLANKETS

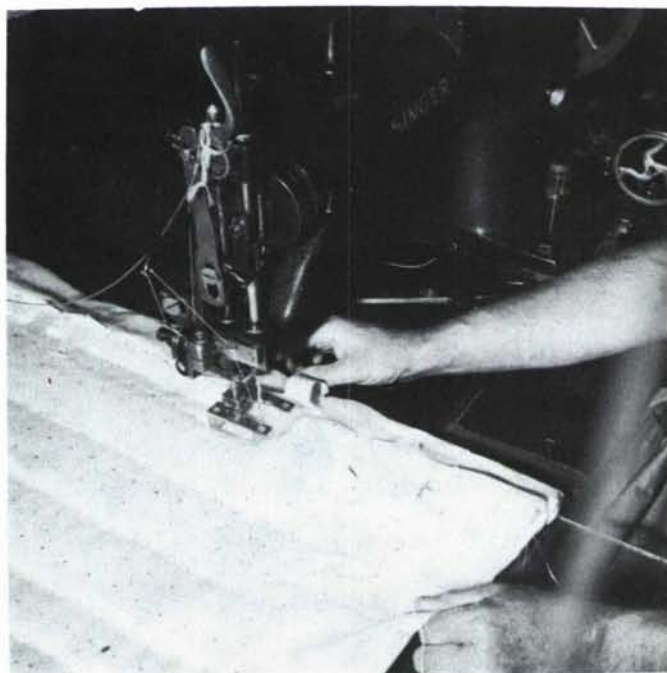


Figure 63 CLOSE-UP VIEW OF INSULATION BLANKET STITCHING

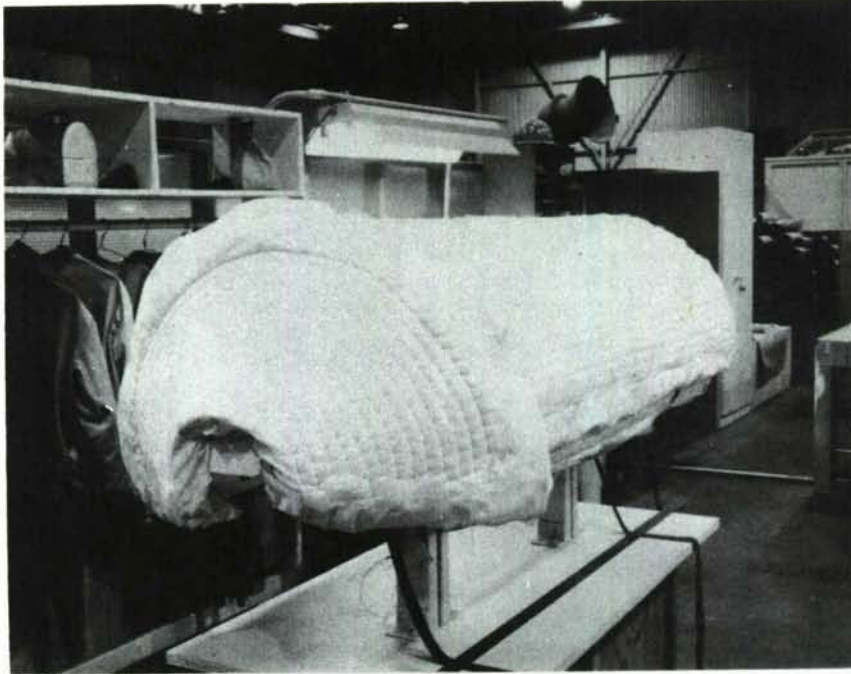


Figure 64 INSULATION BLANKET ASSEMBLY - CONE ENDS

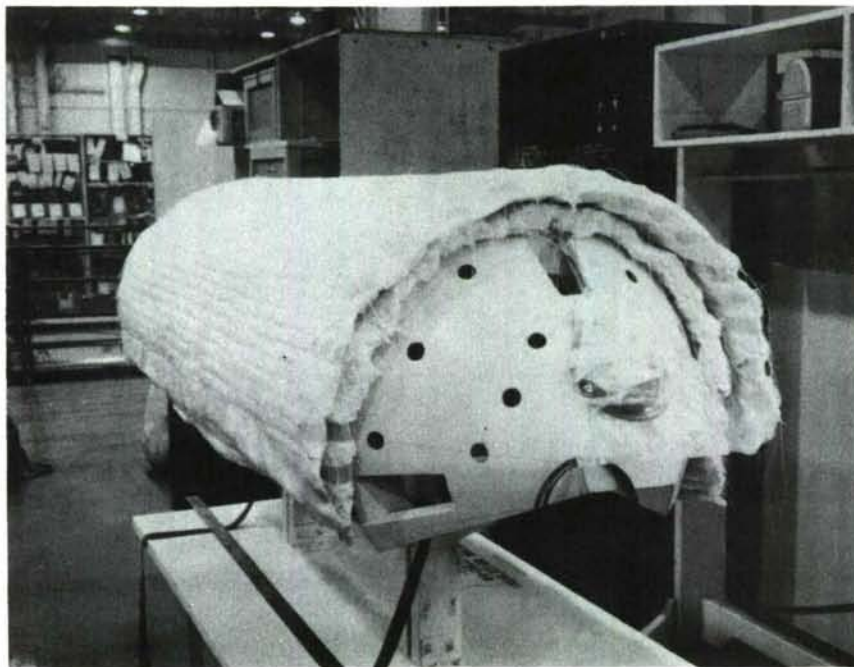


Figure 65. INSULATION BLANKET ASSEMBLY - CYLINDRICAL SECTION



FIGURE 66. INSULATED SUBSCALE TANK #1 IN SUPPORT FIXTURE

5.2.2 FOAM/MICROQUARTZ COMPOSITE SYSTEM. A basic purpose of the cryo-therm tests (see Appendix I) was the development of sufficient thermal data on the foam/Microquartz composite to allow design of a reliable system. As pointed out earlier, under Preliminary Design in Section 3.0, the composite insulation has two temperature limits at the interface between the Microquartz and the foam. A low limit occurs at ground hold where the interface temperature must be greater than 140° R. to prevent cryopumping nitrogen. The high limit occurs in-flight where the interface temperature must not exceed 660° R. (200° F.) to protect the foam and adhesive. The interface temperature is determined by the thicknesses and thermal conductivities of the two materials:

$$\frac{l_f}{l_m} = \frac{k_f}{k_m} \left(\frac{T_i - T_t}{T_o - T_i} \right)$$

The cryogenic tank compartment will be purged with nitrogen. This inerts or removes oxygen from the compartment and minimizes the possibility of an ignition in the event of a hydrogen leak. It also purges moisture from the compartment which would otherwise condense and freeze in the insulation. Cryopumping a small amount of nitrogen, in itself, is not particularly detrimental. The condensing nitrogen will tend to hold the interface temperature at 140°R. This will limit the maximum heat flux into the tank by maintaining a constant temperature difference across the foam layer. A potentially more significant problem relative to cryopumping is the possibility of air entering the tank compartment. Since oxygen condenses at a higher temperature than nitrogen, the condensed product will tend to have a higher oxygen concentration than the gaseous oxygen/nitrogen mixture in the compartment. The resulting oxygen concentration could involve a greater safety hazard than otherwise would exist.

The interface must be prevented from overheating during flight. The outer insulation temperature is fixed by flight parameters. The maximum interface temperature is fixed by material design limit at 660°R, thus the controlling temperature is the inner tank wall. The greater the relative amount of foam, the greater will be the temperature drop across it. Thus, as the amount of foam is increased to prevent cryopumping on the ground, the temperature at the tank wall during flight must be reduced to maintain 660°R at the interface. Cooling is required to hold the upper tank wall temperature at the required level.

The temperatures at the interface during ground hold, the resultant tank wall temperature during flight, and the required cooling are shown in Figure 67, as a function of the foam/Microquartz thickness ratio, l_f/l_m . Other temperatures relative to the insulation system are shown below:

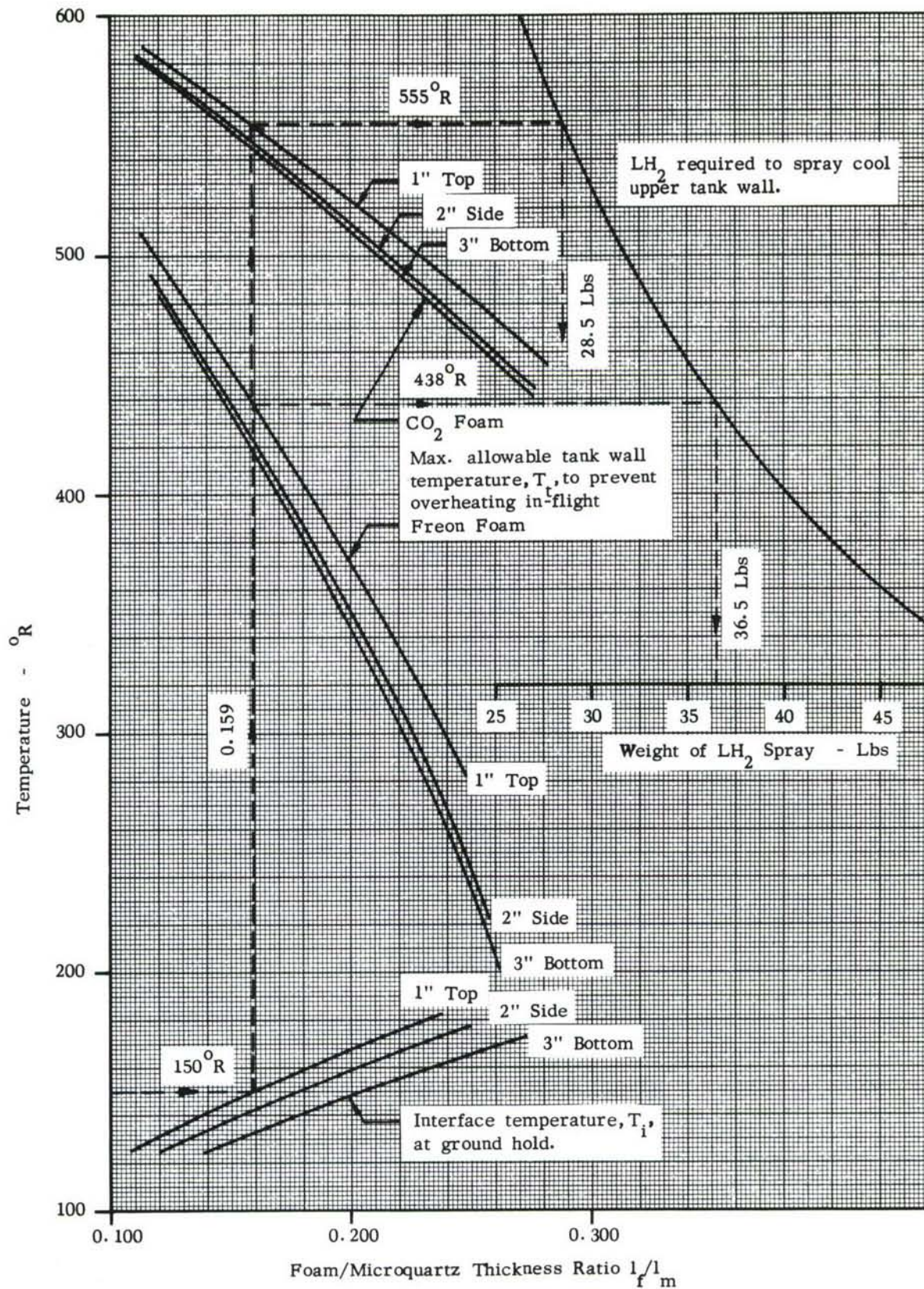
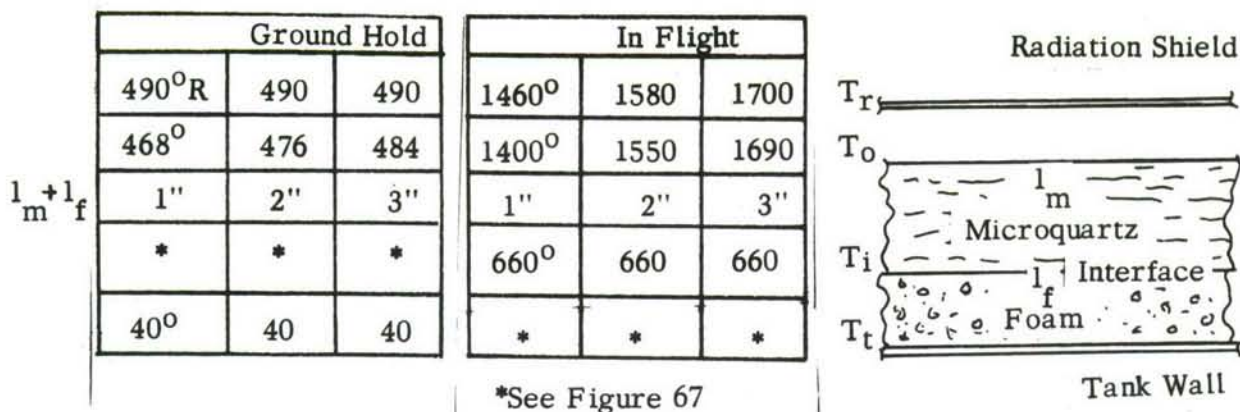


Figure 67. CRYOPUMPING AND OVERHEATING CRITERIA FOR FOAM/MICROQUARTZ INSULATION



The foam is bonded at the interface and tank wall with adhesive which has been determined to penetrate into the foam 0.020" on each side. This reduces the actual foam thickness, ($l_f = l_{fa} - 0.040$ "). The thickness ratio in Figure 67 is based on effective thickness, l_{fe} .

The cryotherm test results indicate that the conductivity of the Microquartz varies with thickness both at ground hold (760 mm Hg) and in-flight (8 mm Hg). The interface and tank wall temperatures have been determined for nominal Microquartz thicknesses of 1", 2" and 3". These thicknesses correspond approximately to the top, side, and bottom of the tank. Thus, the radiation shield, T_r , and the outer insulation, T_o , temperatures used for the in-flight analysis correspond to the actual values representative of these locations.

The cooling requirements shown in Figure 67 are based on continuous spray cooling 200 ft² of upper tank surface for 1.25 hours, assuming a heat transfer coefficient of 5 BTU/hr ft² °R. The heat of vaporization and sensible temperature rise of the hydrogen were used to absorb the incoming heat flux. The assumption of continuous cooling is conservative but represents the maximum penalty as a basis for comparison.

The required tank wall temperature for both freon and CO₂ foam is shown in Figure 67 for comparison. The thermal conductivities of the two foams are the same at low temperature. The interface temperature at ground hold applies to both; however, the greater conductivity of the CO₂ foam at room temperature increases the maximum allowable tank wall temperature during cruise, resulting in a lower cooling requirement. While CO₂ foam is not recommended for use in this application because of its mechanical properties, it serves to illustrate the potential improvement in the insulation which might be obtained if the freon could be removed from the freon foam and replaced with another gas.

The recommended limiting interface temperature at ground hold is 150° R, which is 10° above the nitrogen cryopumping point. The cryotherm tests indicated

that the temperature variation at the interface was $\pm 5^{\circ}$ from the mean value based on six measured points. Thus the 150°R design value should keep the interface above the cryopumping point. The dewpoint temperature of an oxygen/nitrogen mixture increases as the quantity of oxygen in the mixture is increased. It can be safely assumed, however, that any air which enters the compartment being purged with nitrogen will be small and would not increase the dewpoint by more than 1° .

The resultant foam/Microquartz thickness ratios for a 150°R interface temperature and the maximum allowable tank wall temperatures are shown below:

Microquartz	l_f/l_m	T_t Max
Thickness - in.		
1.0	0.159	438°R
2.0	0.178	390°R
3.0	0.205	335°R

The thicknesses have been cross-plotted in Figure 68 to show the actual foam thickness required as a function of total insulation. The actual foam thickness includes 0.040" for adhesive penetration.

The insulation on the top tank surface will be seven layers of Microquartz (0.875") and 0.177" of foam. This represents a minimum practical composite thickness when manufacturing tolerances are considered. The insulation on the lower tank surface will be twenty-four layers of Microquartz (3.0") and 0.655" of foam.

Design. The composite system cross-section is shown on Figure 69. The cryotherm tests have shown that foam thickness control and adhesive bond quality are critical elements for successful performance of the system, and the design is geared to satisfy these requirements. The outer Microquartz blanket design is similar to the all-Microquartz system, except that the number of felt layers was reduced to obtain thicknesses of .875 inch and 3.0 inches at the top and bottom, respectively. The blanket is attached to sealing membrane with a continuous adhesive bond. This is mandatory since mechanical attachment methods, such as used for the all-Microquartz system would allow areas of poor contact leading to either cryopumping or overheating of the foam and Zero-Perm.

The low temperature insulation consists of rigid polyurethane foam panels formed to the tank contour by heat and vacuum bag pressure, and then bonded to the tank. The joints between individual panels are insulated by a pour-in-place foaming technique. Simple butt joints had to be avoided since adhesive penetration up between panels would create a heat short and result in local cryopumping.

Materials. The materials used for the outer blanket manufacture were described earlier in Paragraph 5.2.1.

The material used for the inner insulation freon-blown foam, is manufactured

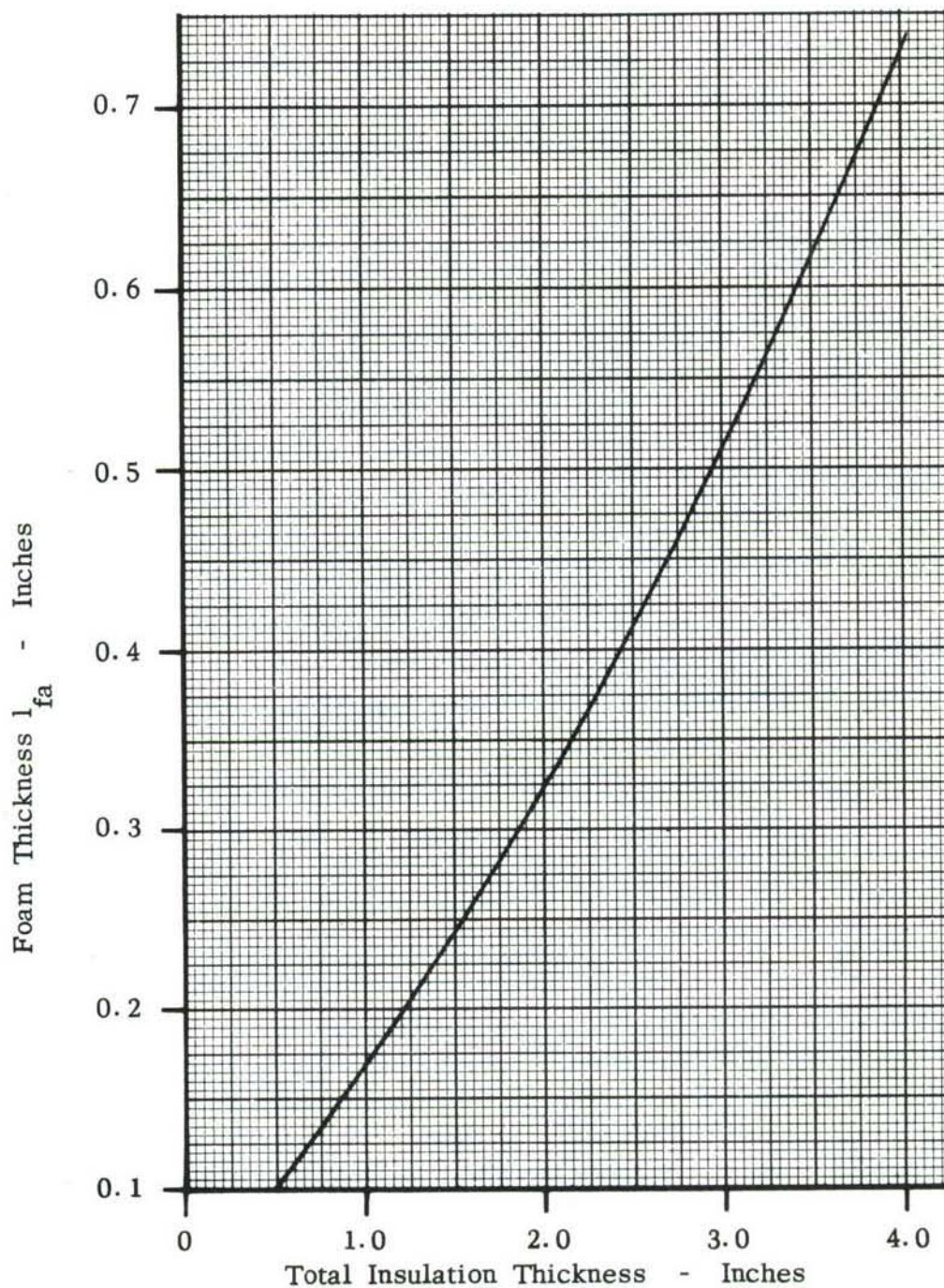


Figure 68. MICROQUARTZ/FOAM COMPOSITE INSULATION - FOAM THICKNESS REQUIRED TO MAINTAIN THE INTERFACE TEMPERATURE AT 150° R DURING GROUND HOLD CONDITION

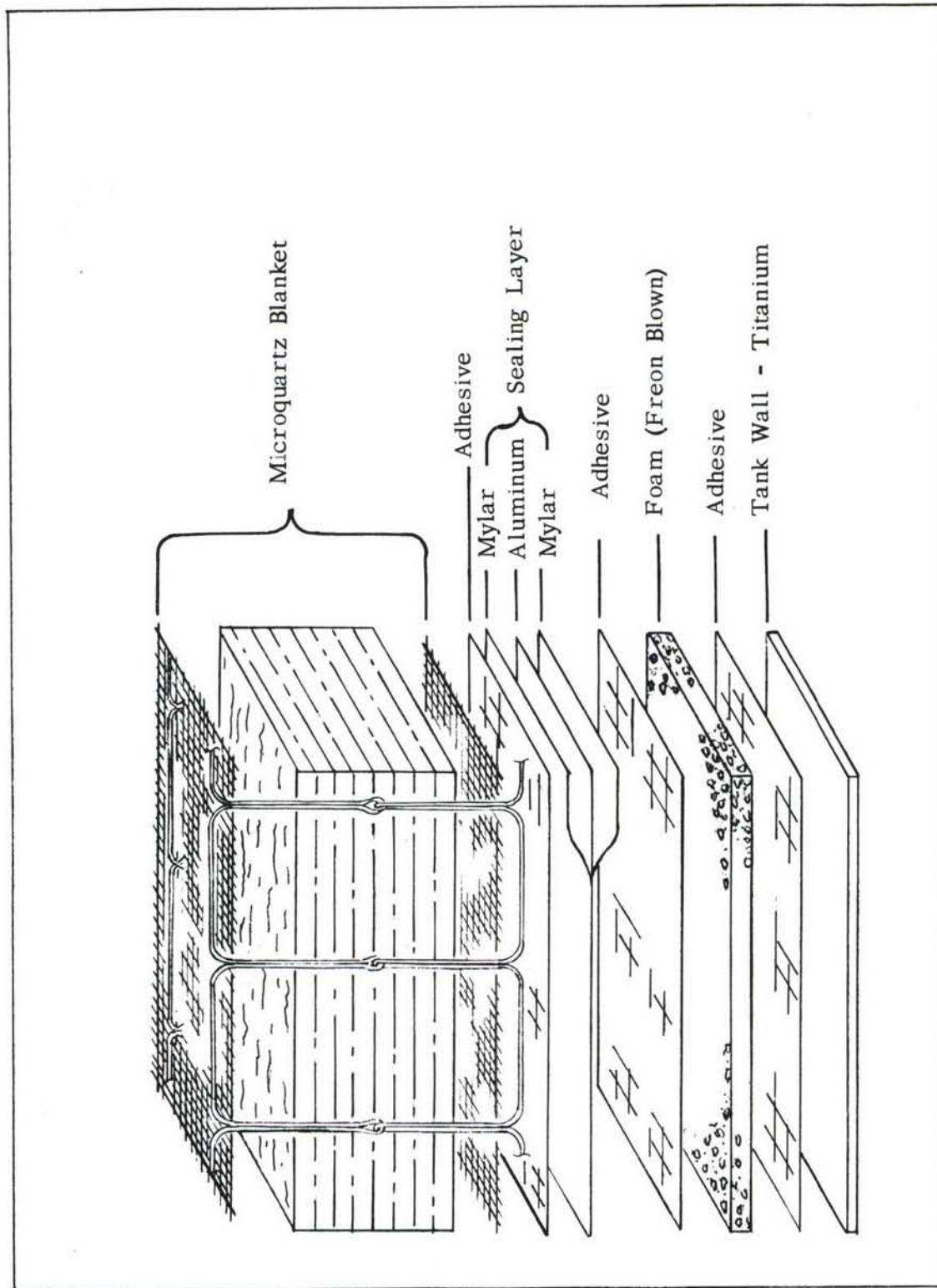


Figure 69. MICROQUARTZ/FOAM COMPOSITE INSULATION SYSTEM - TANK # 2

by the CPR Division of the Upjohn Company. This particular foam was selected since it has good forming characteristics, uniform cell size, and adequate flexibility at cryogenic temperature. The foam density is 4 lb/ft³ to gain additional strength for the cruise condition, when pressures of 15 to 20 psi exist in the cells with associated temperatures of 60° F. to 200° F. The tensile strength of 2 lb/ft³ foam varies between 30 and 50 psi at room temperature, and decreases significantly at 200° F. Since the physical properties vary directly with density, the tensile strength is doubled for 4 lb/ft³ foam. The total insulation system weight penalty incurred is small in view of the relatively thin layer foam required. The denser foam has the added advantage of better machining characteristics, allowing closer thickness tolerance control. The thermal conductivity is not affected by foam density variations, according to available data. Other types of foam were investigated, particularly the CO₂ blown polyurethanes. It was found the CO₂ blown foams have good high-temperature strength and stability characteristics, at the price of increased brittleness and poor forming characteristics. The cell sizes tend to be larger and more irregular than freon-blown foam. It was concluded that the freon-blown foam was the best compromise for the present application.

The foam is sealed by a bonded vacuum tight film consisting of a Mylar-Aluminum-Mylar composite trade-named Zero-Perm. This film has the necessary toughness and strength to remain leak-free through fabrication processes and service environment. The temperature limit of this material is 300° F., imposed by the Mylar.

The adhesive used throughout is Narmco 7343/7139 room temperature curing polyurethane. It has outstanding cryogenic properties, and will withstand temperatures in excess of 200° F. in the present application. This adhesive is solvent-free and, therefore, not susceptible to failures induced by trapped solvent vapor pressure. The Narmco adhesive also forms excellent bonds to Mylar and the tank material.

Sealed Foam Specimen Environmental Tests. A series of environmental tests were performed to verify the adequacy of the freon-blown foam and the Narmco 7343 adhesive at the temperature design limit of 200° F, and to establish the mode of failure of the foam sandwich in case of overheating. Narmco 7343 was used to bond the sandwich under vacuum bag pressure. Six candidate types of polyurethane foam were used to determine the behavior of foams with different densities and blowing agents. The test specimen design is shown in Figure 70.

The specimens were simultaneously tested in an environmental chamber provided with a view port and lights for observation during test. The procedure was to heat the specimens by convection to a predetermined temperature, and then evacuate the chamber to 8 mm Hg. The chamber controls did not allow simultaneous heating and evacuation. Four test runs were made from 150°F to 300°F, in 50° increments. All specimens survived the 200°F test condition without failure. At 250°F and 300°F both foam and adhesive failures occurred. The test results are shown in Table 3 and the failed specimens are shown in Figure 71.

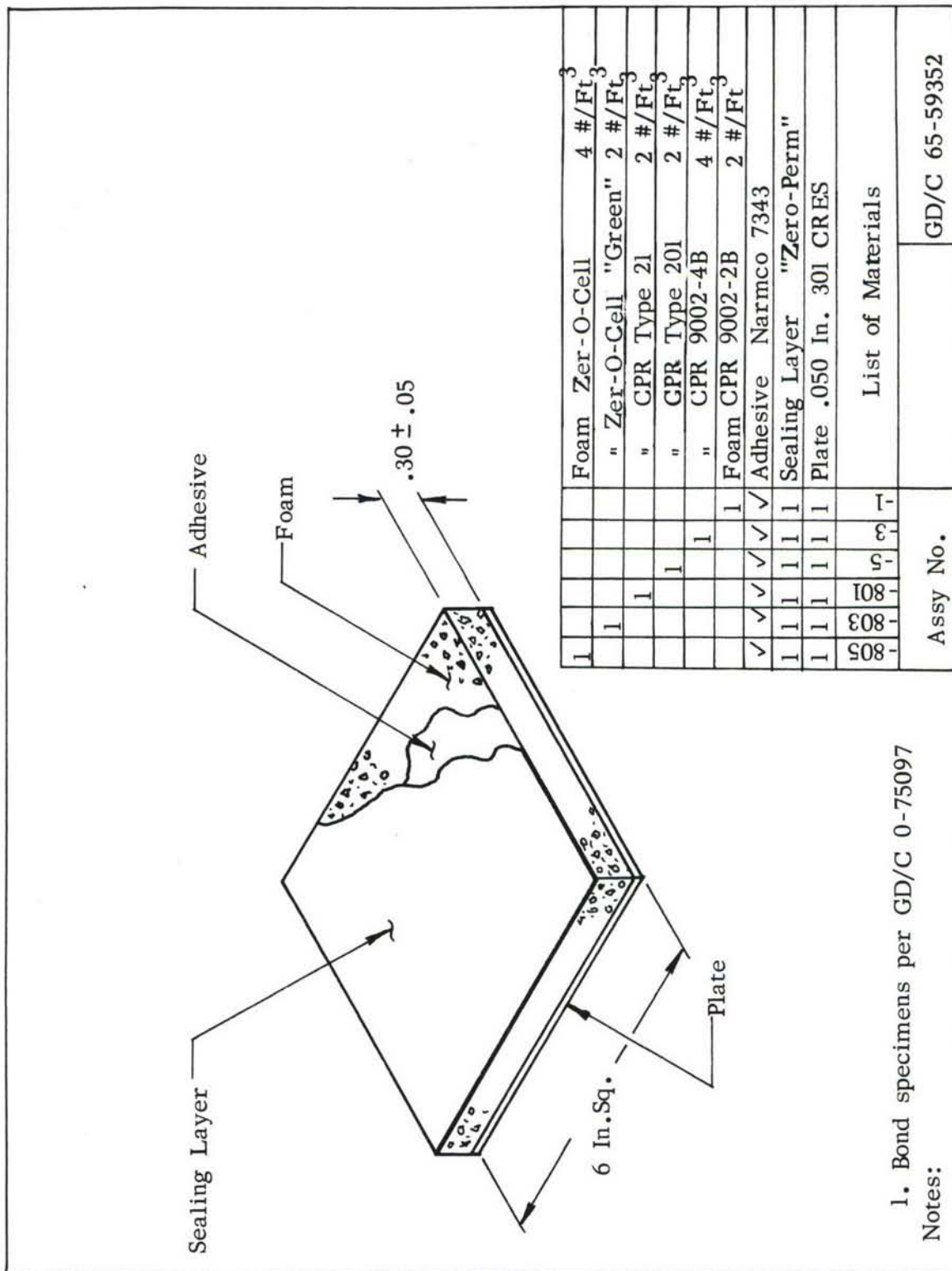


Figure 70 SEALED FOAM TEST SPECIMENS

Table 3 - SEALED FOAM SPECIMENS - TEST RESULTS

Assy No.	Foam			Failure Conditions			Remarks
	Density #/Ft ³	Blowing Agent	Mfg.	Type	Temp °F	Press mm Hg	
-1	2	Freon	CPR	9002-2B	300	760	"Bubble" developed during heat soaking, and expanded during evacuation.
-3	4	Freon	CPR	9002-4B	300	10	Bubble appeared after 10 mm Hg pressure was reached, and expanded gradually at low pressure
-5	2	Freon	CPR	201	250	10	Explosive rupture of foam at end of evacuation cycle.
-801	2	CO ₂	CPR	21	-	-	No Failure This foam shrunk in all directions during test. All other specimens expanded slightly.
-803	2	Freon	Zer-O-Cell National Gypsum Co	"Green"	300	10	Rapid failure of foam at end of evacuation cycle.
-805	4	Freon	Zer-O-Cell	4 Lb.	300	10	Small bubble developed at 10 mm Hg pressure and expanded gradually. Examination after test revealed that foam had also failed by bubble formation.

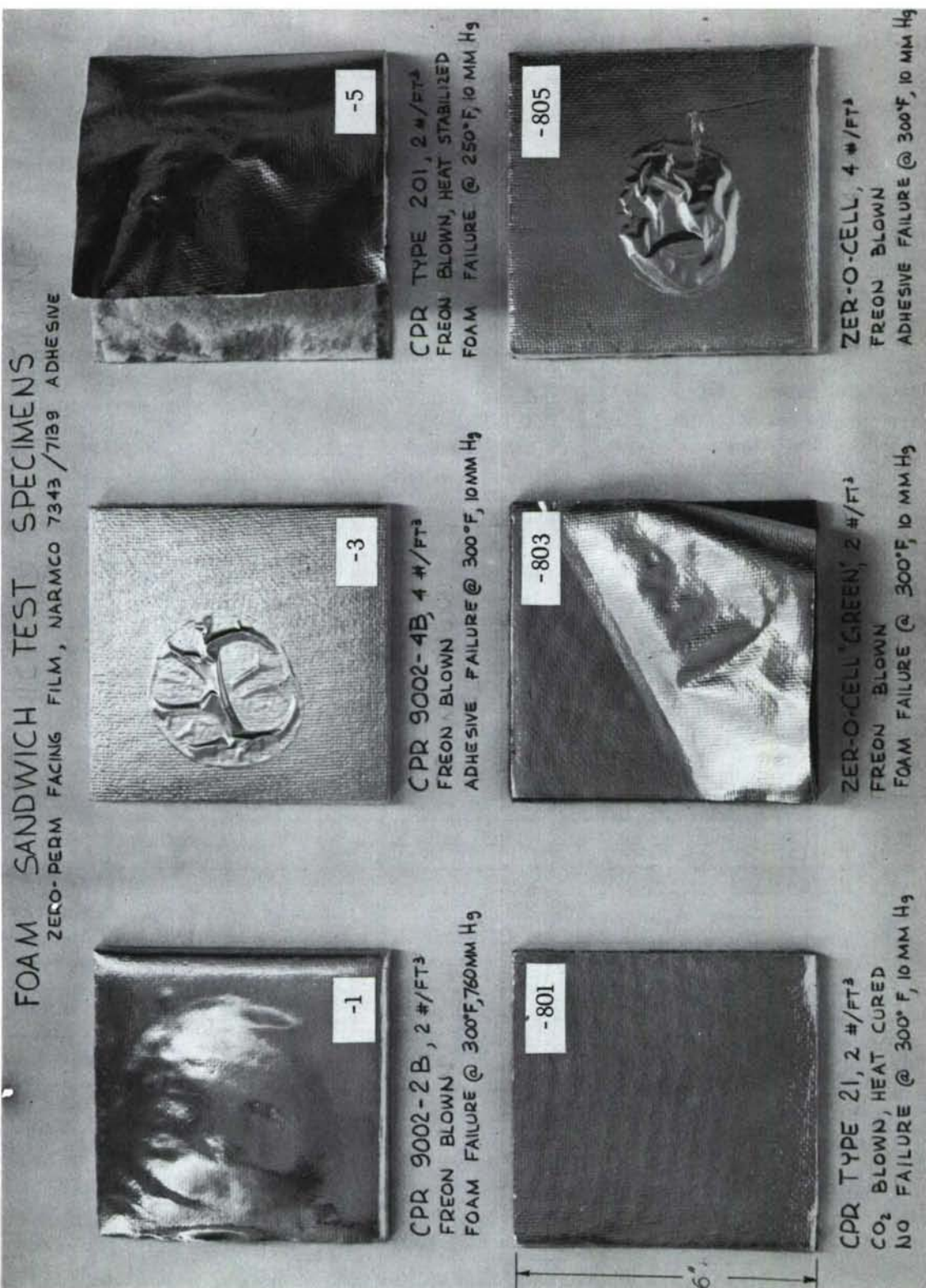


Figure 71 SEALED FOAM SPECIMENS - ENVIRONMENTAL TESTS

The adhesive failure always occurred between the Zero-Perm and the foam layer. These failures are attributed to softening of the adhesive, and were probably initiated by small air pockets in the bond layer. Foam failures were due to a combination of reduced material tensile strength at elevated temperature, and the bursting pressure developed in the cells. The explosive failure of the CPR 201 foam is attributed to brittleness developed during the heat-stabilization process used in material manufacture.

The CPR type 201 CO₂ blown material is identical to the foam used for the Saturn S-II external insulation. The foam is quite coarse-celled and brittle, but possesses good strength at high temperature. The thickness of the foam decreased gradually and uniformly during the tests, from .300 inch to .220 inch. No positive explanation has been found for this effect.

The tests indicated that 200⁰ F. is a realistic design limit temperature for the sealed foam layer, with a margin of the order of 50⁰. The tests also emphasize the importance of a continuous, void-free bond.

Fabrication. The insulation system detail fabrication was partially completed when Air Force Flight Dynamics Lab. discontinued work on Tank #2.

The Microquartz blanket fabrication was concluded, using the same procedure as employed for the all-Microquartz system. The sizing mockup was modified by addition of a layer of flexible foam to simulate the foam thickness on the tank. The foam details were completed to the point of forming the panels to the tank contour. The foam panel manufacturing sequence consisted of the following steps:

- a) Heat cure 2 feet x 4 feet foam sheets at 180⁰ to stabilize dimensions.
- b) Cut sheets to proper thickness.
- c) Layout and cut foam to flat pattern dimensions.
- d) Form sheets to contour on a mold by application of heat and vacuum pressure.

The following operations necessary to conclude the installation were not performed.

- a) Cut Zero-Perm to conform to foam sheet.
- b) Apply adhesive to the tank and outside face of foam, apply Zero-Perm, and bond assembly under vacuum bag load of 10 to 15 psi.
- c) Remove excess adhesive from panel joint areas, and trim adhesive - penetrated foam from panel edges.
- d) Fill gaps between panels with pour-in-place foam.
- e) Trim foam to proper thickness, and seal over with strips of Zero-Perm.
- f) Apply adhesive to Zero-Perm and bond Microquartz blanket under vacuum bag pressure of .50 psi.

5.2.3 CONCLUSIONS AND RECOMMENDATIONS FROM FABRICATION OF INSULATION

1. Fabrication of Microquartz insulation blankets in thickness above 1.38 inches requires the use of multiple blankets due to sewing machine limitations. This leads to additional weight for glass or quartz cloth. Future work will consider improved methods of blanket manufacture.

2. The use of adhesives for insulation attachment results in restrictive temperature limitations of the tank structure. Mechanical attachment methods which do not rely on adhesives will be investigated.

3. The quartz thread and quartz cloth have the required high temperature resistance, but cloth abrasion resistance and thread strength are barely adequate for this application.

4. The foam/Microquartz composite system is more sensitive to overheating than had been estimated. The tank wall temperature must be controlled to 438°R at the top and 335°R at the bottom in order to maintain a 200°F interface temperature. A wall cooling system is thus required. Future work on composite insulations should be directed towards development of materials with greater temperature tolerance.

5. The composite system integrity depends on void-free bonds between foam and sealing membrane. Adequate methods for verification of bond quality have yet to be developed. The effects of thermal cycling and tank structure flexure on service life must be established before the composite can be recommended for this application.

5.3 SUBSCALE TANK TESTING

The basic purpose of the subscale tank test program was to ensure tank structural integrity, verify the insulation system performance estimates, and verify the accuracy of the predictions regarding temperature stratification of the liquid and the ullage. The thermal test results provide the necessary tools for refining the optimization procedure prior to large scale tank final design. The tests also served to establish the compatibility of the insulation with the environment, and verify the soundness of structural design for application to liquid hydrogen tankage.

5.3.1 Structural Integrity and Leak Testing

5.3.1.1 Subscale Tank #1

The tank was hydrostatically tested with deionized water to the proof pressure of 135 psig. The procedure consisted of pressurizing the tank with nitrogen gas to between 10 and 20 psig, thus maintaining structural stability, and filling the tank with water.

The pressure was then increased in 20 psi increments from 20 to 120 psig, and held at each increment to obtain strain gage readings. The pressure was finally increased to 135 psig and held for 5 minutes. The tank was drained while the pressure was being reduced from 100 to 20 psig.

A leak was discovered at the aft frame joint with the cylindrical skin section. After completion of repairs, the tank was again proof tested to 135 psig at ambient temperature with water. Leaks were noted at the fill-drain and vent line flanges. The tank flanges were resurfaced and new seals were installed. The tank was then pressurized to 10 psig with nitrogen gas and the flanges were checked with bubble soap. No leaks were noted.

Strain gage readings taken during the water proof test indicated no appreciable permanent deformation of the material.

The tank was also proof tested with liquid nitrogen. The procedure was the same as that for the water test described above except that the tank was drained at a pressure of 20 to 40 psig. A bubble soap leak check was performed after the tank returned to ambient temperature. No leaks were noted.

The tank was then leak tested with a helium mass spectrometer. The tank was pressurized to 12 psig with helium gas. Polyethylene sheet was taped to the tank exterior, Figure 72, to collect any helium gas which might leak out of the tank. Leaks were noted at the fill-drain and vent flanges. The flanges were removed. New seals were installed using a thin film of Dow-Corning silicone vacuum grease to fill surface irregularities in the seal and mating flanges. The test was repeated and no leaks were noted.

5.3.1.2 Subscale Tank #2. The tank was subjected to water and LN_2 proof pressure tests at 135 psig. On the initial water test leaks were noted at tank welds. These were repaired and the water test was successfully repeated. The test procedure for these tests was the same as for Tank #1 except that strain gage readings were taken on the initial water test only. No other leakage was noted during the tests including a helium mass spectrometer check.

5.3.2 THERMAL TESTS. A series of tests were conducted on Subscale Tank #1 in the Space Simulation Chamber at the Convair Kearney Mesa Plant.

The purpose of these tests was to establish propellant thermal behaviour in the tank and insulation performance under transient temperature and pressure conditions.

5.3.2.1 Thermal Testing Approach. Various techniques for thermal scale modeling were investigated as possible approaches to the small scale tests. The investigation showed that conditions necessary to obtain thermal similarity involve significant differences in insulation materials and/or environmental conditions between the small and large scale tanks. A true thermal modeling technique requires either the use of fluids or insulating materials with properties that are non existent in nature, or the test parameters of time and temperature must be changed drastically to the

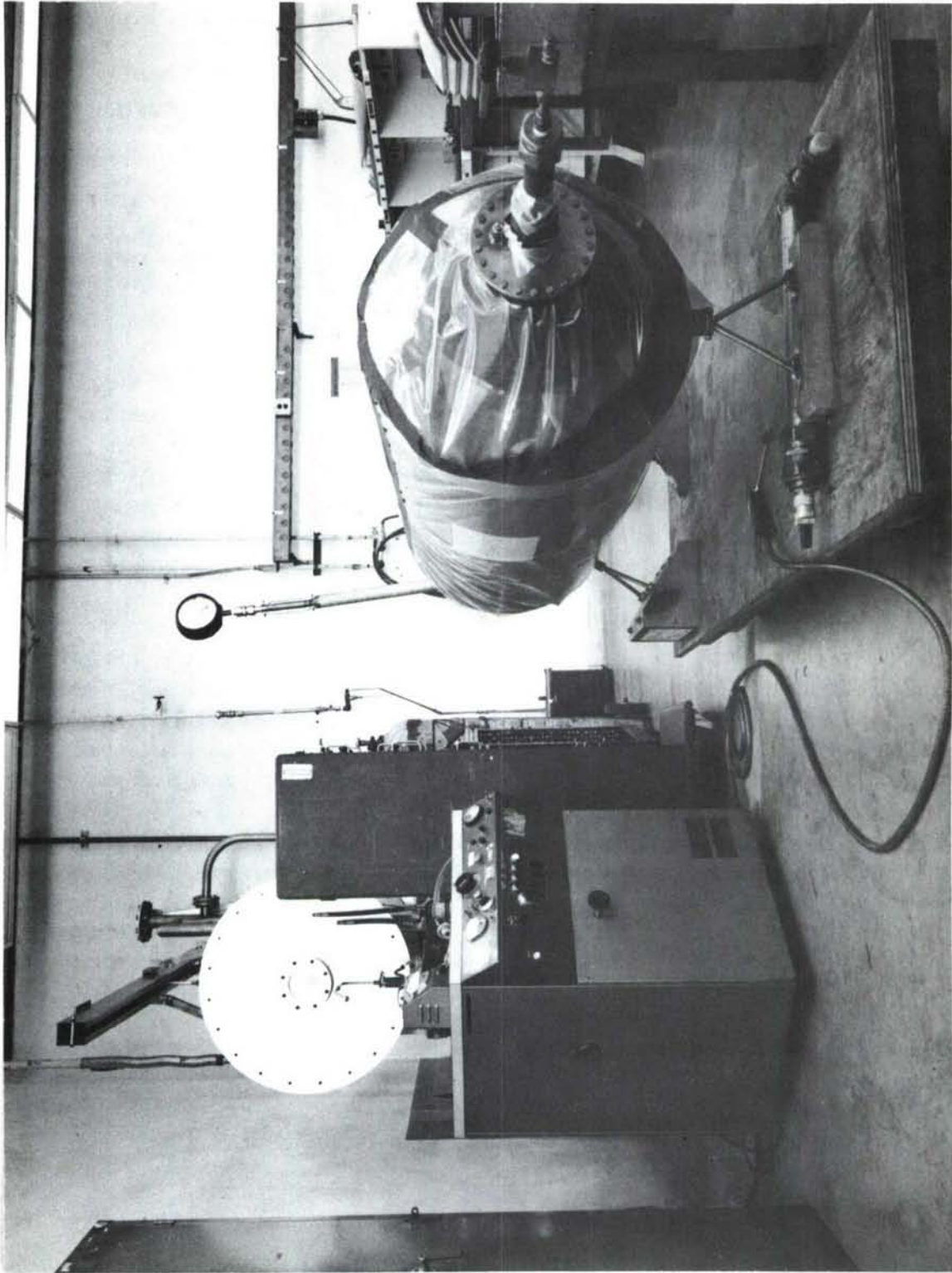


Figure 72. TANK # 1 HELIUM MASS SPECTROMETER LEAK CHECK.

point of infeasibility. It was concluded the objectives could best be met by performing separate tests to determine the heat flux to the ullage and liquid volumes.

The selected method enables the use of full-scale tank insulation material and thickness as well as the same environmental condition of heat flux, temperature, pressure and time imposed on the full-scale tank.

Three types of tests were used to provide the necessary data for optimization and design of the large scale tank.

LH₂ Stratification/Boil-off Cooling Effects Test. This test primarily investigated stratification in the horizontal tank geometry and the influence of both top and bottom heating on the bulk liquid temperature. The test was conducted by self-pressurizing to the tank operating pressure of 30 psia, and checking the temperature stratification in the liquid and the ullage. The test was concluded when the bulk liquid temperature reached the boiling point.

An additional objective of the stratification test was to determine the effects of boil-off cooling of the upper tank surface. The boil-off test was performed immediately after conclusion of the liquid stratification test. Since the amount of boil-off gas varies with the tank liquid level, the amount of tank cooling derived from the boil-off gas will also vary. The test established experimentally the structural temperatures as a function of time and liquid level.

LN₂ and LH₂ Conduction Tests. These tests were conducted to determine the transient temperatures in, and the heat leak to, the surface area of the tank covered with liquid. To minimize the influence of heat transfer to the ullage space, it was desirable to maintain the tank as full as possible during the test. This was accomplished by intermittent liquid topping. The heat flux thru the insulation was established by measuring the boil-off rates except during the topping period.

Transient Temperature Rise Test. The purpose of this test was to determine the transient temperature rise of the upper tank surface and the extent of ullage gas stratification under stagnant conditions. Since the subscale tank has a much smaller volume to surface area ratio than the large-scale tank, the liquid and gas temperatures will increase at a faster rate, and venting will occur earlier than in the large-scale tank.

For a representative experiment, the time at which boiling begins should be the same for the test tank and the full-scale tank. This objective was met by closing the vent valve at the beginning of the test and allowing the ullage to self-pressurize to 50 psia. After this point the liquid was drained at a rate to maintain 50 psia in the ullage. Thus the ullage space was allowed to stagnate and stratify to obtain a good simulation of the conditions at the upper tank wall.

5.3.2.2 Test Procedure. The following procedures are those which were used in conducting the tests in the space simulation chamber. The procedures are written

for liquid hydrogen tests with the differences for liquid nitrogen tests noted. Details such as valve designations have been eliminated to clarify the actual operations.

FACILITY CHECKOUT

1. Install the test tank in the chamber and connect all plumbing and electrical lines.
2. Check instrumentation.
3. Close the space simulation chamber
4. Evacuate the chamber below 10^{-3} Torr and leak test the chamber.
5. Maintain chamber pressure below 10^{-3} Torr for three hours to outgas all equipment.
6. Measure chamber leakup rate by closing pumping valves and observing chamber pressure rise rate.

LIQUID NITROGEN PROOF PRESSURE CYCLE

1. Fill the test tank to 80% with liquid nitrogen having a vapor pressure of 10 psig or greater.
2. Maintain 10^{-3} Torr or lower pressure in the chamber.
3. Pressurize the test tank to 100 psia using helium gas, if necessary.
4. Test relief and fill drain valves as pressure increases. Note relief valve set points.
5. Return liquid nitrogen to the storage dewar.
6. Vent test tank to atmospheric pressure.
7. Evacuate test tank to 0.1 Torr or less.
8. Pressurize test tank with helium gas and check chamber helium content with a mass spectrometer leak detector.
9. Pressurize test tank to above 14.7 psia.
10. Pressurize chamber to 700 mm Hg with helium gas.

FILL AND GROUND HOLD STABILIZATION

1. Purge and pressurize test tank to 16.7 psia (20 psia for liquid nitrogen tests) with helium gas.
2. Evacuate chamber and pressurize to 700 mm Hg with helium gas.

3. Fill tank to 90% level (95% for liquid nitrogen tests).
4. Maintain 16.7 psia tank pressure (20 psia for liquid nitrogen tests)
5. Maintain liquid level at 75 to 90% (85 to 95% for liquid nitrogen tests) by intermittent topping.
6. Maintain radiation shield at 490°R .
7. Allow tank to stabilize.

TRANSIENT CONDUCTION TRAJECTORY

1. Complete ground hold stabilization.
2. Fill tank to 95% (100% for liquid nitrogen test).
3. Allow level to drop to 90% (95% for liquid nitrogen tests).
4. Maintain 16.7 psia tank pressure (20 psia for liquid nitrogen tests).
5. Start chamber evacuation program.
6. Four minutes after step 5 start aerodynamic heating program.
7. Maintain liquid level between 75 and 90% by intermittent topping. (No topping required for liquid nitrogen tests).
8. Terminate test when:
 - a) 90 minutes have elapsed since step 5, or
 - b) Tank skin temperature exceeds 760°R .
9. Turn off heat lamps.
10. Pressurize chamber to 700 mm Hg with helium gas.
11. Allow the tank insulation to cool.
12. Drain residual liquid from the tank.
13. Purge test equipment to remove residual hydrogen gas (not required for LN_2 tests).

LIQUID STRATIFICATION INVESTIGATION

1. Complete ground hold stabilization.
2. Fill tank to 95% level.
3. Maintain a liquid level of 90 to 95% for 30 minutes by intermittent topping.
4. Maintain tank pressure at 16.7 psia.
5. Maintain chamber pressure at 700 mm Hg.
6. Maintain radiation shield temperature at 30°F.
7. Fill tank to 95% level.
8. When level drops by boiloff to 90%, close vent and allow tank to self-pressurize to 30 psia.
9. Maintain 30 psia tank pressure by venting until liquid temperatures stabilize.
10. Continue with boiloff cooling effects test.

BOILOFF COOLING EFFECTS TEST

1. Maintain 30 psia tank pressure by venting.
2. When liquid temperatures stabilize begin chamber evacuation program.
3. Four minutes after step 2 start aerodynamic heating program.
4. Terminate test when:
 - a) 91 minutes have elapsed since step 2, or
 - b) Tank skin temperature exceeds 860°R, or
 - c) Tank liquid level drops below 40%.
5. Turn off heat lamps.
6. Pressurize chamber to 700 mm Hg. with helium gas.

7. Allow the tank insulation to cool.
8. Drain the residual liquid from the tank.
9. Purge test equipment to remove residual hydrogen gas.

TRANSIENT ULLAGE TEMPERATURE RISE TEST

1. Complete ground hold stabilization.
2. Fill tank to 95% level.
3. Maintain 16.7 psia tank pressure.
4. When level drops to 90% by boiloff simultaneously do steps 5 and 6.
5. Close vent and allow tank pressure to rise to 50 psia.
6. Start chamber evacuation program.
7. Four minutes after step 6 start aerodynamic heating program.
8. When tank pressure reaches 50 psia begin draining liquid at a rate to maintain 50 psia tank pressure.
9. When liquid level reaches 40% stop draining and allow tank pressure to rise to a maximum of 90 psia.
10. Vent tank pressure slowly to 16.7 psia.
11. While venting turn off heat lamps.
12. Pressurize chamber to 700 mm Hg.
13. Allow the tank insulation to cool.
14. Drain the residual liquid from the tank.
15. Purge test equipment to remove residual hydrogen gas.

5.3.2.3 Test Setup. The subscale tank tests required a facility capable of simulating the temperature and pressure profile predicated for the vehicle tankage. The tests were performed in a large environmental test chamber which provided the pressure environment. This chamber is 12 feet in diameter by 19 feet long, and uses both diffusion

and mechanical pumps for evacuation, with a capability of 10^{-5} torr. A schematic diagram of the test tank installation is shown in Figure 73. Since the test facility is located within the General Dynamics Convair main plant at Kearny Mesa, an investigation was made of the possible safety hazards associated with liquid hydrogen testing. The results of this study showed that the tests did not involve a safety hazard provided the specified operating procedures are followed.

A schematic of the subscale tank test setup is shown in Figure 74. The setup consists of a vacuum jacketed fill and drain system, a vent and boiloff measuring system, and a purge system using both helium and nitrogen. The majority of the control valves were located outside of the test chamber for easy access and maintenance. The liquid hydrogen and nitrogen were supplied directly from ground support trailers and the helium from standard bottles.

The vent and boiloff measuring system incorporates a pressure relief valve, a motor operated tank pressure control valve, and a flowmeter circuit to measure the boiloff rate.

The test tank was mounted on a triangular platform with three columns, Figure 66. The platform was in turn mounted through three load cells to a steel cradle which rested on the chamber structure.

A furnace assembly consisting of a 60-inch diameter by 72-inch long cylinder was also mounted to the cradle and surrounded the central portion of the test tank. One hundred thirty-six type 500 T3/CL/HT 500 watt quartz infrared lamps were mounted in the furnace to heat the 35-inch diameter, 72-inch long radiation shield. The radiation shield served as a simulated vehicle "hot structure". The furnace shell was protected from excessive heat by two inches of Thermoflex 300 insulation. The insulation was held in place between the shell and the lamps by polished nickel reflectors attached to the shell at each heat lamp location. The reflectors served to minimize local "hot spots" on the insulation and radiation shield.

Heat lamp power was controlled by two THERMAC and nine LABAC temperature controllers. The use of these controllers made possible eleven zones of temperature control on the radiation shield to minimize temperature gradients. The controllers were programmed using two DATA TRACK units to simulate transient vehicle structure temperatures on the radiation shield.

5.3.2.4 Instrumentation. Recorded instrumentation consisted of chromel-alumel and copper-constantan thermocouples, platinum temperature probes, strain gage type pressure transducers, strain gage type load cells, carbon resistor liquid level sensors, a capacitance liquid level sensing system, a 10,000 cubic foot per hour positive displacement gas flowmeter, and temperature compensated strain gages. In addition visual

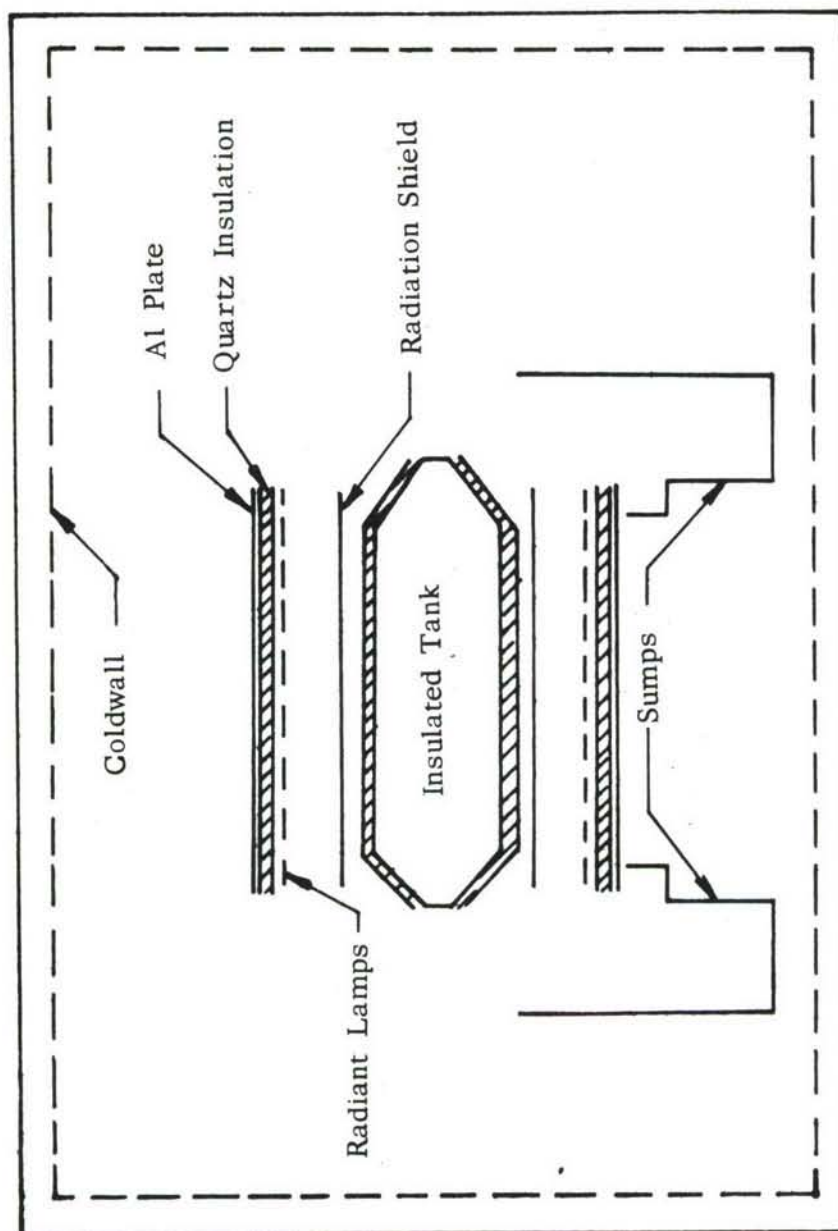
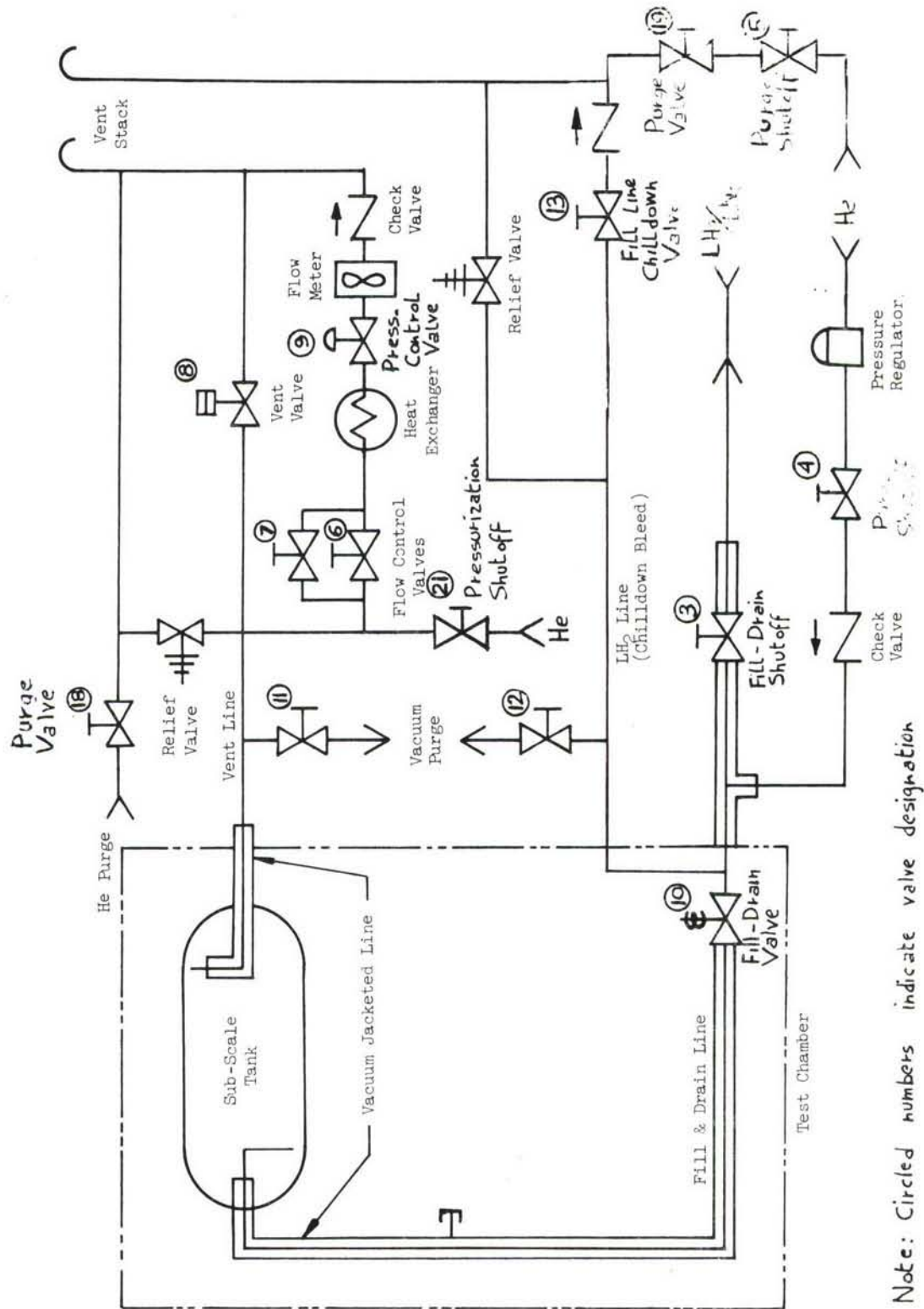


Figure 73. SCHEMATIC DIAGRAM OF TEST TANK INSTALLATION



Note: Circled numbers indicate valve designation

FIGURE 74. SUBSCALE TANK FUEL SYSTEM SCHEMATIC

gages were used to monitor test tank and chamber pressure.

The instrumentation locations, transducer selection and measurement range for the Inconel tank tests have been tabulated and are presented in Table 4. The location dimensions are in inches from a reference point located at the aft end of the cylindrical portion of the tank on the tank centerline, Figure 75. Test data was recorded in digital form on a Dymec Model 2010G recorder. The punched paper tape record was reduced using the IBM 7090 digital computer system and program number 3530. This program converts the recorder voltage output to engineering units and tabulates and plots selected data channels. The plotting portion of the program uses an SC 4020 plotter.

Transducers at locations in the liquid and ullage were supported on tubular frameworks mounted in the tank from the frames. Those on the tank skin and penetrations were mounted directly on the surface. The thermocouples in the insulation blanket were stitched into the blanket during fabrication.

Copper constantan and chromel alumel thermocouples were selected for the majority of the temperature measurements because of their availability, low cost, accuracy, and electrical output characteristics. Since greater accuracy in the measurement of liquid temperatures is required during the liquid stratification tests, a miniature platinum resistance transducer was selected for these measurements. The transducer is manufactured by Rosemount Engineering Company under the model designation 118L. A special bridge circuit was designed to permit high sensitivity in the liquid hydrogen temperature range while still permitting coverage of the entire temperature span.

The FNB-50-12E strain gages were used primarily for evaluation of the gage performance under field test conditions. For this reason the gages have been placed at locations in the tank where discontinuities are at a minimum. Strain gage results are presented in Appendix II.

Figure 76 shows some of the internal and external instrumentation installed on the tank.

Several instrumentation failures were encountered which, while significant, did not invalidate the tests. The capacitance liquid level system did not perform satisfactorily on any test. The probable cause of this failure was changes in lead wire capacitance with variations in temperature and pressure. The load cells were found to be sensitive to external pressure changes and therefore are not sufficiently accurate to provide liquid level or boiloff data better than that which was obtained by other measurements. Three platinum probes failed at various times during the first eight tests. These failures were probably a result of lead wire breaks or shorts. A failure in the

Channel	Measurement	Transducer	Range	Recorder Range	Location			Remarks
					X	Y	Z	
1	Temperature	Cu. Cn.	0 - 880°R	-10 to + 10 MV	55.80	0	11.50	Ullage Temperature
2					30.00	0	11.50	Ullage Temperature
3					4.30	0	11.50	Ullage Temperature
4					55.80	0	12.00	Tank Top
5					42.80	0	12.00	Tank Top
6					31.60	0	12.00	Tank Top
7					17.30	0	12.00	Tank Top
8					4.30	0	12.00	Tank Top
9					55.80	-10.40	6.00	Tank 30°
10					43.30	-10.40	6.00	Tank 30°
11					4.30	-10.40	6.00	Tank 30°
12					42.30	-6.00	10.40	Tank 60°
13					30.00	-12.00	0	Tank 0°
14					63.60	0	9.00	Cone Skin
15					67.30	0	6.00	Cone Skin
16					-13.25	0	-1.75	Vent Flange
17					-13.25	0	0	Vent Gas Temperature
18					73.25	0	-1.75	Fill Flange
19	Temperature	Chr. Al.	0 - 880°R	-10 to + 10 MV	0	.77	-13.53	Lateral Support Lug
20					59.23	-6.77	-11.72	Long. Support Lug
21					30.00	0	12.25	Top Insul.
22					30.00	0	12.50	Top Insul.
23					30.00	0	12.88	Top Insul.
24					30.00	0	13.25	Top Insul.
25					30.00	0	-12.38	Bottom Insul.
26					30.00	0	-12.88	Bottom Insul.
27					30.00	0	-13.38	Bottom Insul.
28					30.00	0	-14.75	Bottom Insul.
29					30.00	0	-16.00	Bottom Insul.
30					30.00	12.38	0	Side Insul.
31					30.00	12.75	0	Side Insul.
32					30.00	13.25	0	Side Insul.
33					30.00	14.50	0	Side Insul.
34					55.80	0	12.25	Top Insul.
35					55.80	0	13.25	Top Insul.
36					4.30	0	13.25	Top Insul.
40					12.00	0	-16.00	Bottom Insul.
41					12.00	0	-12.38	Bottom Insul.
42					55.80	12.38	0	Side Insul.

TABLE 4. SUBSCALE TANK INSTRUMENTATION

Channel	Measurement	Transducer	Range	Recorder Range	Location			Remarks
					X	Y	Z	
44	Temperature	Chr. Al.	0 - 1800°R	-10 to + 30 MV	4.30	12.38	0	Side Insul. Side Insul. Cone Insul. Cone Insul. Long. Support Leg Lateral Support Leg Radiation Shield Radiation Shield Top Insul. Side Insul. Bottom Insul. Bottom Insul.
45					4.30	14.50	0	
46					63.80	0	9.20	
47					64.60	0	10.00	
48					67.60	0	6.00	
49					65.20	10.80	0	
50					63.80	9.20	0	
51					67.60	6.00	0	
52					65.90	0	-11.70	
53					63.80	0	-9.20	
54					67.60	0	-6.00	
55					58.70	-7.50	-13.42	
56					.25	1.30	-15.50	
57					3.00	10.24	-15.59	
58					3.00	3.58	-18.53	
59					3.00	-10.24	-15.59	
60					52.90	-10.24	-15.59	
61					52.90	10.24	-15.59	
62					57.00	15.29	-9.91	
63					30.00	-3.58	-18.53	
64					30.00	16.92	-5.87	
65					57.00	-13.43	9.82	
66					3.00	-13.43	9.82	
67					3.00	-3.04	15.83	
68					30.00	-3.04	15.83	
69					4.3	0	12.25	
70					55.80	14.50	0	
71					55.80	0	-12.38	
72					55.80	0	-16.00	
80	Temperature Boiloff Rate Cum. Boiloff Cum. Boiloff Tank Pressure Chamber Pressure Flowmeter Exhaust Continuous Liq. Level Weight Weight Weight	Chr. Al.	0 - 1800°R	-10 to + 30 MV	-	-	-	Tests 4 through 9 only
81		Rockwell	0 - 20,000 CFH	0 to 100 MV	-	-	-	
82		Rockwell	0 - 1000 SCF	0 to 10 MV	-	-	-	
83		Rockwell	0 - 10 SCF		-	-	-	
84		Statham	0 - 100 psia		-	-	-	
85		Statham	0 - 15 psia		-	-	-	
86		Statham	0 - 10 psid		-	-	-	
87		Capacitor	1 to 23 inches		1.30	-2.25	-11 to + 11	
88		Baldwin			-4.00	0	-36.40	
89		Baldwin		0 to 10 MV	47	47	-36.40	

TABLE 4. SUBSCALE TANK INSTRUMENTATION (CONTINUED)

Channel	Measurement	Transducer	Range	Recorder Range	Location			Remarks
					X	Y	Z	
90	Point Liq. Level	Carbon Resistor	17.25 ft ³ , 94.96%	-10 to +10 MV	.30	3.25	9.50	Tests 1 through 4
91			16.50 ft ³ , 90.93%		.30	3.25	8.25	Not used for Tests 5 through 9
92			17.25 ft ³ , 94.96%		.30	3.25	9.50	Tests 1 through 4
93			15.61 ft ³ , 85.90%		.30	3.25	7.00	Tests 5 through 9
94			16.50 ft ³ , 90.93%		.30	3.25	8.25	Tests 1 through 4
95			14.62 ft ³ , 80.40%		.30	3.25	5.75	Tests 5 through 9
96			15.61 ft ³ , 85.90%		.30	3.25	7.00	Tests 1 through 4
	Point Liq. Level	Carbon Resistor	13.74 ft ³ , 75.61%		.30	3.25	5.75	Tests 5 through 9
			14.62 ft ³ , 80.40%		.30	3.25	3.75	Tests 1 through 4
			12.81 ft ³ , 70.53%		.30	3.25	4.75	Tests 5 through 9
			13.74 ft ³ , 75.61%		.30	3.25	-1.75	Tests 1 through 4
			7.31 ft ³ , 40.23%		.30	3.25		Not used for Tests 5 through 9
97	Flowmeter Vent Temp. Temperature	Cu. Cn. Platinum Res.	0 - 880°R		29.00	0	8.00	
180			0 - 660°R		29.00	0	7.50	
181					29.00	0	7.00	
182					29.00	0	6.00	
183					29.00	0	5.00	
184					29.00	0	4.00	
185					29.00	0	0	
186					29.00	0	-4.00	
187					29.00	0	-8.00	
188					29.00	4.10	8.00	
189					29.00	6.70	6.00	
190					29.00	8.00	4.00	
191					29.00	9.00	0	
192					29.00	4.00	0	
193	Temperature Strain	Platinum Res. FNB-50-12E	0 - 660°R	-10 to +10 MV	43.60	-10.40	6.00	Longitudinal Outside
194			0 - 10,000 μ in/in	0 to +10 MV	43.60	-10.40	6.00	Longitudinal Inside
195					42.80	-10.40	6.00	Hoop Outside
196					42.80	-10.40	6.00	Hoop Inside
197					42.80	-6.00	10.40	Hoop Outside
198	Strain	FNB-50-12E	0 - 10,000 μ in/in	0 to +10 MV	42.80	-6.00	10.40	Hoop Inside
199								

TABLE 4. SUBSCALE TANK INSTRUMENTATION (CONTINUED)

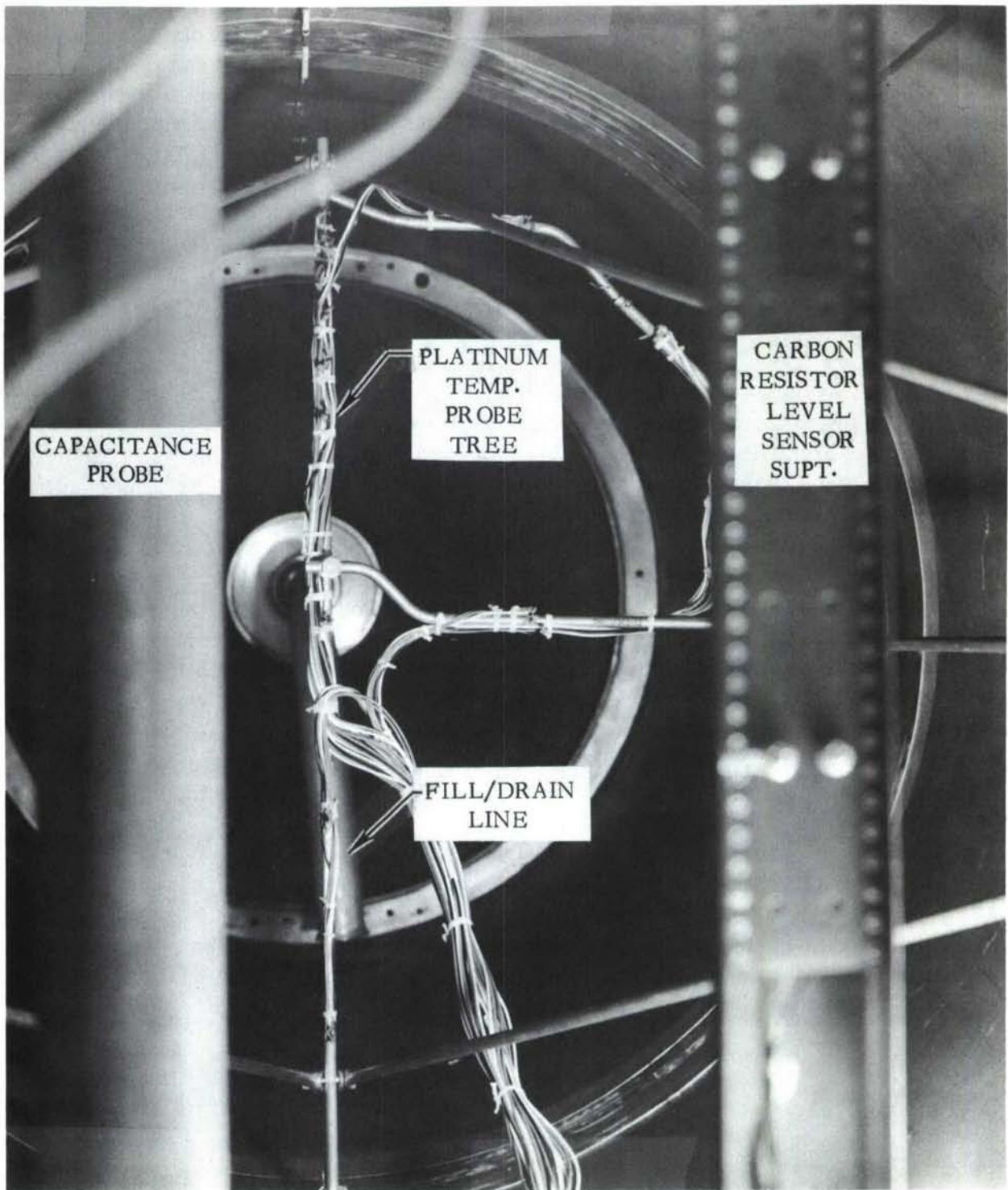


FIGURE 76. SUBSCALE TANK #1 - LIQUID LEVEL & TEMPERATURE SENSORS

platinum probe power supply between tests eight and nine damaged a zener diode in the signal conditioning system and resulted in the loss of all platinum probe data for test nine. A connector was improperly installed during reinstallation of the tank for test four. This resulted in the loss of ullage and vent gas temperature measurements for test 4. This was repaired prior to test 5. Two strain gages failed at various times during the test series probably due to broken or shorted lead wires. The 40% level carbon resistor level sensor did not perform on any test. A rotation of wiring between tests 4 and 5 resulted in the loss of the 70% carbon resistor and misidentification of the other sensors. The power supply failure between tests 8 and 9 also damaged the tank pressure transducer. Tank pressures for test 9 were manually recorded from a mercury manometer. All other instrumentation either performed satisfactorily or failed only at times when it was not significant in evaluating the test results.

One-half hour after the start of Test 3 the wiring inside the chamber which supplied power to the heat lamps was observed smoking. The test was stopped and the chamber was backfilled with helium gas. Damage to the power wiring was extensive. The test tank and fixture were removed from the chamber for repairs. The cause of the electrical insulation damage was due to the reduced convective heat transfer and outgassing (or boiling) in the rarified (8 mm Hg) atmosphere. The insulation was also charred and blistered where it was near the aluminum shell of the furnace assembly. This apparently resulted from the overheating which caused a dielectric breakdown of the insulation permitting arcing to occur between the wire and the furnace assembly. The insulated wire was qualified for 270° C. However, this qualification is based on an environment of 1 atm pressure in air. The furnace was rewired with bare #10 solid copper wire installed to provide a large gap between the wire and the furnace. The furnace shell was blackened to increase the heat transfer rate to the chamber wall, thereby reducing the plate temperatures. A view of the test tank and wiring installed in the chamber is shown in Figure 77.

5.4 THERMAL TEST RESULTS

Nine tests were conducted on Tank #1 in the space simulation chamber. These were as follows:

- | | |
|--------|--|
| Test 1 | Facility checkout and proof pressure cycle to 100 psi with liquid nitrogen in the test tank. |
| Test 2 | Liquid nitrogen fill and stabilization at ground hold conditions. |
| Test 3 | Liquid nitrogen transient conduction trajectory run. |
| Test 4 | Repeat of Test 2 and Test 3 |
| Test 5 | Liquid hydrogen fill and stabilization at ground hold conditions. |

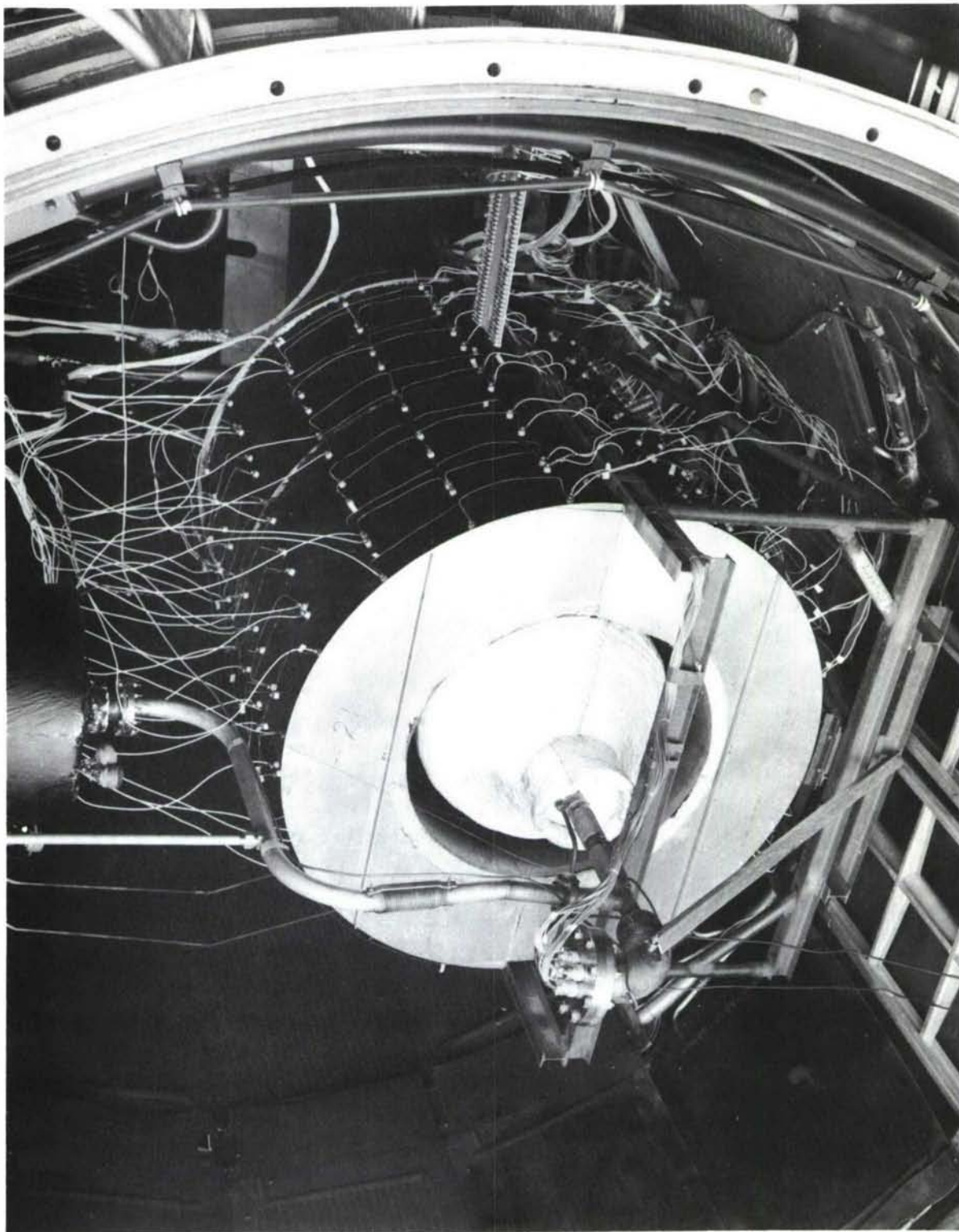


Figure 77. TEST TANK INSTALLED IN ENVIRONMENTAL CHAMBER

Test 6	Liquid hydrogen transient conduction trajectory run.
Test 7	Liquid hydrogen stratification investigation at ground hold conditions.
Test 8	Liquid hydrogen boiloff cooling effects trajectory run.
Test 9	Liquid hydrogen transient ullage temperature rise trajectory run.

All data recorded during tests 2 through 9 was reduced to engineering units and by digital computer and plotted on the SC 4020 plotter. A complete set of this data (approximately 300 graphs) is on file in the Flight Dynamics Laboratory, Wright-Patterson Air Force Base, Ohio. The data presented in this report is limited to that which is used to correlate with pre-test predictions and to illustrate problem areas or unusual conditions of interest.

5.4.1 TEST 1. Test 1 was completed on 13 August 1965. A small leak was noted in the liquid fill line. The leak was between the fluid portion of the line and the vacuum jacket which made it difficult to locate and repair. The decision was made to continuously evacuate the vacuum jacket to prevent the accumulation of cryogenic fluid in the jacket and proceed with the liquid nitrogen tests. The vacuum jacket was therefore connected to a vacuum pumping system through an existing chamber pass-through fitting. No other significant problems were encountered. Since this was primarily a checkout test, no data of any importance was generated. The peak tank pressure was 100.6 psia.

A practice chamber pump down was made to determine the proper pumping schedule for trajectory simulation. It was found that six pumps (maximum system capacity) was required to maintain the trajectory schedule with a slight lag at about 1.0 psia. It was therefore decided to turn the radiant lamps on four minutes after start of pump down to obtain the best pressure temperature relationship.

5.4.2 TEST 2. Test 2 was run with LN_2 to check out the radiant lamp furnace and the automatic power control system. The power control system was turned "on" and set to control to the ground hold temperature of $490^{\circ} R$. The test tank was filled with LN_2 and chilled down. Before the radiation shield had reached $490^{\circ} R$, the power came "full on" inadvertently while the instrumentation was being checked. The power control was found defective. This discrepancy was corrected while the test tank was maintained full of LN_2 . Test data was recorded for about four hours while the checkout was completed and repairs made.

5.4.3 TEST 3. Test 3 was the first complete trajectory run with LN_2 . The test was performed immediately following Test 2. The circuit breaker on one ignitron power supply tripped at approximately 4.45 hours. The breaker was reset and the test continued, although a deviation from the temperature trajectory existed, Figure 78.

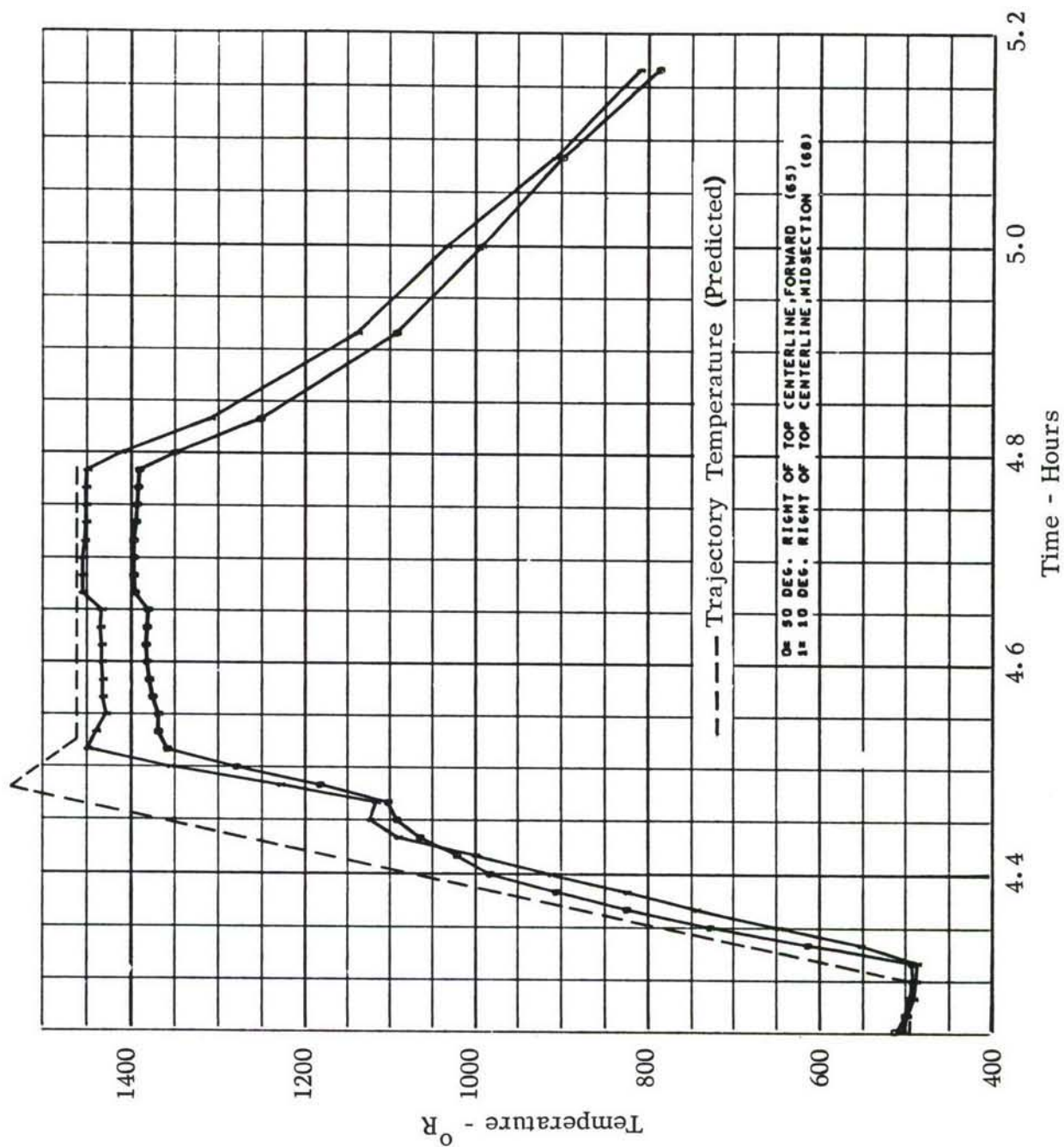


FIGURE 78. RADIATION SHIELD TEMPERATURE - TOP - TEST 3

The test was terminated at 4.78 hours due to a heat lamp power wiring failure and high tank skin temperatures. The subscale tank pressure is presented in Figure 79. Initial pressure data was found to be approximately 4 psia low. The data presented is corrected for this discrepancy by shifting all values 4.0 psi. Liquid level in the test tank, Figure 80, was established by the carbon resistors and by using the platinum probes as point level sensors. Values of liquid level were extrapolated from these points by using integrated boiloff values. Figure 81 presents the heat flux rate to the liquid, boiloff, and predicted heat flux rate. Boiloff was established from the total boiloff gas measured at the flow meter and converted, using heat of vaporization at test tank pressure, to heat flux rate. Pressure variations in the tank during the test resulted in changes in the sensible heat of the liquid. Since these changes represent a sizable portion of the total heat flux to the liquid, they have been accounted for in the heat flux curve in Figure 81. The average bulk temperature of the liquid was computed by assigning portions of the total liquid volume to each of the platinum probes and computing a weighted mean temperature at each data time. The temperatures were then smoothed and the heat flux rate representing the rate of temperature change was computed. These values were added to the boiloff to represent the total heat flux rate to the liquid. The heat flux in Figure 81 is a smoothed curve of these values. The heat flux prediction was computed using actual values of liquid level during the test.

It was necessary after Test 3 to remove the test tank from the chamber to repair the power wiring. During this period, several other discrepancies were also corrected. The liquid fill line leak was located and repaired. The test tank pressure transducer was recalibrated. One of the two chamber pressure transducers was relocated to measure gas pressure at the flowmeter. The test tank was leveled in the chamber. Data indicates that the tank was approximately one inch out of level during Tests 1, 2 and 3.

5.4.4 TEST 4. Test 4 was performed on 25 August. This was a second liquid nitrogen trajectory run. Because of the extent of the repairs and modifications made following Test 3, it was advisable to check the systems with another liquid nitrogen test before proceeding with the liquid hydrogen tests. Figure 82 presents the chamber pressure and the predicted trajectory pressure. The actual and predicted radiation shield temperatures are presented in Figure 83 for the bottom surface. Limited power to the bottom heat lamps prevented achieving the desired temperature rise rate from about 1300°R to 1700°R . This did not, however, significantly affect the test results. The chamber pressure and bottom radiation shield temperature depicted here are representative of the values obtained during all tests with trajectory simulation. The test tank pressure is presented in Figure 84. Liquid level was the same as during Test 3 (Figure 80). Boiloff, heat flux, and predicted heat flux are presented in Figure 85. The relatively large absolute pressure change during the test accounts for the difference between the equivalent heat flux due to boiloff and the actual heat flux to the liquid. Tank skin temperatures at various locations along the top of the tank are presented in Figure 86. The highest tank skin temperatures during all of the testing occurred in this test, 750°R .

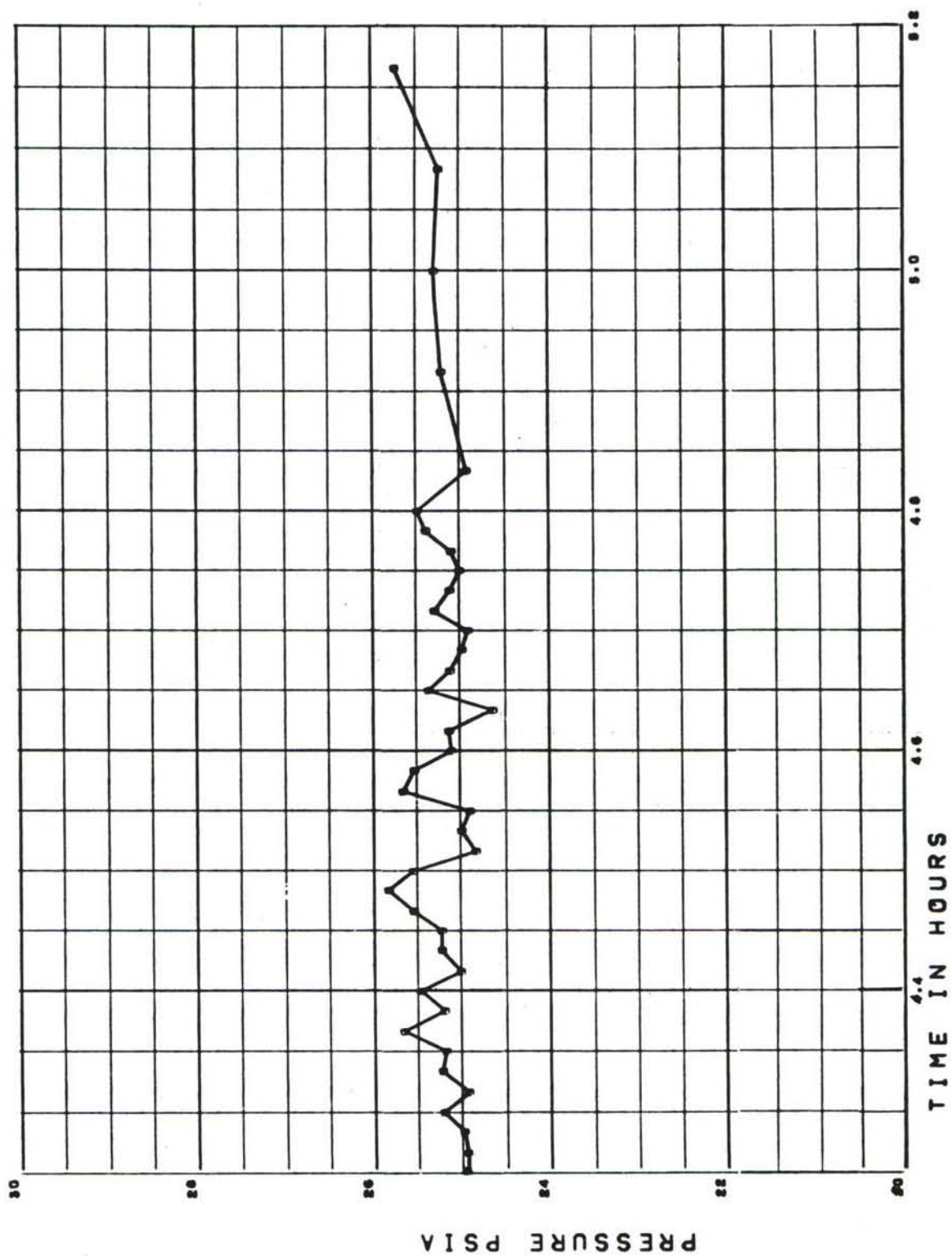


Figure 79. SUBSCALE TEST TANK PRESSURE - TEST 3

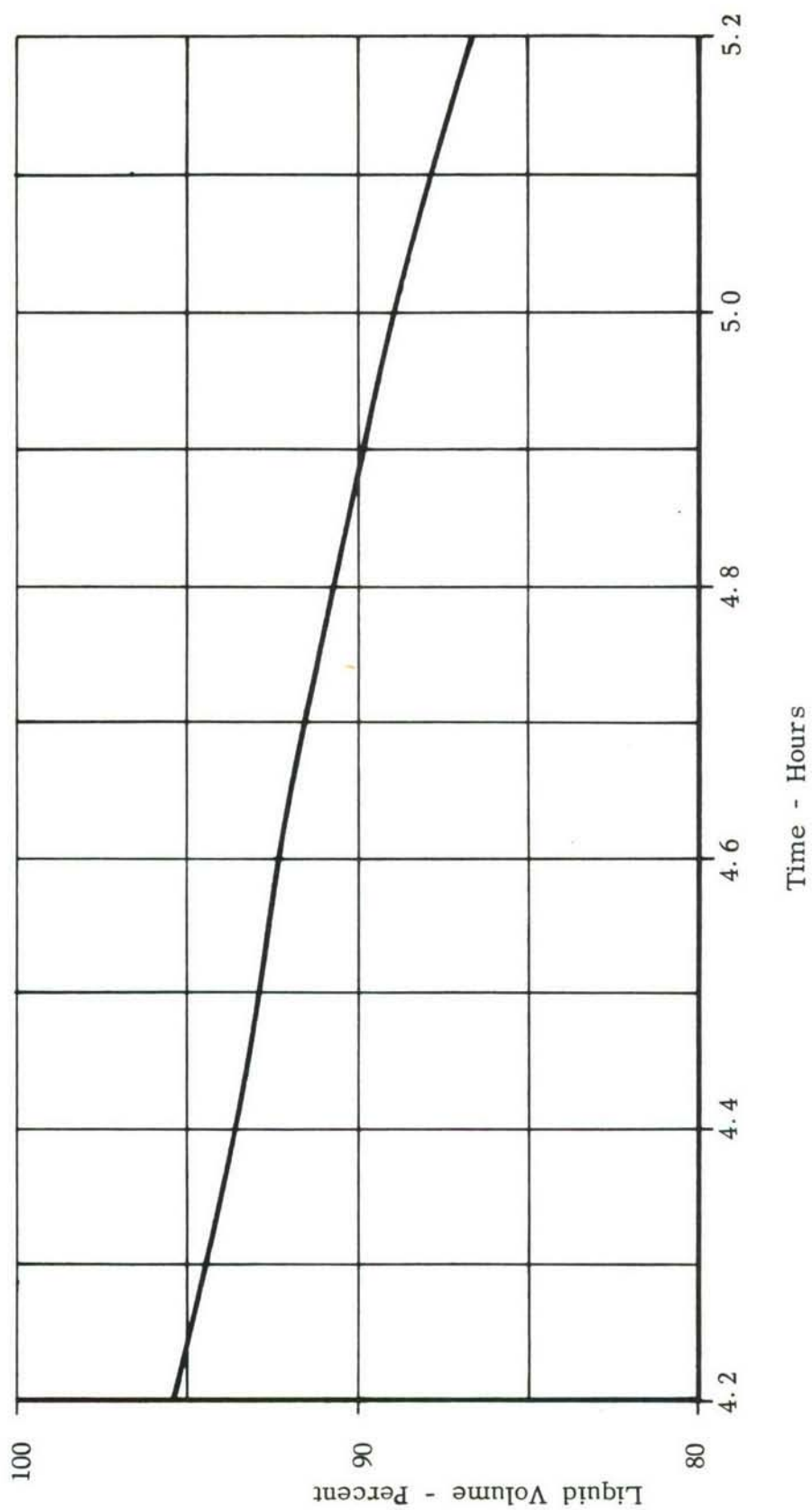


Figure 80. SUBSCALE TANK LIQUID LEVEL - TEST 3

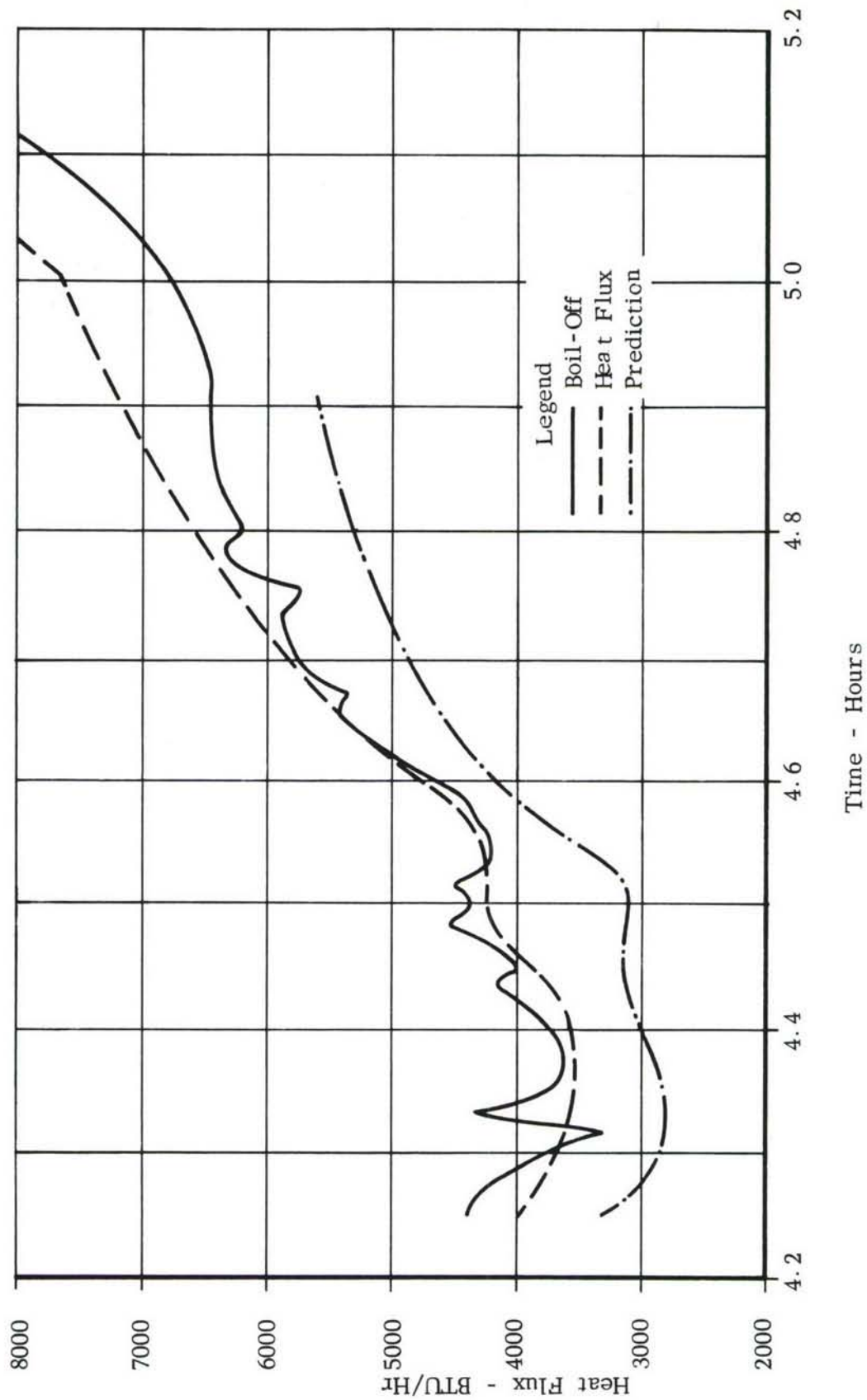


Figure 81. LIQUID HEAT FLUX RATE - TEST 3

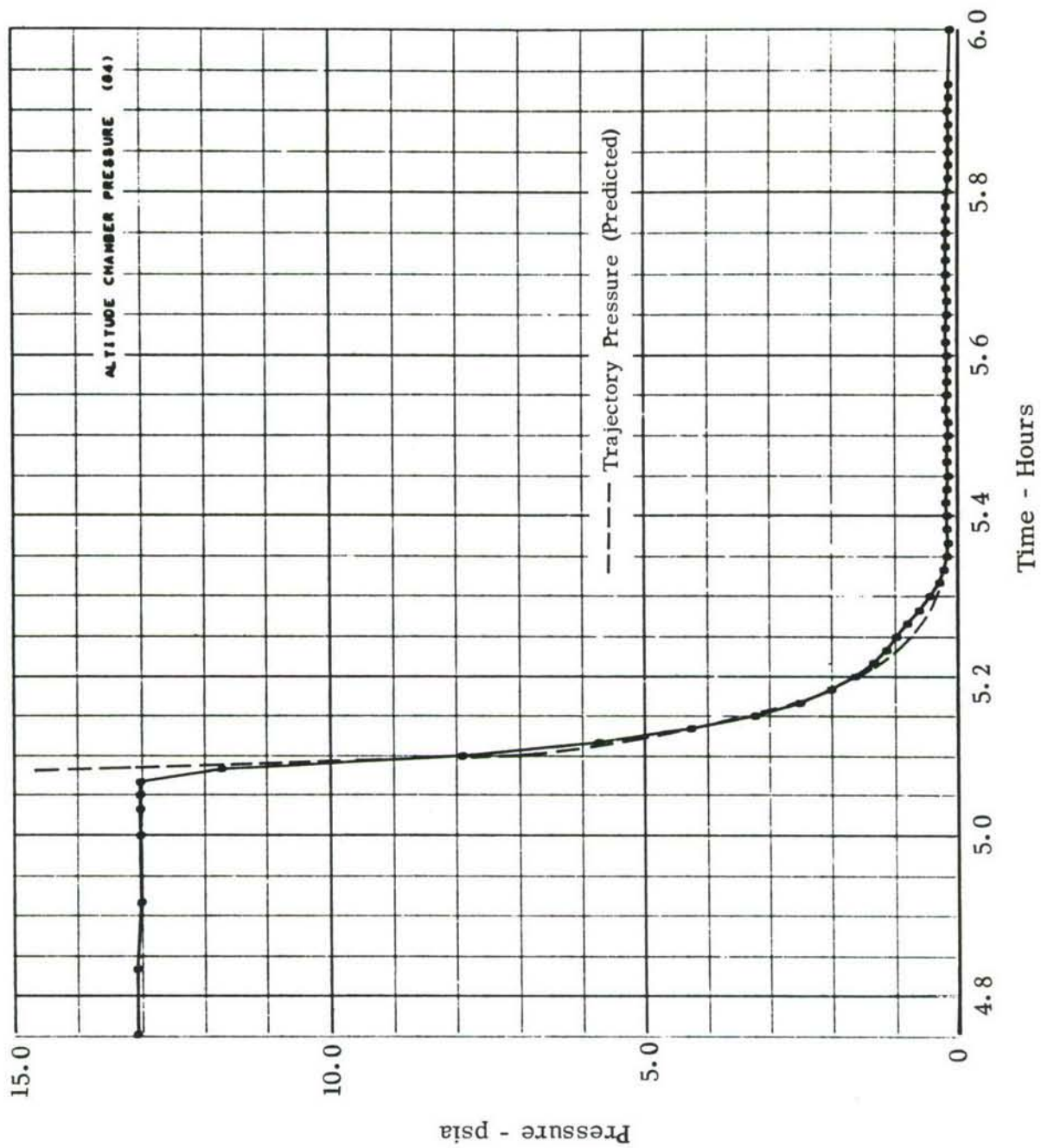


FIGURE 82. ALTITUDE CHAMBER PRESSURE - TEST 4

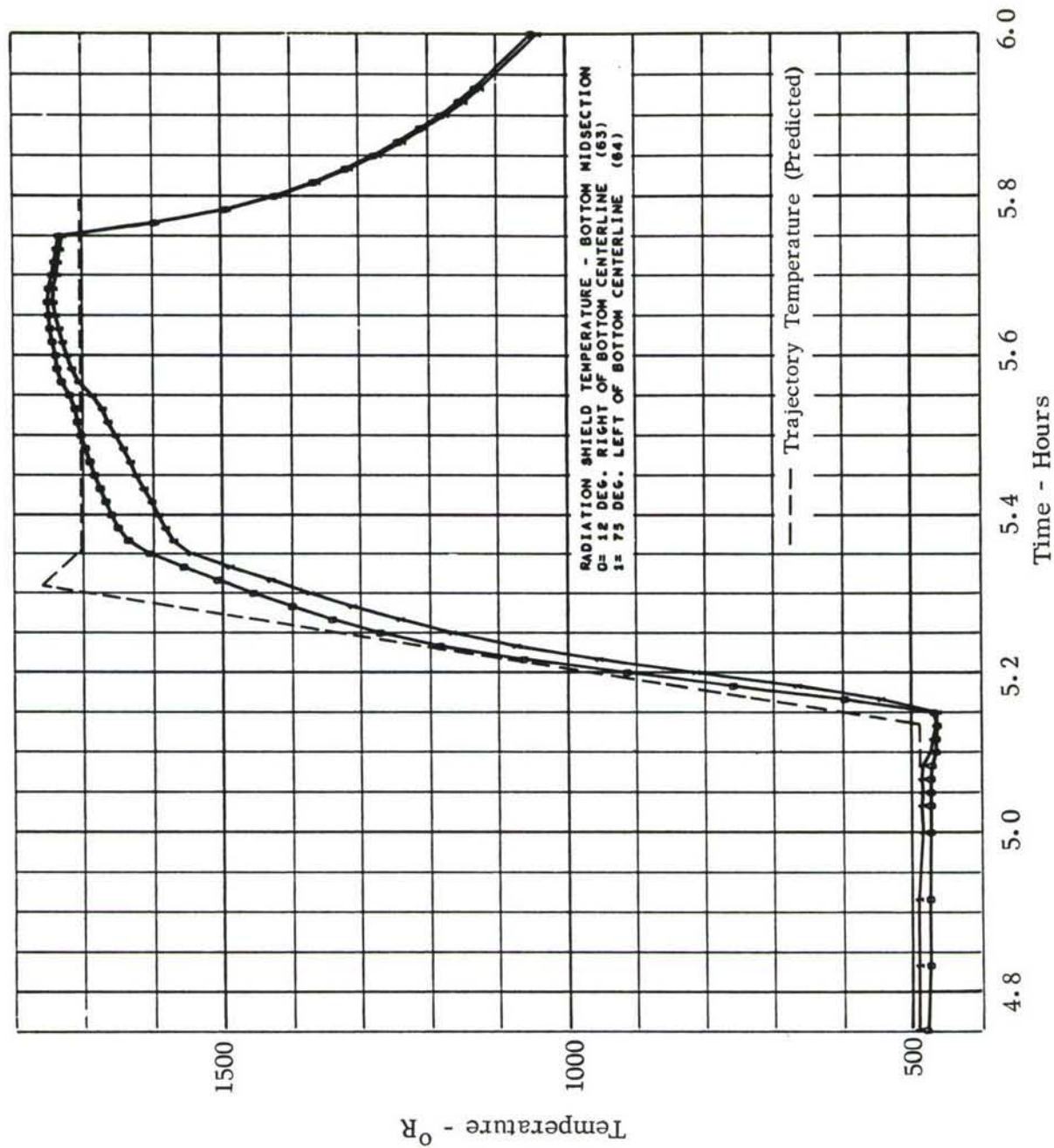


FIGURE 83. RADIATION SHIELD TEMPERATURE - BOTTOM - TEST 4

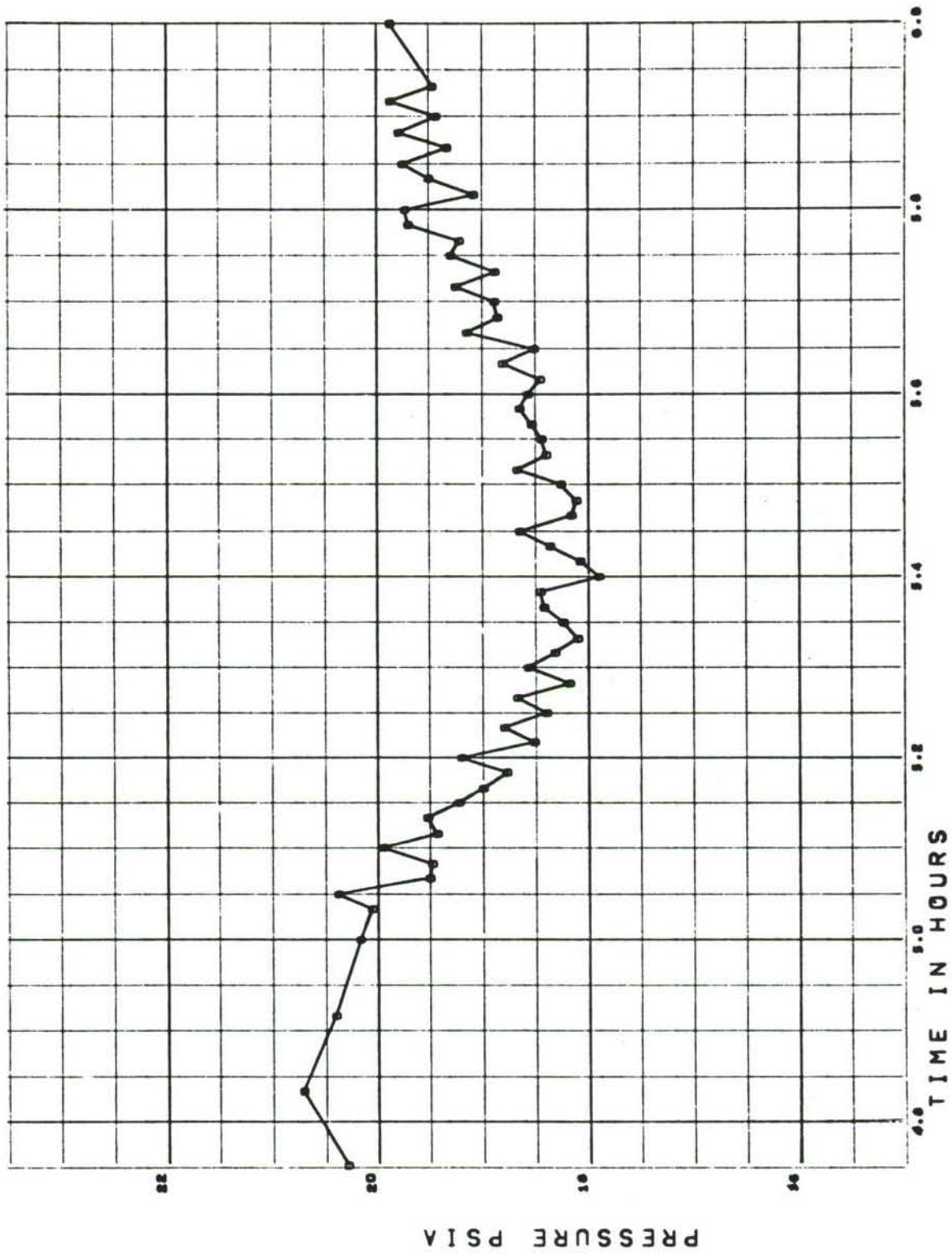


Figure 84. SUBSCALE TEST TANK PRESSURE - TEST 4

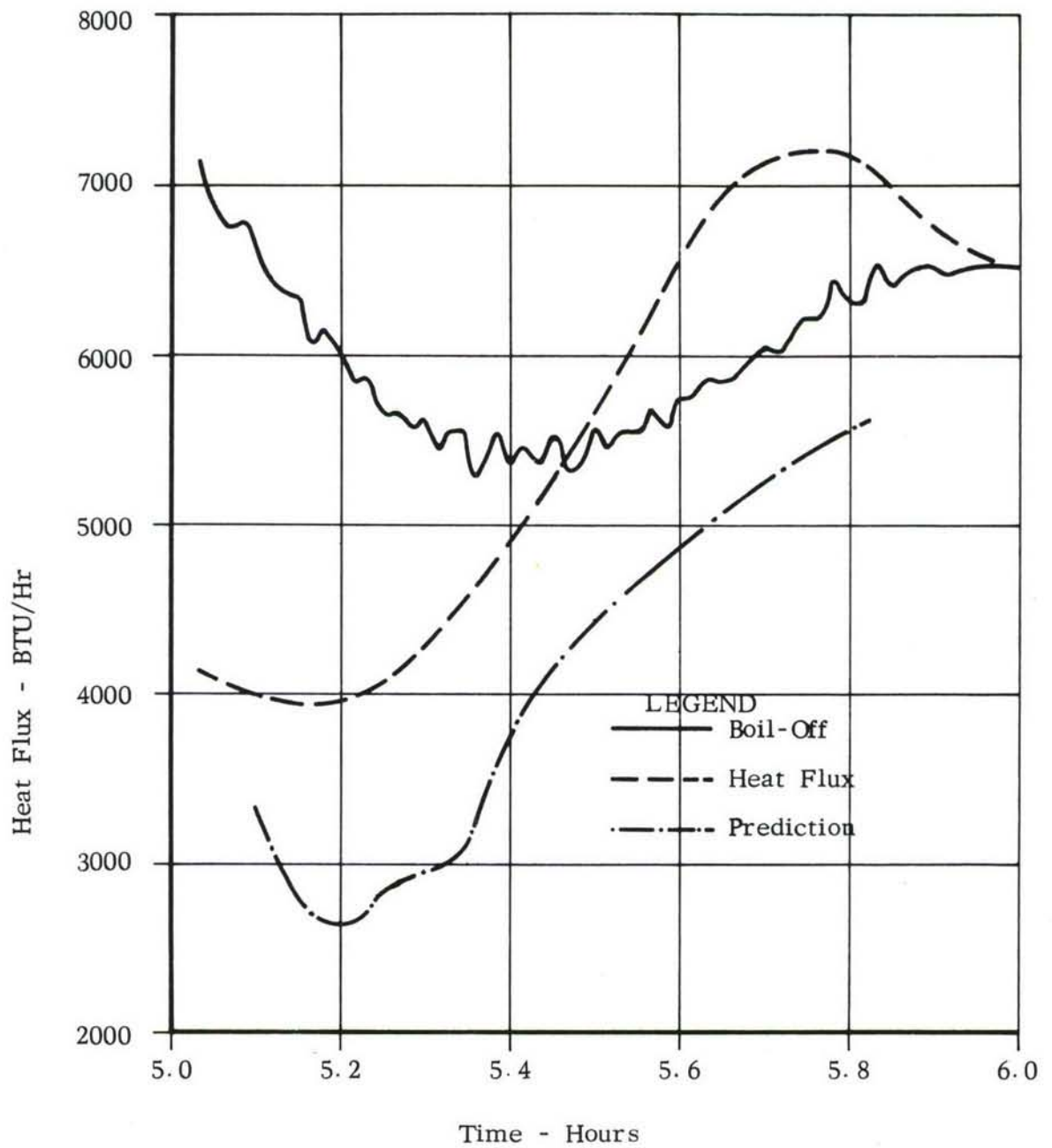


Figure 85. LIQUID HEAT FLUX - TEST 4

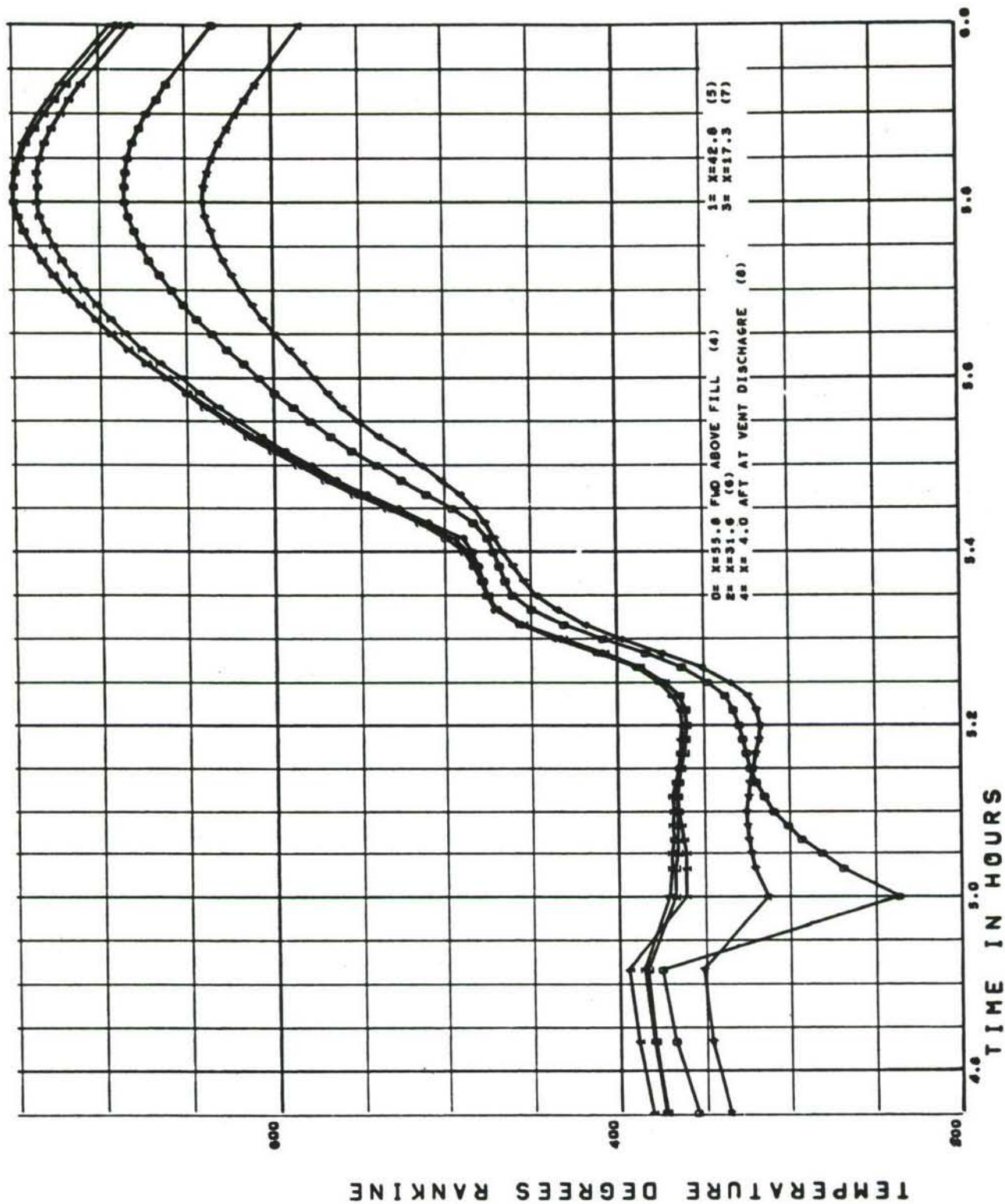


Figure 86. TOP TANK SKIN TEMPERATURE - TEST 4

The ullage and vent gas thermocouples did not work during Test 4. These were repaired prior to Test 5. The vent valve and pressure controller were also repaired. The chamber was closed and purged with helium gas to perform a mass spectrometer leak check. Due to absorbed helium in the insulation, the leak detector could not be brought on scale. The system was established as adequately leak-tight on the basis of chamber leak up rate and the absence of detectable hydrogen in the chamber with the test tank pressurized with hydrogen gas.

5.4.5 TEST 5. Test 5 was a liquid hydrogen fill and ground hold stabilization. It was conducted on 27 August. The test tank pressure was maintained between 15 and 20 psia. The tank was filled and the liquid level maintained between 80 and 90 percent. The measured temperature profile through the bottom insulation is shown in Figure 87. Predicted temperatures are also shown. The data shows a typical chilldown rate in the insulation. Approximately one hour is required for chilldown. Differences between measured and predicted temperatures are discussed in Section 5.5.1.2.

5.4.6 TEST 6. Test 6 was a liquid hydrogen conduction trajectory. It was conducted immediately following Test 5. Tank liquid level is presented in Figure 88. It was necessary to top the tank twice during the trajectory which corresponds to predictions prior to the test. The boiloff, heat flux, and predicted heat flux were generated as previously described. The rate of change of hydrogen bulk temperature immediately after topping was rather large. This accounts for the large difference between the boiloff and heat flux curves immediately after topping, as shown in Figure 89. Gas temperatures in the ullage and vent line are presented in Figure 90. Insulation temperature profile at the top of the tank is shown in Figure 91. These temperatures also show the effects of the intermittent topping.

5.4.7 TEST 7. Test 7 was a ground hold liquid hydrogen stratification investigation. The primary purpose of the test was to establish the rate at which the liquid temperature at various points in the tank would rise when the ullage pressure was increased. The test tank pressure is shown in Figure 92. Pressurization was actually started just prior to 20.33 hours, but since the last preceding data point was at 20.25 hours, the pressure change between these two times had to be estimated. The dashed line on the graph represents the probable pressure vs time curve during this period. The initial pressure control set point was low, approximately 27 psia. It was re-set at 20.37 hours to 30 psia. Liquid level during the test is shown in Figure 93. The discontinuity between 20.3 and 20.4 hours is a result of suppressing boiling during pressurization and liquid expansion due to increase in bulk temperature. The boiloff and liquid heat flux rate are shown in Figure 94. The total heat flux should not have changed greatly during the test. The dip in the heat flux curve, therefore, probably represents heating of liquid at locations not measured by the platinum probes. Typical liquid temperature data is presented in Figure 95. Indication of lower heating rates near the bottom of the tank is apparent. The primary emphasis in these liquid temperature curves is the rate of change, rather than absolute temperature. The absolute temperature values are, however, well within the rated accuracy of the probes.

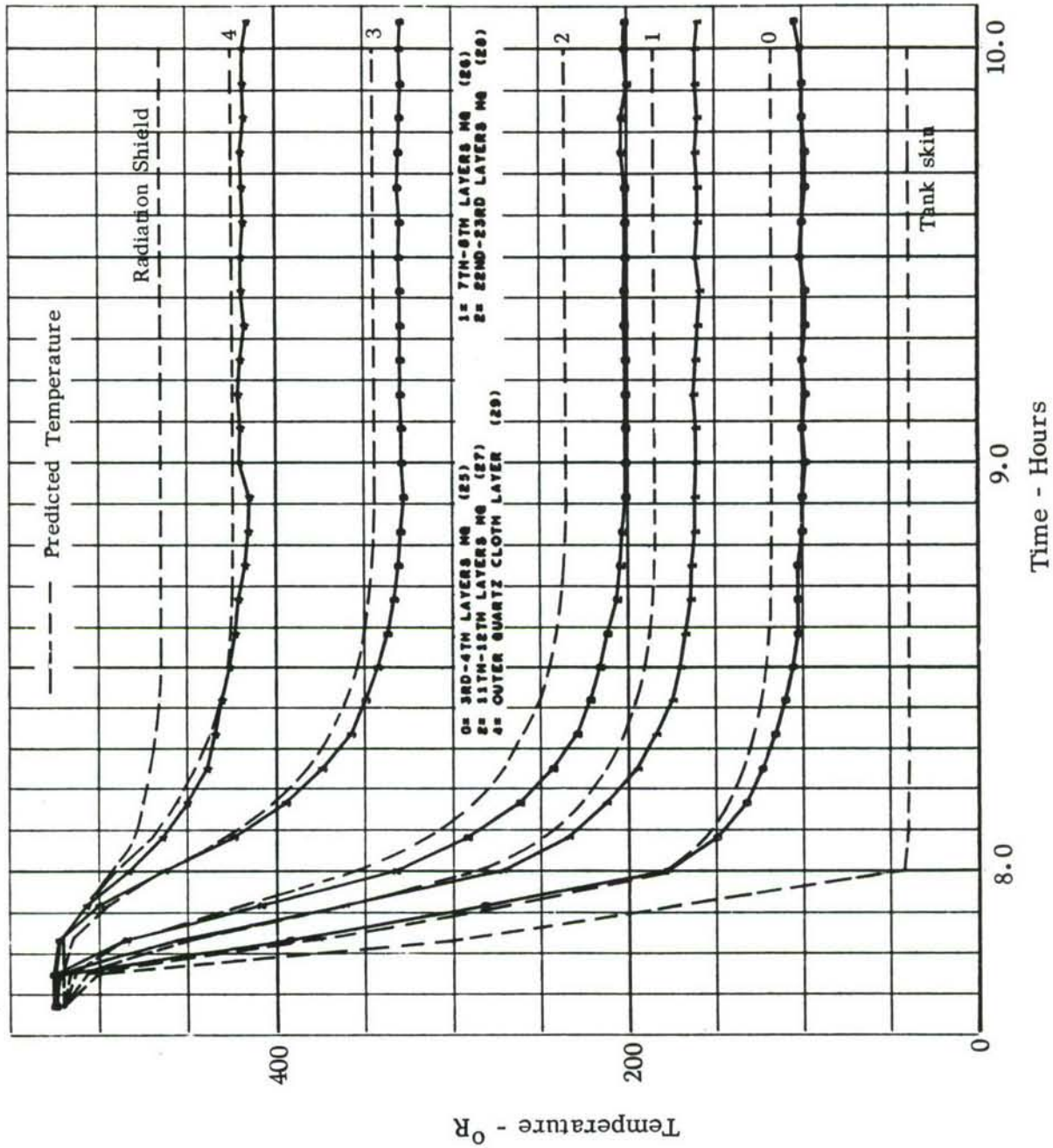


FIGURE 87. BOTTOM INSULATION TEMPERATURE - TEST 5

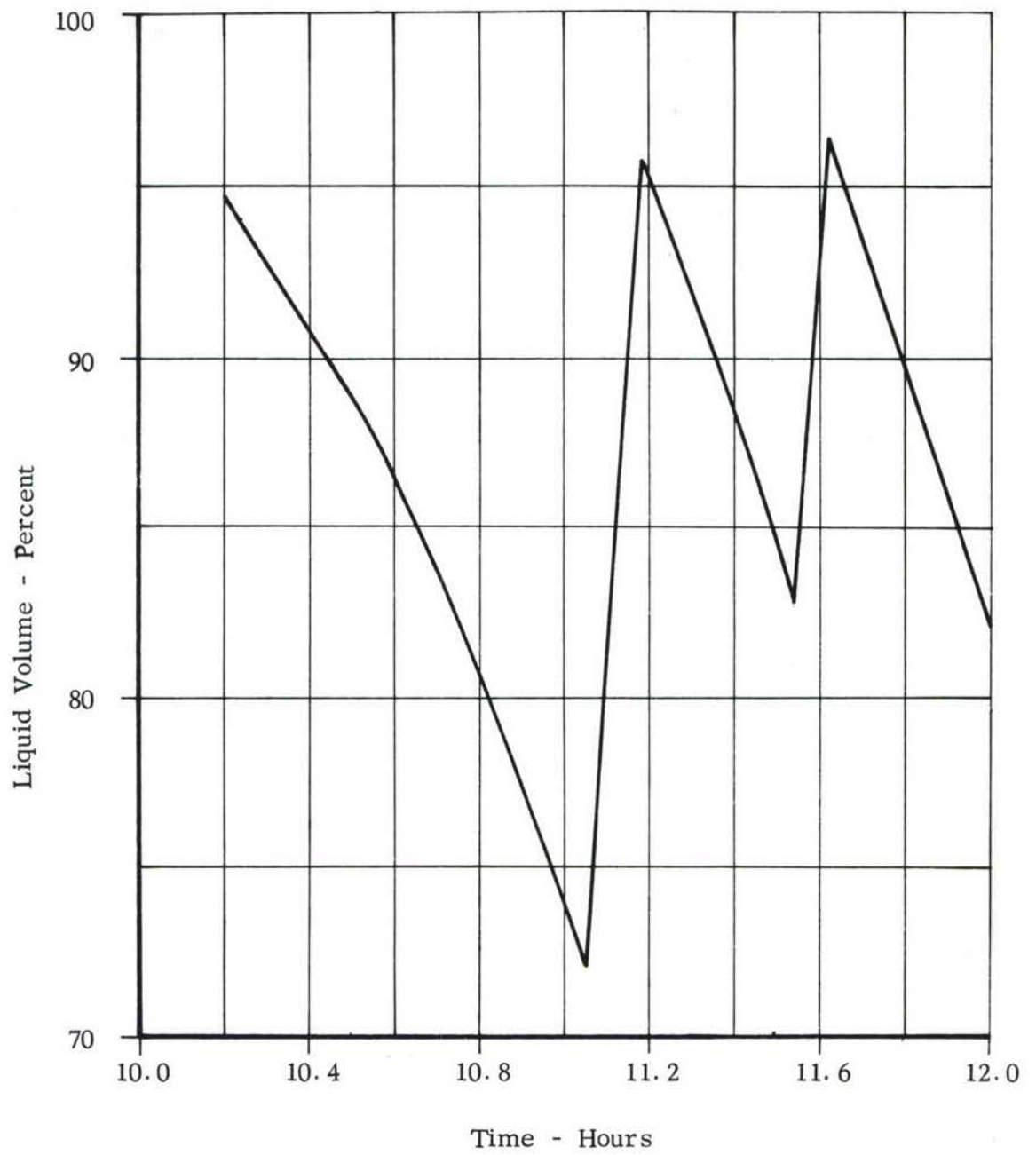


Figure 88. SUBSCALE TANK LIQUID LEVEL - TEST 6

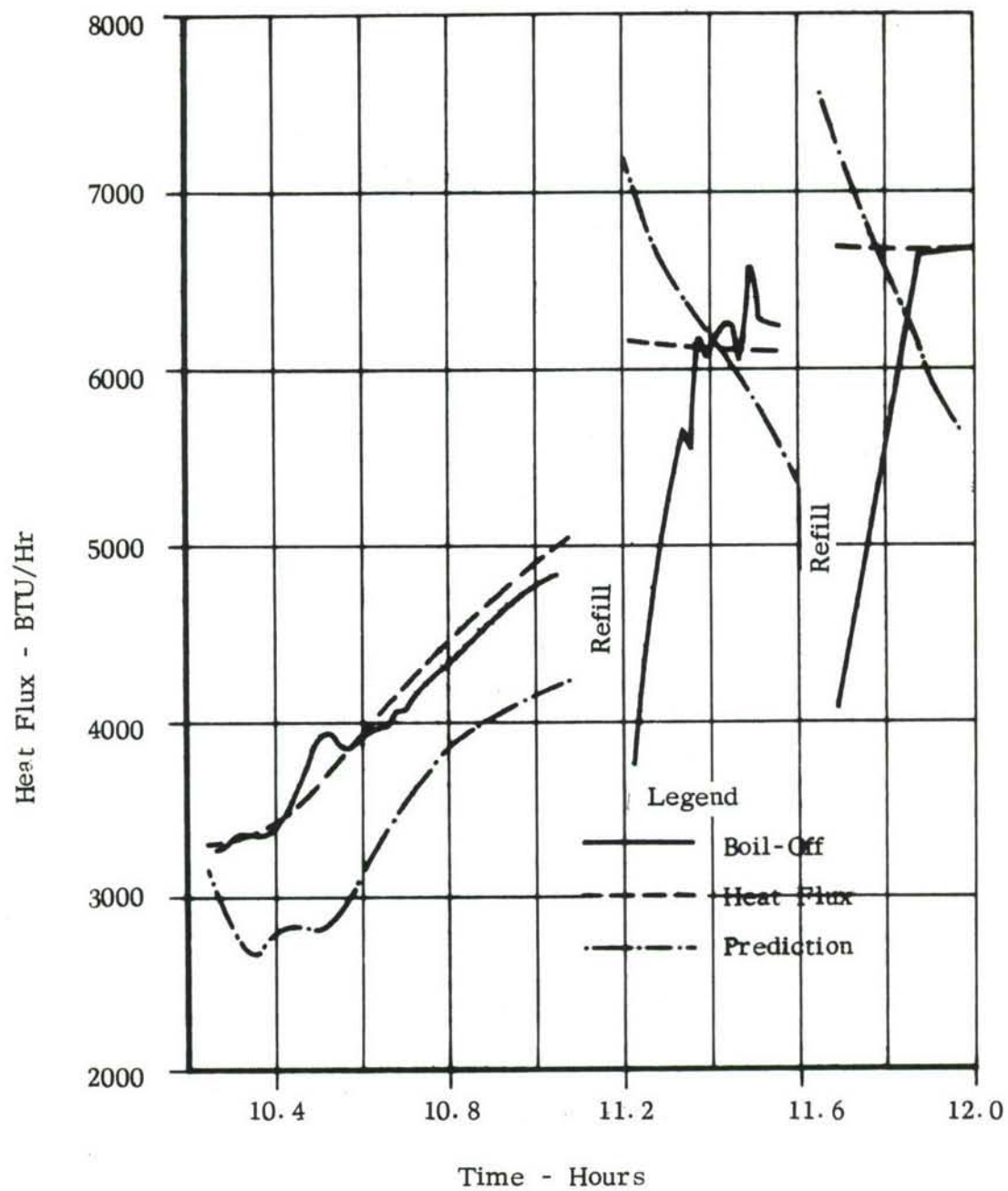


Figure 89. LIQUID HEAT FLUX RATE - TEST 6

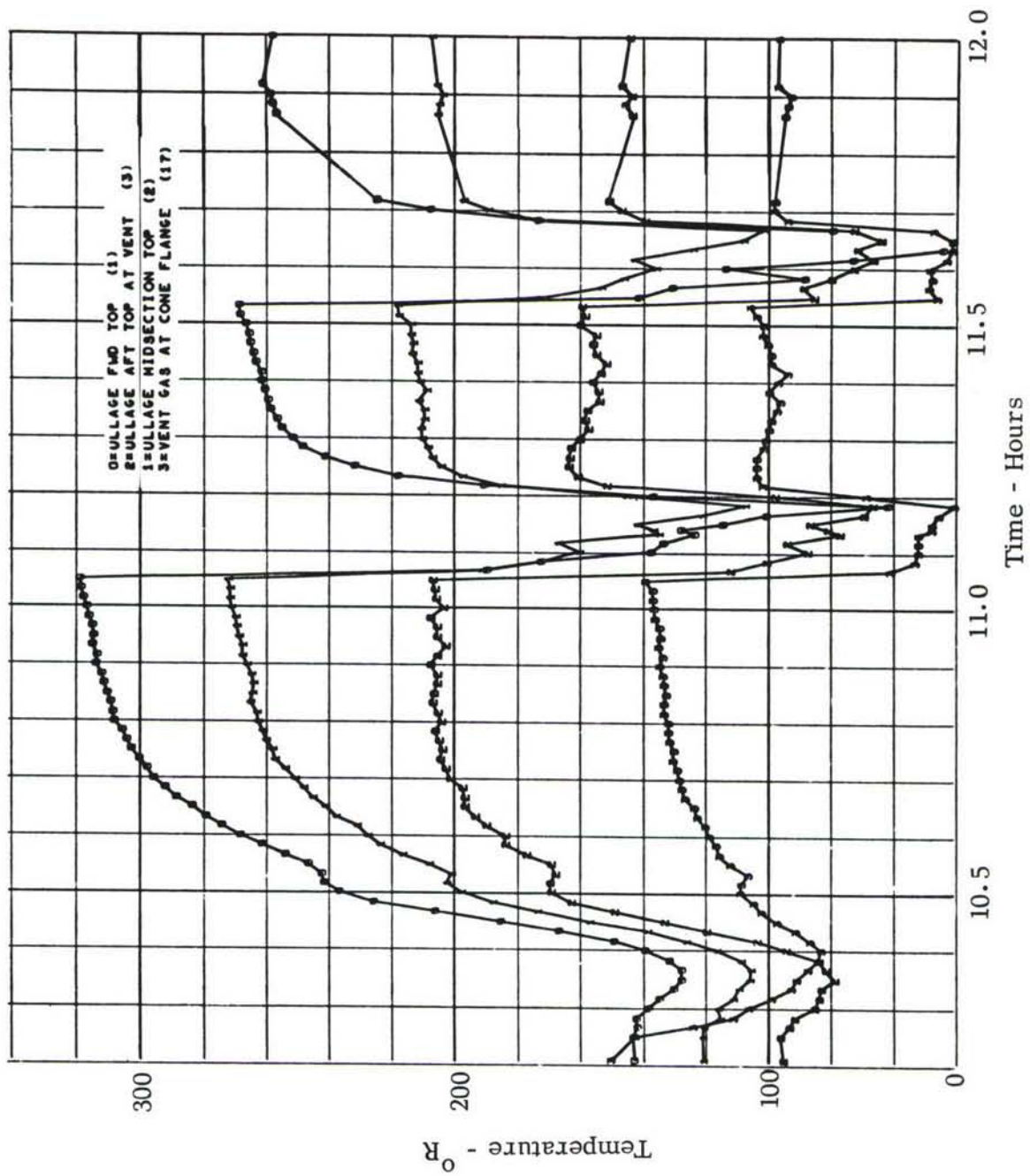


FIGURE 90. ULLAGE AND VENT GAS TEMPERATURE - TEST 6

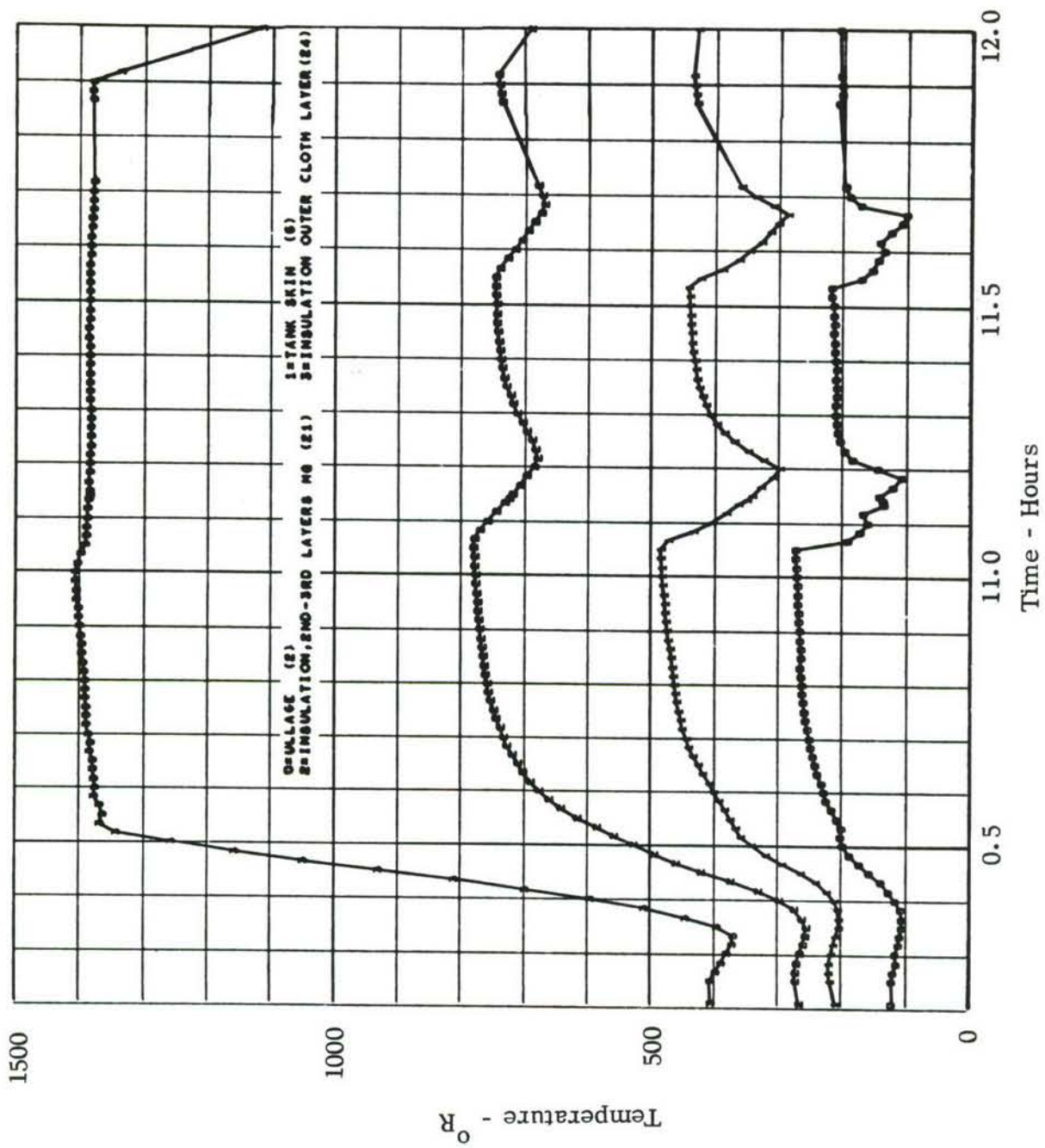


FIGURE 91. TOP INSULATION, SKIN AND ULLAGE TEMPERATURE - TEST 6

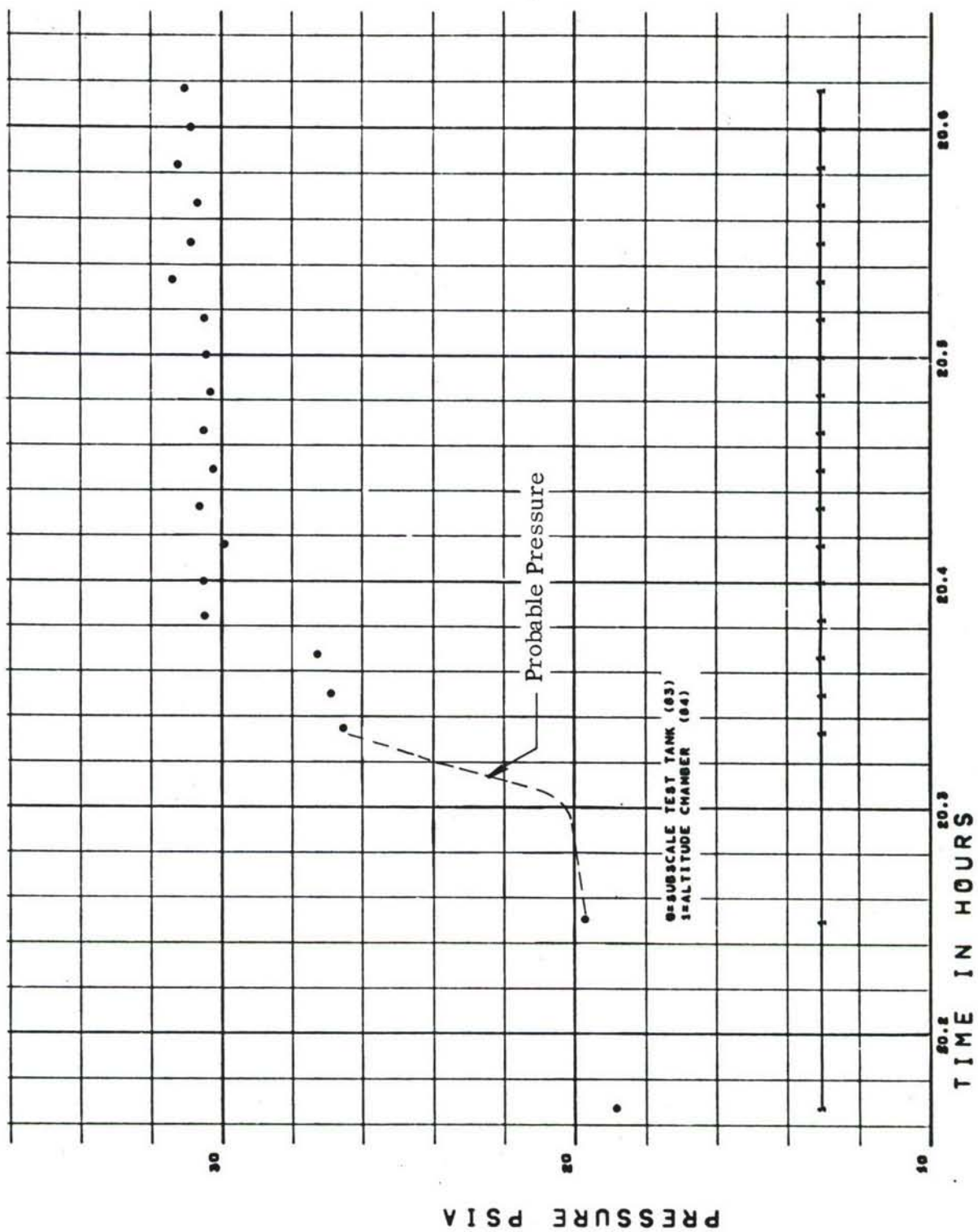


Figure 92. TEST TANK AND CHAMBER PRESSURE - TEST 7.

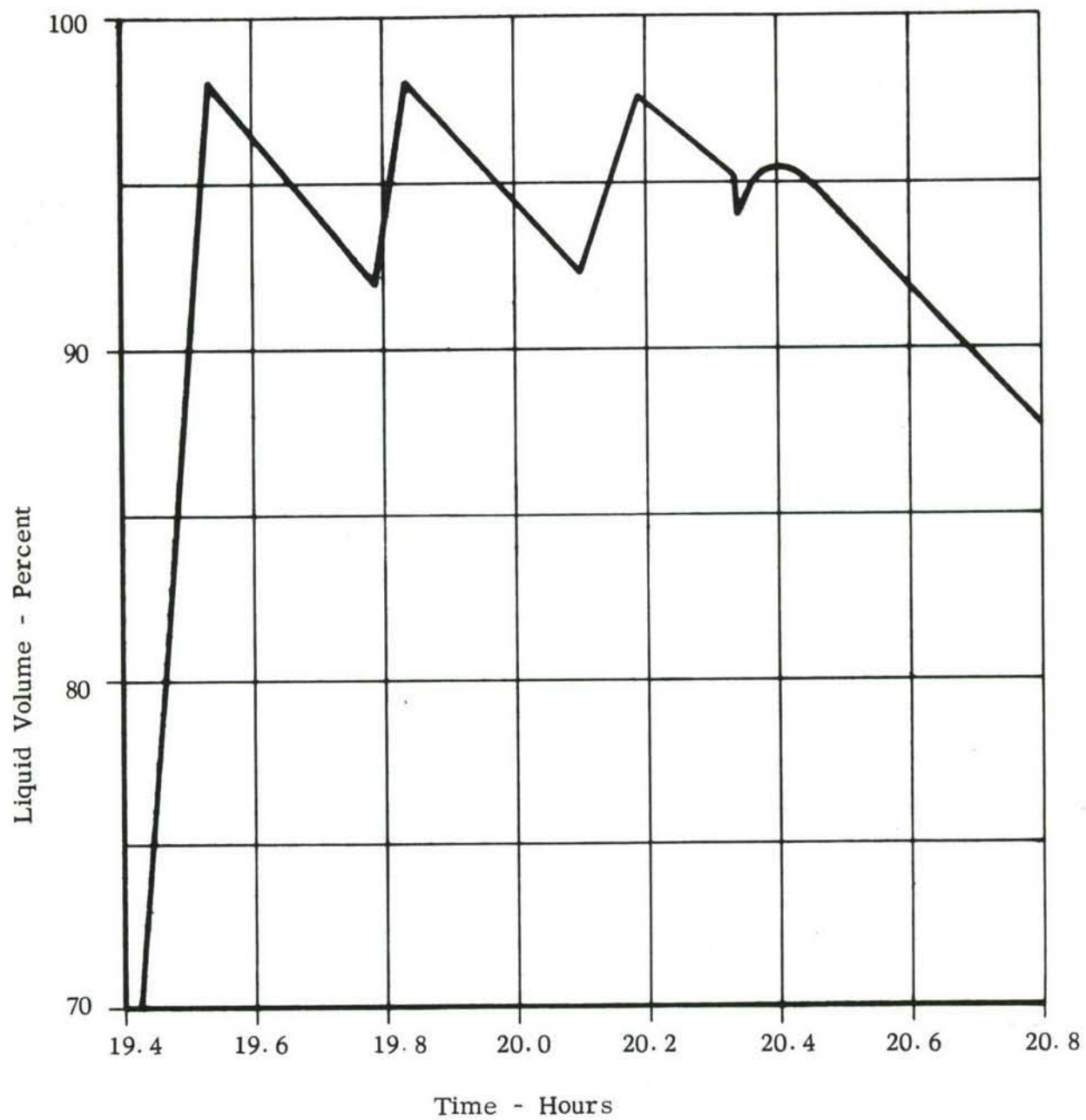


Figure 93. SUBSCALE TANK LIQUID LEVEL - TEST 7

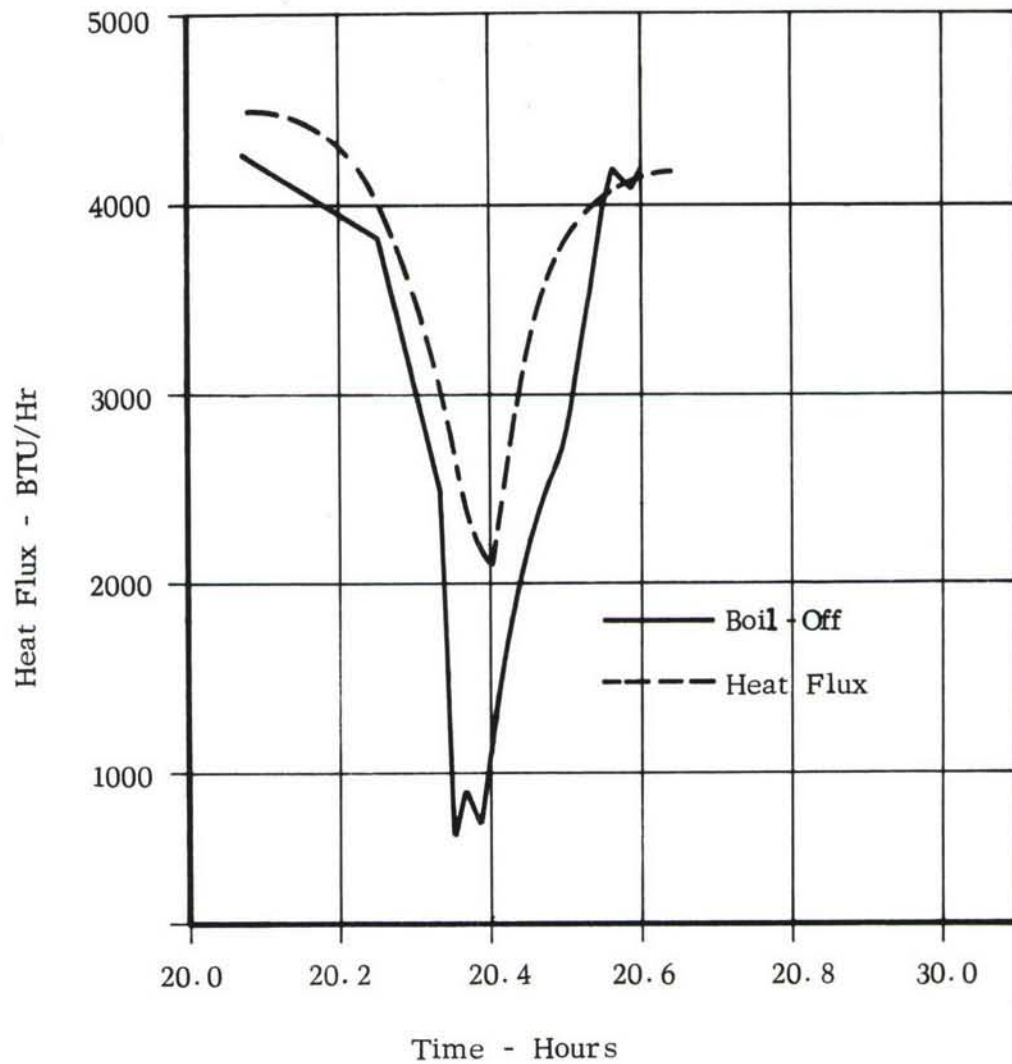


Figure 94. LIQUID HEAT FLUX RATE - TEST 7

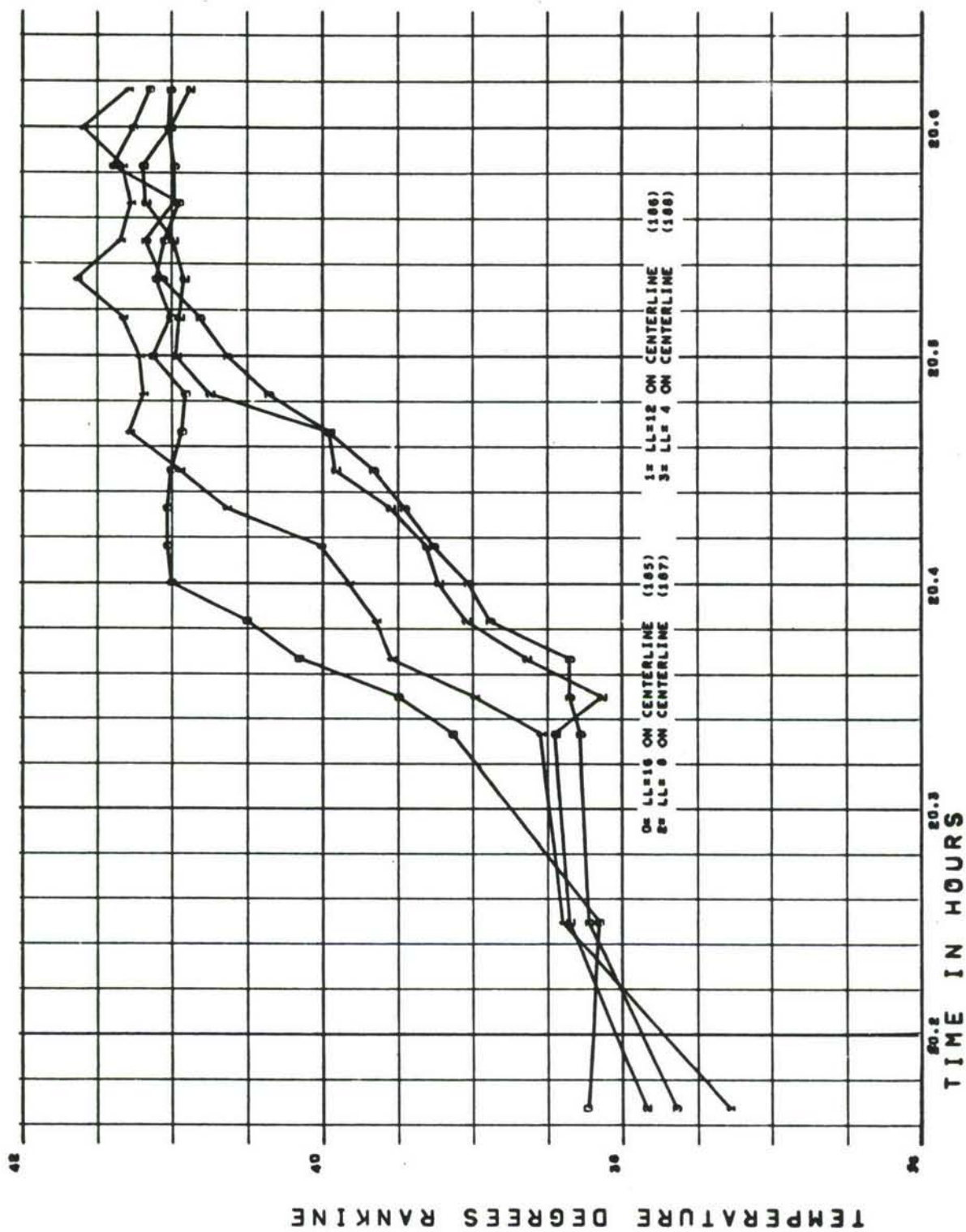


Figure 95. LIQUID/ULLAGE TEMPERATURE - TEST 7.

5.4.8 TEST 8. Test 8 was a liquid hydrogen trajectory run to investigate the effects of boiloff gas cooling on the upper tank skin. The test was performed immediately following Test 7 since Test 7 established the desired initial equilibrium conditions. Subscale tank ullage pressure is shown in Figure 96. The ullage pressure shown here is typical of the rate and magnitude of the cyclic pressure variations encountered in the testing. This undoubtedly had an effect on liquid flashing and sloshing inside the tank. Liquid level as a function of time was established as in test 3 and is presented in Figure 97. Boiloff, heat flux, and predicted heat flux is presented in Figure 98. These curves demonstrate the reduced heat flux to the liquid near the end of the trajectory which results from decreasing liquid level.

5.4.9 TEST 9. This test was an investigation of transient temperature rise in the tank ullage. In order to force a maximum rate of temperature increase, the vent was closed and liquid was drained to prevent excessive tank pressure. Chamber pressure and radiation shield temperature trajectory parameters were the same as for the other trajectory tests. Tank pressure was manually recorded due to failure of the tank pressure transducer. The tank pressure is plotted in Figure 99. Venting was stopped at 14.983 hours, drain was started at 15.063 hours and stopped at 15.25 hours. Venting was resumed at 15.263 hours. Liquid level, Figure 100, was established from the carbon resistors and the tank skin thermocouples. Liquid levels below 50% are estimated and are shown as a dashed-line. Temperatures in the ullage and on the tank skin are discussed in Section 5.5.1.2.

5.5 CORRELATION OF TEST RESULTS

The objectives of the test program were (1) to establish the heat flux rates to the cryogenic liquid in order to predict boil-off losses (2) to determine heat transfer rates from the upper tank skin to predict structure temperatures for design and cooling requirements and (3) make a comparison between nitrogen and hydrogen for the purposes of cryogenic tank testing. The tendency for cryogenic fluids to stratify after pressurization reduces their capability to absorb incoming heat flux into the bulk liquid and effectively limits the advantage of pressurization to reduce boil-off losses. Thus the measurement of liquid stratification was an additional objective of the test program.

The heat flux rates to the liquid and resultant boiloff in the tests were generally within 20% of the predicted values for the LH_2 tests and within 40% for the liquid nitrogen tests. The predicted values were generally lower than the test results. Differences between the predicted and actual heat flux rates were as much as 50% during the transient period where the environmental pressure changed from 1.0 to 0.01 atm. These differences are attributed primarily to (1) unaccounted for convective heat transfer in the insulation at high (1.0 atm) environmental pressure (2) insufficient data on the thermal conductivity of the insulation as a function of pressure during the transient part of the trajectory (3) the possibility of vigorous boiling at

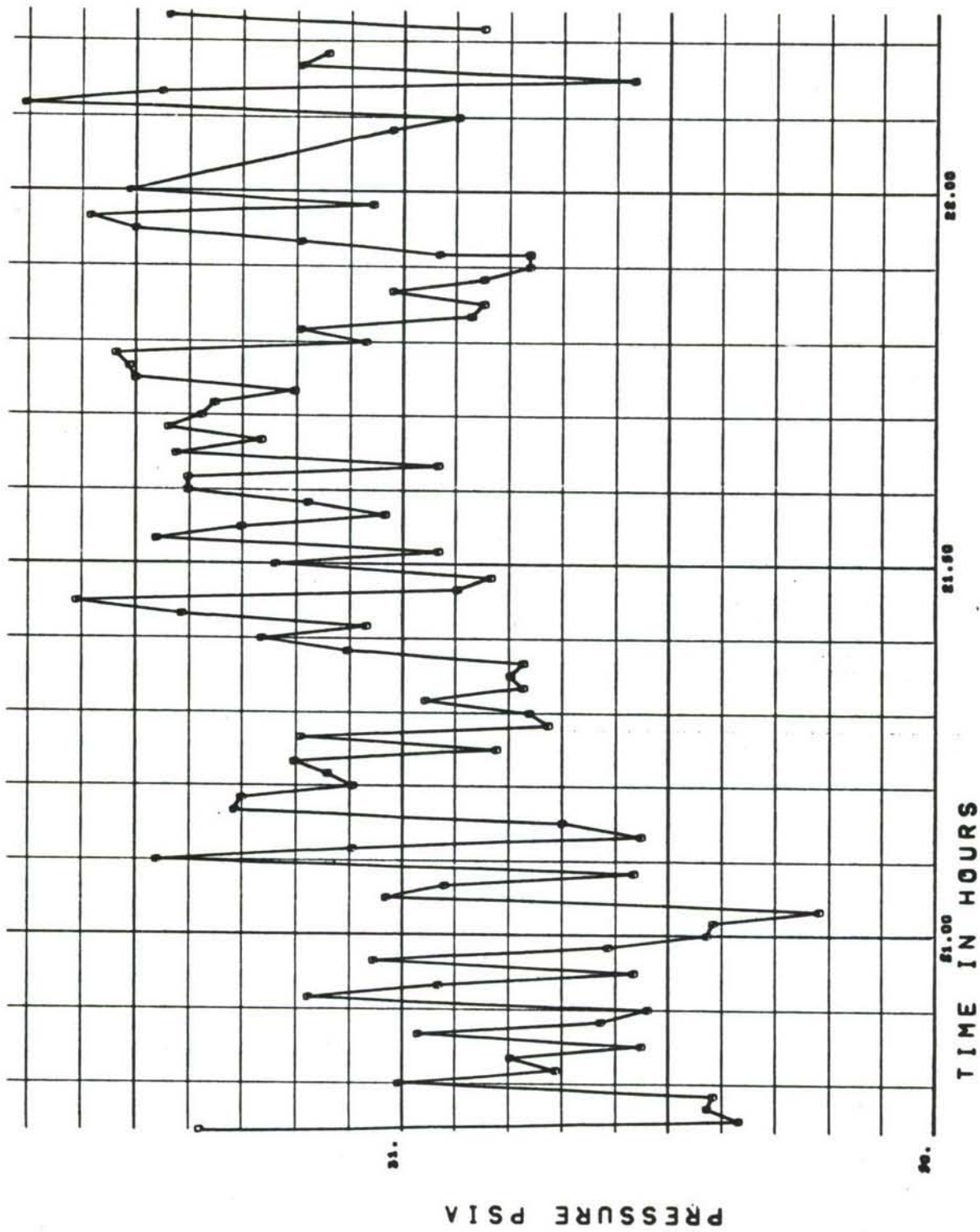


Figure 96. SUBSCALE TEST TANK PRESSURE - TEST 8

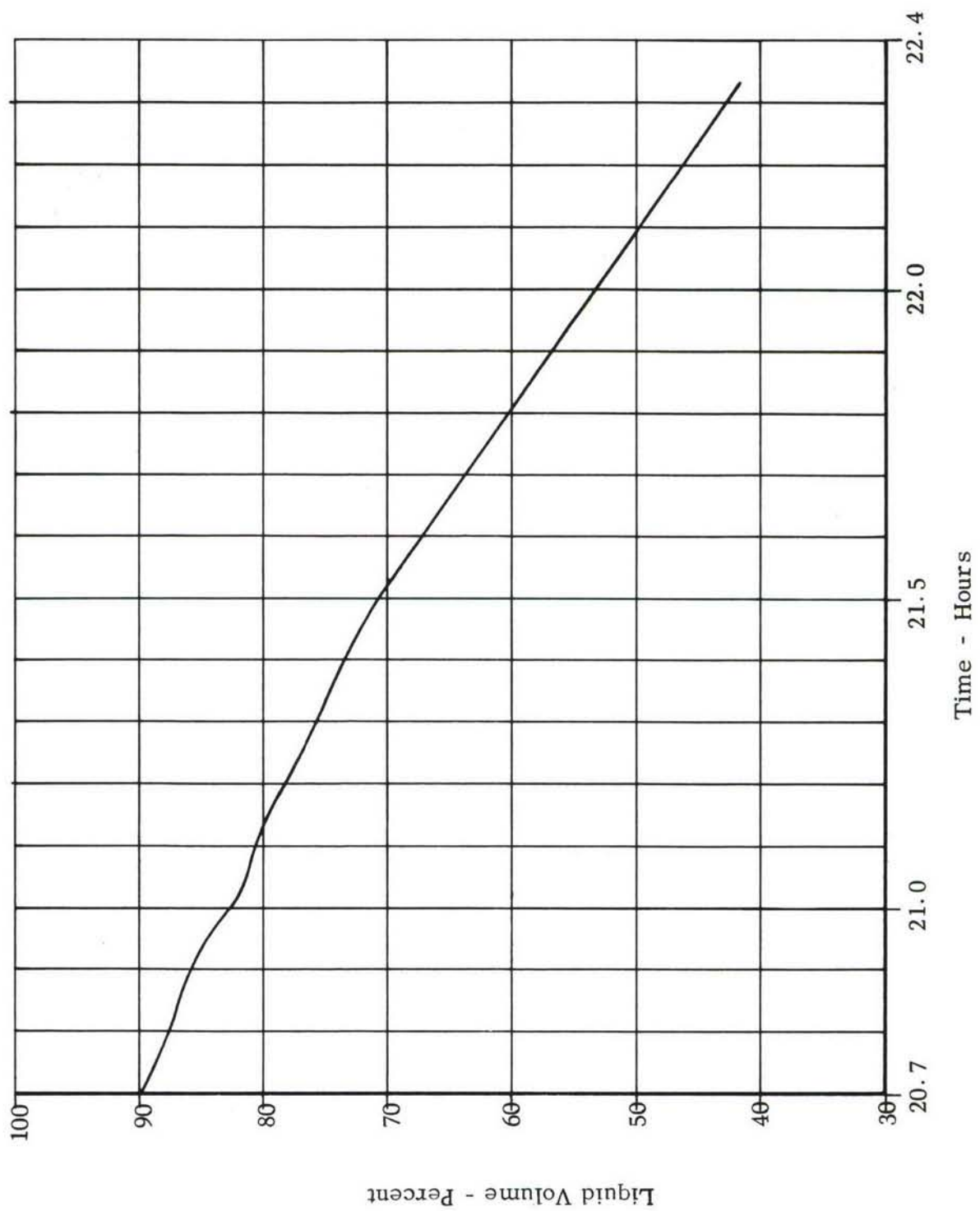


Figure 97. SUBSCALE TANK LIQUID LEVEL - TEST 8

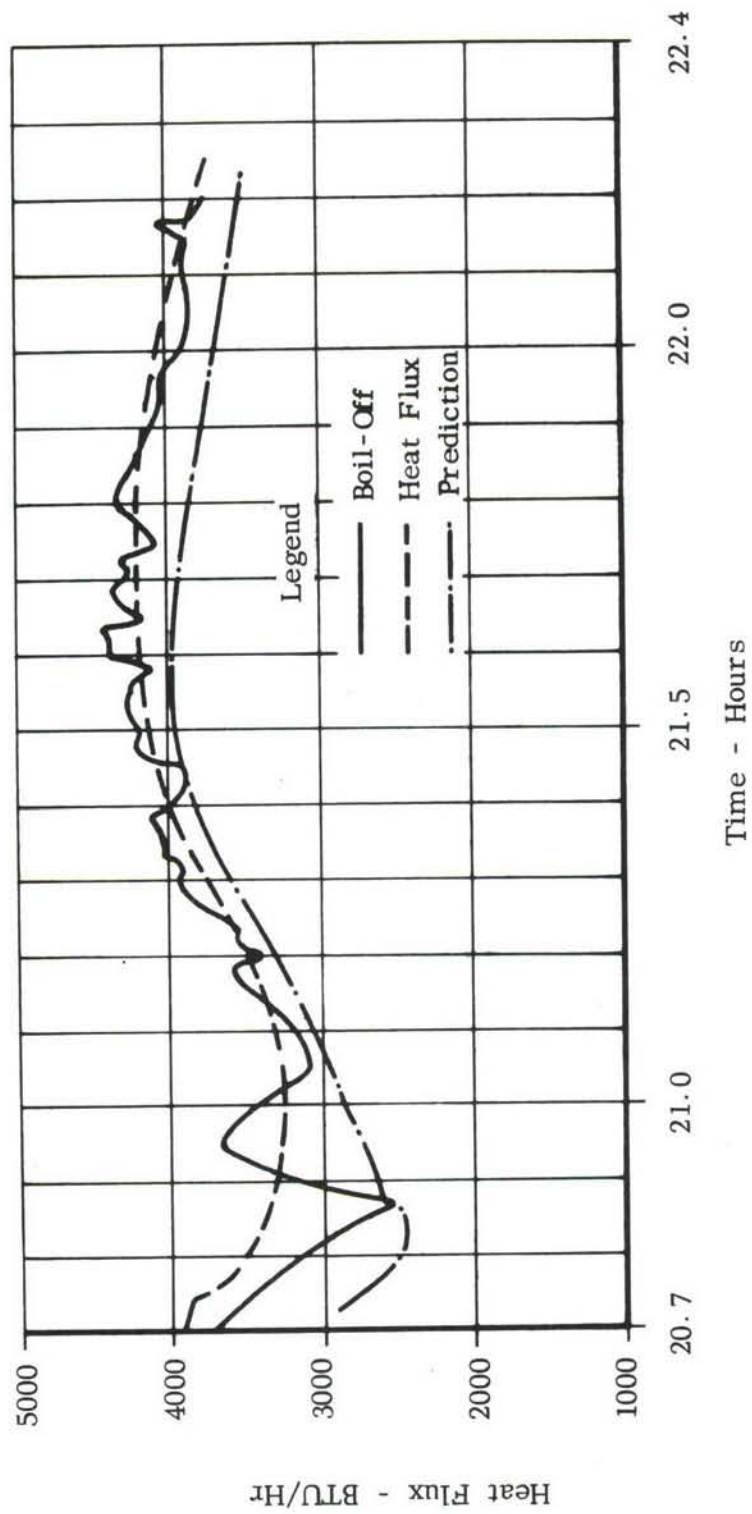


Figure 98. LIQUID HEAT FLUX RATE -TEST 8

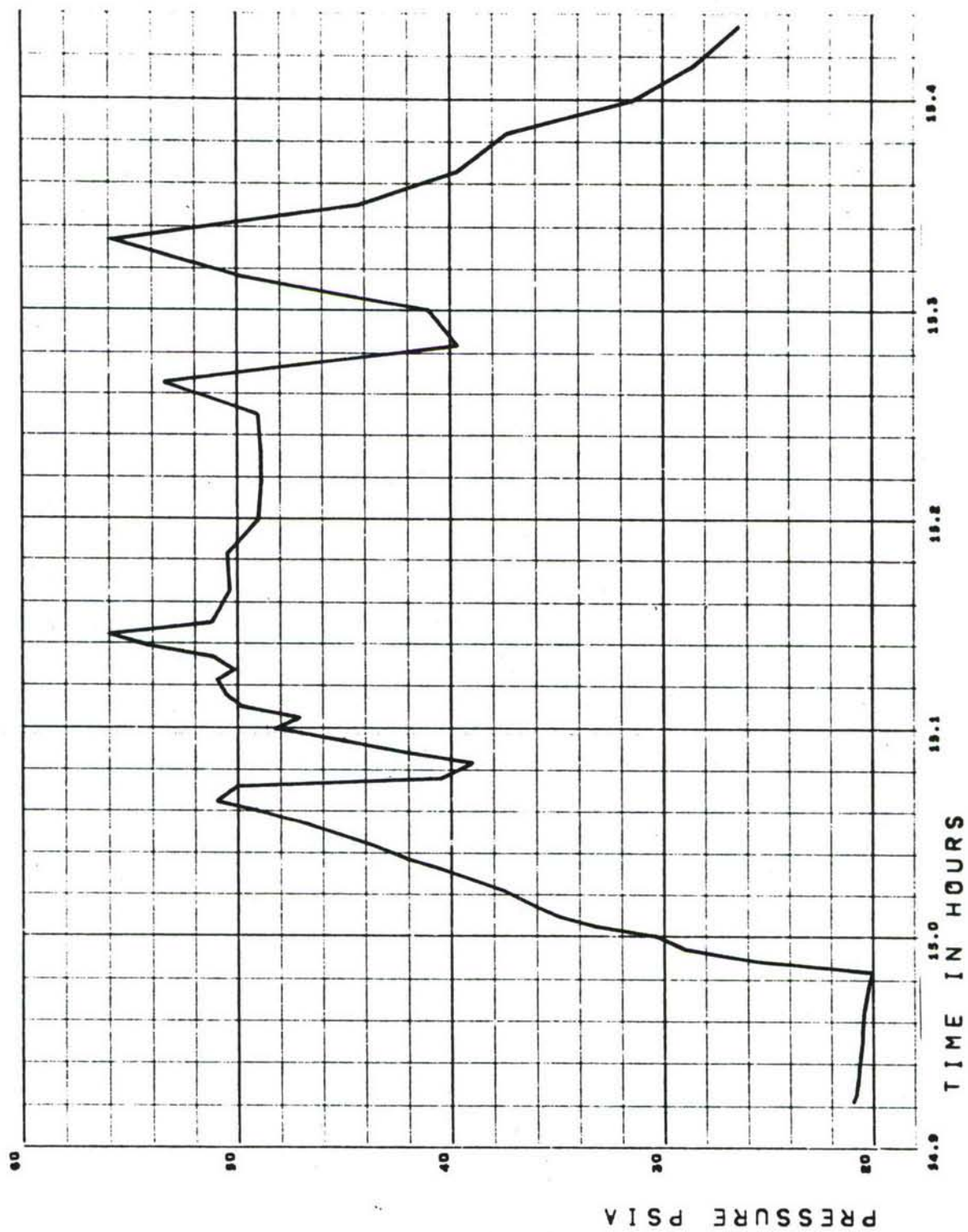


Figure 99. TEST TANK PRESSURE — TEST 9

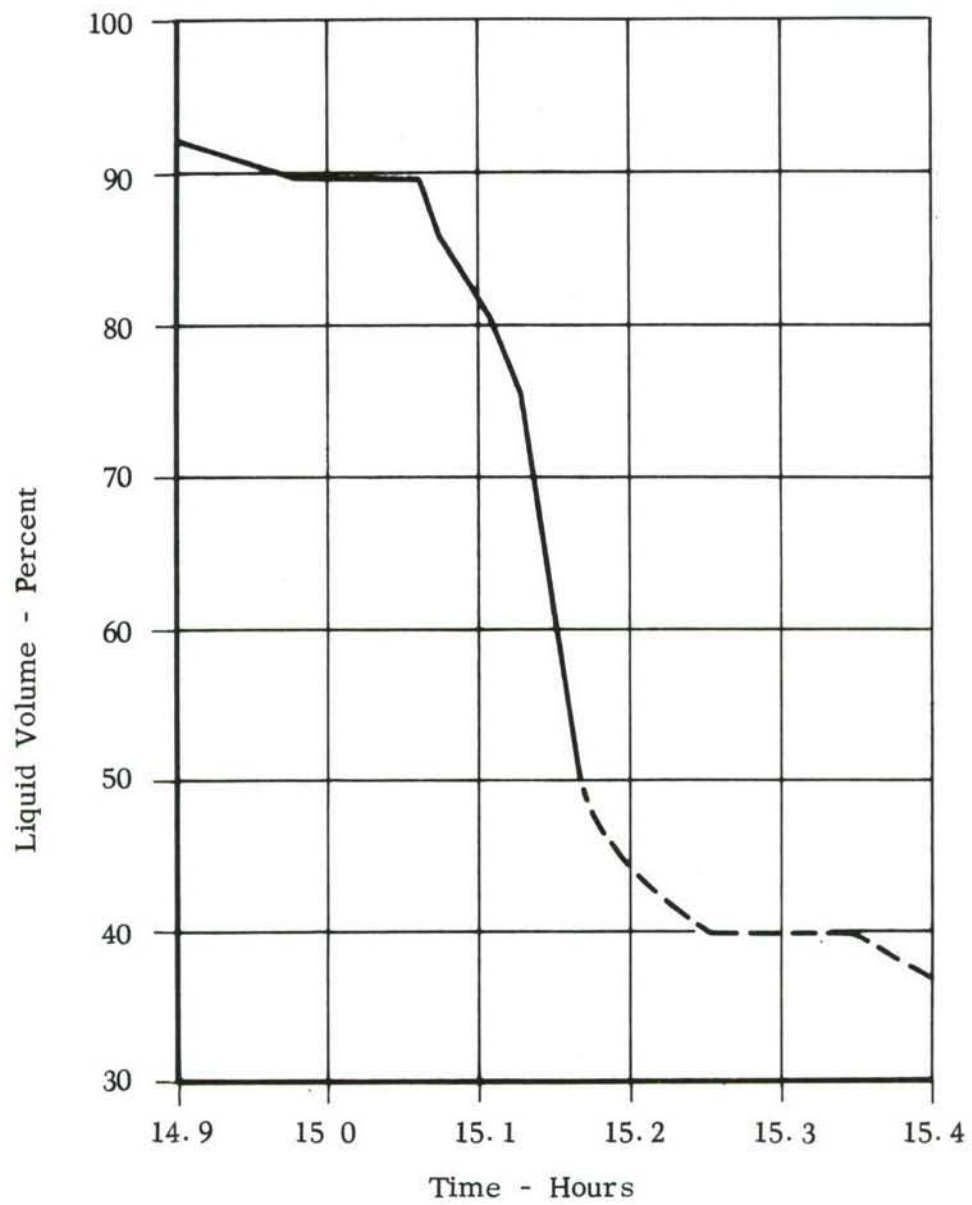


Figure 100. SUBSCALE TANK LIQUID LEVEL -TEST 9

the liquid/tank skin interface which effectively increases the wetted tank area (predictions are based on measured liquid levels in the center of the tank) and (4) rapid pressure variations in the tank which resulted in liquid droplets or fog being transferred into the ullage due to violent boiling which occurs during a flash-off period.

The measured dry tank skin temperatures on the upper surface exhibited predictable temperature changes on a qualitative basis. Attempts to correlate convective heat transfer rates to the measured data resulted in some inconsistencies.

Reasonably good measurements were obtained on liquid stratification. The liquid tended to stratify in layers as a function of time and heat flux rate. There was no apparent convective transfer of liquid from lower to upper sections as occurs in vertical tanks. The tests show that stratification must be considered in evaluating a horizontal tank configuration. This will reduce the maximum liquid level at topping, result in boil-off during ground hold, and increase the total losses due to boiloff.

The use of nitrogen to evaluate hydrogen tankage is a satisfactory substitute for evaluating heat flux rates thru the insulation where a single insulation is used such as the all microquartz system used in this test. However, if a composite system is used where interface temperatures are significant, especially in the cryopumping region, then thermal properties of the system in the hydrogen temperature region must be determined accurately for design purposes. The high temperatures which result in nitrogen ullage space preclude its use as an adequate substitute for hydrogen in evaluating the dry tank area and structural temperatures.

5.5.1 HEAT FLUX TO LIQUID. Heat flux rates to the liquid for each test have been presented in the previous section 5.4. Included on those curves are the measured boil off rate, the actual heat flux rate which included a correction for variations in liquid temperature, and the predicted heat flux rate. The predicted heat flux rate is a revised value from the original prediction.

The revised prediction includes (1) the total penetration heat leak which was inadvertently omitted from the original summation in Figure 104, (2) the effect of pressure on the insulation k value, and (3) radiation from the upper tank surface. Additional heat fluxes which have not been accounted for in the predictions but may have contributed to the discrepancy between measurement and prediction are discussed in the following paragraphs.

5.5.1.1 Predicted Performance. The thermal performance of subscale tank #1 with Microquartz insulation in a helium environment was analytically determined prior to testing. The time-temperature profile for the radiation shield used for the analysis is shown in Figure 3. The radiation shield temperature profile used for the side of the tank is the average of the top and bottom temperature. Heat transfer and boil-off rates were calculated for both the liquid nitrogen and liquid hydrogen tests. Heat flux rates to the cylindrical section of the tank, top 1.25 inch insulation, side 2.6 inch insulation and bottom 4.0 inch insulation are shown in Figure 101. It is noted that the predicted heat flux to a 40° R (LH₂) cold wall is only slightly greater

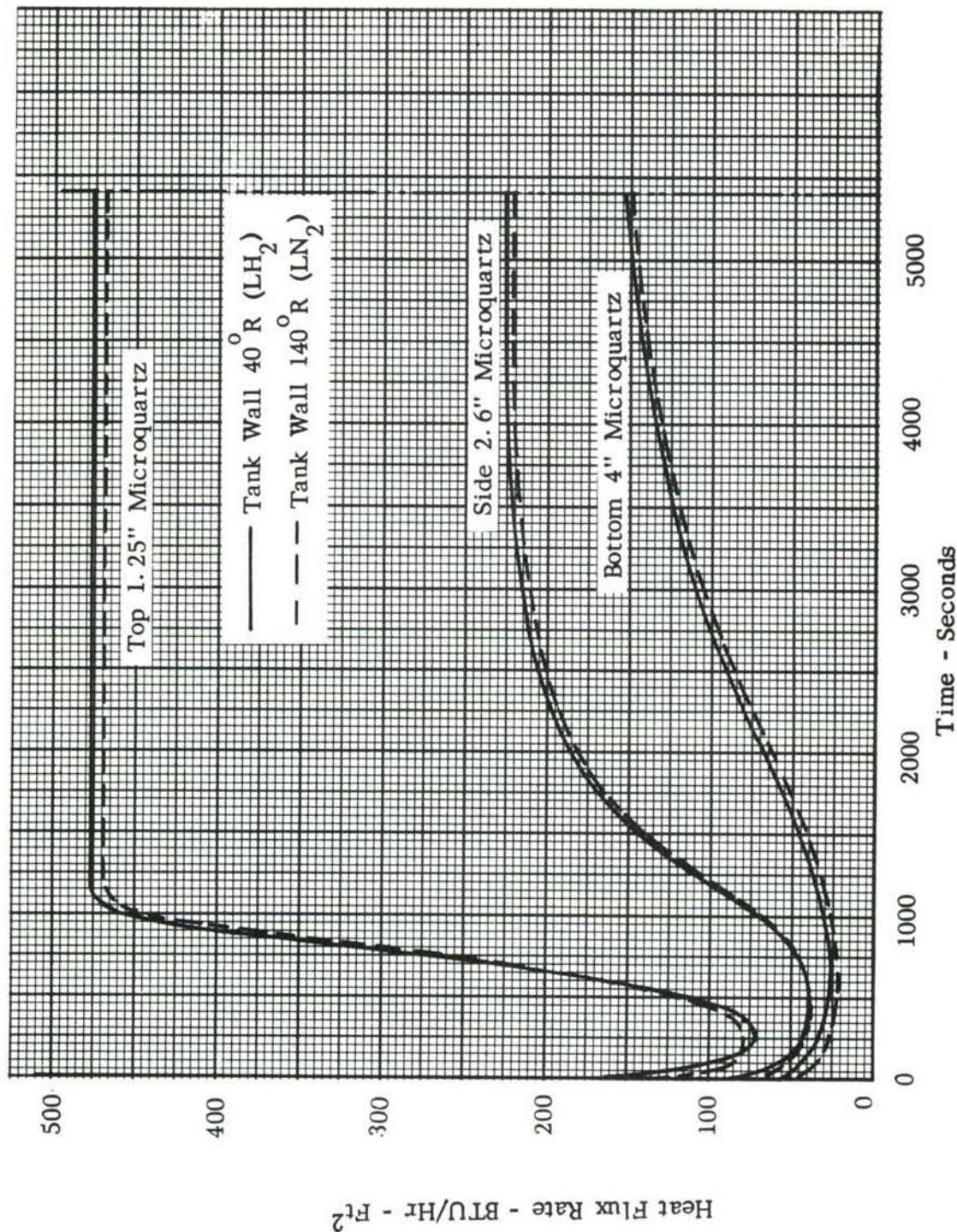


FIGURE 101. HEAT FLUX RATE TO CYLINDRICAL AREAS - TANK # 1

than that to a $140^{\circ}\text{R. (LN}_2\text{)}$ cold wall. The cone section of the tank was analyzed in four segments along with one segment on the cylinder and one segment on the six-inch diameter cone extension. Typical heat flux rates to the bottom part of the cone are shown in Figure 102. Segments 1 through 6 are analyzed simultaneously permitting heat conduction both normal to and parallel to the tank skin. Heat transfer to the outside surface of the insulation on the cone end includes radiation interchange with the radiation shield and with the test chamber walls. The test chamber walls were assumed to be a 530°R. black body. Heat conduction to the cylinder is shown as segment 0 in Figure 102 for comparison. The predicted penetration heat leaks are shown in Figure 103. These include the supports, the vacuum jacket on the fill line and the vent line, and the 6-inch diameter extensions on the cone ends. Heat transfer from the vent pipe to its vacuum jacket, submerged in liquid, is very small and was neglected. The heat transfer rate to the liquid for various wetted areas or liquid levels is shown in Figure 104 for a LH_2 tank wall temperature. The predicted heat transfer rates to LN_2 (140°R.) are about 4% less than that to LH_2 .

5.5.1.2 Insulation Thermal Conductivity. The predicted performance discussed above constituted the original prediction based on thermal conductivity, k , of Microquartz in helium obtained from the cryotherm testing. Values were obtained at 1.0 atm and 0.01 atm from the cryotherm tests (Appendix I, Figures 126 and 127. After the subscale tank test data was reduced it became apparent that the large decrease in heat flux during the transient portion of the trajectory which had been predicted (Figure 104) was not evident. This was also noted when an attempt was made to analytically reproduce the transient temperatures measured in the inner insulation layers. The k value of the insulation as a function of pressure had been used analytically as a straight line interpolation between the two known values at 760 and 8 mm Hg pressure. This is illustrated in Figure 105. Measured values of the thermal conductivity of Dynaquartz, a material similar to Microquartz, in helium at 760 and 55 mm Hg are given in Reference 8. This data indicates approximately a 15% reduction in k when the pressure is reduced to 55 mm Hg. Thus for the revised boil-off prediction this value was used in addition to the two test values. This curve is also shown in Figure 105. A theoretical analysis of the gaseous contribution to k in a fibrous insulation is currently being developed by General Dynamics Convair under Contract AF33(615)-1672 (Reference 8). This method was used to calculate the apparent k of Microquartz in helium as a function of pressure. The results are also shown in Figure 105. Both the test results and the theoretical calculation indicate that k remains large until the pressure is reduced to near 0.01 atm.

Typical transient measured and predicted temperatures in the top insulation are shown in Figure 106. Temperature predictions were calculated using the revised insulation k value. Good agreement is shown between the predicted and measured temperatures throughout the trajectory. The measured rate of temperature change in the bottom insulation, Figures 107 and 108, is greater than the predicted value. This may be due in part to both lower initial temperature at ground hold and an incorrect low temperature specific heat. Good agreement is indicated between the predicted and measured temperatures at low pressure during the hydrogen tests, Figure 108. The temperature depression in the bottom insulation during the nitrogen tests, Figure 107,

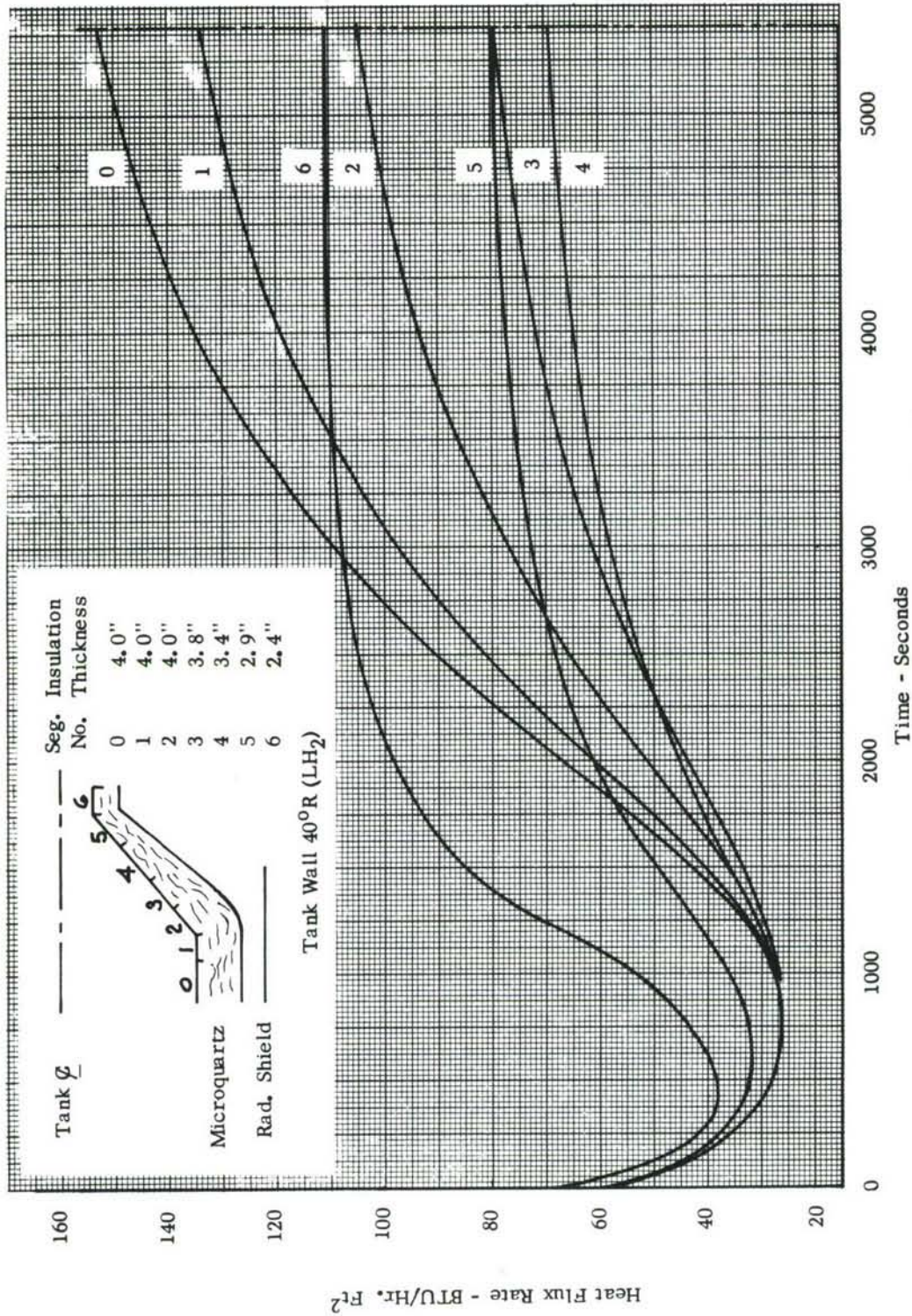


Figure 102. HEAT FLUX RATE TO CONE END - TANK # 1

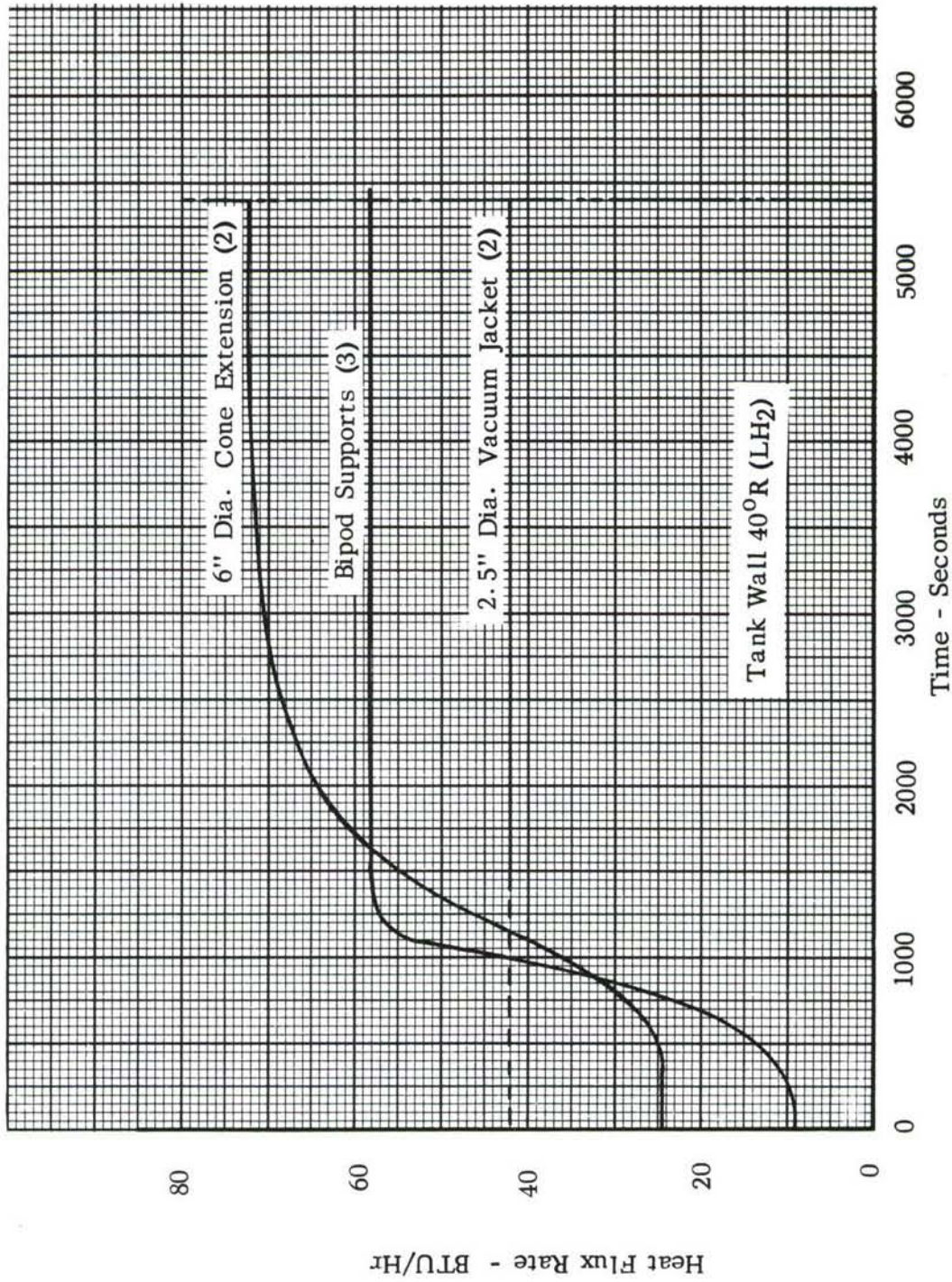


FIGURE 103. HEAT FLUX THROUGH PENETRATIONS - TANK #1

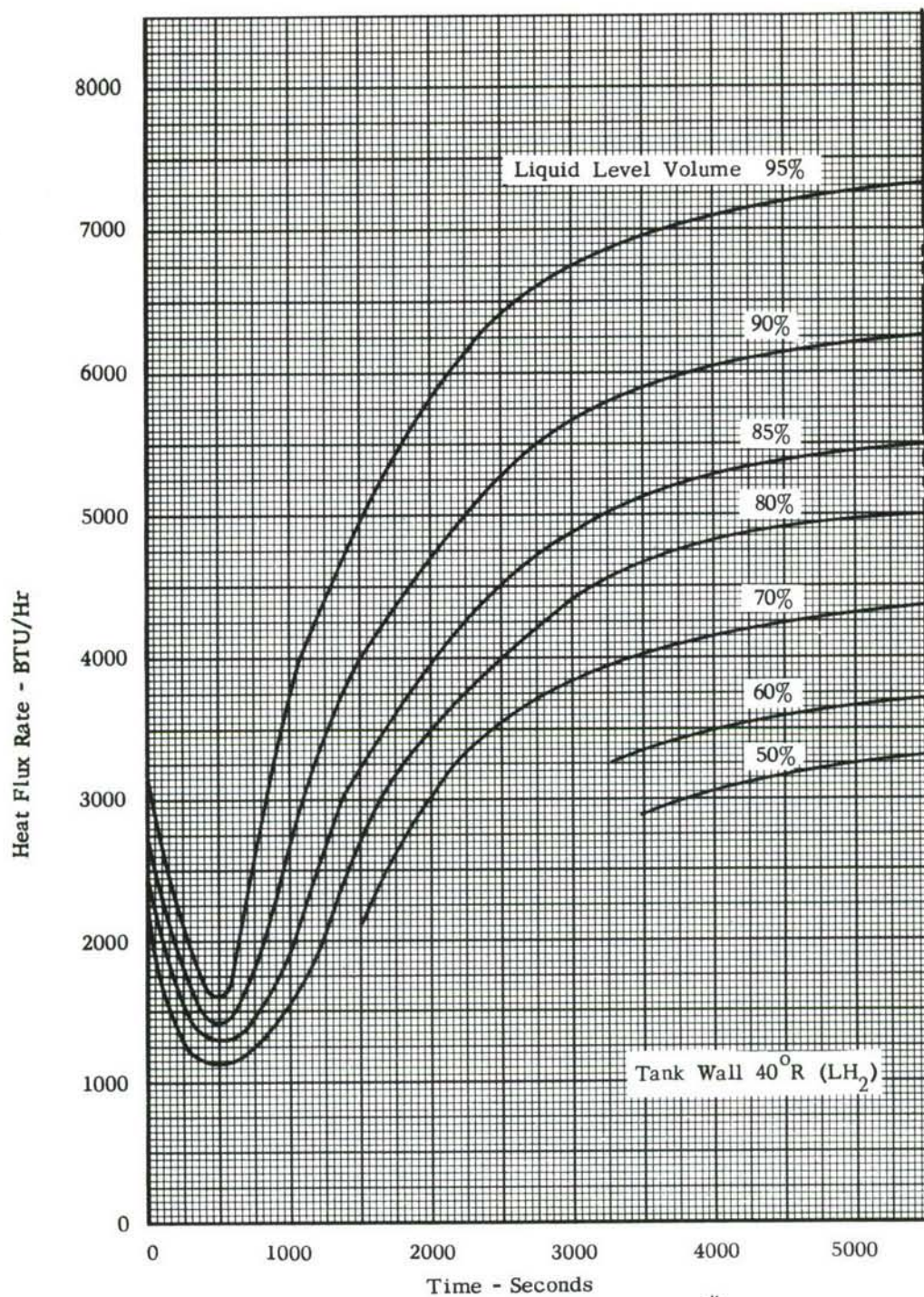


Figure 104. HEAT FLUX TO LIQUID -TANK # 1

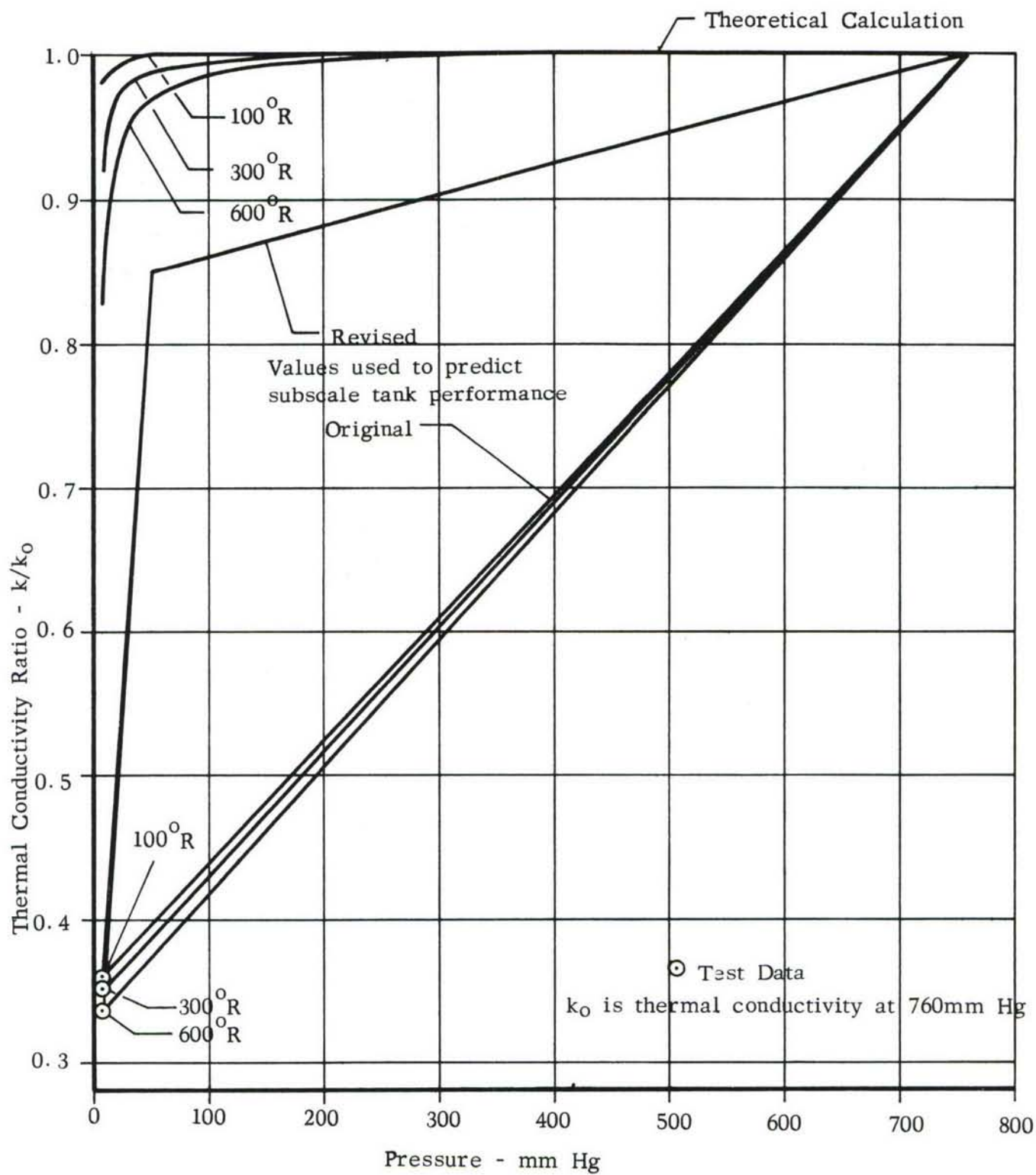


Figure 105. THERMAL CONDUCTIVITY RATIO OF MICROQUARTZ IN HELIUM
Vs PRESSURE - TANK #1

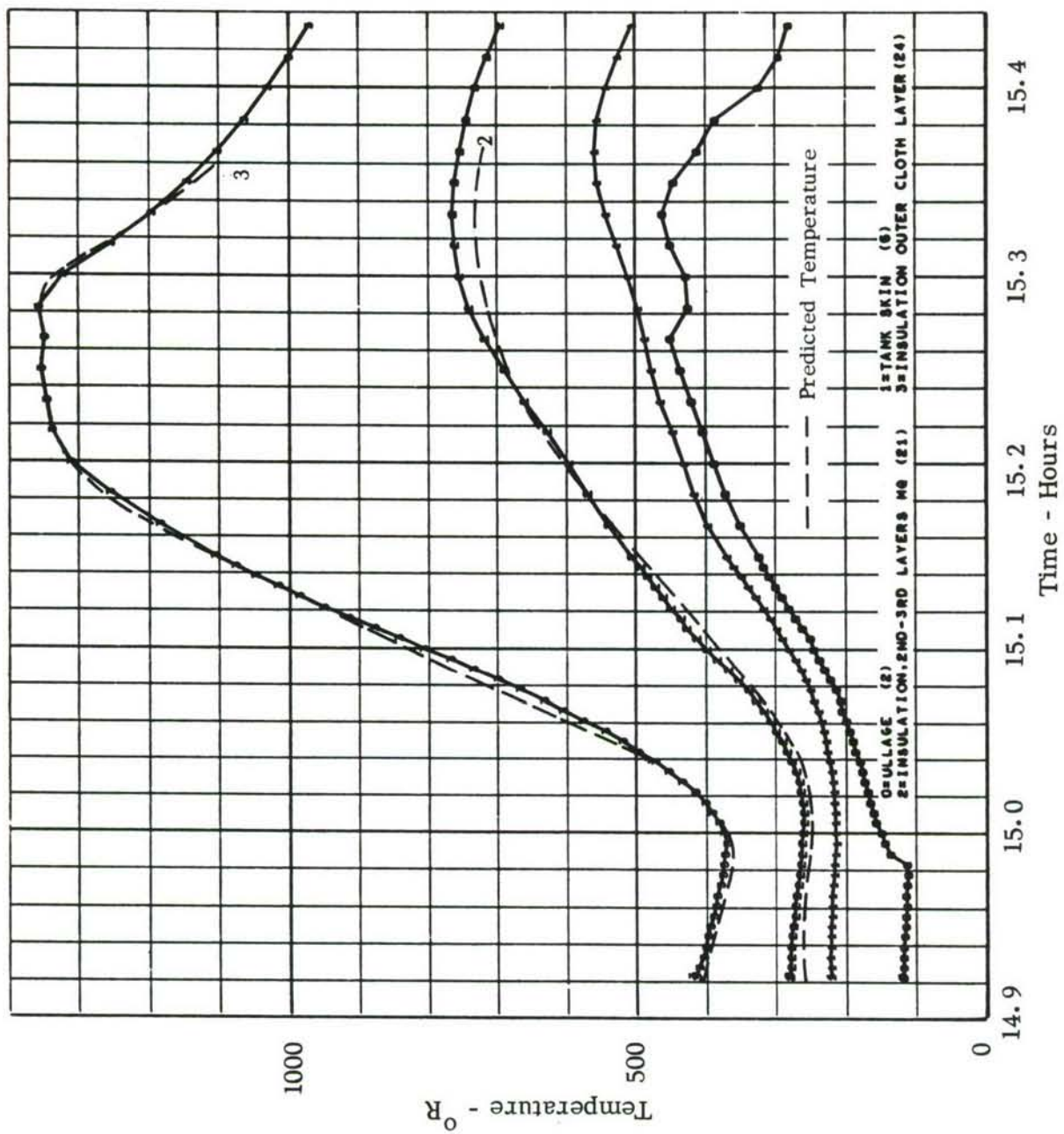


FIGURE 106. TOP INSULATION, TANK SKIN AND ULLAGE TEMPERATURE - TEST 9

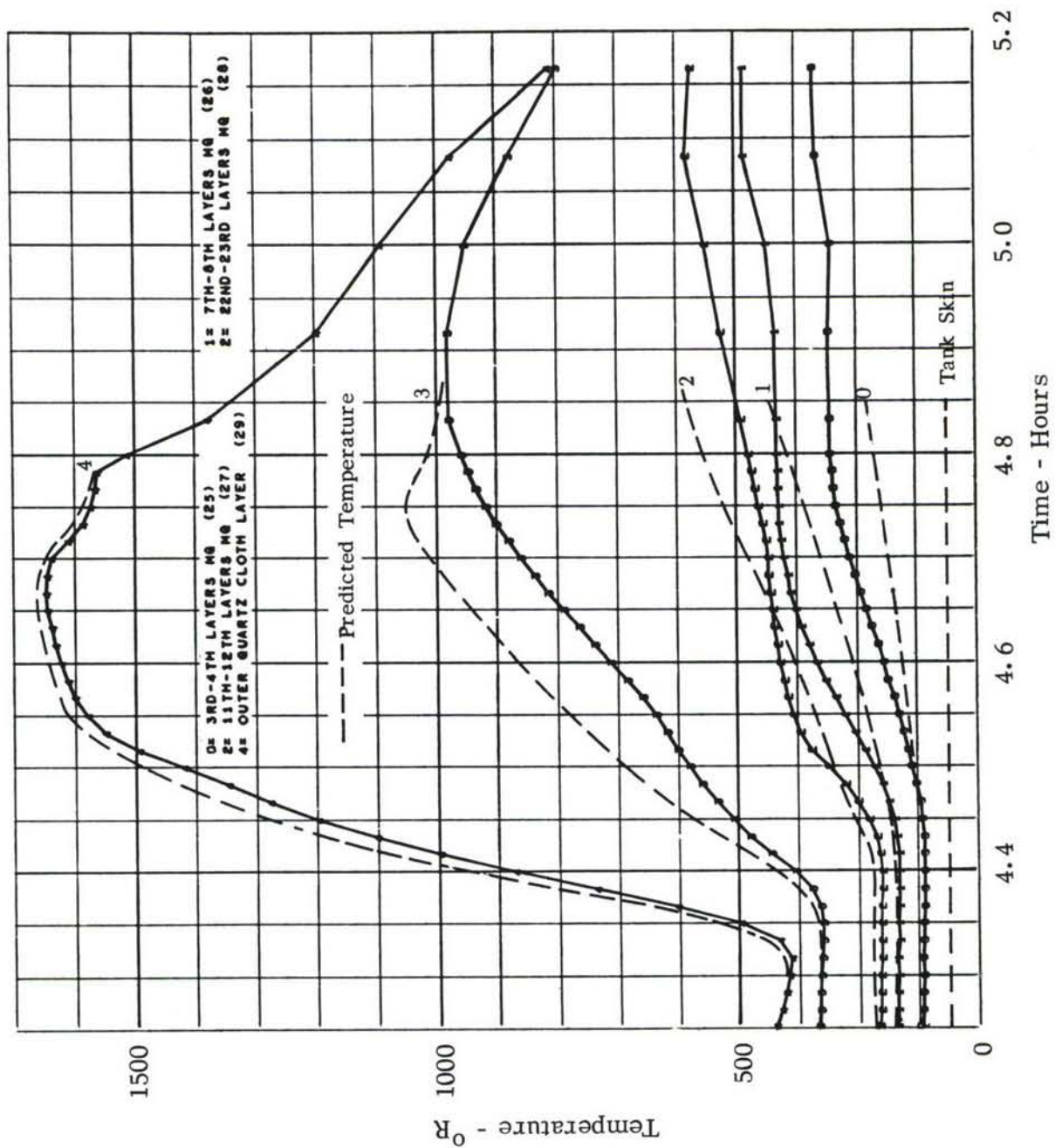


FIGURE 107. BOTTOM INSULATION TEMPERATURE - TEST 3

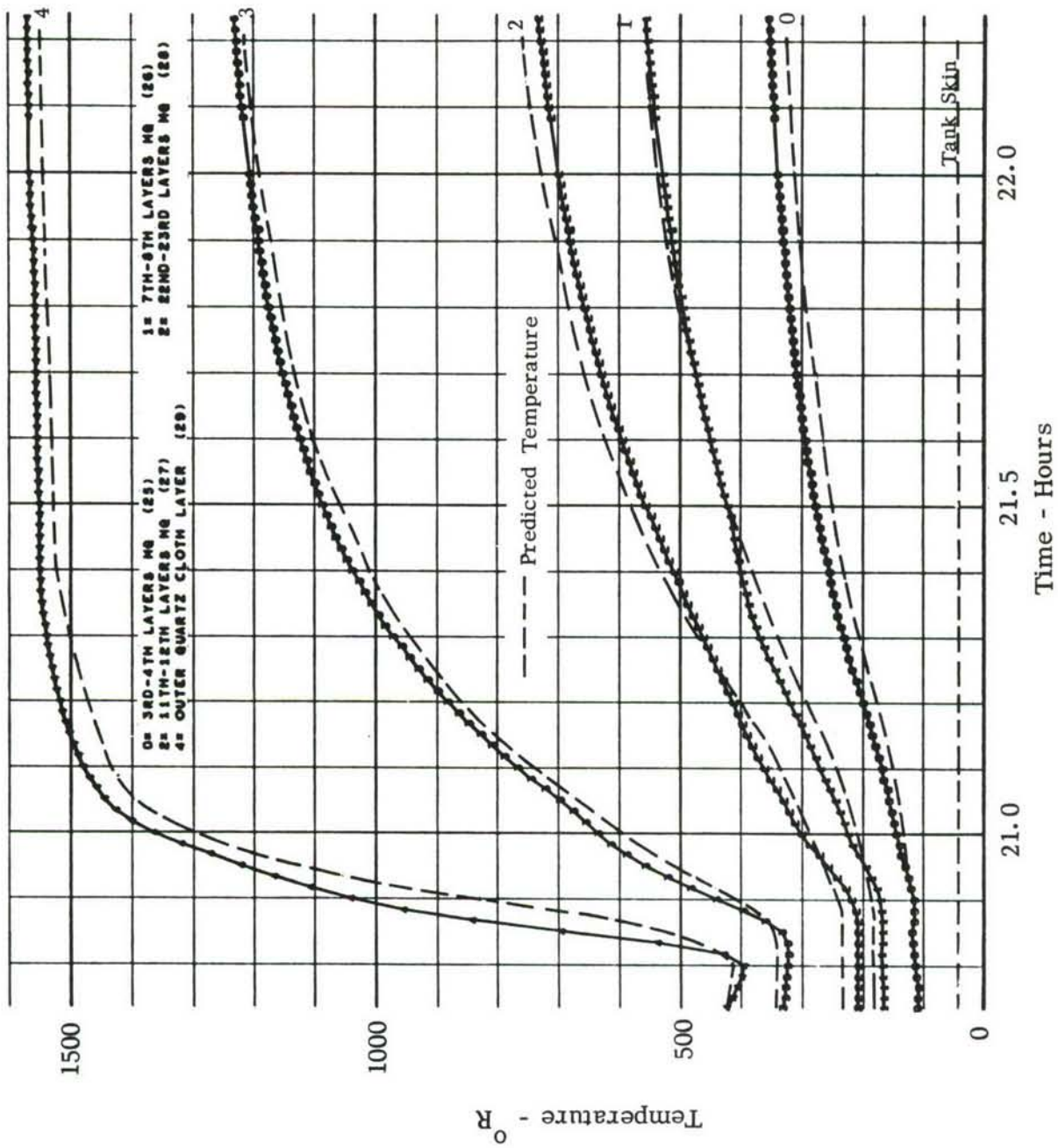


FIGURE 108. BOTTOM INSULATION TEMPERATURE - TEST 8

has not been explained. It appears that moisture may have been frozen in the insulation and evaporated somewhere above 400° R causing a lag in temperature.

The effect of changing the k value of the insulation as a function of pressure is shown in Figure 109. The measured heat flux rate, the original and the revised prediction are shown for Test 6. The original prediction shows a large reduction in heat flux rate during the transient portion of the trajectory. This has been substantially eliminated by properly representing the insulation conductivity as a function of pressure.

The measured heat flux rate during ground hold during most of the tests was near 4000 BTU/hr, whereas the predicted value was nearer 3000 BTU/hr. This is shown in Figures 81, 85, 89, 94, and 98. Since the thermal conductivity has only recently been determined for the Microquartz material in helium in the cryotherm tests, it seems unlikely that the handling and installation on the test tank would have caused such a large deterioration in the insulation quality. It was noted that the measured temperatures in the bottom insulation during ground hold were considerably lower than the predicted values, Figure 87. It is considered possible that the convection currents in the insulation may contribute in part to the increased heat flux. A hypothetical example of this is illustrated in Figure 110 with the subscale tank as a model. The environmental gas (in this case, helium) is assumed to enter the insulation on the upper section of the tank, and as a result of cooling inside the insulation along the tank's surface, flow downward and out the bottom. In the example chosen, a heat loss of 1000 BTU/hr can easily be obtained with gas velocities less than one foot per minute. This will result in high heat flux to the upper area of the tank and as the cold gas flows out the bottom reduce the heat flux and decrease the insulation temperature at the bottom. The test results support this concept. It should be possible to reduce this convective effect by including a barrier in the outer insulation layer. It must be pointed out, however, that a barrier which will prevent convective flow will also limit the outflow of gas as the external pressure is reduced and could result in a stress being applied to the insulation and barrier unless it is adequately vented. The material must also be capable of withstanding the high temperature associated with the external insulation layers.

5.5.1.3 Supports and Penetrations. The heat loss through the support was predicted prior to testing to be 10 BTU/hr at ground hold and 58 BTU/hr in flight. These predictions were based on calculated temperatures of the support flanges welded to the tank; 100° R at ground hold and 200° R at the high temperature. The measured values during a test are shown in Figure 111. These are 210° R at ground and 500° R at high temperature. The resultant heat fluxes are now estimated to be 40 and 175 BTU/hr.

The heat loss by conduction through the vacuum jackets on the vent and fill lines was predicted to be 42 BTU/hr, based on an estimated temperature of 300° R. The measured temperature is 200° R maximum. This heat leak is now estimated to be about 20 BTU/hr.

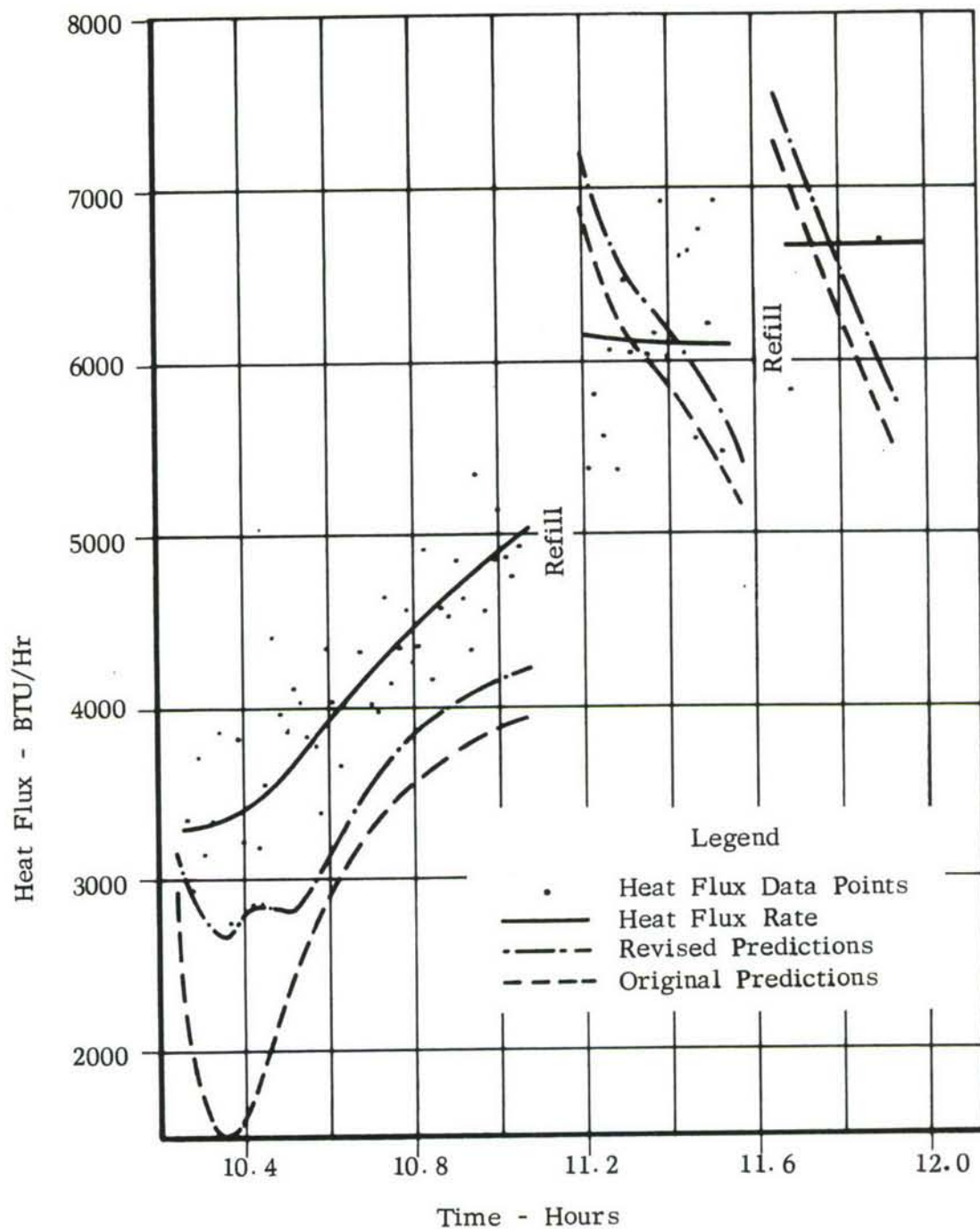
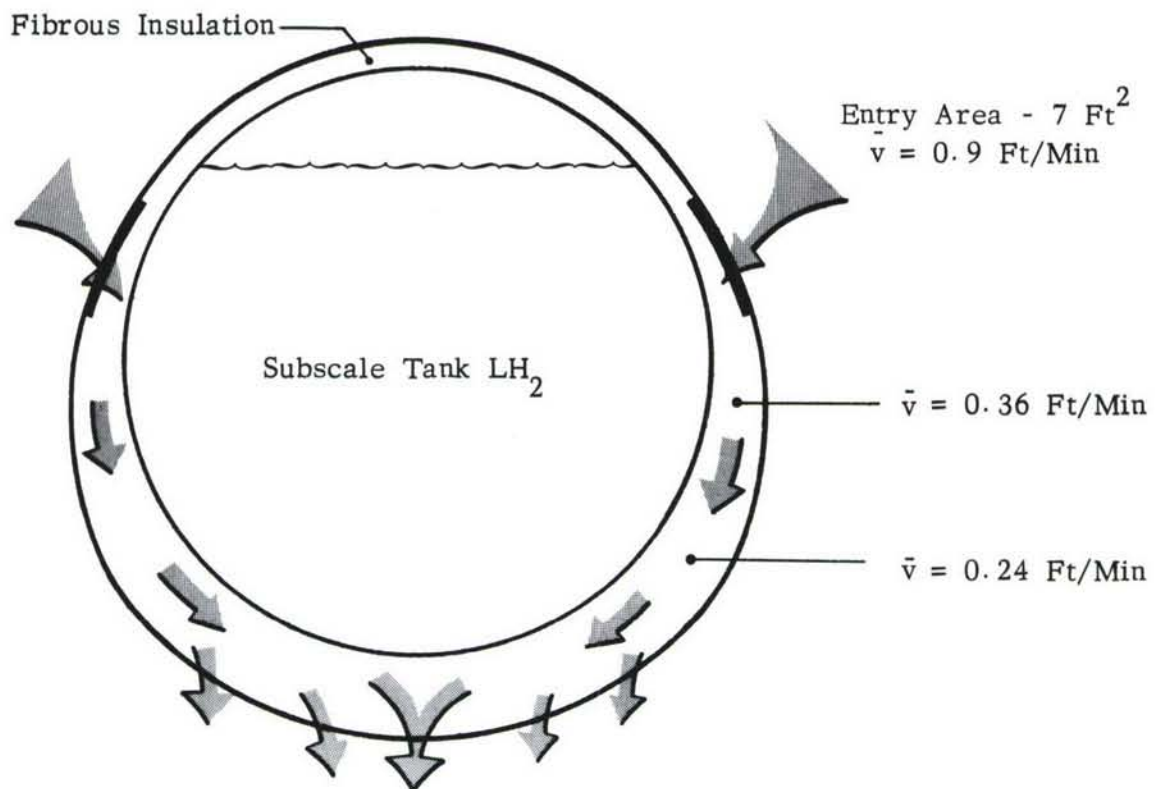


Figure 109. HEAT FLUX RATE TO LIQUID - TEST 6

Environment - Helium, 490°R , 700 mm Hg

Assume: Heat Loss = 1000 BTU/Hr
He ΔT = 200°R

Resultant Mass Flow Rate = 4.0 Lbs/Hr



Note : Sketch intended only to illustrate relatively large heat loss which can result from a very small convective mass flow and velocity.

Figure 110. CONVECTIVE HEAT LOSS IN SUBSCALE TANK AT GROUND HOLD.

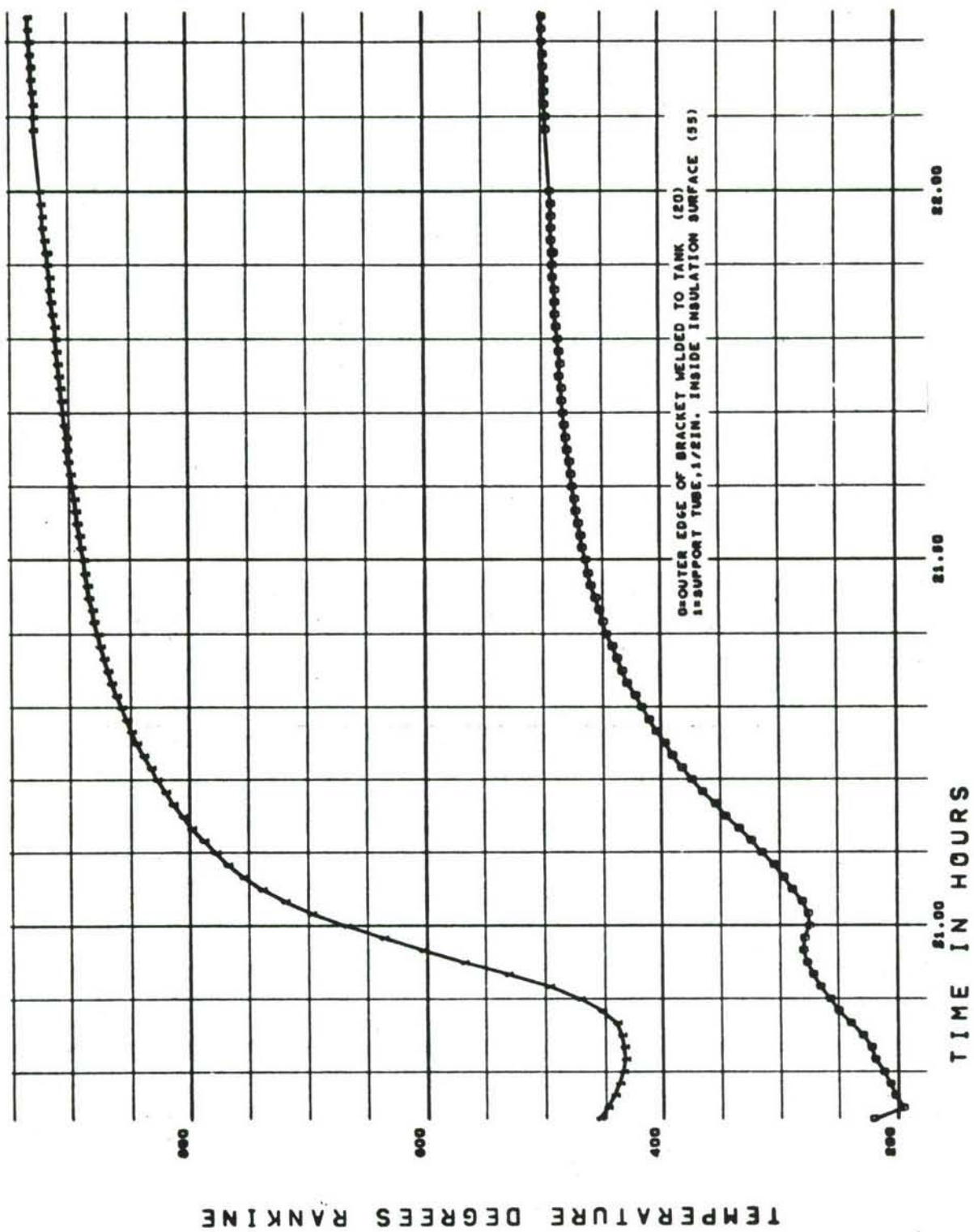


FIGURE 111. FORWARD LONGITUDINAL SUPPORT TEMPERATURE - TEST 8

The resultant penetration and support heat leaks are 85 BTU/hr and 360 BTU/hr at ground hold and high temperature operation vs the predicted values of 65 BTU/hr and 170 BTU/hr.

5.5.1.4 Radiation from Tank Upper Surface. The radiated heat flux to the liquid from the tank upper surface was calculated for each test where the tank temperatures were 500° R or more. These were based on an assumed emissivity of 0.2 for the tank wall and an absorbtivity of 1.0 into the liquid. The maximum heat flux which resulted was 300 BTU/hr during Test 4 where the tank temperature reached 750° R, Figure 86. The radiative heating has been included in the revised predictions for the total heat flux rate to the liquid.

5.5.1.5 Additional Heat Fluxes. The discrepancy between the predicted heat flux rates and the measured heat flux rates at ground hold have been estimated to be due to convection. The discrepancy at high temperature and low environmental pressure is quite variable. Since the predicted temperatures in the insulation at this condition are in reasonably good agreement with the measured values, it is assumed that the heat conduction through the insulation is correct. The other sources of heat have been accounted for; viz., radiation and penetrations. Thus, some additional factors may be influencing the apparent heat flux or boiloff rates.

It should be pointed out that in reducing the test data to obtain the "measured" heat flux rates, considerable data scatter resulted. The actual data points have been plotted in Figure 109 for Test 6. The faired curves through these points represent, at best, a $\pm 10\%$ approximation. The measured mass flow rate through the flow meter was corrected for liquid temperature changes. When the temperature increased as a result of an increase in tank pressure, the heat flux rate was reduced to account for this sensible heat. When the temperatures decreased, the heat flux rate was increased to account for flashing.

The predicted values still are substantially less than measured values for all tests, except Test 8, Figure 98, where good correlation was obtained. This test was run at a tank pressure above 30 psia, Figure 96. This was the highest pressure used during any of the boiloff tests. The liquid level also dropped below 50% at the end of the test.

Two additional factors may have increased the boiloff rates. The predicted heat flux rate is based on a tank wetted area measured by the level sensors in the center of the tank. A boiling (bubbling) layer of liquid along the tank wall could have increased the effective wetted area, thereby increasing the boiloff an indeterminate amount. The other factor which may have increased the boiloff is the rapid pressure variation in the test tank during most tests (Figure 96). When the ullage pressure is suddenly reduced below the vapor pressure in liquid hydrogen, the liquid flashes and becomes turbulent throwing liquid droplets into the warm ullage and against the dry tank surface. Any droplets which absorb heat from the ullage and vaporize are lost liquid and will result

in an increase in actual boiloff.

The dynamics of the vent system pressure control apparently caused surges which resulted in the pressure variations evident in the test data. The transducer measuring tank pressure was on a long piece of tubing outside the altitude chamber. This may have caused a time lag in the system. A rapid reduction in pressure at times might have caused flashing, overloading the vent, causing the control valve to go full open. Then, as the pressure rose, the boiling quickly subsided which suddenly dropped the pressure. The vent system in future testing will be designed to correct this problem.

5.5.1.6 Liquid Heating Summary. The heat input to the liquid which results in boil-off losses are tabulated in Table 5. Insulation, penetrations and radiation are normal predictions and typically account for 70 to 80% of the over-all boiloff measured during the tests. Measurement and prediction error will always exist in any analysis or test but, statistically, would be expected to yield values both greater and less than actual, thus, hopefully average out. The unaccounted losses which can be seen qualitatively are primarily the result of dynamic behavior of the liquid. Since these may account for 20 to 30% of the over-all loss, methods of predicting or preventing them need to be developed. The propellant loss due to boiloff is not the only problem. Inaccurate boil-off predictions will also result in incorrect vent system sizing. A vent system oversized 30% to provide for contingencies could be a substantial penalty in a system which may be one to three feet in diameter. On the other hand, a system undersized 30% could be dangerous.

TABLE 5. TYPICAL BOIL-OFF LOSSES DURING A TEST

1.	CONDUCTION THROUGH INSULATION	3000
2.	PENETRATIONS AND SUPPORTS	300
3.	RADIATION FROM TOP INTO LIQUID	150
4.	UNACCOUNTED	
	INDETERMINATE LIQUID LEVEL	
	FLASHING (LIQUID DROPLETS)	1000
	MEASUREMENT ERROR	
		<hr/> 4450

5.5.2 LIQUID STRATIFICATION. Liquid stratification occurs in cryogenic tanks when the ullage pressure is raised above the liquid vapor pressure. As the liquid heats, the warm lower density fluid tends to rise to the top, displacing the more dense colder liquid. Tank geometry, as well as the rate and location of the incoming heat flux, influence stratification. Stratification measurements have been made and thermodynamic models developed for vertical cryogenic tanks. Vertical tanks with side heating have a high degree of stratification as the liquid heats along the sidewalls and rises through a convective boundary layer to the top. Stratification can be minimized in vertical tanks

by bottom heating which tends to keep the bulk liquid mixed. Horizontal tanks with cylindrical cross section have little vertical surface on which to develop a boundary layer and at the same time, a large "bottom" area; thus, if uniformly heated, should exhibit little tendency for stratification. It was assumed in the thermal analysis of the double-bubble tank in this program that the liquid heated uniformly with no stratification.

The optimized insulation system resulted in a variable insulation thickness with 1.25 inches on the top and 4.0 inches on the bottom. It is to be expected then that an upper volume of liquid will heat more rapidly than a lower volume in contact with the same area. This naturally would result in stratification without any liquid displacement. The volume of liquid in the bottom, however, is in contact with a very large area which offsets the lower heat flux rate through the thick bottom insulation. This, then, should result in mixing in the lower half of the tank and cause a uniform heating rate with little stratification.

Liquid stratification was measured for a ground hold condition in Test 7. Typical platinum probe measurements are shown in Figure 95. These have been smoothed and corrected (Figure 112) to an initial temperature of 38.5°R (20 psia) before lock-up and a final temperature of 41.4°R (30.5 psia) after all liquid has reached the boiling point. The significant parameters are rate of temperature increase and the time each volume segment reached the boiling point. It is noted that the stratification is uniform from top to bottom and that the mixing and a uniform temperature which might have been expected in the lower half of the tank did not occur. The sketch on Figure 112 shows the tank volume segments considered, the location of the platinum probes and the time in minutes after lock-up that a particular probe reached the boiling point. It is noted that the probes in the tank center and at the side reached the boiling point at the same time, indicating that the liquid layers heated uniformly with very little circulation or liquid displacement; the only significant exception being the probe at the 12-inch liquid level four inches from the centerline. It appeared to be warmer and reached its boiling point two minutes before the other probes at that level. Thus, an internal circulation pattern may have existed. There is, however, no other evidence to support this since the probes lower in the liquid heated very slowly.

The test data; i.e., the time required for each volume segment to reach its boiling point, was used to calculate the heat flux rate required to heat that volume segment without any mixing from liquid above or below. This tabulation is shown in Table 6 as 'heat flux rate, \dot{q}_t '. The total heat flux is also shown for each segment, \dot{Q}_t , and the summation for the over-all tank, 3900 BTU/hr. Also listed in Table 6 is the theoretical time, θ_p , required to heat each segment to its boiling point under the same conditions; i.e., no mixing. The heat flux rate, \dot{q}_p , used to calculate the theoretical time is that based solely on the thermal conductivity of the insulation. There are two significant differences between the test data and the predicted values:

Table 6

HEAT FLUX RATES RESULTING FROM LH₂ STRATIFICATION TESTS

(Refer to Figure 112.)

Tank Segment	Depth Inches	Wetted Area, A Ft ²	Volume, V Ft ³	Test Data			Predicted		
				Time, θ_t Hours	Heat Flux Rate, \dot{q}_t BTU/Hr Ft ²	Heat Flux $\dot{Q}_t = \dot{q}_t A$ BTU/Hr	Time, θ_p Hours	Heat Flux Rate, \dot{q}_p BTU/Hr Ft ²	Heat Flux $\dot{Q}_p = \dot{q}_p A$ BTU/Hr
1	21.5-16.5	7.50	3.75	0.083	191	1431	0.106	150	1125
2	16.5-14.0	3.29	2.40	0.117	197	650	0.178	130	428
3	14.0-10.0	4.94	4.04	0.167	155	766	0.260	100	494
4	10.0-6.0	5.44	3.71	0.200	108	587	0.288	75	408
5	6.0-0	12.38	3.35	0.230	37	461	0.143	60	743
				Total		3900		Total	3200

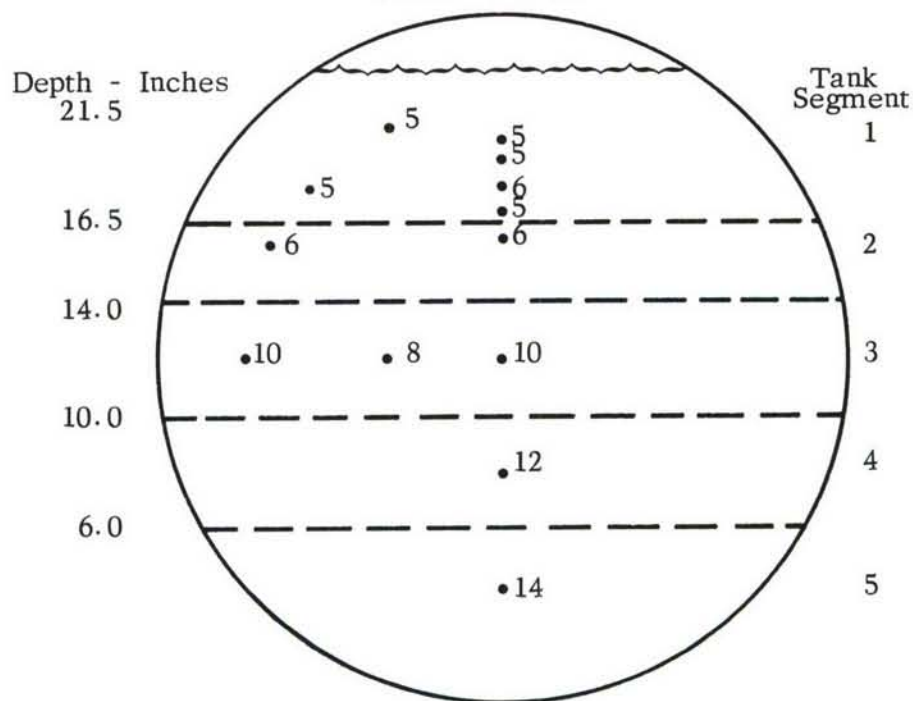
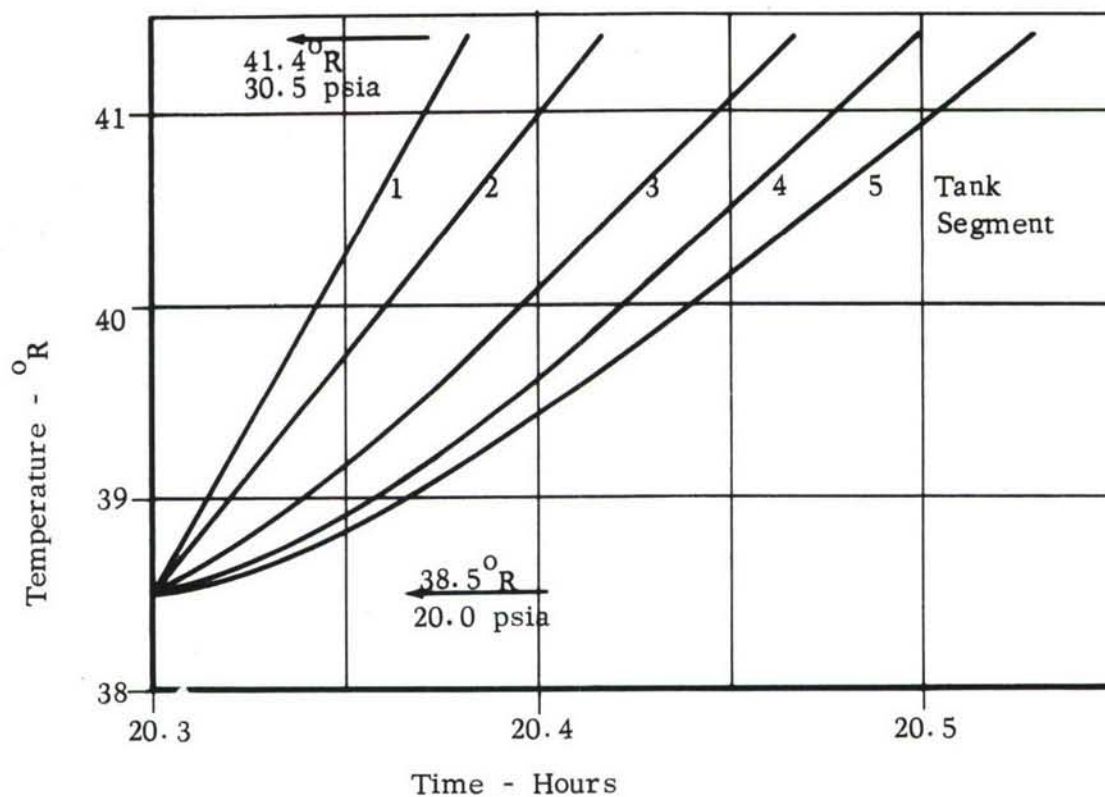
$$*\dot{q}_t = \rho C_p \Delta T \frac{V}{A \theta_t}$$

$$**\theta_p = \rho C_p \Delta T \frac{V}{A \dot{q}_p}$$

$$\rho = 4.2 \text{ Lbs/Ft}^3 \text{ (Nominal)}$$

$$C_p = 2.6 \text{ BTU/Lb } ^\circ\text{R (Nominal)}$$

$$\Delta T = 41.4 - 38.5 = 2.9 ^\circ\text{R}$$



- Pt Probe : Minutes after lock-up that probe indicated liquid reached boiling point
- Figure 112. LH_2 STRATIFICATION AT GROUND HOLD - TEST 7

1) The bottom layer theoretically should have heated rapidly with a "bottom heating" effect which would have resulted in mixing, thus heating the layer above at approximately the same rate. The test data therefore indicates that the heat flux into the bottom of the tank was in fact less than predicted.

2) The total heat flux rate to the tank is predicted to be 3200 BTU/hr., whereas the test data indicates 3900 BTU/hr., a value much closer to the measured heat flux 4100 BTU/hr., Figure 94.

The stratification data further supports the ground hold heat flux model which includes convection in the insulation. That is, an overall higher heat flux rate into the tank with a reduced heat flux rate on the bottom.

5.5.3 ULLAGE AND TANK SKIN TEMPERATURES. The use of the boil-off ullage gas to cool the dry upper tank wall is significant because: (1) the tank structure weight is dependent on the maximum or design temperature; and (2) the heat flux radiated into the liquid from a hot tank surface increases boil-off. The ullage and skin temperatures measured during the tests indicate that the heat transfer to the ullage even in the stagnant area at the top of the tank is quite large. This tends to keep the tank wall cool, and minimizes the need for a special spray cooling mechanism. The top tank skin temperatures at the mid-section of the tank 30 inches from the vent are shown in Figure 113 for Test 3, LN_2 boil-off; Test 8, LH_2 boil-off and Test 9, LH_2 transient temperature rise test with no venting. The test results show that the heat transfer to the ullage is substantial. The calculated time to reach 520°R is 0.25 hours assuming no heat transfer to the ullage. Even with the vent locked up the time to reach 520°R is 0.4 hours with a hydrogen ullage. The LN_2 boiloff test resulted in higher tank skin temperature than the LH_2 tests. This is to be expected since nitrogen has a lower heat capacity and thermal conductivity than hydrogen.

The ullage temperature distribution during the LN_2 boiloff test is shown in Figure 114 and during the LH_2 boiloff test in Figure 115. A similar plot is not available for the LH_2 transient temperature rise Test 9, because the platinum probes failed. The only ullage temperatures available in this test are the thermocouples one-half inch from the skin. The ullage temperature distribution in both LN_2 and LH_2 tests was considerably different than had been anticipated. The high heat flux rates associated with the upper tank surface had been expected to rapidly heat and form a hot stratified layer of gas which would effectively insulate the tank upper surface.

The temperature distribution down through the ullage and the tank skin temperature at the top are illustrated in Figure 115 for three different times during the trajectory during Test #8, the hydrogen boiloff test. The liquid level at each time is noted on the sketches at the right, along with the location of the temperature measurements. A dashed line connects the highest measured ullage temperature with the tank skin temperature above it. Note that the ullage remains very cold up to within an inch of the top of the tank. Even after 1.5 hours with the liquid level more than a foot below the tank surface, the ullage one inch from the top is 300° colder than the tank surface ($500^\circ - 200^\circ\text{R}$). The calculated horizontal average gas velocity at the particular

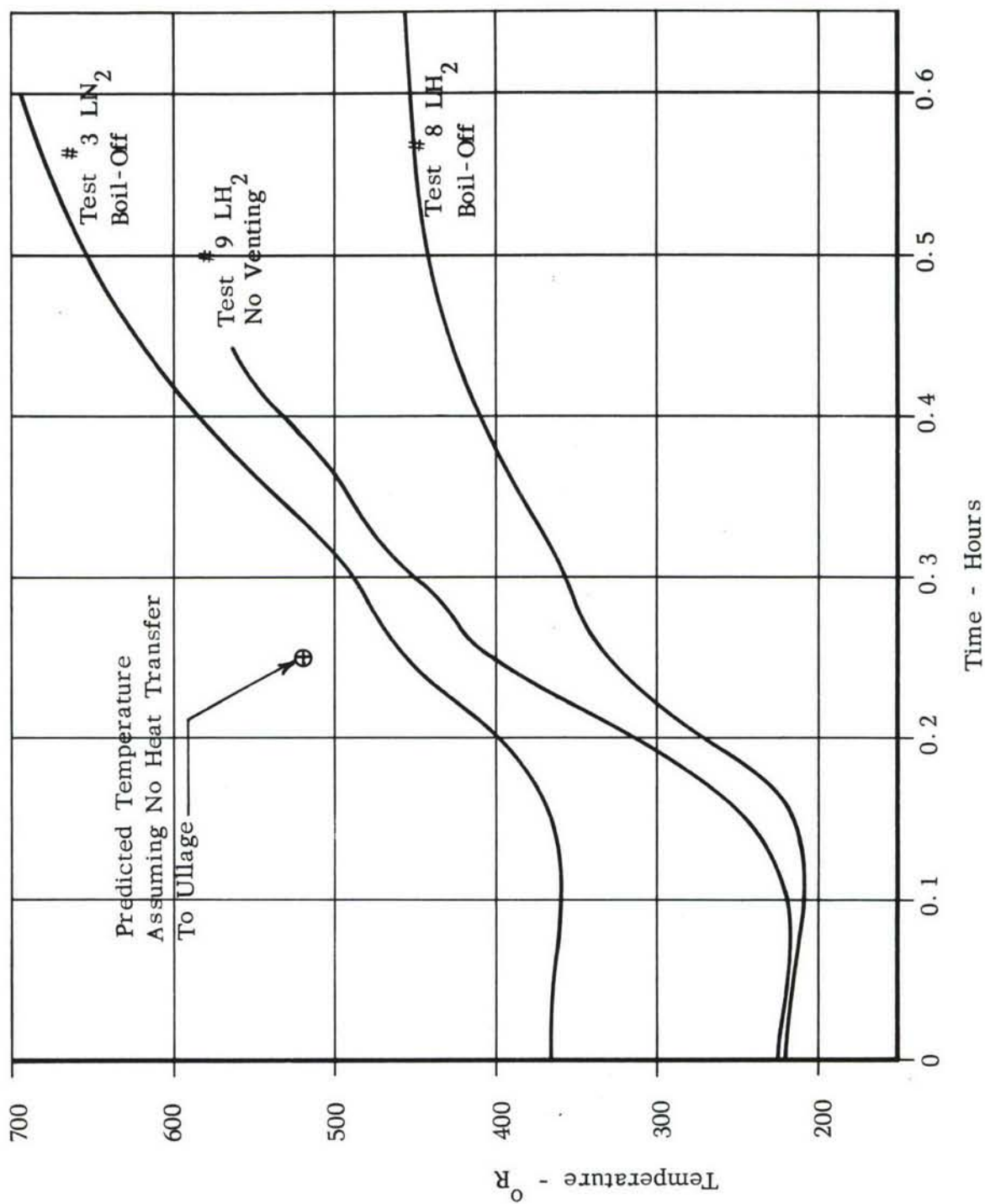


Figure 113. TOP TANK SKIN TEMPERATURE - MID-SECTION

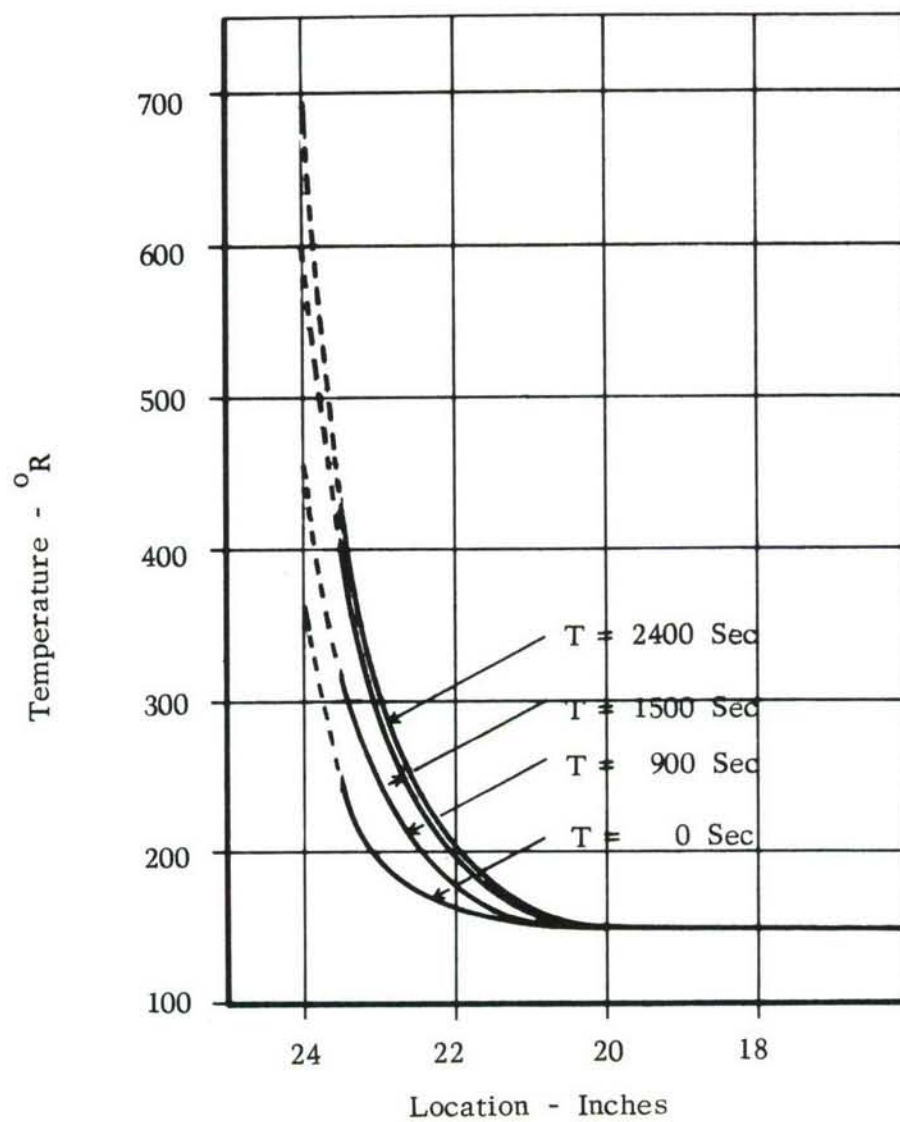


Figure 114. NITROGEN ULLAGE TEMPERATURES - TEST 3

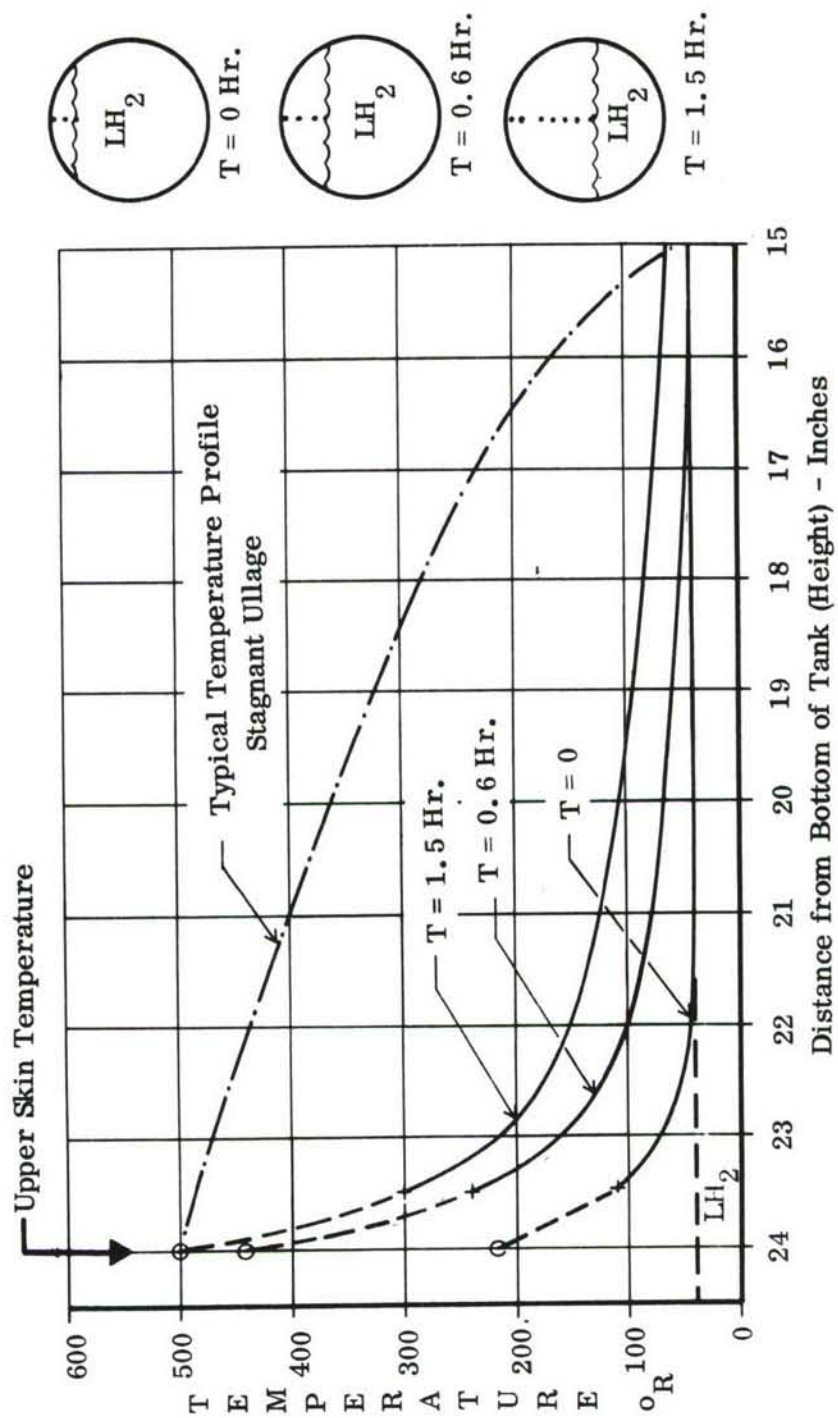


FIGURE 115. HYDROGEN ULLAGE TEMPERATURES - TEST 8

station (30") where the temperatures were measured is about 3 ft/min. Thus, mixing due to mass movement would not be expected to contribute significantly to the low temperature. If the ullage were completely stagnant, a hypothetical curve is depicted showing the temperature distribution due to conduction through hydrogen gas. It is possible that the boiling rate may have been high enough to inject liquid droplets into the ullage, thus maintaining the very low temperatures.

The convective heat transfer rate to the ullage was calculated for each of the three tests shown in Figure 113. Using the measured transient tank skin temperature and top radiation shield temperature, the radiative and convective heat transfer rate from the skin was calculated. The emissivity of the upper tank skin was assumed to be 0.2. The results are tabulated below for the trajectory time of 0.2 hours:

	Radiative Heat Flux BTU/hr. ft^2	Convective Heat Flux BTU/hr. ft^2	Tank Skin Temp. $^{\circ}\text{R}$	Ullage Temp. $^{\circ}\text{R}$	h $\text{BTU/hr. ft}^2 \text{ }^{\circ}\text{R}$
Test 3	25	290	520	360	1.8
Test 8	7	357	370	210	2.2
Test 9	19	301	480	440	7.5

The calculation of the heat flux rate also included the predicted temperatures in the insulation layers, Figure 106. The temperature difference between the ullage and the skin used to compute the convective heat transfer coefficient is the thermocouple measurement one-half inch from the skin. Under the temperature conditions tabulated above, the calculated heat transfer coefficient is of the correct order of magnitude for free convection in Tests 3 and 8, but the value of $7.5 \text{ BTU/hr. ft}^2 \text{ }^{\circ}\text{R}$ for Test 9 is substantially higher than normal free convection. However, using the gas temperature one-half inch from the skin to obtain a heat transfer coefficient is arbitrary and does not necessarily represent the correct bulk gas temperature which should be used. The significant result is that the heat transfer rate did provide upper tank wall cooling.

The measured temperature distribution in the ullage is different than had been anticipated and the bulk gas temperature was quite low. The possibility, mentioned in Section 5.5.1.5, that liquid was being injected into the ullage because of pressure fluctuations and flashing may have contributed to the low ullage temperatures. If this is true, then the ullage and skin temperature may have been too low; however, the results of Test 9, where no venting occurred, represents an upper limit which can be used to evaluate the heat transfer rates.

5.5.4 NITROGEN/HYDROGEN SIMILARITY IN TESTING

Testing insulated cryogenic hydrogen tankage and its associated fuel system in its total environment is complex and can be hazardous. The use of nitrogen to test this tankage is obviously desirable. Testing with nitrogen, because it is inert, is obviously far

safer than testing with hydrogen. Nitrogen costs less than hydrogen and facility costs are also less primarily because of safety requirements.

The primary reasons for testing are:

- 1) Evaluate the insulation installation in its environment throughout the range of temperatures and pressures including thermal shock and rapid pressure changes.
- 2) Evaluate the thermal protection of cryogenic liquid or insulating quality of the insulation to minimize boil-off.
- 3) Evaluate the cooling system necessary in the ullage or dry areas of the tankage to prevent overheating.
- 4) Evaluate the fuel system; pumps, vent and pressurization.
- 5) Evaluate the structural integrity of the tank installation, including supports.

The areas to be evaluated in a test program itemized above are inter-related and all must be properly accounted for in order to develop a safe and optimum system.

The use of nitrogen as a test substitute for hydrogen is most compatible in the first two areas mentioned above; insulation compatibility with the environment and thermal protection of the liquid. Pressure and temperature cycling which must be done to determine the life or reliability of an insulation system will not be significantly affected by the temperature difference between nitrogen (140°R) and hydrogen (40°R) provided, of course, the basic materials are compatible with 40°R temperature. The heat flux rate through an insulation to liquid hydrogen or nitrogen are practically the same. Predicted heat flux rates through both the all Microquartz and the Microquartz/foam system differed by only about 5% from hydrogen to nitrogen. This is because of the characteristic reduction in thermal conductivity of almost all materials as the temperature is lowered from 140° to 40°R . Since heat flux is proportional to the product of thermal conductivity, k , and temperature difference, ΔT , across the insulation, the increase in ΔT is offset by the decrease in k to yield a practically constant heat flux.

One exception to the foregoing has become apparent as a result of the work done on the composite Microquartz/foam system. A sealed or composite insulation system is intended to eliminate the need for helium which has a high thermal conductivity and is in short supply. A substitute gas such as air or nitrogen must be prevented from cryopumping at the sealed interface. Most sealed systems will include the use of materials which are temperature limited and therefore must be prevented from overheating at high operating temperatures, especially on the dry upper tank surfaces. Thus nitrogen is not recommended for use in cyclic environmental tests of a composite system. Nitrogen will not demonstrate non-cryopumping capability nor would an ullage cooling system designed for use with high heat capacity hydrogen be likely to perform satisfactorily with low heat capacity nitrogen.

The predicted heat flux rates through the insulation to both liquid hydrogen and liquid nitrogen were practically the same for a given liquid level and time after the start of a test. A considerable amount of time and funds were expended to obtain data which would yield an accurate prediction. Cryotherm tests were run to obtain good thermal conductivity data. A relatively complex analysis was made on the cone end configuration to obtain accurate heat fluxes. Corrections were made in the predictions after the tests in such areas as radiation from the upper tank skin, increase in support heat, and incorrect assumptions in variation of thermal conductivity with pressure. The error in the predicted boiloff rate compared to the measured values is shown in Figure 116. During the latter part of Test 8 with LH_2 the prediction was good. Generally, however, the predictions for the LN_2 tests were considerably less accurate than those for the LH_2 tests. The error in the predictions is believed to result, at least in part, from the characteristics of the boiling liquids; i.e., liquid being thrown into the ullage during flashing and a high effective liquid level at the tank wall due to rising vapor carrying liquid. Since, as a practical matter, neither ullage pressure variations nor boiling liquid at the walls can be eliminated, the use of liquid nitrogen to predict liquid hydrogen thermal performance could result in a largely indeterminate error.

Effective use of the boiloff gases is necessary to maintain a low structure temperature, thus preventing overheating the tank upper surface and reduce radiation into the liquid which will cause increased boiloff. The mass flow rate into the ullage due to boiloff is given by:

$$\dot{M} = \dot{q}_1 A_1 / H_v$$

and the heat balance in the ullage is given by the equation

$$T_u - T_\ell = \frac{\dot{q}_u A_u}{\dot{M} C_p}$$

where \dot{M} - boil-off mass flow rate
 A_u, A_1 - dry and wetted areas, respectively
 \dot{q}_u, \dot{q}_1 - heat flux rates to dry and wetted areas, respectively
 H_v - heat of vaporization (85 BTU/lb. N_2) (190 BTU/lb. H_2)
 C_p - heat capacity of gas (0.25 BTU/lb. $^\circ\text{R}$, N_2) (3.0 BTU/lb. $^\circ\text{R}$, H_2)
 T_ℓ - liquid boiling temperature (140 $^\circ\text{R}$, N_2) (40 $^\circ\text{R}$, H_2)
 T_u - temperature ullage at vent

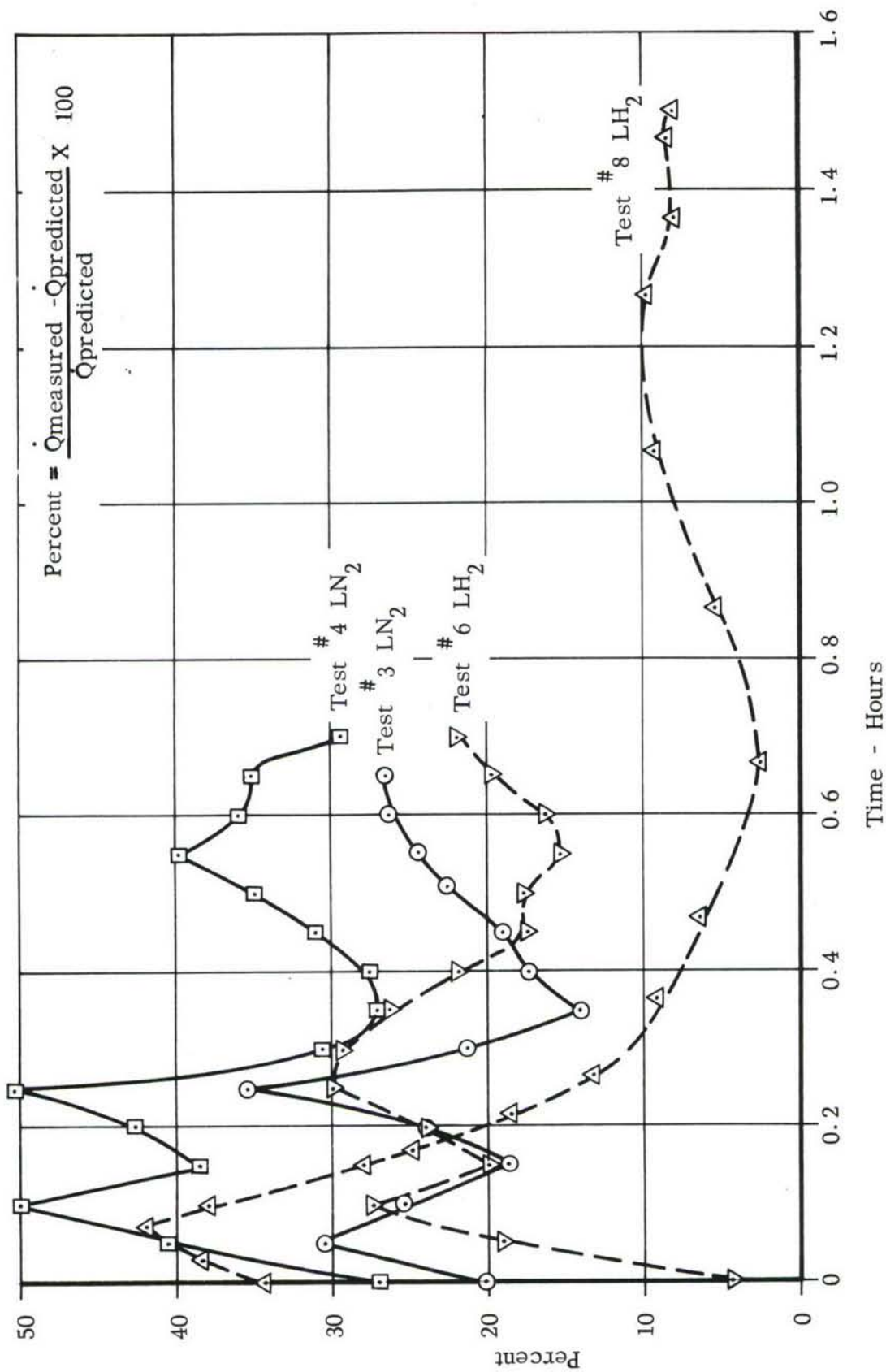


Figure 116. DEVIATION OF MEASURED BOIL-OFF RATE FROM PREDICTED BOIL-OFF RATE

As a first approximation it can be assumed that the heat flux, \dot{q} , into the liquid and the ullage for both nitrogen and hydrogen are equal. Combining the above equations, substituting in the values and taking the ratio nitrogen temperature rise to hydrogen temperature rise gives

$$\frac{[T_u - 140]}{[T_u - 40]} \frac{N_2}{H_2} = 5.4$$

Thus for a case where the hydrogen boiloff gas is discharging at 140°R , the nitrogen would be discharging at 680°R . It is obvious that the use of nitrogen to evaluate ullage conditions and tank wall cooling is not a suitable substitute for hydrogen. Identical conditions of heat flux rate and liquid level are not available from the test results but the tank skin temperature curves in Figure 113 illustrate the large difference between the two fluids during boil-off tests.

The use of nitrogen to evaluate a hydrogen fuel system would be impractical. In the vent system, for the reasons discussed above, the nitrogen would be hotter than hydrogen resulting in different system pressures. A hydrogen fuel pump is not suitable for pumping nitrogen. Thus special components compatible with nitrogen would be required if nitrogen were used for thermal evaluation of the insulation. The use of nitrogen in the large scale, 6000 gallon tank for test purposes, has been investigated and found to be impractical. It is intended that the tank be of light weight aerospace type construction. The difference in the weights or static heads of the two fluids precludes the use of nitrogen in a light weight hydrogen tank. Inserting light weight materials into the tank to displace most of the nitrogen was investigated. If the foam blocks are unsupported, they float to the top leaving the cryogenic fluid all in the bottom. If the foam could in some way be supported, the buoyancy forces would have to be carried into the tank structure. Thus if nitrogen is used for thermodynamic purposes it would have to be in a boiler-plate tank. This would result in non-representative support systems and heavier material gauges which would result in changes in the transient heating and cooling rates especially in the ullage or dry areas of the tankage system.

5.5.5 CONCLUSIONS AND PHASE II LARGE SCALE TANK RECOMMENDATIONS

1. The predicted thermal performance of the insulation was good during simulated flight at low environmental pressure. Predicted performance during ground hold was low by as much as 50%. Helium convection in the fibrous insulation is believed to have significantly affected the local heat flux rates; an increase at the top and a decrease at the bottom of the tank.
2. Liquid stratification was different than predicted. The liquid stratified from top to bottom in horizontal layers. No significant liquid circulation was detected with the instrumentation used in these tests. Very little stratification

had been predicted especially in the bottom of the tank exposed to a large "heated" surface. The postulated external helium convection in the insulation correlates with the character of the stratification.

3. Liquid turbulence is believed to have contributed to the difference between measured and predicted boil-off rates. This turbulence increased the effective wetted area, thus the boil-off rate.
4. Bulk ullage temperatures were lower than predicted, due to greater than predicted boil-off and possibly due to liquid turbulence. The turbulence was caused by pressure fluctuations resulting from vent control problems. Pronounced ullage stratification occurred above the level of the vent. Temperature gradients in the top tank skin were as high as 50°R per inch. The stratification occurred both in the vent and non-vent end of the tank. This poses a potentially difficult problem in efficient utilization of boil-off gas to cool the upper tank surface.
5. Use of liquid nitrogen to evaluate a liquid hydrogen tank installation is of limited value. The weight or static head of nitrogen will probably overload most tanks designed for lightweight hydrogen. The low heat capacity of nitrogen boil-off will not satisfactorily cool the dry upper tank surface. Liquid nitrogen will not permit evaluation of cryopumping limits imposed on composite insulation systems by liquid hydrogen
6. The quality of the Microquartz insulation system after repeated temperature cycling under static conditions was excellent.

The above conclusions and recommendations which follow are based on the evaluation and test of the fluid dynamics associated with a static horizontal tank. Vehicle motion and acceleration are certain to have a profound effect on ultimate hydrogen tank design. Liquid sloshing will cause large sudden variations in vent rates. Vents must be sized and located to provide for this sloshing. Thermal shock of the hot tank surfaces is a consideration in structural design.

7. Install a convection shield over the fibrous insulation to minimize convection during ground hold.
8. Install instrumentation at the top of the tank in the liquid and near the liquid interface to detect the magnitude of liquid turbulence. Although not practical in this installation, a camera will probably be necessary to properly evaluate surface liquid turbulence.
9. Install instrumentation in the liquid which will better describe the stratification process; especially in the bottom of the tank.

10. Design a vent and spray system to provide maximum tank surface cooling. A piccolo vent will uniformly distribute the vent gas along the tank surface. Spray system will be based on assumption of liquid flow. The possibility of two phase flow will limit effectiveness and efficiency of spray system.
11. Make provisions in the thermal performance analysis to compute both liquid and ullage stratification.

6.0 PHASE I CONCLUSIONS AND LARGE-SCALE TANK RECOMMENDATIONS

All of the objectives of Phase I have been met. Design criteria were established, tank design studies performed, optimization program developed, and an experimental test program conducted which now allows orderly progression into Phase II. The conclusions reached and recommendations being made for design and fabrication of the large-scale tank are given below:

Structural Concept and Material.

- 1) On the basis of a non-buckling criteria for the skin, low operating pressures, and the need to support inertia loading without internal pressurization, a frame/stringer stiffening of the main shell evolved as the minimum structural weight concept. The removal of bonding requirements - feasible only with an all-fibrous insulation - would allow a frame-only concept to be employed. This recommended structural concept allows the skins to buckle and the majority of tank bending be taken by the center beam. This would provide a minimum - weight structural concept, and one not restricted to temperature limitations when the bonding requirements are removed.
- 2) The 718 nickel alloy, 30 per cent cold rolled plus aged condition, was shown to have the best attributes as a structural material. Investigations of empty tanks, during or after cruise, and ullage stratification influences on upper tank wall temperatures, indicate that the optimum material must have high strength at elevated temperatures. For this reason, the aluminum alloy which loses strength rapidly above 200°F is a poor candidate material. The indicated efficiency of the titanium alloy is also reduced due to its susceptibility to hydrogen embrittlement and strength loss at temperature. Extended material procurement lead time and lack of any existing material specifications on the cold-rolled plus aged condition are not compatible with Phase II schedule commitments and it is recommended that an annealed plus double aged condition be employed.
- 3) Optimum tank pressures are low (20 to 30 psia) for hypersonic cruise vehicle applications. The lower limit likely will be restricted by fuel system requirements on venting control. The structure sees a changing pressure differential, depending upon the atmospheric pressure.

- 4) Heat leaks through the tank supports and penetrations are not a problem area for hypersonic vehicle applications. The significance of such losses is related to the thermal efficiency of the insulation system used and, as such, constitutes a very small percentage of the total fuel loss. Boil-off resulting from these items does not justify elaborate investigation of low-conductivity designs.

Insulation

- 1) The all-Microquartz, helium environment insulation system was chosen as the best compromise of thermal efficiency, reliability, and fabricability. This system is not temperature-limited within the imposed environment, thus easing bonding requirements. The composite insulation was ruled out because of its temperature limitations, which demand tank cooling to maintain a temperature at the foam/Microquartz interface well below room temperature. Other detrimental attributes of the composite insulation include extreme sensitivity to thickness tolerances, the need for exacting manufacturing control to prevent voids in the adhesive bond areas, cryo-pumping problems at discontinuities and penetrations, an absolute lower thickness limitation of one inch, and lack of adequate methods to predict long-term integrity under cycling temperature and flexure conditions.
- 2) Insulation thickness distribution around a tank is an important consideration in determining minimum tankage system weight. Essentially, an optimum thickness exists for any given location on the tank, depending upon the time that point sees the liquid and upon the associated environment.

Fuel System

- 1) Maximum use of fuel boil-off to restrict upper tank wall temperatures will require a vent manifold system. Test results clearly indicate this need. Without such a system, cold boil-off gas is vented without any appreciable effect upon the stagnated ullage in the top inch of the tank. A vent manifold would induce the boil-off to the tank upper wall and supply cooling in a reasonable uniform manner. The penalties of not using boil-off gas include increased spray requirements or an increased tank structural weight caused by decreased material strength and increased heat flux into the fuel from radiation.

- 2) A booster pump is mandatory for hypersonic vehicle applications to contend with mass boiling of the fuel and to supply liquid fuel to the main pumps.
- 3) The need for a spray-cooling system in connection with the all-quartz insulation system has not been fully established. The need for such a system depends upon the efficiency of a vent manifold system (not yet ascertained) and empty-tank cooling requirements. This requirement is expected to be resolved during the Phase II continuation of the work on this program.

Fabrication

- 1) Fabrication experience with the thin-gauge subscale tanks clearly indicates the need for automatic weld operations, rigid welding procedures, and fixtures that afford good chill-down and gas coverage on the backside of welds. Quality tooling is necessary at all levels of work to maintain good fit-up of parts. Resistance welds were found difficult to repair and to inspect, although TIG fusion spotwelds were used satisfactorily to repair resistance welds in restricted-access areas of the closed tank.
- 2) Fabrication of the present design of Microquartz insulation blankets, greater than 1 3/8 inches in thickness, requires the use of multiple blanket build-up due to sewing machine limitations. Use of adhesives to bond insulation blankets to the tank places a restriction on the tank operating temperature. Although the present quartz thread stitching and cloth covering have the required high temperature capability, they were found to be barely adequate from a handling standpoint in abrasion resistance and thread strength. A solution to these problems is offered in the use of wire mesh to replace the quartz cloth, tufting with wire in place of the quartz thread, and mechanical attachment to replace the previous adhesive bonding.

Testing

- 1) Testing showed potentially large losses will occur if good vent system control is not provided. These losses are also significant from the standpoint of structural integrity, since the tank design must employ the maximum or upper limit as the operating pressure.

- 2) Boil-off losses were greater than predicted, a fact attributed in part to the liquid being injected into the ullage by violent surface action, and to the effective increase in wetted surface caused by liquid level rise at the side-walls. Another source of loss was helium mass flow transfer down the sidewalls during the ground hold condition.
- 3) Liquid stratification occurred in layers, as a function of heat flux rate and time, during the tests without apparent convection transfer. Stratification influences the storage penalties of liquid hydrogen, resulting in earlier boil-off and reduces the liquid level at topping. Liquid stratification was in part attributed to convective helium mass flow down through the insulation. Flow of this kind can be prevented by a shield over the upper part of the tank.
- 4) Stratified ullage temperature distribution was considerably different from that predicted. In part, the variation can be accounted for by agitated liquid surface conditions.
- 5) The implications of a dry tank at the end of cruise is significant. The thermal energy stored in the insulation can result in tank structure temperatures which exceed the cruise design conditions, with detrimental effects on instrumentation and tank integrity. Suitable steps must be taken to circumvent possible problems by such means as maintaining sufficient residual fuel for cooldown, venting the tank to a lower pressure, or providing cool-down from an external source.

7.0 REFERENCES

1. Air Force Contract AF(615)-2048, "Design, Fabrication and Experimental Verification of Cryogenic Tankage Applicable to Manned Aerospace Systems", dated 1 July 1964.
2. MIL-A-8861 (ASG), "Airplane Strength and Rigidity - Flight Loads", dated 18 May 1960.
3. MIL-A-8865 (ASG), "Airplane Strength and Rigidity - Miscellaneous Loads", dated 18 May 1960.
4. "NOVA Study Program - Supporting Hardware Investigations - Welding Test Program", Final Report on Contract NAS 8-5136, General Dynamics/Astronautics Report No. 63-0705, August 1963
5. Lange, R. A. , et al, "Lightweight Thermal Protection System Development", ASD-TDR-63-596, Vol. II, GD/Astronautics, June 1963.
6. O'Neill, R. F. , and Brown, B. S. , "The Variable-Boundary Transient Heat Conduction Program", General Dynamics/Astronautics Report No. AY63-0065, 17 June 1963.
7. Fortran Program for the Analysis of a Single-Propellant Tank Pressurization Program, Rocketdyne, A Division of North American Aviation, Inc. , R-5727, S&ID IDWA, 5835, 15 June 1964.
8. "Research on Optimization of Thermal Composites," Interim Progress Report No. 3, Contract AF33(615)-1672, General Dynamics/Convair Report No. GD/C-DCB-65-035.
9. Ferrigno, T. H. , "Rigid Plastic Foams", Reinhold Pub. Corp. , 1963.
10. Christian, J. L. , and Kerr, J. R. , "Selection of Optimum Materials for Use in Liquid-Hydrogen Fueled Aerospace Vehicles", Report No. ASD TDR-63-798, for USAF under Contract AF33(657)-9445 by GD/Astronautics, October 1963.
11. Watson, J. F. , and Christian, J. L. , "Cryostat and Accessories for Tensile Testing at -423°F ," ASTM Bulletin, February 1961.

APPENDIX I

CRYOTHERM TESTING

1.0 OBJECTIVES

In order to obtain practical design data on the foam/Microquartz and the helium environment Microquartz insulation systems, a series of tests were performed using the Cryotherm II test apparatus. This apparatus measures heat flux through insulation specimens using a guarded liquid nitrogen calorimeter. Flat specimens 26 inches square were tested with hot side temperatures from 0 to above 1500°F. The specimen temperature, gas environment, and pressure were varied to obtain transient or steady-state performance under a variety of conditions.

The need for this test program became evident during the design phase when it was realized that the composite foam/Microquartz insulation system is very sensitive to variations in material properties and fabrication method. The thickness of the foam layer is governed by the requirement to prevent cryopumping during ground hold and to protect the temperature limited sealing material from overheating during flight. The minimum thickness is fixed by the need of cryopumping prevention. Calculations based on available conductivity data show that even this minimum foam thickness will allow overheating of the interface between the foam and Microquartz when the tank wall is maintained at room temperature. The only practical way to prevent overheating at the Microquartz/foam interface is to control the tank wall temperature. The control temperature should be as high as possible to minimize the cooling weight penalty. Accurate conductivity data on foam and Microquartz is required to design an optimized composite with sufficient confidence in long-term integrity. Thermal performance change of the foam or of the Microquartz as a result of adhesive penetration, density variations, or inaccurate conductivity data could result in insulation system failure. The possible failures which could result are either cryopumping during ground hold, or overheating the seal during simulated flight.

Since the foam layer thickness for optimum performance is only 0.125 inches, very small deviations in the effective thickness will produce a large variation in the foam performance. Consideration must be given to thickness tolerance, adhesive penetration, density, cell size, and handling damage.

Conductivity data of Microquartz in a helium environment was also obtained to provide a good basis for performance evaluation of the actual stitched blankets.

Since the cryotherm uses liquid nitrogen rather than liquid hydrogen, it was necessary in the case of the foam composite to extrapolate the test data to the lower temperature. This was done within a reasonable degree of accuracy and provided a prediction of effective thickness to be used in a composite insulation system.

2.0 TEST SPECIMEN DESIGN AND FABRICATION

2.1 DESIGN

The test specimens were 26-inch square flat panels using the materials and fabrication techniques advocated for the subscale tanks. For the foam/Microquartz composite system, three specimens were designed to represent the upper tank insulation, with different foam/Microquartz thickness ratios, and one specimen each for the tank side and bottom insulation configuration. Two specimens, representing the tank bottom and tank top insulations, were designed for the helium environment Microquartz system.

The overall insulation thickness and thickness ratio for the composite system were taken from the optimization study results, with minor adjustments to allow for Microquartz blanket thickness in increments of .125 inches.

The materials employed were determined earlier in the preliminary design phase. Johns-Manville Microquartz felt of 3 lb/ft³ density was enclosed between cloth facings and compressed by stitching with quartz thread to a final density of 4.5 lbs/ft³. Multiple blankets were used to obtain the required total thicknesses above 1.5 inches due to sewing machine limitations.

In the composite system, the low temperature insulation layer consists of closed cell (Freon-blown) polyurethane foam. The foam density was 4 lb/ft³ in all specimens except the tank bottom configuration which was 2 lb/ft³. This was done to take advantage of the high tensile strength of the denser foam for the areas where high temperatures are likely to be encountered. The foam layer was sealed with Zero-Perm film, consisting of .001 inch aluminum foil sandwiched between two layers of .0005 inch Mylar.

Two types of polyurethane adhesive were selected for specimen assembly. A solvent-free adhesive, Narmco 7343 was employed for bonding of the foam to the back-up plate and the Zero-Perm. A less viscous adhesive with thinner, APCO 1252 was selected for bonding of the Microquartz blankets.

Design details of the specimen assemblies are shown in Figure 117.

2.2 FABRICATION

Microquartz Blankets. The original intent was to sew the individual blankets by machine. However, the quartz thread available proved too fragile for machine sewing and the blankets

Specimen No.	Foam Thickness (Inches)	Microquartz Nominal Thickness (inches) & Number of Layers	Remarks
GD/A 65-59343-1	.125	.875, 7	Assembly not completed
-3	.165	.875, 7	-
-5	.200	.875, 7	Two specimens fabricated
-801	.330	2.00, 16	-
-803	.490	3.125, 25	-
-805	-	.875, 7	-
-807	-	3.125, 25	-

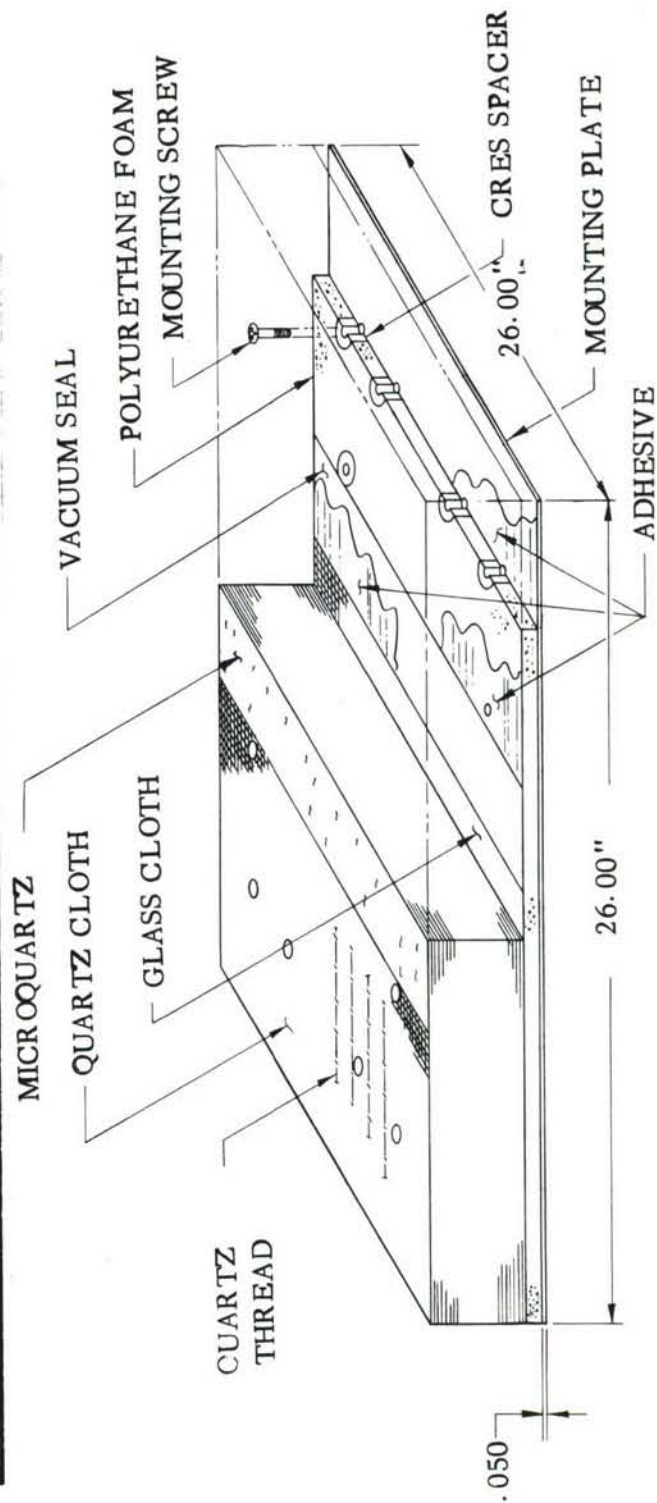
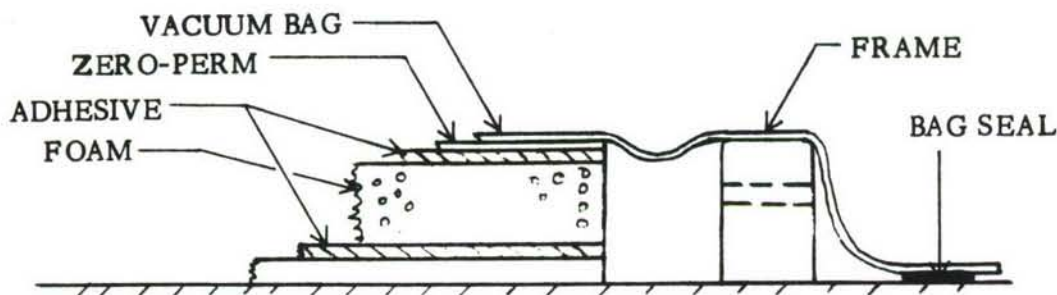


FIGURE 117. CRYOTHERM SPECIMEN CONFIGURATION

were therefore hand-stitched on a pattern simulating machine-stitch geometry. This procedure was extremely time consuming, and also resulted in considerable density variations between individual blankets. Figure 118 shows the completed GD/C 65-59341-1 blanket.

Foam Layer. The foam was cut to the proper thickness on a precision band saw, within a tolerance of $\pm .005$ inches. For bonding, the adhesive was applied to both sides of the foam in a minimum thickness. All excess adhesive that could be scraped off with a flat wooden scraper was removed. The Zero-Perm, foam and mounting plate were placed on a flat surface under a plastic bag and the bag was evacuated to provide uniform bonding pressure while curing. The assembly of the first test specimen, GD/A 65-59343-1, resulted in air and excess adhesive being trapped between the Zero-Perm and the foam. This was because the vacuum bag tended to form a tight seal around the edges of the specimen. This specimen with 0.125 inches of foam was not completed. The problem was alleviated by placing a frame around the specimen (see sketch below) which eliminated the edge sealing and permitted outgassing between the layers.



The remaining assemblies were fabricated without any difficulty. A total of 7 specimens were completed, one each of -3, -801, -803, -805, -807, and two -5 assemblies. Two -5 specimens were required since the first unit failed during the test. Figure 119 shows the -3 test specimen components prior to assembly. The foam sheet is shown after it had been cut to the 0.165 inch thickness, but before it was trimmed to the 26 x 26 inch assembly size. Figure 120 shows the detail of the thermocouple installation on the mounting plate.

3.0 TEST APPARATUS AND PROCEDURE

3.1 APPARATUS

The Cryotherm II is a test facility designed specifically to evaluate thermal protection system performance in a simulated flight environment, from take-off conditions to hypersonic velocity at high altitude.

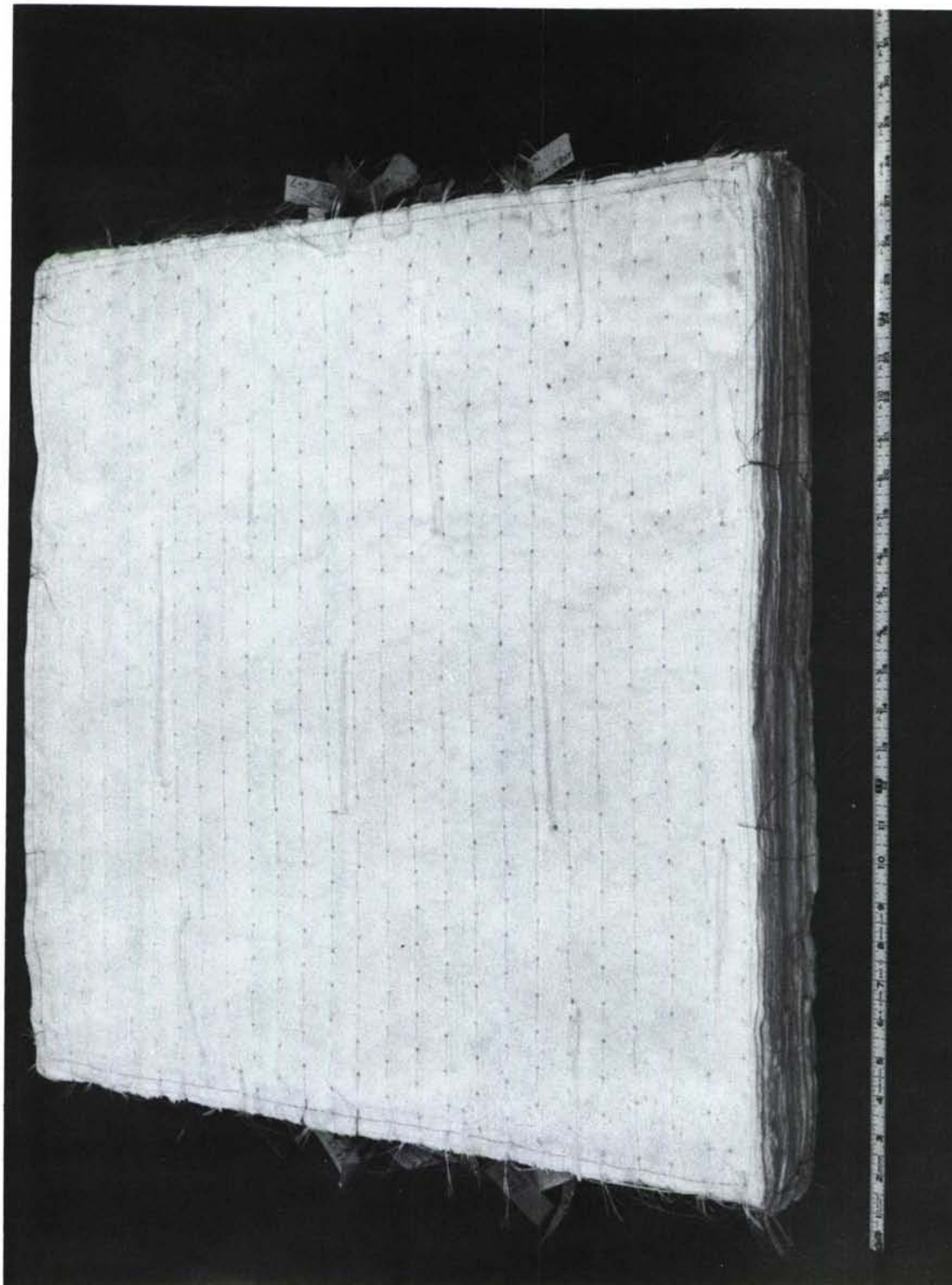


Figure 118. INSULATION BLANKET - TEST SPECIMEN GD/C 65-59341-1

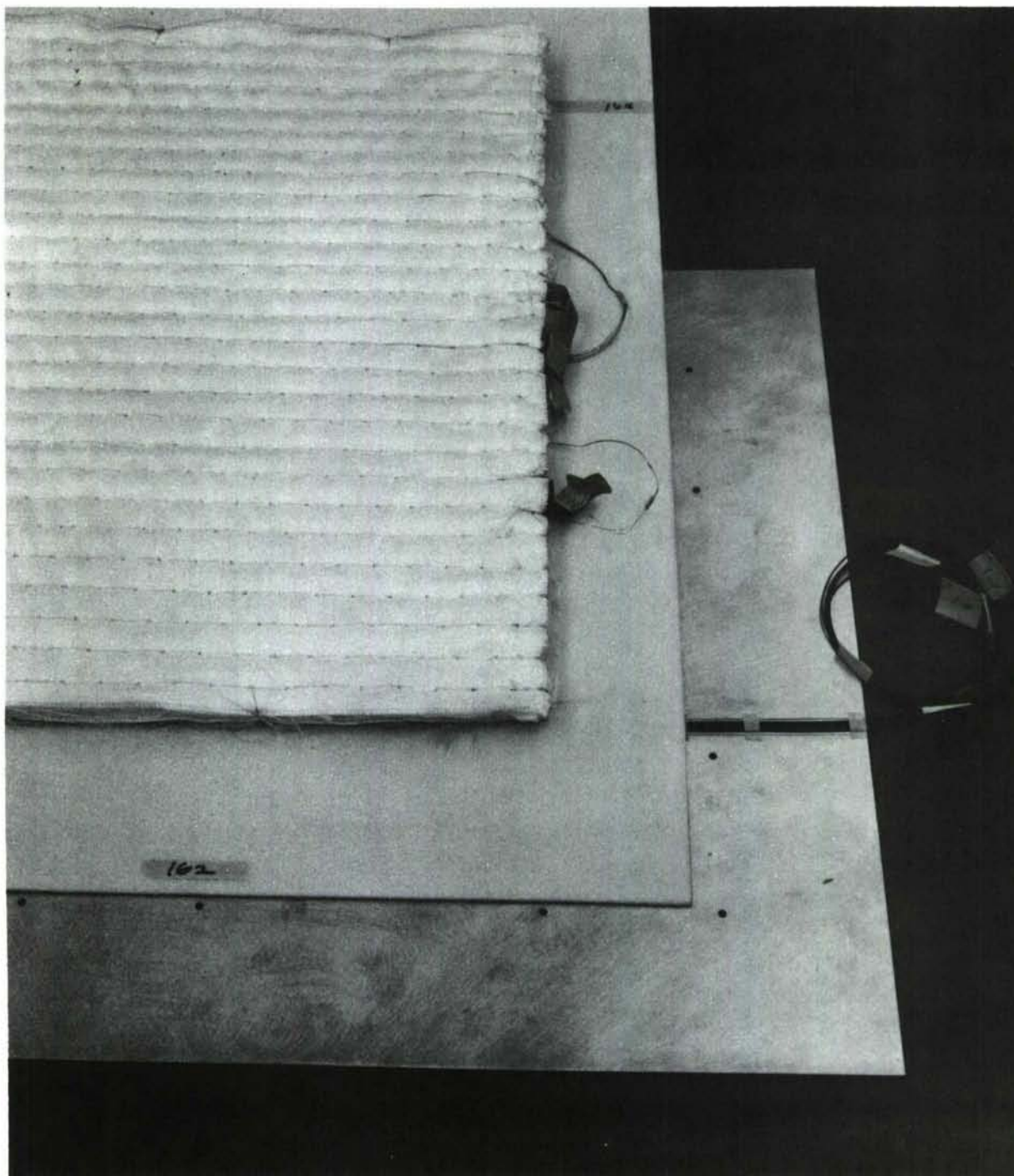


Figure 119. DETAILS FOR INSULATION TEST SPECIMEN GD/C 65-59343-3

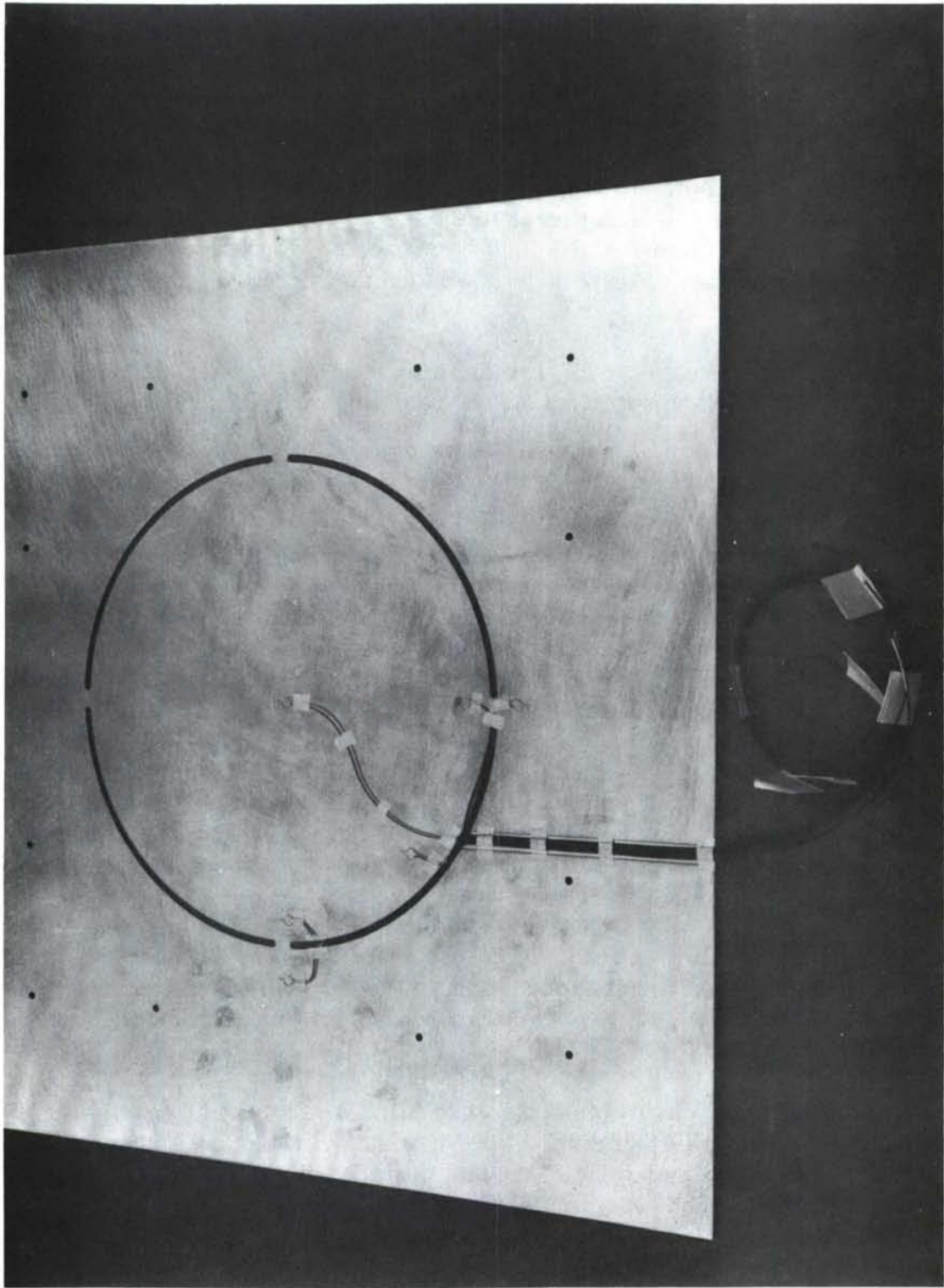


Figure 120. MOUNTING PLATE - INSULATION TEST SPECIMEN

The test specimen is mounted below two cryogenic tanks, in a chamber in which the surrounding gas composition and pressure can be controlled to simulate environmental conditions. Quartz tube heat lamps in this chamber simulate aerodynamic heating on the lower surface of the test panel. Heat flowing through the specimen boils the saturated liquid nitrogen in the calorimeter tanks. The resultant gas flow from the center (meter) tank is proportional to the heat flux. Measurement of boil-off gas flow and the temperature distribution in the test specimen provides the data for evaluating the thermal performance of the insulation system. The outer (guard) tank surrounds the meter tank and reduces side heat leaks to the meter tank to a minimum value. The metering section has an effective area of .969 square feet. The surrounding guard section is 25 inches square. Figure 121 shows the cryotherm with its associated control equipment.

For the current set of tests, a radiation shield was installed between the specimen and the heating lamps to simulate the radiating mode of heat transfer between the vehicle hot structure and the tanks.

3.2 TEST PROCEDURE

The procedure consisted of allowing the system to stabilize under ground hold conditions to obtain low temperature steady state data. Each specimen was then subjected to conditions of pressure and temperature simulating the flight trajectory for determination of the transient properties of the insulation. At the conclusion of the transient test, the system was allowed to stabilize at the terminal trajectory conditions to obtain high temperature steady state performance data.

One specimen was subjected to four simulated flight missions to determine if any deterioration would occur upon cycling. A thermal barrier between the specimen and the calorimeter was used to raise the temperature of the back face of the specimen simulating the conditions expected in the tank ullage area.

The sequence of operations consisted of mounting the specimen in the apparatus, evacuating the test chamber for a rough leak check and back filling to one atmosphere pressure with the desired gas for the test. The evacuation and back fill cycle were then repeated to ensure a high concentration of the gas medium for the test (helium or nitrogen).

The guard and calorimeter tanks were filled with liquid nitrogen. The radiation shield temperature was programmed to 30°F and maintained until the specimen temperatures and heat flux stabilized. The test chamber pressure and the radiation shield temperature were then programmed to the trajectory parameters, Figure 122 for the upper or lower surface as applicable to the specimen being tested. The terminal (steady state) trajectory temperature and pressure were maintained until the specimen temperature and heat flux again stabilized. Data was recorded periodically through the

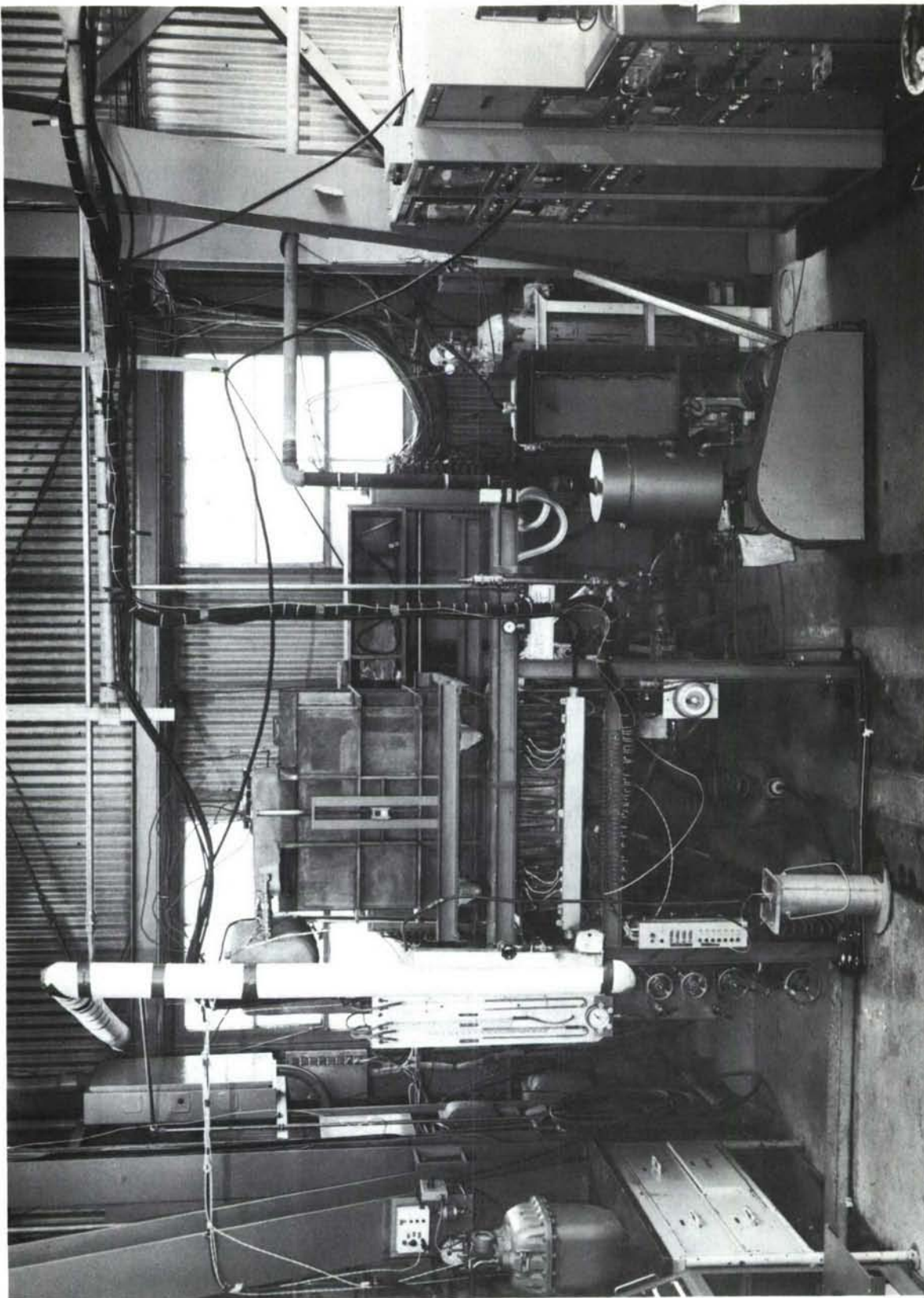


FIGURE 121. CRYOTHERM APPARATUS

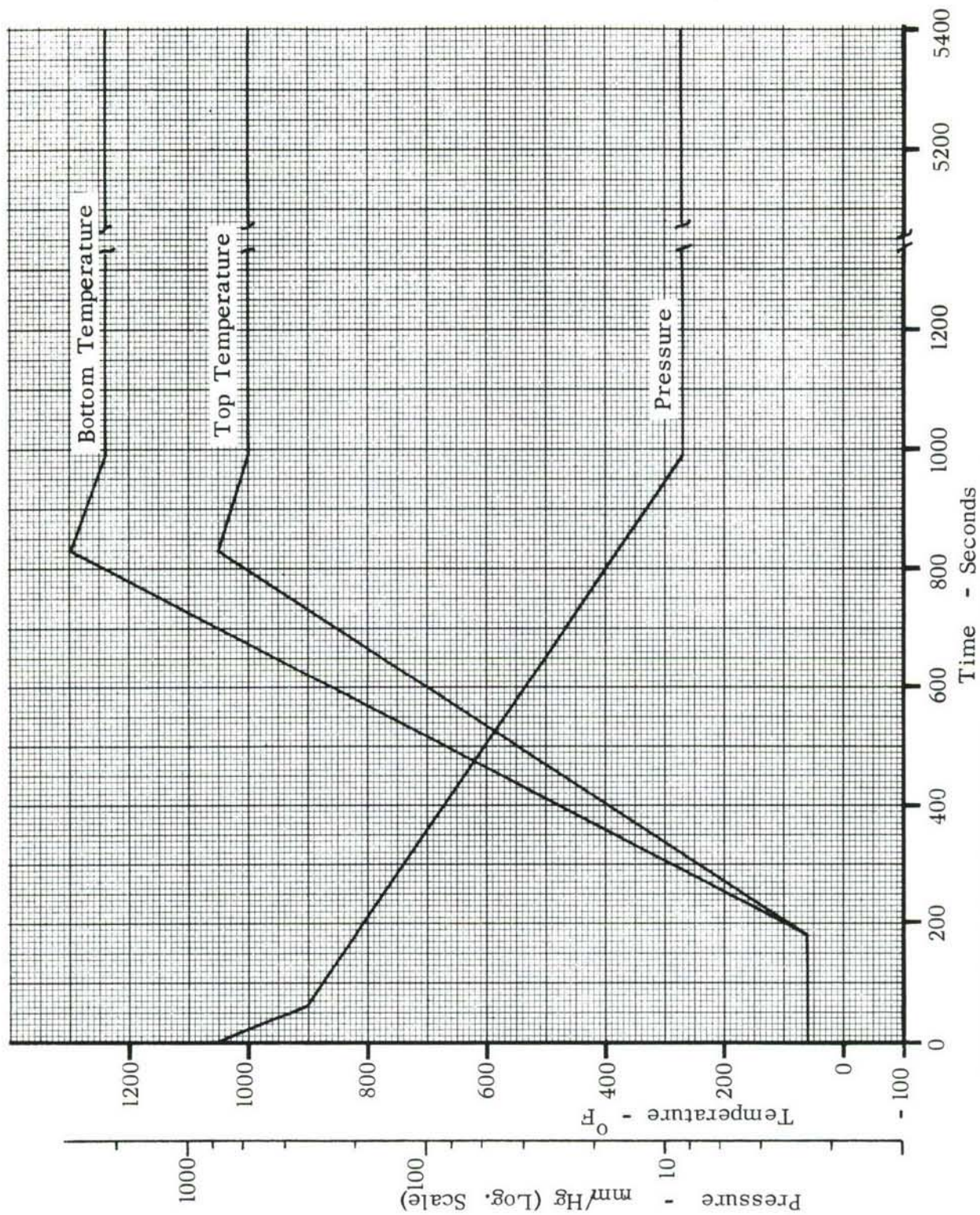


FIGURE 122 -TEMPERATURE and PRESSURE PROGRAM - SUB-SCALE TANK TESTS

above operations from the conclusion of filling the apparatus until high temperature stabilization was achieved. The radiation shield temperature was then reduced to 30°F, and the chamber pressure raised to one atmosphere to permit stabilization for repeat runs, or the liquid nitrogen was drained if the specimen was to be removed from the apparatus.

4.0 TEST RESULTS

4.1 CONDUCTIVITY TESTS

A summary of the test results in Table 7 shows the stabilized temperatures and heat flux rates at 760 and 8 mm Hg pressure. The predicted performance shown is based on the previously available Dynaquartz data.

The foam conductivity in the specimens tested was very consistent between specimens and agreed well with the published data when the thickness of the foam was reduced to compensate for adhesive penetration by an amount equivalent to one cell depth on each side (0.040 inches total). The average of the six measured points on each of two runs are plotted in Figure 123 for the three composite systems tested. The curve was shaped to conform to the best available published data for freon blown polyurethane foams. Based on this curve the interface temperatures extrapolated from the -5 test data for a 40°R tank wall temperature would be from 146° to 156°R at various locations. Since nitrogen gas would be expected to cryopump at 140°R, the foam-Microquartz ratio used in this specimen is the minimum which will reliably prevent cryopumping.

The mean density of the Microquartz in the blankets in the test specimens varied from 3.78 to 4.46 lbs. per cubic foot after the test. The mean thickness per layer and equivalent density for each specimen were:

GD/A-65-59343	After Test		Before Test	
-3	0.0114 ft./layer	4.11 lb/ft ³	0.0119 ft./layer	3.94 lb/ft ³
-5	0.0119 ft.	3.94 lb/ft ³	0.0119 ft.	3.94 lb/ft ³
-803	0.0105 ft.	4.46 lb/ft ³	0.0107 ft.	4.40 lb/ft ³
-805	0.0124 ft.	3.78 lb/ft ³	0.0131 ft.	3.57 lb/ft ³
-807	0.01073 ft.	4.37 lb/ft ³	0.0100 ft.	4.69 lb/ft ³

Conductivity data for Microquartz based on the cryotherm test results is presented in Figures 124 through 127 for nitrogen and helium gas at 760 and 8 mm of mercury absolute pressure. The conductivity curves were derived from the steady-state boundary temperatures and heat flux rates shown in Table 7. Dynaquartz conductivity curves are shown for comparative purposes. The difference between the conductivity of Microquartz and Dynaquartz at low temperature is attributed to the added solid conduction in the sintered material (Dynaquartz).

Table 7. TEST RESULTS SUMMARY

Test			Results						Prediction			
GD/C 65	Run No.	Thermal Barrier	Test Press/Gas mm Hg	Cold Face °R	Inter-face °R	Hot Face °R	Q/A Btu/Hr.Ft ²	Cold Face °R	Inter-face °R	Hot Face °R	Q/A Btu/Hr.Ft ²	
-805	1	No	760 N ₂	171	-	458	32.8	140	-	490	97	
	2A			169	-	488	30.6					
	2B			177	-	486	29.0					
-805	1	No	8 N ₂	603	-	1455	205	140	-	1460	453	
	2B			541	-	1455	216					
-805	1	No	760 He	182	-	414	147	140	-	490	133	
	2A			195	-	416	145					
	2B			190	-	421	157					
-805	1	No	8 He	369	-	1447	523	140	-	1460	715	
	2B			354	-	1408	510					
-807	1	No	760 N ₂	165	-	499	7.5	140	-	490	27	
-807	1	No	8 N ₂	373	-	1817	108	140	-	1700	157	
-807	1	No	760 He	159	-	474	58.9	140	-	490	89	
-807	1	No	8 He	240	-	1924	212	140	-	1700	241	
-3	1	No	760 N ₂	156	209	492	34.9	140	240	490	74	
	2			155	208	488	31.0					
-3	1	No	8 N ₂	180	502	1450	294	140	475	1460	368	
	2			177	502	1457	286					
-5	1	No	760 N ₂	154	222	462	34.9	140	255	490	69	
-5	1	No	8 N ₂	216	539	1428	267	140	520	1460	342	
	2			218	541	1433	243					
-5	3	Yes	760 N ₂	181	257	464	32.0	236	315	490	54	
-803	1	No	760 N ₂	154	204	484	8.8	140	240	490	21	
	2			153	202	483	7.2					
-803	2	No	8 N ₂	170	475	1692	72.8	140	535	1700	131	

Test Specimen	Foam Thickness (ρ)		Adhesive
	Actual	Corrected *	
GD/C 65-59343-3	● 0.165	○ 0.125	Narmco 7343
" -5	▲ 0.200	△ 0.160	"
" -803	■ 0.490	□ 0.450	"
GD/C 64-59201-3	◆ 0.140	◇ 0.100	APCO 1252

* Allowance for adhesive penetration -.040 inches.

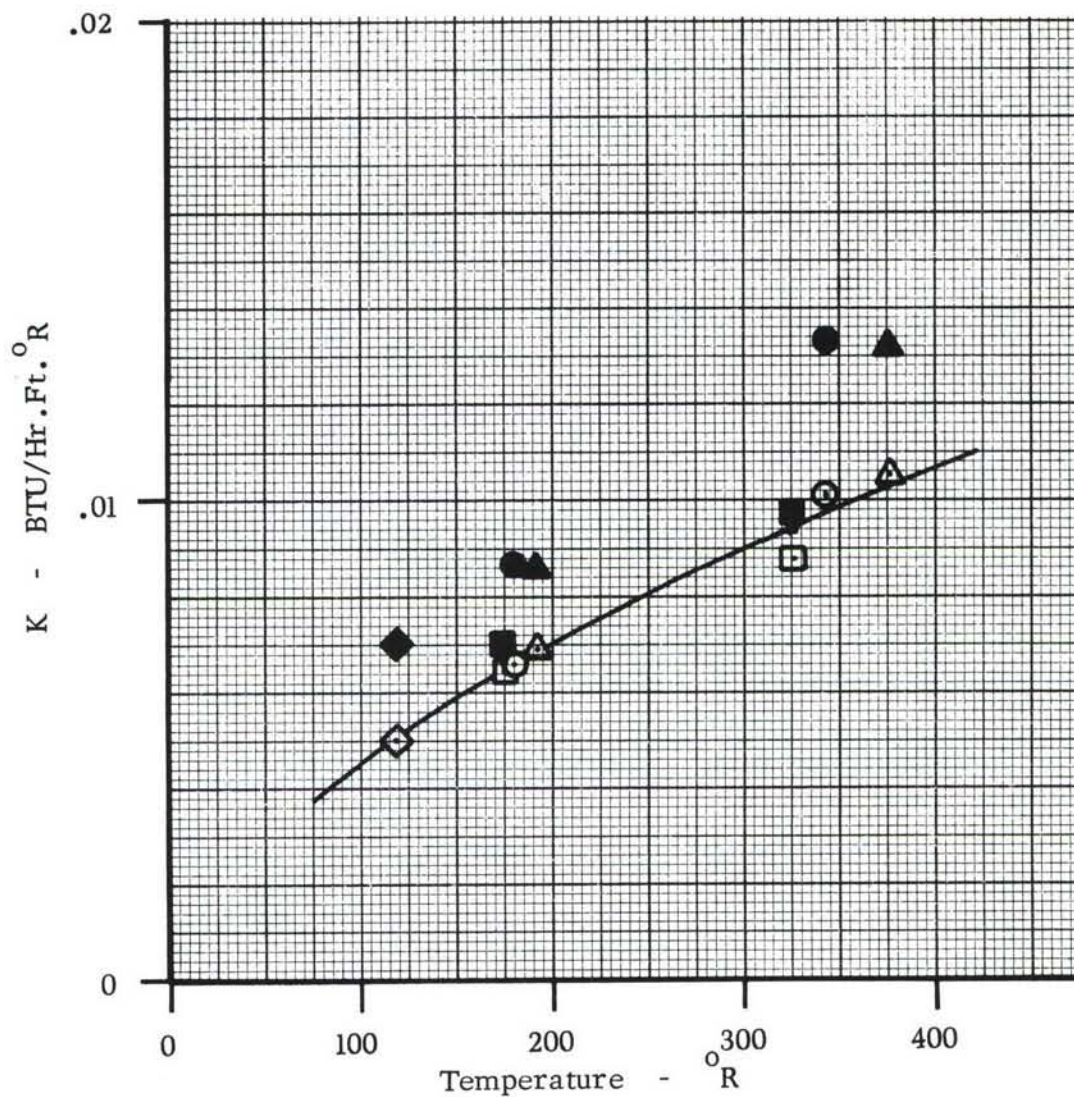


Figure 123. THERMAL CONDUCTIVITY (K) OF POLYURETHANE FOAM (FREON BLOWN) - CORRECTED FOR ADHESIVE PENETRATION

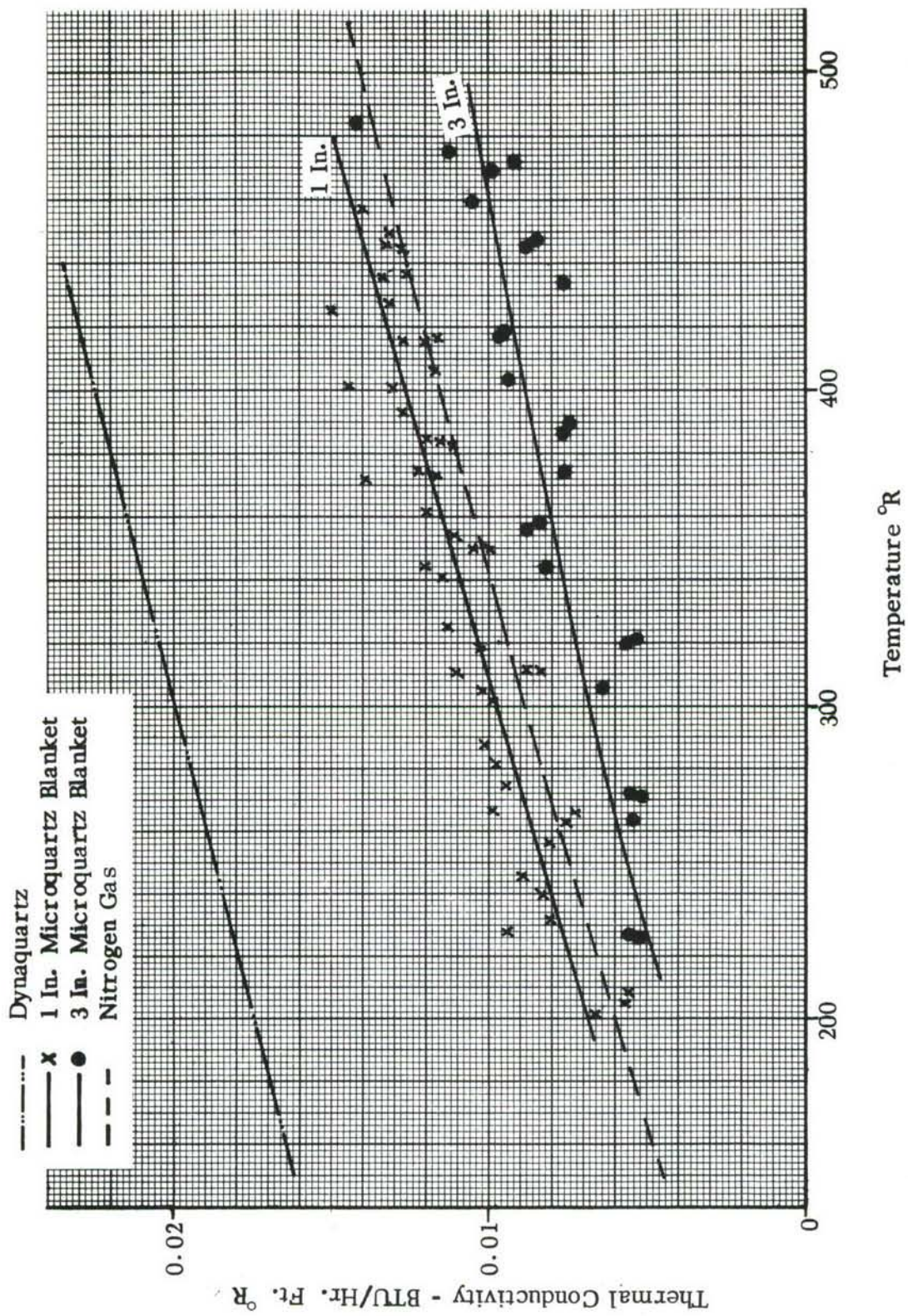


FIGURE 124 THERMAL CONDUCTIVITY (K) AT 760 mm Hg IN NITROGEN

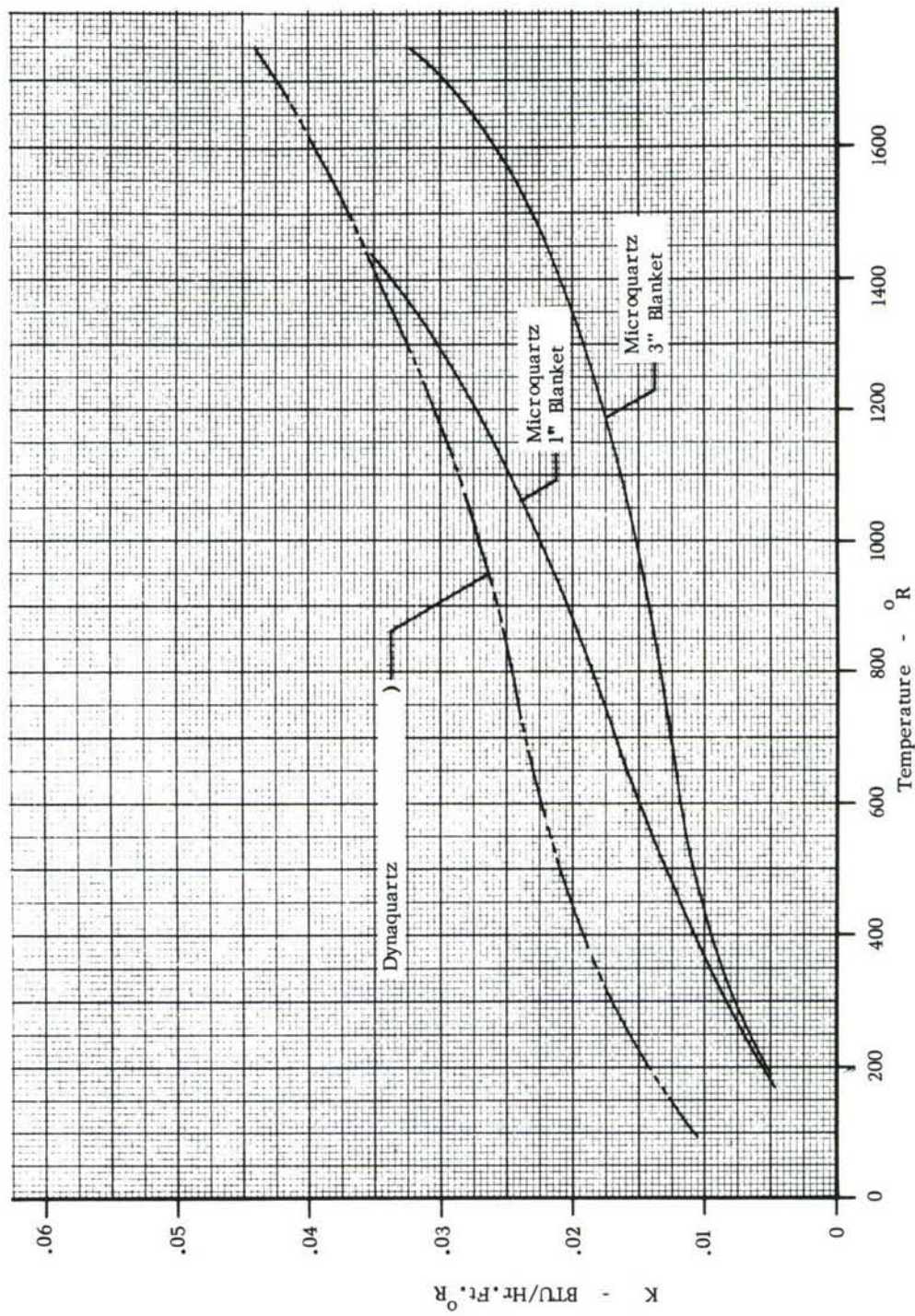


Figure 125 THERMAL CONDUCTIVITY (K) AT 8mm Hg IN NITROGEN

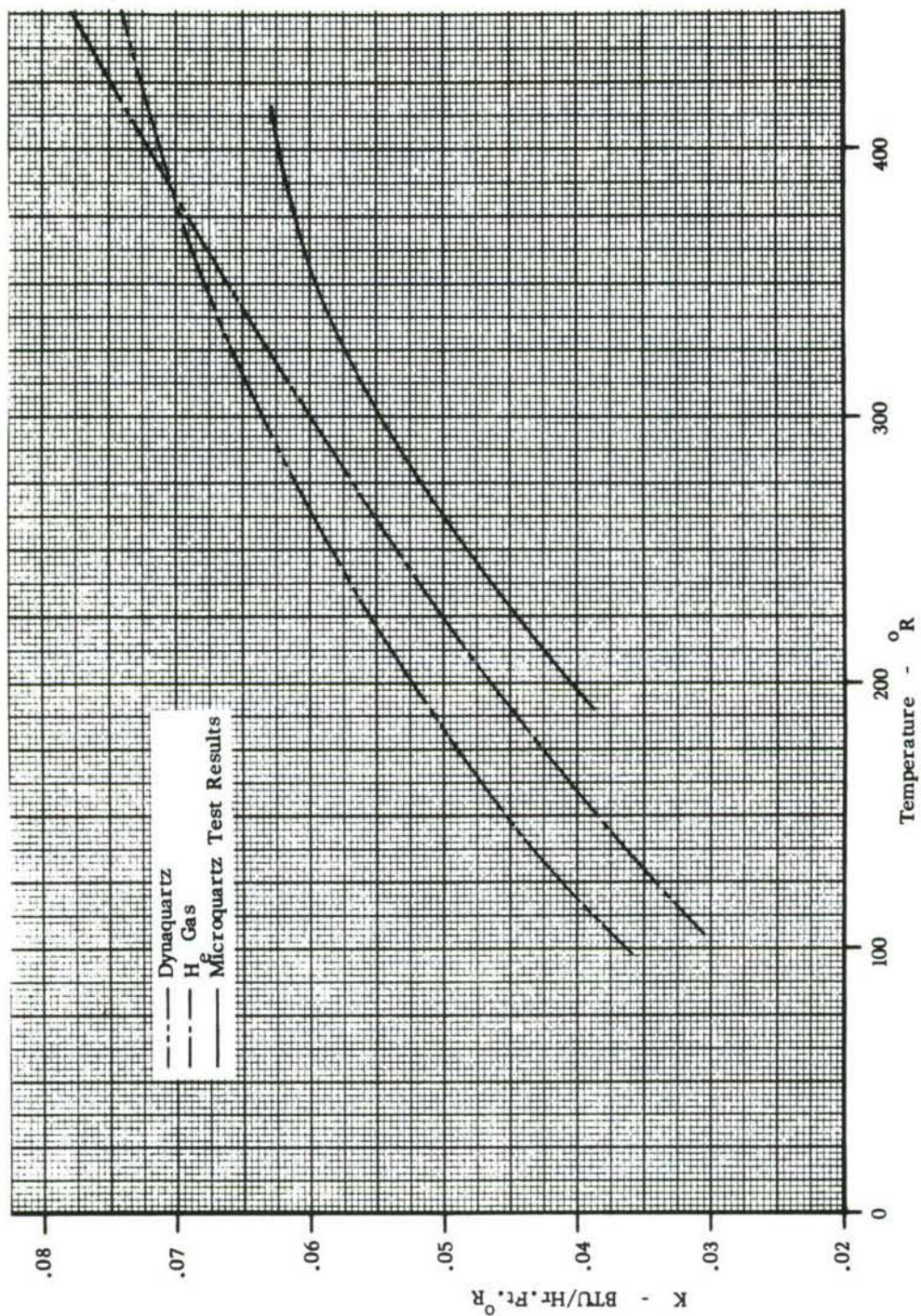


Figure 126 THERMAL CONDUCTIVITY (K) AT 760mm Hg IN HELIUM

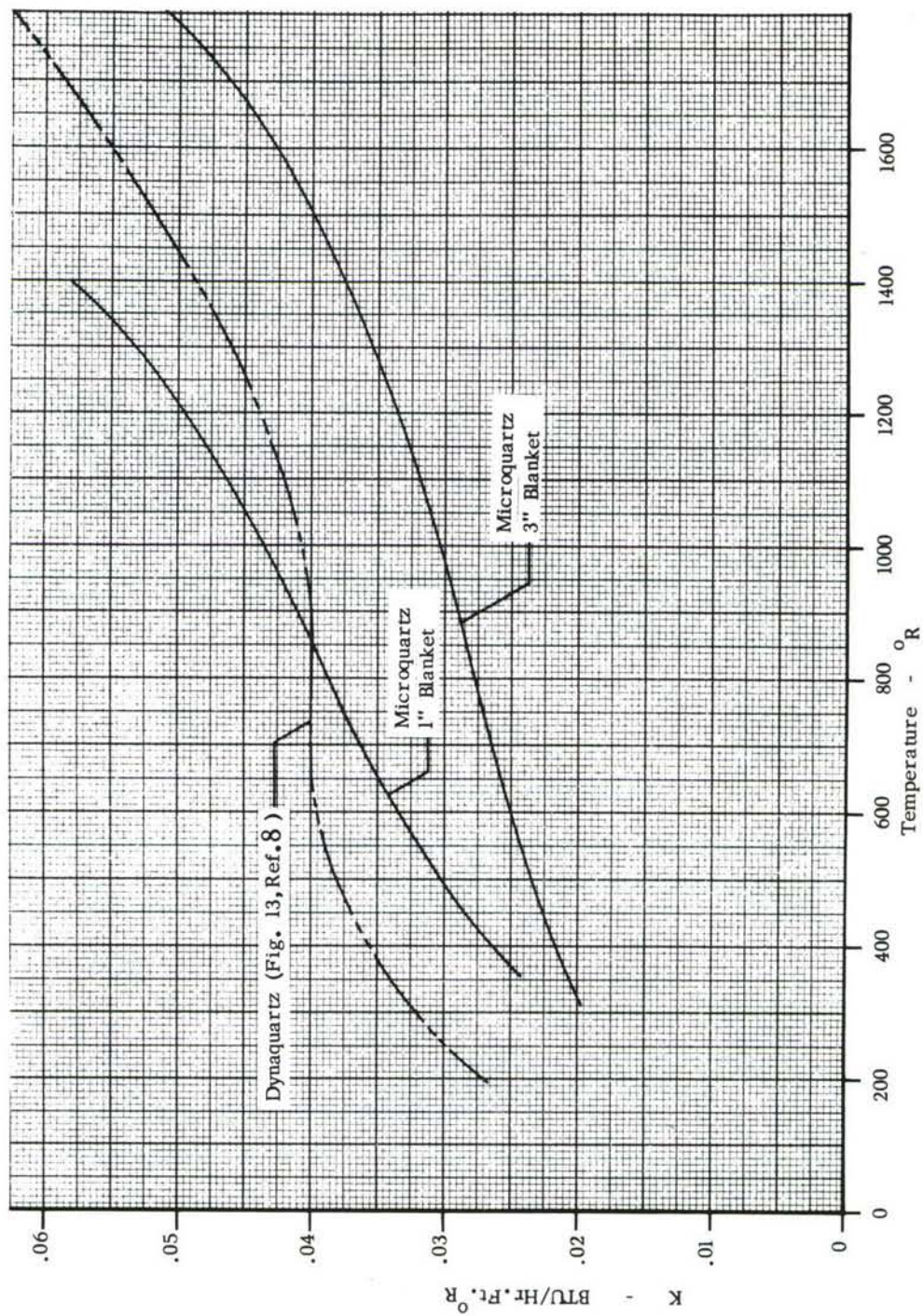


Figure 127 THERMAL CONDUCTIVITY (K) AT 8mm Hg IN HELIUM

The conductivity of Microquartz is affected to a large degree by the thermal gradient (thickness) at high hot face temperatures. Greater radiation attenuation in the thicker blankets reduces the apparent thermal conductivity. This difference in conductivity was noted at both high and low temperature levels in the insulation for tests run in nitrogen and helium environments at low pressure (8 mm Hg) where the hot face temperature was 1400°R or higher.

A difference in conductivity between the one-inch and three-inch Microquartz blankets at 760 mm Hg pressure was noted in the first cryotherm tests with the -805 and -807 test specimens. Test runs with the -5 and -803 specimens with foam also show the same difference in thermal conductivity between the one-inch and three-inch Microquartz blankets. The heat flux through the three-inch blankets is quite low. The conductivity difference had been generally attributed to the difficulty in accurate measurement of very low heat fluxes in a cryotherm type apparatus. Heat transfer between the metering and guard tanks due to difference in liquid level (static head) and heat transfer down the wall between the two tanks make it necessary to introduce correction factors to obtain the actual heat flux through the test specimen. The cryotherm correction factor has been determined analytically and by test calibration with favorable correlation between the predicted and test results. However, it is considered possible that variations in the correction factor can occur. The conductivity of the -5 and -803 specimens was checked by assuming that foam is a standard reference. The heat flux, \dot{q} , values were determined using the measured temperature difference across the foam layer and the foam conductivity. These heat flux values were used to determine the Microquartz conductivity. This evaluation still showed the thermal conductivity of the three-inch blankets to be substantially lower than the one-inch blankets. The conductivity is shown in Figure 124.

The heat transport through fibrous insulation is generally represented by three modes; solid conduction, gas conduction and radiation. None of these, however, account for the difference in apparent conductivity with varying blanket thickness at low temperature. Radiation is not significant because if the difference could be attributed to radiation in the temperature range below 500°R then the radiation at higher temperatures would be well in excess of measured values. The absolute temperature and the temperature difference across both blankets is similar, therefore, both gaseous and solid conduction should be the same in either blanket. The only thermal difference between the blankets is the temperature gradient. One possible explanation then is that part of the heat transport attributed to gaseous conduction is actually convective heat transfer. Free convection, as described empirically by relationships containing Grashof's number, is a function of local temperature difference between solid and gas. A variation in temperature gradient might result in a difference in convective heat transfer. One would expect, however, that the heat transfer by convection would result in an apparent conductivity in the insulation greater than pure gas conduction. This is not the case with the 3 inch blanket; its conductivity is less than that of nitrogen. The test specimens are mounted horizontally, in the cryotherm with the cold face on top. The buoyancy forces on the gas are in the opposite direction to the heat flow which could have the effect of convective heat transfer opposing the conductive heat flow. Effects similar to this have been noticed in other test data on fibrous insulation. As yet, no really satisfactory explanation has been developed.

The transient conduction and temperature data for the -5 and -803 specimen configurations are presented in Figures 128, 129, and 130. The heat flux was considerably lower and stabilization time longer than the original predictions. This is due primarily to the lower thermal conductivity of the microquartz.

An apparent failure of the adhesive was noted during testing of the 65-59343-5 specimen. The specimen was cut apart after the failure to examine the foam layer for signs of damage. No damage was visible. The thermocouples at level 2 (between the "Zero-Perm" layer and the Microquartz blanket) were held in place during fabrication by taping them to the Zero-Perm. The blanket was then bonded with adhesive to the subassembly. When the area reached a sufficiently high temperature, approximately 700°R , bubbles of gas formed between the Zero-Perm and the blanket. The thermocouples apparently stuck to the tape which was bonded to the blanket. The thermocouples were, therefore, registering the temperature on the hot side of the bubble and not the temperature of the foam layer. Figures 131 and 132 are plots of these temperature indications. The test provided definite proof that the composite system will require tank wall cooling below the 520°R level which was originally planned. The -5 specimen had the minimum foam ratio which can reliably prevent cryopumping under ground hold conditions, but the interface was above the 660°R limit for reliable operation with a cold side temperature of 430°R at the termination of the thermal barrier test. The thermal barrier used with the -5 specimen consisted of 0.125 inches of Microquartz with spacers at each of the 12 bolts to prevent excessive compression of the Microquartz felt.

Cold face thermal contact between the apparatus and the test specimen mounting plate was a problem, especially with the -805 and -807 specimens.

All specimens were installed using Dow-Corning 340 heat sink compound between the cryotherm colorimeter and the specimen cold face, except for the -5 thermal barrier test. The -805 specimen was run through one test series, removed, reinstalled, and re-run in an effort to improve the thermal contact. No significant change in the results was observed. While contact would be made initially, the two specimens without foam tended to sag after a period of time such that the unsupported area in the center metering section dropped away from the cryotherm. The test specimens with foam have been less problem because the bonded foam layer gives greater specimen rigidity.

A ceramic cement, Saureisen No. 78, was used to bond thermocouples to the hot side of the -805, -807 and -3 test specimens. A reaction of the cement with the quartz cloth and the first layer of microquartz was discovered after the specimens had been subjected to a hot trajectory cycle. The quartz tended to form a dark rigid mass which crumbled and powdered when handled. Hot face thermocouples on subsequent test specimens were installed by slitting the quartz cloth about 1.5 inches from the thermocouple location and slipping it into position between the cloth and first layer of Microquartz.

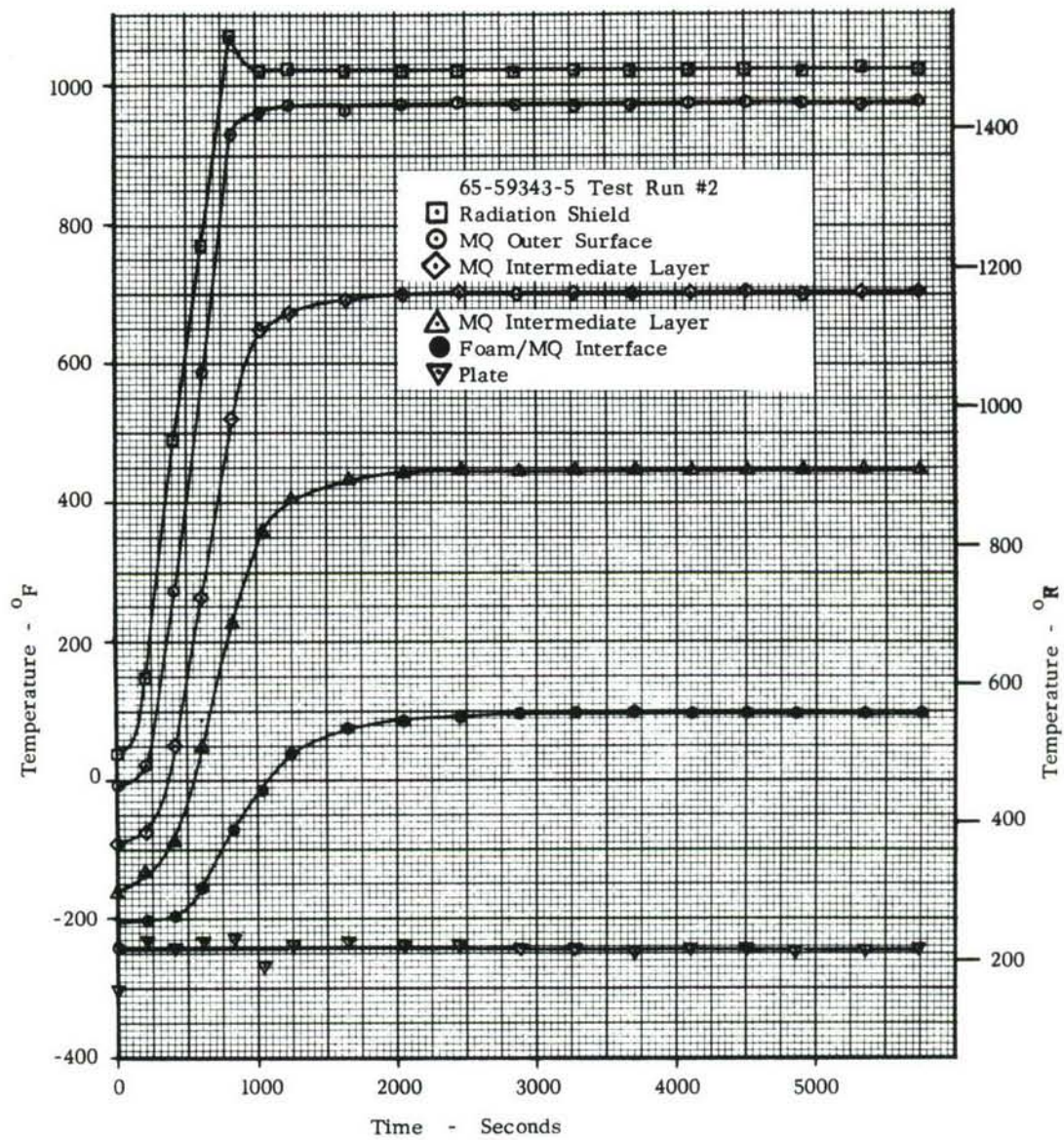


Figure 128 TEMPERATURE PROFILES FOR -5 SPECIMEN - CRYOTHERM TESTS

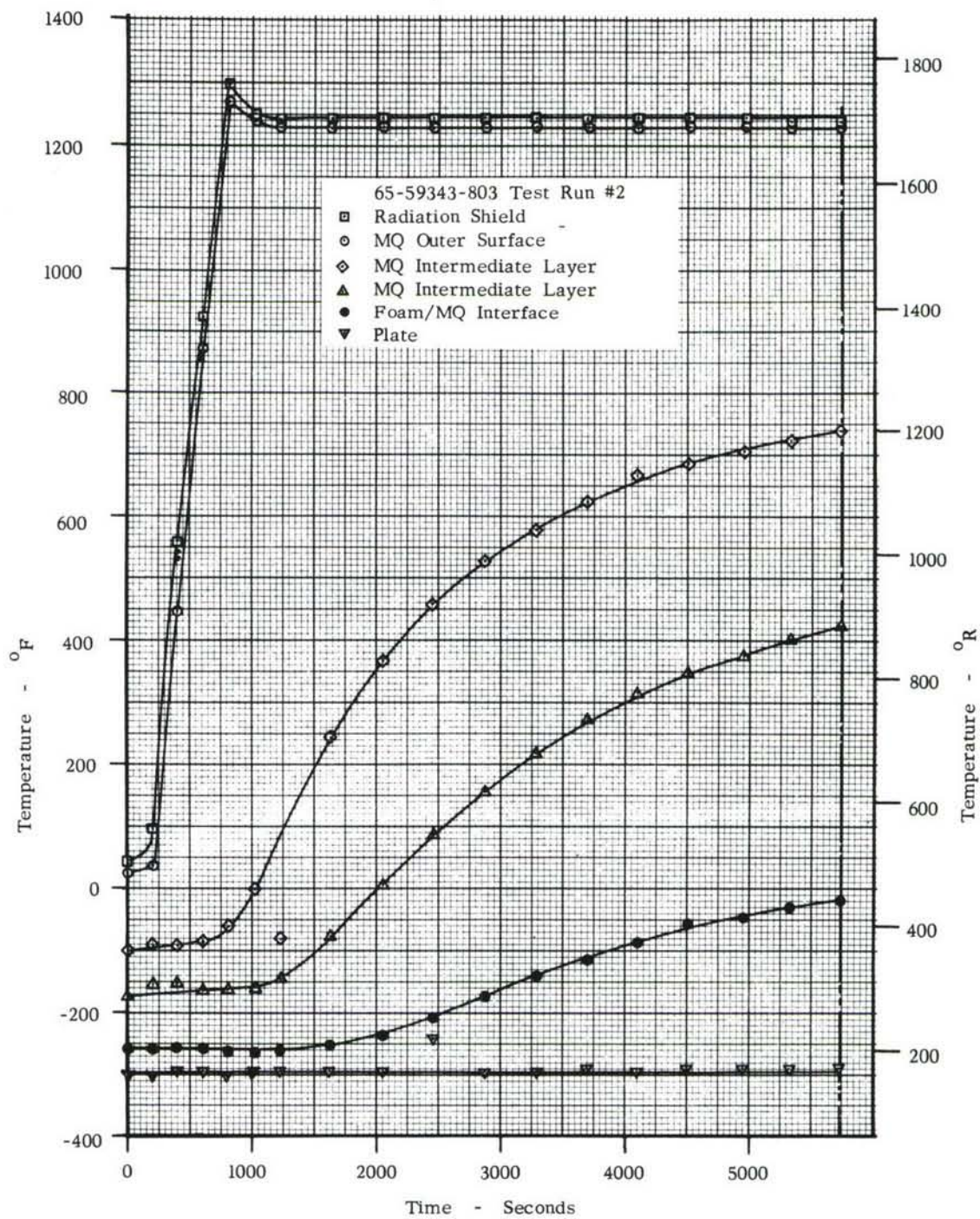


Figure 129 TEMPERATURE PROFILES FOR -803 SPECIMEN - CRYOTHERM TESTS

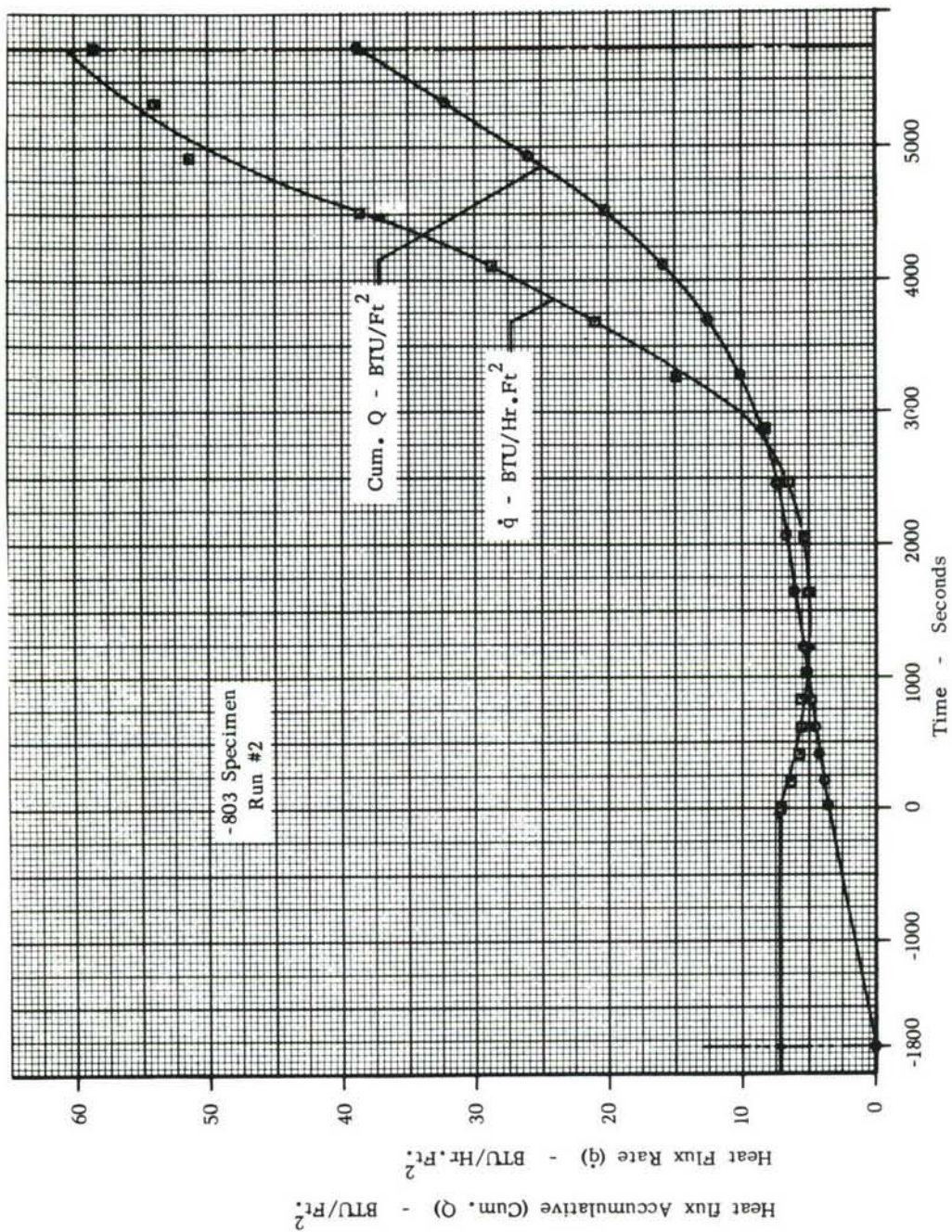


FIGURE 130 - HEAT FLUX RATE AND ACCUMULATIVE HEAT FLUX FOR -803 SPECIMEN (RUN # 2) - CRYOTHERM TESTS

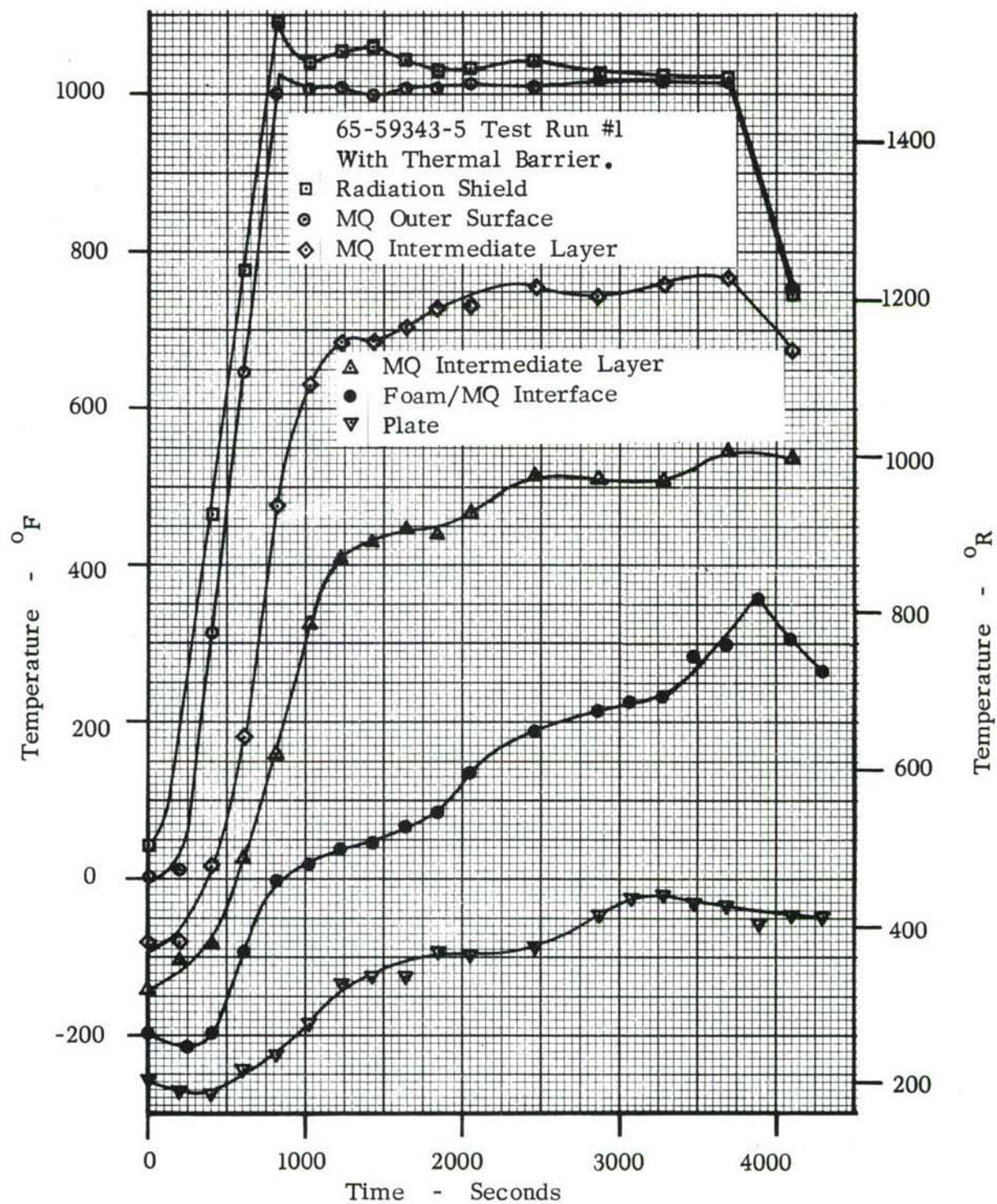


Figure 131 TEMPERATURE PROFILES FOR -5 SPECIMEN WITH THERMAL BARRIER - CRYOTHERM TESTS

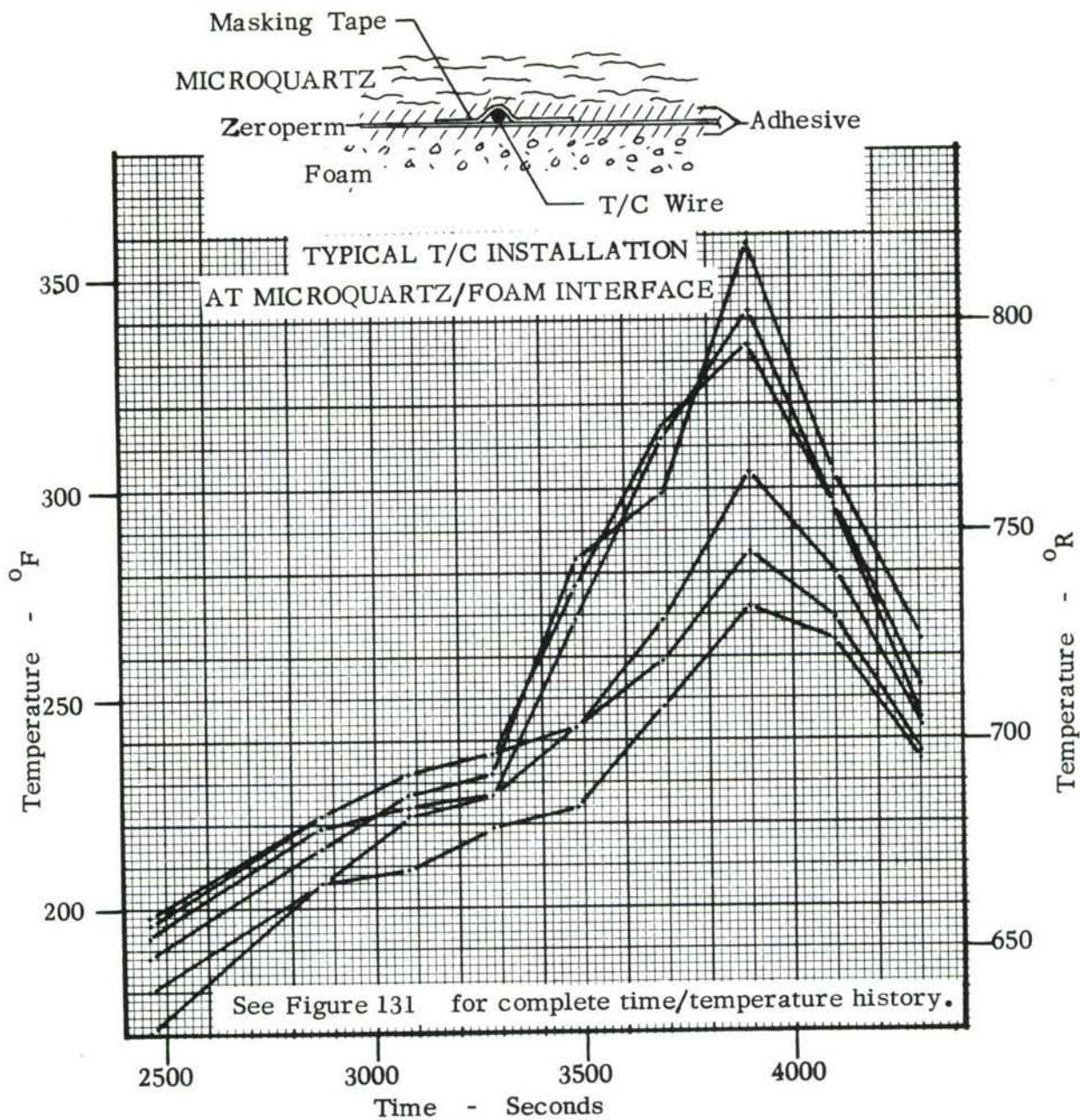


Figure 132 TEMPERATURES OF THE -5 SPECIMEN AT THE MICROQUARTZ/FOAM INTERFACE - ADHESIVE FAILURE.

Power programming problems on the first test specimen resulted in surface temperatures greater than 1500°F. This had no effect on the quality of the material. Aside from the cement problem discussed above, the high temperatures have resulted in no apparent deterioration of the quartz material.

4.2 THERMAL CYCLING

The second 65-59343-5 specimen was tested to verify the wall temperature required to protect the foam/microquartz interface from overheating, and also to demonstrate the durability of the system under cyclic temperature conditions.

The specimen was subjected to four trajectories with a thermal barrier to simulate the fatigue effects which will be encountered by the top surface insulation. The test data, Table 8, was consistent with the results for previous test specimens. A failure was noted at the conclusion of the third run. This resulted in the temperature at one of the six interface thermocouples rising above the value for the previous run. The temperature at this location was still higher on the fourth run. Examination of the specimen after the test revealed that an adhesive failure had occurred between the Zero-Perm and the foam. Since the other five instrumented locations showed no sign of such a failure even though some of the locations reached higher temperatures than that at which the failure occurred, the failure can be attributed to a locally defective joint. The cause of the defect cannot be definitely determined. The most probable causes are oil or grease on the Zero-Perm (hand prints, etc.) or excessive cure prior to application of the Zero-Perm.

Test			Results			
Run Number	Thermal Barrier	Test Press/Gas (mm. Hg)	Cold Face °R	Inter - face °R	Rad. Shield °R	Q/A BTU Hr. Ft. ²
1	Yes	760/N ₂	191	252	490	33.5
1	Yes	8/N ₂	361	619	1354	231
2	Yes	760/N ₂	191	250	491	35.9
2	Yes	8/N ₂	371	638	1388	239
3	Yes	760/N ₂	190	250	500	33.3
3	Yes	8/N ₂	366	703	1390	228
4	Yes	760/N ₂	193	254	500	33.5
4	Yes	8/N ₂	347	763	1388	211

TABLE 8. THERMAL CYCLING TEST RESULTS, 65-59343-5 SPECIMEN

The value of thermal conductivity for the foam at a mean temperature of 502° R was 0.0121 BTU Ft./Hr. Ft. ² °R from the high temperature steady state condition at the end of Run 2. The low temperature conductivity of the foam agreed within 2% of the value in Figure 182. The Microquartz blanket had a mean thickness per layer of 0.0105 feet, which is equivalent to a density of 4.46 lb/ft³. The Microquartz

conductivity was approximately 6% higher than the values shown in Figures 124 and 125. The trajectories were run at a temperature slightly below the 1460°R level to prevent heating the interface above 660°R . The failure occurred at a temperature of 649°R . The highest temperature at the other interface locations reached 665°R .

4.3 TEST DATA EXTRAPOLATION

The test results from the microquartz/foam specimens were extrapolated from actual test conditions to the projected operating conditions. The test data and extrapolated temperatures are shown in Table 9. The temperatures at 760 mm Hg were extrapolated to a liquid hydrogen cold face temperature of 40°R . The temperatures at 8 mm Hg were extrapolated to a microquartz/foam interface temperature of 660°R .

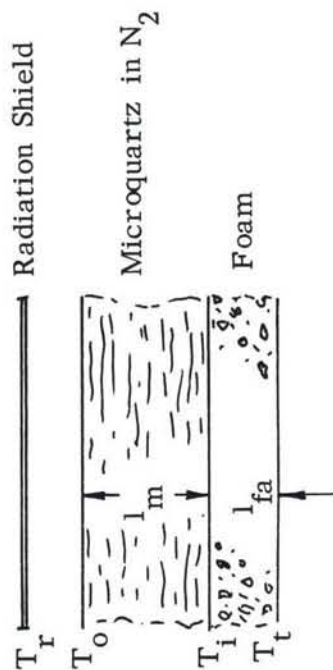
The liquefaction temperature of nitrogen at 760 mm Hg is 140°R . The -3 specimen with an effective foam/microquartz thickness ratio of 0.130 will cryopump since the interface temperature is 127°R . The -803 specimen with a thickness ratio of 0.143 also will cryopump with an interface temperature of 130°R . The -5 specimen resulted in an interface temperature of 150°R and a thickness ratio of 0.160. The six temperature measurements made on each side of the foam indicated a variation of $\pm 5^{\circ}\text{R}$. Thus this thickness ratio is considered to be the lower limit which will prevent cryopumping.

Extrapolating the test results for the -5 specimen at the high temperature operating condition and 8 mm Hg results in a required tank wall temperature of 378°R in order to limit the Microquartz/foam interface temperature to 660°R . This is well below the 520°R tank wall temperature originally predicted. The cause of this marked temperature reduction is the very low room temperature thermal conductivity of the freon blown polyurethane foam. The conductivity of freon and CO_2 blown foam and the gases, air, CO_2 and freon are shown in Figure 133. The low temperature S shaped curve is data from the foam manufacturer, CPR Division of Upjohn Co. It is apparent from the data in Figure 133 that the foam conductivity is influenced largely by the gas which it contains. Thus, if the freon could be removed and replaced by CO_2 or air and still retain the desirable mechanical properties of the freon blown foam, the temperature drop across it would be substantially reduced. Data published in the book "Rigid Plastics Foams", Reference 9, indicates that freon diffuses very slowly from closed cell foams. The conductivity of freon foam increased a maximum of about 25% after aging in air at 140°F for three months. It is possible that this aging time could be reduced and the conductivity increased even more by aging at elevated temperature in a partial vacuum. It is apparent that an increase in foam conductivity will improve the overall insulation system by minimizing the need for cooling.

TABLE 9 MICROQUARTZ/FOAM TEST SPECIMEN TEMPERATURES.

Test Specimen	Thickness - Inches			Ratio
	l_{fa}	l_{fe}	l_m	l_{fe}/l_m
-3	0.165	0.125	0.96	0.130
-5	0.200	0.160	1.00	0.160
-803	0.490	0.450	3.15	0.143

$$l_{fe} = l_{fa} - 0.040$$



* 'Operation' indicates temperatures have been extrapolated to actual operating conditions.

	-3 Test Specimen			-5 Test Specimen			-803 Test Specimen		
	Run # 1	Run # 2	Operation*	Run # 1	Run # 2	Operation	Run # 1	Run # 2	Operation
	N ₂ pressure in Microquartz - 760 mm Hg						N ₂ pressure in Microquartz - 8 mm Hg		
T_r	489	490	490	505	-	490	499	500	490
T_o	492	488	467	462	-	469	484	483	484
T_i	209	208	127	222	-	150	204	202	130
T_t	156	155	40	154	-	40	154	153	40
N ₂ pressure in Microquartz - 8 mm Hg									
T_r	1456	1470	1460	1480	1477	1460	-	1695	1700
T_o	1450	1457	1400	1428	1433	1400	-	1692	1690
T_i	502	502	660	539	541	660	-	475	660
T_t	180	177	443	216	218	419	-	170	451

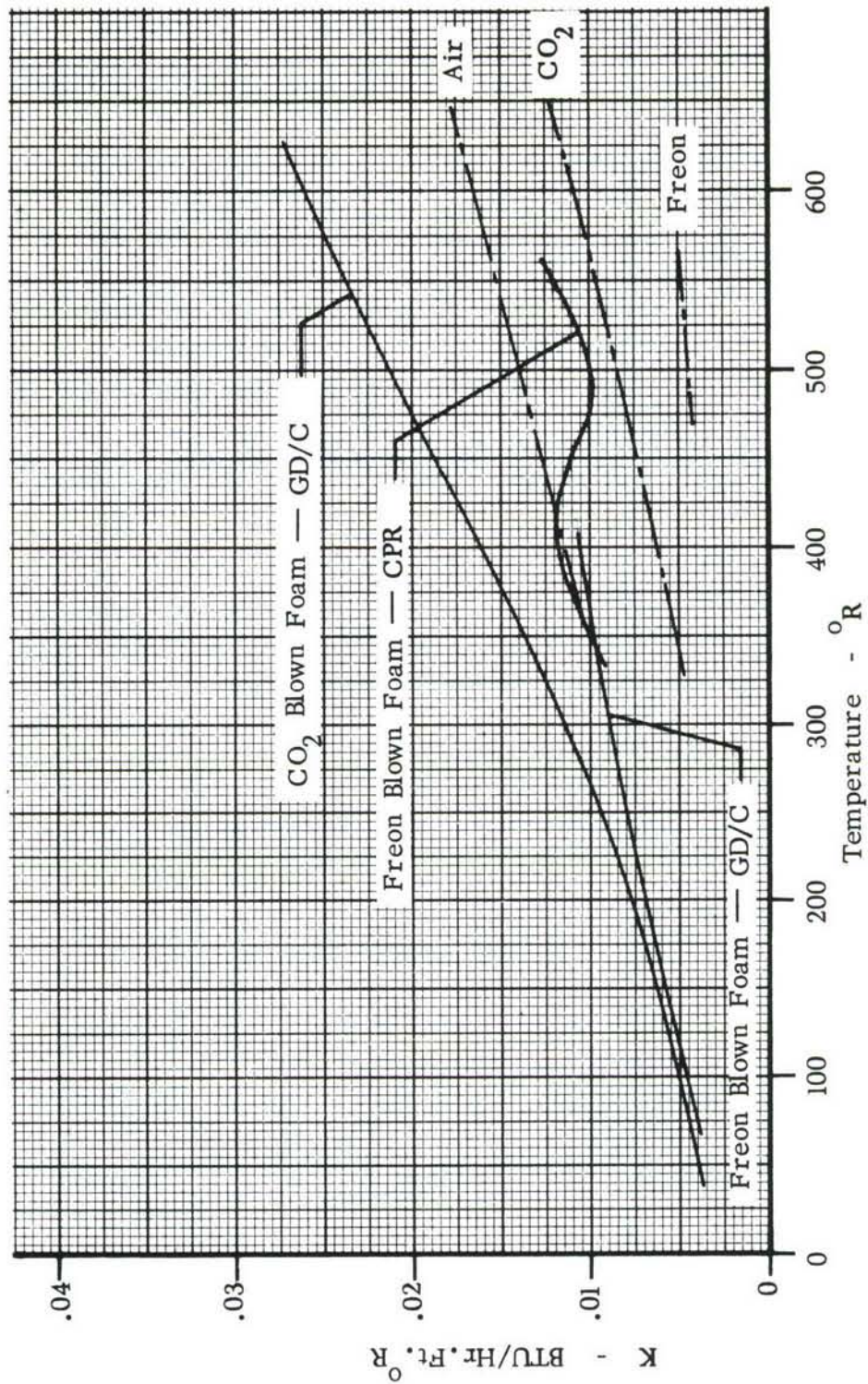


Figure 133 THERMAL CONDUCTIVITY (K) OF FOAM AND ASSOCIATED GASES

APPENDIX II

STRAIN GAGE EVALUATION

INTRODUCTION

The measurement of strains using resistance type strain gages at a temperature other than room temperature generally imposes additional requirements on the installed gage. These range from satisfactory bonding cements to changes in the gage output characteristics. The unknowns and problems can usually be resolved by appropriate evaluation testing of the gage at the temperature at which the installation is to be used. It is also often possible to "adjust out" any shift in the gage output resulting from changing the temperature from room to test temperature.

A more difficult requirement, the task of using the strain gage over a spectrum of temperatures, requires knowledge of the gage characteristics at all points of the spectrum. Again, a test program, will provide the required information. To "adjust out" the gage output resulting from temperature changes is not so easily accomplished when the temperature is subject to continual changes, however. To give satisfactory performance then, a gage is needed that produces zero output as a function of temperature. This is an idealized property of course. There are, however, means of approaching this ideal condition. One method is by the selection of material for the gage grid that is thermally compensated with respect to the structural material to which the gage is bonded. A second approach is to maintain a thermally balanced measuring circuit by utilizing a compensating element. It was this latter technique that was investigated for the present task of developing a strain gage system capable of accurately measuring strains on a tank structure subject to temperatures from ambient to minus 423°F.

A commercially available strain gage was subjected to a series of tests and evaluations that provided the required information.

DEFINITION AND NOMENCLATURE:

Thermal Constant-symbolized by $\frac{\Delta T}{\Delta G}$ - it is the ratio of the change in resistance of the platinum compensating element to that of the active strain element of the strain gage per unit temperature change. Dimensionless. (The value of this constant is used in computing the value of the circuit ballast resistor for any strain gage from the specified manufacturers lot, mounted on the preselected material, to give temperature compensation for a typical gage installation).

Ballast Resistance - R_B - the resistance placed in series with the compensating element of the strain gage to provide proper thermal compensation. Calculated using the thermal constant, $\frac{\Delta T}{\Delta G}$.

Thermal Output - the indicated output (or strain) of the strain gage resulting from inherent changes in the grid material and expansion or contraction of the material on which the gage is bonded (unrestrained) caused by temperature changes. Micro-inches/inch.

Thermal Hysteresis - the difference in indicated strain between an increasing and decreasing temperature cycle when measured at the same true strain level between the two temperature limits. Micro-inches/inch.

Indicated Strain - the quantity available directly from the analog signal after instrumentation errors have been adjusted from the indicator reading. Micro-inches/inch.

Strain limit - the maximum strain an installation may be subjected to while continuing to indicate true strain. Micro-inches/inch.

Mechanical Hysteresis - the difference in indicated strain between an increasing and decreasing mechanical strain cycle when measured at the same real strain level between zero and a specified maximum limit. Micro-inches/inch.

Creep - the change in output of the gage installation with time under constant applied load and constant temperature. Micro-inches/inch.

Gage Factor - G. F. - the ratio of the unit change in resistance of a strain gage to the unit elongation of the surface to which the gage is bonded caused by a uni-axial stress in the direction of the gage axis. Dimensionless.

Mathematically:
$$\frac{\Delta L}{L} \times G. F. = \frac{\Delta R}{R}$$

where: L = Initial length of specimen under the gage.

R = Resistance of the strain gage at length L .

ΔL = Change in length L of the test surface.

ΔR = Change in resistance R , caused by ΔL .

PRINCIPLES OF COMPENSATION

Temperature compensation by maintaining a thermally balanced circuit may be accomplished by having two identical strain measuring grids electrically located in adjacent arms of a Wheatstone bridge circuit. Both gages are mounted on the same material and subject to the same temperatures but with only one grid being sensitive to the structural strains. While this would theoretically give the desired results, isolation of one grid from the mechanical strains while maintaining the thermal atmosphere at both grids is not easily accomplished. A single strain gage that performs the compensating function to a large degree is the type FNB 50-12E now described.

The FNB 50-12E strain gage, manufactured by the Baldwin-Lima-Hamilton Instrument-Division, is a dual grid element combining a thermometer grade platinum wire and a nickel-chromium alloy foil grid to produce a half-Wheatstone bridge. A close-up photo of the gage is presented in Figure 134. A ballast resistor placed in series with the platinum element is used to control the percentage change in resistance of this compensating bridge arm caused by changes in temperature, and thus cancels the unwanted temperature induced resistance change in the Nichrome active strain element.

Normally there will be only two temperatures at which the thermal output will be exactly zero, within a specified range. Between these two points the thermal output is predictable as determined from experimental results. Likewise, the two zero points are experimentally determined for typical gage installations. The zero points and thermal output will, in general, be different for each material to which the strain gage is bonded for a specified ballast resistor. This is because of differences in the coefficient of thermal expansion of the material.

The value of the ballast resistor to give the desired compensation may be calculated for each operating strain gage circuit based on the thermal constant $\frac{\Delta T}{\Delta G}$ when the gage and lead wire resistances are known. The thermal constant is found by testing strain gages from the same manufacturers lot on the material that will be used for operational gages.

The Budd Instrument Company 700 Series and Micro Measurement SK series gages were considered as alternates to the preferred FNB-50-12E. These gages could not, however, be obtained within the time scheduled for the strain gage evaluation work.

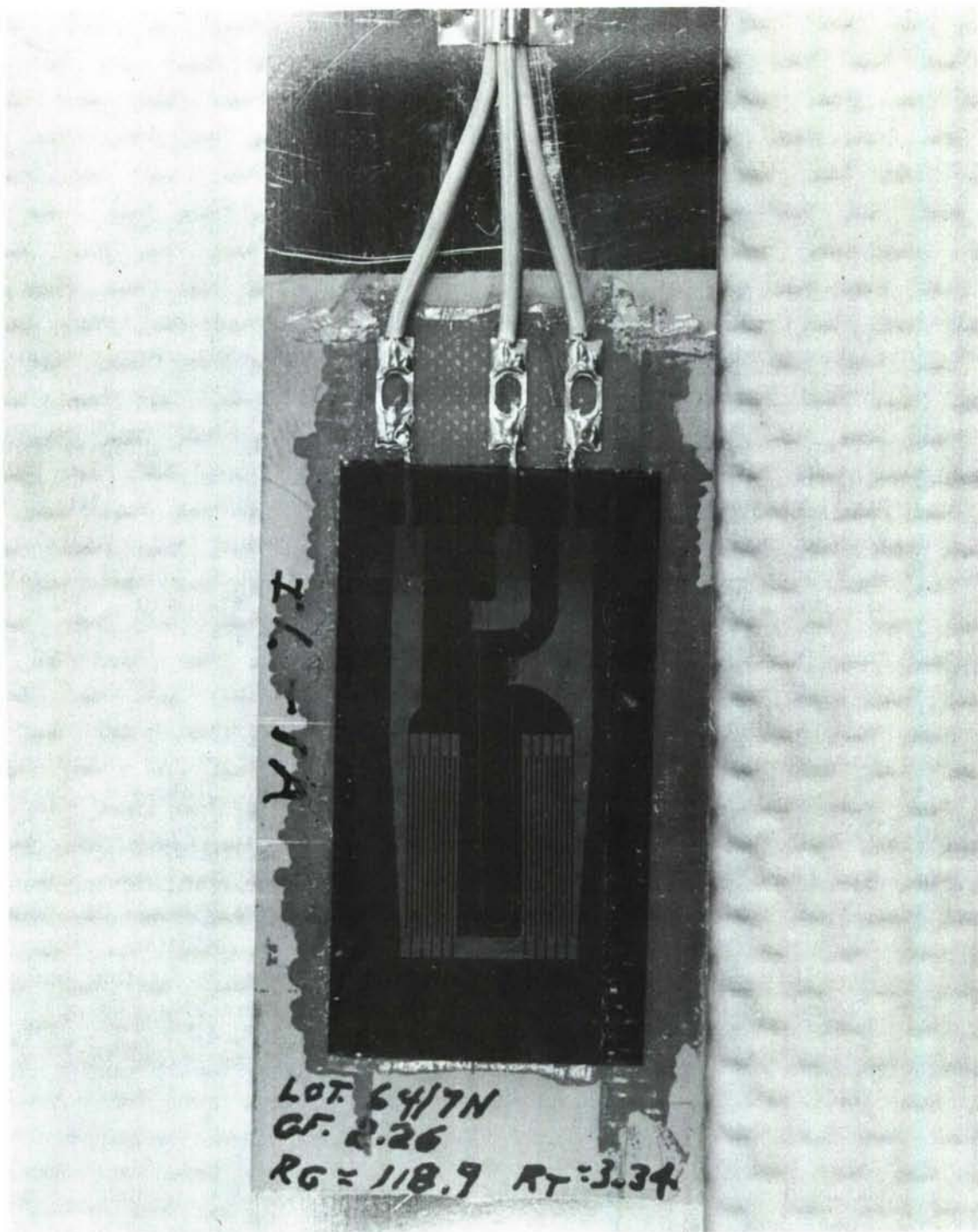


Figure 134. MOUNTING OF FNB-50-12E STRAIN GAGE, PRIOR TO SPRAYING ON PROTECTIVE COAT COVER.

STRAIN GAGE EVALUATION SPECIMENS:

A total of 10 FNB-50-12E strain gages were initially evaluated. Six gages were bonded to 0.025 inch thick 30% rolled Inconel 718 and 4 gages were bonded to 0.025 inch thick 5 Al 2.5 Sn ELI titanium. The material coupons were 12 inch long tensile specimens with a 1-inch wide test section. This configuration of test specimen was selected so that all testing could be performed on the same installations. Figure 135 is a sketch of a typical installation.

A single gage was mounted on each of four Inconel specimens and two gages were located back-to-back on either side of a fifth specimen. Three specimens were cut from the longitudinal grain direction and two from the transverse grain direction.

Two gages were mounted back-to-back on one longitudinal and on one transverse specimen of titanium.

The gage mounting surface was prepared by "Velvetizing" the area with 27 micron aluminum oxide. The gages were bonded with GA-5 epoxy cement. The cement cure was: two hours at room temperature, a temperature rise of one degree F. per minute to 180°F., then two hours at 180°F. The installation was then allowed to cool slowly in the oven.

A very thin protective coat of GA-5 cement was sprayed over the completed installation with an artist's air brush. The same cure cycle applied to the cement bond was used on the protective coat.

The lead wires were stranded, 26 gage, teflon insulated copper and attached to the integral ribbon leads of the gage through a printed circuit type tab. A photograph of the gage installations in various stages is presented in Figure 136.

INSTRUMENTATION:

Strain gage output was read directly using null balance type strain indicators in all tests. A typical circuit schematic is presented in Figure 137. A switching unit was used in one test to selectively connect the strain gages to a single strain indicator.

The ballast resistor and one balance resistor for each circuit were decade resistors with 0.1 ohm steps.

The thermocouples used in the thermal output test were read on a null balance potentiometer.

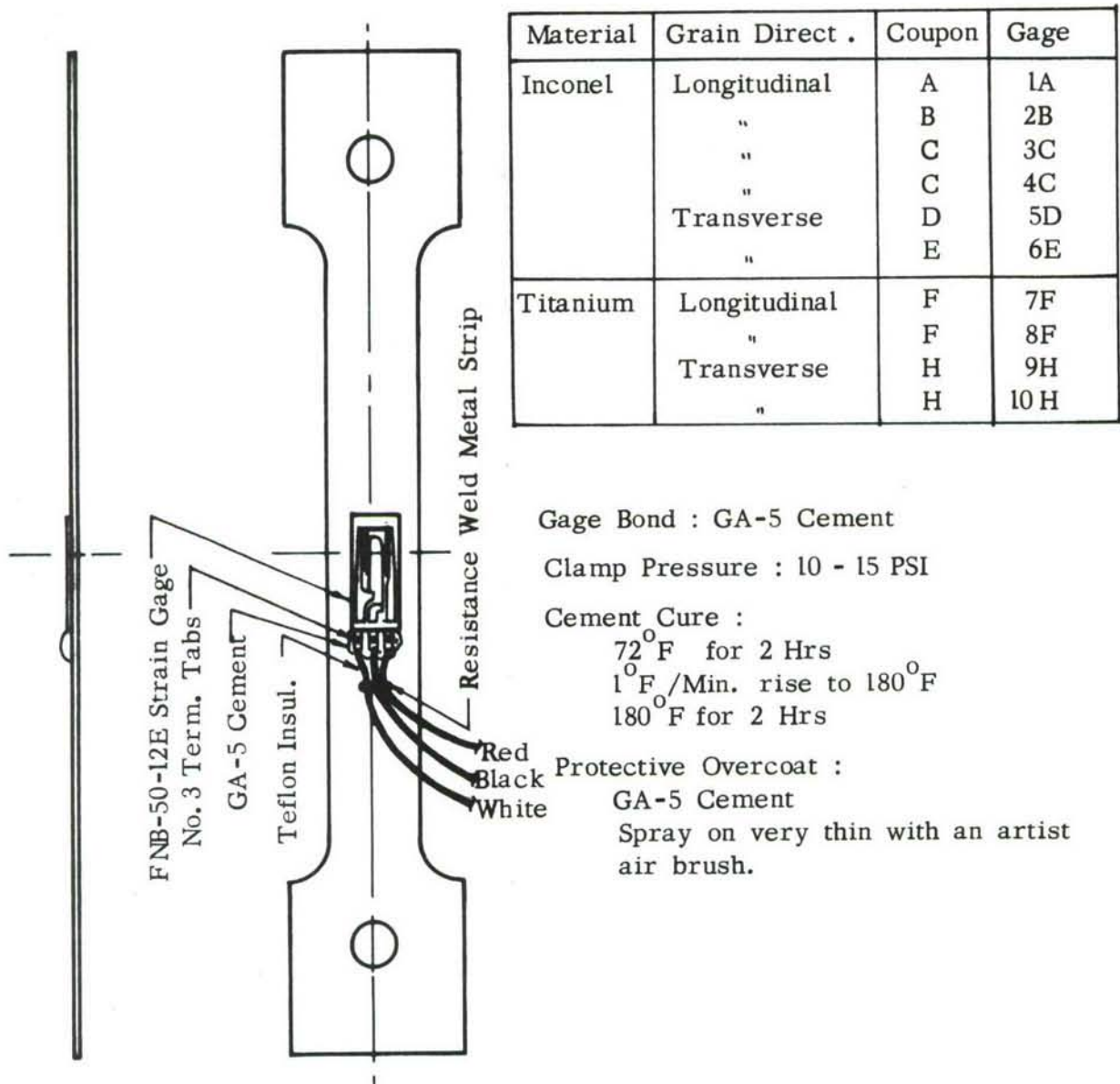


Figure 135. STRAIN GAGE INSTALLATION ON TENSILE COUPONS

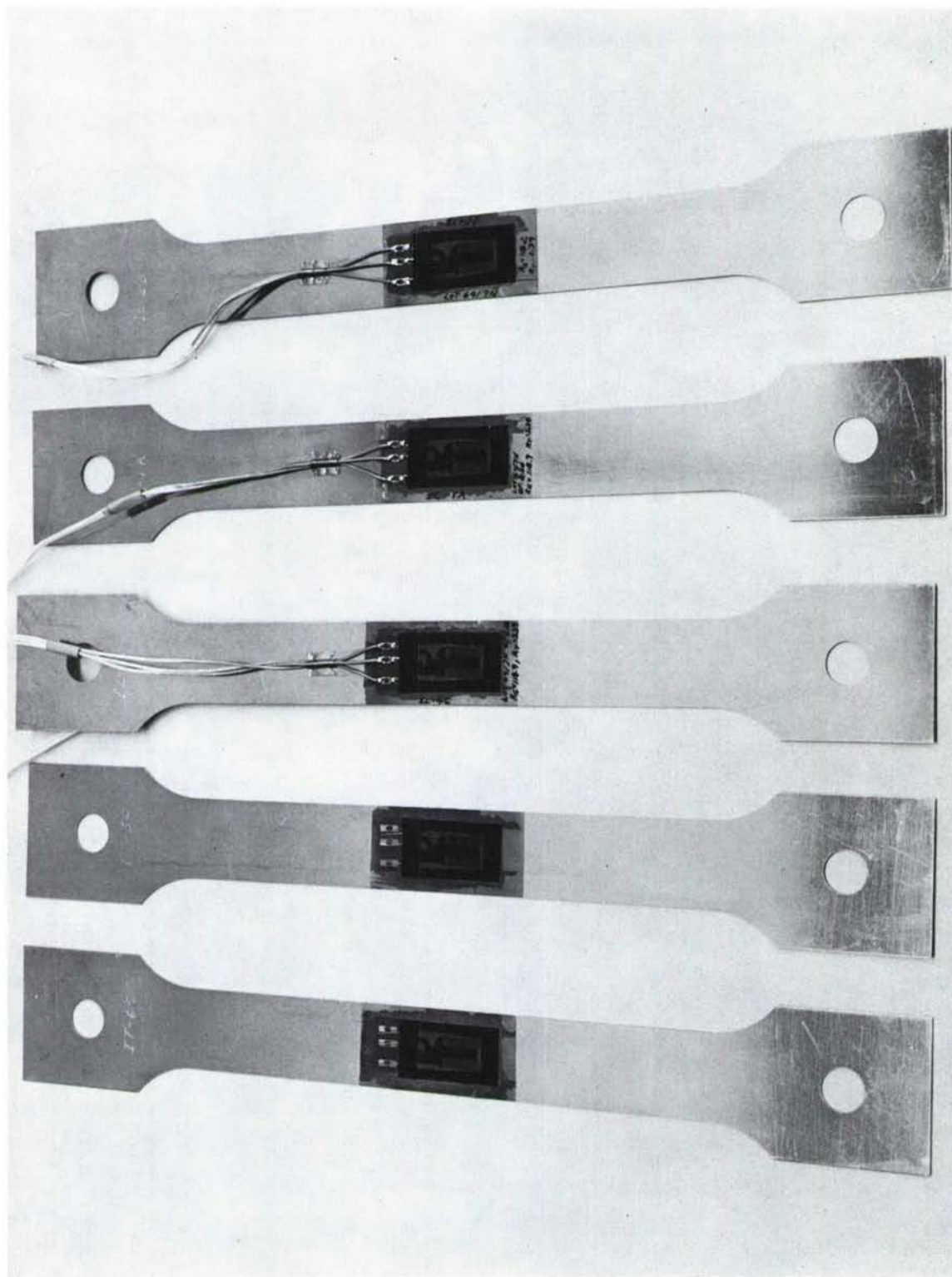
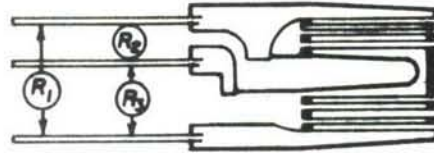


Figure 136. FNB-50-12E STRAIN GAGES IN VARIOUS PHASES OF MOUNTING ON TEST COUPONS.

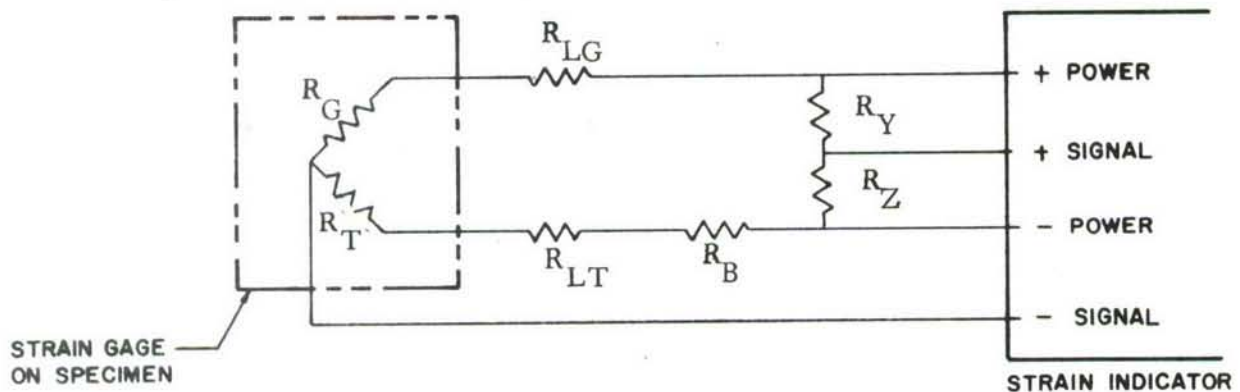


FNB-50-12E Strain Gage

R_1, R_2 & R_3 Represent resistance measurements on the installed strain gage.
 Values of R_T and R_G used in the calculation of $\Delta T/\Delta G$ are as follows:

$$R_T = \frac{R_2 + R_3 - R_1}{2}$$

$$R_G = \frac{R_1 - R_2 + R_3}{2}$$



- R_G - Strain Sensitive Element (Ohms).
- R_T - Temperature Compensating Element (Ohms).
- R_B - Ballast Resistor (Ohms).
- R_{LG} - Line in Series with R_G (Ohms).
- R_{LT} - Line in Series with R_T (Ohms).
- R_Y, R_Z - Balance Resistors (Ohms).

Figure 137. TYPICAL CIRCUIT FOR FNB-50-12E STRAIN GAGE

RESULTS

Installation Performance:

All strain gages performed satisfactorily throughout the evaluation tests. There was no indication of physical damage to the GA-5 cement overcoat as a result of the repeated immersions in liquid nitrogen and immersion in liquid hydrogen. The data presented in the following sections is valid for strain gages from manufacturers lot number 64/7N.

$\frac{\Delta T}{\Delta G}$ Determination

Room temperature (72°F.) and minus 320°F. were selected as the two points where zero thermal-output was desired. These temperatures satisfied the range of the proposed "field" test and were readily available.

Two independent system set-ups permitted testing two gages simultaneously. The purpose was to find a value of the ballast resistor, R_B , that resulted in zero thermal output of the gage at minus 320°F. and room temperature. The minus 320°F. was achieved by submerging the gage in liquid nitrogen.

Figure 138 is a photograph of the set up for determining $\frac{\Delta T}{\Delta G}$ as the specimen is immersed in liquid nitrogen.

The test procedure for finding R_B was to physically vary the value of the R_B in the test circuit in known steps at both room temperature and minus 320°F. For each value of R_B the strain was noted. The indicated strain difference (referred to as zero shift) noted at the two temperatures for a set R_B was then plotted against R_B . The curve was then read for an R_B representative of zero strain difference. With knowledge of the test circuit parameters a calculation of $\frac{\Delta T}{\Delta G}$ was made.

The formula was as follows:

$$\frac{\Delta T}{\Delta G} = \frac{R_B + R_T + R_{LT}}{R_T (1 + \frac{R_{LG}}{R_G})}$$



Figure 138. INSTRUMENTATION AND SPECIMEN BEING LOWERED INTO LN₂ FOR $\frac{\Delta T}{\Delta G}$ DETERMINATION

where: R_B = Ballast resistor (ohms)
 R_T = Platinum temperature sensing element of gage (ohms)
 R_{LT} = Lead wire connecting platinum sensor into circuit (ohms)
 R_{LG} = Lead wire connecting strain sensing element into circuit (ohms)
 R_G = Strain sensing element of gage (ohms)

R_G and R_T are obtained by resistance measurements and calculations defined in Figure 137.

The graphical representations of R_B versus the zero shift are presented in Figures 139 and 140 for Inconel and titanium respectively. The values of $\frac{\Delta T}{\Delta G}$ of each test gage are also tabulated. The average $\frac{\Delta T}{\Delta G}$ from all test gages mounted on Inconel was 40.78. The average $\frac{\Delta T}{\Delta G}$ for the gages bonded to titanium was 44.18.

The results of test work for the thermal constant, $\frac{\Delta T}{\Delta G}$, were very good. The average $\frac{\Delta T}{\Delta G}$ of the six strain gages mounted on Inconel was within 0.4 percent of any of the individual values. Titanium test specimens average $\frac{\Delta T}{\Delta G}$ was a maximum of about 0.8 percent from the results on any single gage. These values would reflect maximum errors in the ballast resistor of approximately the same magnitude. In the case for titanium, then, referring to Figure 140, an 0.8% error would cause a thermal output (zero shift) of about 70 micro-in./in. at liquid nitrogen temperatures.

The fact that the ballast resistor is different for the various gages as the curve passes through zero strain is not scattered data, but represents the effect of nominal gage resistance differences.

Specimens were carefully selected with respect to the orientation of the gage grid to the base material grain direction. It was concluded with certainty that the grain direction did not affect the thermal constant, $\frac{\Delta T}{\Delta G}$, on either Inconel or titanium.

Gage Factor Correction Due to R_B

When an FNB strain gage is used in a readout circuit designed for a symmetrical bridge, such as the strain indicators used in this evaluation, the circuit is less

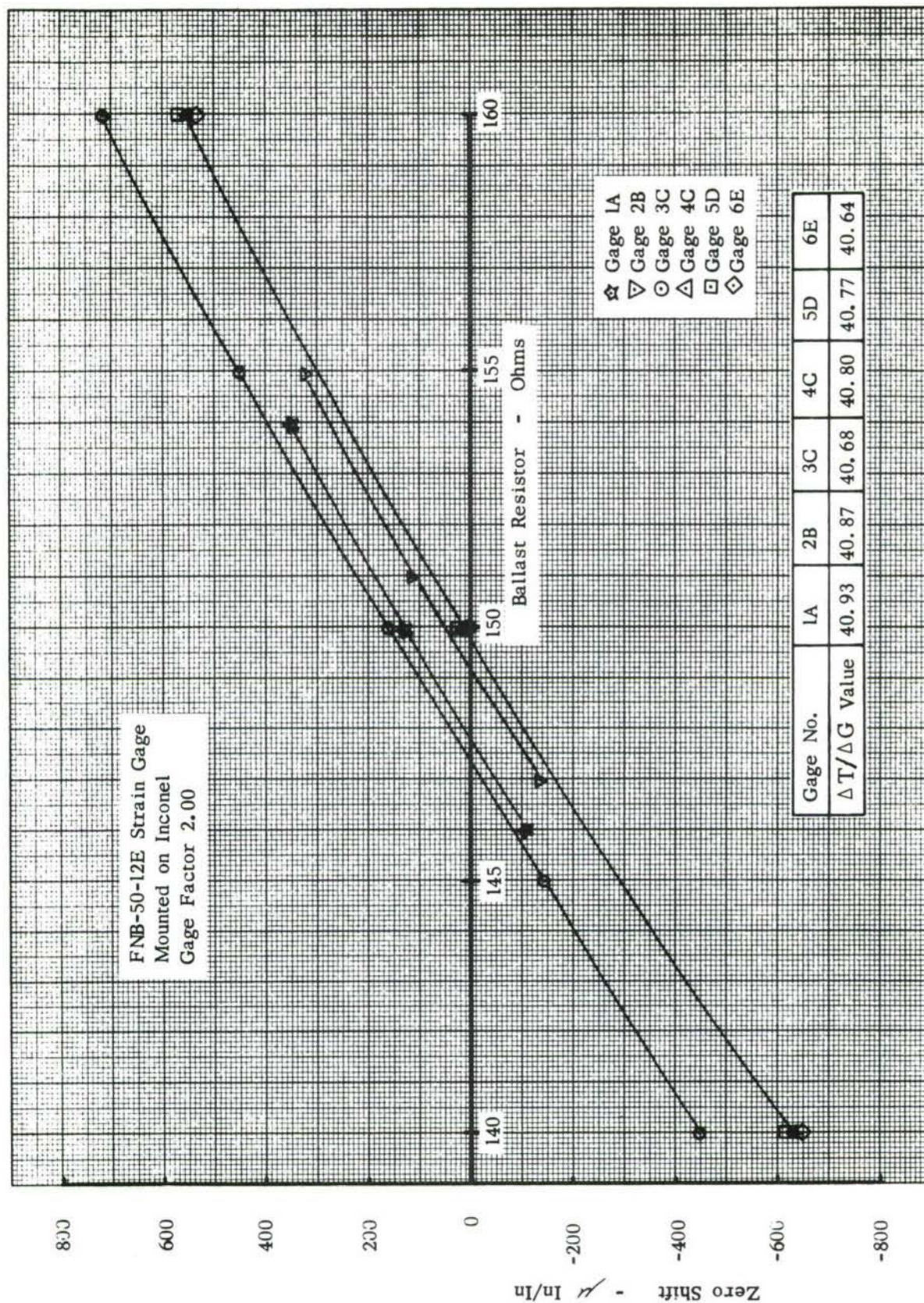


Figure 139. ZERO SHIFT Vs. BALLAST RESISTOR - INCONEL (72 to -320°F)

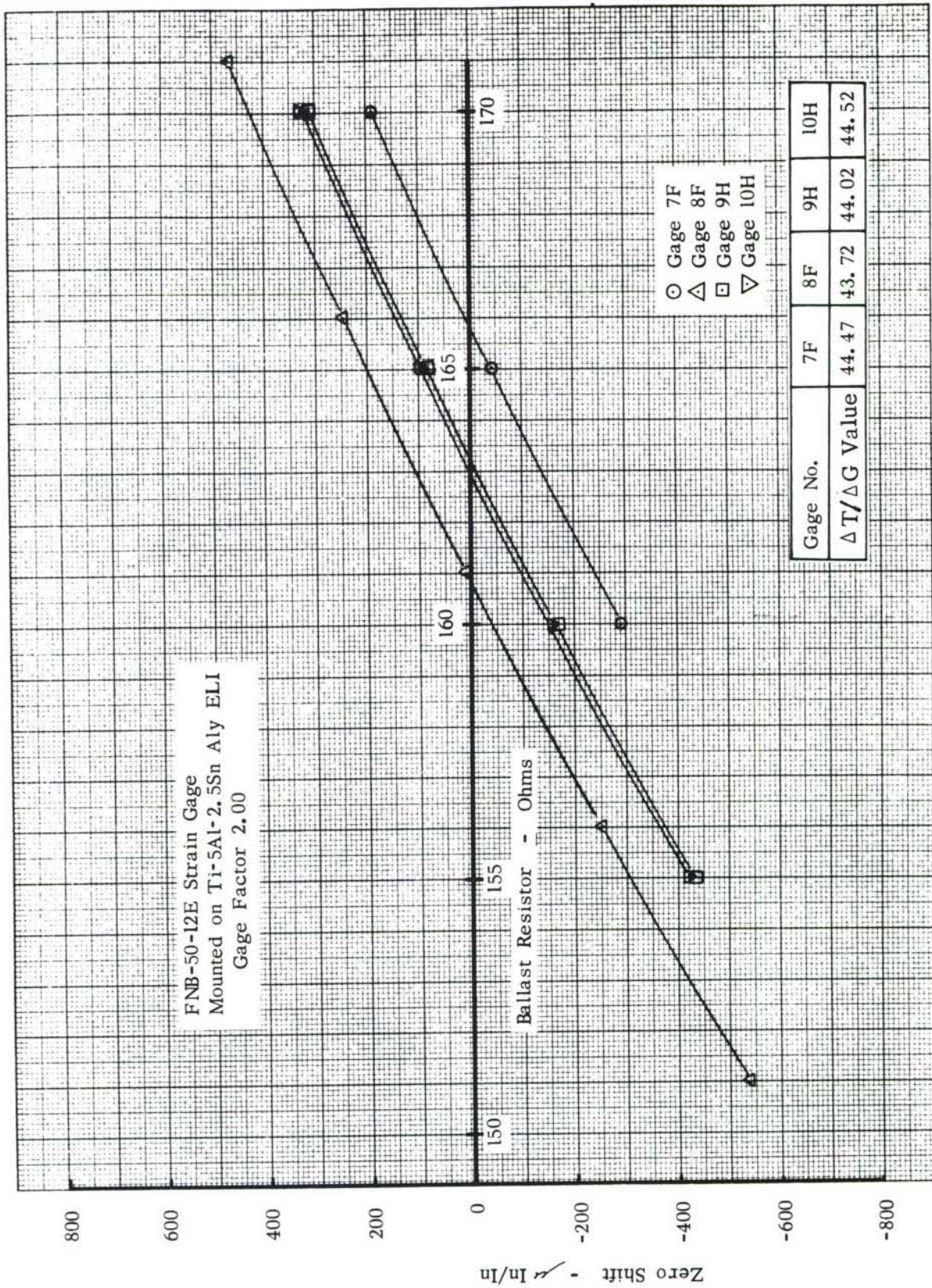


Figure 140. ZERO SHIFT Vs. BALLAST RESISTOR - TITANIUM (72 to -320°F)

sensitive as the value of the compensating resistance (R_B) deviates from the gage resistance (R_G). The sensitivity assuming typical values of R_G , R_L and R_T of 120, 2.0 and 3.4 ohms, respectively, is plotted in Figure 141 as a function of R_B .

Thermal Output

The test of thermal output versus temperature was done in three phases. The thermal output at minus 320°F and minus 423°F was determined with the specimen immersed in cryogenic fluids. The temperature range from room temperature to minus 280°F and return was completed as one phase. The third phase was a temperature cycle from room temperature to + 200°F.

To find the thermal output of the gage for temperatures from -280°F to +200°F, four gage mount specimens containing six test gages were placed in an environmental chamber. The test included three gages on Inconel and three on titanium.

Copper-constantan thermocouples were attached to three of the specimens for the purpose of monitoring their actual temperature. The temperature was varied in 50°F increments and thermal output recorded.

The experimental value previously determined for the ballast resistor to give zero thermal output at 70°F and minus 320°F for each gage was used in the test circuit.

The results of the thermal output tests are plotted in Figures 142 through 145. Figure 146 represents composites of the applicable curve segments. It is constructed from the average data of test points taken for temperature changes diverging from room temperature and is corrected for gage factor variation with temperature.

The thermal output of strain gage 5D, mounted on Inconel, shows considerable difference from the other two similar mounts. The wide variance from the more typical curves of the other gages during the warmup portion of the cycle makes this data questionable.

On both titanium and Inconel, the gage that exhibited the largest thermal hysteresis below room temperature also had the largest hysteresis at higher temperatures. The present test work was not broad enough to show conclusive evidence that the thermal output and thermal hysteresis of the strain gage is affected by the grain direction of the specimen material. It should be noted, however, that in cases of both titanium and Inconel the data of the most consistency between gages was for gages that were mounted in a similar grain direction.

Thermal output was the only testing done above room temperature. There was no indication that this cycle at elevated temperature affected the operation of the gage. No other work to verify satisfactory use or evaluation of the gage at elevated temperatures was attempted.

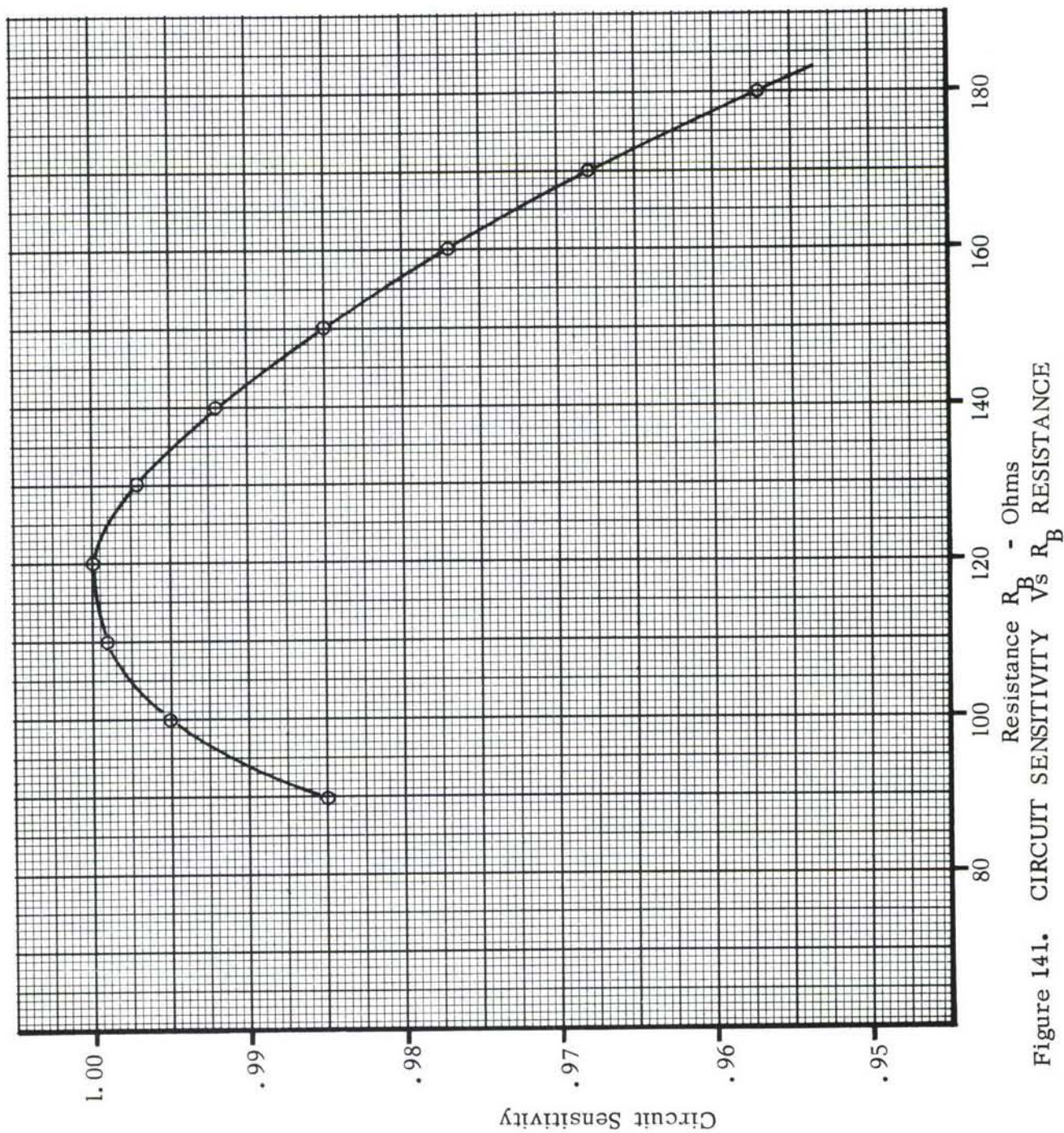


Figure 141. CIRCUIT SENSITIVITY $V_s R_B$ RESISTANCE

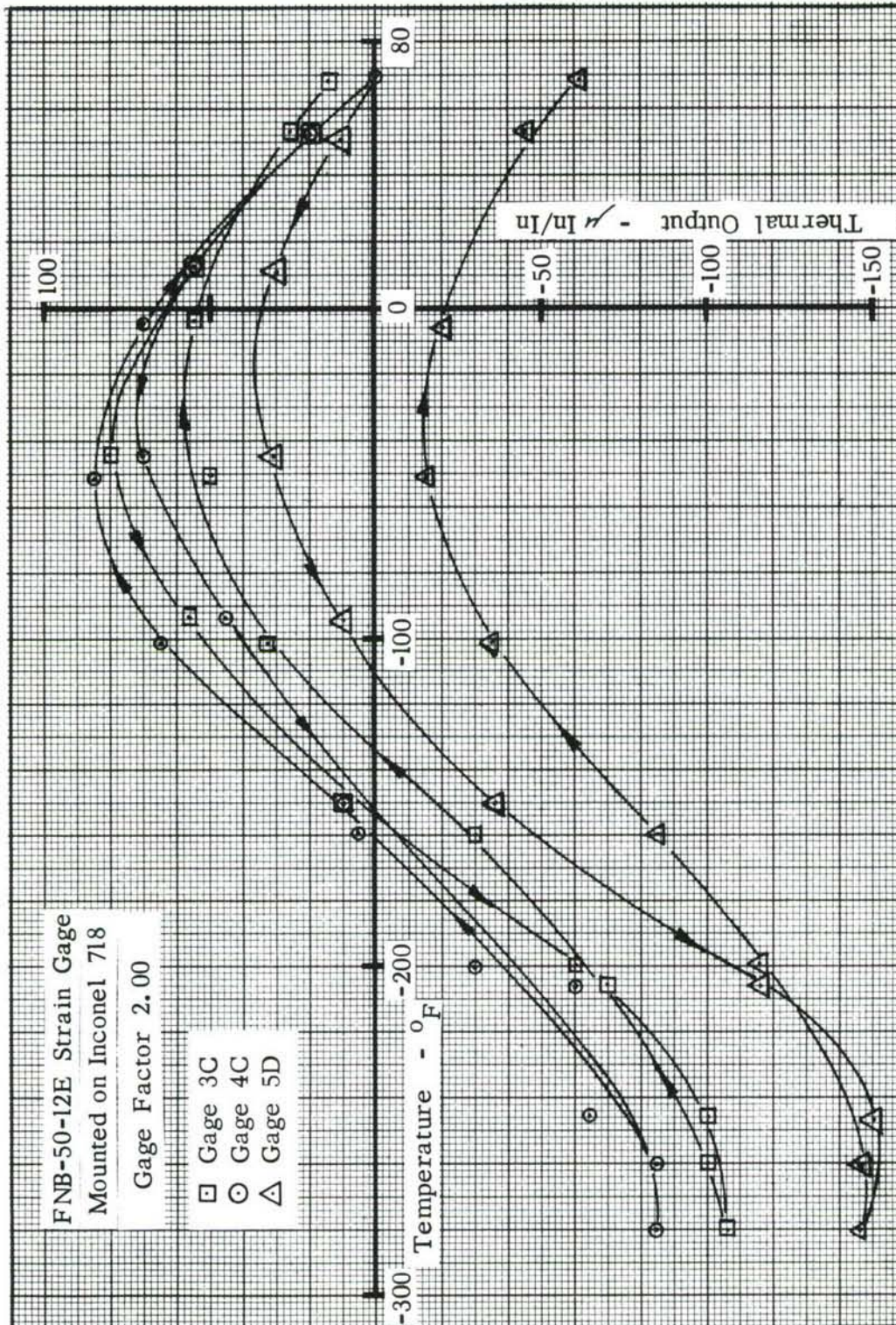


Figure 142. THERMAL OUTPUT Vs TEMPERATURE - STRAIN GAGE ON INCONEL 718.

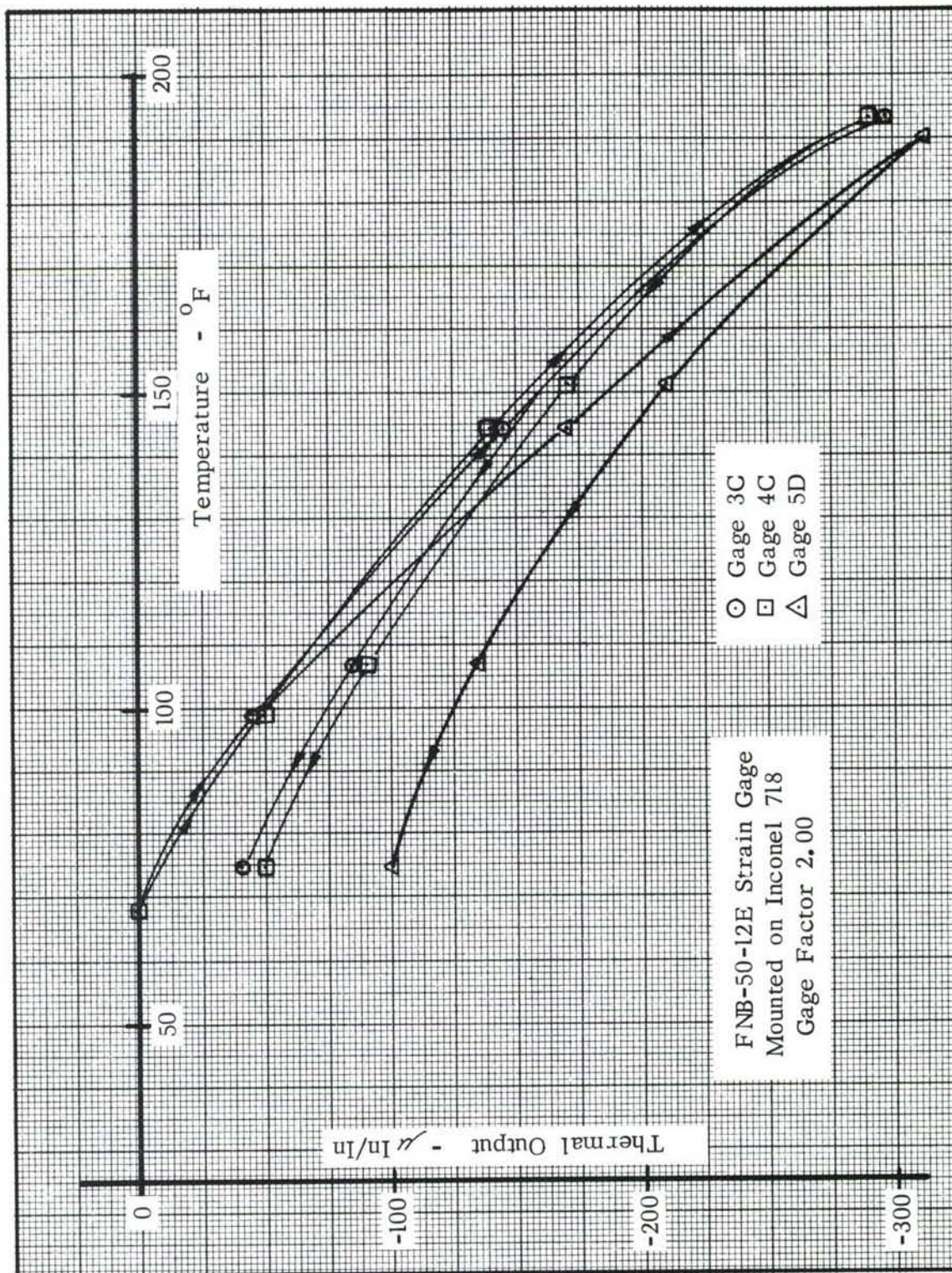


Figure 143. THERMAL OUTPUT Vs TEMPERATURE - STRAIN GAGE ON INCONEL 718

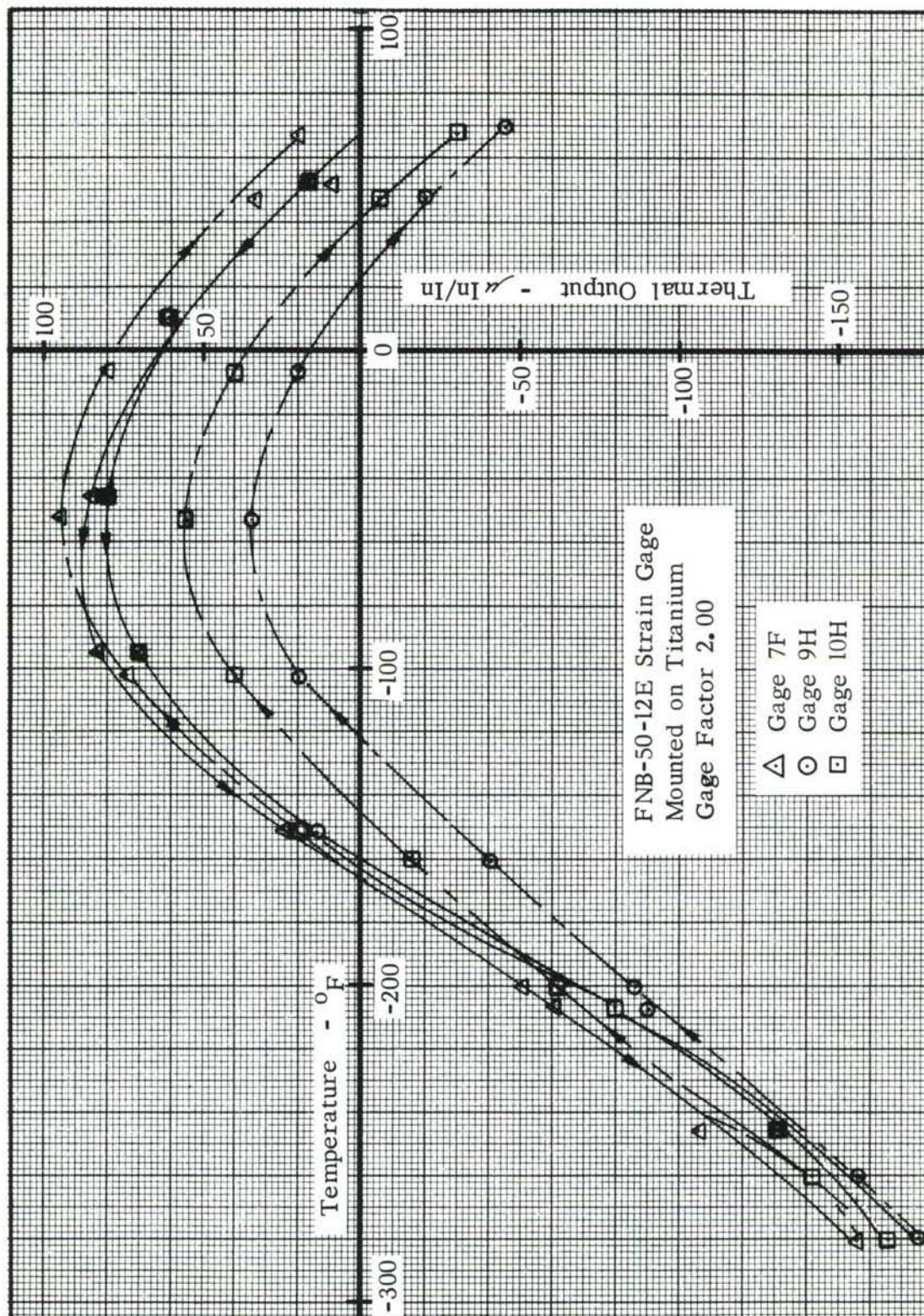


Figure 144. THERMAL OUTPUT Vs TEMPERATURE - STRAIN GAGE ON TITANIUM

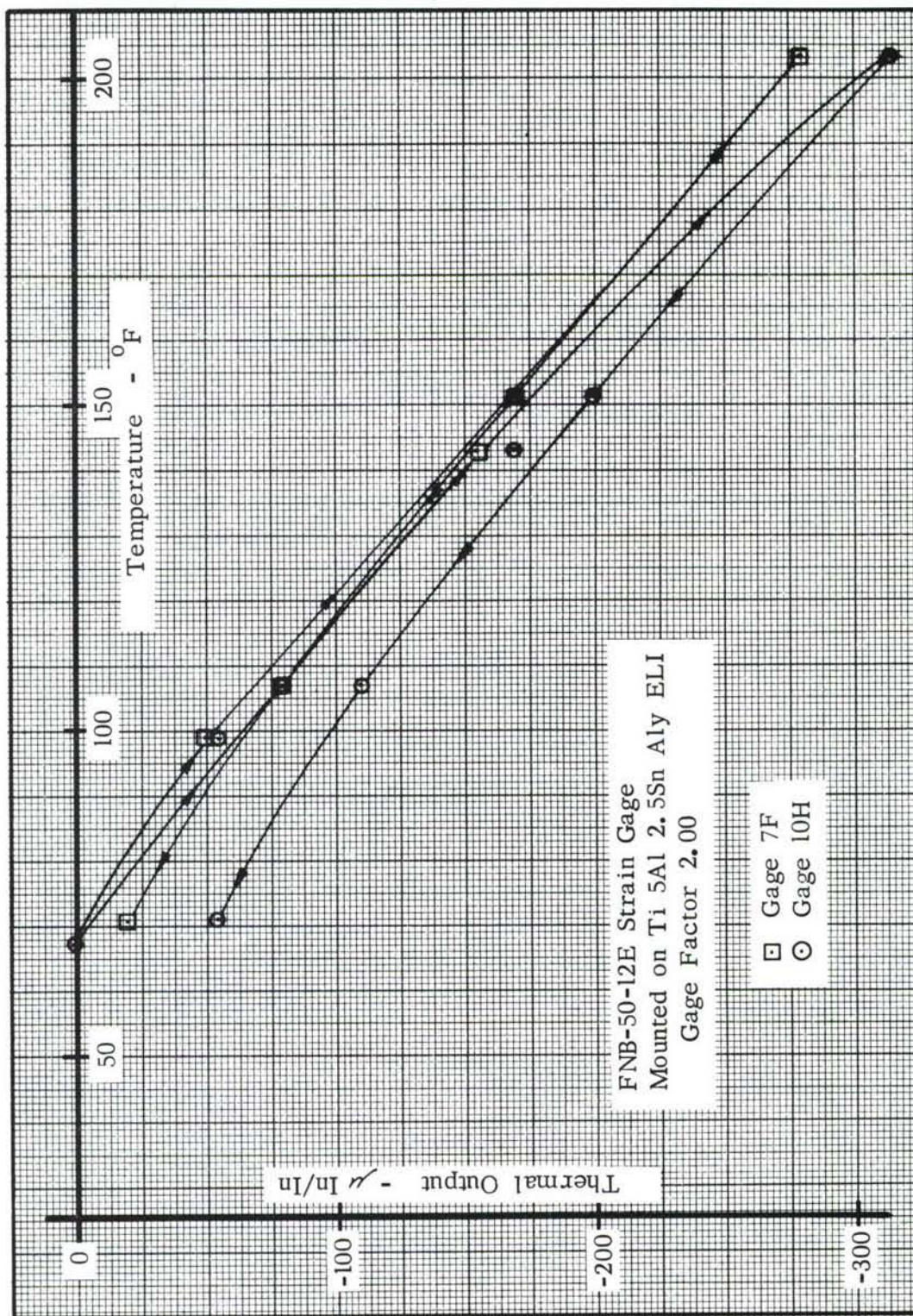


Figure 145. THERMAL OUTPUT Vs TEMPERATURE - STRAIN GAGE ON TITANIUM

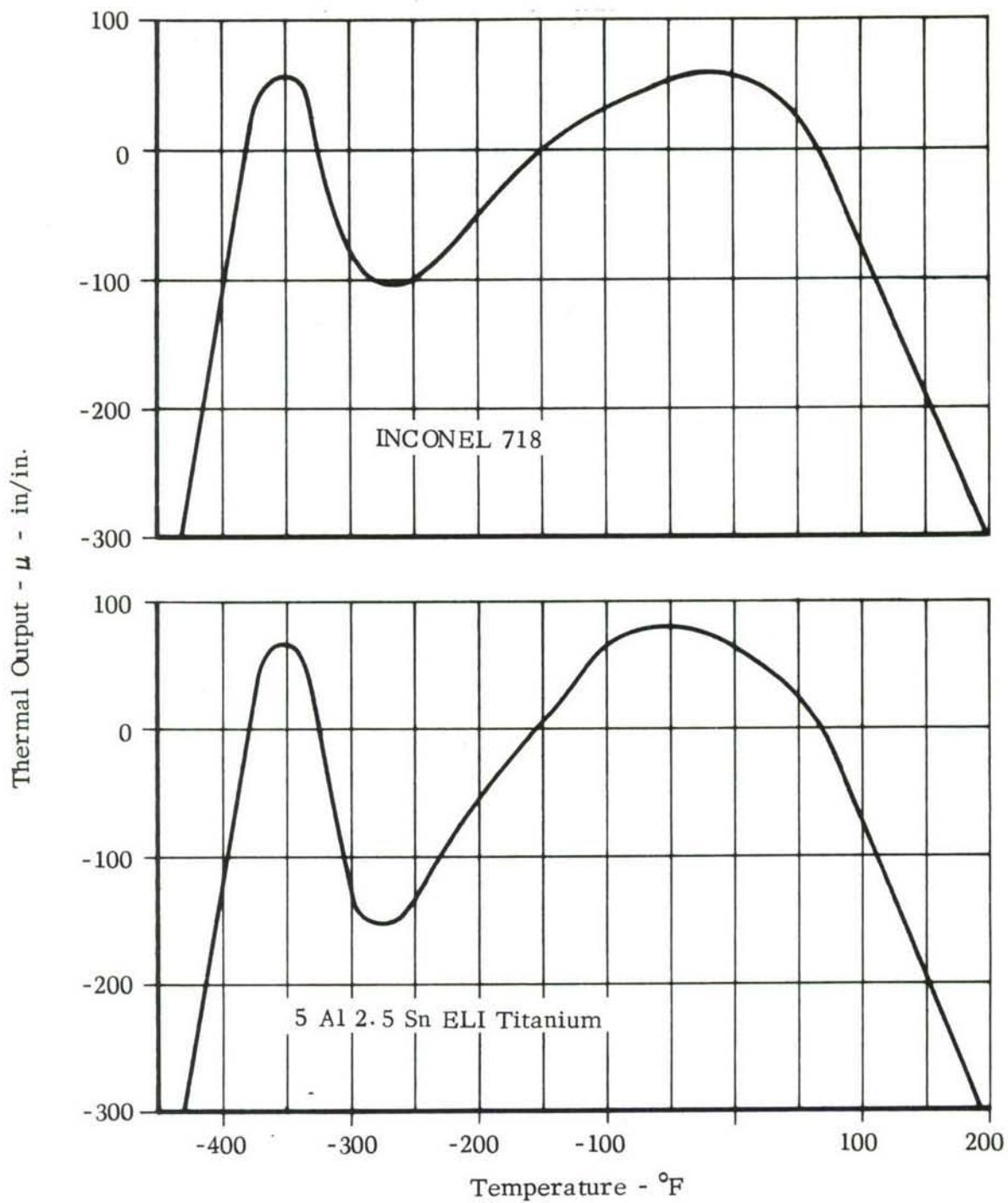


Figure 146. FNB-50-12E STRAIN GAGE THERMAL OUTPUT

Thermal Hysteresis

Strain gage 5D demonstrated thermal hysteresis of about 50 micro-in/in. on Inconel in the low temperature range (Figure 142). The other two test gages on Inconel exhibited less than 20 micro-in/in. thermal hysteresis at the low temperatures.

Above room temperature the thermal hysteresis was nearly 100 micro-in/in. for gage 5D but only about 40 micro-in/in. for the other two test gages (Figure 143).

The thermal hysteresis of the three test gages bonded on titanium was different for each gage at low temperatures. It ranged from 20 micro-in/in. to 45 micro-in/in. (Figure 144). In the area above room temperature, two gages exhibited thermal hysteresis values of 20 and 55 micro-in/in. (Figure 145).

There was no indication of thermal hysteresis at room temperature after the specimens were cycled to cryogenic temperature by immersion of the gages in the cryogenic fluids.

Gage Factor

Since the electrical properties of the strain gage grid material change with temperature, it would be expected that the gage factor will also change.

In order to measure the change in gage factor, gages were mounted in a constant strength cantilever beam apparatus, Figure 147. The apparatus has an eccentric cam which deflects the beam end in sixteen calibrated steps through approximately ± 0.5 inches. Due to the beam design the strain at any point on the surface of the beam is proportional to the deflection at the end. The deflection apparatus is then mounted on a vacuum jacketed cryostat to permit immersion of the strain gaged beam in any desired fluid.

The test procedure was to deflect the beam in a series of steps and record the strain. This was accomplished for each temperature medium (ambient air, 72°F; liquid nitrogen, -320°F; liquid hydrogen, -423°F). Ballast resistances to accommodate zero thermal output at 72°F and -423°F for strain gages on Inconel and titanium were used (except in the LH_2 test environment).

A graph of beam deflection vs. strain was plotted for each run. The absolute gage factor at room temperature, for a ballast resistor based on the $\frac{\Delta T}{\Delta G}$ ratio found by

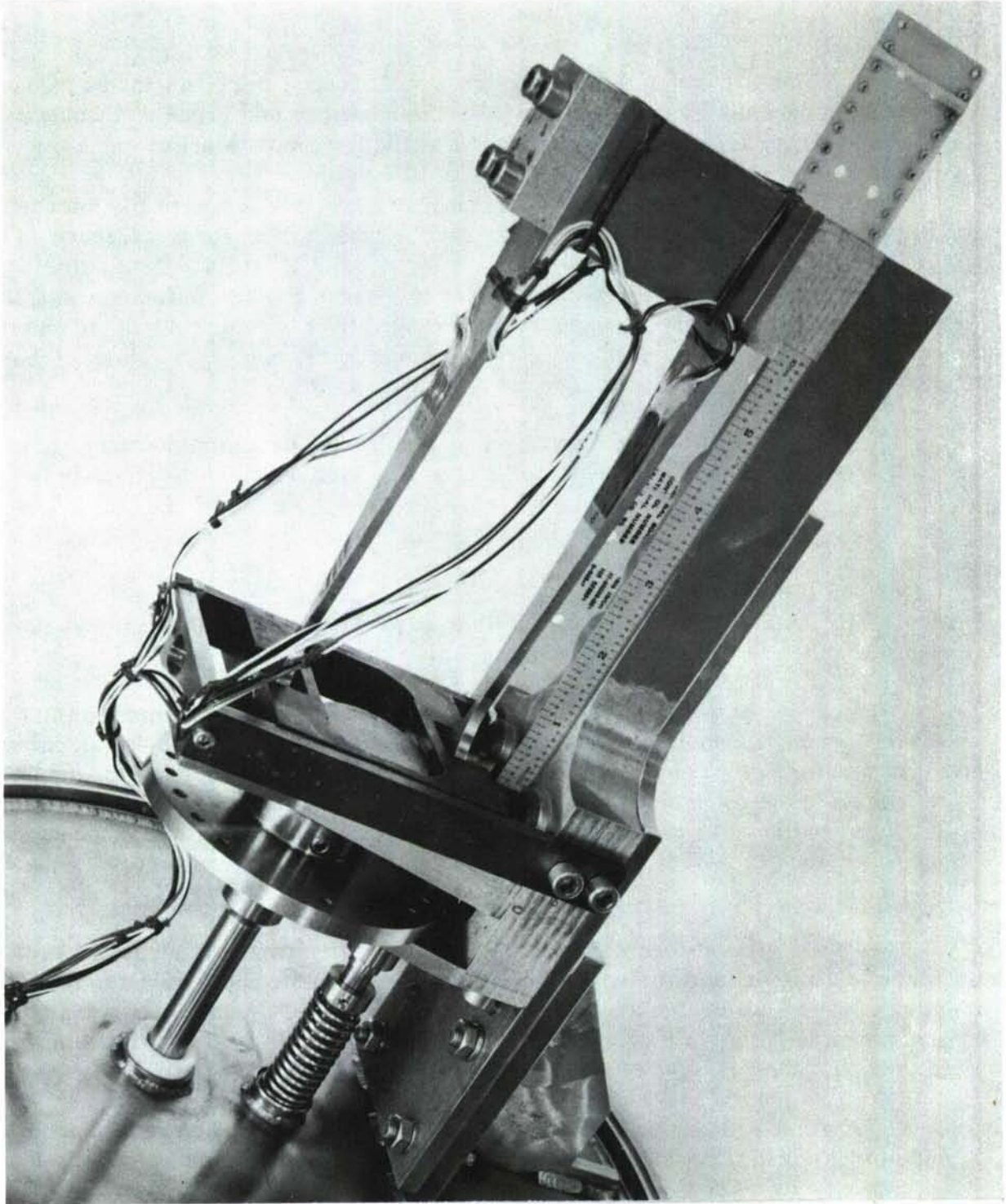


Figure 147. CONSTANT STRENGTH BEAM APPARATUS

experimental techniques, was calculated by taking the ratio of the theoretical beam strain to the measured strain at 72°F. This value was also normalized by eliminating the desensitization caused by the R_B used during the test.

The data from the 72°F and -320°F runs include strain information using ballast resistor values that are used with strain gages mounted on both Inconel and titanium.

The data was analyzed by extrapolating the measured strain on the graph to 0.5 inches beam deflection along the straight part of the curve.

Summary tables of the results are given below:

INDICATED STRAIN AT 0.5 IN BEAM DEFLECTION					
Test Temp. °F	Compression	Strain at 0.5 In. Beam Deflection		Ballast Resistance	
	Tension	Gage 11X	Gage 12X	Gage 11X	Gage 12X
72	Tension	2025	2020	153.7	158.1
72	Compression	2005	2000	153.7	158.1
-320	Tension	2175*	2205	153.7	158.1
-320	Compression	2210*	2210	153.7	158.1
-423	Tension	2160	2195	163.4	169.1
-423	Compression	2160	2160	163.4	169.1

*Lower curve slope.

TEMPERATURE EFFECT ON GAGE FACTOR				
Temperature °F	Tension	Gage Factor Ratio (ϵ at T/ ϵ at 72°F)		
	Compression	Gage 11X	Gage 12X	Average
-320	Tension	1.07	1.08	1.08*
-320	Compression	1.10	1.10	1.10
-423	Tension	1.05	1.07	1.06
-423	Compression	1.06	1.07	1.07

*Data from gage 12X was most consistent

NORMALIZED GAGE FACTOR *AT 72°F			
Tension Compression	Gage 11X	Gage 12X	Average
Tension	1.934	1.939	1.94
Compression	1.915	1.916	1.92

$$*G. F. = \frac{\text{Indicated Strain} \times G. F. (\text{Set on Strain Indicator})}{S \times \text{Theoretical Strain}} = \frac{\epsilon \times 2.00}{S \times 2133}$$

where S = Desensitization caused by R_B

Figure 148 is a plot of the gage factor over the temperature range from 72°F to -423°F.

Waterproofing of Strain Gage Installation

Prior to the cryogenic test on the subscale tanks, each tank was subjected to a proof test with internal water pressure of about 135 psi. Thus, the protective coating over the strain gages had to be capable of keeping the grids and wire connections free of water as well as withstanding the cryogenic conditions during later testing.

Several types of possible waterproof agents were tried. They were Sylgard, Silastic 140, R. T. V. 732, Hysol-Urethane casting compound XCU-A123, GA-5 cement directly over the strain gage and solder joints, 2 mil thick teflon cemented to the strain gages and solder joints with GA-5 cement, and PT 201 thermoset resin.

The test procedure was to cover the strain gage installation with the waterproofing and then submerge the test area into tap water at one atmosphere pressure. Resistance to ground readings were taken at periodic intervals. Specimens that survived this water test (about 50 hours) were then cycled in LN_2 (-320°F) 3 times, followed by more water immersion tests. As a final test, the good specimens were dipped in LH_2 (-423°F) for 3 cycles.

Some waterproof samples, such as Sylgard, were initially subjected to LN_2 .

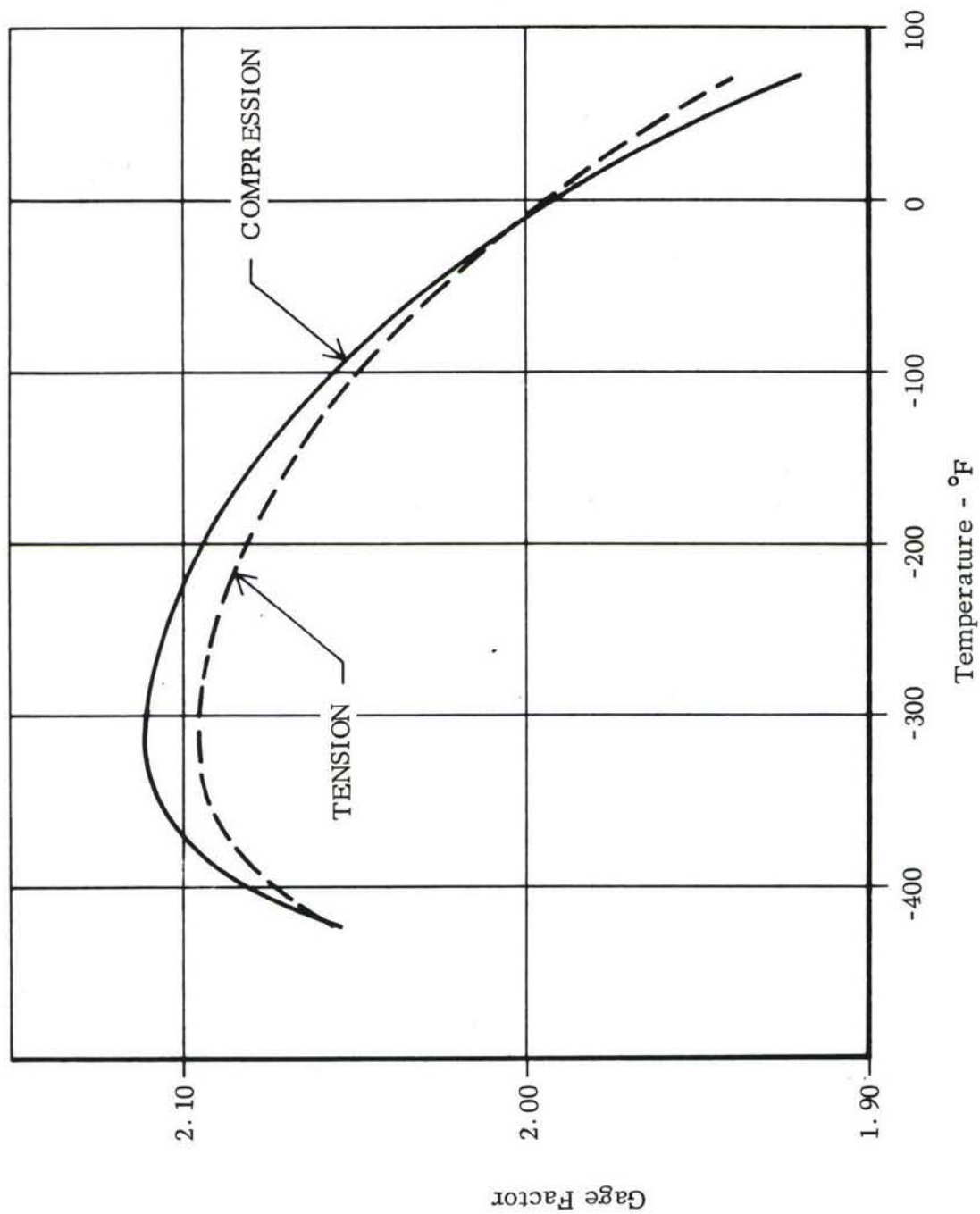


Figure 148. GAGE FACTOR VS. TEMPERATURE - FNB-50-12E STRAIN GAGE

The following table summarizes the results of the waterproof tests:

Waterproof Agent	Water	LN ₂	LH ₂	Remarks
Sylgard	-	All (3) specimens cracked	-	Unsatisfactory
Silastic 140	2 specimens failed after 2 hours	-	3 specimens	Unsatisfactory
RTV 732	Good	Good	No test	-
Nysol-urethane	10 specimens failed after 1 hour	-	-	Unsatisfactory
GA-5 Cement	Failed	-	-	Solder joints not covered
GA-5 Teflon	Good*	Good	Good	Proper Installation techniques vital
PT 201 Thermoset	6 specimens failed	-	-	Unsatisfactory

*Some of the original GA-5 Teflon samples failed because of inadequate sealant around the lead wires. Improved techniques of installation made this waterproofing method satisfactory.

Lead Wire Correction

The inherent bridge arm resistances used with the FNB-50-12E gages allows bridge circuit unbalance from temperature changes in the lead wire. The lead wire (R_{LG}) connected to the nichrome element and lead wire (R_{LT}) connected to the platinum element both realize identical temperature changes; however, because the resistance change (ΔR_{LG} and ΔR_{LT}) due to temperature constitutes a different change in percentage of the respective bridge arms, the bridge becomes unbalanced. Tests were performed to learn the characteristic resistance change of lead wire with temperature changes. This change can then be translated to bridge output.

The lead wire resistance change is plotted against temperature in terms of the ambient temperature resistance in Figure 149. This permits an easy interpretation

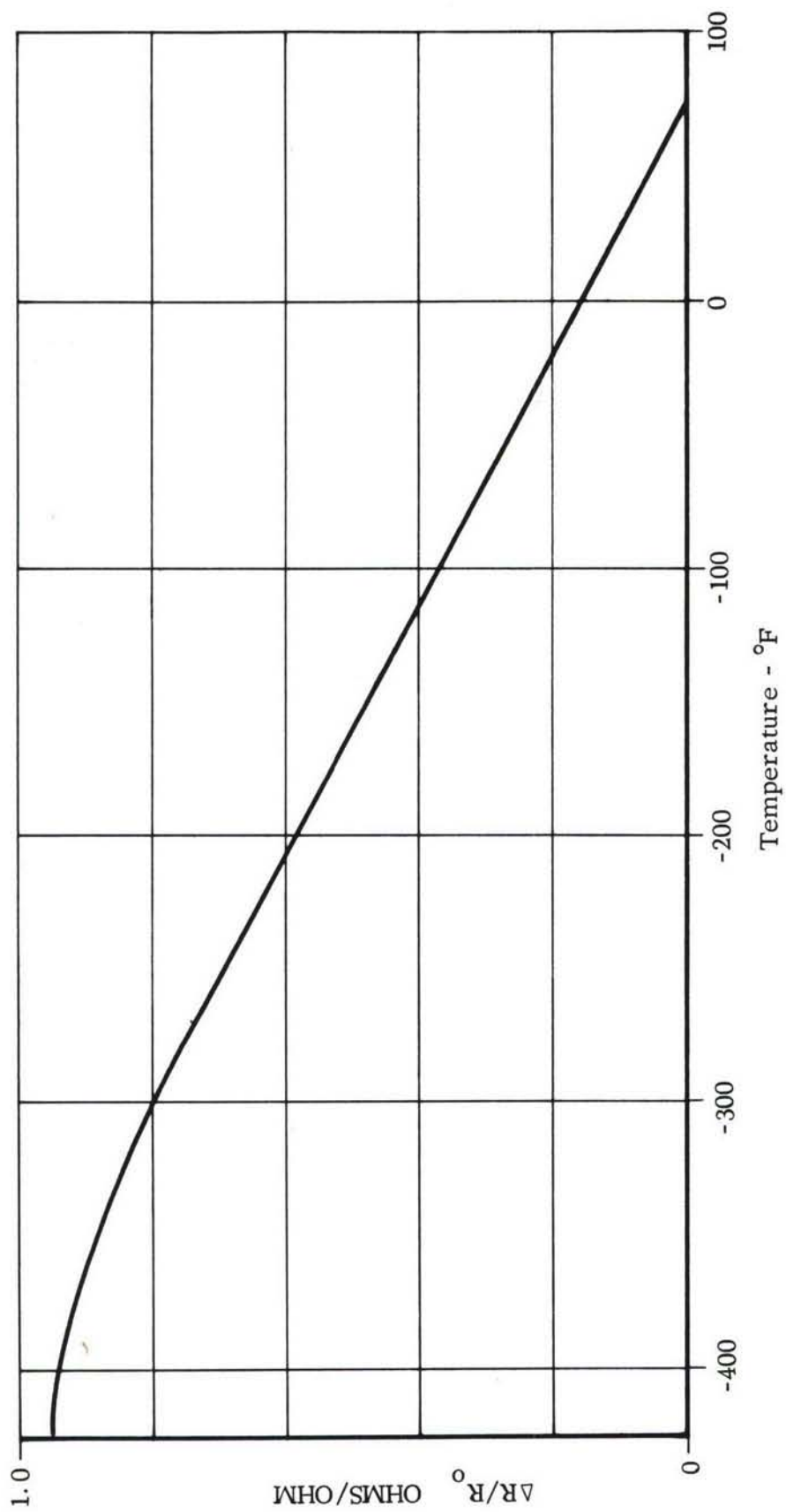


Figure 149. RESISTANCE CHANGE OF COPPER WIRE

of the resistance change in any length of lead wire if the ambient temperature resistance and the test temperature of that length of wire are known.

The bridge output can be computed in terms of strain by a formula derived from simple circuit considerations.

$$\epsilon_L = \frac{\Delta R_L}{G.F. (R_G + R_{LG})} \frac{R_T + R_B - R_G}{R_T + R_{LT} + R_B}$$

where

ΔR_L = Change of lead wire resistance due to temperature change (ohms).

ϵ_L = Strain resulting from ΔR_L (micro-in/in.)

G. F. = Gage factor (dimensionless)

In future installations the circuit can be made self-compensating by varying the lead wire sizes. This would eliminate the uncertainties in lead wire temperature distribution and the necessity for making the additional correction to the measured strain values. The condition of self-compensation can be achieved by satisfying the equation

$$R_{LT} = R_{LG} \left(\frac{R_B + R_T + R_{LT}}{R_G + R_{LG}} \right)$$

Transverse Sensitivity

In a biaxial stress field the strain gage can have an error in output because its sensitivity (gage factor) is based on a uniaxial stress field. No experimental work was included within the project; however, transverse sensitivity error is given to aid in more accurate data analysis. This data was derived from other evaluation programs using the FNB-50-12E strain gage.

$$E = \frac{-2.9}{1 + 2.9\mu} \left(\mu + \frac{\epsilon_N}{\epsilon_A} \right)$$

E is the percent error in the indicated strain along the principal axis.

μ is the poisson's ratio for the material.

-2.9 is the experimentally derived transverse sensitivity factor for the FNB-50-12E gage.

ϵ_A is the principal axis strain.

ϵ_N is the strain normal to the principal axis.

Limit Strain, Mechanical Hysteresis and Creep

The limit strain test was accomplished by subjecting two strain gages, mounted on either side of a titanium tensile coupon to a strain of about 10,000 micro-inches/in. while immersed in liquid nitrogen. Three load cycles were applied to the specimen in a universal testing machine. The load was uniformly increased (or decreased) while strains were read at 500 pound intervals. Prior to testing at LN₂ temperatures, three cycles at room temperature to about 6,000 micro-inches/inch were made.

A short duration creep test was made by maintaining maximum load on the specimen during the third cryogenic cycle for 20 minutes.

Testing of two gages demonstrated satisfactory results to strains of about 9,600 micro-inches/inch at a temperature of minus 320°F.

Mechanical Hysteresis:

Maximum mechanical hysteresis was about 200 micro-inches/inch for strain levels to a maximum of 9,600 micro-inches/inch for the first cycle at temperatures of minus 320°F. For the second and third run the mechanical hysteresis was only about 100 micro-inches/inch.

At room temperature, the mechanical hysteresis was about 75 micro-inches/inch at the first cycle to maximum strain of 5,000 micro-inches/inch. The hysteresis was negligible for the second strain cycle.

Creep:

There was no detectable creep in the gage installation while maintaining a strain of 9,600 micro-inches/inch for 20 minutes.

STRAIN GAGE INSTALLATION ON THE SUB-SCALE TANKS:

Six FNB-50-12E strain gages were installed on each of the sub-scale tanks. On the Inconel tank the gages were located about 17 inches from the end of the cylindrical portion of the tank at 30° and 60° above a horizontal plane through the center. At the 30° location two longitudinal and two circumferential gages were placed back-to-back (inside and outside). At 60° two circumferential gages were placed back-to-back.

Strain gages on the titanium tank were all mounted on the inside. The gages were about 17 inches from the end of the cylindrical section of the tank. At the top and at the horizontal plane through the center on one side, a longitudinal and a circumferential gage were mounted. A circumferential gage was located at 45° above the horizontal, and a single longitudinal gage was mounted at the bottom. A thermocouple was located adjacent to each gage location.

The procedure for installation of the strain gages, in general, was the same as used for the evaluation specimens. GA-5 cement was cured with heat lamps and the pressure was maintained on the strain gages with a vacuum system.

The following is the detailed procedure used in installing strain gages on the subscale tanks:

Gage Locations:

- a) Locate approximate location of gages.
- b) Wipe area thoroughly with acetone.
- c) Layout strain gage locations per installation request.
- d) Mask areas for gage alignment, 4" x 4" strain gage area if on large area.
- e) Wash enclosed areas with acetone soaked wiper. Do not touch thereafter.
- f) Mask a square area (for velvetizing) and transfer alignment marks with pencil.
- g) Cover area with polyethylene.
- h) Engineer to inspect and initial installation log if O. K.

Surface Preparation:

- a) Set up "velvetizer" with No. 3 powder. Use dry nitrogen at 80 psig.
- b) Velvetize sample material before starting on specimen.
- c) Velvetize surface to a uniform light grey color. Hold nozzle 2-1/2 to 3 inches from surface at approximately 45°. Catch dust with vacuum cleaner. Feather out velvetizing to masked area.
- d) Blow off area with dry nitrogen. Recover with polyethylene until ready for cleaning.

Cleaning for Cement Coat :

- a) Use detergent wash and rinse with distilled water. Repeat wash and rinse three times. Do not wipe dry. Do not wash over tape on last wash and rinse. Just wash velvetized area.

NOTE: Cleaning to be done immediately before cement application .

Gage Preparation:

- a) Clean working surface just prior to laying gages down for tape pickup.

- b) Remove gage carrier if applicable.
- c) Roughen gage mounting surface with pumice powder.
- d) Trim gage if required.
- e) Wipe gage mounting surface with acetone.
- f) Place in proper alignment on the cellophane tape.
- g) Align and place terminal strips on same tape with gage.

Cement Mounting Coat:

- a) Mix 3 gm. GA-5 resin with 9 - 10 drops of activator thoroughly in glass container. Allow mixture to sit for 5 minutes minimum before use to minimize air bubbles.
- b) Brush a thin layer of cement on installation area.
- c) Do not use cement which has been mixed more than one half hour.

Gage Mounting:

- a) Place gages in position (use alignment marks on masking tape) and secure one end. Be sure that ends of cellophane tape extend beyond cement area. Slide finger from secured end of tape to other end, to mount gage and drive air bubbles and excess cement out.
- b) Place teflon film, sponge rubber pad (approximately 1/4" over lapping gage) over gage installation and hold tightly in place with tape.
- c) Place a Mylar sheet over gage area and seal three edges with 1 inch wide glass tape. Install vacuum inlet on fourth side and seal sheet. Pull a vacuum of 15 inch Hg (a mechanical clamping device may be used in cases where specified by the engineer).
- d) Allow to room temperature cure for 2 hours.
- e) Raise temperature slowly to 180°F over 1-1/2 hour period (30°F per 1/2 hour). Cure at 180°F for 3 hours.
- f) Allow to cool to ambient temperature. Remove tape and inspect for appearance suitability. Notify engineer of discrepancies.
- g) Engineer to inspect and initial installation log if O. K.
- h) Protect with cover until ready for electrical check.

Initial Electrical Check:

- a) Check continuity with Triplet multimeter. Use blunt probes.
- b) Check resistance to ground with Weston insulation tester. (Minimum value 100 megohms).

Gage Ribbon Leads - Terminal Strip to Gage:

- a) Touch tab and wire lightly and quickly with soldering iron (slight amount of solder on end).
- b) Clean with brush and alcohol to remove flux. Allow to dry and cover.

Electrical Check:

- a) Measure resistance of each gage with digital ohmmeter and record on check list.
- b) Measure resistance to ground of each gage with Weston insulation tester and record. 100 megohms is acceptable minimum.

Lead Wire Attachment:

- a) Locate lead wire near gage, hold down with green tape.
- b) Spot weld strap over lead wire near gage.
- c) Route lead wires to appropriate areas per Installation Request.
- d) Solder leads to terminal strip.
- e) Clean with alcohol followed by acetone using brush to remove flux.

Electrical Check:

- a) Check continuity with Triplet multimeter.
- b) Check resistance to ground with Weston insulation tester. (100 megohms minimum)
- c) Engineer to witness and initial log if wiring is O. K.

Absolute Waterproofing:

- a) Wash with detergent and rinse with distilled water (use brush). Air dry one hour or with heat gun (do not exceed 100°F).
- b) Mix 3 gm GA-5 resin with 9 - 10 drops of activator thoroughly and let stand for 5 minutes.
- c) Cut a 2 Mil thick piece of teflon the size of the velvetized area and extending 1/2" up the lead wires, etch teflon for bonding if necessary.
- d) Place a piece of unetched teflon over the bondable piece (1/4" to 1/2" overlap).
- e) Place a piece of "rough surfaced" sponge rubber over the teflon.
- f) Secure a 6" x 6" sheet of Mylar over the gage area using green tape to seal three edges.
- g) Install the vacuum inlet on the fourth side and seal that side.
- h) Pull a vacuum of 15" Hg.
- i) Allow to room temperature cure for 2 hours.

- j) Raise temperature 10°F per 10 minutes to 180°F .
- k) Cure at 180°F for 2 hours.
- l) Shut off vacuum.
- m) Remove Mylar sheet, sponge rubber, etc.
- n) Inspect that good bonding of teflon was attained.

Electrical Check - Final Inspection:

- a) Measure resistance of each gage with lead wire and record value. Engineer to witness and initial log.
- b) Measure resistance to ground at each circuit and record value. Engineer to witness and initial log.
- c) Hook up strain indicator to each circuit and check sensitivity. Engineer to witness and initial log.
- d) Secure leads until test.

Figure 150 is a photograph of the vacuum system during cure on the Inconel tank. A typical completed installation is shown in Figure 151.

The lead wires were routed along the side at the horizontal center plane. All leads were made the same length by doubling back as required. The wires on the Inconel tank were secured by patches of GA-5 cement every few inches. This is shown in the photograph, Figure 152. Figure 153 is an overall photograph of Tank #1 with the outside strain gages in view. Wires were held to the titanium tank by small metal clips of titanium "Unitec" welded to the surface. Figure 154 shows the strain gages, lead wires and thermocouples on the inside of Tank #2.

Results

Data was obtained for four different conditions on the Inconel tank and one condition in the titanium tank. The strain was recorded on both tanks during proof tests with water to about 135 psi. A proof test to about 135 psi with liquid nitrogen was also performed on the Inconel tank. The third and fourth conditions of testing were with the tank in the chamber filled with liquid nitrogen and liquid hydrogen, respectively.

Data from the proof tests were analyzed by hand, while the data from the evaluation tank tests were machine processed. Ten of the twelve strain gages performed well during all tests. No data was obtained from one gage during testing in the chamber and a second gage failed to produce good data during the LH_2 tests in the chamber. It was not determined whether the failures were in the strain gage or in the landlines.

Proof Tests - Tank #1

Plots of strain vs. tank pressure for the proof tests are presented in Figures 155 through 160. In each case the curve is drawn through points of data corrected for thermal output, lead wire error, gage factor, etc.

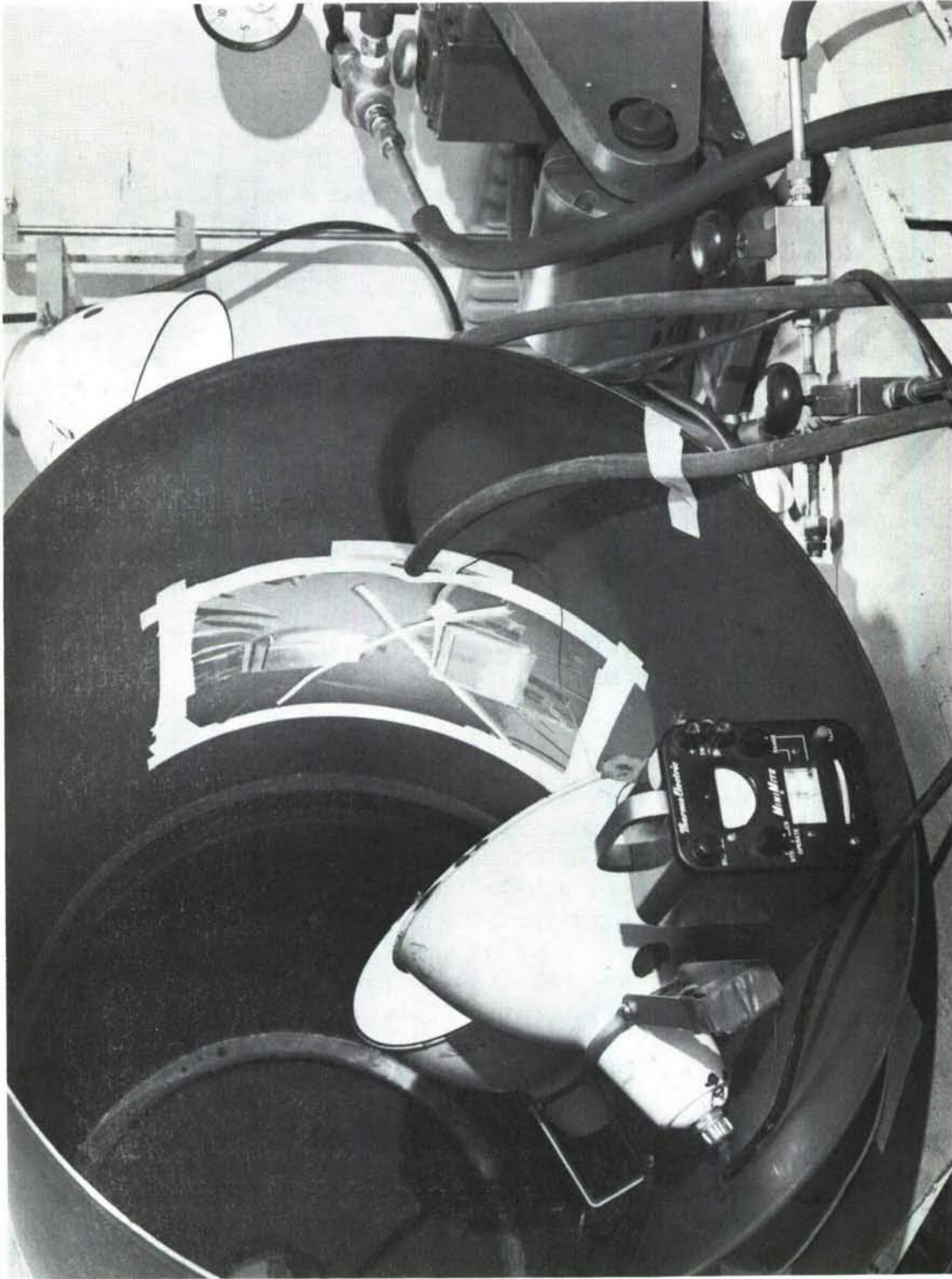


Figure 150. CURING STRAIN GAGE INSTALLATIONS ON TANK # 1.

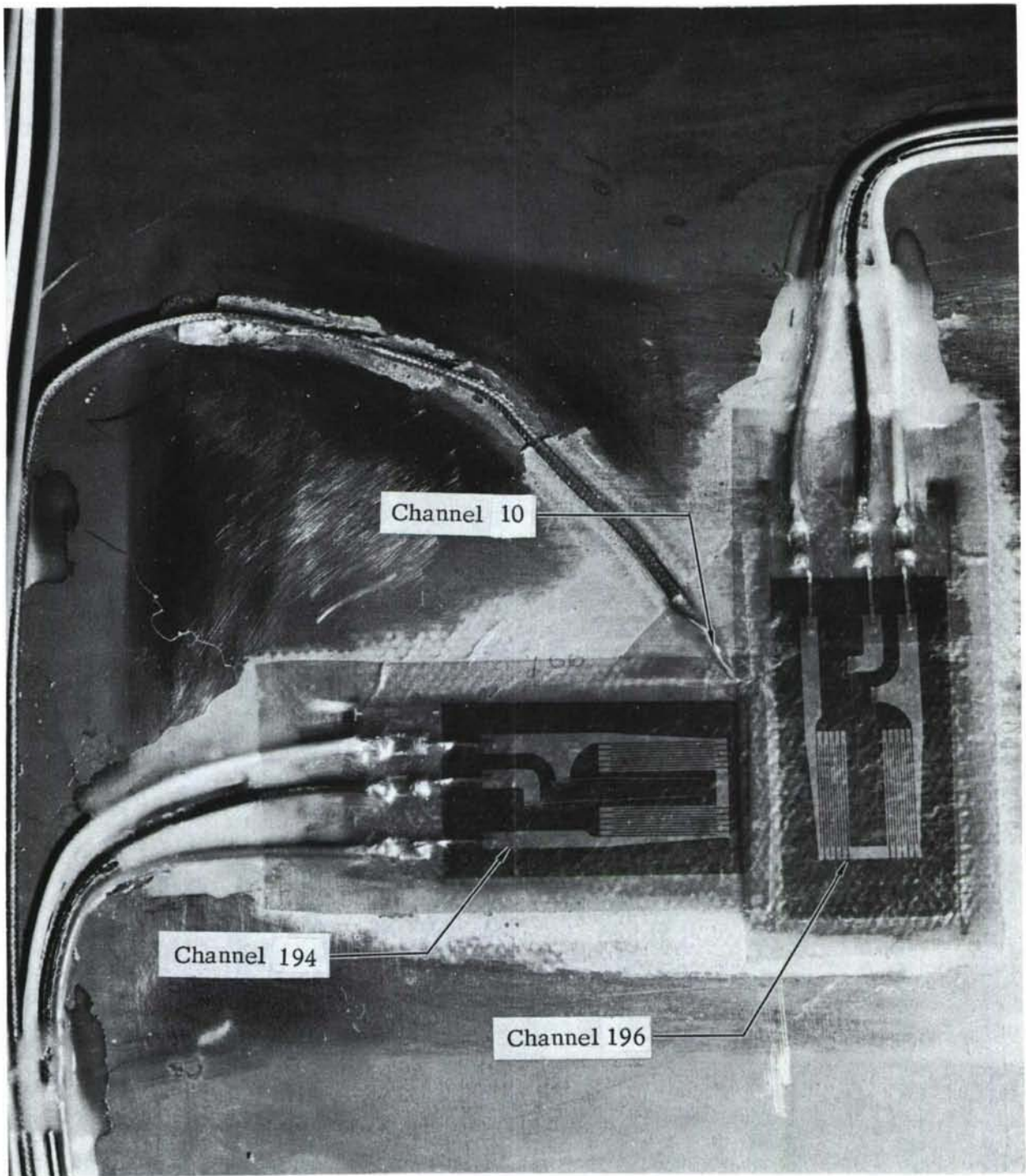


Figure 151. STRAIN GAGE INSTALLATION - SUBSCALE TANK #1

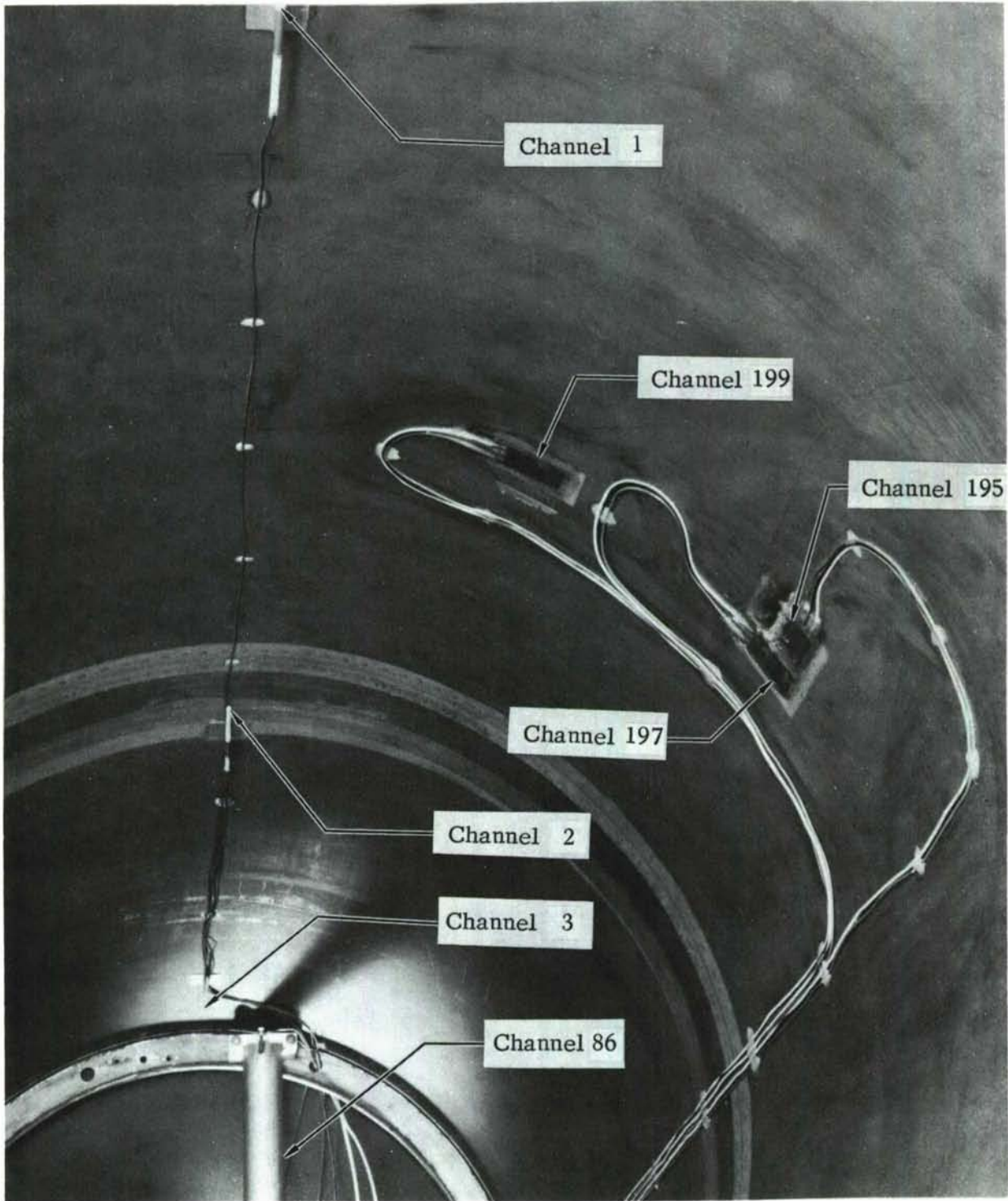


Figure 152. INSIDE INSTRUMENTATION - SUBSCALE TANK # 1

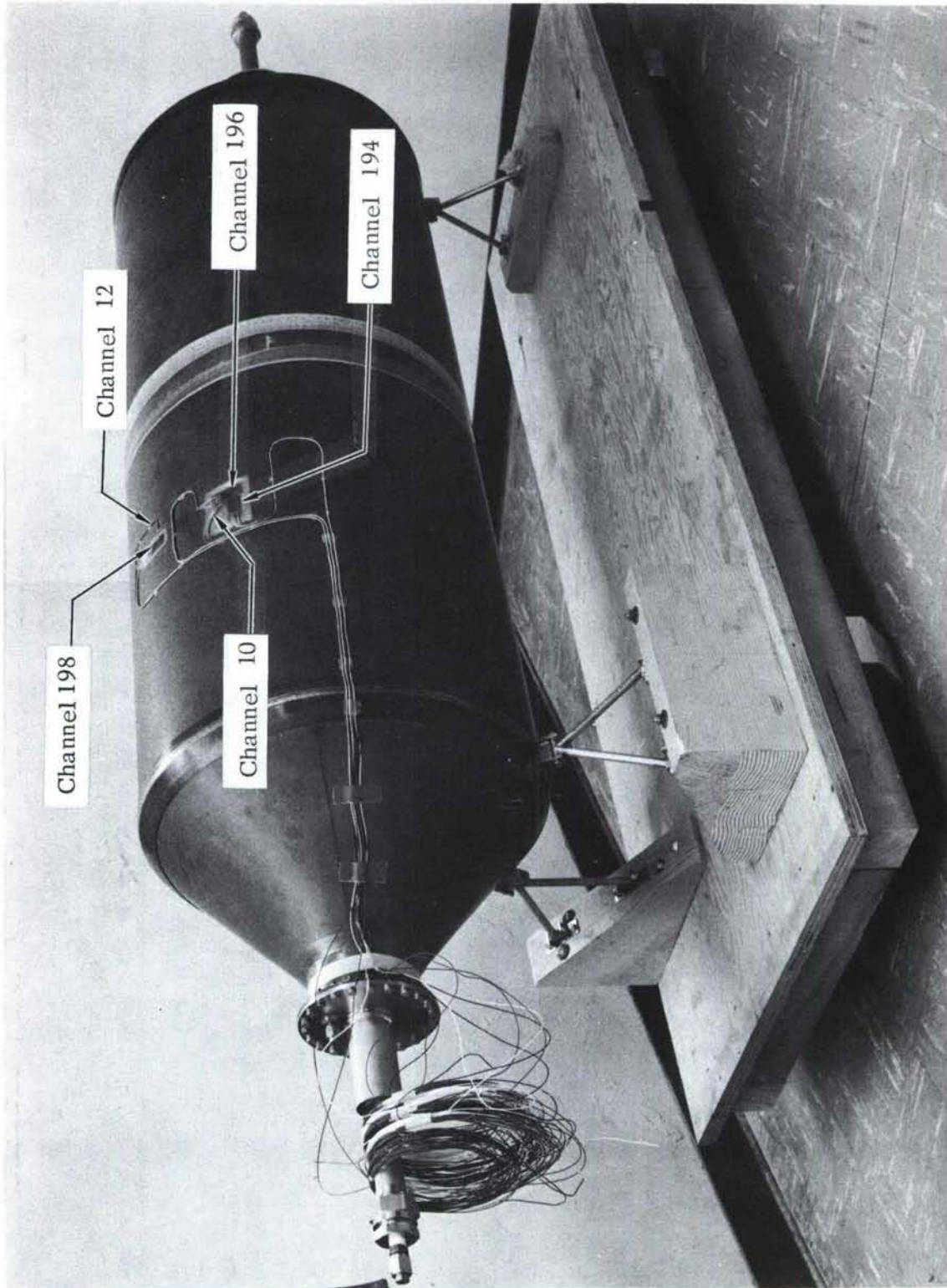


Figure 153. OUTSIDE INSTRUMENTATION - SUBSCALE TANK #1

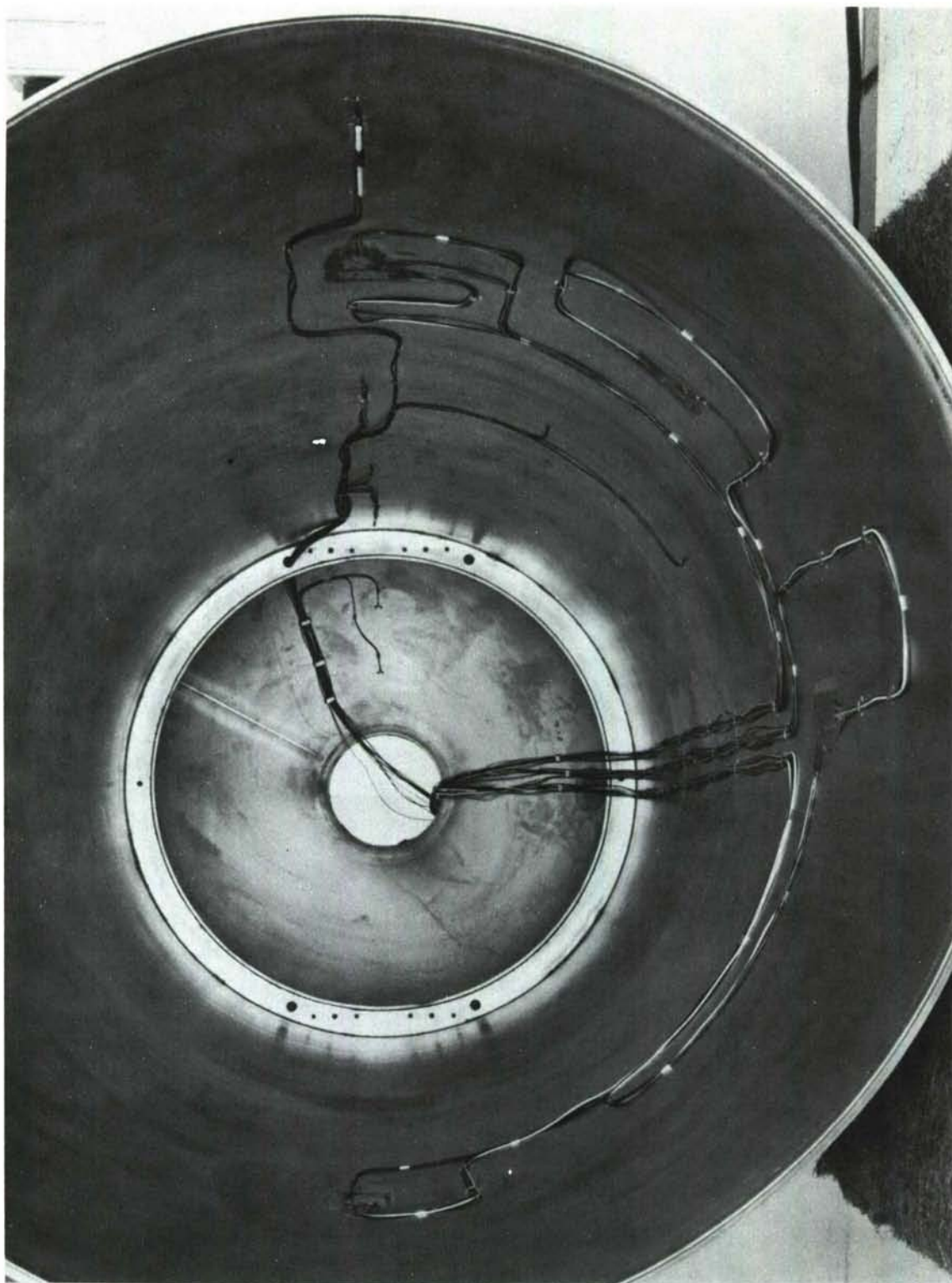


Figure 154. STRAIN GAGE & THERMOCOUPLE INSTALLATION - TANK #2.

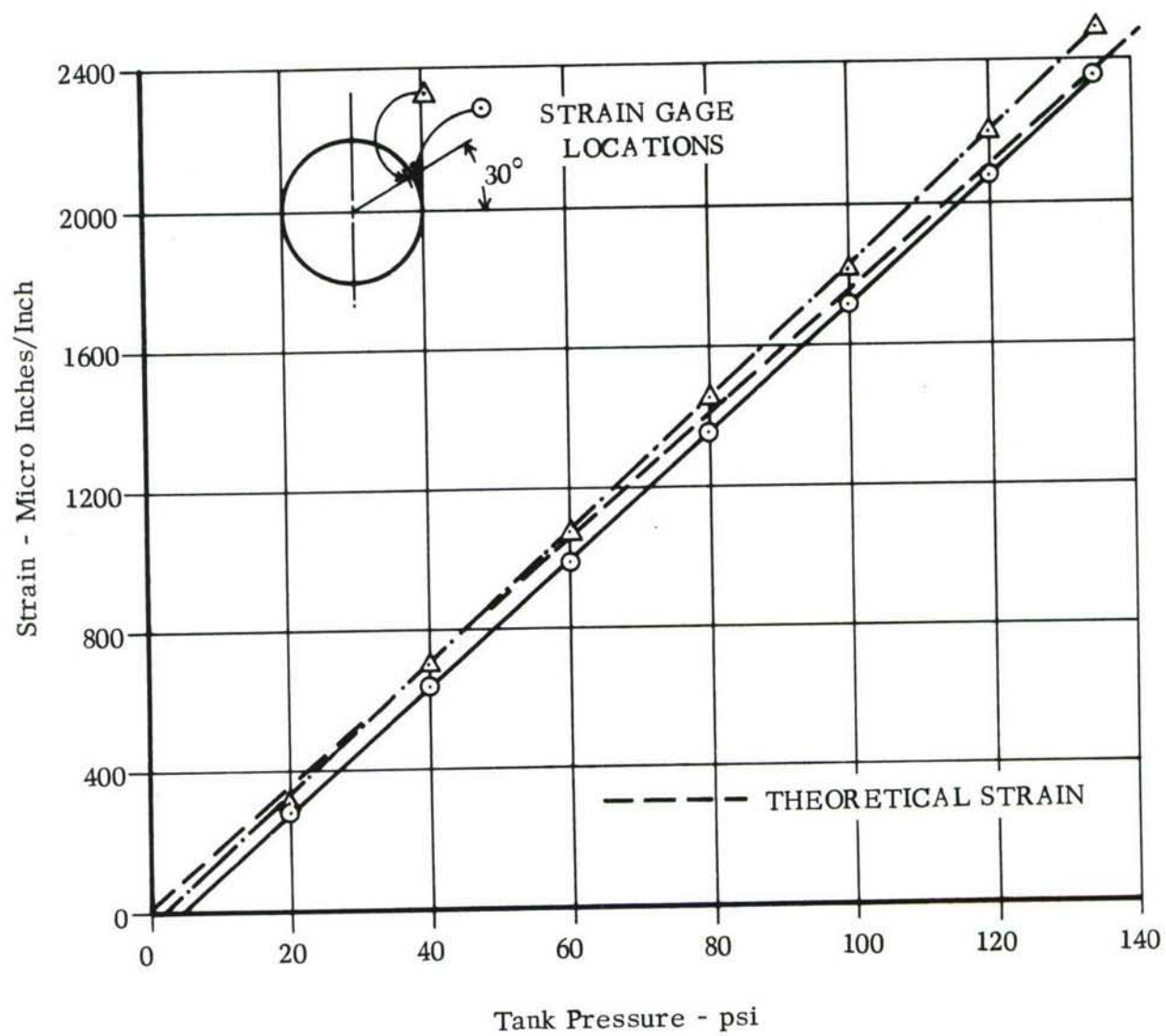


Figure 155. HOOP STRAIN - WATER PROOF TEST (INCONEL 718)

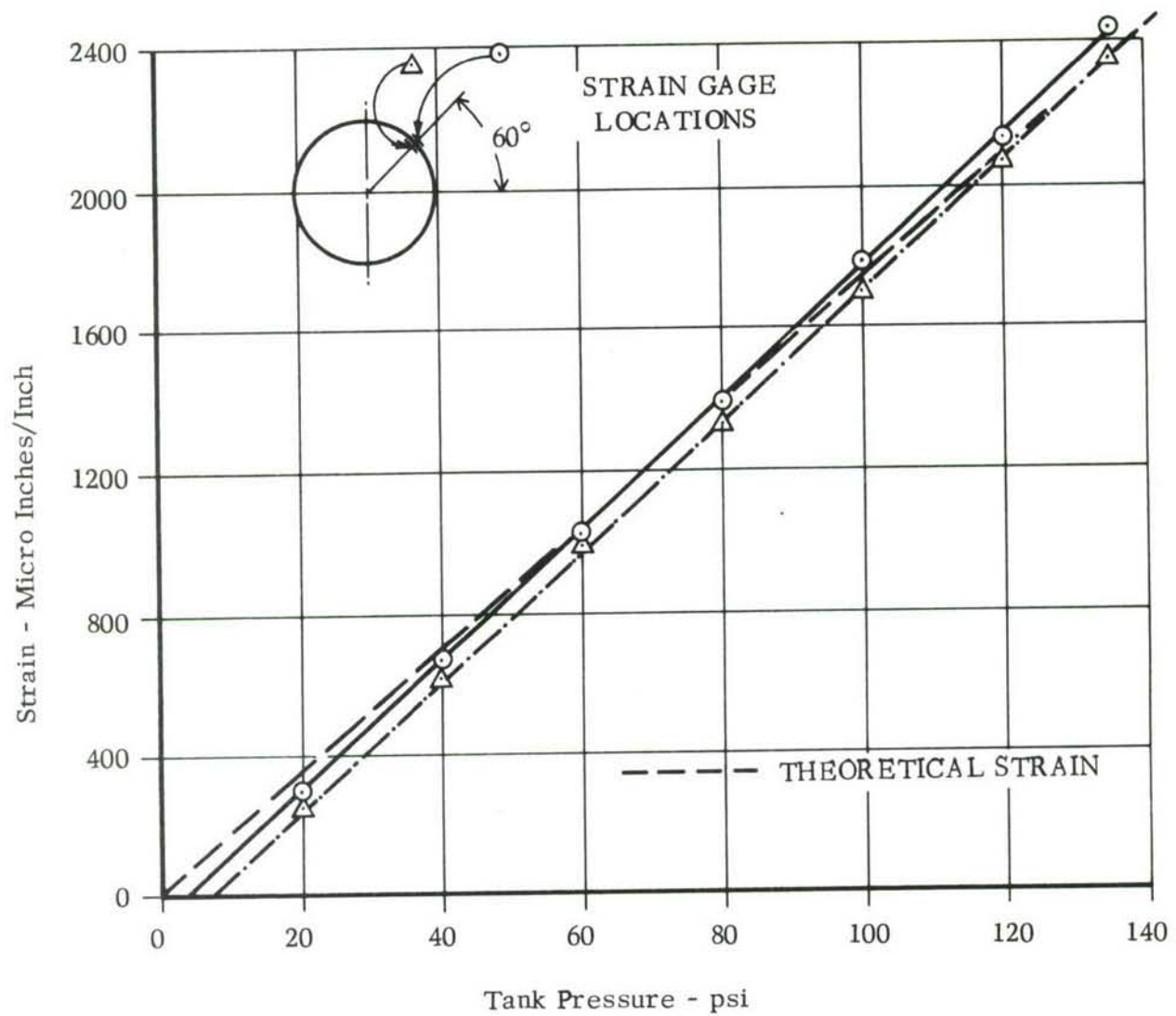


Figure 156. HOOP STRAIN - WATER PROOF TEST (INCONEL 718)

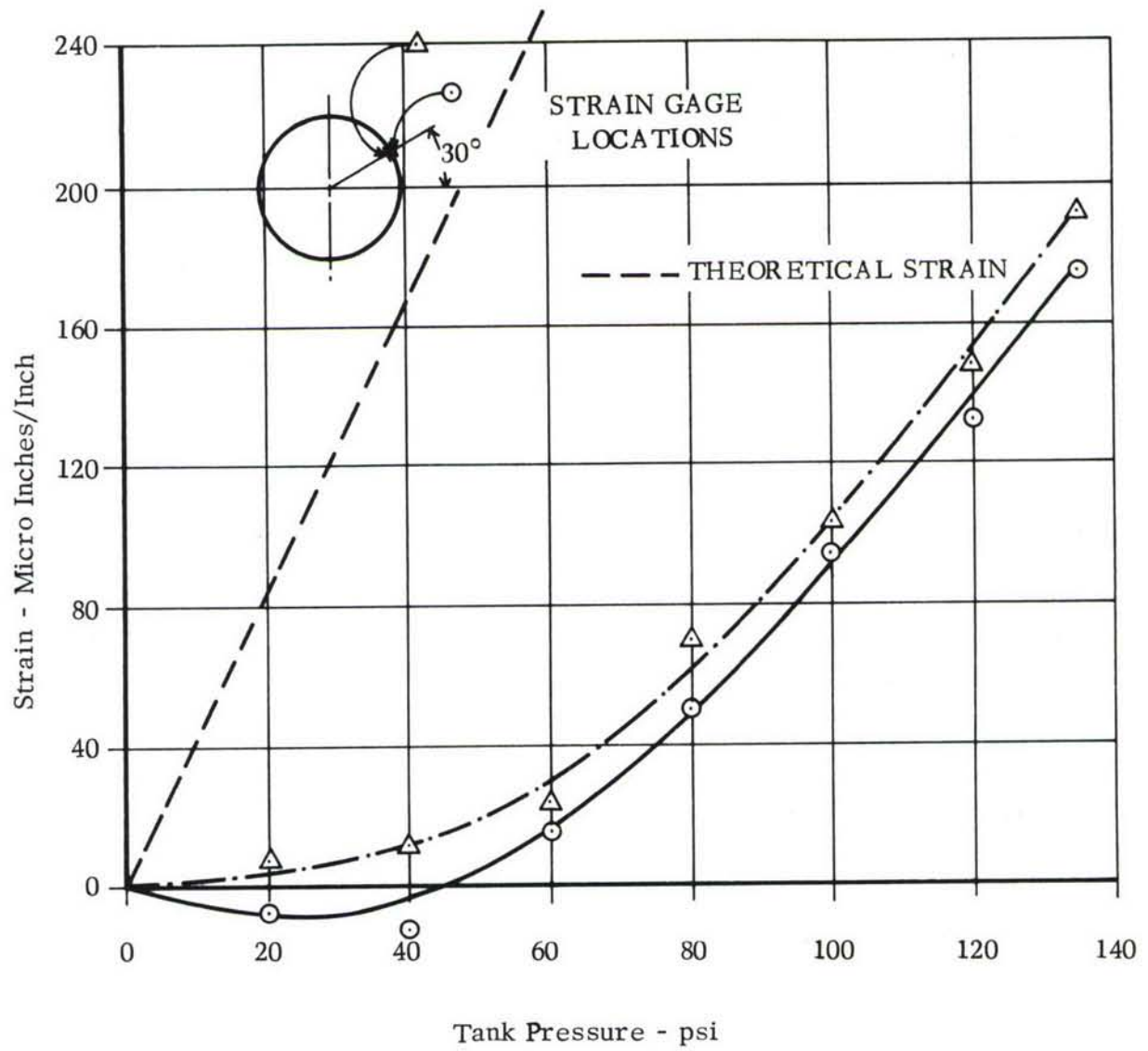


Figure 157. LONGITUDINAL STRAIN - WATER PROOF TEST
(INCONEL 718)

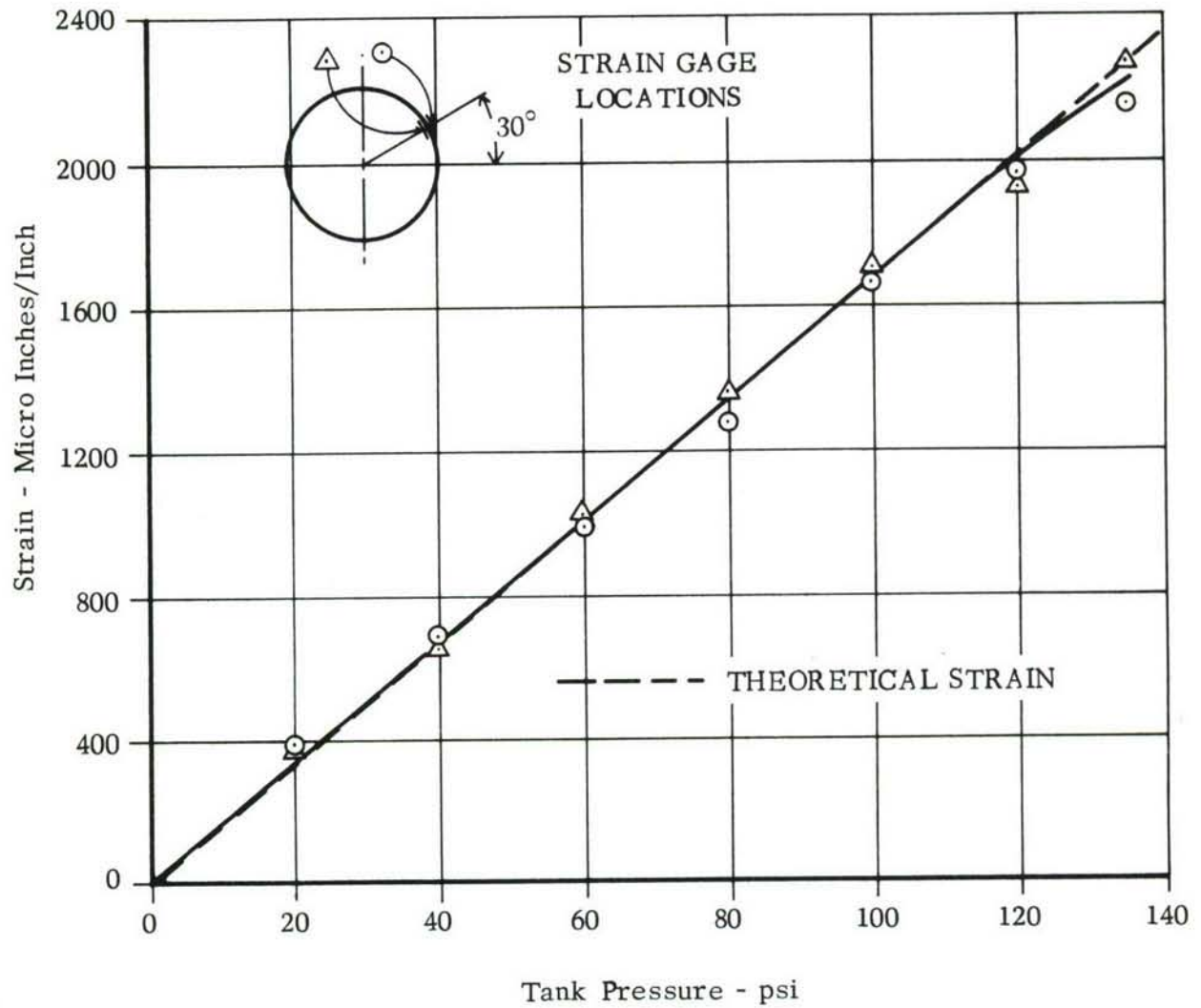


Figure 158. HOOP STRAIN - LN₂ PROOF TEST (INCONEL 718)

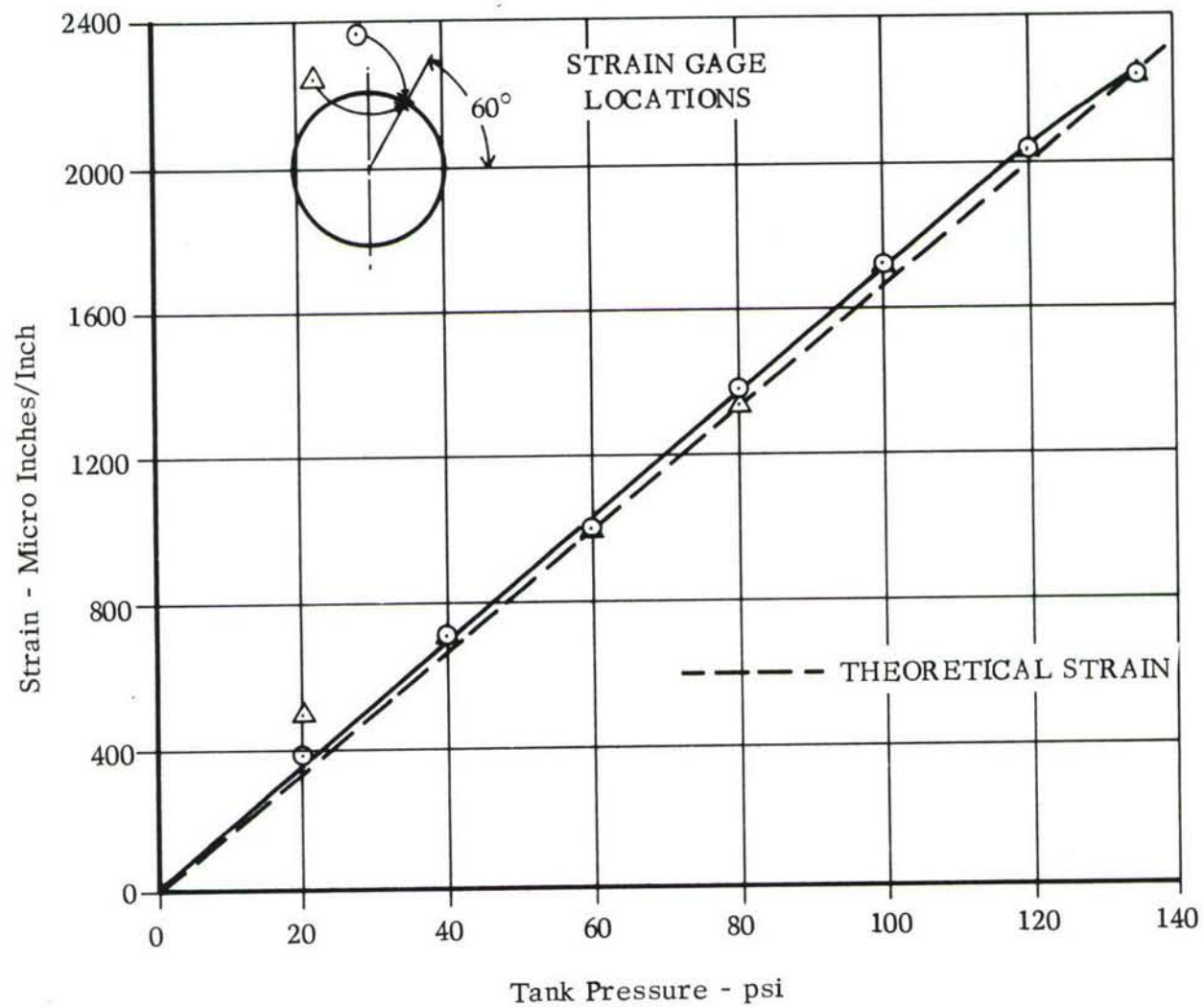


Figure 159. HOOP STRAIN - LN₂ PROOF TEST (INCONEL 718)

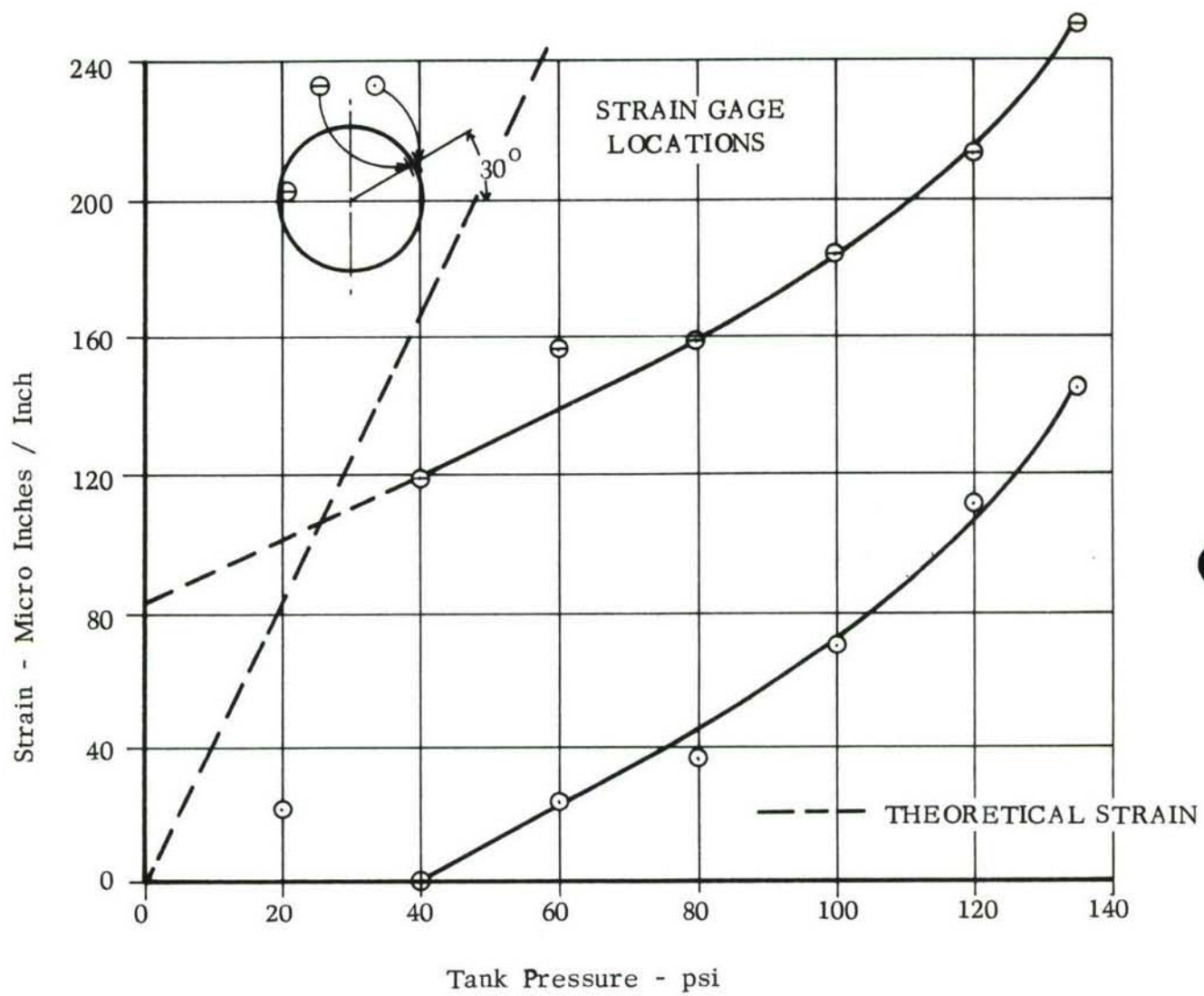


Figure 160. LONGITUDINAL STRAIN - LN₂ PROOF TEST (INCONEL 718)

The hoop strains for the water proof test were well defined linear functions for increasing pressure. The strain does not pass through zero for zero pressure; this was attributed to instrumentation drift. Figure 157 is a plot of the two longitudinal strains. Large discrepancy between the actual and theoretical longitudinal strains is attributed to uneven circumferential distribution as a result of localized buckling and small change in actual skin length between end frames. This observation is supported by small changes in the longitudinal strain measurement between 0 and 60 psig, and that strain linearity is not indicated until a 80 psi tank pressure is reached.

The hoop strains for the LN_2 proof test, Figures 158 and 159, are plotted as a single curve through both the inside and outside strain gage at the respective locations. There is a slight drop in strain at 135 psi pressure; this may be because of inaccurate relation passes through zero. The longitudinal strains are plotted against tank pressure in Figure 160. They have zero shift which, while small in terms of absolute strains, is large when compared to the total strain recorded.

The theoretical strains were calculated by the strain equations:

$$\epsilon_H = \frac{1}{E} (\sigma_H - \mu \sigma_L)$$

$$\epsilon_L = \frac{1}{E} (\sigma_L - \mu \sigma_H)$$

where σ_H and σ_L are calculated from stress considerations on a thin walled pressure vessel, neglecting the bending moment of the fluid weight which is small.

The theoretical strains were calculated on the basis of a skin thickness of 0.020 inches, modulus of elasticity 29.4×10^6 at 72°F and 30.5×10^6 at -320°F , and poisson's ratio .293 at 72°F and .310 at -320°F .

Proof Tests - Tank #2

The strains from the water proof tests on the titanium subscale tank are plotted against tank pressure in Figures 161 and 162. The strain magnitudes of the three hoop gages were in good agreement. There was evidence of zero shift of the readout instrumentation between the time the strain gage circuit was "zeroed" and the start of the pressure cycle.

The longitudinal strains indicated by two strain gages are very near the theoretical strain for a thin pressure vessel. The other strain gage showed higher strains, but the consistency of data points verifies that a good measurement was obtained. The discrepancy between the actual and theoretical strain indicated for this gage supports the conclusions reached earlier in the test, that a uneven distribution of longitudinal strains exist around the circumference of the tank due to small change in actual skin length between the frames and small initial imperfections.

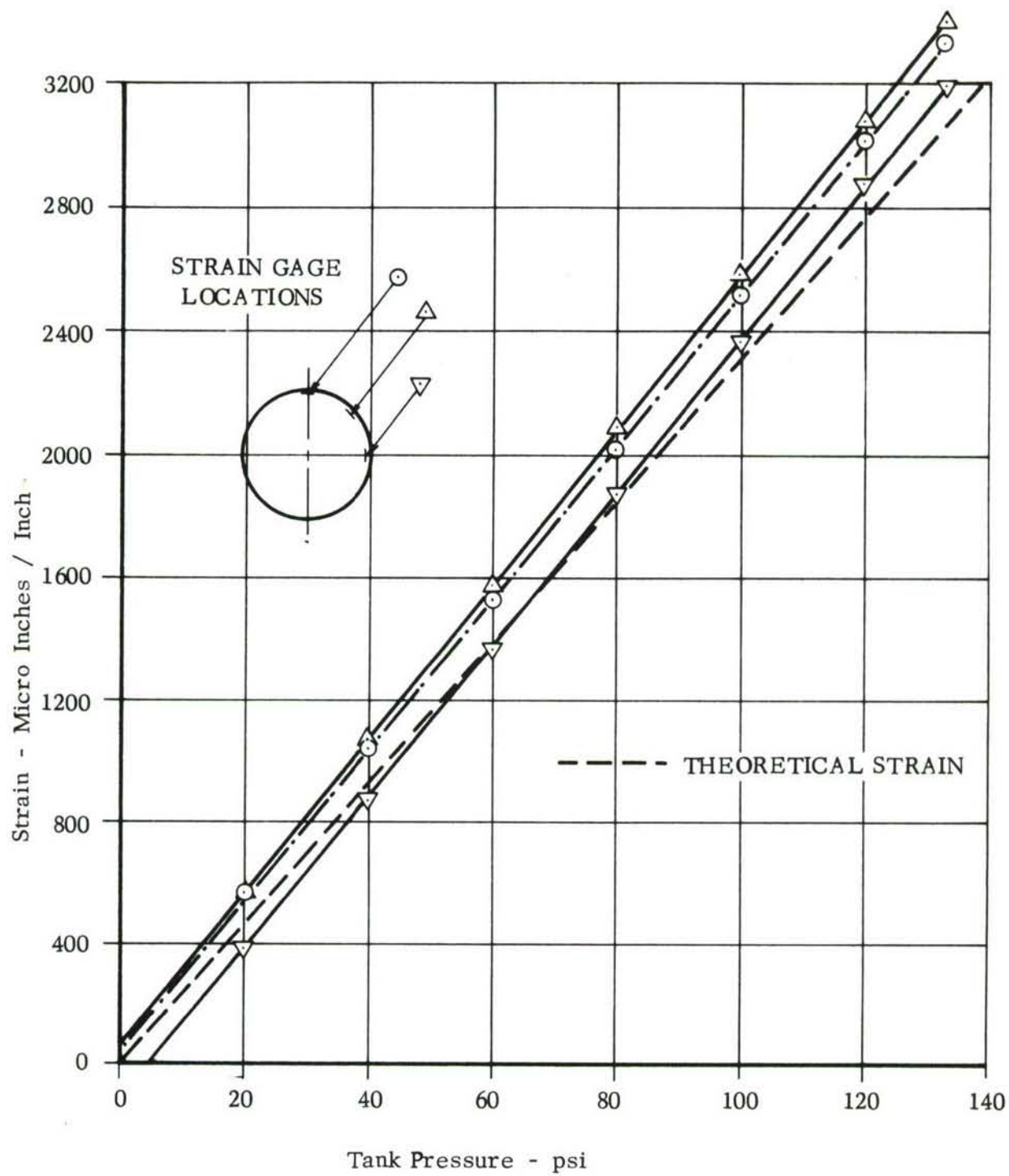


Figure 161. HOOP STRAIN - WATER PROOF TEST (TITANIUM)

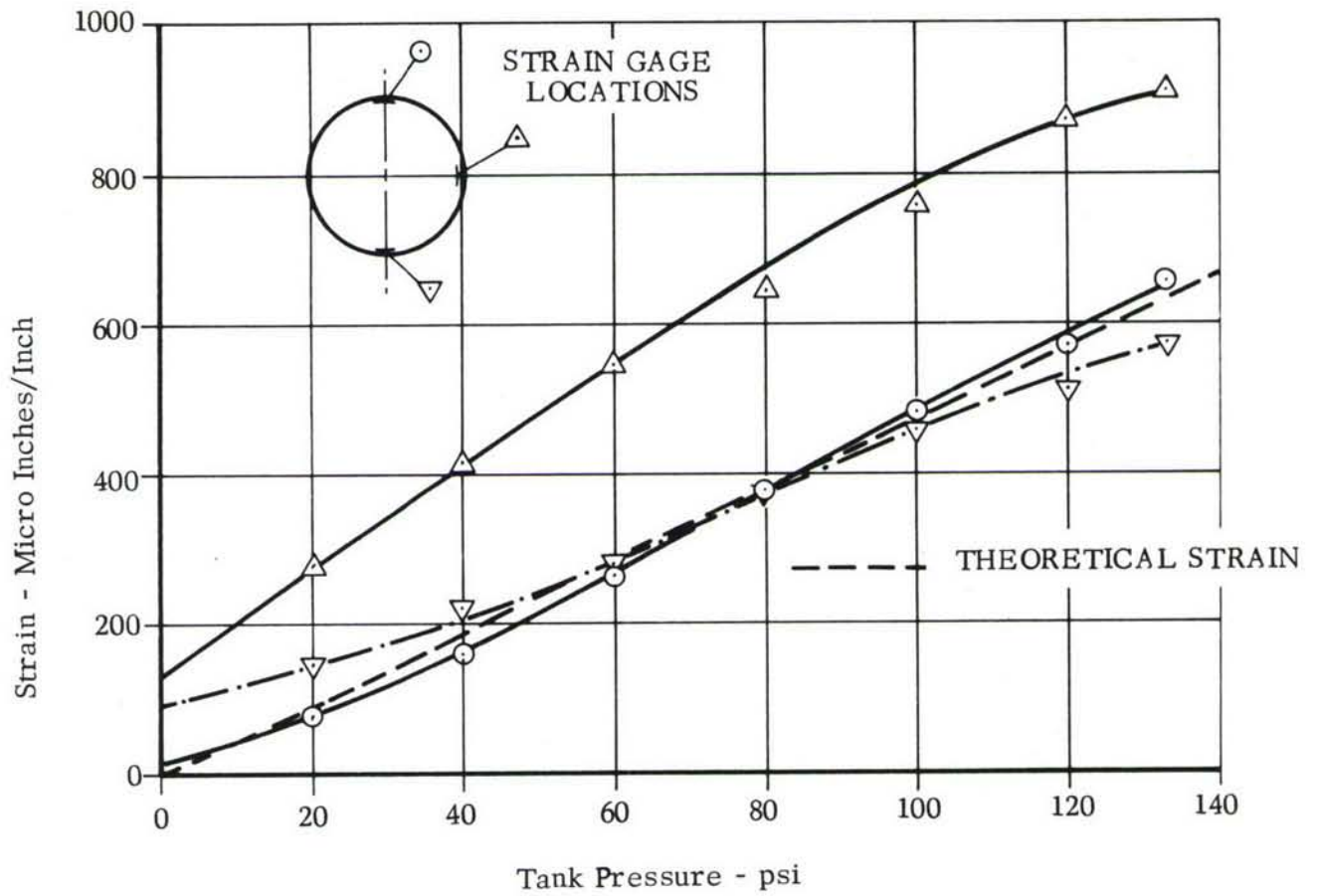


Figure 162. LONGITUDINAL STRAIN - WATER PROOF TEST (TITANIUM)

This gage actually experiences higher initial longitudinal strains than those obtained theoretically whereas previous discrepancies were the reverse. The theoretical values are based on a modulus of elasticity of 15.5×10^6 psi, a tank skin thickness of .028 inches, and a poisson's ratio of .327.

Large variations in published values for the material properties of 5 Al 2.5 Sn ELI titanium may account for some of the deviation of the measured strains from the theoretical strains. Additional error might have been introduced as a result of material loss in tank fabrication and strain gage installation.

Chamber Tests - Tank #1

Figures 163 through 171 present strain vs. tank pressure data for Tank #1. Locations of strain gages are given in Table 4 Page 137 by reference to channel number. The scatter of data points represents variations in temperature effects on the lead wire and on the strain gages as shown in the thermal hysteresis tests. The scatter was about ± 100 micro-inches/inch.

The data for each gage was corrected for lead wire, thermal output and gage factor variations and plotted on two graphs for liquid nitrogen and liquid hydrogen environments.

Theoretical strains were calculated using the same properties as those used in analysis of the proof test data with the addition of values of modulus of elasticity of 30.5×10^6 and poisson's ratio of .315 at -423°F .

The stress values at 100 psi, calculated from the measured strain, were 57,500 psi hoop and 21,200 psi longitudinal, which are lower than the theoretical for each gage. While uncertainties in the mechanical properties of the tank material would give errors, the difference in this case was attributed to the low measured value of the longitudinal strains. The measured strains from the liquid nitrogen proof test and the chamber test are in close agreement. Confidence is thus given in accuracy of the reduced data since the same results were obtained and the two test conditions used different correction factors (thermal output, gage factor, and lead wire) resulting from different temperatures.

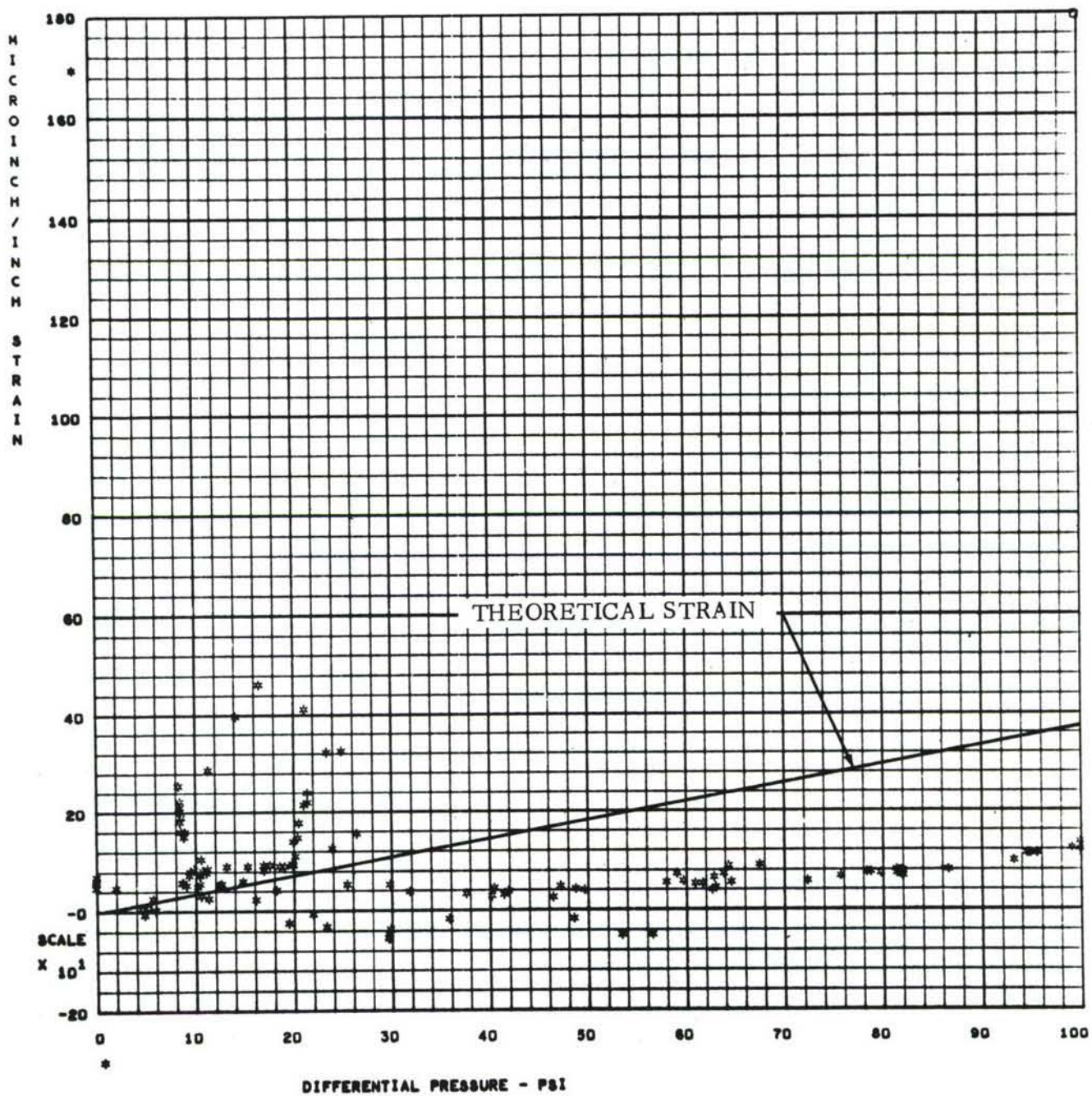


Figure 163. STRAIN GAGE OUTPUT (194) - LN₂ TESTS

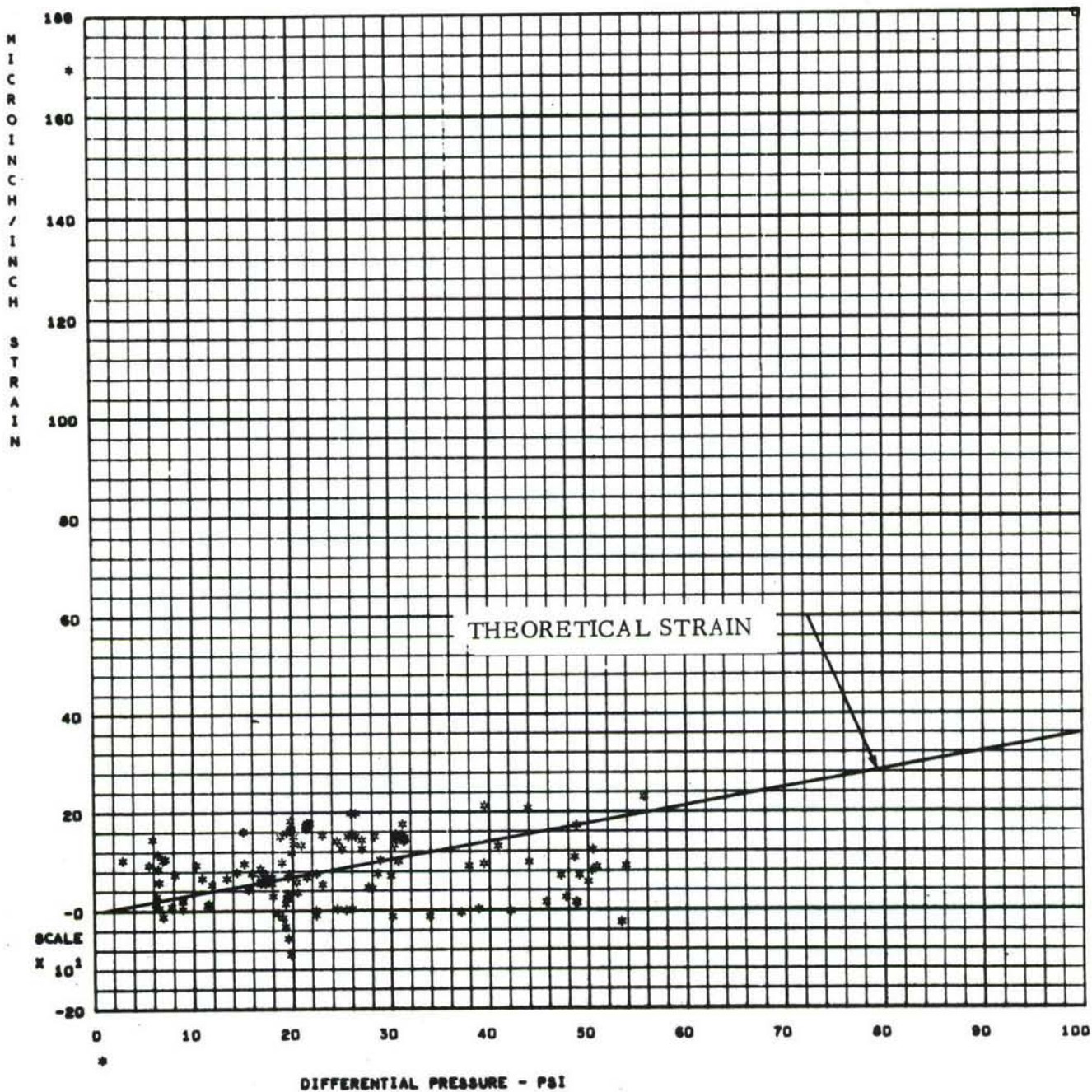


Figure 164. STRAIN GAGE OUTPUT (194) - LH₂ TESTS.

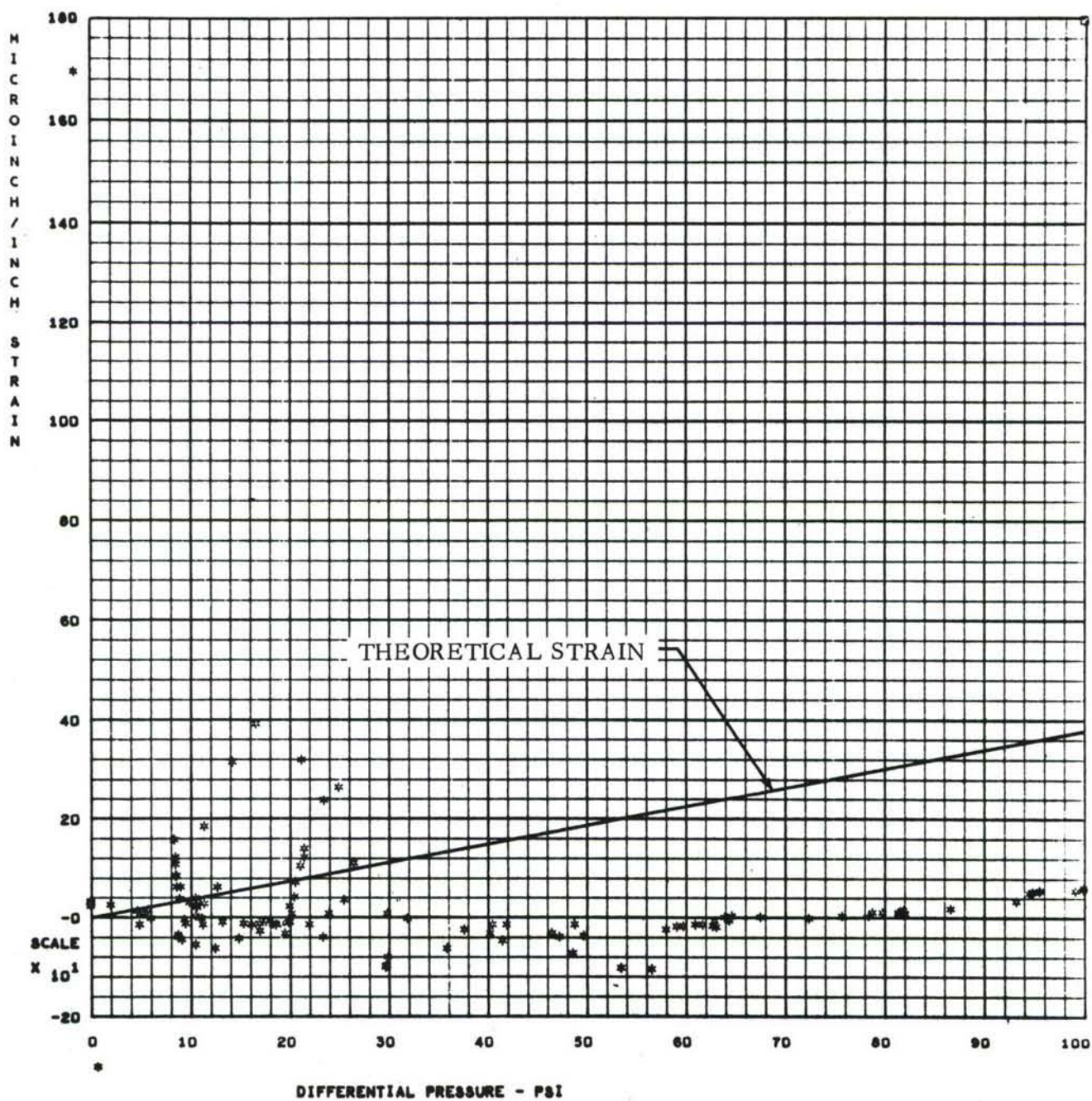


Figure 165. STRAIN GAGE OUTPUT (195) - LN₂ TESTS.

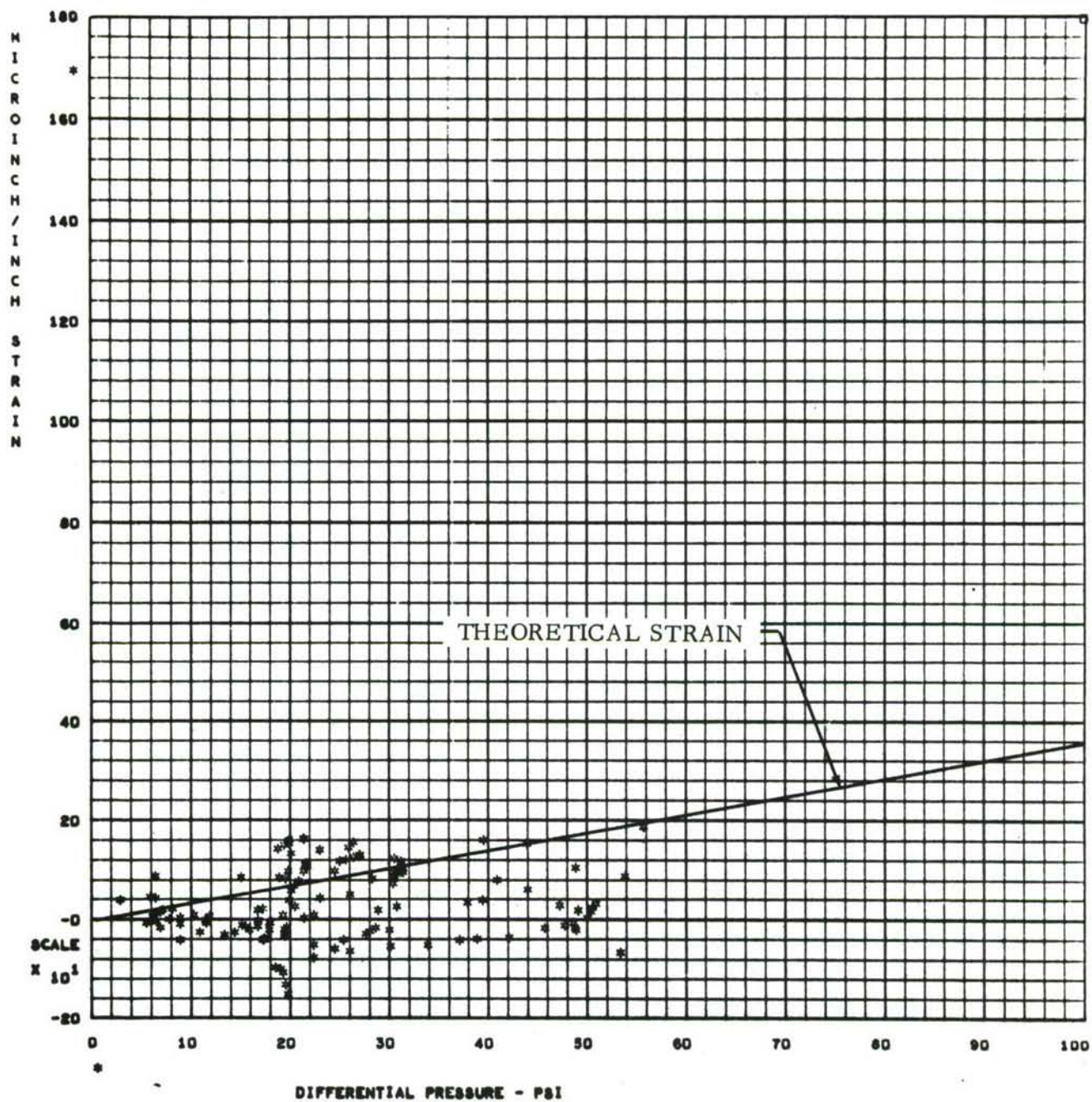


Figure 166. STRAIN GAGE OUTPUT (195) - LH₂ TESTS

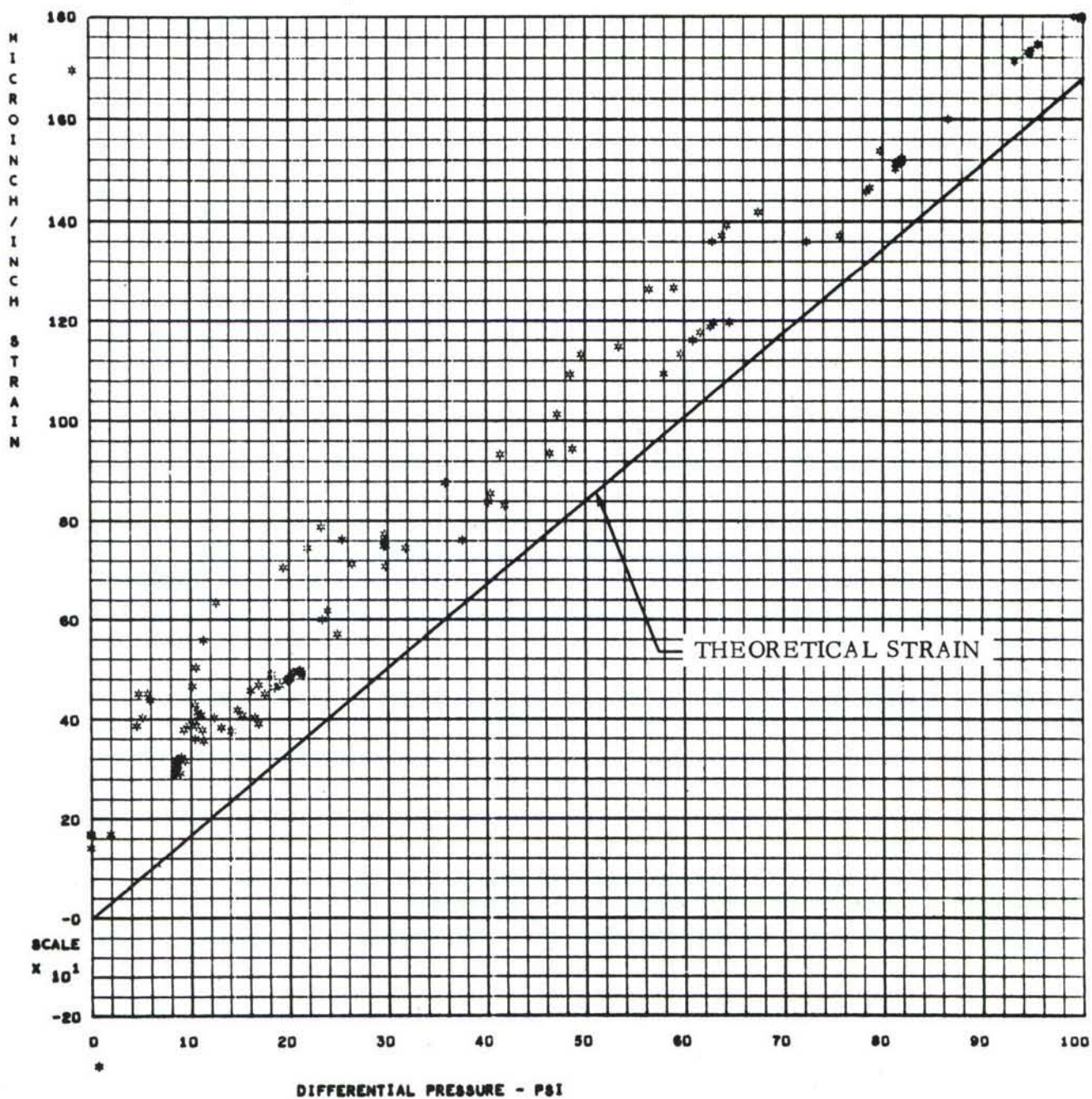


Figure 167. STRAIN GAGE OUTPUT (196) - LN₂ TESTS

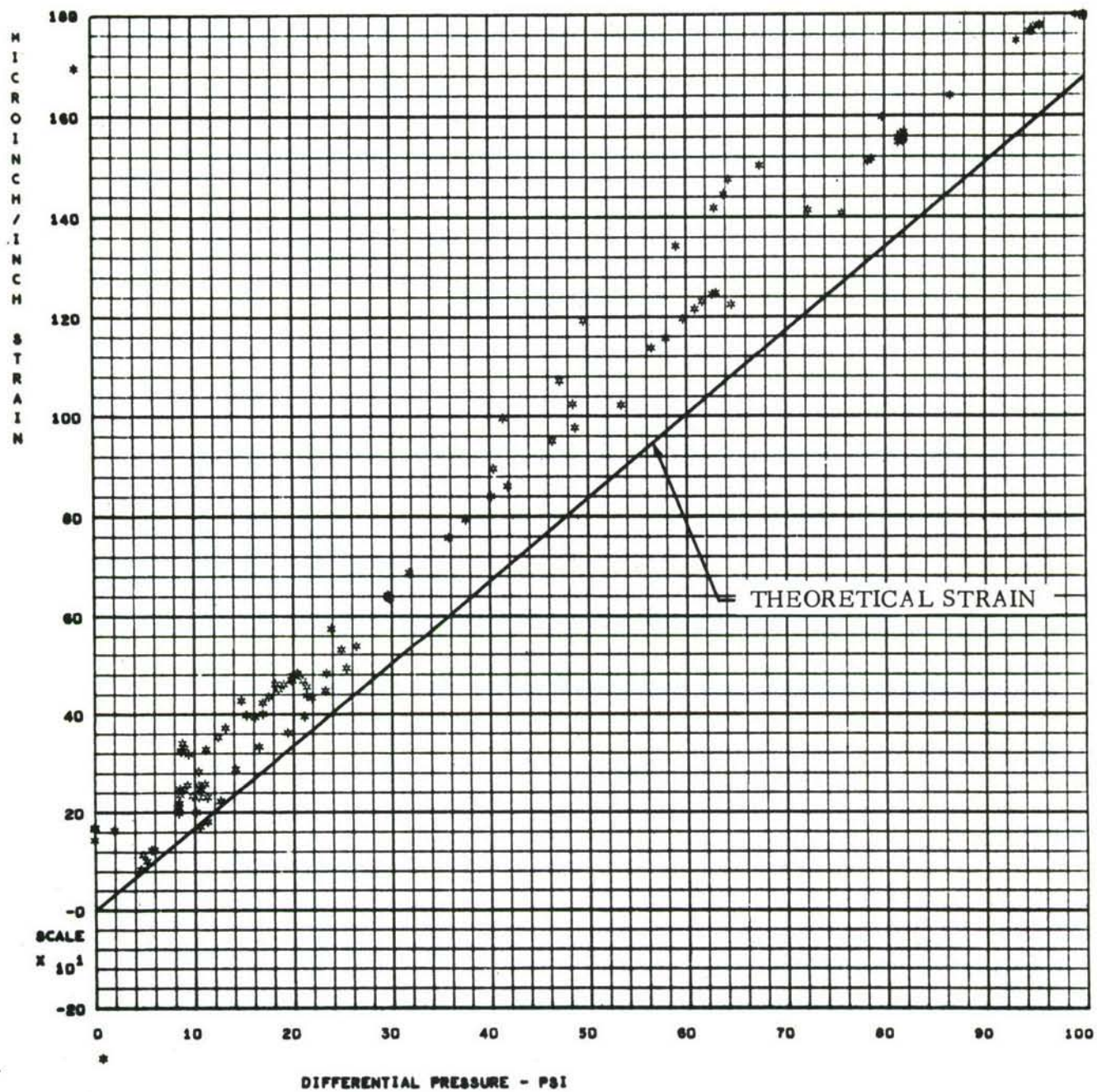


Figure 168. STRAIN GAGE OUTPUT (198) - LN₂ TESTS

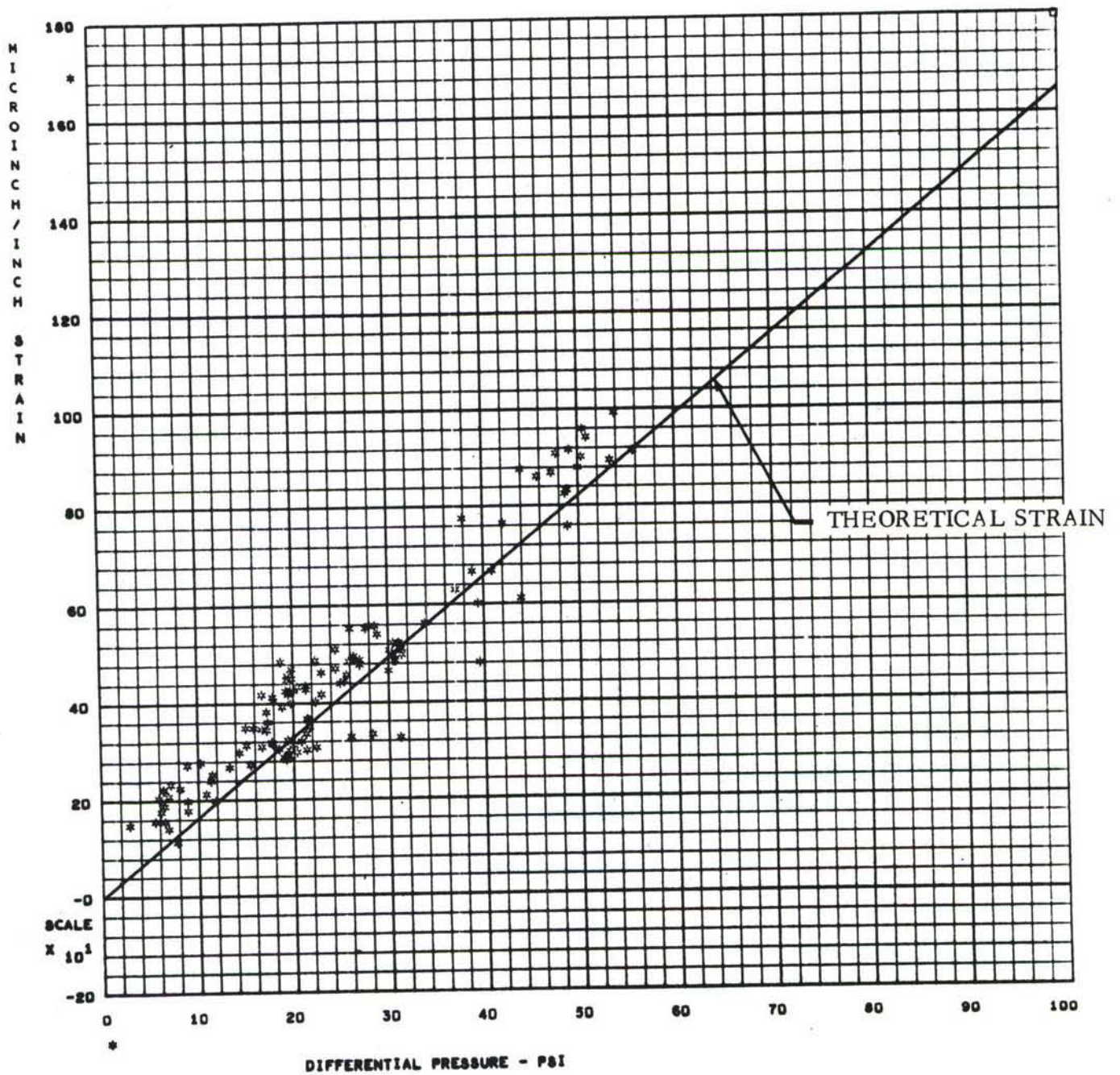


Figure 169. STRAIN GAGE OUTPUT (198) - LH₂ TESTS

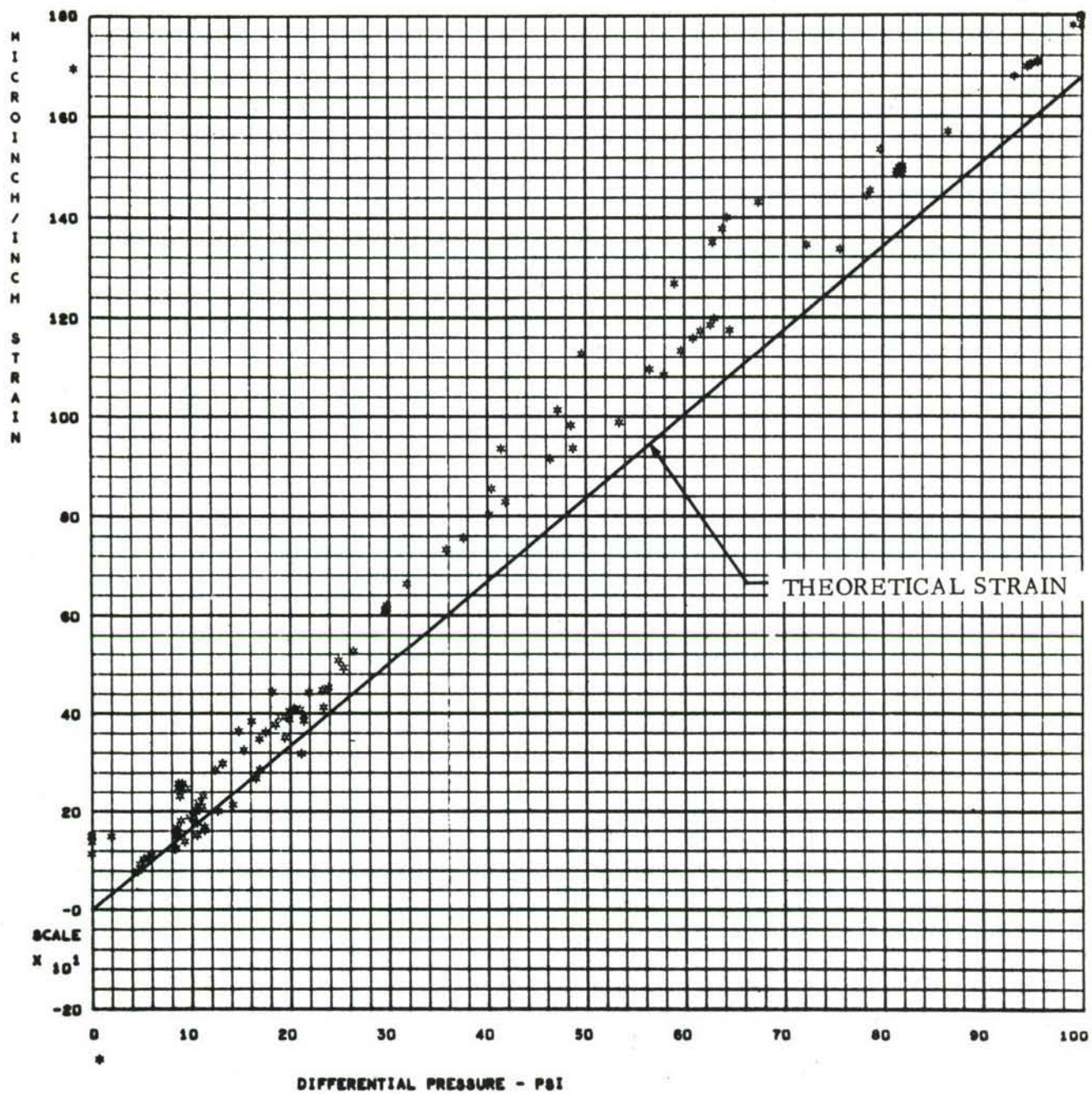


Figure 170. STRAIN GAGE OUTPUT (199) - LN₂ TESTS

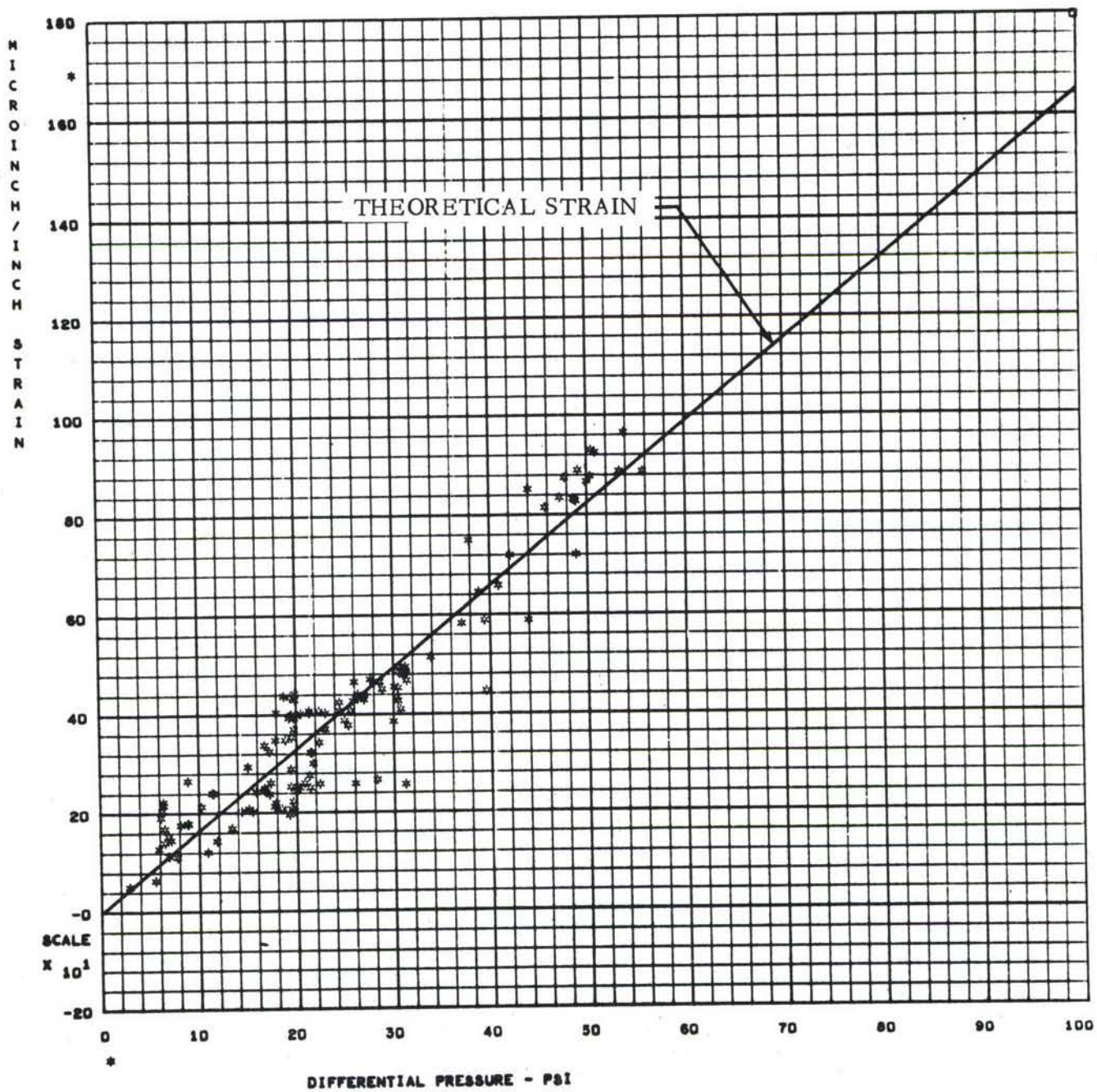


Figure 171. STRAIN GAGE OUTPUT (199) - LH_2 TESTS

APPENDIX III

EVALUATION OF THE EFFECTS OF HYDROGEN EXPOSURES ON THE MECHANICAL PROPERTIES OF TITANIUM 5A1 2.5 Sn ELI ALLOYS

INTRODUCTION

About two years ago a study was performed to select and evaluate optimum structural materials for application in liquid hydrogen-liquid oxygen fueled recoverable aerospace vehicles. This study was performed by General Dynamics/Convair (formerly Astronautics) for the Air Force Materials Laboratory under Contract AF33(657)-9445. A portion of this study was concerned with a determination of the effects of hydrogen exposures at elevated temperatures on the mechanical properties of the titanium 5A1 2.5 Sn ELI alloy. The Ti 5A1 2.5 Sn ELI alloy was selected for fabrication of liquid hydrogen tankage in preference to other candidate materials (e.g., 300 series stainless steels and 2000 series aluminum alloys) because of its superior mechanical and physical properties.

The results of this initial evaluation of the effects of gaseous hydrogen exposures at elevated temperatures on the mechanical properties of Ti 5A1 2.5 Sn ELI alloy are reported in Reference 10. The conclusions from that study are quoted as follows:

"Long-time (100-hour) thermal exposures at 400°, 600°, and 800° F in various pressures of hydrogen gas resulted in significant decreases in notched tensile strength and crack-propagation properties at -423° F. However, a more severe exposure occurred as a result of applying a mechanical load during thermal exposures at 600° F in various pressures of hydrogen gas. The application of the load caused failure in nearly half of the notched tensile specimens during exposure. The poor creep-rupture life during 600° F exposure and the decrease in toughness resulting from these exposures is believed to be due to hydrogen absorption. Microstructural studies substantiated this deficiency by showing the formation of large numbers of titanium hydride platelets. The decrease in toughness and the poor creep-rupture life caused by exposure to hydrogen gas is felt to be a serious problem. For this reason it is recommended that additional studies be performed to more accurately define the effects of hydrogen exposures on the Ti 5A1 2.5 Sn ELI alloy before it is used structurally in an elevated-temperature hydrogen environment".

The purpose of the present investigation was therefore, to more accurately define the effects of hydrogen exposures on the mechanical properties of the titanium 5A1 2.5 Sn ELI alloy, and in particular to evaluate those exposure conditions which are anticipated to occur for the liquid hydrogen test tank being designed, fabricated, and tested by GD/C under this contract.

TEST PROGRAM

The test program originally consisted of performing 204 specimen exposures followed by tensile notched tensile, weld tensile, and crack propagation testing as shown below:

Exposure Conditions:

Temp. (° F)	H ₂ Gas Pressure	Time (Hr.)	Stress
200	1 (+ 12 tests to evaluate effect, if any, of high pressures	5	No load
300		50	Load
500			
+ 1			
4	X	1	X
		2	X
			2 = 16 conditions

Number of screening tests: 16 conditions x 2 types specimens (smooth and notched tensile) x 1.5 test temperature after exposure (both types specimens at -423°F and smooth tensile at room temperature) x 3 replicate tests = 144 + 12 (high pressure tests) = 156 tests.

Number of evaluation tests: 8 conditions (2 temperature x 2 times x 2 loads) x 2 types specimens (weld tensile and crack propagation) x 3 replicate tests = 48 tests.

Total number of tests: 156 + 48 = 204

The hydrogen gas pressure and stress levels were the same as those used in the previous study (Reference 10) for 3 of the 4 temperature exposure conditions. The remaining exposure condition consisted of a temperature, hydrogen gas pressure, and stress level anticipated in the liquid hydrogen test tank being built and tested by GD/C under this contract. All tests were to be performed on one heat and one sheet thickness (about 0.017 inch) of the titanium 5A1 2.5 Sn ELI alloy.

However, upon completion of the screening tests and part of the evaluation tests (the fusion welded specimen tests), it was found that the hydrogen exposures were resulting in little or no effect on the mechanical properties of the Ti 5A1 2.5 Sn ELI alloy. This was in distinct disagreement with previous results (as reported in Reference 10). Possible explanations could only be attributed to differences in the exposure conditions or the test materials. The only changes in the exposure apparatus consisted of 1) the use of a different pressure bottle of hydrogen gas which conceivably could have a different water vapor content; and 2) a new and improved loading mechanism.

It was therefore deemed desirable to evaluate alternate materials and conditions. Two additional heats, with sheet thicknesses of 0.006, 0.013 and 0.032 inches, were in-

cluded in the test program. In addition, a number of exposure tests were conducted with the addition of water vapor in the hydrogen to determine the effects, if any, of increased amounts of water vapor present during the high temperature exposures. No additional tests were performed to evaluate the new loading mechanism since no significant differences were noted in the results of loaded tests as compared to the unloaded specimen exposures.

The revised test program consisted of performing 238 specimen exposures (as compared to 204 originally) followed by tensile, notched tensile, and fusion weld tensile tests at room and cryogenic temperatures. The increased number of tests were partially offset by substituting tensile and notched tensile tests for the crack propagation tests. The remaining testing was performed in conjunction with a company sponsored research and development program.

MATERIALS AND TEST SPECIMENS

The test materials used in this study consisted of three different heats (four different sheet thicknesses) of titanium 5Al 2.5 Sn ELI alloy. The history and chemical analysis of these materials is given in Table 10. The 0.006 and 0.013 inch thick sheet materials were the same as that evaluated in a previous study (see Reference 10 for details). These two gages of titanium 5Al 2.5 Sn ELI alloy were included in order to compare the results of hydrogen exposures with previous results. The 0.017 inch thick sheet material was selected for the major portion of the study since this gage is representative of sheet thicknesses most likely to be employed in large size liquid hydrogen propellant tankage. The 0.032 inch thick material was included because this is some of the actual material being used for fabrication of the liquid hydrogen subscale test tank #2.

The test specimens used in this investigation consisted of unnotched, notched, and fusion welded tensile specimens. The notched tensile specimens had a stress concentration factor (K_t) of 6.3 as determined by the $\sqrt{a/r}$ where a is equal to one half of the distance between the notches and r is equal to the radii at the root of the notches. Both the unnotched and fusion welded test specimens were standard sheet specimens with a test section 0.5 inch wide by about 2 inches long. The weld specimens contained a fusion weld in the center of the test section and perpendicular to the loading axis. Drawings of the test specimens are shown in Figure 172.

Particular care was exercised in the handling, machining, and measurement of the test specimens. Notched tensile specimens were measured by means of an optical comparator. Flat tensile, and weld specimens were measured by means of a

micrometer. Only those specimens conforming to machining prints and free of surface and edge defects were used for testing.

APPARATUS AND PROCEDURE

The apparatus used in the hydrogen exposure tests included a gas tight retort, a resistance heated (glo-bar) furnace equipped with a temperature recorder and automatic (Elect-O pulse) power control, a Heise pressure gage, and bottled helium and hydrogen gas with regulators as shown in Figures 173, 174 and 175. A chemical analysis was made of the hydrogen gas. It was found to contain 1.5% N_2 , 0.13% O_2 , 8 ppm H_2O and the rest H_2 . Hydrogen gas exposures were performed at various pressures (1.0 psig and 15.0 psig hydrogen gas in a helium atmosphere), and 100 percent pure hydrogen gas at 5.0 psig. Specimen exposure temperatures included 200°, 300°, 400°, 500°, 600°, and 800°F, for various periods of time ranging from five to sixty-four hours. Some specimen exposures were made without an applied load. Other exposures were made with a mechanical load (ranging from 10,000 to 50,000 psi) applied to the test specimens. The load was applied by means of a load applicator, as shown in Figure 176. The time elapsed from the gaseous hydrogen exposure to the tensile testing of the specimens was generally 1 hour to 2 days, with a maximum of five days.

Those specimens tested at 75°F were tested on a 50,000 pound Baldwin-Emery universal testing machine equipped with continuous stress strain recorder, strain pacer, and extensometer. The tensile specimens tested at -423°F were tested on a 30,000 pound Tinius-Olsen universal testing machine equipped with continuous stress strain recorder, strain pacer, a special test cryostat, and a cryo-extensometer. See Reference 11 for details of the cryostat and cryo-extensometer. Strain rates for both room temperature and cryogenic tests were 0.005 in/in/min to yield followed by a 0.15 in/min to failure for the smooth tensile specimens, and 0.05 in/min to failure for the notched and fusion welded tensile specimens. Standard test procedures as given in Reference 11, were used for specimen testing.

RESULTS AND DISCUSSION

The results of this investigation are tabulated in Tables 11-13 and graphically presented in Figures 177-184. The major portion of the study was performed on heat number 3920498 (0.017 inch thick sheet material). These data are reported in Table 11, and Figures 177-184. Table 12 contains test data on heat number D-3274 (0.006 and 0.013 inch thick sheet material) and Table 13 presents the test data on heat number D-5907 (0.032 inch sheet thickness). Upon completion of the exposures and tensile

testing, several of the broken test specimens were subjected to a metallographic examination. Photomicrographs resulting from the metallographic work on heat number 3930498 (0.017 inch thick sheet material) are shown in Figures 185-189.

The most significant result of this investigation is that there was little or no effect of the hydrogen exposures on the mechanical properties of the Ti 5Al 2.5 Sn ELI alloy. This is true regardless of heat number, sheet thickness, or exposure condition (i. e., temperature from 200° to 800°F, applied loads from 0 to 50,000 psi, exposure times from 5 to 64 hours, gas pressures from 1.0 to 15.0 psig, and various gas exposures including pure hydrogen and hydrogen-helium or hydrogen-helium-water vapor mixtures). In the previous study (Reference 10), there were significant decreases in strength properties as a result of hydrogen exposures at elevated temperatures (at 400°, 600°, and 800°F). For example, notched tensile strengths at -423°F decreased from 10 to 20%, depending upon exposure conditions, as a result of the hydrogen exposures. In this investigation the largest effects ranged from a 6% increase (in room temperature tensile strength) to a 5% decrease (in notched tensile strength at -423°F after an 800°F exposure). These differences are very nearly within the margin of testing error (based on an average obtained from three replicate specimens). It is therefore concluded that there was little or no effect of hydrogen exposures on the mechanical properties of the titanium 5Al 2.5 Sn ELI sheet material.

Because of the inconsistency with previous results, a number of additional exposures were performed. It will be noted (in Table 11) that exposure conditions simulating those which will be experienced by the liquid hydrogen test tank (i. e., 5.0 psig pure H₂, 50 KSI load, 5-16 hour exposures) had little or no effect on the mechanical properties of the Ti 5Al 2.5 ELI alloy. Likewise, the addition of water vapor during the exposure resulted in no significant effects on the mechanical properties. As may be seen in Tables 12 and 13, there was little or no effect of hydrogen exposures on the mechanical properties of two additional heats (three sheet thicknesses) on the Ti 5Al 2.5 Sn ELI alloy. This was true even of some of the same material as was evaluated in the previous study (the 0.006 and 0.013 inch thick material as reported in Table 12).

A metallographic examination was performed on several of the broken test specimens. The resulting photomicrographs are shown in Figures 185-189. In the previous study (Reference 10) titanium-hydrate platelets were found in the microstructures of exposed specimens. However, in this study no evidence of titanium-hydrate platelets were found in any of the microstructures. The only interesting feature of the microstructures were the voids present in the material, as may be seen in Figures 185-189 (the large black spots are voids). The voids in Figures 186-188

are more plentiful and larger than those in Figures 185 & 189. This is attributed to the sustained mechanical loads which were applied for 50 hours on those specimens shown in Figures 186-188 but only for 5 hours for Figure 189 and 0 hours for Figure 185 (depicting as received material). The few voids which are present in the as received material are believed to be due to the processing (i. e., severe cold rolling) of the material.

SUMMARY AND CONCLUSIONS

Exposures were performed on more than two hundred test specimens in order to determine the effects of gaseous hydrogen exposures on the mechanical properties of titanium 5Al 2.5 Sn ELI sheet material. Exposure conditions consisted of temperatures ranging from 200° to 800°F, applied loads ranging from 0 to 50,000 psi, gas pressures ranging from 1.0 to 15.0 psig of pure hydrogen and hydrogen-helium or hydrogen-helium-water vapor mixtures, and exposure time ranging from 5 to 64 hours. Three heats of Ti-5Al-2.5 Sn ELI alloy in four sheet thicknesses (0.006, 0.013, 0.017, and 0.032 inches) were evaluated. Test specimens consisted of tensile, notched tensile, and fusion weld tensile specimens which were tested at 75° and -423°F after hydrogen exposure. The major results and conclusions are as follows:

- 1) There was little or no effect of hydrogen exposures at elevated temperatures on the tensile, notched tensile or weld tensile properties of Ti 5Al 2.5 Sn ELI alloy at either room or cryogenic (-423°F) temperatures.
- 2) Because of the inconsistency of these results with previous results it is suggested that additional tests be performed to substantiate or negate the present test data before the application of Ti-5Al-2.5 Sn ELI in an elevated temperature gaseous hydrogen atmosphere.
- 3) The above conclusion does not influence testing of the Ti-5Al-2.5 Sn Alloy Subscale Tank #2, since tank wall temperatures will not exceed room temperature while in the presence of gaseous hydrogen.



297

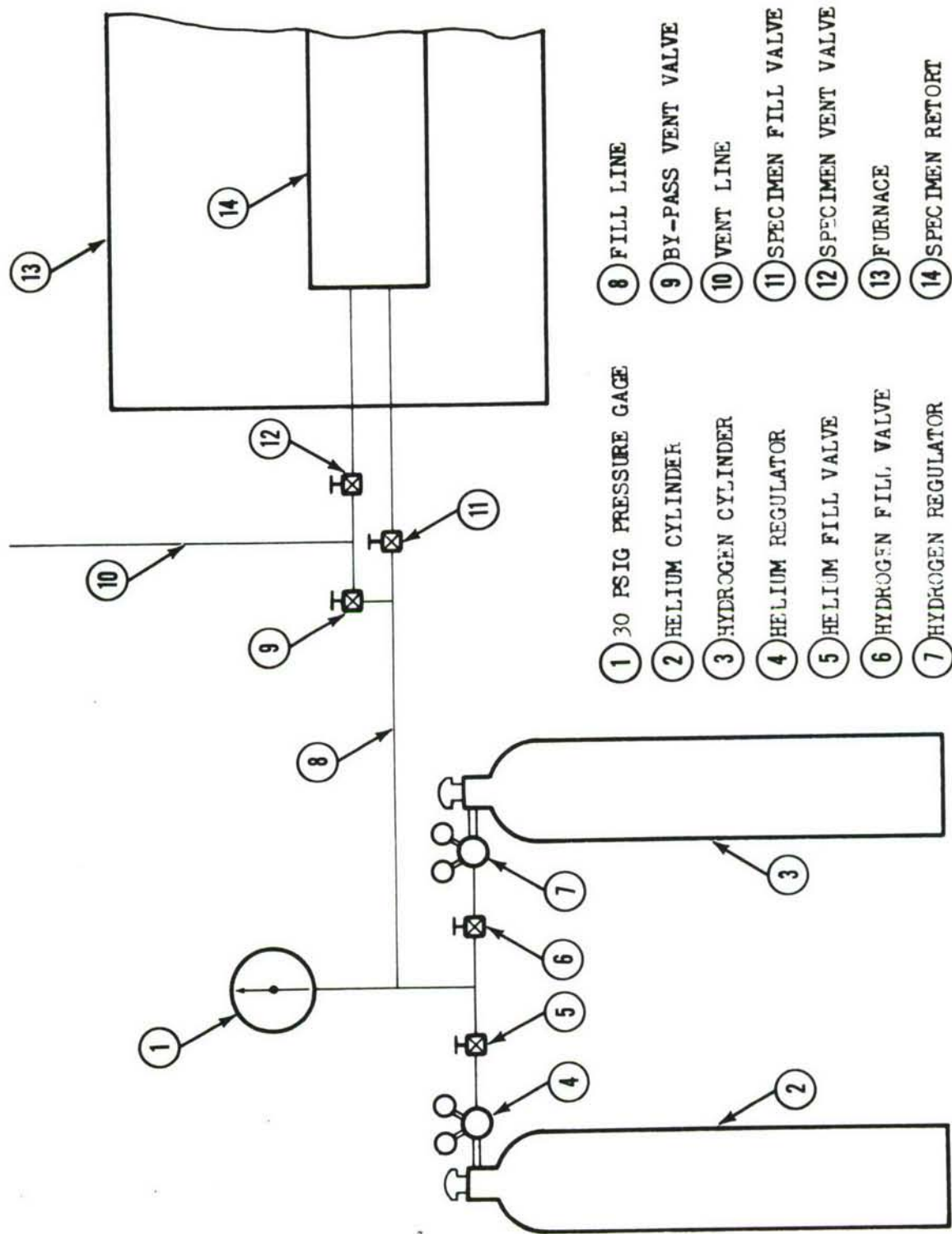


Figure 173. SCHEMATIC VIEW OF HYDROGEN EXPOSURE APPARATUS

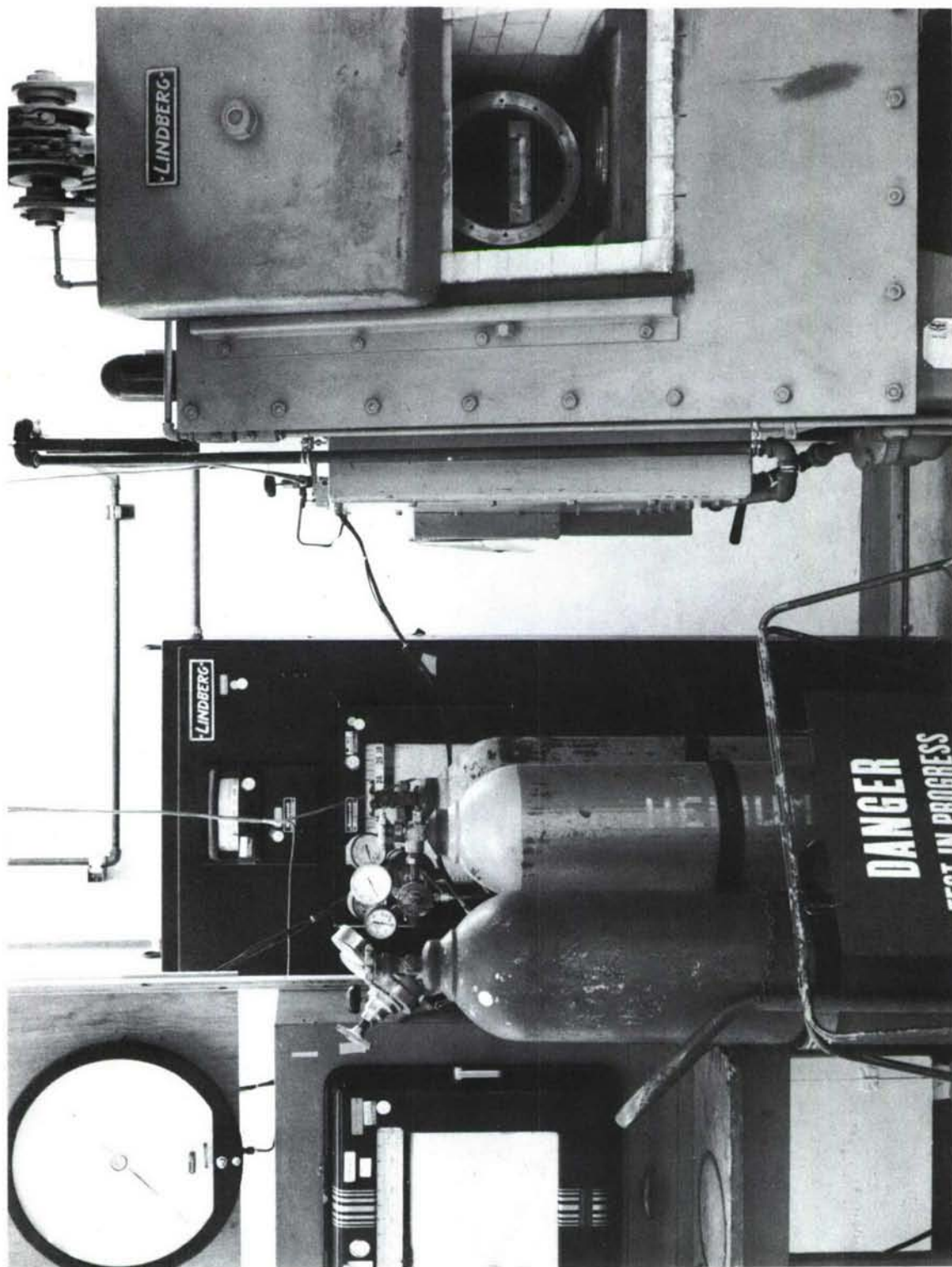


Figure 174. GENERAL VIEW OF GASEOUS EXPOSURE TEST APPARATUS

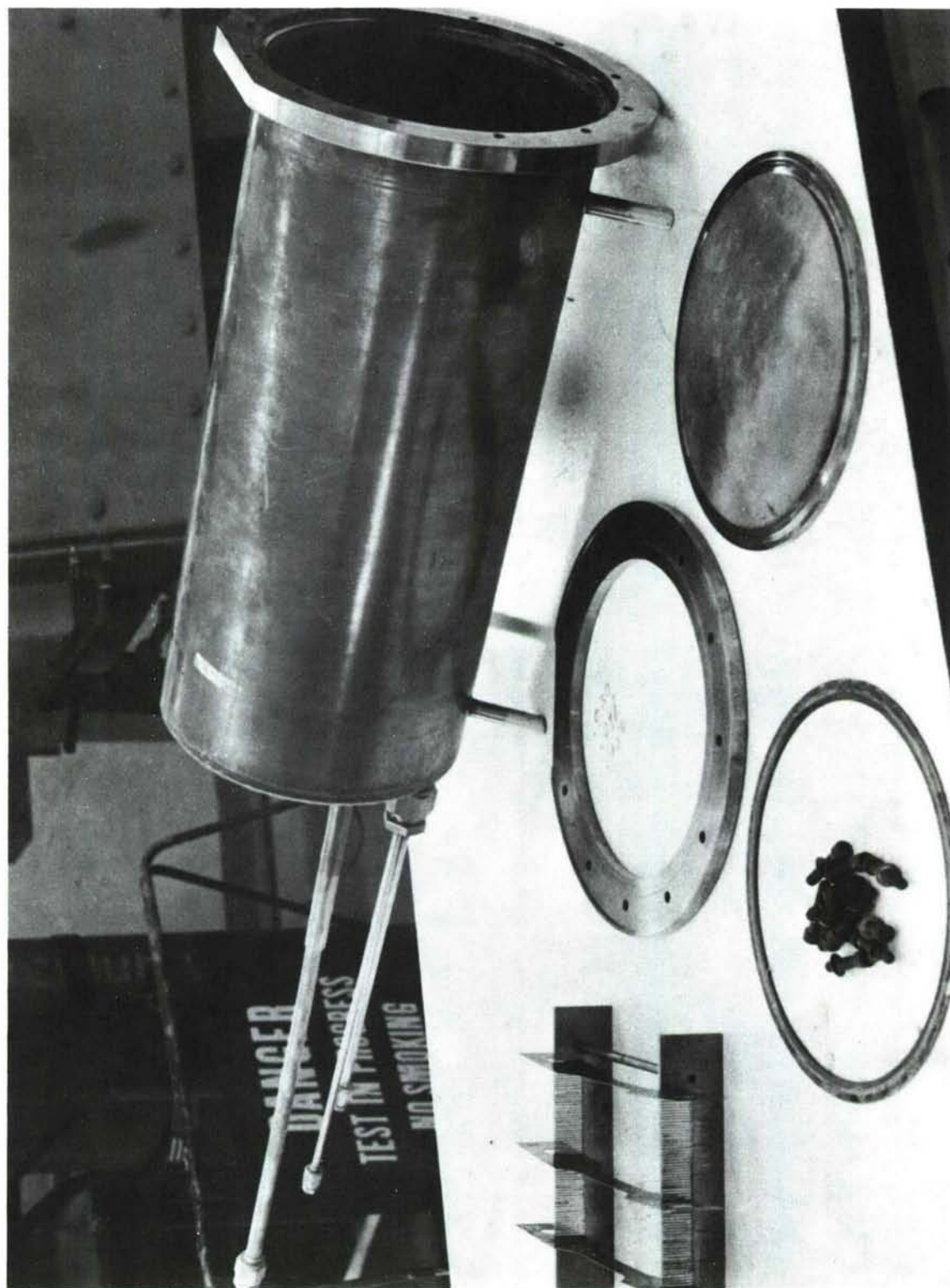


Figure 175. RETORT FOR GASEOUS HYDROGEN EXPOSURES

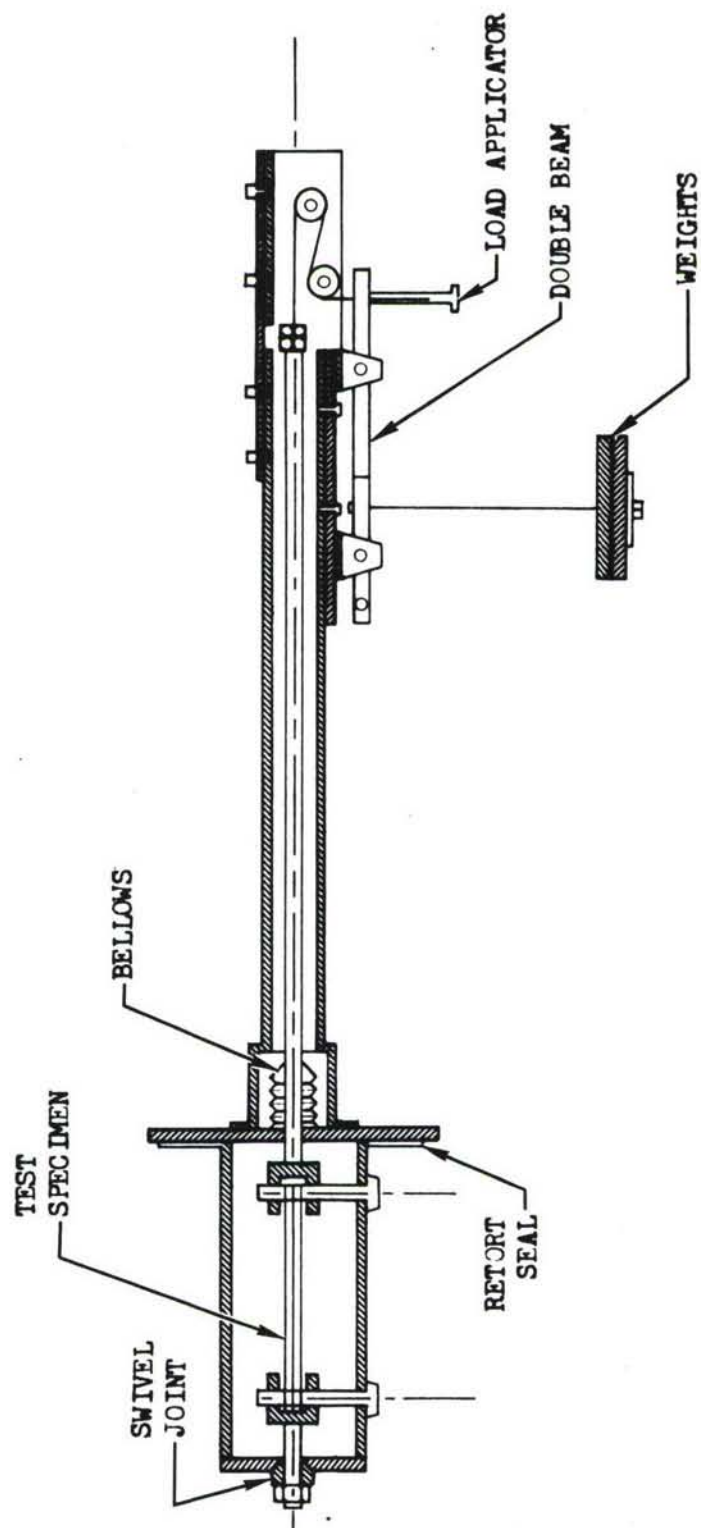


Figure 176. SCHEMATIC VIEW OF LOAD APPLICATOR

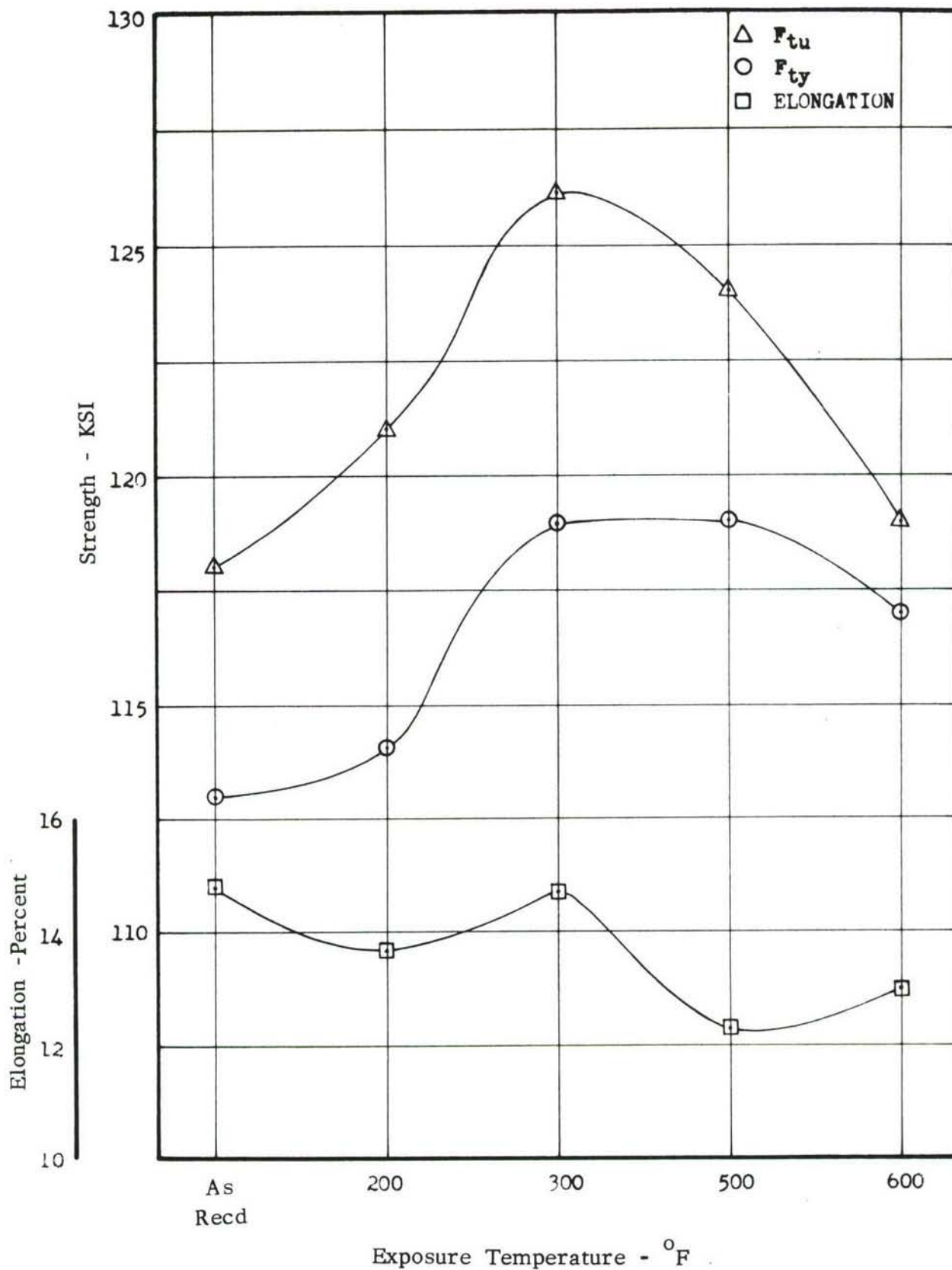


Figure 177. MECHANICAL PROPERTIES AT 75°F, AFTER EXPOSURE TO 1.0 PSIG H₂ GAS FOR 5 HOURS

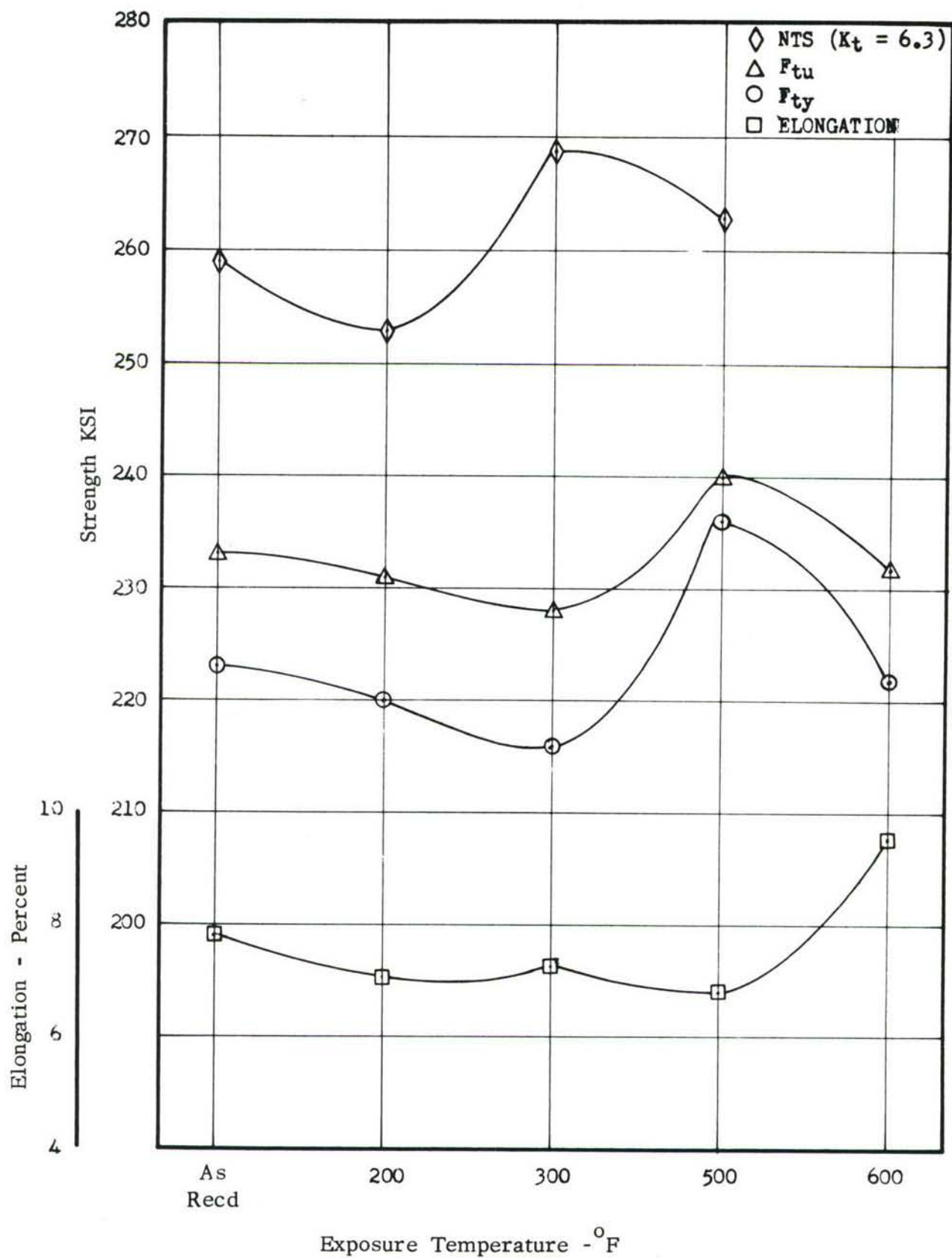


Figure 178. MECHANICAL PROPERTIES AT -423°F , AFTER EXPOSURE TO 1.0 PSIG H_2 GAS FOR 5 HOURS

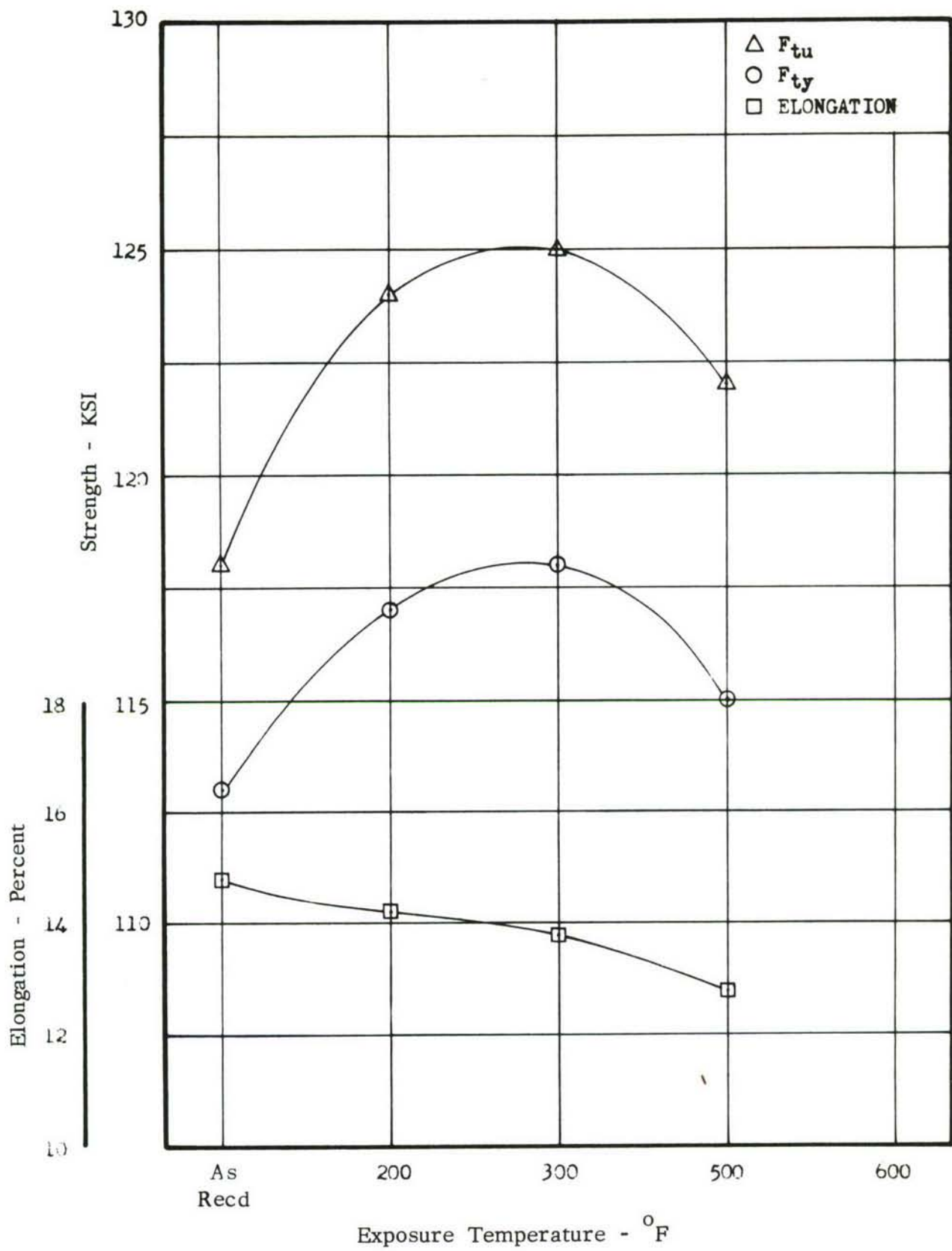


Figure 179. MECHANICAL PROPERTIES AT 75°F, AFTER EXPOSURE TO 1.0 PSIG H₂ GAS FOR 50 HOURS

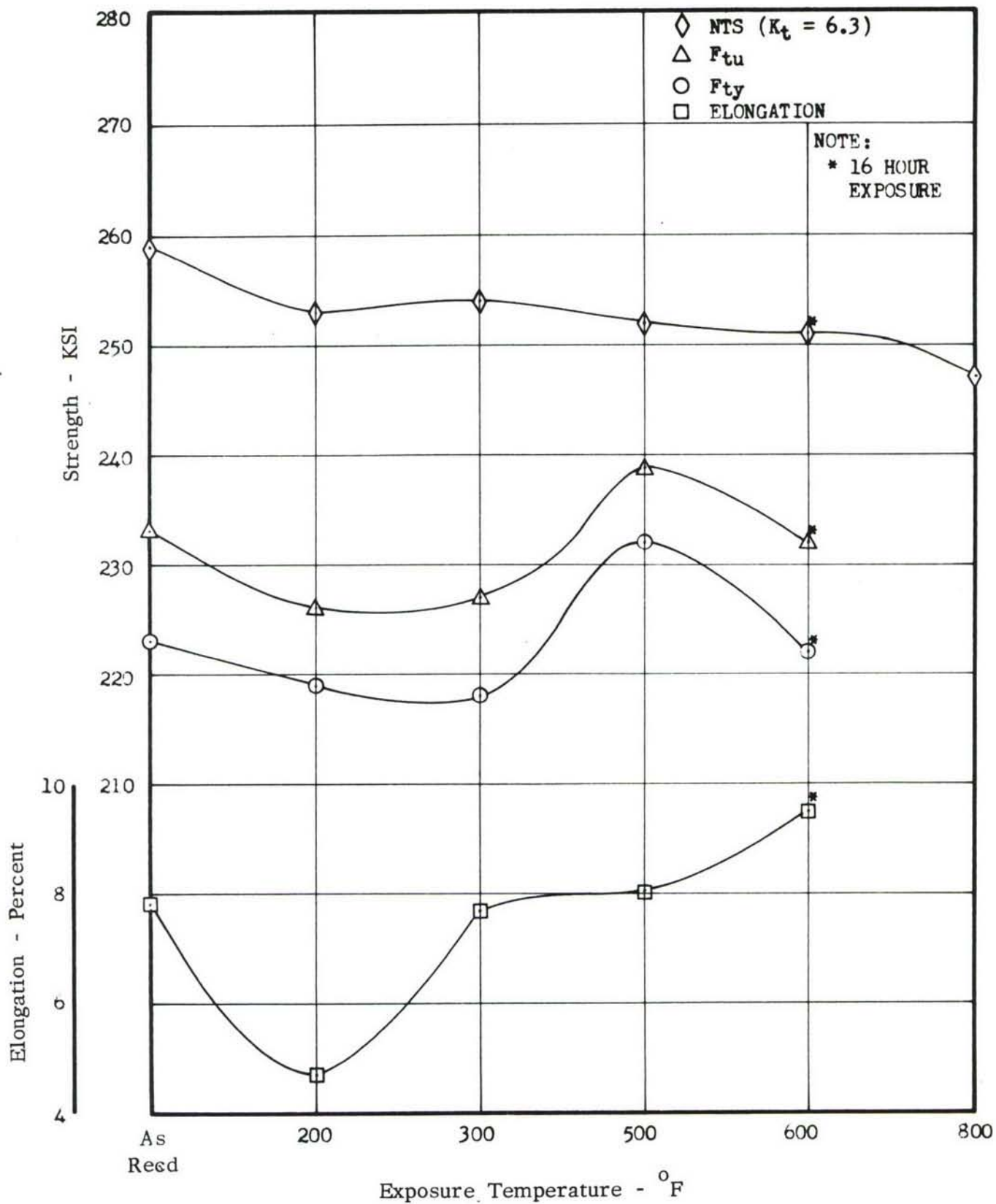


Figure 180. MECHANICAL PROPERTIES AT -423°F , AFTER EXPOSURE TO 1.0 PSIG H_2 GAS FOR 50 HOURS

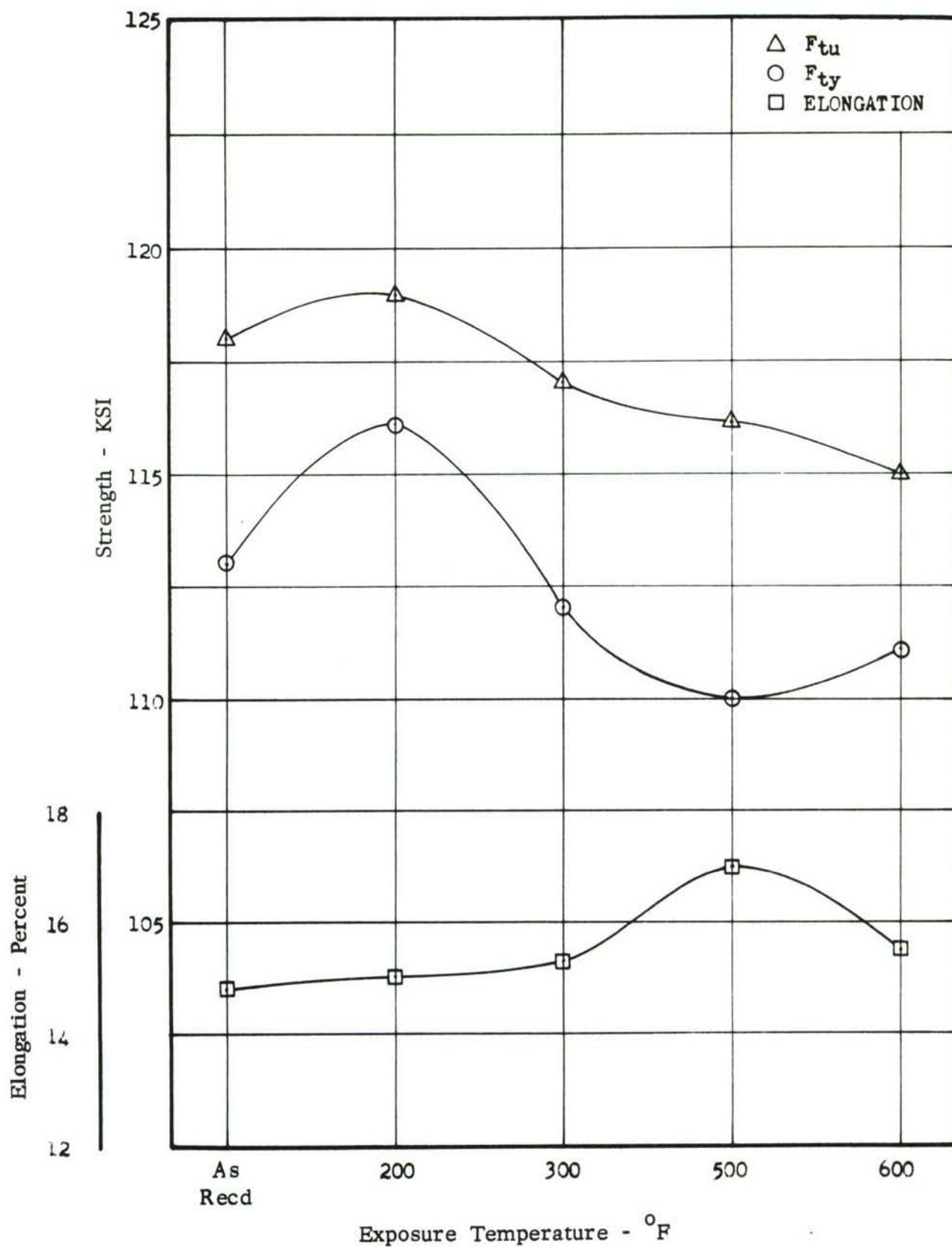


Figure 181. MECHANICAL PROPERTIES AT 75°F, AFTER EXPOSURE TO 1.0 PSIG H₂ GAS FOR 5 HOURS WITH 10 KSI LOAD

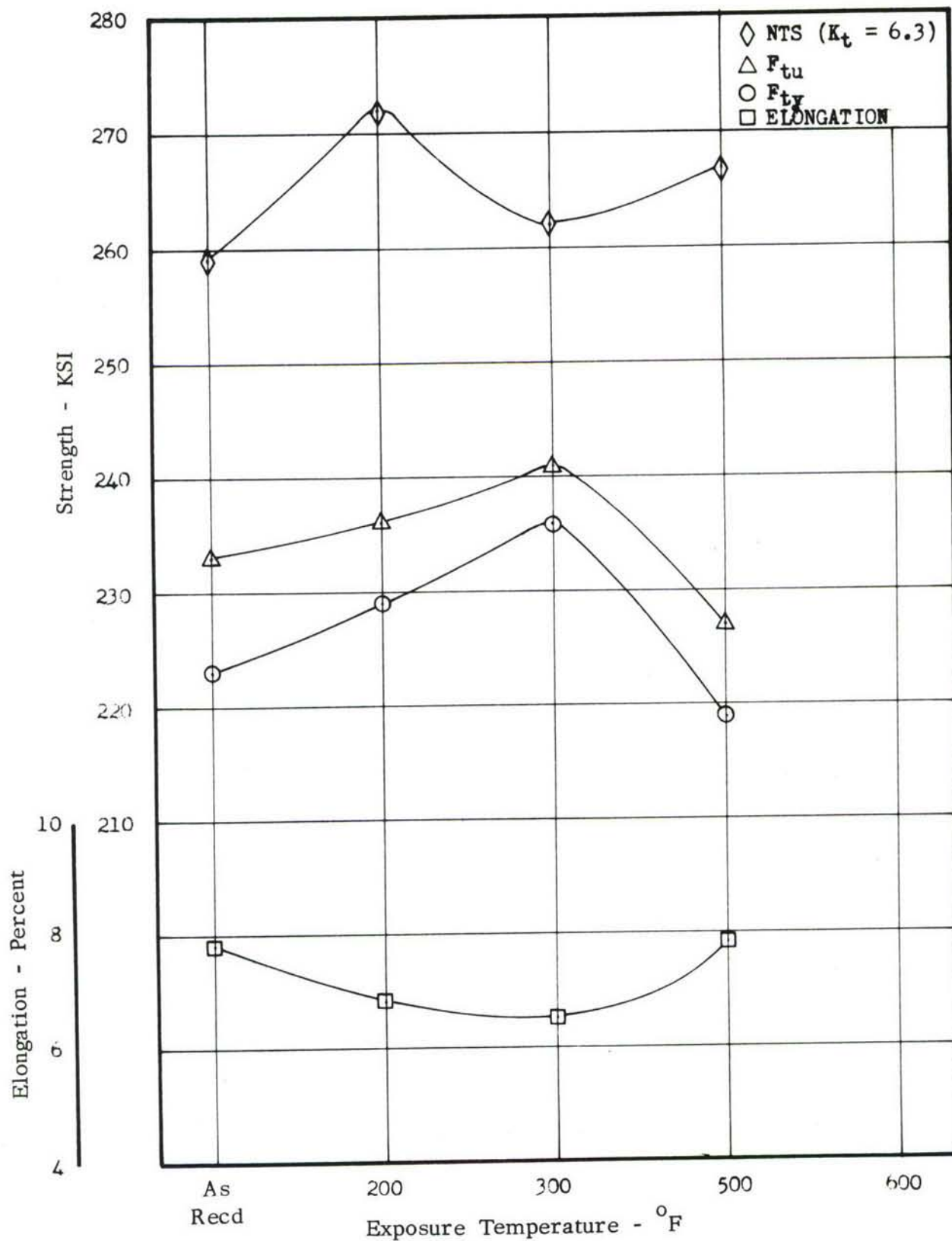


Figure 182. MECHANICAL PROPERTIES AT -423°F , AFTER EXPOSURE TO 1.0 PSIG H_2 GAS FOR 5 HOURS WITH 10 KSI LOAD

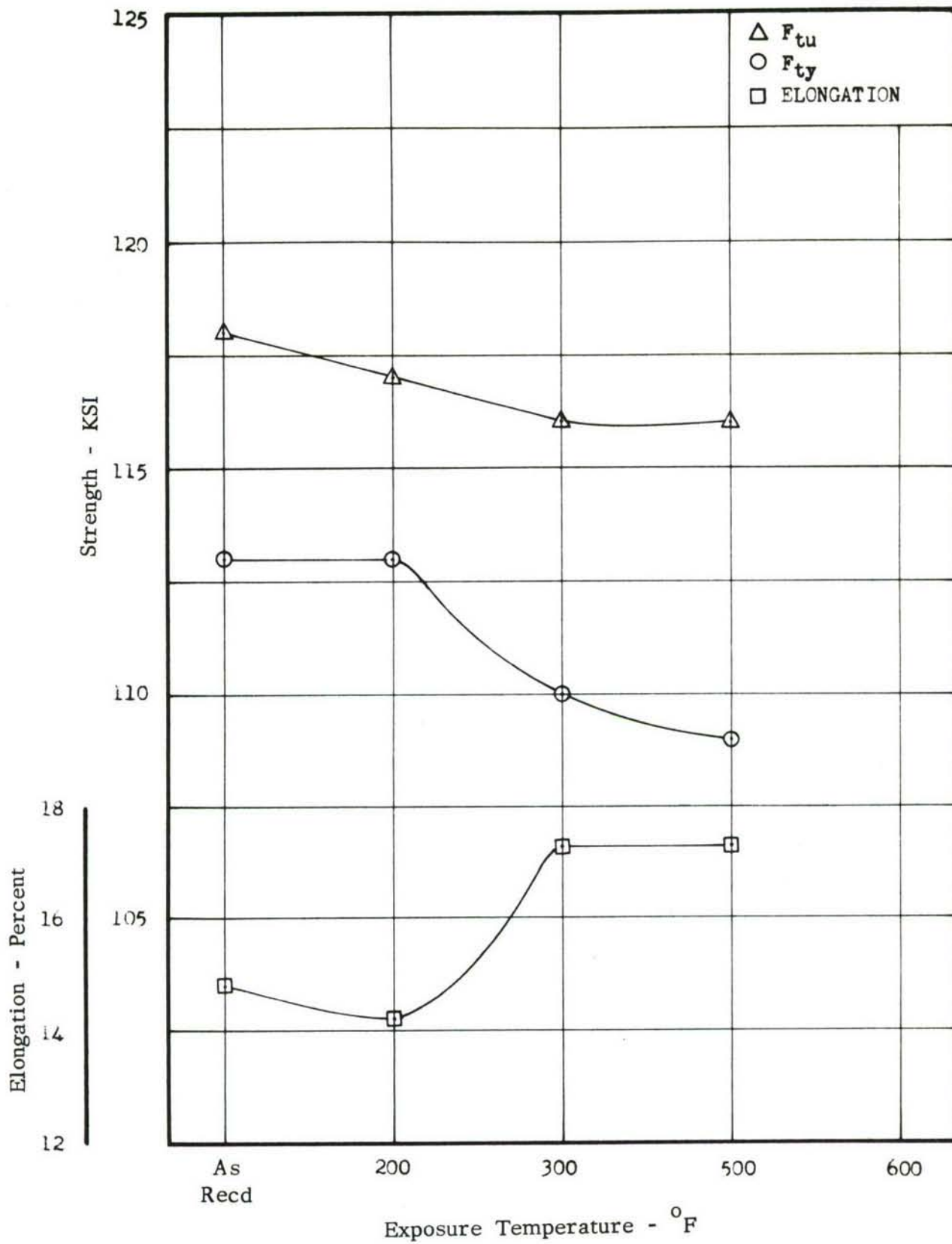


Figure 183. MECHANICAL PROPERTIES AT 75 °F, AFTER EXPOSURE TO 1.0 PSIG H₂ GAS FOR 50 HOURS WITH 10 KSI LOAD

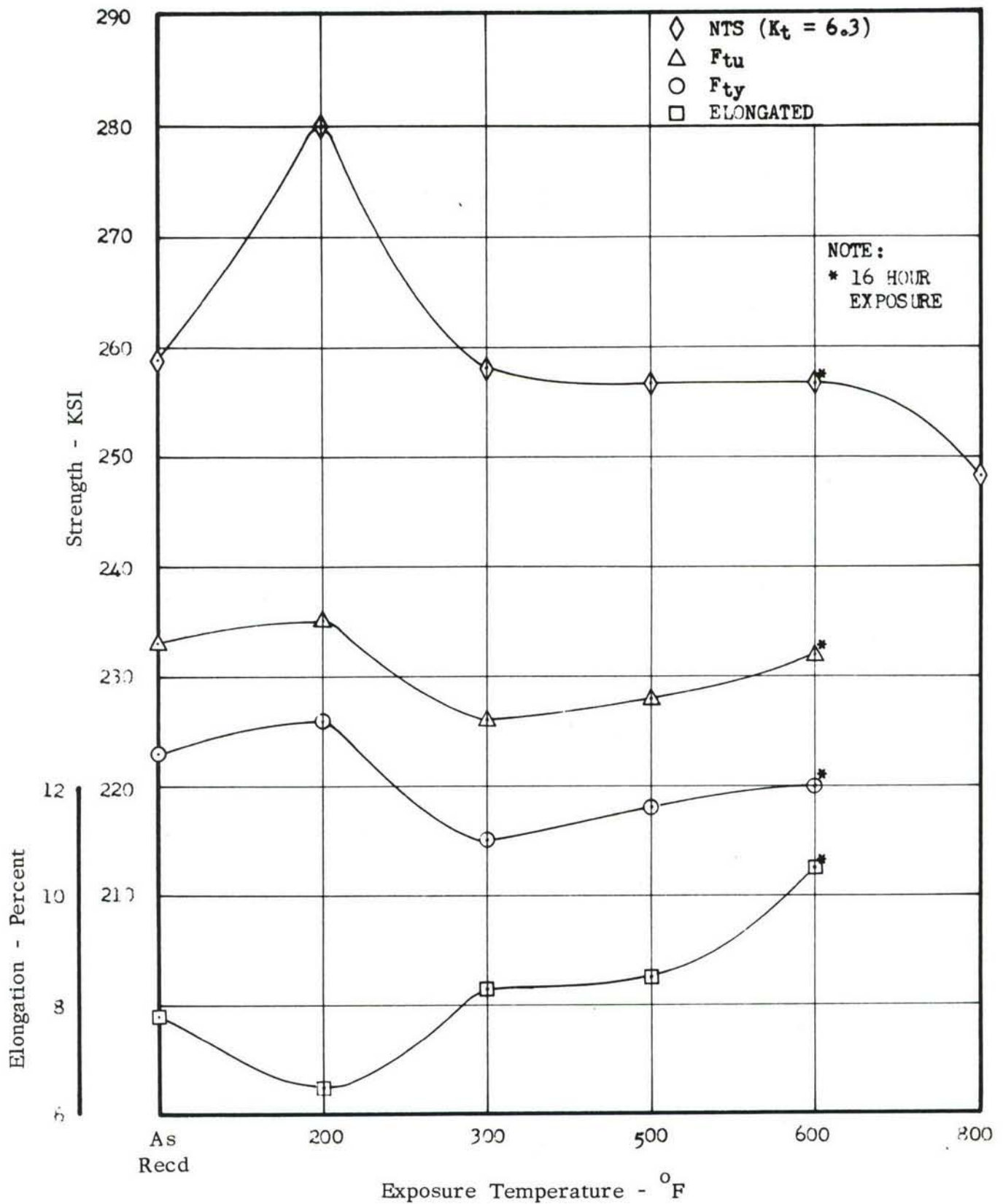
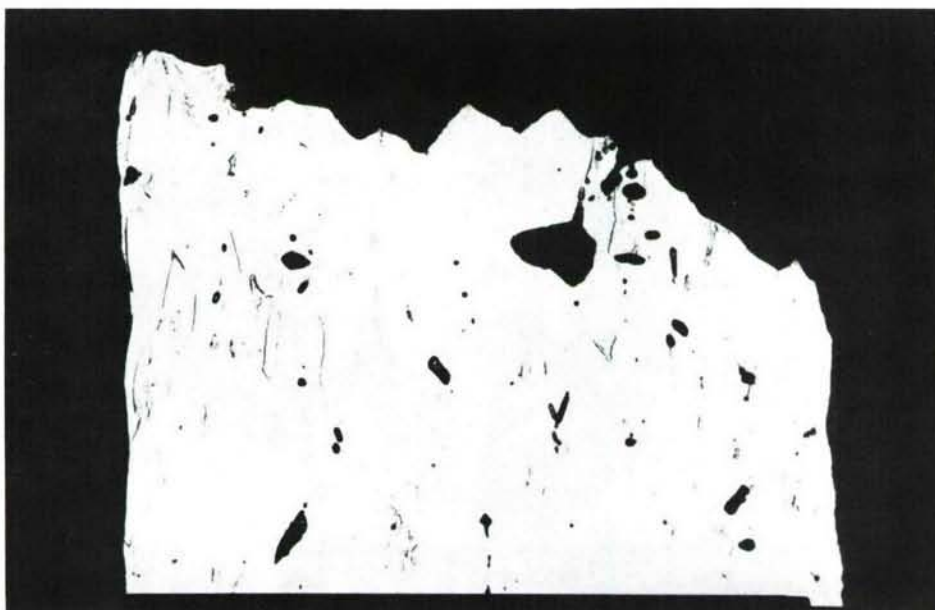


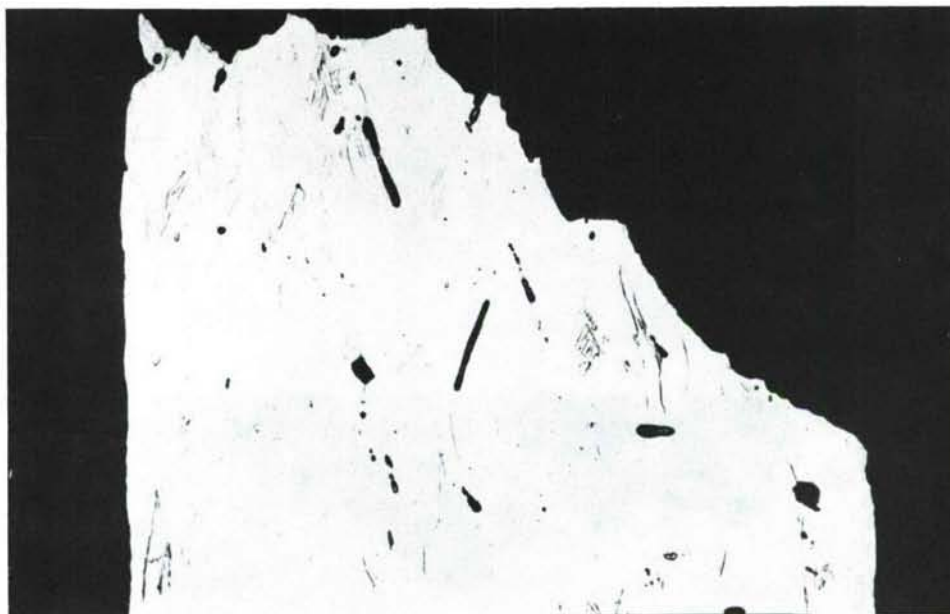
Figure 184. MECHANICAL PROPERTIES AT -423°F , AFTER EXPOSURE TO 1.0 PSIG H_2 GAS FOR 50 HOURS WITH 10 KSI LOAD



Etchant : Kroll's Magnification : 250X
 Figure 185. PHOTOMICROGRAPH OF TITANIUM - AS RECEIVED
 (Heat # 3930498)



Etchant : Kroll's Magnification : 250X
 Figure 186. PHOTOMICROGRAPH OF TITANIUM (Heat # 3930498)
 - AFTER EXPOSURE TO 1.0 PSIG H_2 GAS AT 200°F, FOR 50 HOURS
 WITH 10 KSI LOAD



Etchant : Kroll's

Magnification : 250X

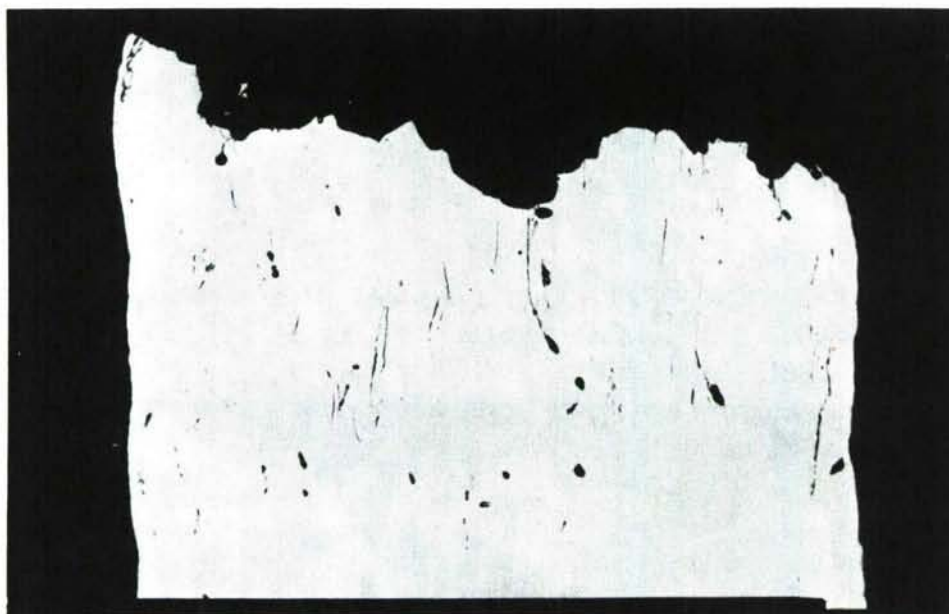
Figure 187. PHOTOMICROGRAPH OF TITANIUM (Heat # 3930498)
AFTER EXPOSURE TO 1.0 PSIG H_2 GAS AT 300 F, FOR 50 HOURS,
WITH 10 KSI LOAD



Etchant : Kroll's

Magnification : 250X

Figure 188. PHOTOMICROGRAPH OF TITANIUM (Heat # 3930498)
AFTER EXPOSURE TO 1.0 PSIG H_2 GAS AT 500 F, FOR 50 HOURS,
WITH 10 KSI LOAD



Etchant : Kroll's Magnification : 250X
Figure 189. PHOTOMICROGRAPH OF TITANIUM (Heat # 3930498)
- AFTER EXPOSURE TO 1.0 PSIG H_2 GAS AT 600° F, FOR 5 HOURS,
WITH 10 KSI LOAD

Table 10. HISTORY AND CHEMICAL ANALYSIS
OF TITANIUM 5Al 2.5Sn ELI ALLOYS

Gage	0.006	0.013	0.017	0.032
Temper	Annealed	Annealed	Annealed	Annealed
Supplier	TMCA	TMCA	Republic	TMCA
Heat No.	D-3274	D-3274	3930498	D-5907
Specification	GD/A-071010	GD/A-071010	GD/A-071010	GD/A-071010
Tensile Prop. F _{ty} (KSI)	96.3	98.7	113	111
(at room temp) F _{tu} (KSI)	104	110	118	121
Elong (%)	18.0	18.2	14.8	17.5
Chemistry (Wt. %)				
Al	5.2	5.2	5.38	5.2
C	0.026	0.026	0.04	0.025
Fe	0.005	0.05	-	0.16
H	0.0012	0.0012	0.0048	0.010
Mn	<0.006	<0.006	-	0.002
N	0.017	0.017	0.007	0.014
O	0.08	0.08	0.012	0.07
Sn	2.5	2.5	2.53	2.5
Ti	Bal	Bal	Bal	Bal

TABLE 11 - MECHANICAL PROPERTIES OF TITANIUM-5Al-2.5Sn ELI ALLOY (Heat No. 3930498, 0.032

Inch Thick Sheet)

EXPOSURE CONDITION	EXPOSURE TEMP (°F)	TEST TEMP (°F)	F _{ty} (Ksi)	F _{tu} (Ksi)	ELONG. (%)	NOTCH T.S. (K _t =6.3) (Ksi)	NOTCH/UN- NOTCHED TENSILE RATIO	WELD T.S. (Ksi)	WELD ELONG. (%)	JOINT EFF. (%)
As Received	-	75	115	119	14.5			109	10.0	
	-	75	111	118	15.5			112	8.5	
	-	75	113	117	14.5			113	14.0	94
Avg.			113	118	14.8			111	10.8	
	-	-423	225	235	8.0	270		214	1.0	
	-	-423	223	232	7.0	247		224	1.0	
	-	-423	222	231	8.5	260	1.11	223	2.0	94
Avg.			223	233	7.8	259		220	1.3	
1.0 PSIG H ₂ for 5 hours	200	75	113	122	14.5					
	200	75	115	123	14.0					
	200	75	114	119	12.5					
Avg.			114	121	13.7					
	200	-423	219	230	6.5	250				
	200	-423	220	231	8.0	256	1.09			
	200	-423	222	231	6.5	253				
Avg.			220	231	7.0					
1.0 PSIG H ₂ for 50 hours	200	75	115	123	14.5					
	200	75	119	127	14.0					
	200	75	116	123	14.0					
Avg.			117	124	14.2					
	200	-423	216	217	1.0	253				
	200	-423	220	231	7.0	264				
	200	-423	221	231	6.0	242	1.12			
Avg.			219	226	4.7	253				

TABLE 11.- CONTINUED

EXPOSURE CONDITION	EXPOSURE TEMP (°F)	TEST TEMP (°F)	F _{ty} (Ksi)	F _{tu} (Ksi)	ELONG. (%)	NOTCH T.S. (K _t =6.3) (Ksi)	NOTCH/UN- NOTCHED TENSILE RATIO	WELD T.S. (Ksi)	WELD ELONG. (%)	JOINT EFF. (%)
1.0 PSIG H ₂ for 5 hours	300	75	120	128	14.0					
	300	75	118	128	15.0					
	300	75	118	125	15.0					
Avg.			119	126	14.7					
	300	-423	216	227	6.5	257				
	300	-423	220	231	9.0	273				
	300	-423	213	225	6.5	276	1.18			
Avg.			216	228	7.3	269				
1.0 PSIG H ₂ for 50 hours	300	75	116	124	13.5					
	300	75	119	126	13.5					
	300	75	118	125	14.5					
Avg.			118	125	13.8					
	300	-423	218	228	7.0	257				
	300	-423	220	231	7.0	251				
	300	-423	217	229	9.0	255	1.12			
Avg.			218	229	7.7	254				
1.0 PSIG H ₂ for 5 hours	500	75	117	125	14.0					
	500	75	121	124	11.5					
	500	75	120	123	11.5					
Avg.			119	124	12.3					
	500	-423	238	241	5.5	258		227	1.5	
	500	-423	228	234	8.0	263		232	1.5	
	500	-423	242	246	-	269		230	1.5	
Avg.			236	240	6.8	263	1.09	230	1.5	96

TABLE 11 - CONTINUED

EXPOSURE CONDITION	EXPOSURE TEMP (°F)	TEST TEMP (°F)	F _{ty} (Ksi)	F _{tu} (Ksi)	ELONG. (%)	NOTCH T.S. (K _t =6.3) (Ksi)	NOTCH/UN- NOTCHED TENSILE RATIO	WELD T.S. (Ksi)	WELD ELONG. (%)	JOINT EFF.. (%)
1.0 PSIG H ₂ for 50 hours	500	75	118	122	13.5					
	500	75	115	122	14.5					
	500	75	111	122	10.5					
Avg.			115	122	12.8					
	500	-423	240	244	6.5	246		228	1.5	
	500	-423	238	242	-	254		226	0.5	
	500	-423	219	232	0.5	256	1.05	230	1.0	94
Avg.			232	239	8.0	252		225	1.0	
15.0 PSIG H ₂ for 5 hours	500	75	116	122	13.5					
	500	75	110	118	14.0					
	500	75	128	128	8.5					
Avg.			118	119	12.0					
	500	-423	239	244	6.0	252		225	0.5	
	500	-423	239	243	6.0	254		229	0.5	
	500	-423	232	237	5.5	272	1.07	230	1.0	93
Avg.			237	241	5.8	259		228	0.7	
1.0 PSIG H ₂ for 5 hours	600	75	116	118	13.0	152				
	600	75	118	120	13.0	149				
	600	75	118	120	13.0	150	1.26			
Avg.			117	119	13.0	150				
1.0 PSIG H ₂ for 16 hours	600	-423	220	231	-	253		230	1.0	
	600	-423	226	234	9.0	258		229	1.0	
	600	-423	220	231	10.0	241	1.08	230	1.0	99
Avg.			222	232	9.5	251		230	1.0	

TABLE 11 - CONTINUED

EXPOSURE CONDITION	EXPOSURE TEMP (°F)	TEST TEMP (°F)	F _{ty} (Ksi)	F _{tu} (Ksi)	ELONG. (%)	NOTCH T.S. (K _t =6.3) (Ksi)	NOTCH/UN- NOTCHED TENSILE RATIO	WELD T.S. (Ksi)	WELD ELONG. (%)	JOINT EFF. (%)
1.0 PSIG H ₂ for 5 hours 10 KSI load Avg.	200 200 200 Avg.	75 75 75	114 122 111 116	117 122 117 119	16.5 13.0 15.5 15.0					
	200 200 200 Avg.	-423 -423 -423	224 223 239 229	233 231 244 236	7.5 7.0 6.0 6.8	280 279 258 272	1.15			
1.0 PSIG H ₂ for 50 hours 10 KSI load Avg.	200 200 200 Avg.	75 75 75	118 111 109 113	122 115 113 117	11.0 15.5 16.0 14.2					
	200 200 200 Avg.	-423 -423 -423	236 216 225 226	247 226 233 235	6.0 6.5 7.0 6.5	272 291 276 280	1.19			
1.0 PSIG H ₂ for 5 hours 10 KSI load Avg.	300 300 300 Avg.	75 75 75	112 107 116 112	118 115 117 117	15.5 16.5 14.0 15.3					
	300 300 300 Avg.	-423 -423 -423	240 236 231 236	246 240 237 241	5.5 7.0 7.0 6.5	276 291 276 280	1.09			

TABLE 11. CONTINUED

EXPOSURE CONDITION	EXPOSURE TEMP (°F)	TEST TEMP (°F)	F _{ty} (Ksi)	F _{tu} (Ksi)	ELONG. (%)	NOTCH T.S. (Kt=6.3) (Ksi)	NOTCH/UN- NOTCHED TENSILE RATIO	WELD T.S. (Ksi)	WELD ELONG. (%)	JOINT EFF. (%)
1.0 PSIG H ₂	300	75	111	117	17.0					
for 50 hours	300	75	109	116	17.5					
10 KSI load	300	75	109	116	17.0					
Avg.			110	116	17.3					
	300	-423	217	237	7.0	264				
	300	-423	218	230	9.5	256				
	300	-423	211	222	8.0	254	1.14			
Avg.			215	226	8.3	258				
5.0 PSIG Pure	300	75	108	114	15.5					
H ₂ for 5 hours	300	75	110	116	15.0					
50 KSI load	300		109	115	15.3					
Avg.										
	300	-423	220	230	8.5	280		226	0.5	
	300	-423	-	-	-	260		229	0.5	
			220	230	8.5	270	1.17	228	0.5	99
5.0 PSIG Pure	300	75	111	113	14.5					
H ₂ for 16 hours	300									
50 KSI load	300	-423	222	233	8.5	263		-	-	
Avg.										
	300	-423	226	230	8.0	247		226	0.5	
			224	232	8.3	255	1.10	226	0.5	98
5.0 PSIG Pure										
H ₂ for 5 hours	400	-423	-	-	-	258	-			
50 KSI load										
5.0 PSIG Pure										
H ₂ for 64 hours	400	-423	-	-	-	262	-			
50 KSI load										

TABLE 11 - CONTINUED

EXPOSURE CONDITION	EXPOSURE TEMP (°F)	TEST TEMP (°F)	F _{ty} (Ksi)	F _{tu} (Ksi)	ELONG. (%)	NOTCH T.S. (Kt=6.3) (Ksi)	NOTCH/UN- NOTCHED TENSILE RATIO	WELD T.S. (Ksi)	WELD ELONG. (%)	JOINT EFF. (%)
1.0 PSIG H ₂ for 5 hours 10 KSI load Avg.	500 500 500 Avg.	75 75 75	109 - 110 110	117 115 117 116	17.5 16.5 17.0 17.0					
	500 500 500 Avg.	-423 -423 -423	219 219 219 219	229 229 230 227	7.5 8.0 8.0 7.8	273 261 266 267	1.18	230 229 221 227	1.5 0.5 0.5 0.8	100
1.0 PSIG H ₂ for 50 hours 10 KSI load Avg.	500 500 500 Avg.	75 75 75	108 106 114 109	116 113 120 116	17.0 17.0 18.0 17.3					
	500 500 500 Avg.	-423 -423 -423	219 214 221 218	229 225 231 228	8.0 9.0 8.5 8.5	254 256 262 257	1.13	225 229 215 223	1.0 1.5 0.5 1.0	98
1.0 PSIG H ₂ for 5 hours 10 KSI load Avg.	600 600 600 Avg.	75 75 75	113 113 108 111	116 116 114 115	15.5 15.5 15.5 15.5	155 154 153 154	134			
1.0 PSIG H ₂ for 16 hours 10 KSI load Avg.	600 600 600 Avg.	-423 -423 -423	226 218 217 220	234 232 230 232	10.0 11.5 10.0 10.5	256 261 254 257	1.10	228 226 230 228	1.0 0.5 0.5 0.7	98

TABLE 11 - Cont.

EXPOSURE CONDITION	EXPOSURE TEMP (°F)	TEST TEMP (°F)	F _{ty} (Ksi)	F _{tu} (Ksi)	ELONG. (%)	NOTCH T.S. (K _t =6.2) (Ksi)	NOTCH/UN- NOTCHED TENSILE RATIO	WELD T.S. (Ksi)	WELD ELONG. (%)	JOINT EFF. (%)
1.0 PSIG H ₂ + H ₂ O vapor for 16 hours Avg.	600 600 600 Avg.	-423 -423 -423				259 238 <u>266</u> 254		237 219 <u>236</u> 231	1.0 1.0 <u>0.5</u> 0.8	
1.0 PSIG H ₂ + H ₂ O vapor for 16 hours 10 KSI load Avg.	600 600 600 Avg.	-423 -423 -423	229 229 <u>221</u> 226	233 233 <u>230</u> 232	8.5 9.5 <u>7.0</u> 8.3	260 246 <u>264</u> 257	1.14			
1.0 PSIG H ₂ for 64 hours Avg.	800 800 800 Avg.	-423 -423 -423				260 230 <u>250</u> 247				
1.0 PSIG H ₂ for 64 hours 10 KSI load	800 800 800	-423 -423 -423				253 251 <u>240</u> 248				

TABLE 12 - MECHANICAL PROPERTIES OF TITANIUM 5Al-2.5Sn ELI ALLOY (Heat No. D-3274, 0.006 and 0.013 inch thick Sheet)

EXPOSURE CONDITION	EXPOSURE TEMP (°F)	TEST TEMP (°F)	F _{ty} (Ksi)	F _{tu} (Ksi)	ELONG. (%)	NOTCH T.S. (K _t =6.3) (Ksi)	NOTCH/UN- NOTCHED TENSILE RATIO	WELD T.S. (Ksi)	WELD ELONG. (%)	JOINT EFF. (%)
As Received	-	75	98.7	110	18.2	143	1.30	111	15.2	100
	-	-423	208	228	10.8	250	1.10	225	2.3	99
	-	-423	191*	207*	8.1*	252*	1.22*	211*	2.5*	100*
1.0 PSIG H ₂ for 50 hours	200	-423						219	1.0	
	200	-423						220	1.0	
	200	-423						220	1.5	
	Avg.							217	1.2	
1.0 PSIG H ₂ for 50 hours	500	75	98.3	107	18.5			106	13.5	100
	500	-423	213	228	11.0	248		224	5.0	
	500	-423	220	233	10.5	247		224	4.5	
	Avg.		216	230	10.8	248	1.08	224	4.8	97
1.0 PSIG H ₂ for 50 hours	500	-423	192*	214*	3.0*	248*				
	500	-423	214*	229*	5.5*	247*				
	Avg.		203*	221*	4.3*	248*	1.12*			

* 0.006 inch thickness

TABLE 13- MECHANICAL PROPERTIES OF TITANIUM - 5Al-2.5Sn ELI ALLOY (Heat No. D-5907, 0.032 Inch Thick Sheet)

EXPOSURE CONDITIONS	EXPOSURE TEMP (°F)	TEST TEMP (°F)	F _{ty} (Ksi)	F _{tu} (Ksi)	ELONG. (%)	NOTCH T.S. (K _t =6.3) (Ksi)	NOTCH/UN- NOTCHED TENSILE RATIO	WELD T.S. (Ksi)	WELD ELONG. (%)	JOINT EFF. (%)
As Received	-	-423	-	-	12.0					
	-	-423	206	230	13.5					
	-	-423	205	231	11.5					
Avg.			206	231	12.3					
	-	-423				195				
	-	-423				203				
	-	-423				207				
	-	-423				185				
	-	-423				196				
	-	-423				202				
Avg.						198	0.86			
1.0 PSIG H ₂ for 16 hours 10 KSI load	600	-423	208	232	12.0					
	600	-423	205	233	15.5					
	600	-423	209	235	-					
Avg.			207	233	13.8					
	600	-423				209				
	600	-423				204				
	600	-423				216				
Avg.						210	0.90			

UNCLASSIFIED

Security Classification

DOCUMENT CONTROL DATA - R&D

(Security classification of title, body of abstract and indexing annotation must be entered when the overall report is classified)

1. ORIGINATING ACTIVITY (Corporate author) Convair Division of General Dynamics Corp. San Diego, California		2a. REPORT SECURITY CLASSIFICATION UNCLASSIFIED	
		2b. GROUP	
3. REPORT TITLE Hydrogen Tankage for Hypersonic Cruise Vehicles Phase I			
4. DESCRIPTIVE NOTES (Type of report and inclusive dates) Phase I, Final Technical Report-Work Period July 1964 to October 1965			
5. AUTHOR(S) (Last name, first name, initial) Heathman, John H., et al			
6. REPORT DATE August 66	7a. TOTAL NO. OF PAGES 322	7b. NO. OF REFS 11	
8a. CONTRACT OR GRANT NO. AF 33(615)-2048	9a. ORIGINATOR'S REPORT NUMBER(S)		
b. PROJECT NO. 651G			
c.	9b. OTHER REPORT NO(S) (Any other numbers that may be assigned this report)		
d.	AFFDL-TR-65-230		
10. AVAILABILITY/LIMITATION NOTICES This document is subject to special export controls and each transmittal to Foreign governments or Foreign Nationals may be made only with prior approval of the AFFDL/FDTS.			
11. SUPPLEMENTARY NOTES		12. SPONSORING MILITARY ACTIVITY AF Flight Dynamics Laboratory FDTS Wright-Patterson AFB, Ohio	
13. ABSTRACT This is the Final Report on Phase I, of a three phase program under contract AF 33(615)-2048 "Hydrogen Tankage for Hypersonic Cruise Vehicles" and covers the design, fabrication and experimental verification of non-integral liquid hydrogen tankage systems applicable to manned aerospace vehicles. The design criteria, results of an optimization program, supporting test and evaluation work, and an experimental test program are summarized. Design studies covered structural materials and concepts, insulation systems and fuel system requirements. Supporting evaluations and test data on strain gages at -423°F and titanium sensitivity to hydrogen gas embrittlement are included.(U) This work provides the basis for establishment of the design requirements of a large-scale tank to be designed, fabricated and proof tested in Phase II and subjected to a simulated vehicle environment with programmed liquid hydrogen defueling in Phase III. (U)			

UNCLASSIFIED
Security Classification

14. KEY WORDS	LINK A		LINK B		LINK C	
	ROLE	WT	ROLE	WT	ROLE	WT
CRYOGENIC TANKS (U)						
INSULATION (U)						
LIQUID HYDROGEN (U)						
HYPERSONIC VEHICLES (U)						
HYDROGEN EMBRITTLEMENT (U)						
PRESSURE VESSELS (U)						

INSTRUCTIONS

1. **ORIGINATING ACTIVITY:** Enter the name and address of the contractor, subcontractor, grantee, Department of Defense activity or other organization (*corporate author*) issuing the report.

2a. **REPORT SECURITY CLASSIFICATION:** Enter the overall security classification of the report. Indicate whether "Restricted Data" is included. Marking is to be in accordance with appropriate security regulations.

2b. **GROUP:** Automatic downgrading is specified in DoD Directive 5200.10 and Armed Forces Industrial Manual. Enter the group number. Also, when applicable, show that optional markings have been used for Group 3 and Group 4 as authorized.

3. **REPORT TITLE:** Enter the complete report title in all capital letters. Titles in all cases should be unclassified. If a meaningful title cannot be selected without classification, show title classification in all capitals in parenthesis immediately following the title.

4. **DESCRIPTIVE NOTES:** If appropriate, enter the type of report, e.g., interim, progress, summary, annual, or final. Give the inclusive dates when a specific reporting period is covered.

5. **AUTHOR(S):** Enter the name(s) of author(s) as shown on or in the report. Enter last name, first name, middle initial. If military, show rank and branch of service. The name of the principal author is an absolute minimum requirement.

6. **REPORT DATE:** Enter the date of the report as day, month, year, or month, year. If more than one date appears on the report, use date of publication.

7a. **TOTAL NUMBER OF PAGES:** The total page count should follow normal pagination procedures, i.e., enter the number of pages containing information.

7b. **NUMBER OF REFERENCES:** Enter the total number of references cited in the report.

8a. **CONTRACT OR GRANT NUMBER:** If appropriate, enter the applicable number of the contract or grant under which the report was written.

8b, 8c, & 8d. **PROJECT NUMBER:** Enter the appropriate military department identification, such as project number, subproject number, system numbers, task number, etc.

9a. **ORIGINATOR'S REPORT NUMBER(S):** Enter the official report number by which the document will be identified and controlled by the originating activity. This number must be unique to this report.

9b. **OTHER REPORT NUMBER(S):** If the report has been assigned any other report numbers (*either by the originator or by the sponsor*), also enter this number(s).

10. **AVAILABILITY/LIMITATION NOTICES:** Enter any limitations on further dissemination of the report, other than those

imposed by security classification, using standard statements such as:

- (1) "Qualified requesters may obtain copies of this report from DDC."
- (2) "Foreign announcement and dissemination of this report by DDC is not authorized."
- (3) "U. S. Government agencies may obtain copies of this report directly from DDC. Other qualified DDC users shall request through _____."
- (4) "U. S. military agencies may obtain copies of this report directly from DDC. Other qualified users shall request through _____."
- (5) "All distribution of this report is controlled. Qualified DDC users shall request through _____."

If the report has been furnished to the Office of Technical Services, Department of Commerce, for sale to the public, indicate this fact and enter the price, if known.

11. **SUPPLEMENTARY NOTES:** Use for additional explanatory notes.

12. **SPONSORING MILITARY ACTIVITY:** Enter the name of the departmental project office or laboratory sponsoring (*paying for*) the research and development. Include address.

13. **ABSTRACT:** Enter an abstract giving a brief and factual summary of the document indicative of the report, even though it may also appear elsewhere in the body of the technical report. If additional space is required, a continuation sheet shall be attached.

It is highly desirable that the abstract of classified reports be unclassified. Each paragraph of the abstract shall end with an indication of the military security classification of the information in the paragraph, represented as (TS), (S), (C), or (U).

There is no limitation on the length of the abstract. However, the suggested length is from 150 to 225 words.

14. **KEY WORDS:** Key words are technically meaningful terms or short phrases that characterize a report and may be used as index entries for cataloging the report. Key words must be selected so that no security classification is required. Identifiers, such as equipment model designation, trade name, military project code name, geographic location, may be used as key words but will be followed by an indication of technical context. The assignment of links, rules, and weights is optional.